AD-A242 827

1

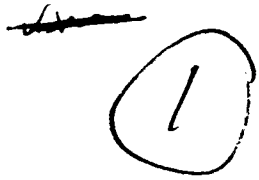

NASA Technical Memorandum 101598

AVSCOM
Technical Memorandum 89-B-001

INFLOW MEASUREMENTS MADE WITH A LASER VELOCIMETER ON A HELICOPTER MODEL IN FORWARD FLIGHT

Volume VI: RECTANGULAR PLANFORM BLADES AT AN ADVANCE RATIO OF 0.35

Danny R. Hoad, Susan L. Althoff, and Joe W. Elliott
Aerostructures Directorate
USAARTA - AVSCOM
Langley Research Center
Hampton, Virginia

Richard H. Sailey
Planning Research Corporation
Aerospace Technologies Division
Hampton, Virginia

DTIC
ELECTE
NOV 08 1991
S D
D

This document has been approved for public release and sale; its distribution is unlimited.

April 1989

91-14725

91 10 31 096

NASA
National Aeronautics and
Space Administration

Langley Research Center
Hampton, Virginia 23665-5225

"Original contains color plates: All DTIC reproductions will be in black and white"

US ARMY
AVIATION
SYSTEMS COMMAND
AVIATION R&T ACTIVITY

SUMMARY

An experimental investigation was conducted in the 14- by 22-Foot Subsonic Tunnel at the NASA Langley Research Center to measure the inflow into a scale model helicopter rotor in forward flight (μ = 0.35). The measurements were made with a two-component Laser Velocimeter (LV) one chord above the plane formed by the path of the rotor tips (tip-path-plane). A conditional sampling technique was used to determine the position of the rotor at the time that each velocity measurement was made so that the azimuthal fluctuations in velocity could be determined. Measurements were made at a total of 179 separate locations in order to clearly define the inflow character. The mean and standard deviation of the induced inflow ratios and the azimuthally dependent induced inflow ratios are included on 5.25 flexible disk in the pocket on the inside of the rear cover of this report. These data are presented herein without analysis.

INTRODUCTION

One of the problems confronting the helicopter industry is the lack of detailed information about the velocity fluctuations around and through rotating blades. This information is needed for two reasons: to ensure a more complete understanding of the flow field environment associated with a thrusting rotor and to provide data for the validation of rapidly emerging computational codes. One explanation for the lack of available data is the absence, until recent years, of a suitable device for making such measurements. Making measurements of the velocity around a system of rotating blades requires an accurate, nonintrusive measurement capability that presents a minimum risk to the systems involved. The LV, which uses high energy light beams to measure velocities, is ideally suited to this task.

The LV has been successfully used to measure specific areas and localized phenomena within the rotor disk (references 1 through 3). In addition, the hotwire anemometer and pressure probe, both having directional measuring limitations, have been used in similar programs (references 4 and 5). This comprehensive program has been conducted to measure the flow into a representative rotor system as a function of azimuth using a two-component (stream-wise and vertical direction) LV system.

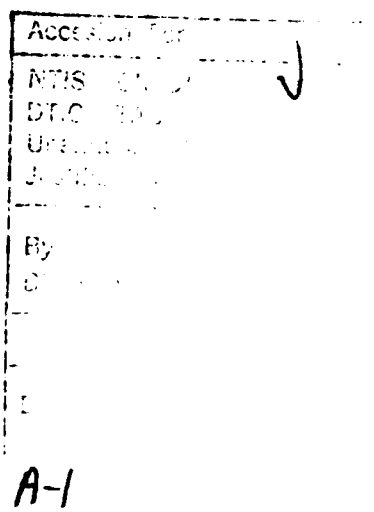

NOTATION

A	rotor disc area, (πR^2), ft^2
A_0	Constant term in Fourier series of blade feathering (collective) at r/R = 0.75, deg
A_1	Coefficient of cosine term in Fourier series of blade feathering, deg
b	Number of blades
B_1	Coefficient of sine term in Fourier series of blade feathering, deg
C_Q	Rotor torque coefficient, $Q/(\rho A(12R)V_{tip}^2)$, nondimensional
C_D	Rotor drag coefficient, $D/(\rho A\ V_{tip}^2)$, nondimensional
C_T	Rotor thrust coefficient, $T/(\rho A\ V_{tip}^2)$, nondimensional
D	Rotor drag, lbf (positive to the rear)
q	Dynamic pressure, lb/ft^2
Q	Rotor torque, in-lbf
r	Local radius of the rotor system, ft
R	Rotor radius, ft
T	Thrust produced by the rotor, lbf
U_∞	Tunnel freestream velocity, ft/sec, (positive downstream)
U	Freestream component of velocity, ft/sec, (positive downstream)
u_i	Induced component of velocity parallel to the tip path plane, ft/sec, (positive downstream)
V	Vertical component of velocity, ft/sec, (positive up)
v_i	Induced component of velocity normal to the tip path plane, ft/sec, (positive up)
V_{tip}	Rotor blade hover-tip velocity, ft/sec, (ΩR)

GREEK

α	Angle between rotor disk and freestream velocity (positive nose up), deg
λ	Inflow Ratio normal to tip path plane (positive up), $(U_\infty \sin \alpha + v_i)/V_{tip}$
λ_i	Induced Inflow Ratio normal to tip path plane (postive up), v_i/V_{tip}
μ_∞	Rotor advance ratio, $U_\infty \cos \alpha/V_{tip}$
μ	Inflow Ratio parallel to tip path plane (positive downstream), $(U_\infty \cos \alpha + u_i)/V_{tip}$
μ_i	Induced Inflow Ratio parallel to tip path plane (positive downstream), u_i/V_{tip}
Ω	Rotor rotational speed, radians/sec
ψ	Rotor azimuth measured from downstream position, positive counterclockwise, as viewed from above, deg
ρ	Air density, slug/ft^3
θ	Blade pitch angle at a specific azimuth (positive nose up), deg, $\theta = A_0 - A_1 \cos \psi - B_1 \sin \psi$
$\overline{XX}$	Mean value

EXPERIMENTAL APPARATUS

The experimental apparatus used in this investigation included the NASA Langley Research Center 14- by 22-Foot Subsonic Tunnel, the 2-Meter Rotor Test System (2MRTS), and a two-component Laser Velocimeter system.

The 14- by 22-Foot Subsonic Tunnel is an atmospheric, closed-circuit wind tunnel of conventional design with enhancements for the testing of powered and high-lift configurations (reference 6). The tunnel is shown in figure 1. When the tunnel is operated in the open configuration, the walls and ceiling of the test section are lifted out of the flow leaving only a solid floor and a flow collector. In this configuration, the tunnel can be driven to about 170 knots. This investigation was conducted with the tunnel in the open configuration to allow complete optical access to the rotor flow field.

The 2MRTS is a general purpose rotorcraft model testing system which was mounted on a strut in the forward part of the test section (see figure 2). The system consists of a 29-horsepower electric drive motor and 90° speed-reducing transmission, a blade pitch remote control system, and two six-component strain gage balances used for measuring forces and moments on the rotor system and the generic fuselage shell (ROBIN). The four-bladed rotor hub is fully articulated with viscous dampers for lead-lag motion and coincident flap and lag hinges. A more detailed description of the 2MRTS and the ROBIN fuselage can be found in reference 7. The characteristics of the rotor blades used during this investigation can be found in table 1. No attempt was made to dynamically scale the rotor blades; rather, they were very rigid to minimize blade aeroelastic response uncertainties.

The LV system used in this investigation was designed to measure the instantaneous components of velocity in the longitudinal (freestream) and vertical directions and is described in reference 8. The system is comprised of four subsystems: optics, traverse, data acquisition, and seeding. The optics subsystem, which is shown in figure 3, operates in backscatter mode and at high power (2 watts in all lines) in order to accommodate the long focal lengths needed to scan the wide test section. The transmitting and receiving optics packages are augmented by a zoom lens system consisting of a 3-inch clear aperture negative lens and a 12-inch clear aperture positive lens. Bragg cells in each of the optical paths provide a directional measurement capability. The velocity measurements are made at a point in space where the four beams cross, called the sample volume. The length of the sample volume (transverse to the flow direction) increases as the sample volume is moved away from the optics assembly. The sample volume length, over the 10- to 20-foot focal length of the system, is less than 1 cm and has a nearly constant diameter of 0.2 mm.

The traverse subsystem provides five degrees of freedom in positioning the sample volume and is controlled by the same computer that is used for data acquisition. Translation of the sample volume in the horizontal and vertical direction is accomplished by displacing the entire optics platform. Translation along the lateral axis is accomplished by displacing the negative lens located in the zoom lens assembly, thus refocusing the sample volume along the axis of optical transmission. The other two degrees of freedom, pan and tilt, are implemented by rotating the final mirror about its vertical and horizontal axes in order to change the direction of optical transmission. The total range of the traversing system is 7 feet vertically, 6 feet streamwise, 16.5 feet laterally, and 10° in both pan and tilt. Measurements can be made outside of this envelope by re-positioning the optics platform, which is mounted on wheels to facilitate such relocations. For this study the traversing system was positioned to the right of the test section when looking upstream as shown in figure 2.

The data acquisition subsystem is shown schematically in figure 4 and interfaces with the optical signal processing equipment to receive two channels of raw LV data and up to five channels of auxiliary data. In this investigation, two auxiliary channels were used for the acquisition of data relative to blade position (one each for the U and V components). The system converts the raw LV data to engineering units and determines the statistical characterstics of the acquired data so that the test results can be evaluated during the acquisition process. The raw data and up to 64 parameters from the tunnel static data acquisition system are written to magnetic tape for later analysis. The final function performed by the data system is to control the five degree-of-freedom scan system.

The seeding subsystem, shown schematically in figure 5 and in the photo in figure 6, is a solid particle, liquid dispensing system (reference 9). Polystyrene latex microspheres are suspended in a mixture containing, by volume, 50 percent water and 50 percent ethyl alcohol. The advantages of the polystyrene particles are their low density, high reflectivity, and precise particle size. The particles used in this investigation were 1.7 microns in diameter with a standard deviation of 0.0239 microns. The particle mixture is pumped to an array of nozzles where compressed air is used to atomize the mixture. These nozzles are mounted on a frame that can be moved about the settling chamber of the tunnel using the remote positioning system recently installed (figure 6). The low vapor pressure of water/alcohol mixture allows it to evaporate as it travels the 85 feet from the settling chamber to the test section. This process provides isolated single particles in the flow field whose velocities are measured as they pass through the sample volume. The local fluid velocity is inferred from the seed particle velocity.

ERROR ANALYSIS

The overall LV system error is obtained by summing the error of all of the components that contribute to an error in the velocity measurement. The error sources are summarized in the table below and are defined in references 10 and 11. The resulting total bias error of -0.806 to 1.820 percent is obtained by adding the percents contributed by each error source. The total random error of 1.120 percent is obtained by taking the square root of the sum of the squared percents of the random sources. Taking the square root of the sum of the squares of the random and bias errors gives a total system error of 1.38 percent to 2.14 percent.

Error Source	Bias Error	Random Error
Cross Beam Angle Measurement	±0.813	N/A
Diverging Fringes	A	A
Time Jitter	N/A	N/A
Clock Synchronization	0.507	± 0.507
Quantization	A	± .999
Velocity Bias	B	B
Bragg Bias	B	B
Velocity Gradient	B	B
Particle Lag	±0.50	B
Total Error	-0.806 to 1.820	1.120

A Not Measured

B Negligible

N/A Not Applicable

TEST PROCEDURES

In all cases measurements were made at azimuthal increments of 30° from ψ = 0, at 3.0 inches (approximately 1 chord) above the plane formed by the tips of the blades. Measurements were made from a radial location of r/R = 0.2 to r/R = 1.10, with the majority of the measurement locations concentrated toward the outboard portion of the disk. Figure 7 shows the measurement locations superimposed on the rotor disk. During the test, the rotor tip path plane angle-of attack was set at -5.7° relative to the freestream by zeroing the blade flapping relative to the shaft and setting the shaft angle to -5.7°. The operating hover-tip speed for the test was held at 624 ft/sec (2113 rpm), the nominal tunnel speed was 219 ft/sec (μ_∞= 0.35), and the nominal rotor thrust coefficient was 0.0064. Table 2 lists the nominal test conditions and selected parameters. The LV data acquisition process consisted of placing the sample volume at the measurement location and acquiring data for a period of 1 minute or until 4096 velocity measurements were made in either the longitudinal or the vertical component. During this process, conditional sampling techniques were used to permanently associate each measured velocity with the location of the rotor blades at the time when the measurement was made. At the conclusion of the process, the measurement location was changed and the acquisition process was repeated.

DATA REDUCTION

Independent velocity measurements in the freestream and vertical direction were made at each measurement location. At the same instant in time that a velocity measurement was made, the location of the blades was recorded for that velocity component. The maximum time required to acquire this data was 1 minute (2113 rotor revolutions for this test) and the minimum was approximately 10 seconds. These data, collected over many revolutions, were sorted into 128 equally spaced azimuth segments (2.81° wide) that are representive of blade position. Careful measurements indicated that the lead-lag motion was well within this azimuth resolution (2.81°); therefore, no corrections to blade position were made due to lead-lag. The velocity value assigned to each interval at a measurement location is the arithmetic mean of all the measurements that were taken in the respective 2.81° wide azimuthal range. The results of this sorting process provide the azimuthally dependent velocity data. The "mean velocity" value refers to the velocity calculated from the arithmetic mean of all the measurements made at a single measurement location.

EXPERIMENTAL RESULTS

Table 3 lists the measurement locations, the mean and standard deviation of the two components of induced inflow ratio, and the number of measurements in each of the measured components (U and V). In figure 8 the mean longitudinal induced component of inflow ratio, μ_i , with a band of ± one standard deviation is plotted vs. blade radius for each radial scan. The standard deviation represents the fluctuation in velocity at a given measurement location. *It is not an indication of the error in the mean measurements.* The size of the symbols used for plotting the mean velocity values is an approximation of the calculated error in the measurements. Figure 9 presents in the same format the mean normal induced component of inflow ratio, λ_i. The same data without the ± one standard deviation is presented in a contour plot format in figures 10 and 11 in order to show more clearly the interactions over the whole disk (viewed from above). Azimuth dependent data are presented in figures 12-190. The format for these include the induced inflow ratio vs azimuth at the top of the figure, the number of measurements that were used in determining the inflow ratio value for each azimuth segment in the center, and a

conditionally sampled amplitude spectrum (order ratio analysis) of the azimuthal variation at the bottom of the figure. The figure numbers for the azimuthal and radial measurement locations are indicated:

r/R	.20	.40	.50	.60	.70	.74	.78	.82	.86	.90	.94	.98	1.02	1.04	1.10
ψ															
0	12	13	14	15	16	17	18	19	20	21	22	23	24	25	26
30	27	28	29	30	31	32	33	34	35	36	37	38	39	40	41
60	42	43	44	45	46	47	48	49	50	51	52	53	54	55	56
90	57	58	59	60	61	62	63	64	65	66	67	68	69	70	71
120	72	73	74	75	76	77	78	79	80	81	82	83	84	85	86
150	87	88	89	90	91	92	93	94	95	96	97	98	99	100	101
180	102	103	104	105	106	107	108	109	110	111	112	113	114	115	
210	116	117	118	119	120	121	122	123	124	125	126	127	128	129	130
240	131	132	133	134	135	136	137	138	139	140	141	142	143	144	145
270	146	147	148	149	150	151	152	153	154	155	156	157	158	159	160
300	161	162	163	164	165	166	167	168	169	170	171	172	173	174	175
330	176	177	178	179	180	181	182	183	184	185	186	187	188	189	190

The mean and standard deviation of the induced inflow ratios (table 3) and the azimuthally dependent induced inflow ratios (figures 12 through 190) are included on a 5.25 flexible disk in the pocket on the inside of the rear cover of this report. The details of the data format and the file structure are located in the file "README.DOC". The disk format is 360 byte double-sided, written using the Microsoft Corporation MS-DOS operating system.

CONCLUDING REMARKS

The Laser Velocimeter provides an effective system for making measurements in the dynamic environment associated with rotor blades. It has been used on numerous occasions to measure the localized flow phenomena encountered in such flows. This investigation demonstrates the use of a matured LV system to map the flow into a representative rotor in forward flight by making velocity measurements at 179 locations above the rotor disk. These measurements provide both the mean and azimuthally dependent velocity values, and they provide a detailed look at the nature of this flow. The mean and standard deviation of the induced inflow velocities and the azimuthally dependent induced inflow velocities are included on a 5.25 flexible disk in the pocket on the inside of the rear cover of this report.

REFERENCES

1. Landgrebe, A. J.; and Johnson, B. V.: Measurement of Model Helicopter Rotor Flow Velocities with a Laser Doppler Velocimeter. American Helicopter Society Journal, Vol 19, July 1974, p. 39-43.

2. Biggers, J. C.; and Orloff, K. L.: Laser Velocimeter Measurements of the Helicopter Rotor-Induced Flowfield. American Helicopter Society, Annual National V/STOL Forum, 30th, Washington, D.C. May 7-9, 1974.

3. Owen F. K.; and Taubert M. E.: Measurement and Prediction of Model-Rotor Flowfields. AIAA, 18th Fluid Dynamics, Plasmadynamics and Laser Conference, Cincinnati, Ohio, July 16-18, 1985.

4. Tangler, J. L.; Wohlfeld, R. M.; and Miley, S. J.: An Experimental Investigation of Vortex Stability, Tip Shapes, Compressibility and Noise for Hovering Models. NASA CR-2305, September 1973.

5. Junker, B.: Investigations of Blade-vortices in the Rotor Downwash. Twelfth European Rotorcraft Forum, Garmish-Partenkirchen, Federal Republic of Germany, September 22-25, 1986.

6. Applin, Z. T.: Flow Improvements in the Circuit of the Langley 4- by 7-Meter Tunnel. NASA TM 85662, December 1983.

7. Phelps, A. E. III; and Berry, J. D.: Description of the U.S. Army 2-Meter Rotor Test System. NASA TM 87762, AVSCOM TM 86-B-4, January 1987.

8. Sellers, W. L.; and Elliott, J. W.: Applications of a Laser Velocimeter in the Langley 4- by 7-Meter Tunnel. Proceedings of the Workshop on Flow Visualization and Laser Velocimetry for Wind Tunnels, NASA CP 2243, March 1982, pp. 283-293.

9. Elliott, J. W.; and Nichols, C. E.: Seeding Systems for Use with a Laser Velocimeter in Large Scale Wind Tunnels. Proceedings of the Workshop on Wind Tunnel Seeding Systems for Laser Velocimeters, NASA CP 2393, March 1985, pp. 93-103.

10. Young, W. H.; Meyers, J. F.; and Hepner, T. E.: Laser Velocimeter Systems Analysis to a Flow Survey above a Stalled Wing. NASA TN D-8408, August 1977.

11. Dring, R. P.: Sizing Criteria for Laser Anemometry Particles. Journal of Fluids Engineering, Vol. 104, March 1982, p. 15-17.

TABLE 1 - 2MRTS ROTOR AND BLADE CHARACTERSTICS

Hub Type	Fully Articulated
Number of blades	4
Airfoil section	NACA 0012
Hinge offset, in, r/R	2.00, .06
Root cutout, in, r/R	8.25, .24
Pitch-flap coupling angle, deg	0.0
Twist linear, deg	-8.0
Radius, R, in	33.88
Airfoil chord, C, in	2.6
Rotor solidity, $bc/\pi R$	0.0977
Blade stiffness	
Flapwise lb-in^2	11500
Torsional lb-in^2	25500
Blade weight, grams	259.3
Lead/lag damping in-lb/deg/sec	182.4

TABLE 2 - NOMINAL ROTOR CONTROL AND PERFORMANCE PARAMETERS

C_T	0.0064
C_Q	0.00048
C_D	0.00
α, deg	-5.70
Coning, deg	1.8
A_0, deg	9.2
A_1, deg	-0.30
B_1, deg	6.8
μ_∞	0.35
U_∞, ft/sec	219.0
V_{tip}, ft/sec	624.0
Lag angle (mean), degrees	1.3

TABLE 3 - INFLOW VELOCITY SUMMARY

		μ_i			λ_i		
Ψ	r/R	Mean	Standard deviation	# of Measurements	Mean	Standard deviation	# of Measurements
0	0.20	0.0199	0.0117	1025	0.0073	0.0146	979
0	0.40	0.0147	0.0106	2102	-0.0150	0.0124	2903
0	0.50	0.0126	0.0109	1981	-0.0210	0.0102	2891
0	0.60	0.0100	0.0107	1961	-0.0251	0.0096	2932
0	0.70	0.0096	0.0107	2049	-0.0270	0.0096	2787
0	0.74	0.0093	0.0107	2261	-0.0280	0.0096	2782
0	0.78	0.0061	0.0110	2232	-0.0251	0.0098	2522
0	0.82	0.0044	0.0103	2256	-0.0272	0.0094	2697
0	0.86	0.0033	0.0102	2280	-0.0289	0.0091	2759
0	0.90	0.0027	0.0097	2192	-0.0292	0.0087	2773
0	0.94	0.0041	0.0146	2473	-0.0318	0.0085	2740
0	0.98	0.0025	0.0142	2370	-0.0325	0.0086	2800
0	1.02	0.0023	0.0153	2512	-0.0316	0.0085	2692
0	1.04	0.0012	0.0154	2440	-0.0305	0.0086	2608
0	1.10	-0.0005	0.0154	2484	-0.0300	0.0083	2623
30	0.20	0.0102	0.0159	2372	0.0067	0.0075	2227
30	0.40	0.0141	0.0147	2383	-0.0139	0.0100	2760
30	0.50	0.0152	0.0136	2024	-0.0229	0.0098	2954
30	0.60	0.0087	0.0135	2429	-0.0205	0.0086	2452
30	0.70	0.0128	0.0148	2415	-0.0233	0.0086	2563
30	0.74	0.0145	0.0157	2291	-0.0242	0.0092	2232
30	0.78	0.0109	0.0150	2302	-0.0221	0.0087	2073
30	0.82	0.0103	0.0149	2312	-0.0236	0.0089	2209
30	0.86	0.0113	0.0148	2327	-0.0233	0.0080	2209
30	0.90	0.0106	0.0148	2311	-0.0233	0.0081	2222
30	0.94	0.0096	0.0151	2344	-0.0243	0.0077	2320
30	0.98	0.0091	0.0157	2428	-0.0240	0.0074	2436
30	1.02	0.0076	0.0152	2380	-0.0234	0.0074	2486
30	1.04	0.0089	0.0167	2448	-0.0235	0.0072	2247
30	1.10	0.0063	0.0172	2425	-0.0218	0.0065	2205
60	0.20	0.0076	0.0139	2303	0.0009	0.0061	2604
60	0.40	0.0144	0.0132	2004	-0.0161	0.0079	2830
60	0.50	0.0130	0.0134	1768	-0.0182	0.0082	2921
60	0.60	0.0123	0.0139	2271	-0.0158	0.0078	2726
60	0.70	0.0099	0.0138	2273	-0.0122	0.0075	2672
60	0.74	0.0088	0.0141	2347	-0.0109	0.0078	2622
60	0.78	0.0080	0.0145	2233	-0.0079	0.0067	2134
60	0.82	0.0082	0.0137	2333	-0.0074	0.0066	2189
60	0.86	0.0081	0.0144	2301	-0.0061	0.0060	2259
60	0.90	0.0045	0.0151	2211	-0.0033	0.0056	1930
60	0.94	0.0035	0.0144	2260	-0.0036	0.0060	2557
60	0.98	0.0053	0.0131	2123	-0.0016	0.0055	2838
60	1.02	0.0038	0.0132	2091	0.0018	0.0045	2808
60	1.04	0.0036	0.0129	2006	0.0035	0.0045	2812
60	1.10	0.0030	0.0135	2335	0.0076	0.0050	2671

TABLE 3 - CONTINUED

ψ	r/R	μ_i Mean	μ_i Standard deviation	μ_i # of Measurements	λ_i Mean	λ_i Standard deviation	λ_i # of Measurements
90	0.20	0.0031	0.0143	2004	0.0002	0.0052	2348
90	0.40	0.0084	0.0138	2064	-0.0080	0.0066	2537
90	0.50	0.0075	0.0137	2222	-0.0062	0.0059	2454
90	0.60	0.0041	0.0139	2154	-0.0029	0.0058	2474
90	0.70	0.0044	0.0137	2074	-0.0004	0.0052	2399
90	0.74	0.0035	0.0139	2107	0.0005	0.0052	2516
90	0.78	0.0031	0.0140	2241	0.0020	0.0051	2485
90	0.82	0.0036	0.0135	2340	0.0032	0.0052	2583
90	0.86	0.0028	0.0136	2312	0.0041	0.0055	2566
90	0.90	0.0007	0.0137	2398	0.0052	0.0055	2521
90	0.94	0.0006	0.0136	2419	0.0058	0.0056	2596
90	0.98	0.0011	0.0135	2403	0.0052	0.0053	2522
90	1.02	-0.0011	0.0136	2311	0.0051	0.0052	2543
90	1.04	-0.0006	0.0135	2439	0.0045	0.0052	2527
90	1.10	0.0012	0.0134	2341	0.0025	0.0051	2406
120	0.20	0.0015	0.0113	2086	0.0020	0.0042	2754
120	0.40	0.0108	0.0101	1414	-0.0030	0.0043	2891
120	0.50	0.0078	0.0097	1226	-0.0028	0.0045	2998
120	0.60	0.0063	0.0100	2624	0.0004	0.0034	2931
120	0.70	0.0041	0.0102	2659	0.0022	0.0034	2619
120	0.74	0.0028	0.0107	2602	0.0026	0.0034	2612
120	0.78	0.0003	0.0108	2561	0.0025	0.0036	2483
120	0.82	-0.0003	0.0101	2659	0.0032	0.0033	2553
120	0.86	-0.0009	0.0101	2678	0.0032	0.0032	2558
120	0.90	0.0000	0.0099	2657	0.0028	0.0031	2337
120	0.94	0.0009	0.0091	2760	0.0030	0.0032	2874
120	0.98	-0.0004	0.0099	2679	0.0020	0.0030	2596
120	1.02	-0.0027	0.0102	2572	0.0013	0.0031	2523
120	1.04	-0.0025	0.0095	2729	0.0018	0.0029	2590
120	1.10	-0.0018	0.0100	2678	0.0012	0.0029	2721
150	0.20	-0.0085	0.0132	2336	0.0081	0.0066	2382
150	0.40	0.0041	0.0130	2522	-0.0004	0.0068	3015
150	0.50	0.0045	0.0129	2440	0.0008	0.0069	3066
150	0.60	0.0039	0.0128	2343	0.0022	0.0076	3105
150	0.70	0.0041	0.0119	2121	0.0034	0.0075	2997
150	0.74	0.0014	0.0123	2130	0.0038	0.0075	2995
150	0.78	0.0017	0.0119	2002	0.0044	0.0067	2864
150	0.82	0.0031	0.0147	2186	0.0017	0.0065	2304
150	0.86	0.0011	0.0141	2214	0.0033	0.0067	2473
150	0.90	0.0006	0.0151	2233	0.0026	0.0067	2415
150	0.94	-0.0032	0.0139	2059	0.0023	0.0065	2439
150	0.98	-0.0007	0.0107	2462	0.0013	0.0038	2601
150	1.02	-0.0017	0.0108	2426	0.0014	0.0036	2791
150	1.04	-0.0044	0.0108	1887	0.0013	0.0037	2139
150	1.10	-0.0042	0.0109	2343	0.0003	0.0034	2681

TABLE 3 - CONTINUED

		μ_i			λ_i		
Ψ	r/R	Mean	Standard deviation	# of Measurements	Mean	Standard deviation	# of Measurements
180	0.20	-0.0100	0.0094	2530	0.0079	0.0055	3043
180	0.40	-0.0027	0.0130	2453	0.0061	0.0055	2326
180	0.50	-0.0009	0.0141	2517	0.0104	0.0092	2351
180	0.60	-0.0060	0.0137	2509	0.0108	0.0103	2538
180	0.70	-0.0073	0.0112	2334	0.0114	0.0100	3066
180	0.74	-0.0090	0.0117	2102	0.0108	0.0094	3019
180	0.78	-0.0087	0.0109	1731	0.0097	0.0088	3074
180	0.82	-0.0105	0.0113	2025	0.0093	0.0077	3019
180	0.86	-0.0122	0.0108	2469	0.0092	0.0072	3112
180	0.90	-0.0136	0.0103	2502	0.0088	0.0065	3075
180	0.94	-0.0139	0.0102	2587	0.0080	0.0055	3086
180	0.98	-0.0144	0.0098	2499	0.0072	0.0051	3100
180	1.02	-0.0150	0.0094	2265	0.0064	0.0047	3059
180	1.04	-0.0144	0.0095	2182	0.0059	0.0045	3061
210	0.20	-0.0107	0.0096	1205	0.0092	0.0047	2458
210	0.40	-0.0055	0.0126	2203	0.0060	0.0066	2812
210	0.50	-0.0061	0.0125	2273	0.0058	0.0083	2687
210	0.60	-0.0062	0.0128	2133	0.0054	0.0086	2767
210	0.70	-0.0077	0.0126	2018	0.0052	0.0079	2760
210	0.74	-0.0053	0.0124	2021	0.0044	0.0072	2777
210	0.78	-0.0069	0.0123	1990	0.0040	0.0065	2749
210	0.82	-0.0078	0.0118	2144	0.0037	0.0060	2794
210	0.86	-0.0077	0.0124	2228	0.0035	0.0056	2779
210	0.90	-0.0093	0.0129	2380	0.0036	0.0053	2766
210	0.94	-0.0080	0.0120	2065	0.0042	0.0052	2924
210	0.98	-0.0076	0.0113	2204	0.0038	0.0044	2943
210	1.02	-0.0085	0.0110	2297	0.0036	0.0043	2873
210	1.04	-0.0086	0.0104	2273	0.0034	0.0044	2918
210	1.10	-0.0084	0.0097	2456	0.0021	0.0041	2926
240	0.20	-0.0075	0.0100	1609	0.0066	0.0045	3010
240	0.40	0.0015	0.0099	2448	0.0012	0.0080	3073
240	0.50	0.0020	0.0112	2262	-0.0004	0.0095	3213
240	0.60	0.0001	0.0114	2589	-0.0002	0.0106	3015
240	0.70	0.0011	0.0109	2443	-0.0001	0.0093	2868
240	0.74	0.0002	0.0106	2494	-0.0010	0.0086	2802
240	0.78	-0.0017	0.0108	2354	-0.0008	0.0079	2810
240	0.82	0.0020	0.0126	2485	-0.0031	0.0126	3418
240	0.86	0.0034	0.0123	2920	-0.0020	0.0118	3480
240	0.90	0.0035	0.0118	2813	-0.0008	0.0106	3172
240	0.94	0.0033	0.0115	2823	0.0004	0.0091	3182
240	0.98	0.0026	0.0111	2821	0.0016	0.0076	3108
240	1.02	0.0011	0.0113	2849	0.0031	0.0056	2821
240	1.04	0.0006	0.0115	2529	0.0023	0.0054	2241
240	1.10	-0.0003	0.0111	2556	0.0025	0.0051	2914

TABLE 3 - CONCLUDED

ψ	r/R	μ_i Mean	μ_i Standard deviation	μ_i # of Measurements	λ_i Mean	λ_i Standard deviation	λ_i # of Measurements
270	0.20	0.0065	0.0113	2135	0.0067	0.0051	3425
270	0.40	0.0043	0.0114	2171	-0.0004	0.0073	3477
270	0.50	0.0040	0.0117	2460	-0.0029	0.0071	3102
270	0.60	0.0043	0.0119	2415	-0.0053	0.0078	3346
270	0.70	0.0051	0.0123	2622	-0.0067	0.0092	3391
270	0.74	0.0029	0.0126	2476	-0.0071	0.0100	3515
270	0.78	0.0041	0.0126	2591	-0.0061	0.0100	3145
270	0.82	0.0023	0.0127	1851	-0.0059	0.0112	3356
270	0.86	0.0044	0.0122	2100	-0.0055	0.0107	3132
270	0.90	0.0045	0.0126	2104	-0.0049	0.0107	3155
270	0.94	0.0055	0.0128	2178	-0.0031	0.0098	3134
270	0.98	0.0052	0.0124	2177	-0.0011	0.0081	3069
270	1.02	0.0033	0.0116	2193	0.0017	0.0058	2819
270	1.04	0.0022	0.0116	2373	0.0026	0.0057	2854
270	1.10	0.0026	0.0128	2351	0.0033	0.0055	2863
300	0.20	0.0126	0.0122	2448	0.0029	0.0061	3040
300	0.40	0.0083	0.0136	2225	-0.0005	0.0061	2235
300	0.50	0.0089	0.0124	2147	-0.0029	0.0055	2299
300	0.60	0.0075	0.0133	2260	-0.0052	0.0052	2653
300	0.70	0.0073	0.0122	2148	-0.0082	0.0055	2848
300	0.74	0.0040	0.0119	2222	-0.0090	0.0060	2798
300	0.78	0.0037	0.0136	2081	-0.0103	0.0063	2370
300	0.82	0.0193	0.0111	2089	-0.0129	0.0059	1705
300	0.86	0.0098	0.0117	2095	-0.0132	0.0066	2213
300	0.90	0.0045	0.0125	2191	-0.0144	0.0076	2506
300	0.94	0.0051	0.0127	2114	-0.0150	0.0073	2610
300	0.98	0.0029	0.0118	2054	-0.0142	0.0067	2381
300	1.02	0.0043	0.0135	2017	-0.0134	0.0066	2444
300	1.04	0.0050	0.0117	2008	-0.0113	0.0057	2428
300	1.10	-0.0039	0.0113	1826	-0.0063	0.0053	2328
330	0.20	0.0205	0.0123	2252	0.0055	0.0066	2406
330	0.40	0.0157	0.0131	2191	-0.0047	0.0040	1991
330	0.50	0.0118	0.0143	2325	-0.0066	0.0044	2120
330	0.60	0.0137	0.0135	2428	-0.0074	0.0048	2577
330	0.70	0.0082	0.0139	2395	-0.0069	0.0050	2686
330	0.74	0.0149	0.0150	2051	-0.0069	0.0053	2710
330	0.78	0.0101	0.0140	2000	-0.0070	0.0058	2666
330	0.82	0.0095	0.0139	1983	-0.0076	0.0061	2697
330	0.86	0.0098	0.0131	2119	-0.0089	0.0070	2699
330	0.90	0.0144	0.0153	2034	-0.0094	0.0073	2755
330	0.94	0.0185	0.0153	1980	-0.0126	0.0087	2623
330	0.98	0.0189	0.0129	2095	-0.0177	0.0098	2540
330	1.02	0.0139	0.0135	1746	-0.0191	0.0092	2569
330	1.04	0.0163	0.0126	1751	-0.0190	0.0089	2527
330	1.10	0.0058	0.0138	1567	-0.0192	0.0082	2467

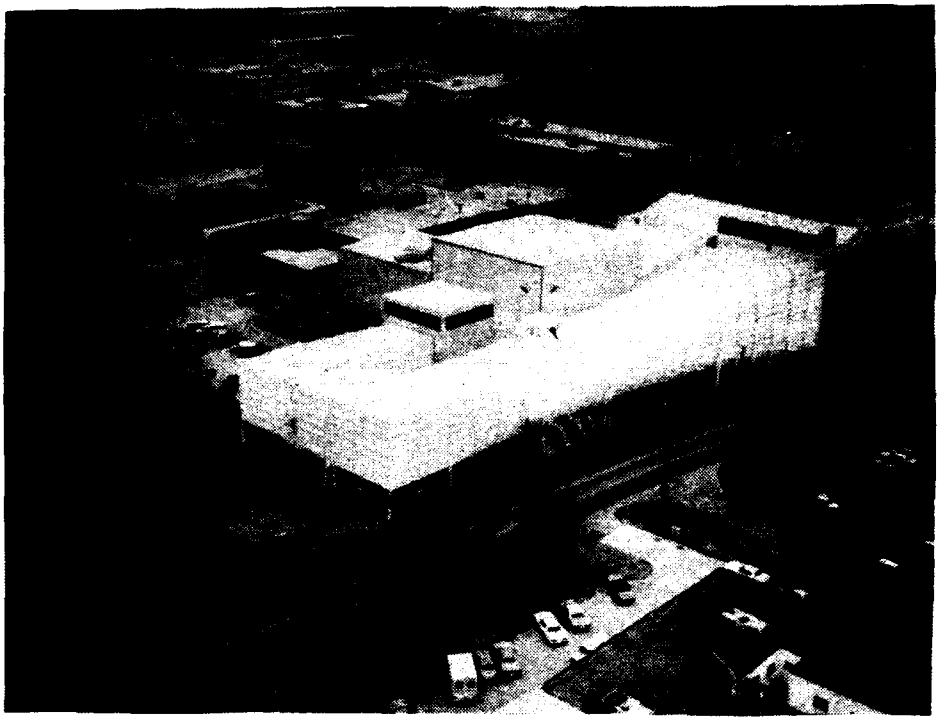

Figure 1. Aerial view of 14- by 22- Foot Subsonic Tunnel.

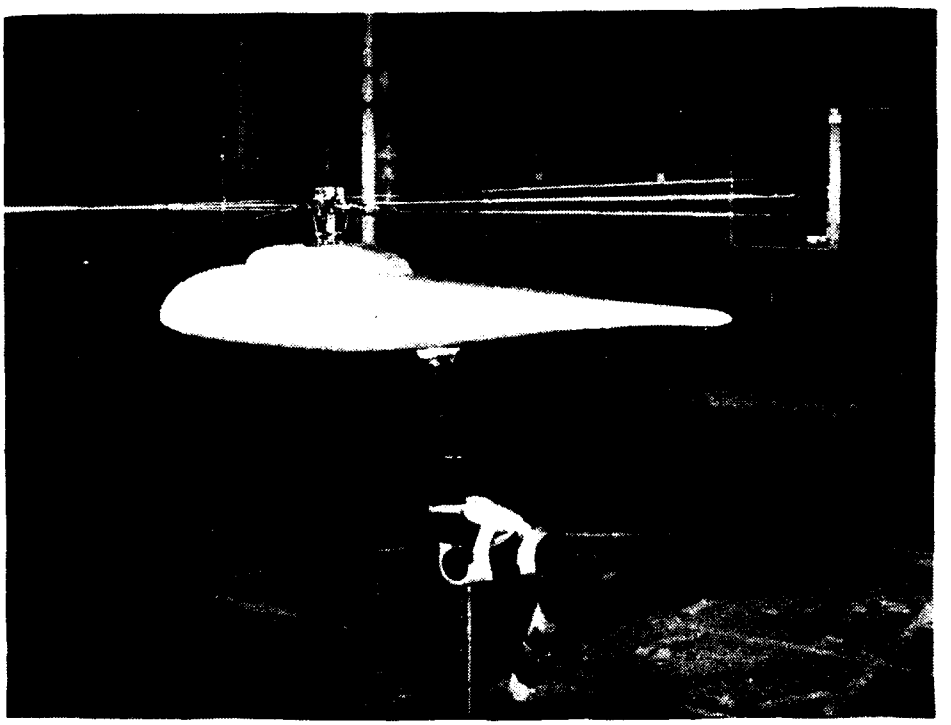

Figure 2. 2 MRTS mounted in forward bay of the test section.

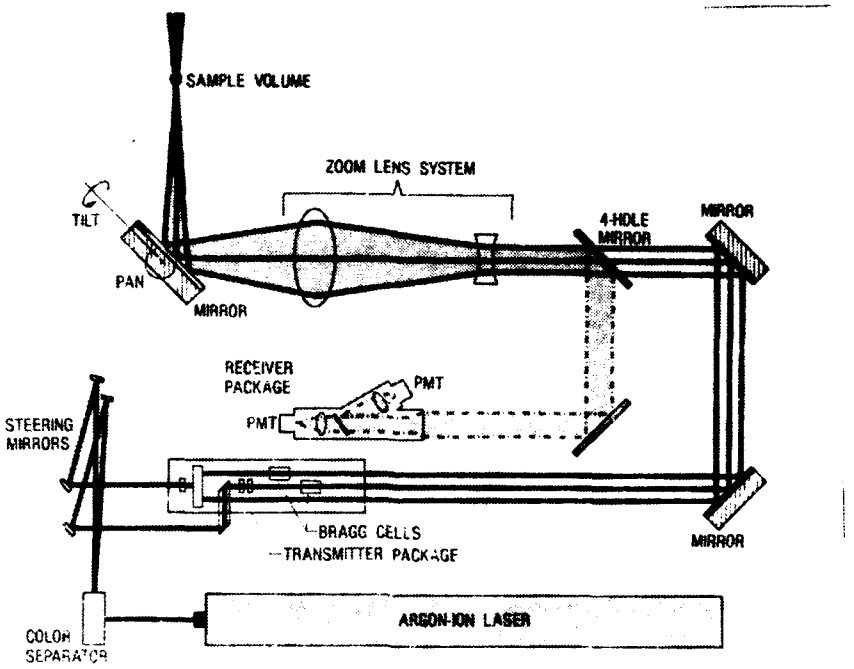

Figure 3. Schematic of Laser Velocimeter optics subsystem.

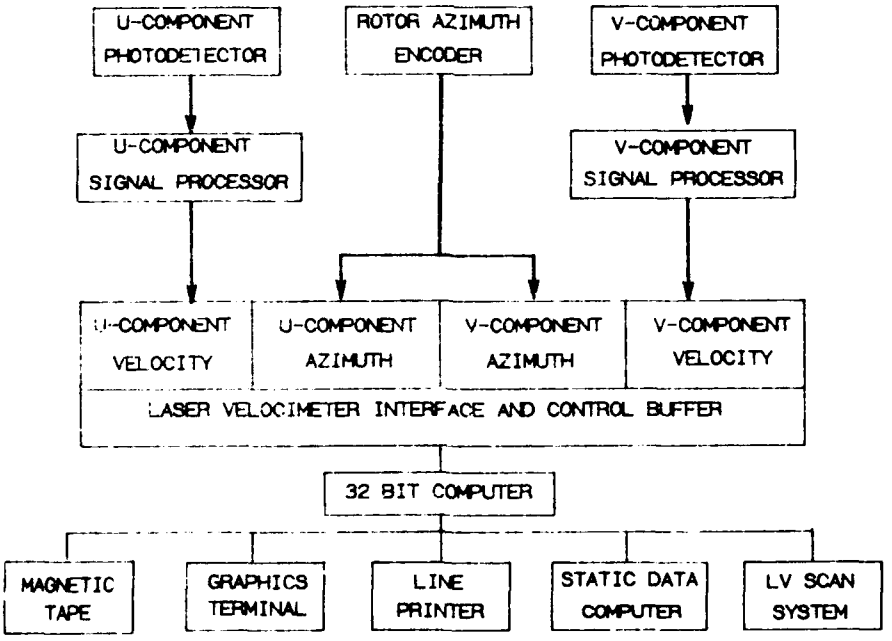

Figure 4. Schematic of data acquisition and control subsystem.

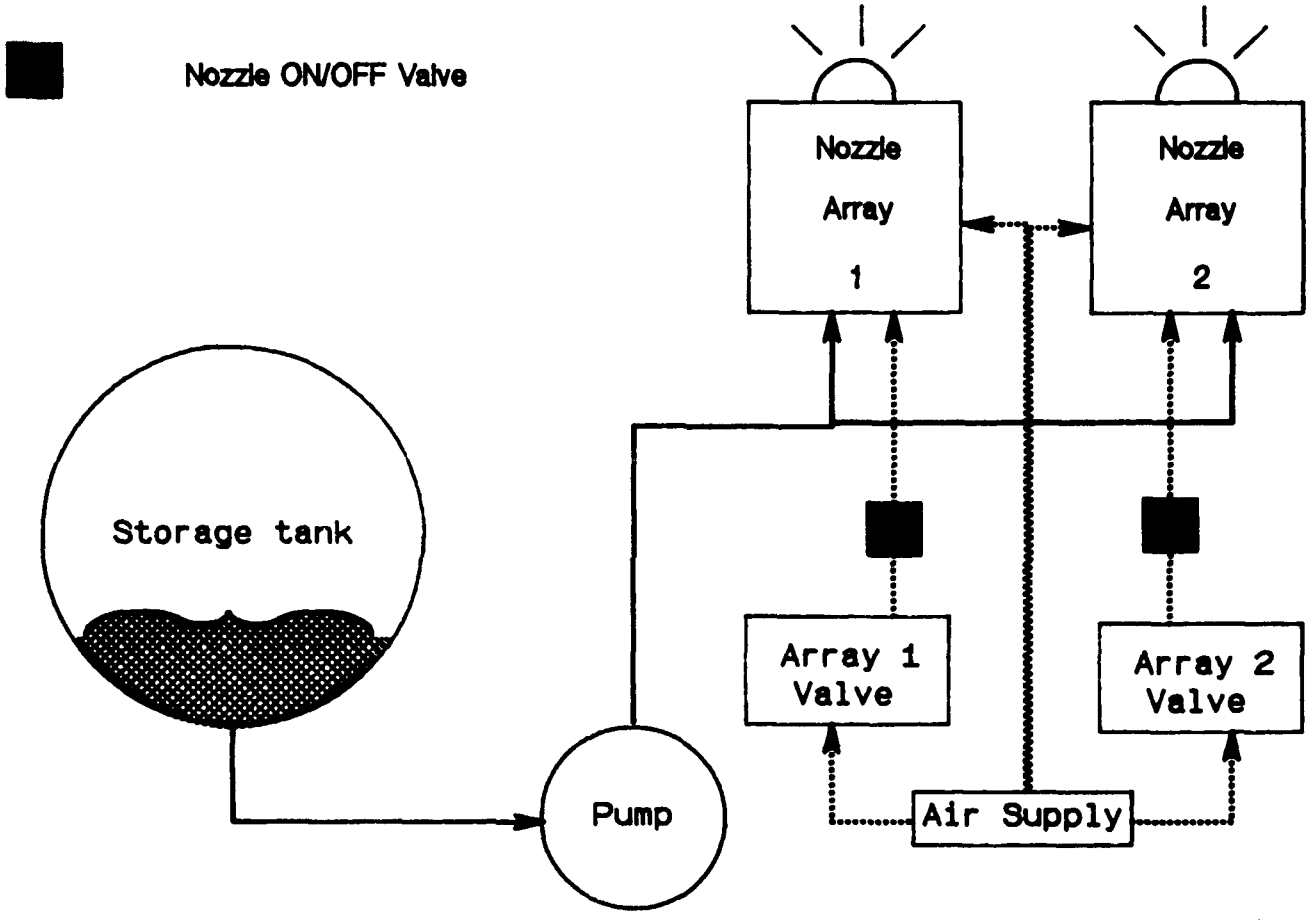

Figure 5. Schematic of seeding system.

Figure 6. Photograph of remote control positioner for seeding system.

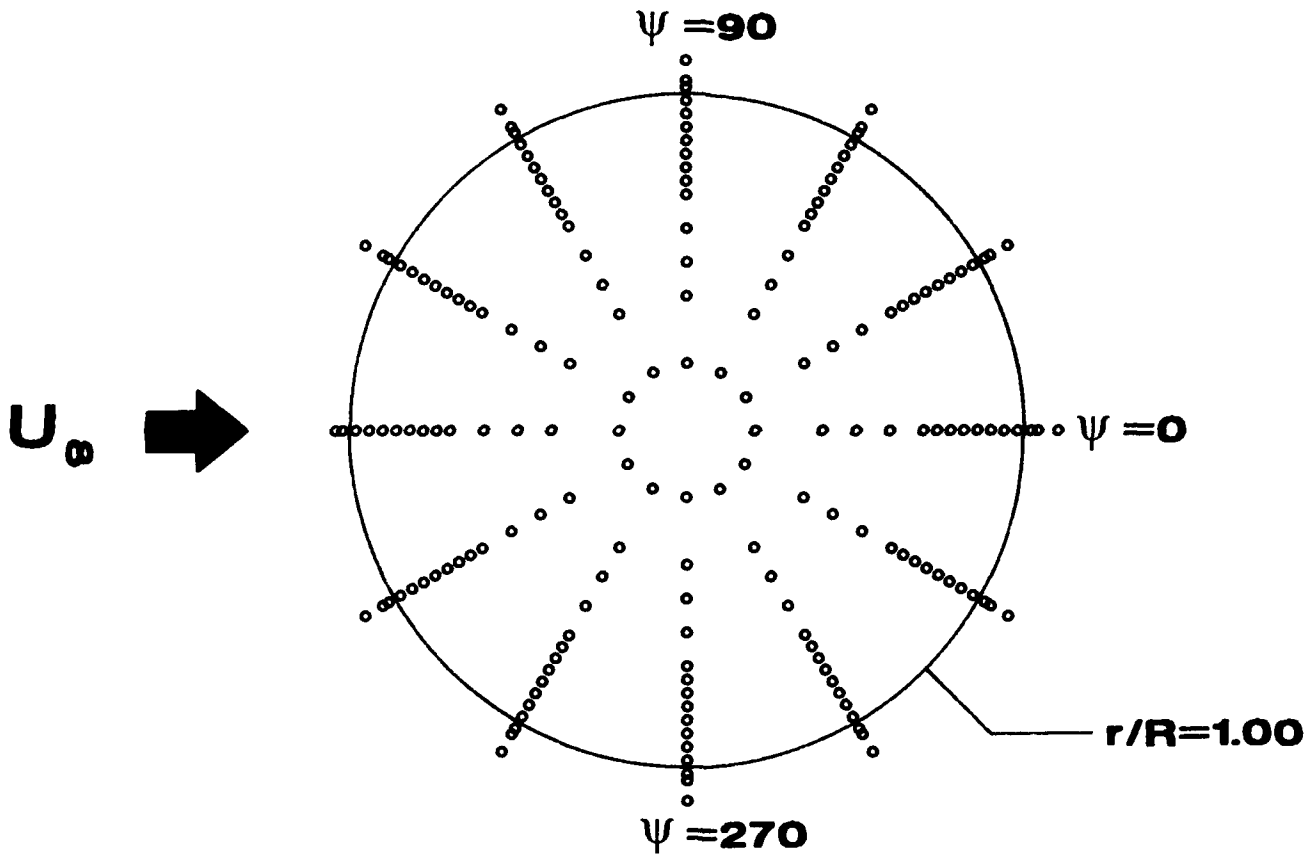

Figure 7. Locations of velocity measurements, 3.0 inches above rotor tip path plane.

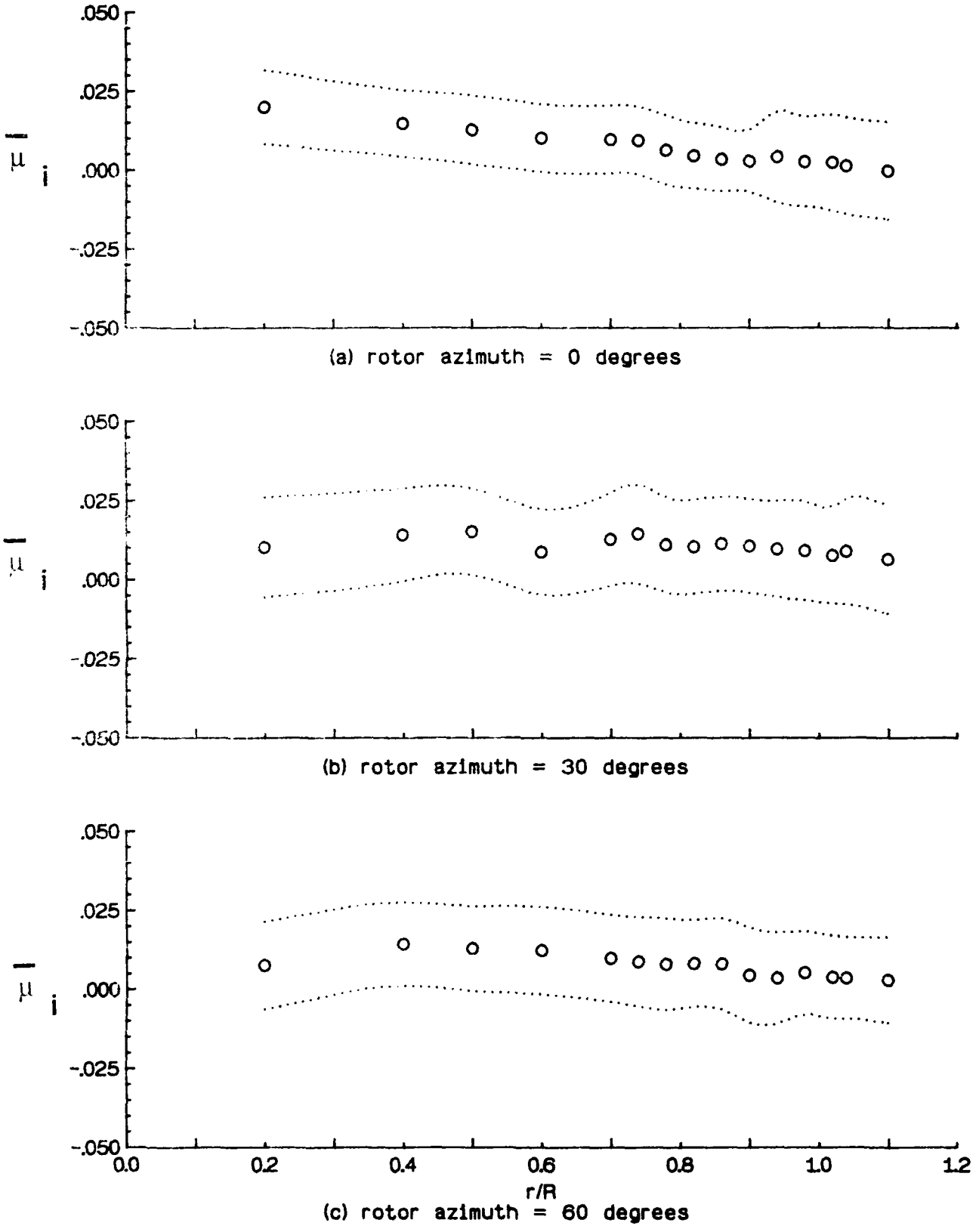

Figure 8. Radial distribution of mean induced inflow ratio - $\bar{\mu}_i$.

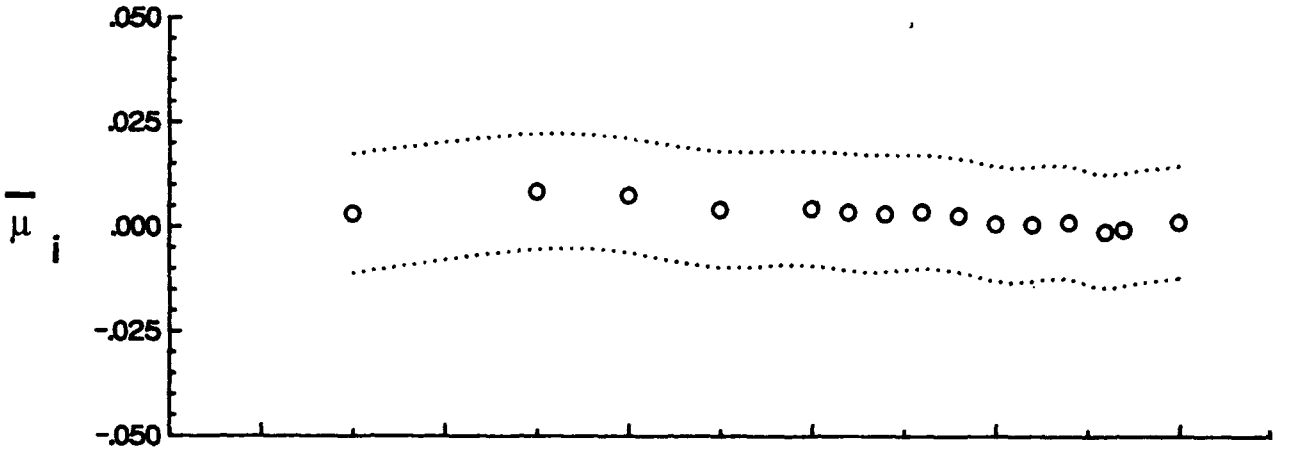

(d) rotor azimuth = 90 degrees

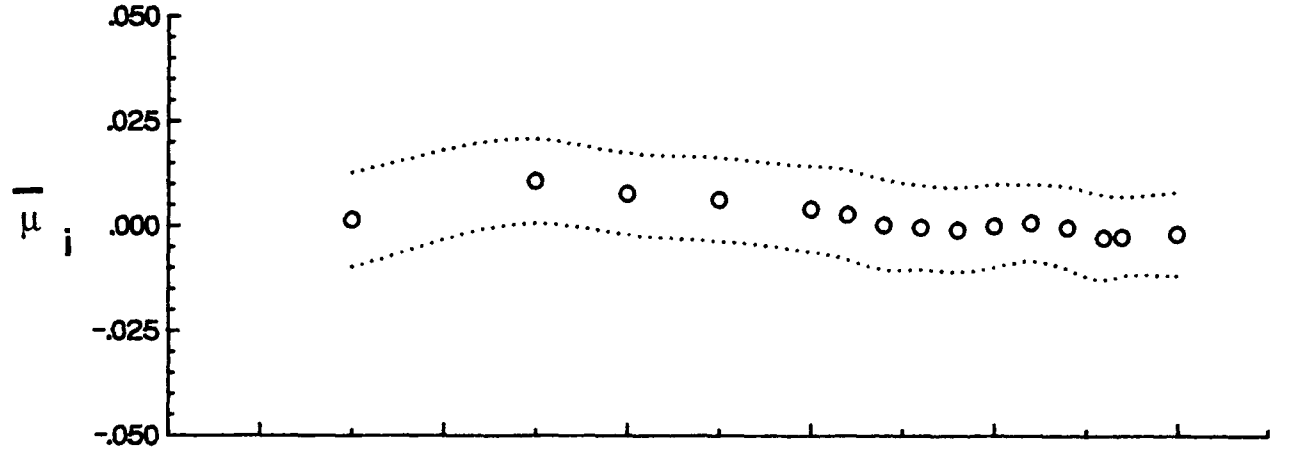

(e) rotor azimuth = 120 degrees

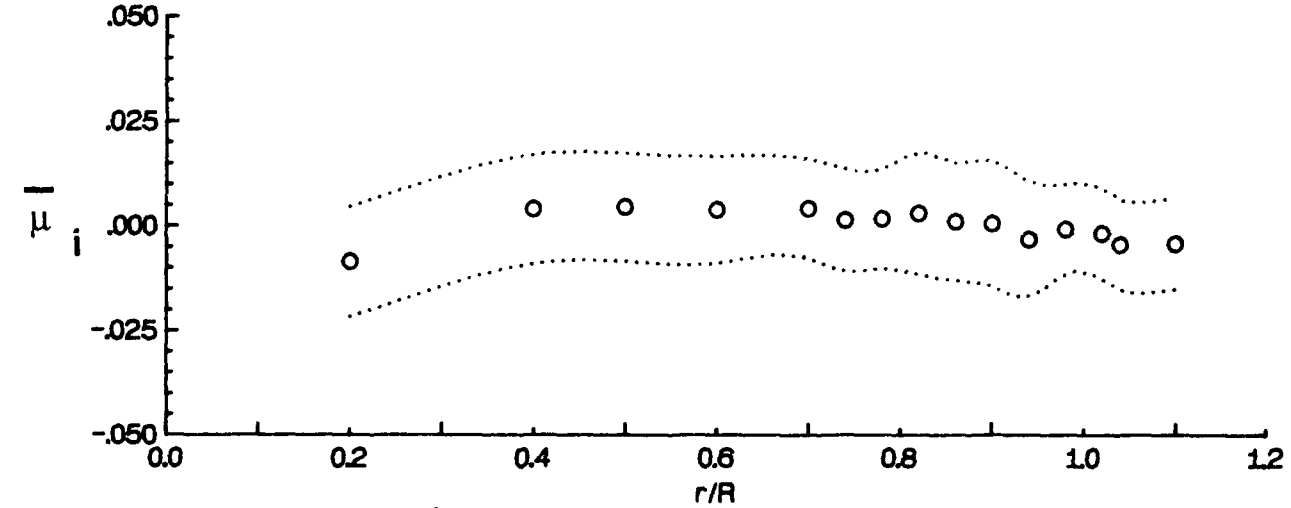

(f) rotor azimuth = 150 degrees

Figure 8. Continued.

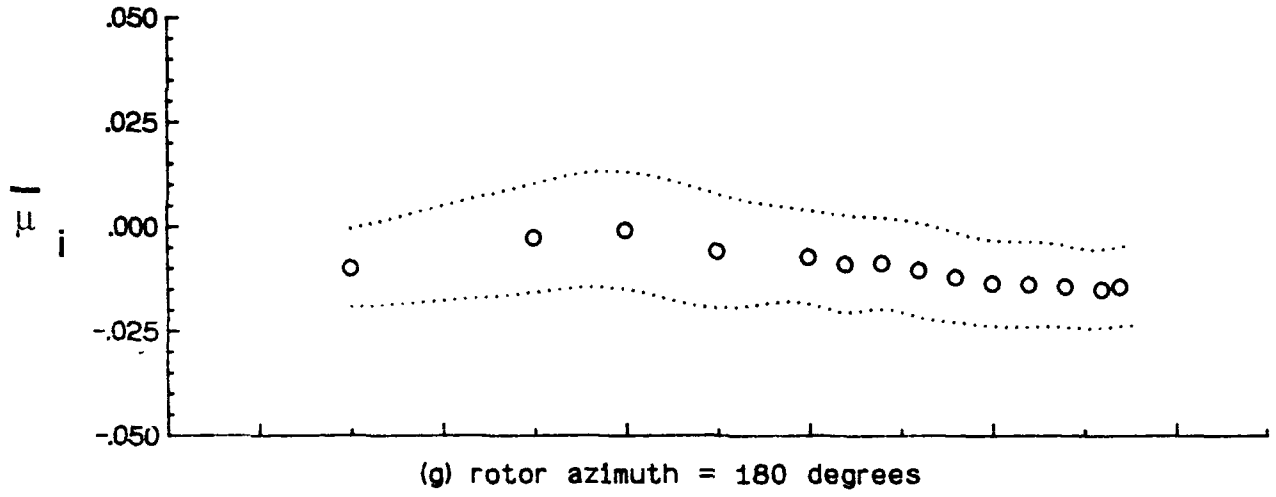

(g) rotor azimuth = 180 degrees

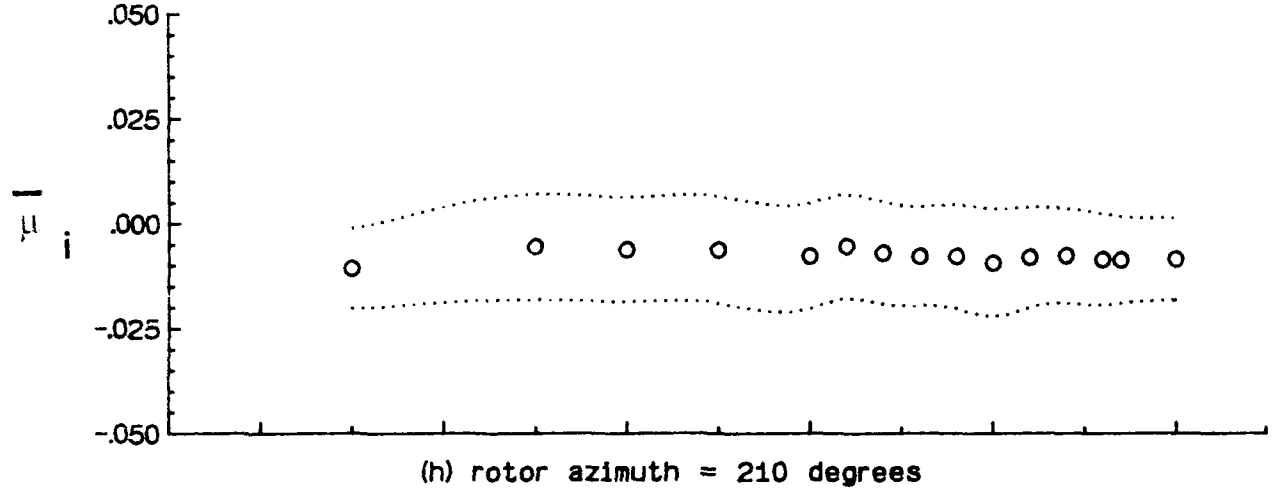

(h) rotor azimuth = 210 degrees

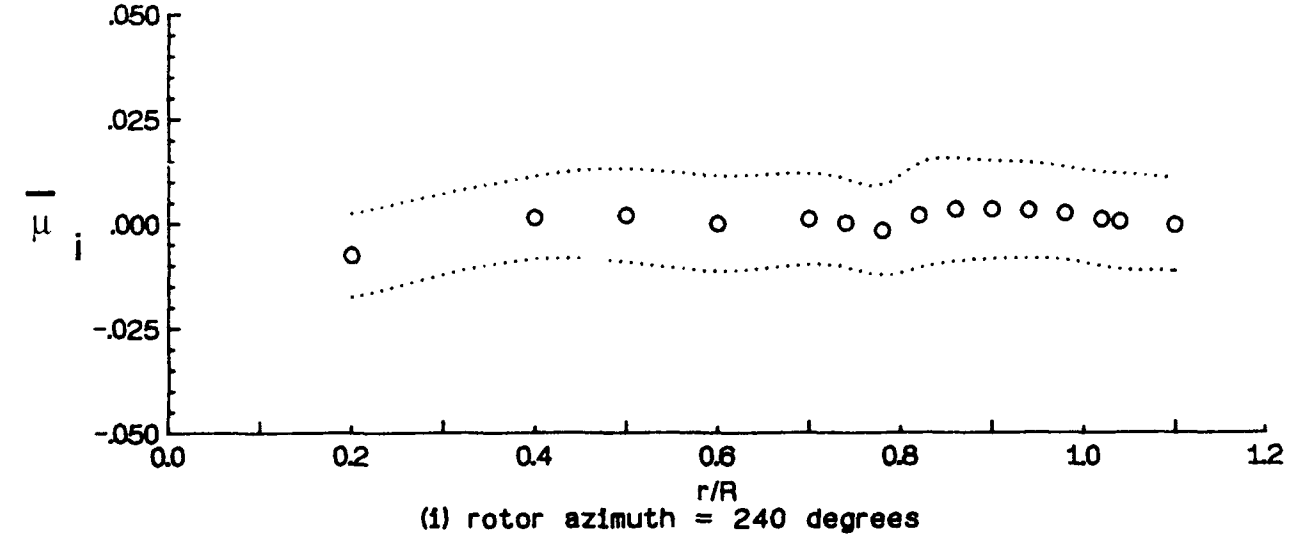

(i) rotor azimuth = 240 degrees

Figure 8. Continued.

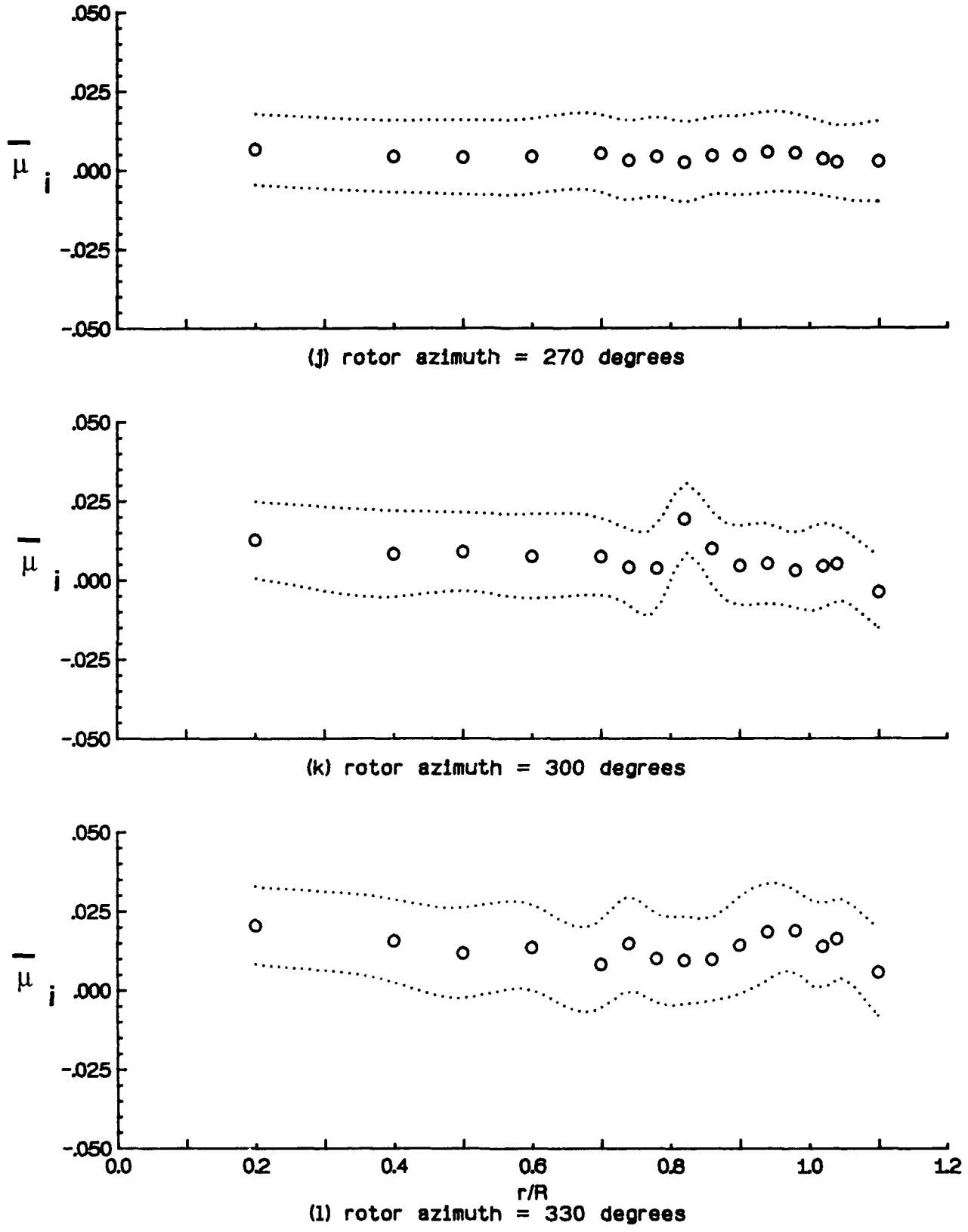

Figure 8. Concluded.

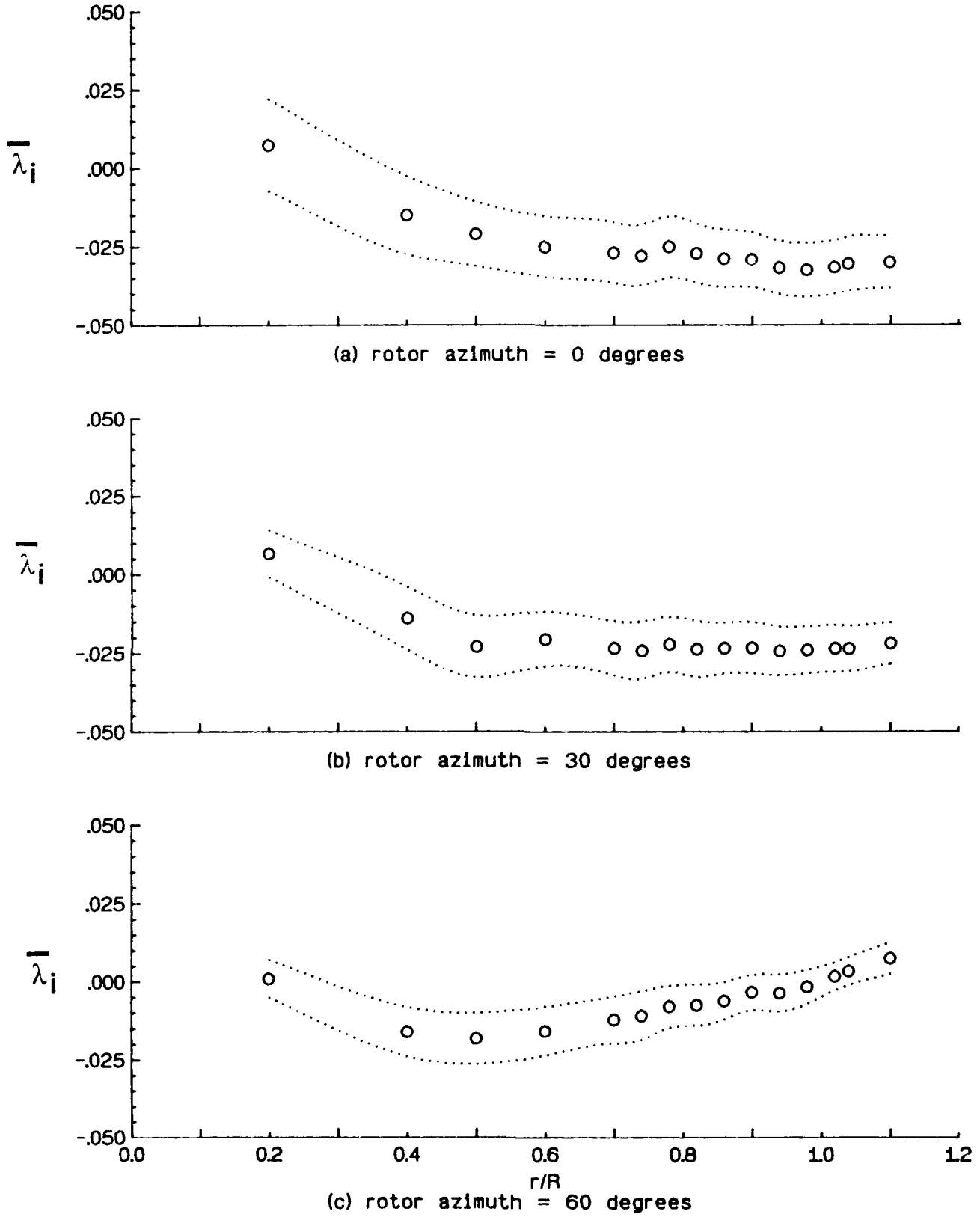

Figure 9. Radial distribution of mean induced inflow ratio - $\overline{\lambda}_i$.

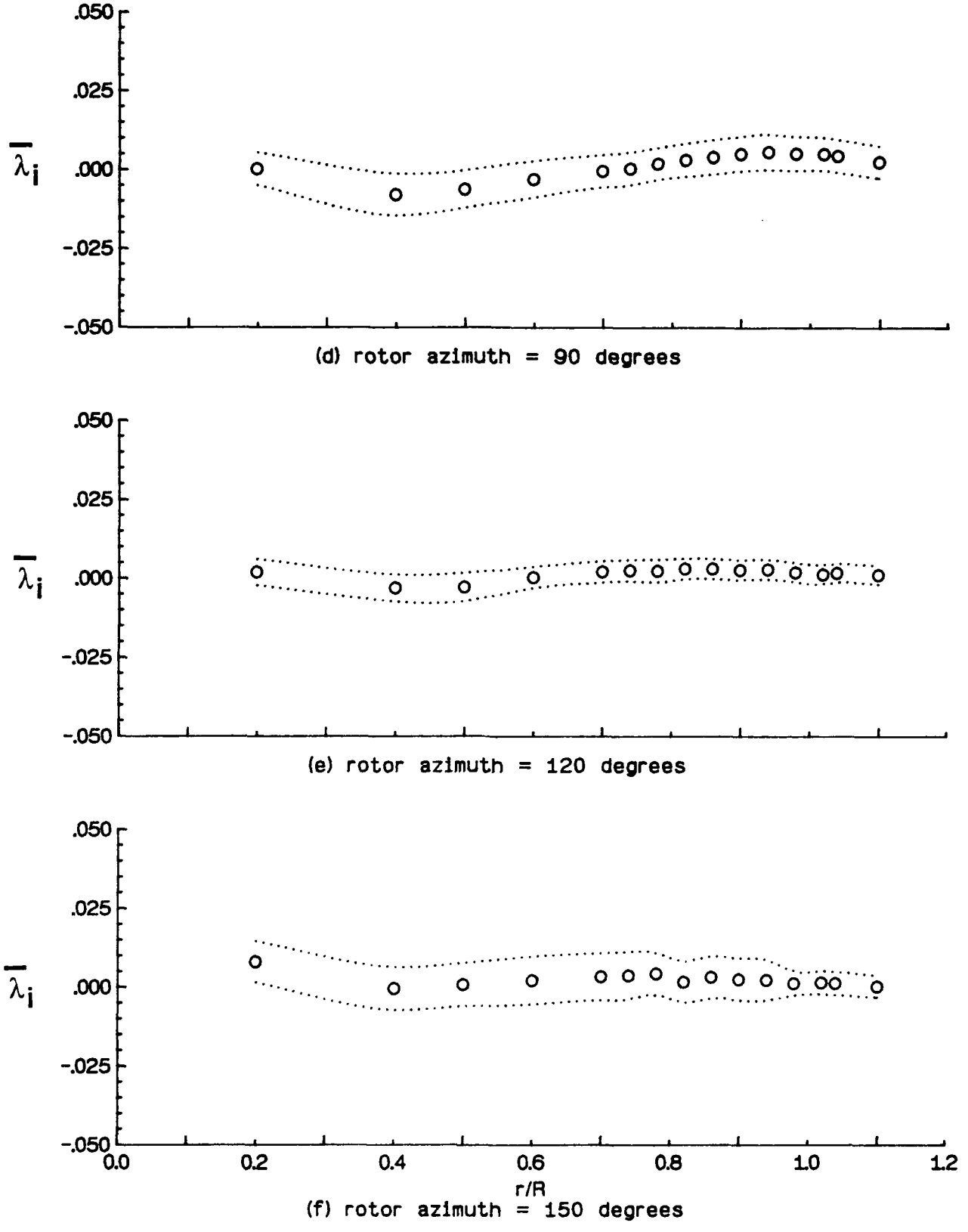

Figure 9. Continued.

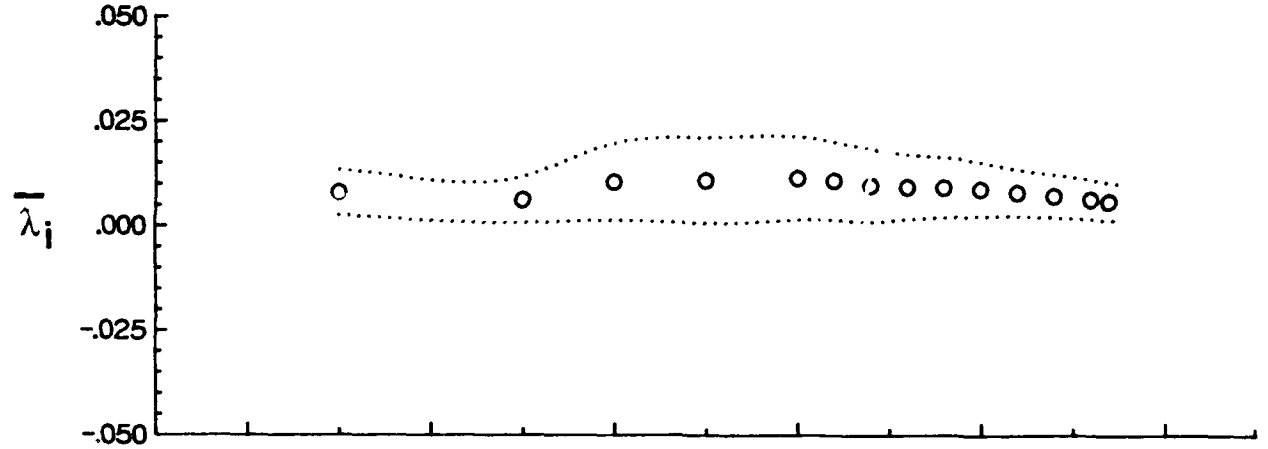

(g) rotor azimuth = 180 degrees

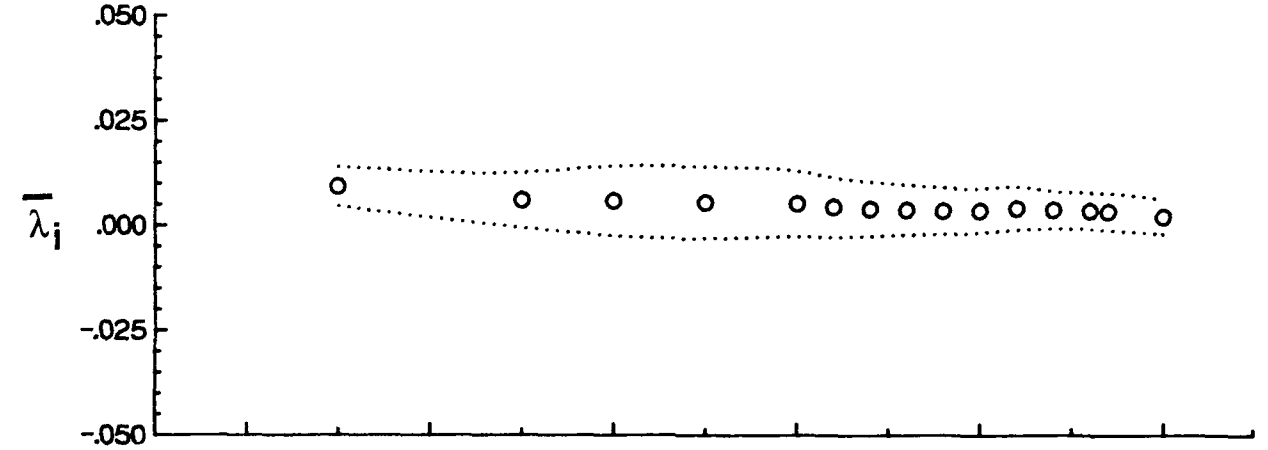

(h) rotor azimuth = 210 degrees

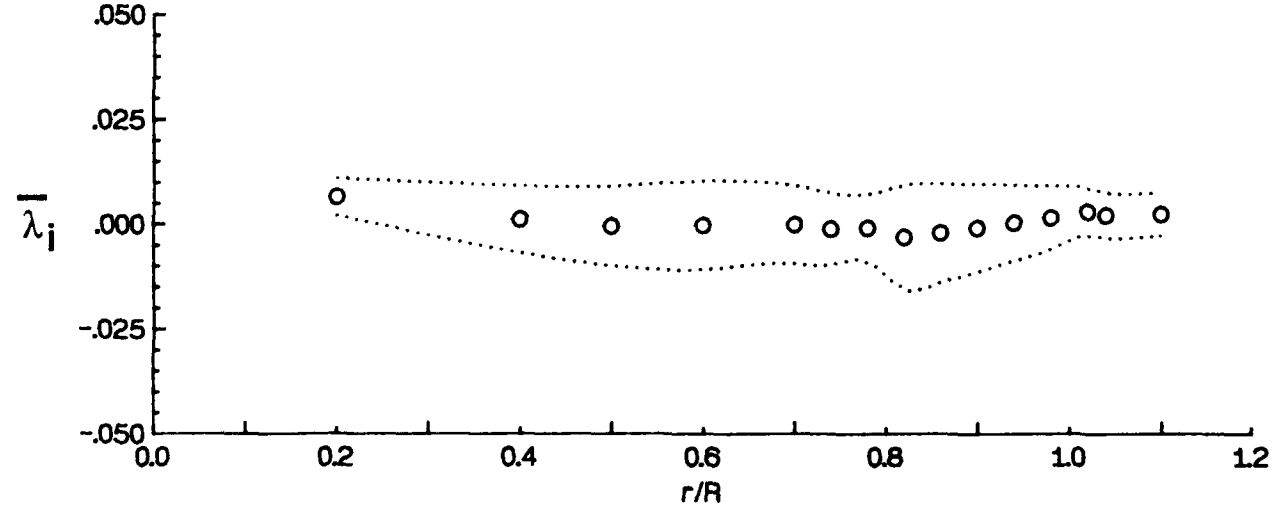

(i) rotor azimuth = 240 degrees

Figure 9. Continued.

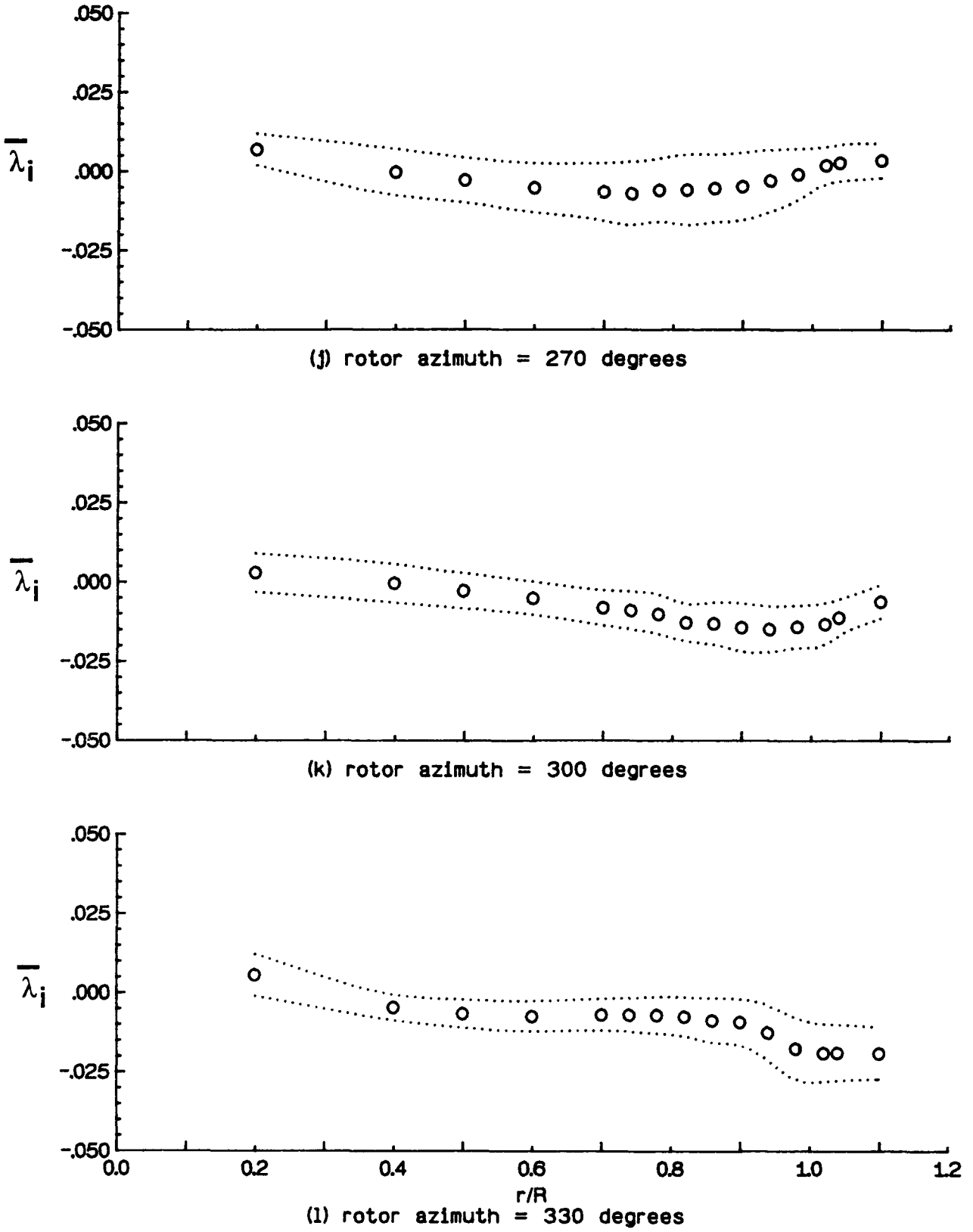

(j) rotor azimuth = 270 degrees

(k) rotor azimuth = 300 degrees

(l) rotor azimuth = 330 degrees

Figure 9. Concluded.

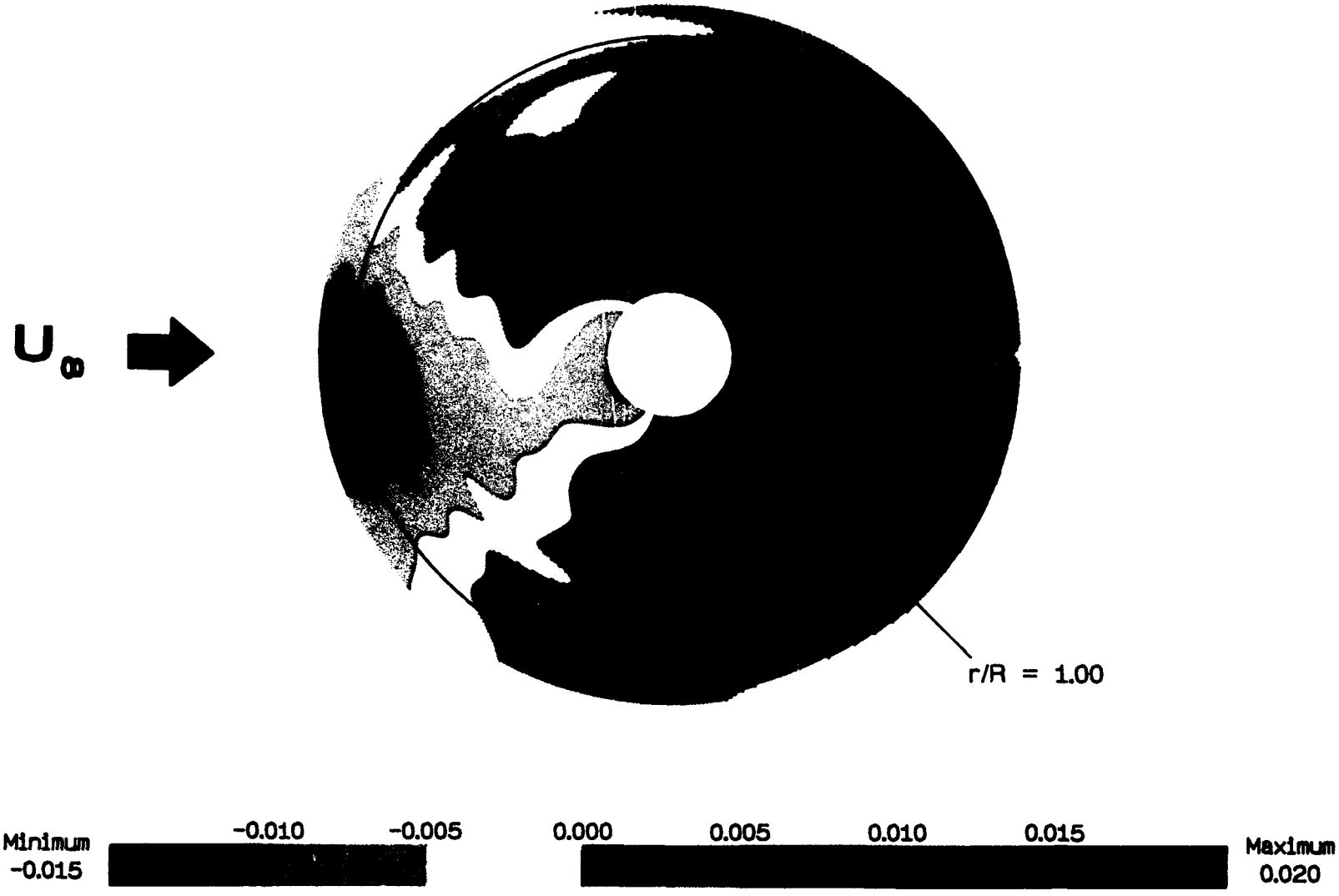

Figure 10. Contour plot of mean induced inflow ratio $\bar{\mu}_i$.

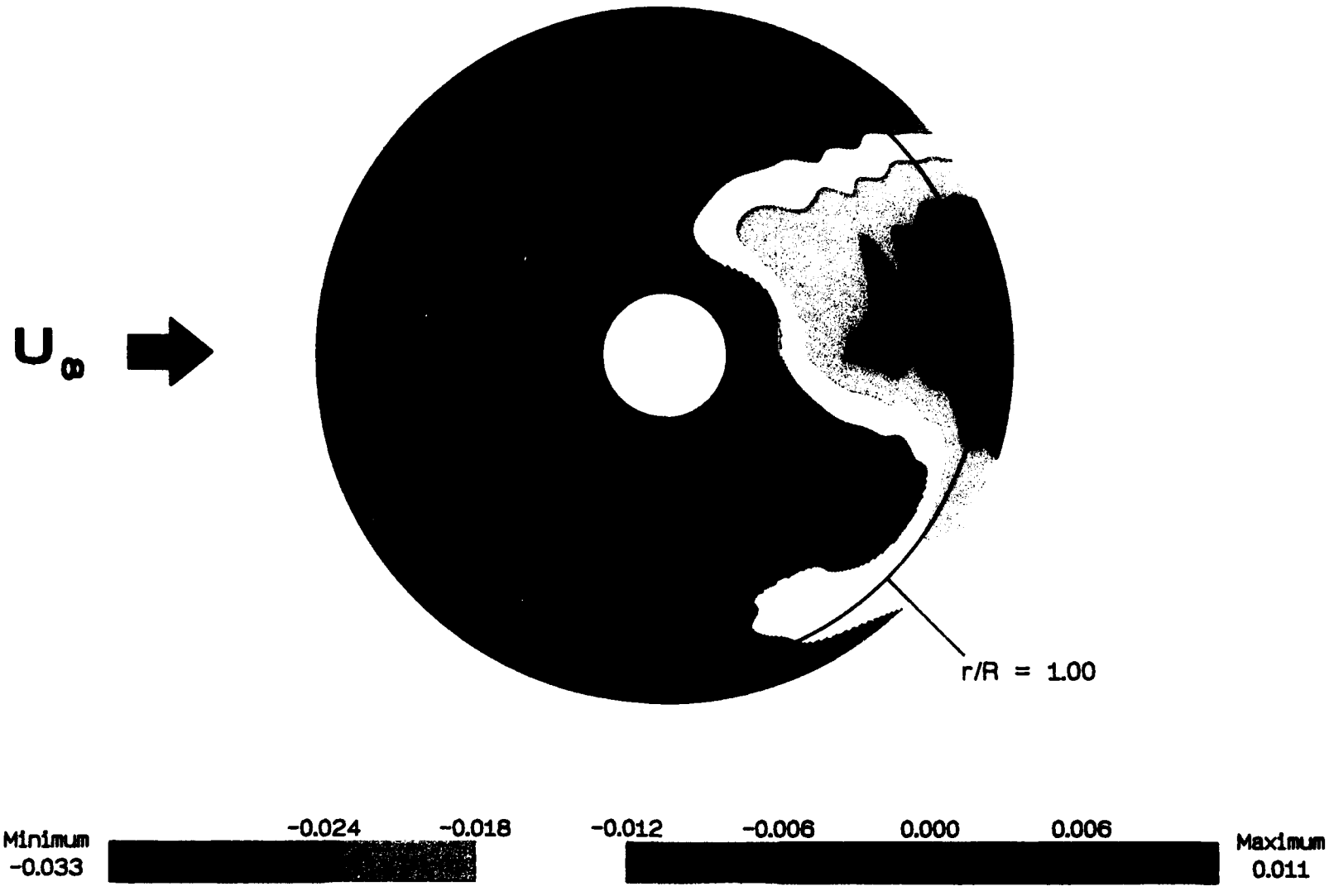

Figure 11. Contour plot of mean induced inflow ratio $\overline{\lambda_i}$.

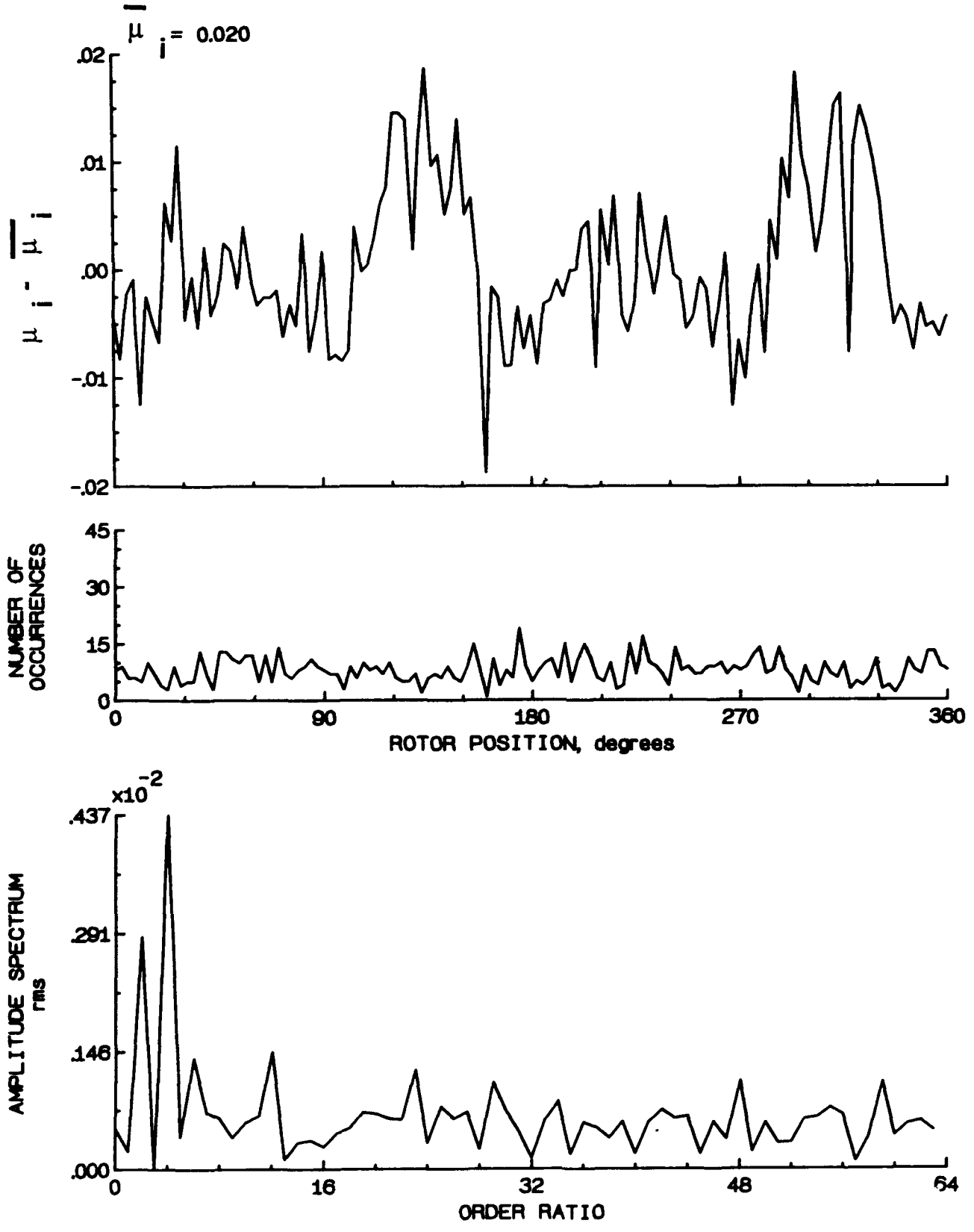

Figure 12.- Induced inflow velocity measured at 0 degrees and r/R of 0.20.

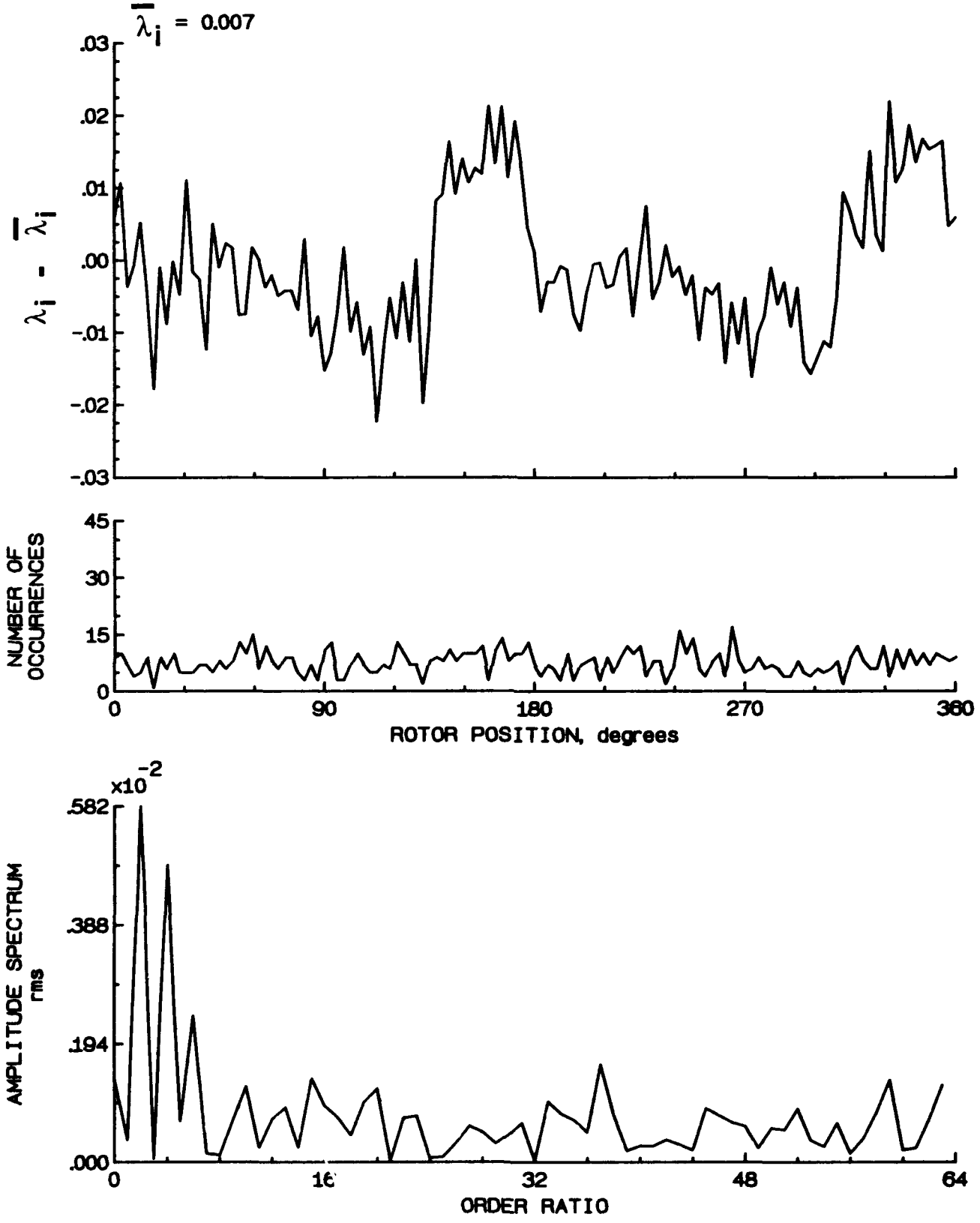

Figure 12.- Concluded.

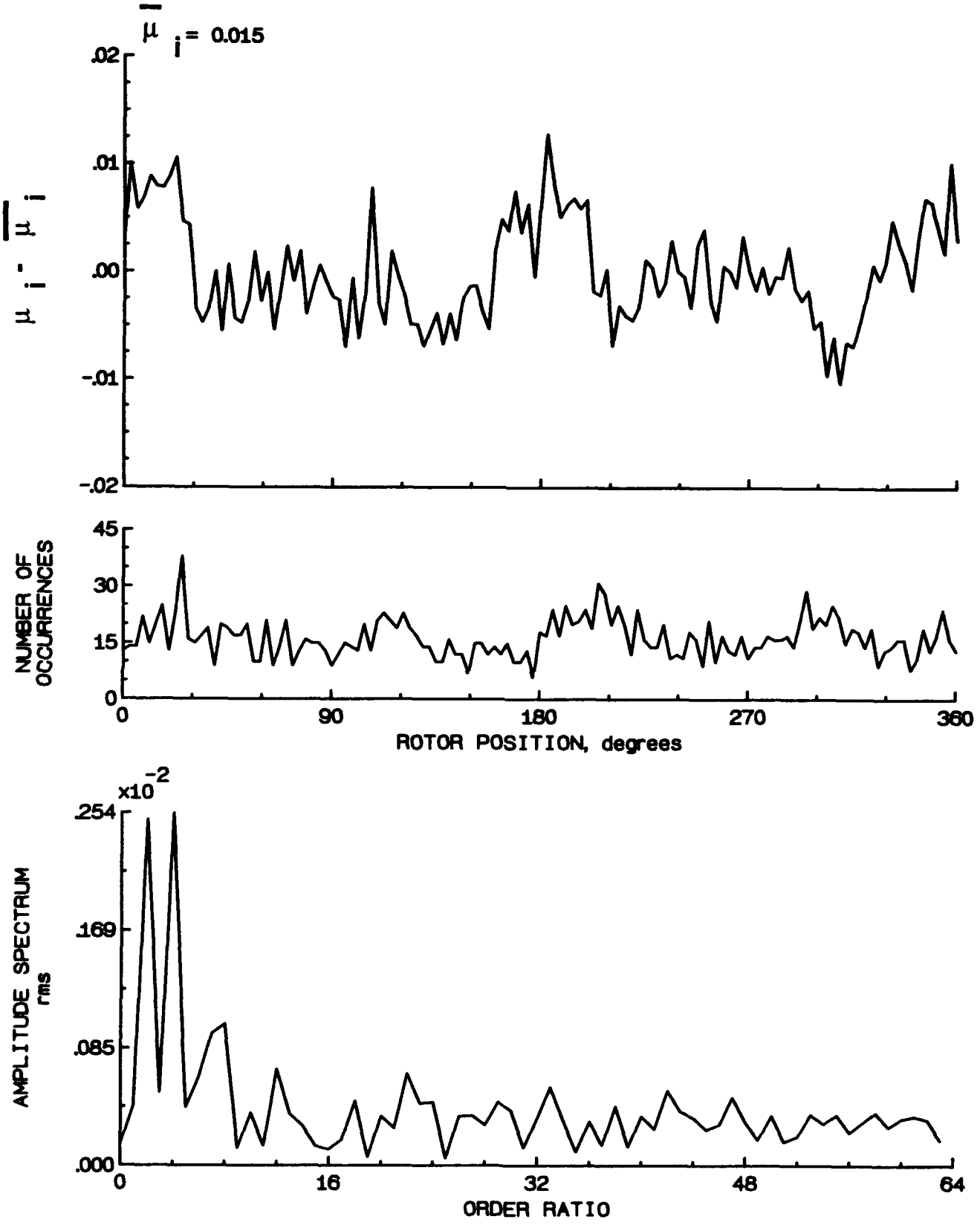

Figure 13.- Induced inflow velocity measured at 0 degrees and r/R of 0.40.

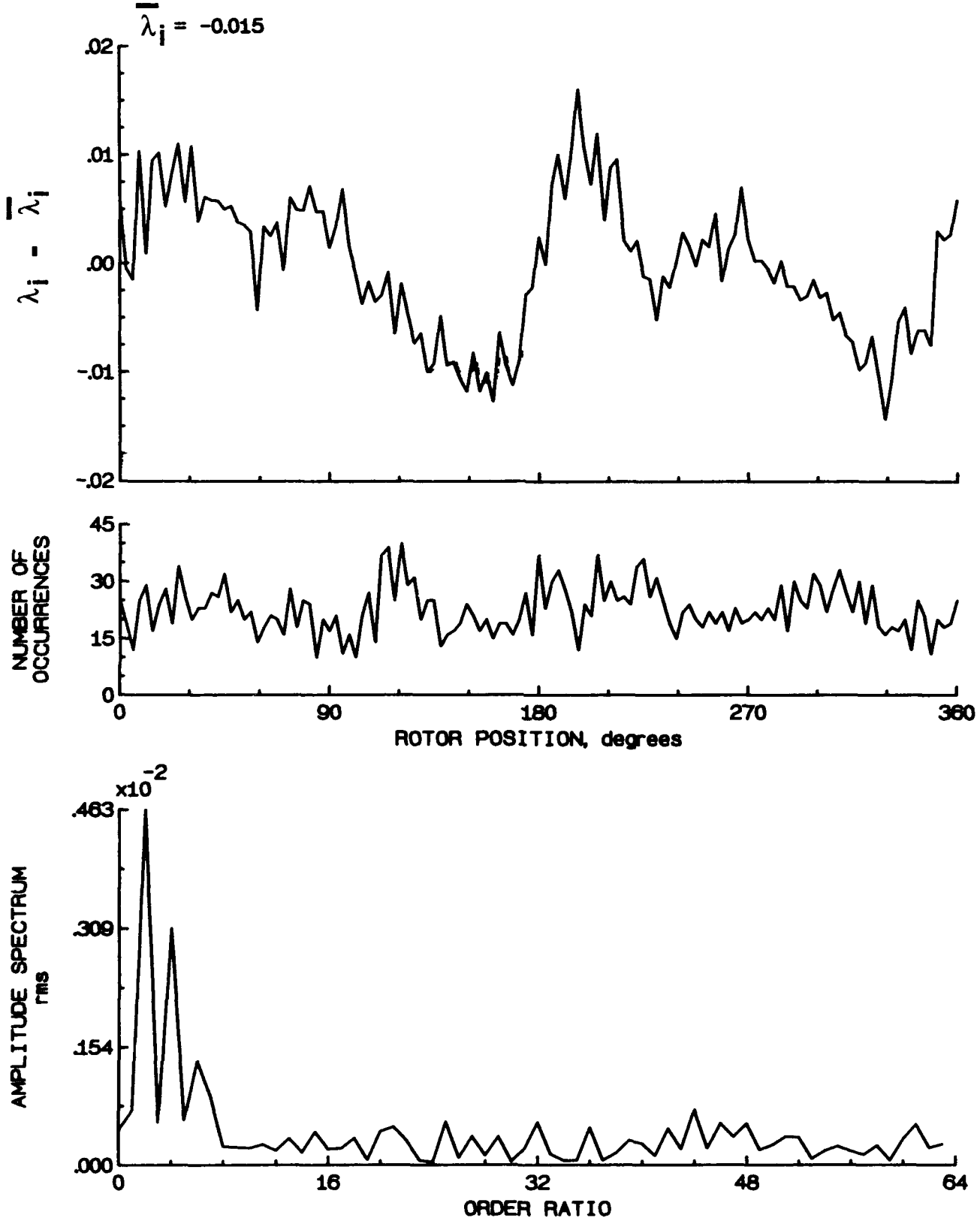

Figure 13.- Concluded.

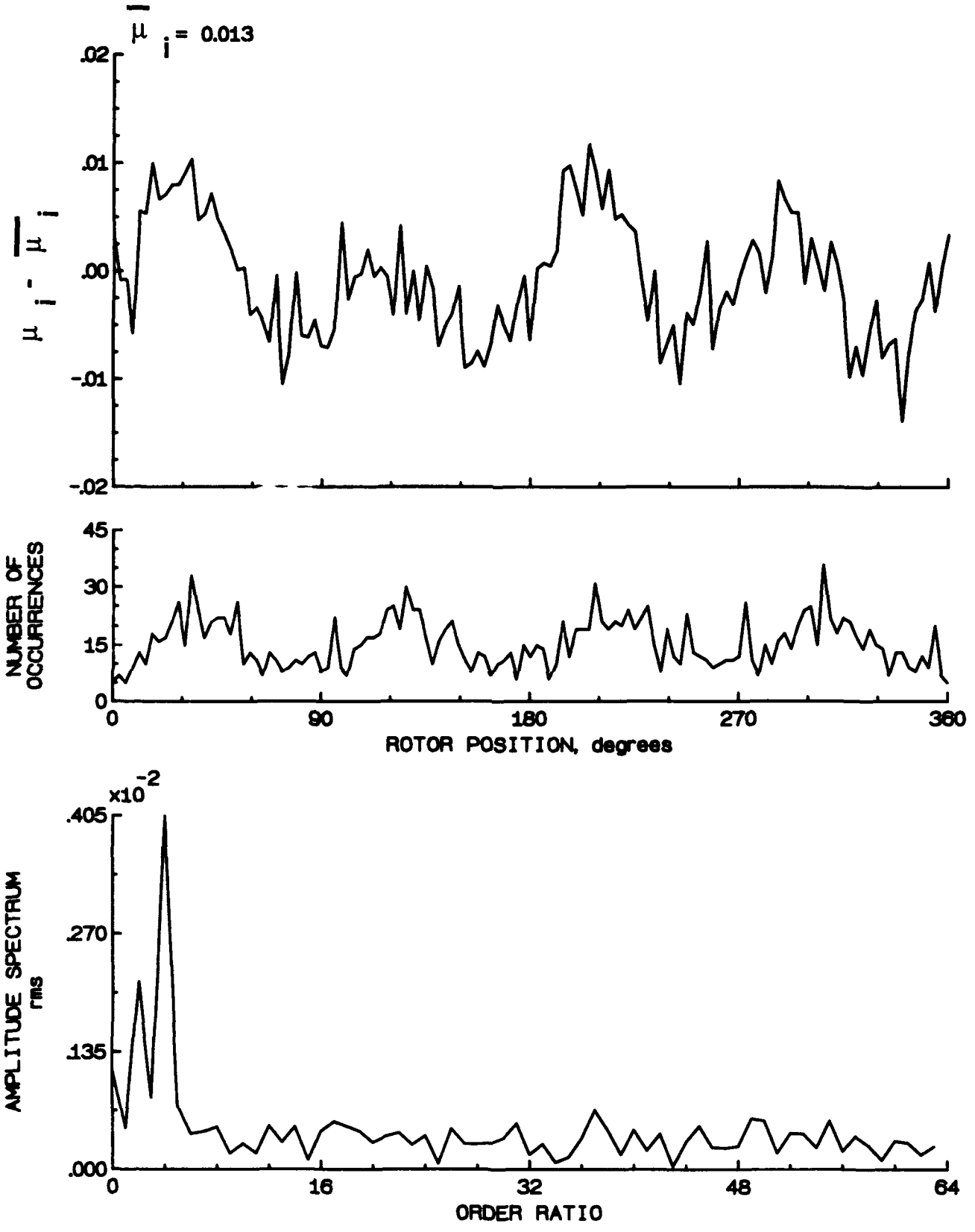

Figure 14.- Induced inflow velocity measured at 0 degrees and r/R of 0.50.

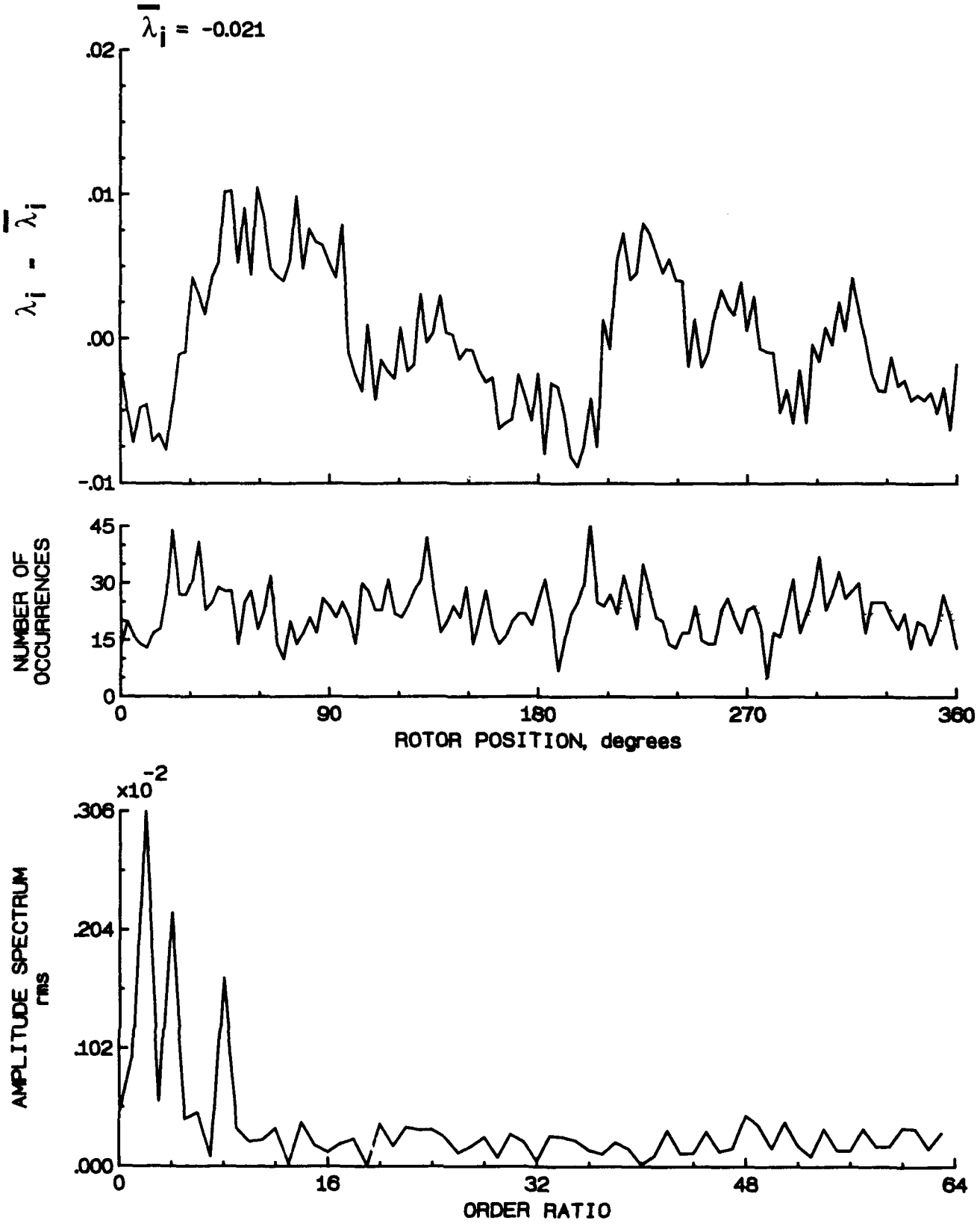

Figure 14.- Concluded.

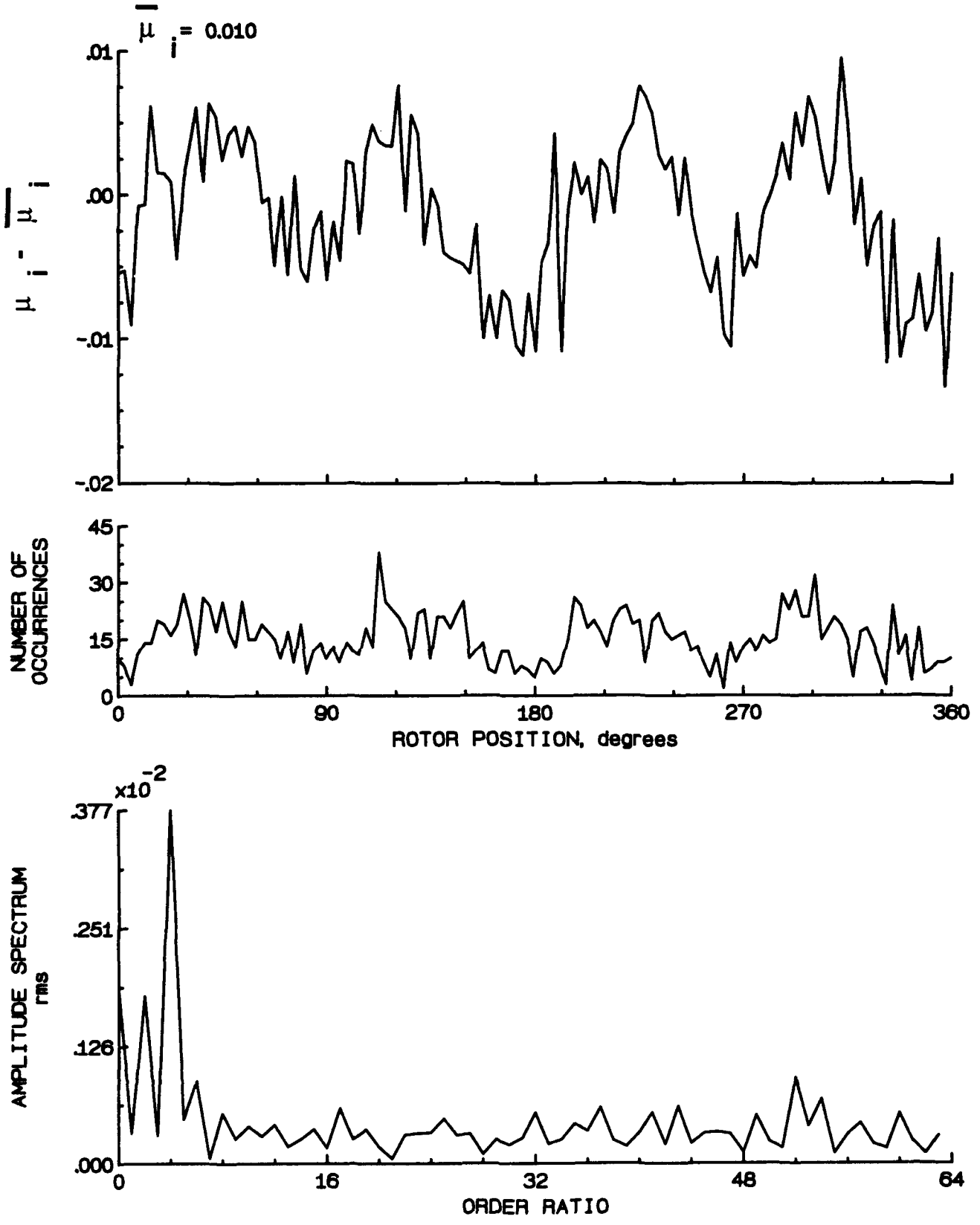

Figure 15.- Induced inflow velocity measured at 0 degrees and r/R of 0.60.

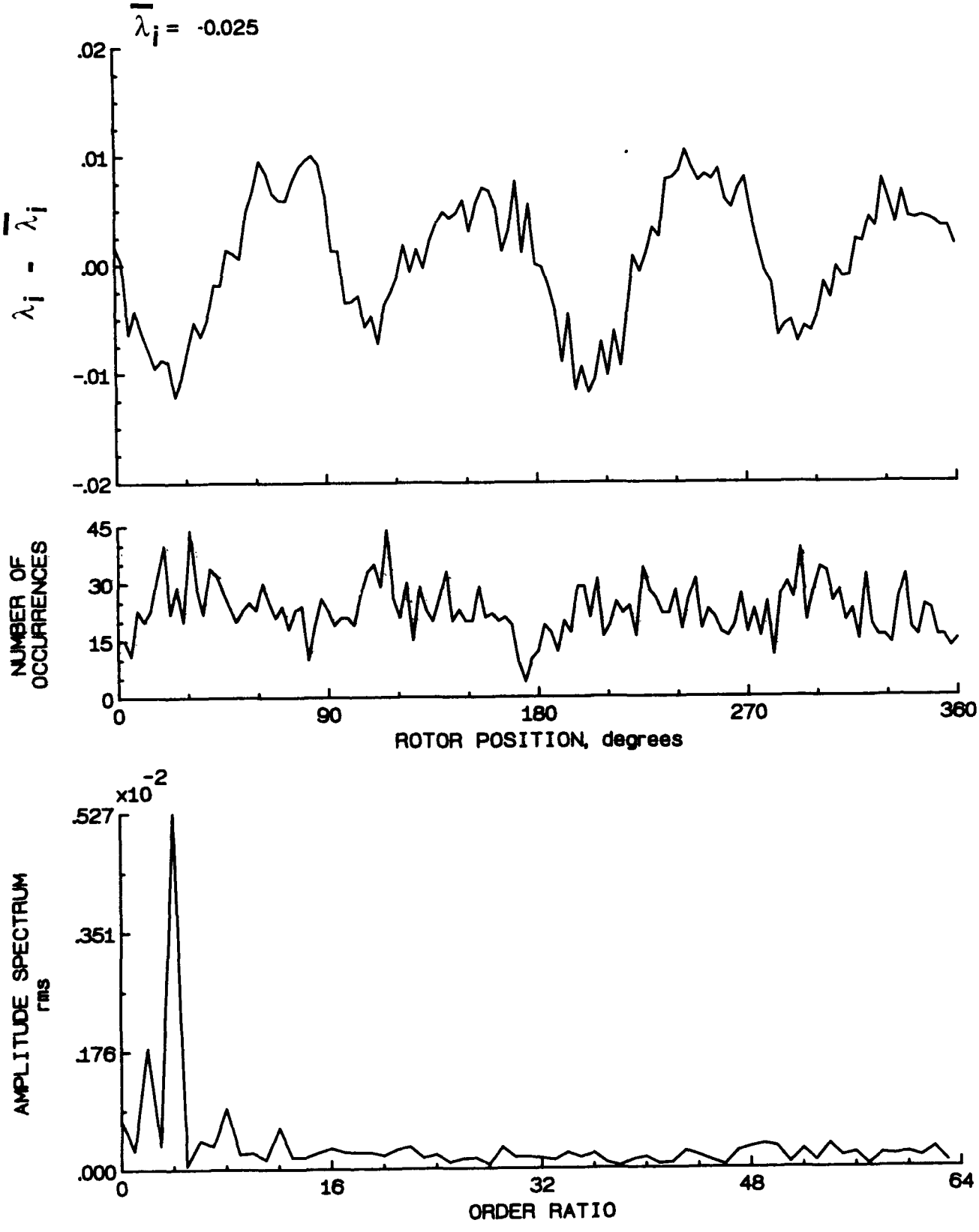

Figure 15.- Concluded.

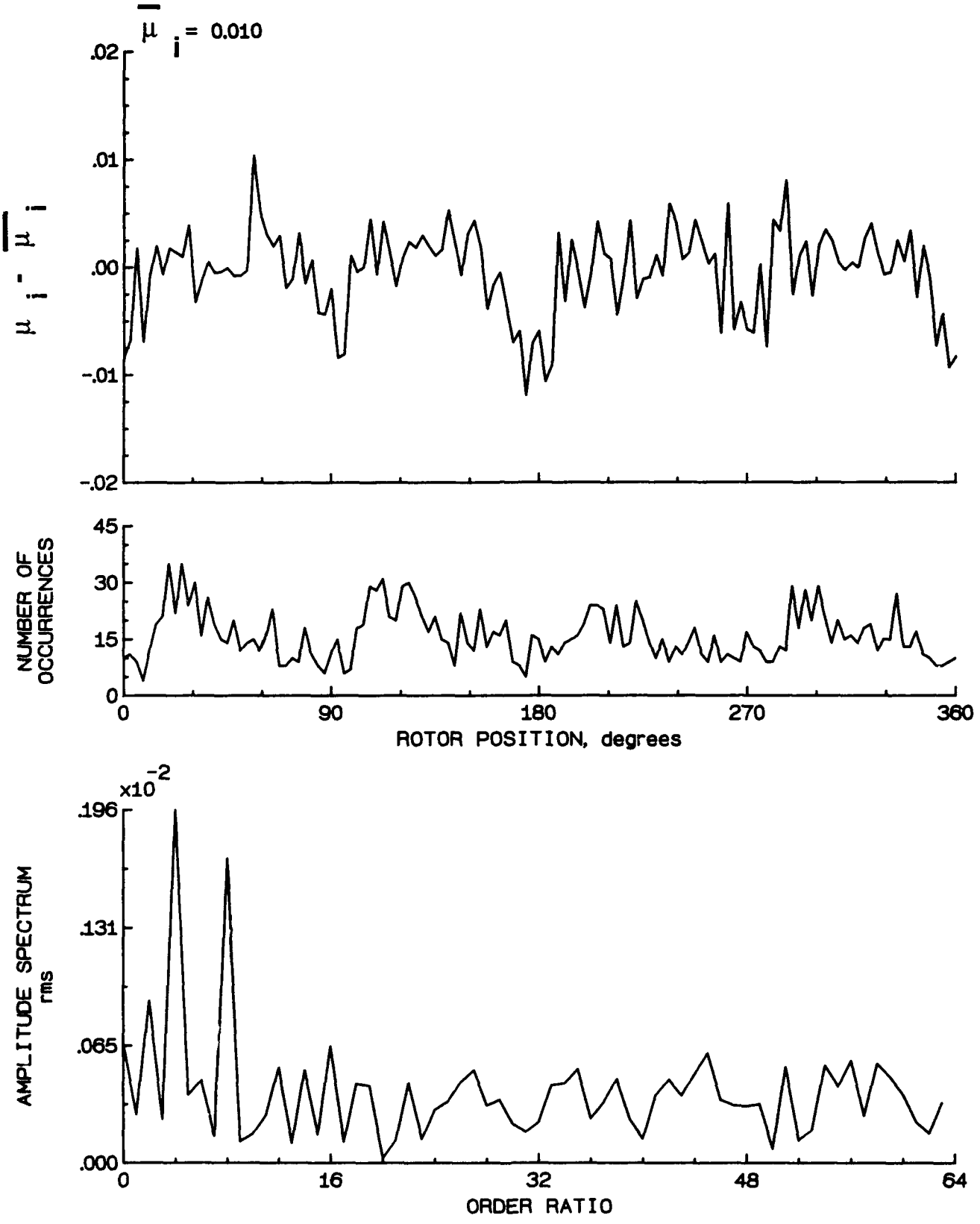

Figure 16.- Induced inflow velocity measured at 0 degrees and r/R of 0.70.

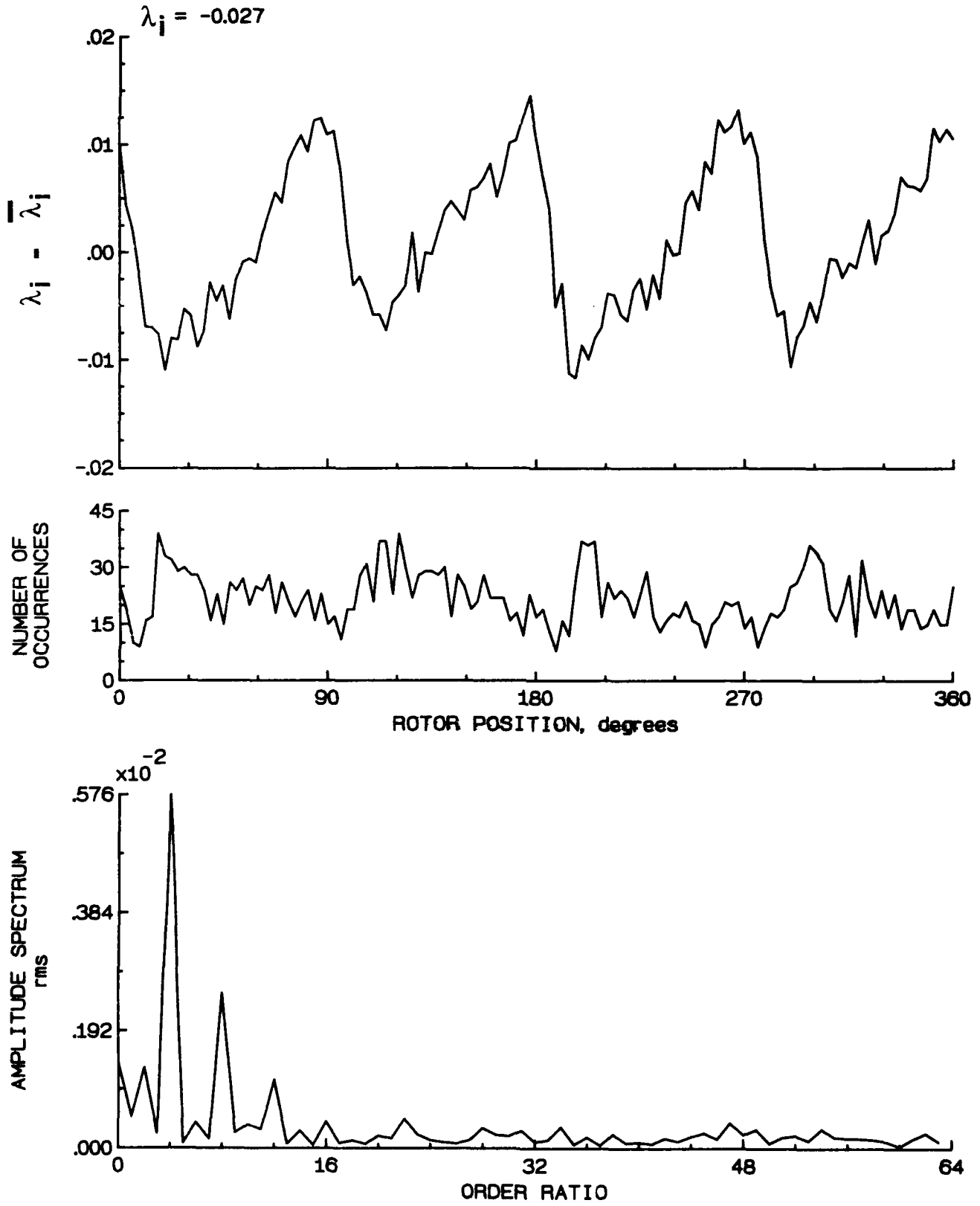

Figure 16.- Concluded.

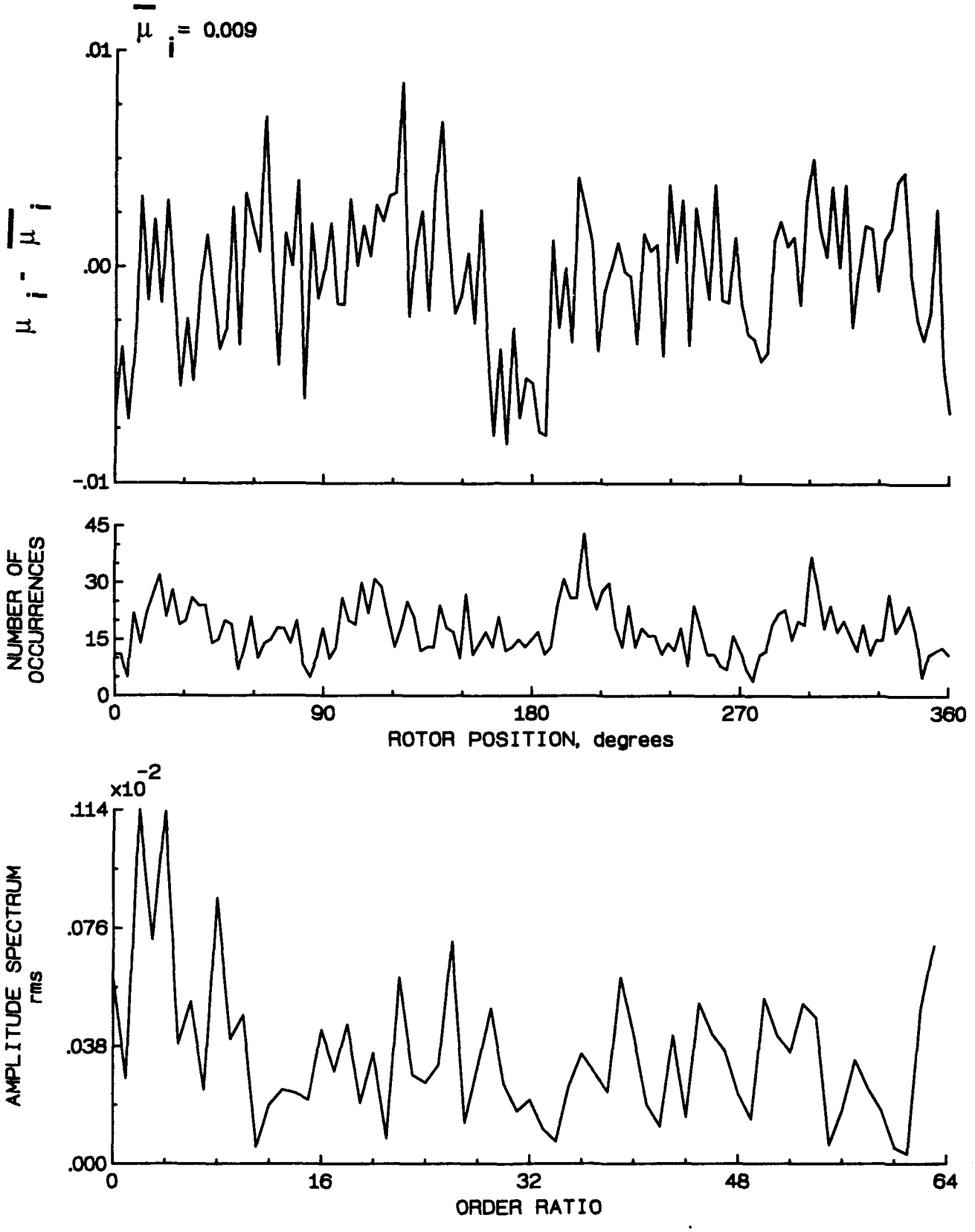

Figure 17.- Induced inflow velocity measured at 0 degrees and r/R of 0.74.

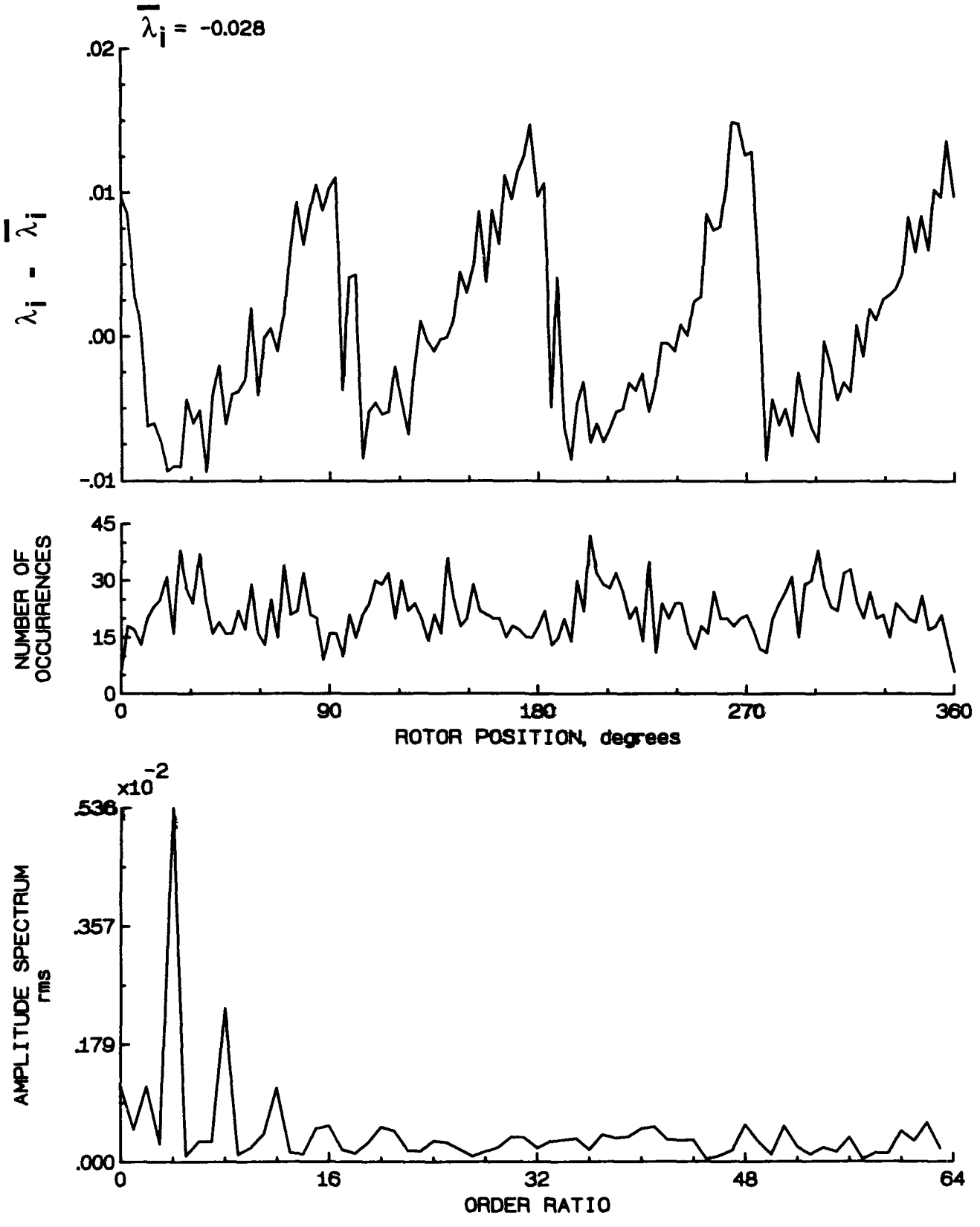

Figure 17.- Concluded.

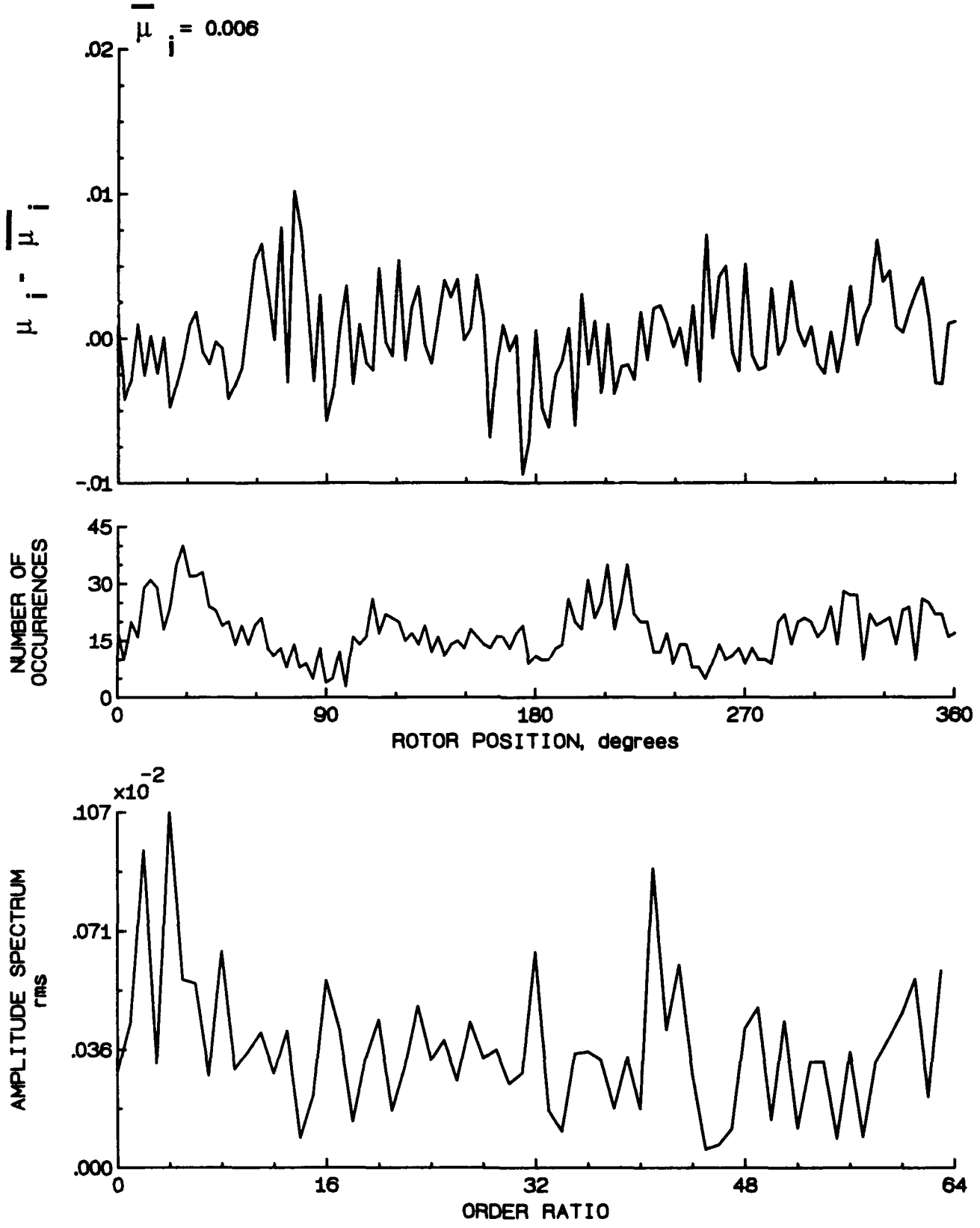

Figure 18.- Induced inflow velocity measured at 0 degrees and r/R of 0.78.

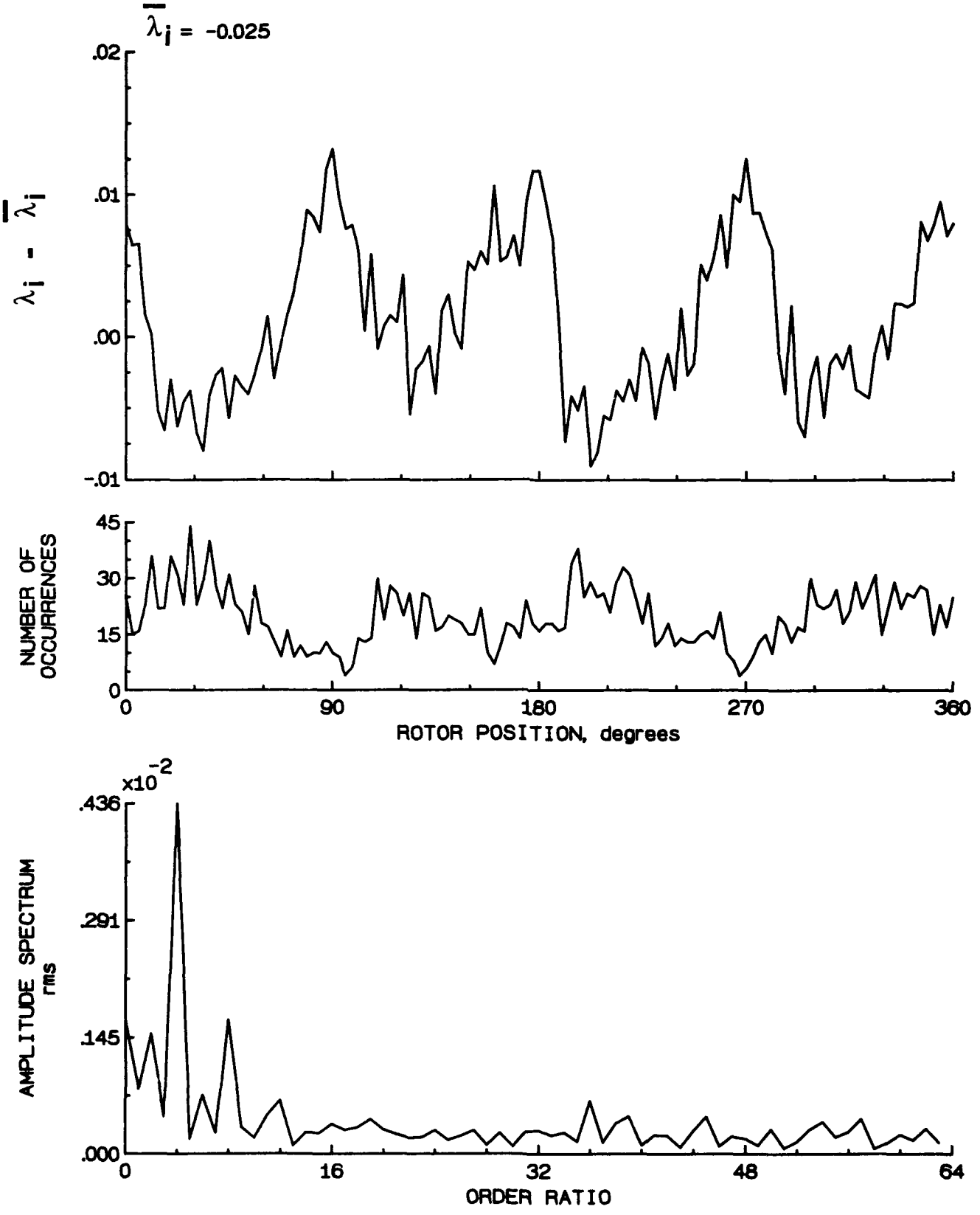

Figure 18.- Concluded.

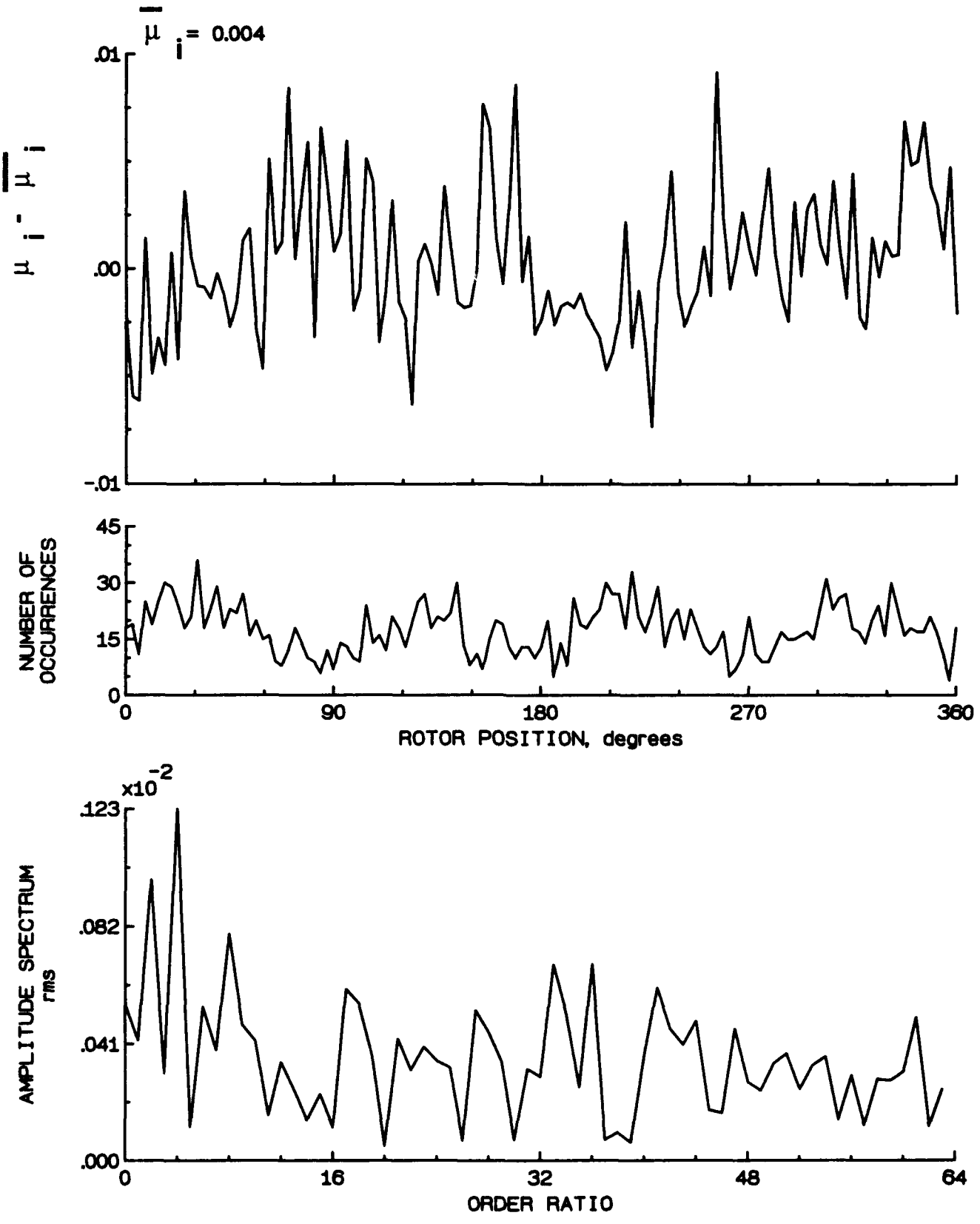

Figure 19.- Induced inflow velocity measured at 0 degrees and r/R of 0.82.

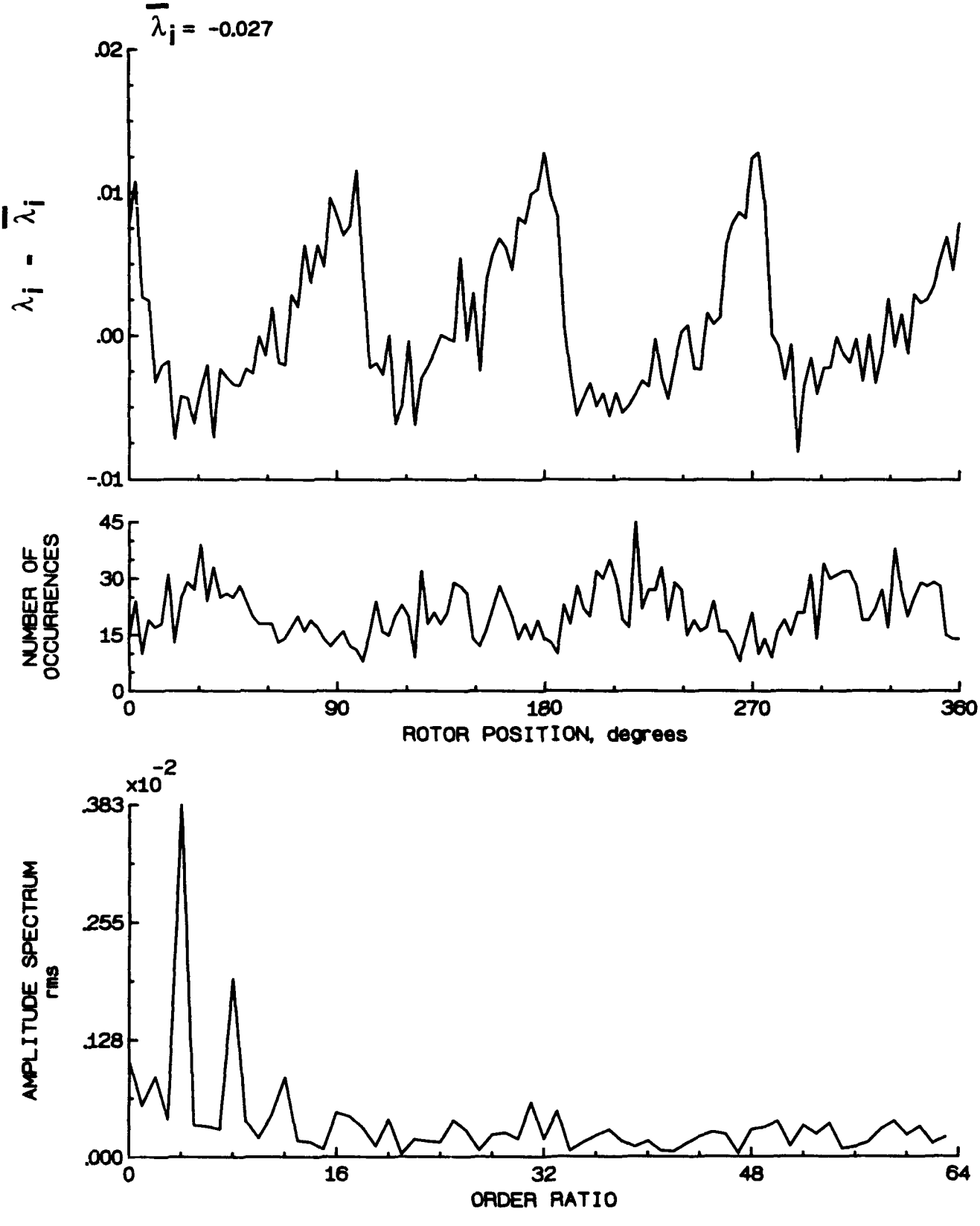

Figure 19.- Concluded.

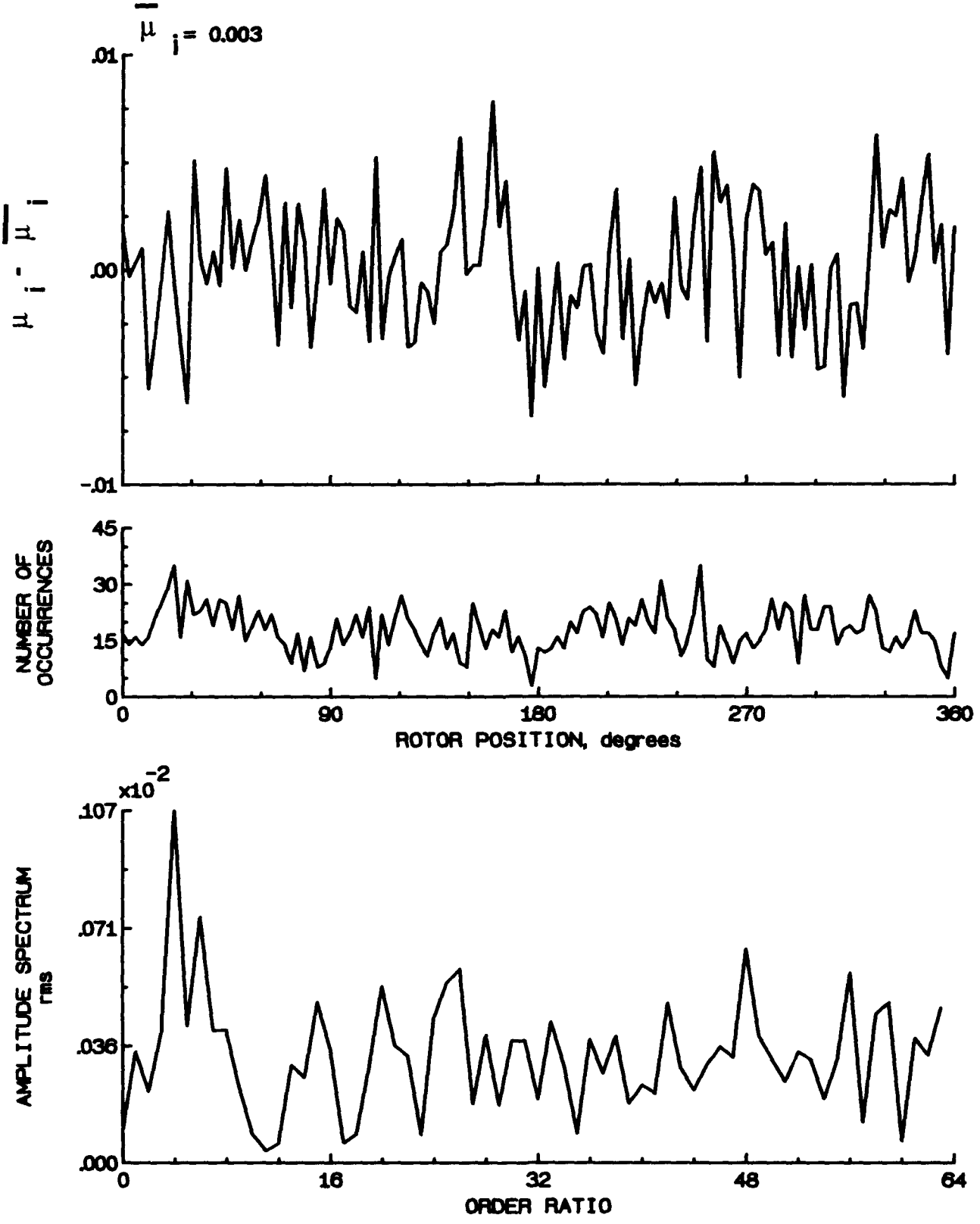

Figure 20.- Induced inflow velocity measured at 0 degrees and r/R of 0.86.

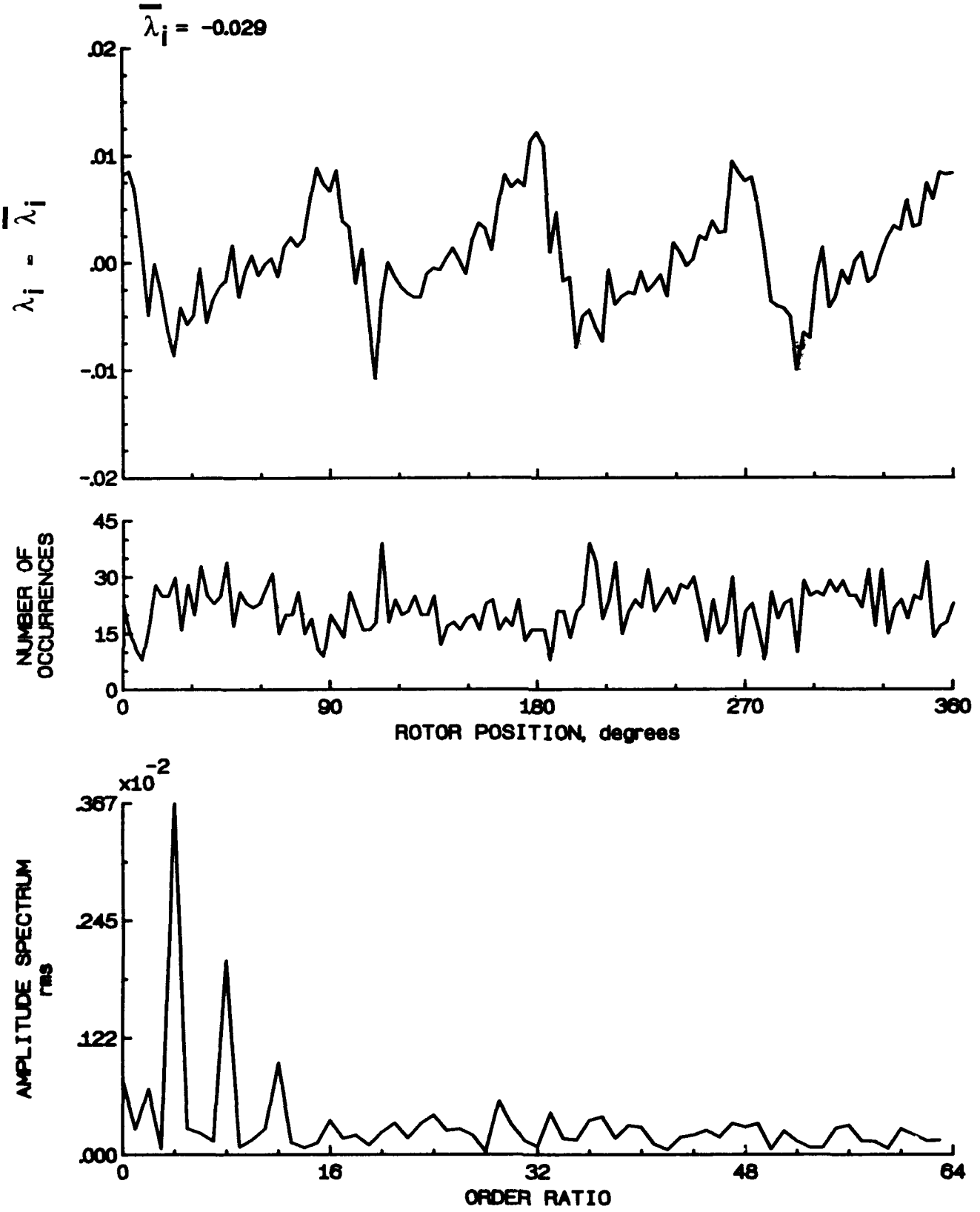

Figure 20.- Concluded.

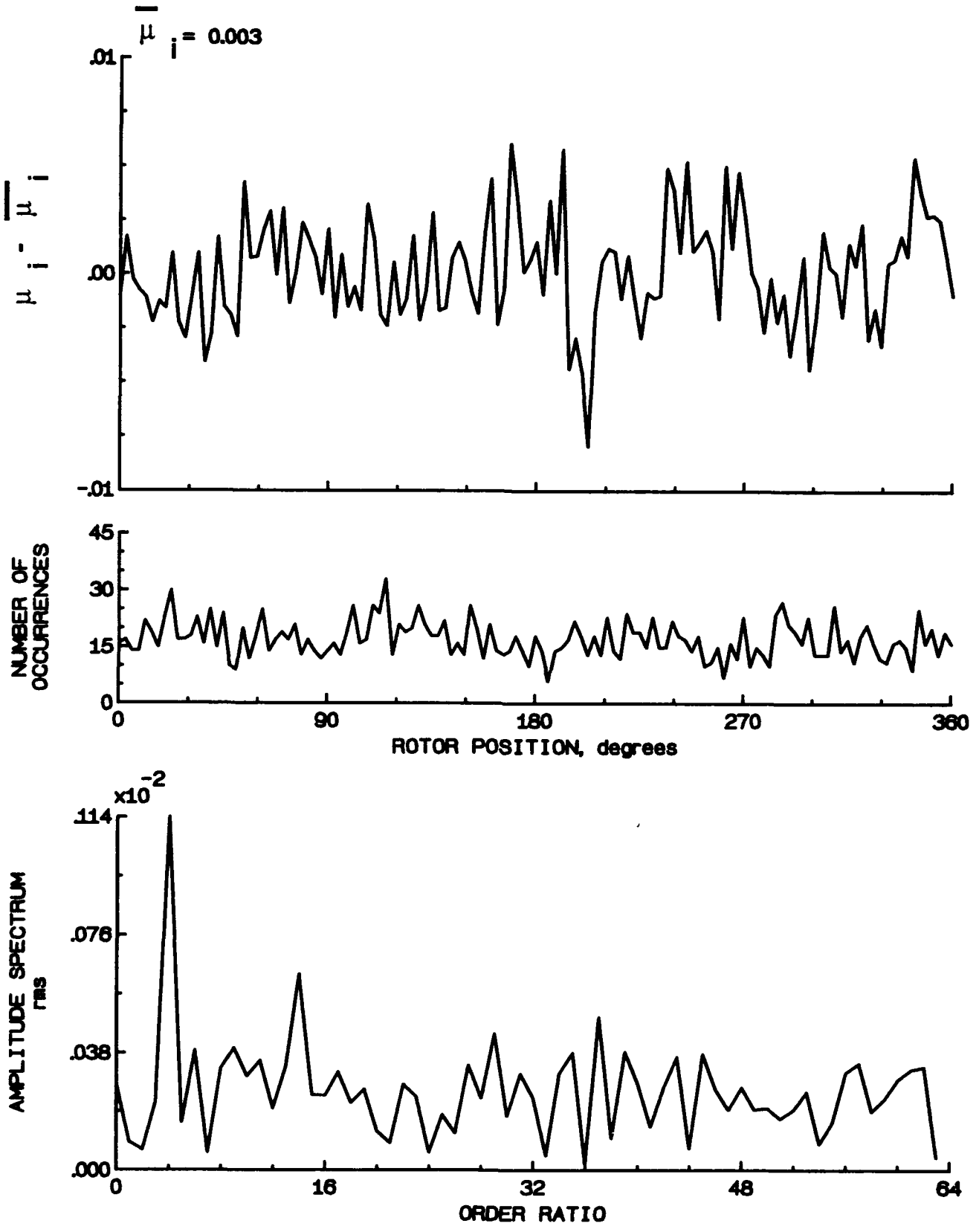

Figure 21.- Induced inflow velocity measured at 0 degrees and r/R of 0.90.

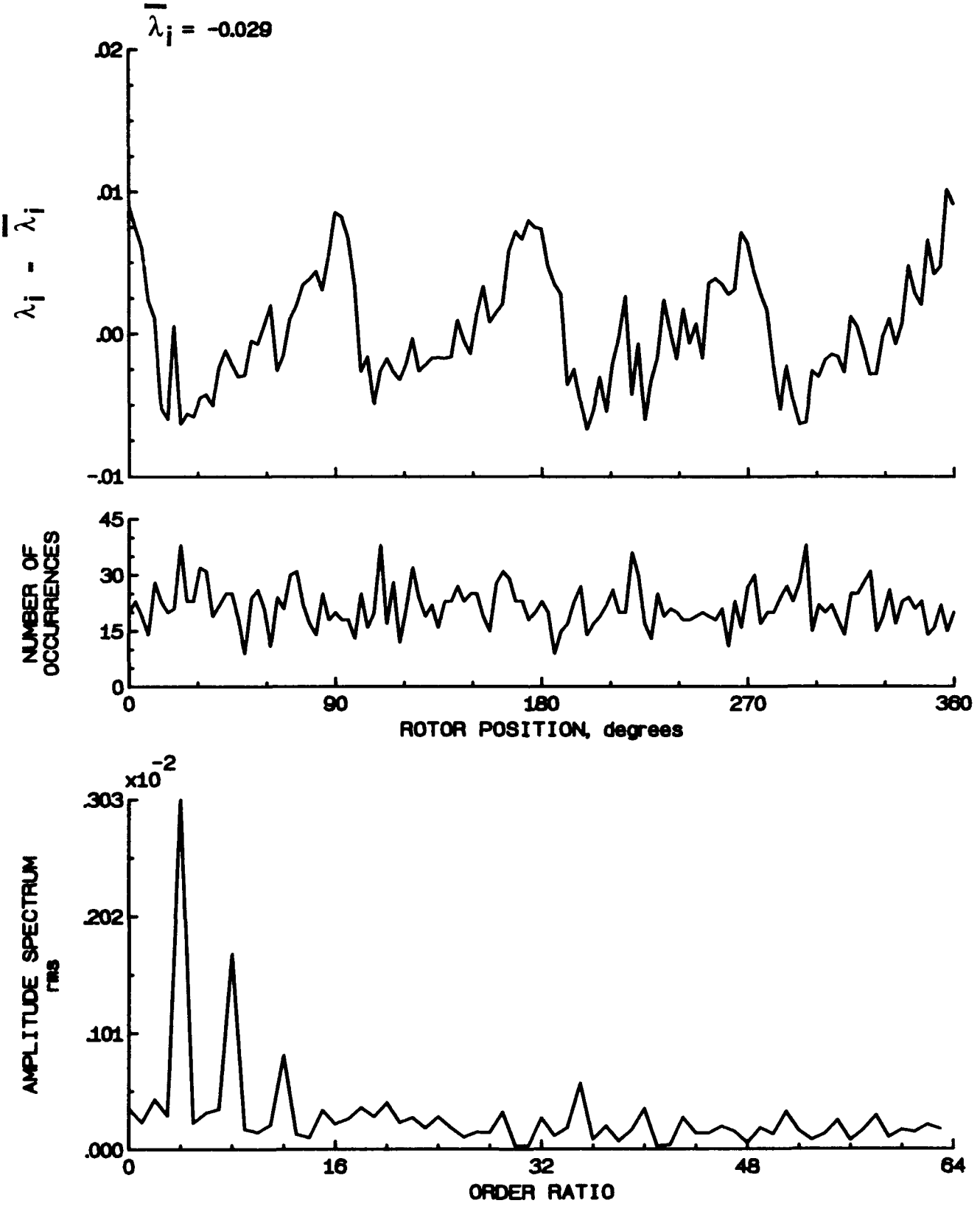

Figure 21.- Concluded.

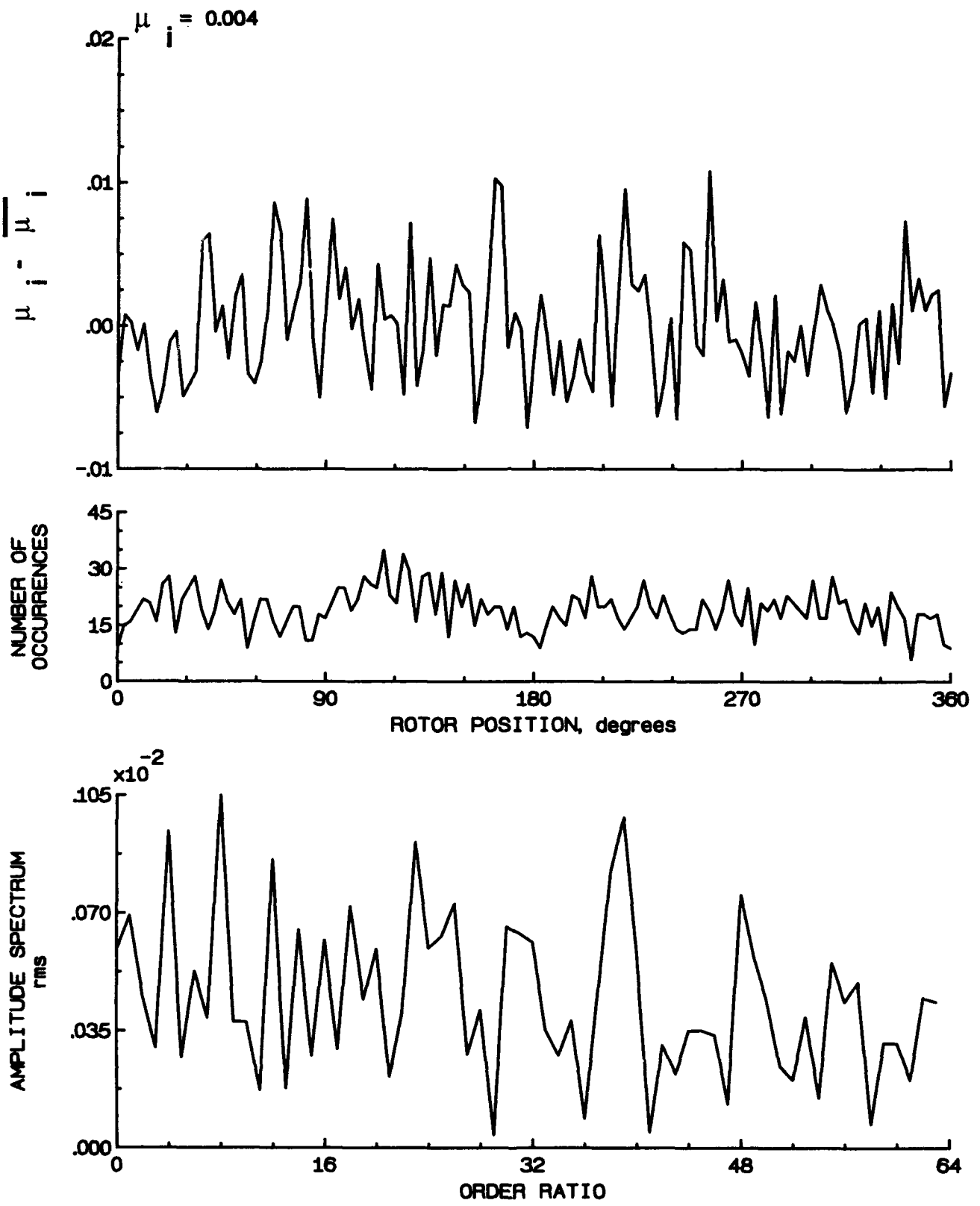

Figure 22.- Induced inflow velocity measured at 0 degrees and r/R of 0.94.

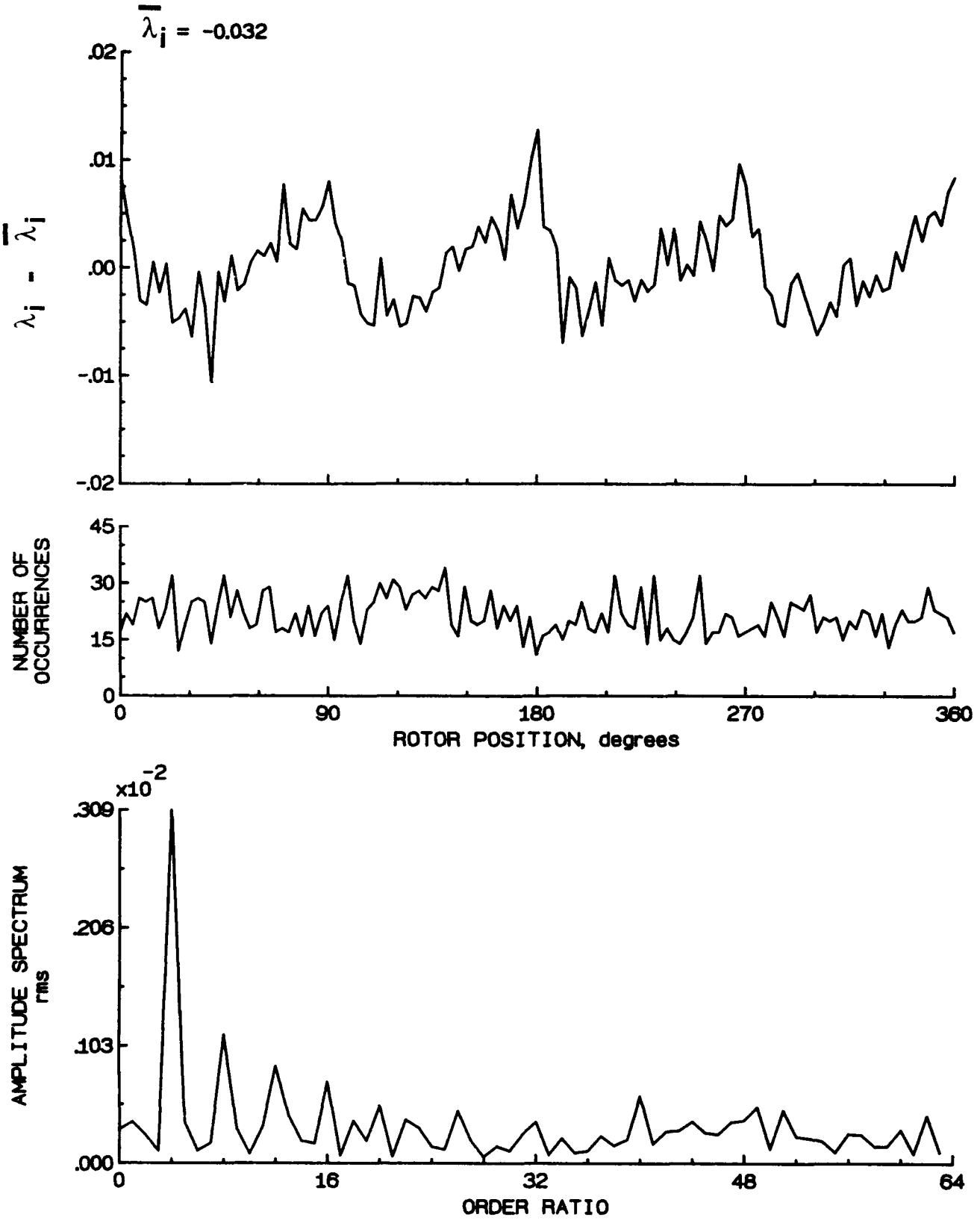

Figure 22.- Concluded.

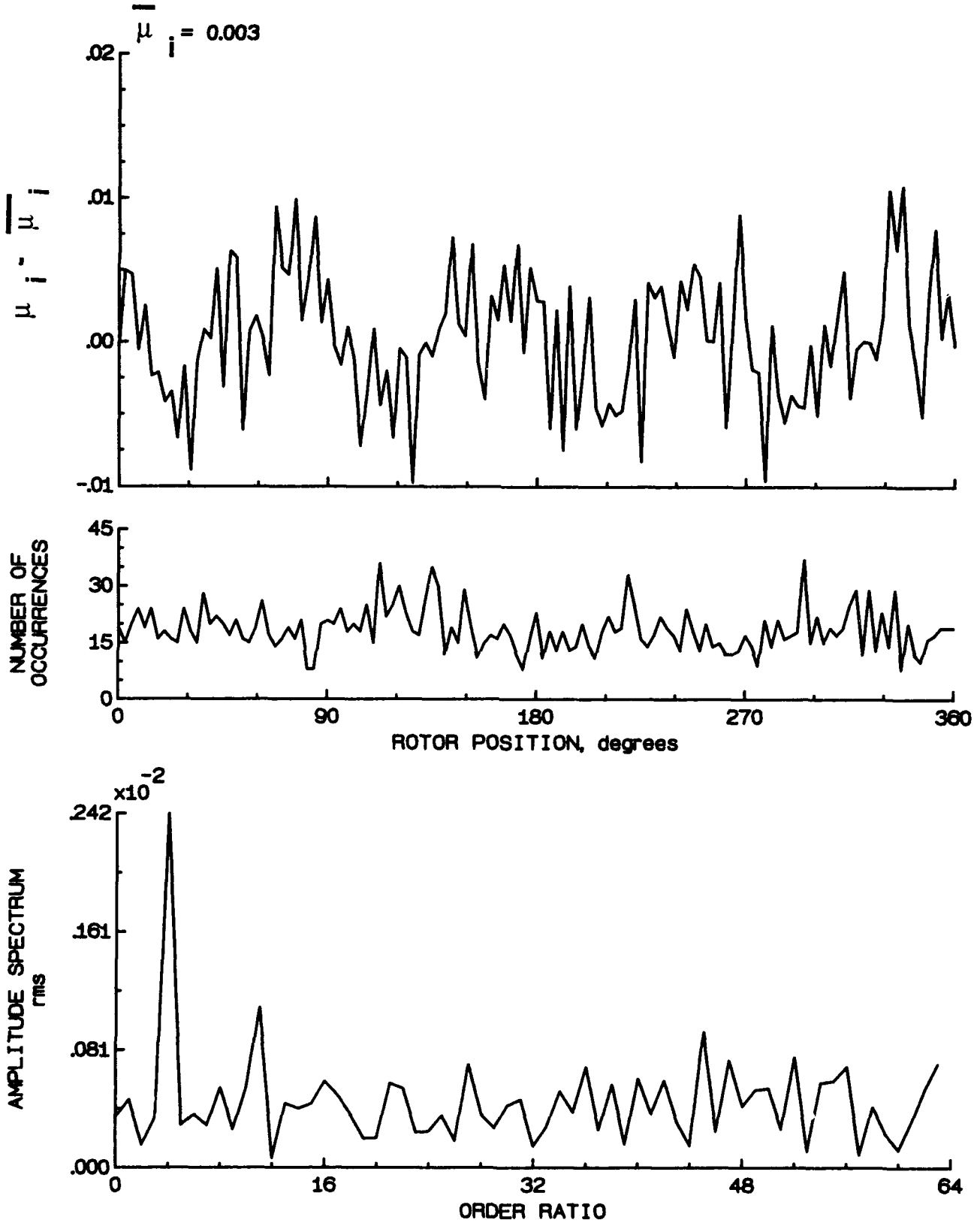

Figure 23.- Induced inflow velocity measured at 0 degrees and r/R of 0.98.

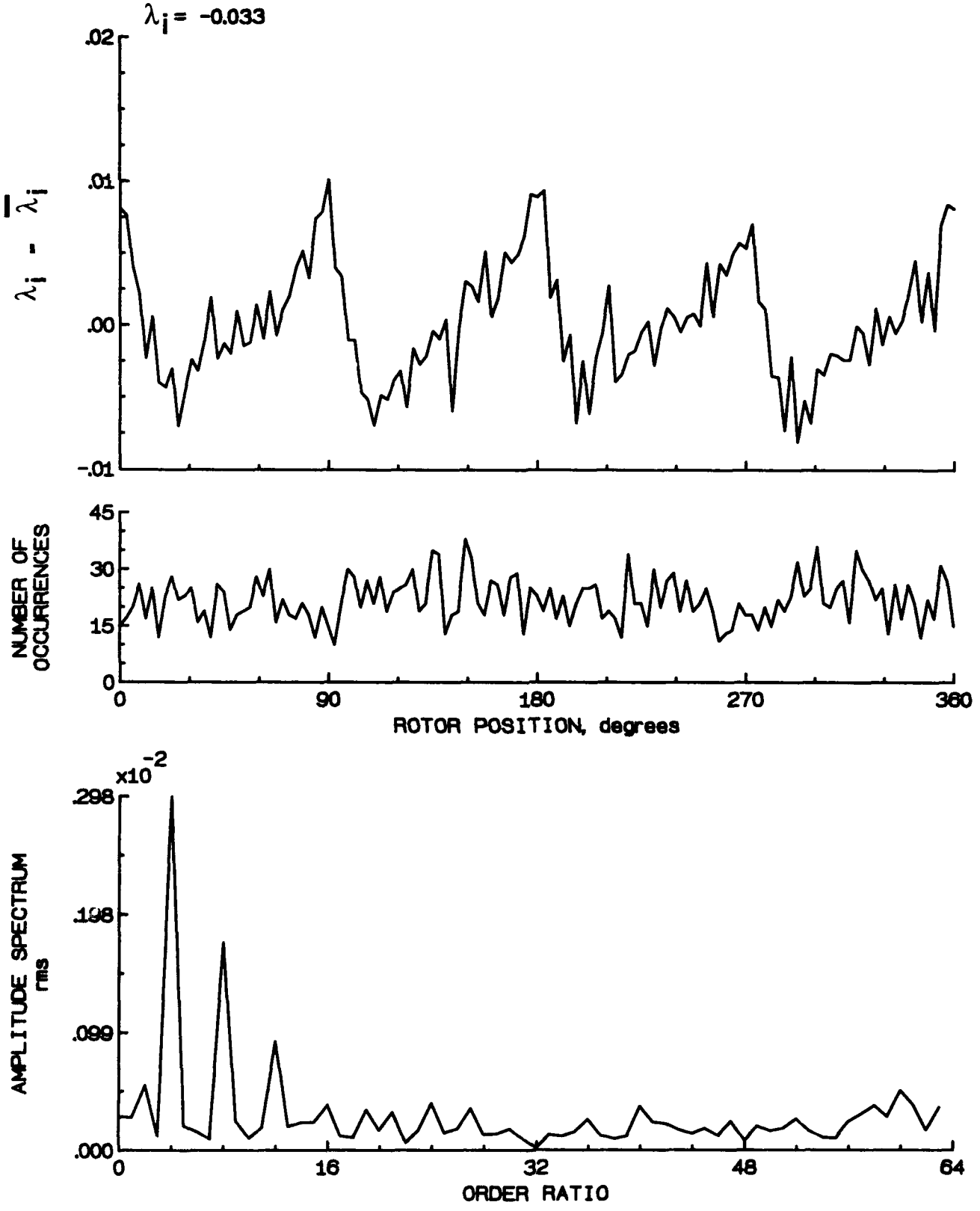

Figure 23.- Concluded.

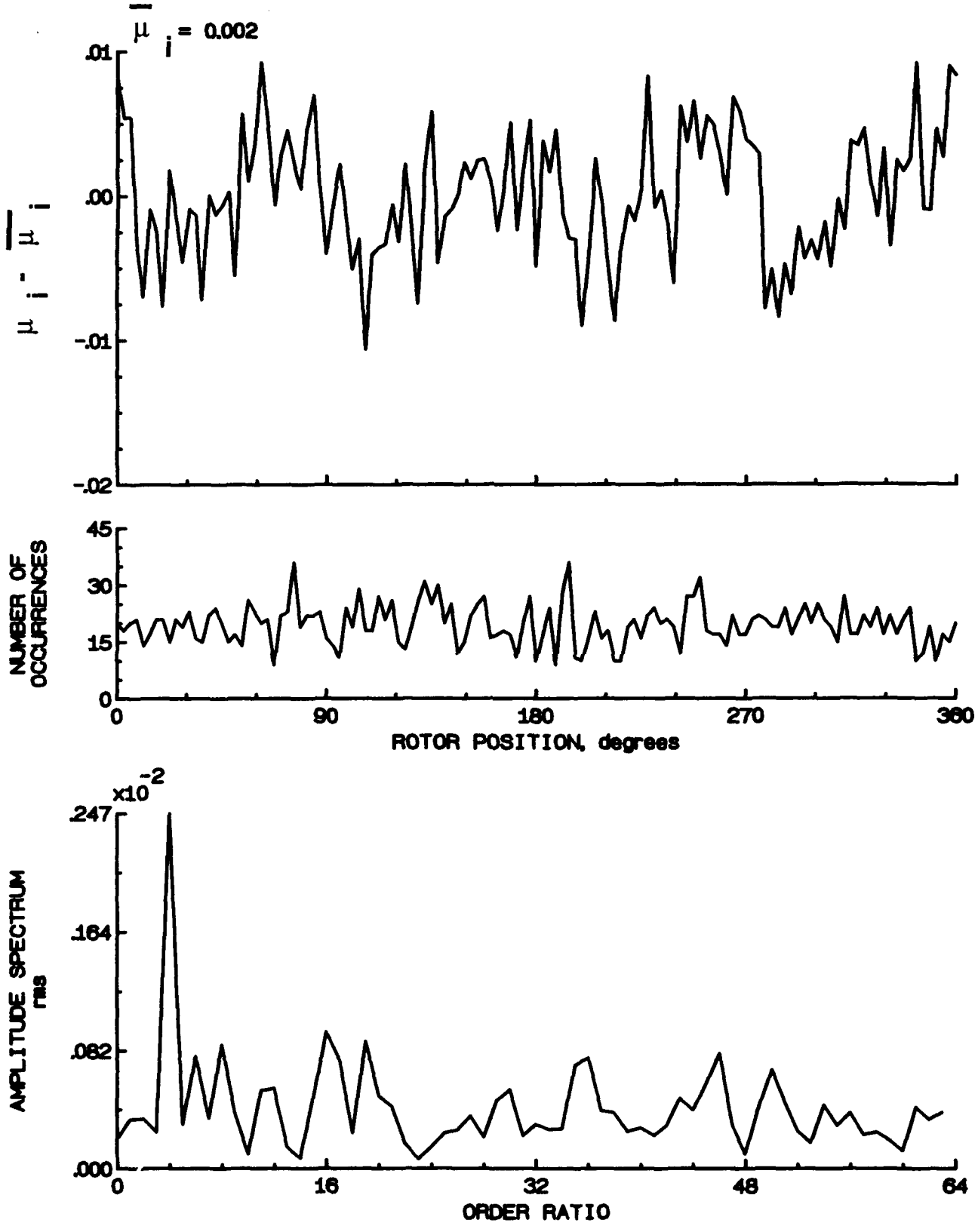

Figure 24.- Induced inflow velocity measured at 0 degrees and r/R of 1.02.

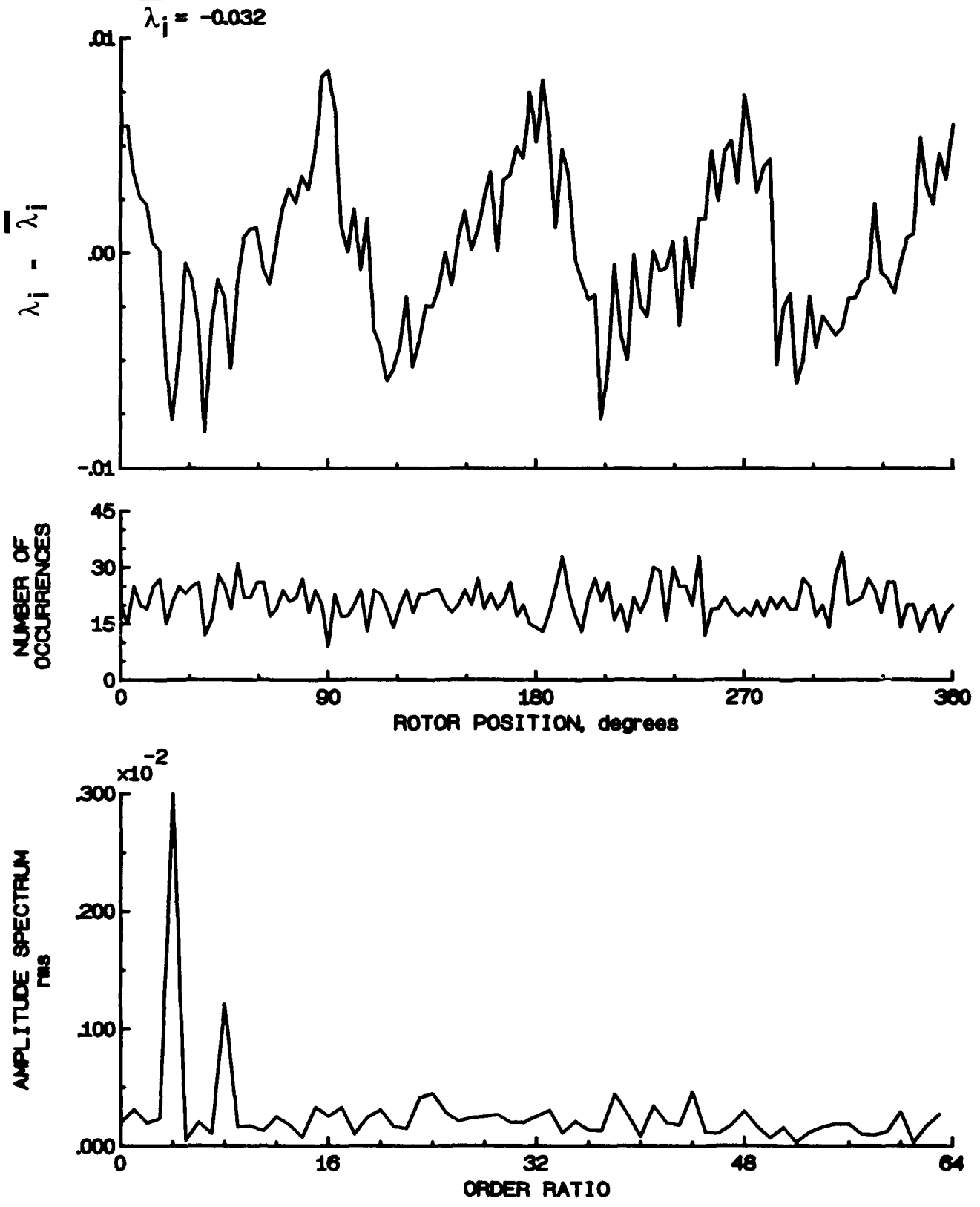

Figure 24.- Concluded.

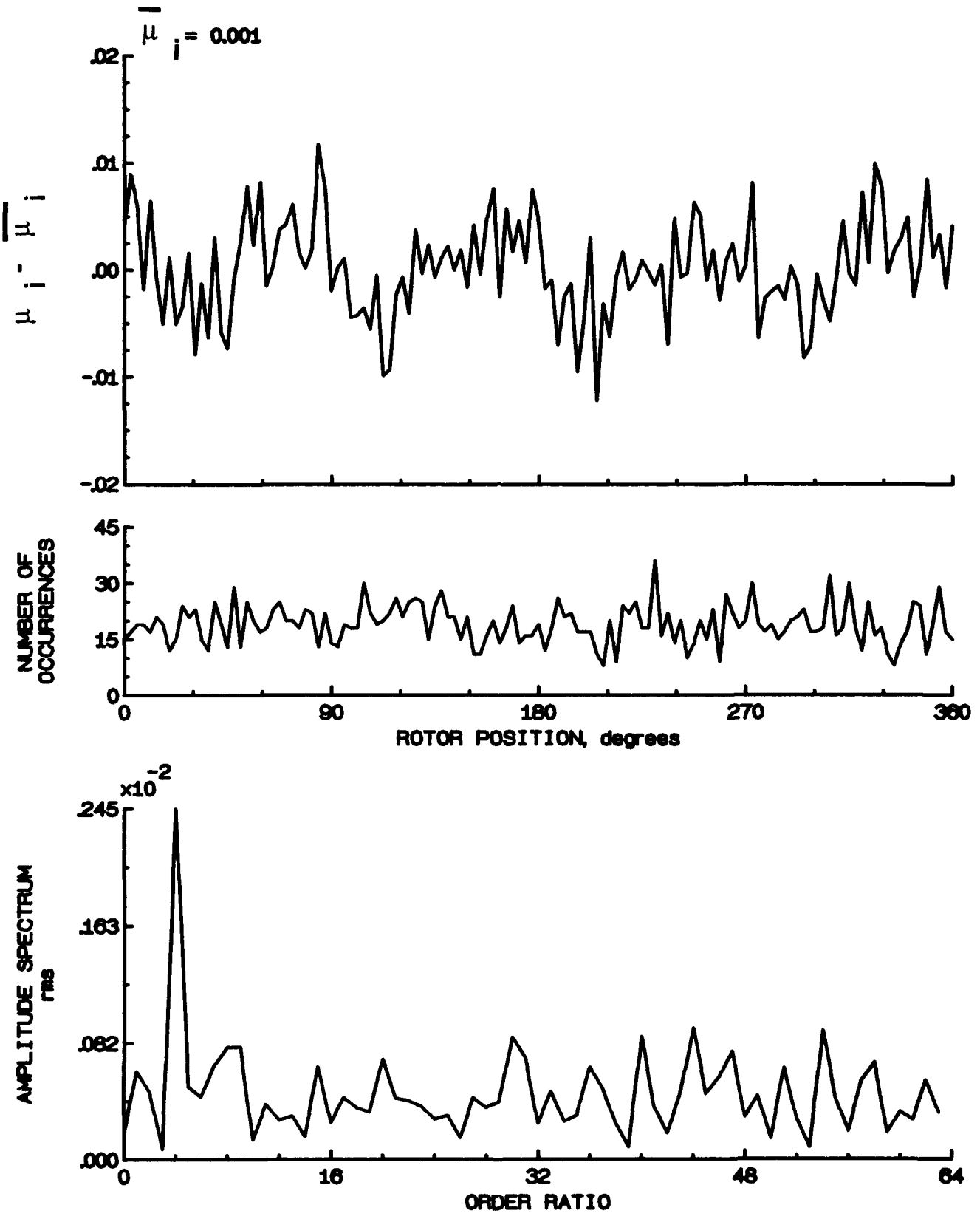

Figure 25.- Induced inflow velocity measured at 0 degrees and r/R of 1.04.

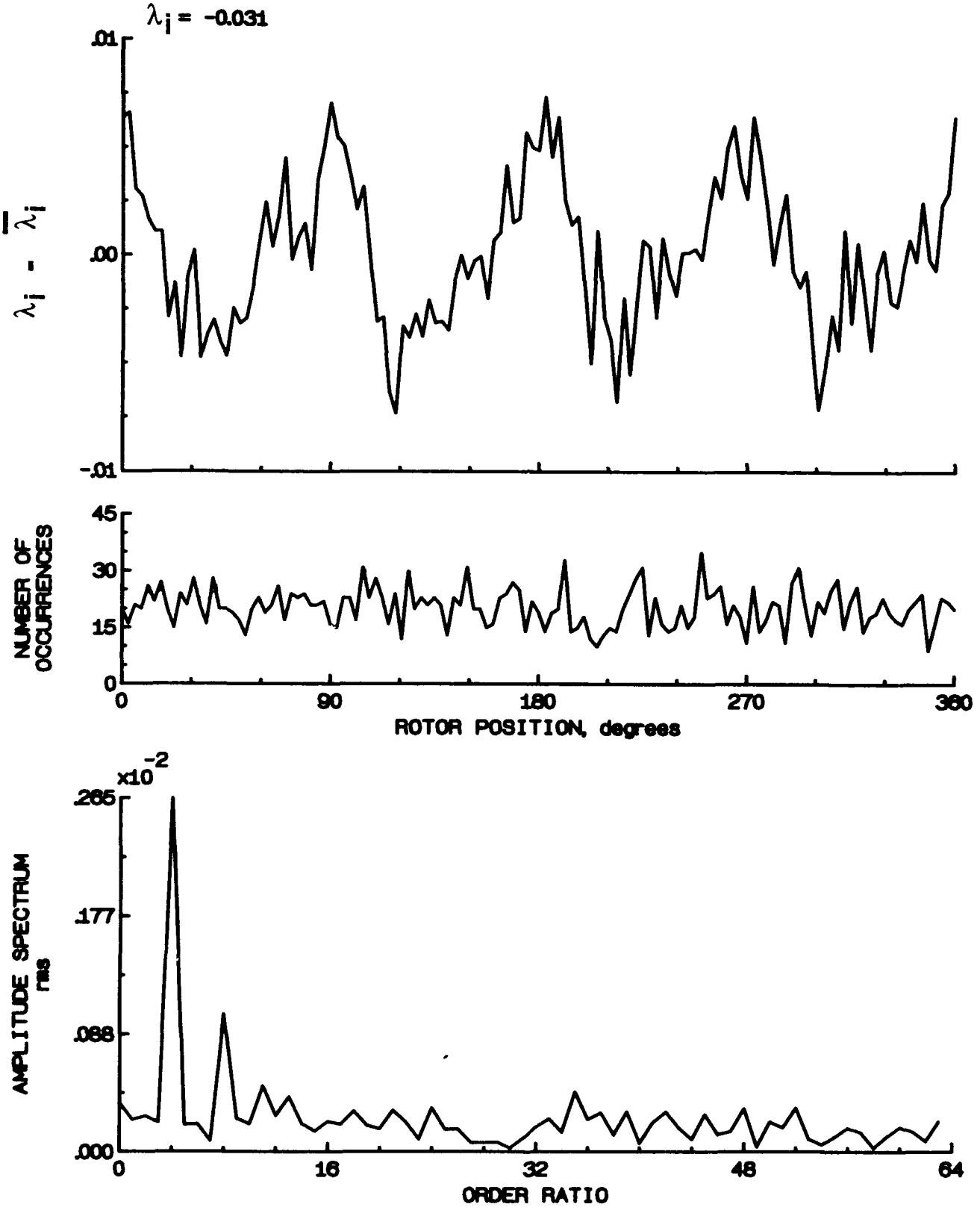

Figure 25.- Concluded.

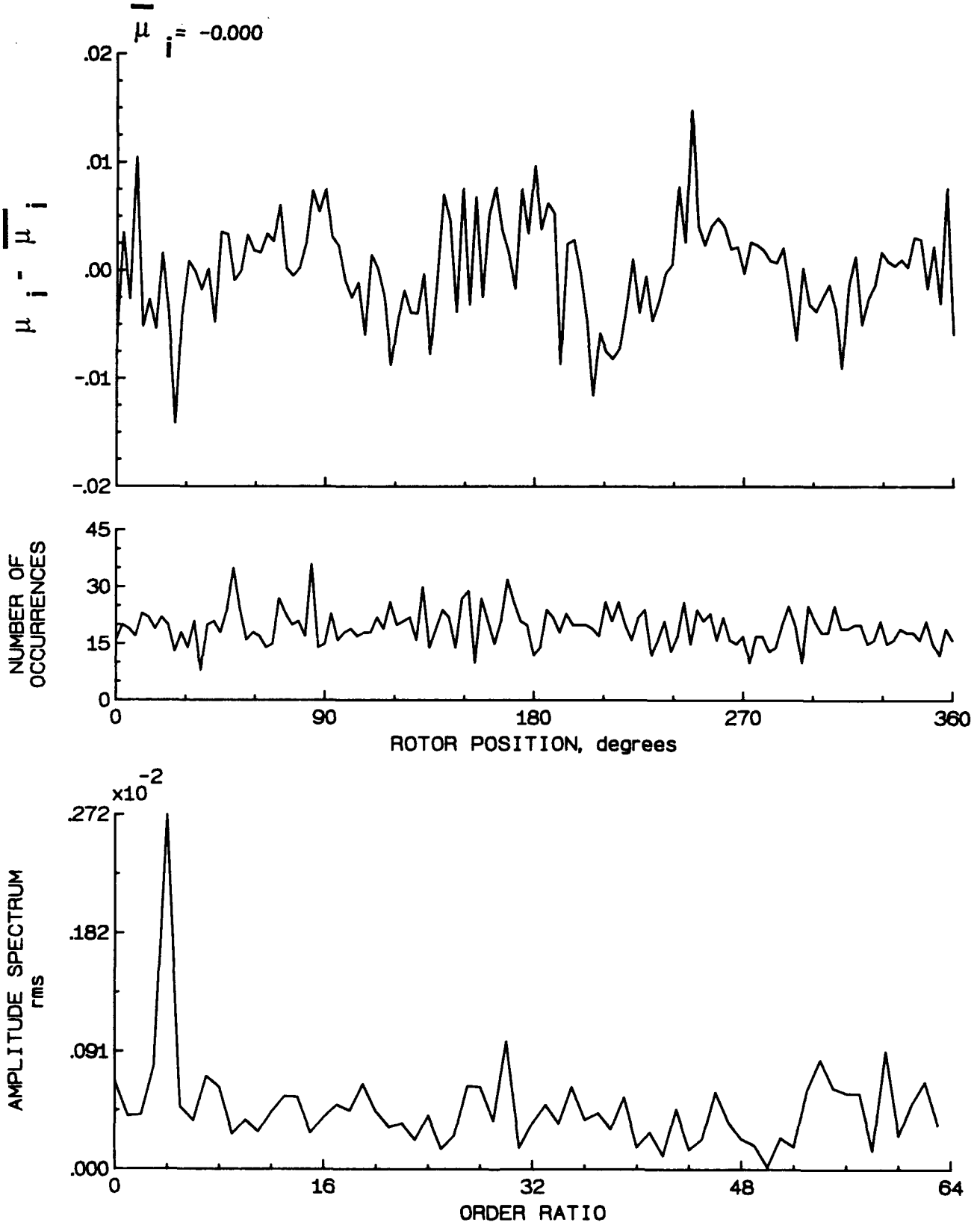

Figure 26.- Induced inflow velocity measured at 0 degrees and r/R of 1.10.

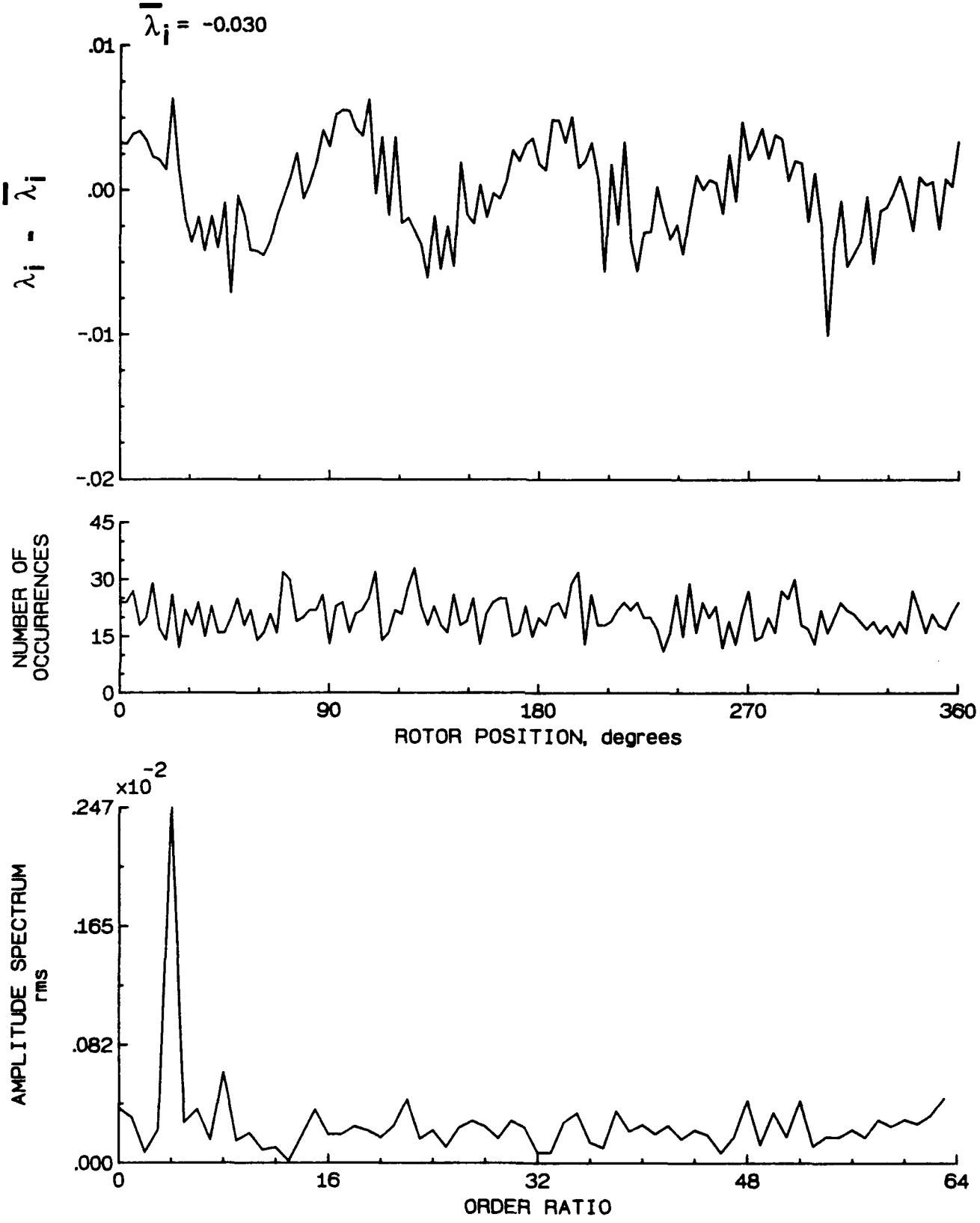

Figure 26.- Concluded.

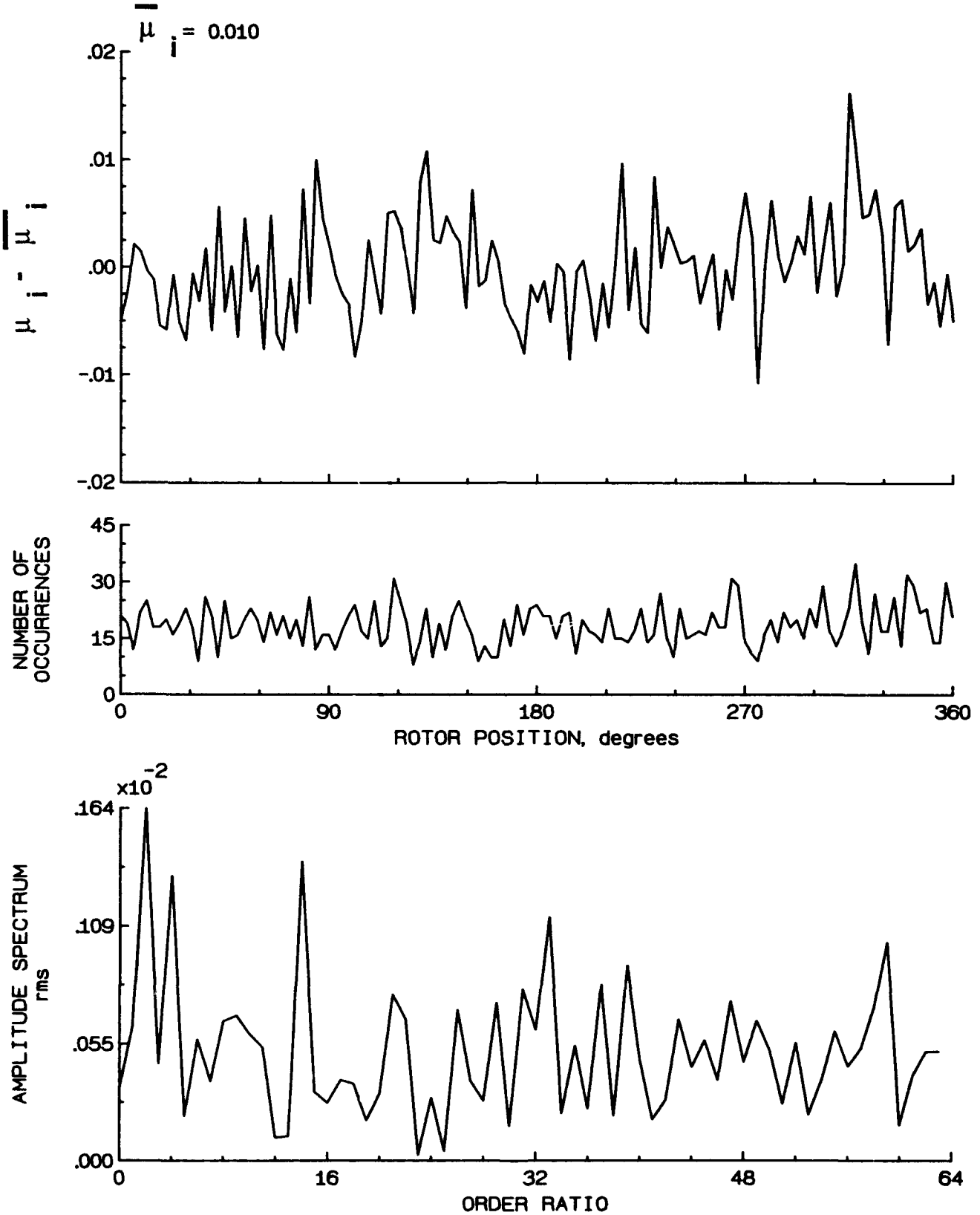

Figure 27.- Induced inflow velocity measured at 30 degrees and r/R of 0.20.

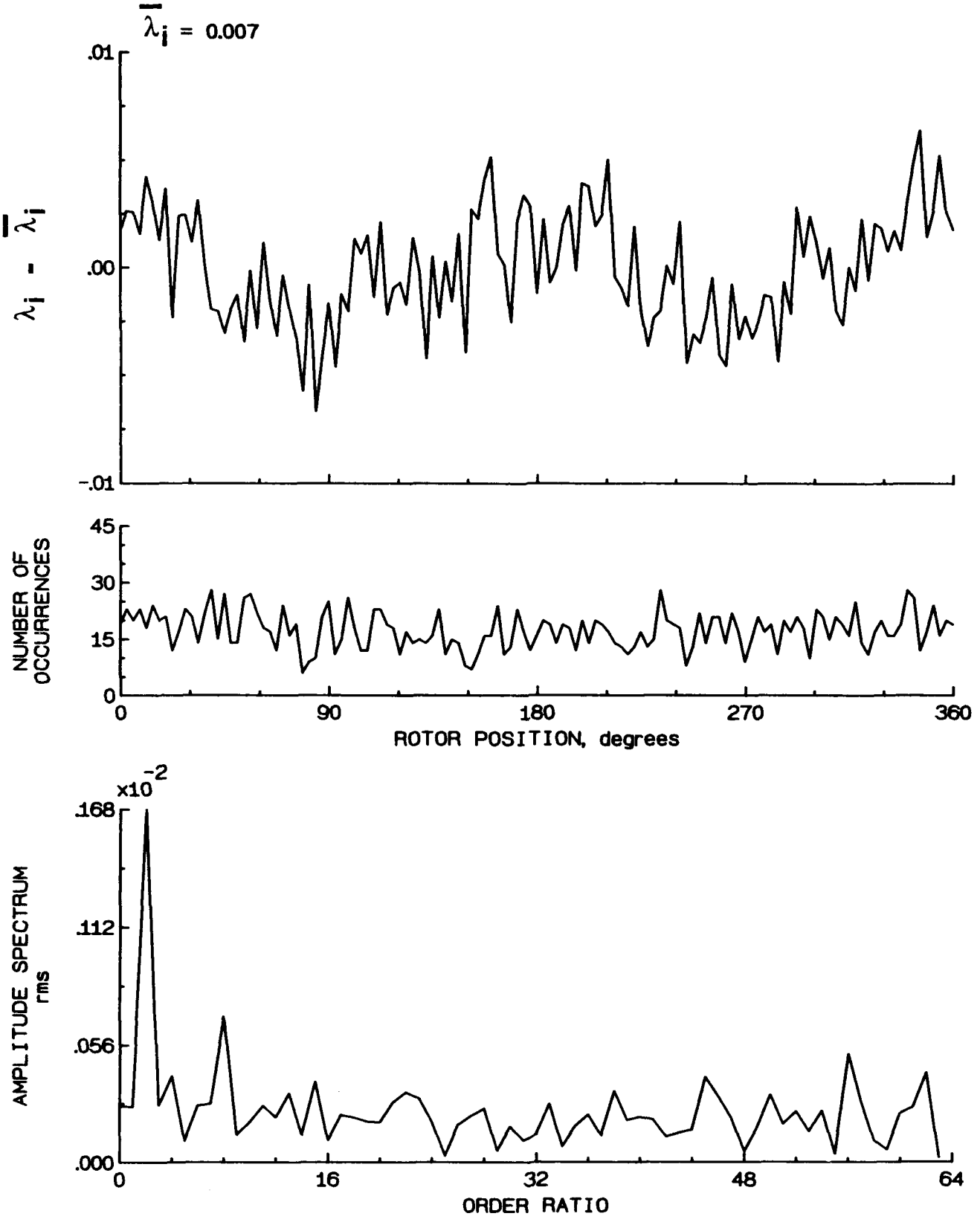

Figure 27.- Concluded.

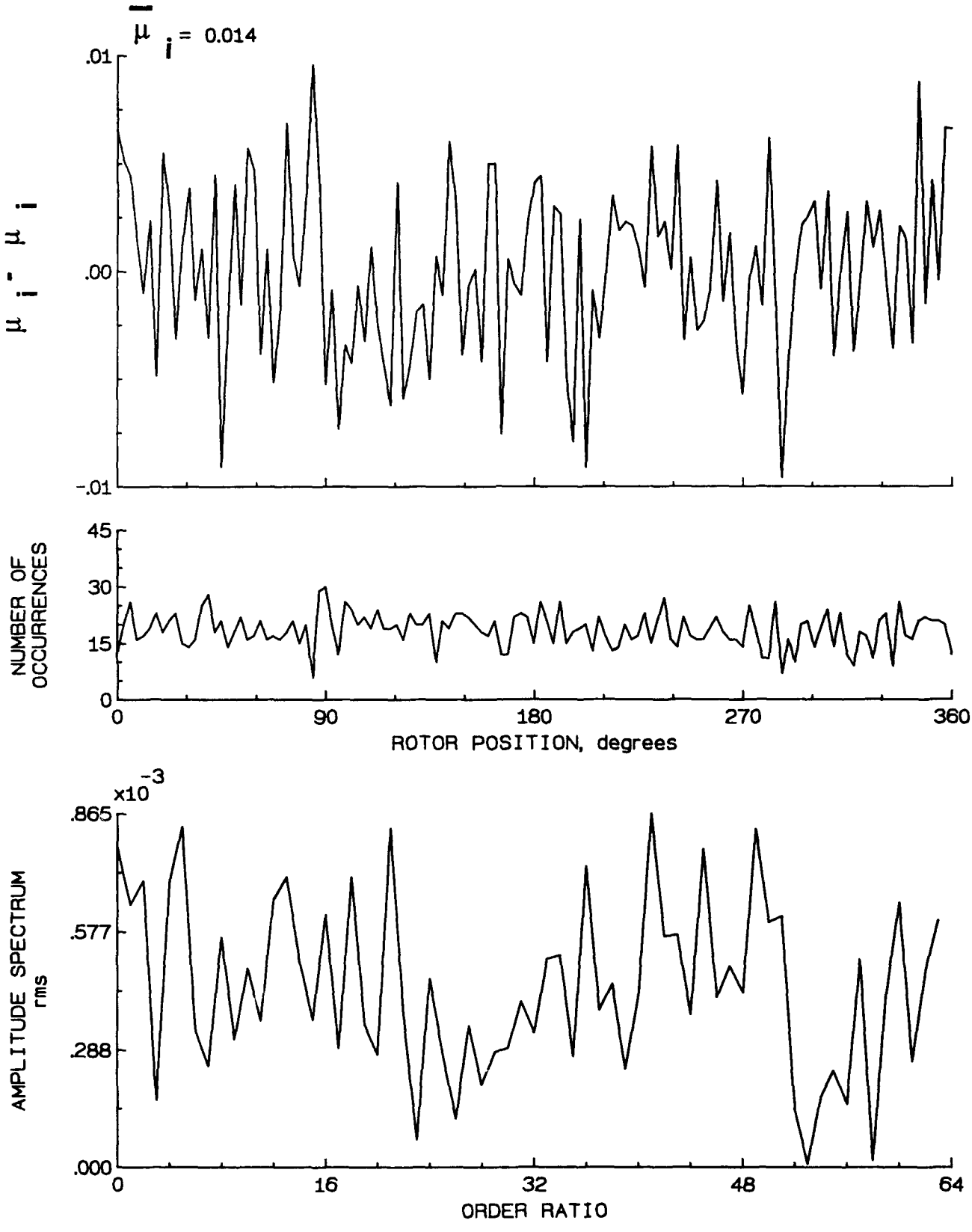

Figure 28.- Induced inflow velocity measured at 30 degrees and r/R of 0.40.

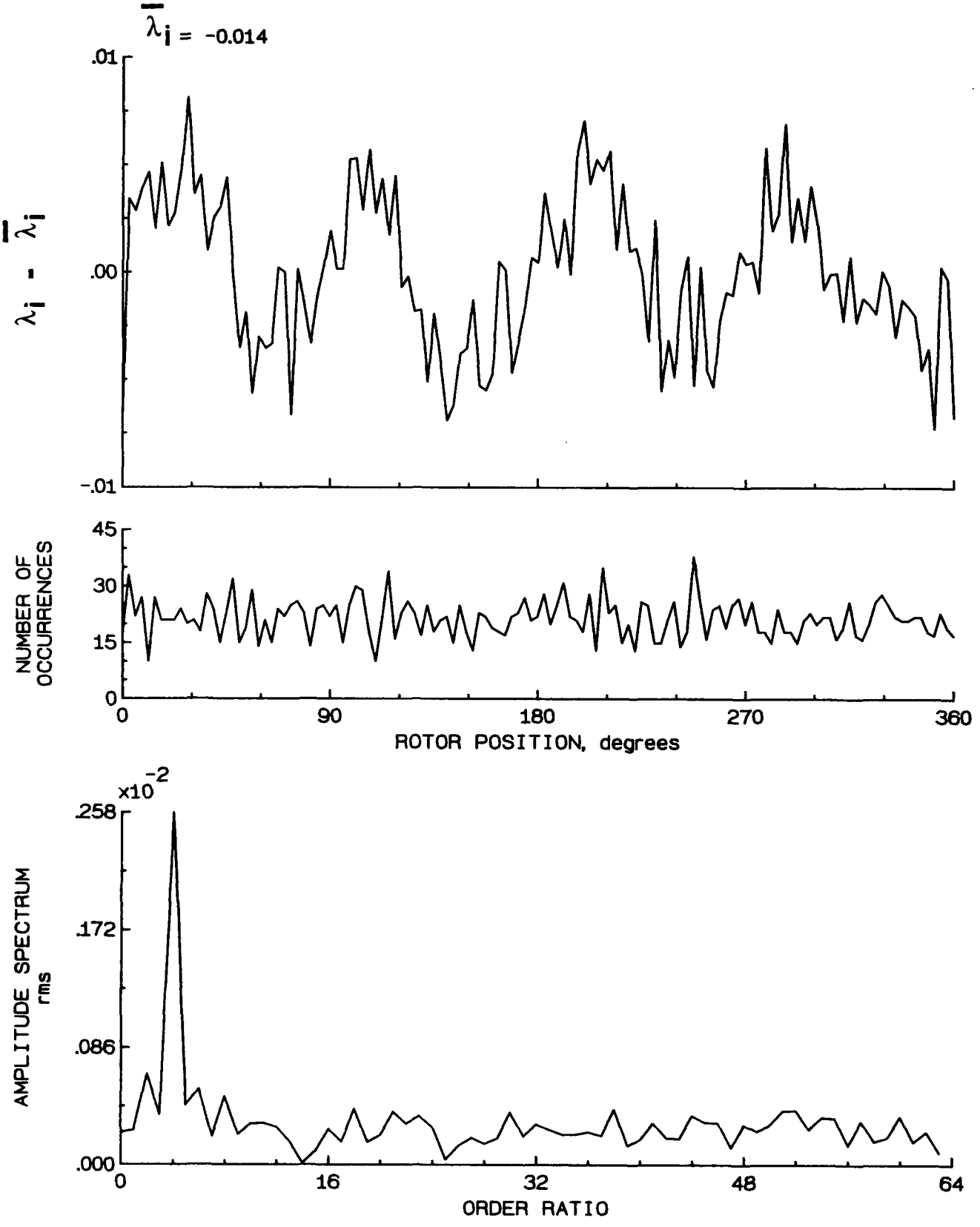

Figure 28.- Concluded.

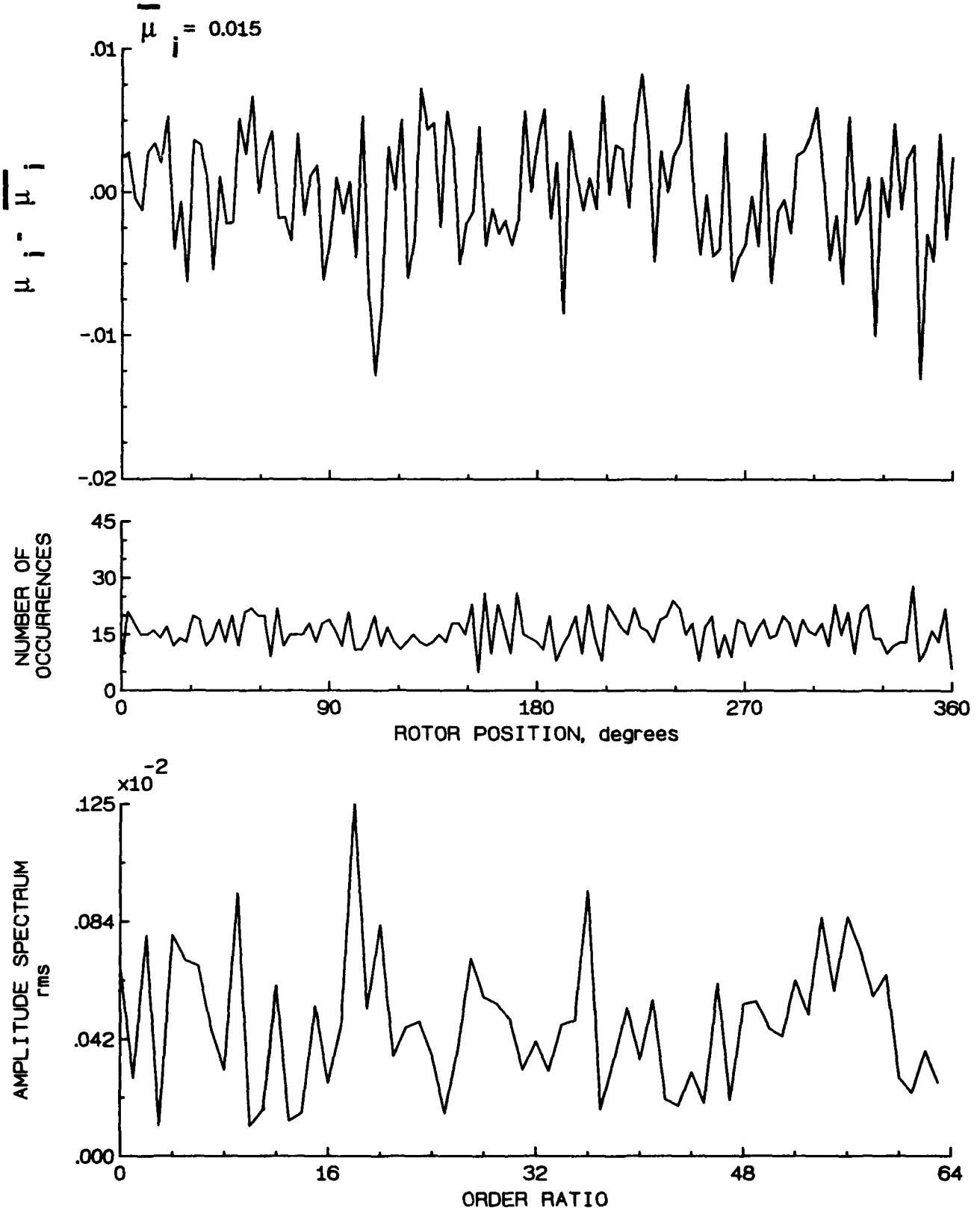

Figure 29.- Induced inflow velocity measured at 30 degrees and r/R of 0.50.

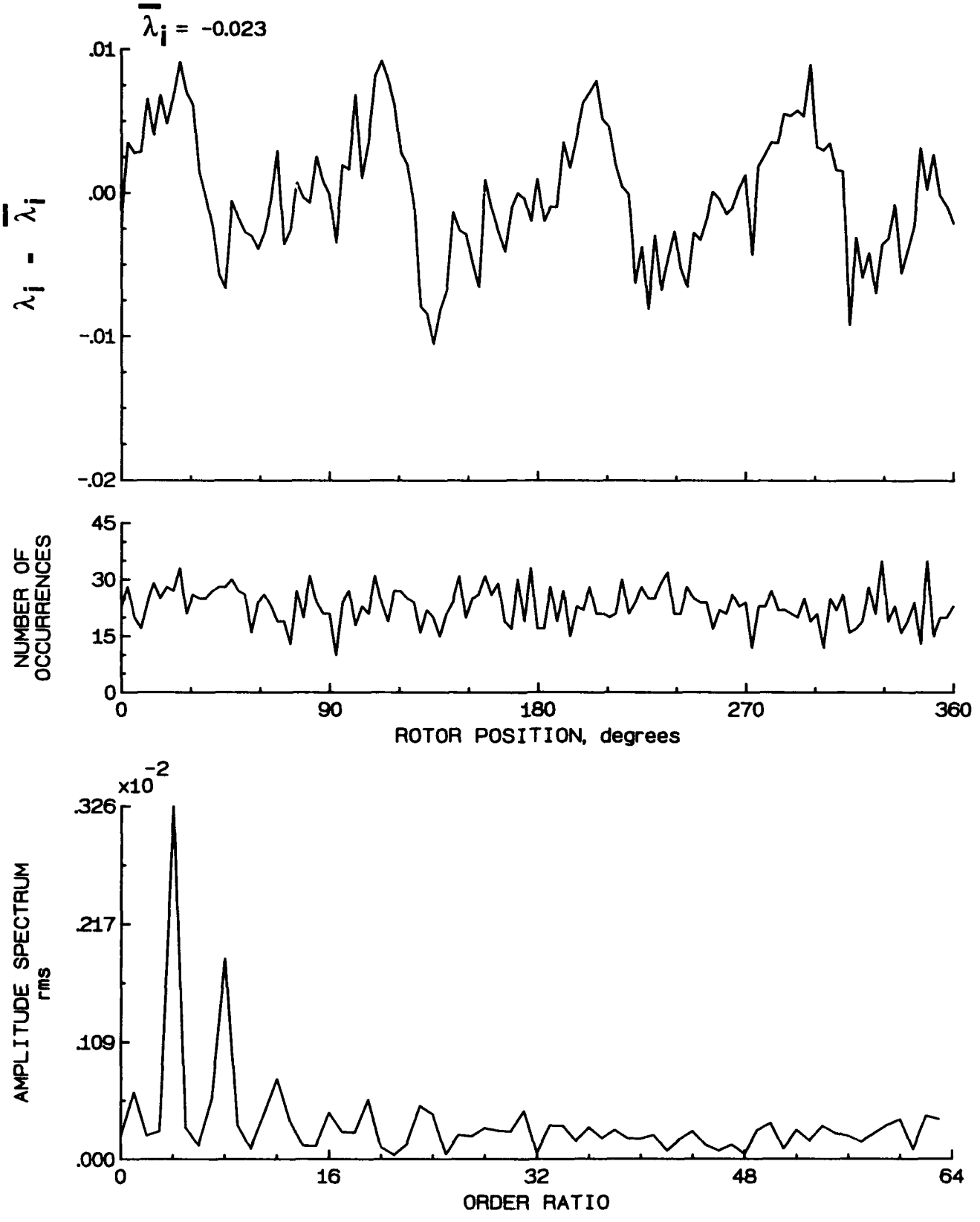

Figure 29.- Concluded.

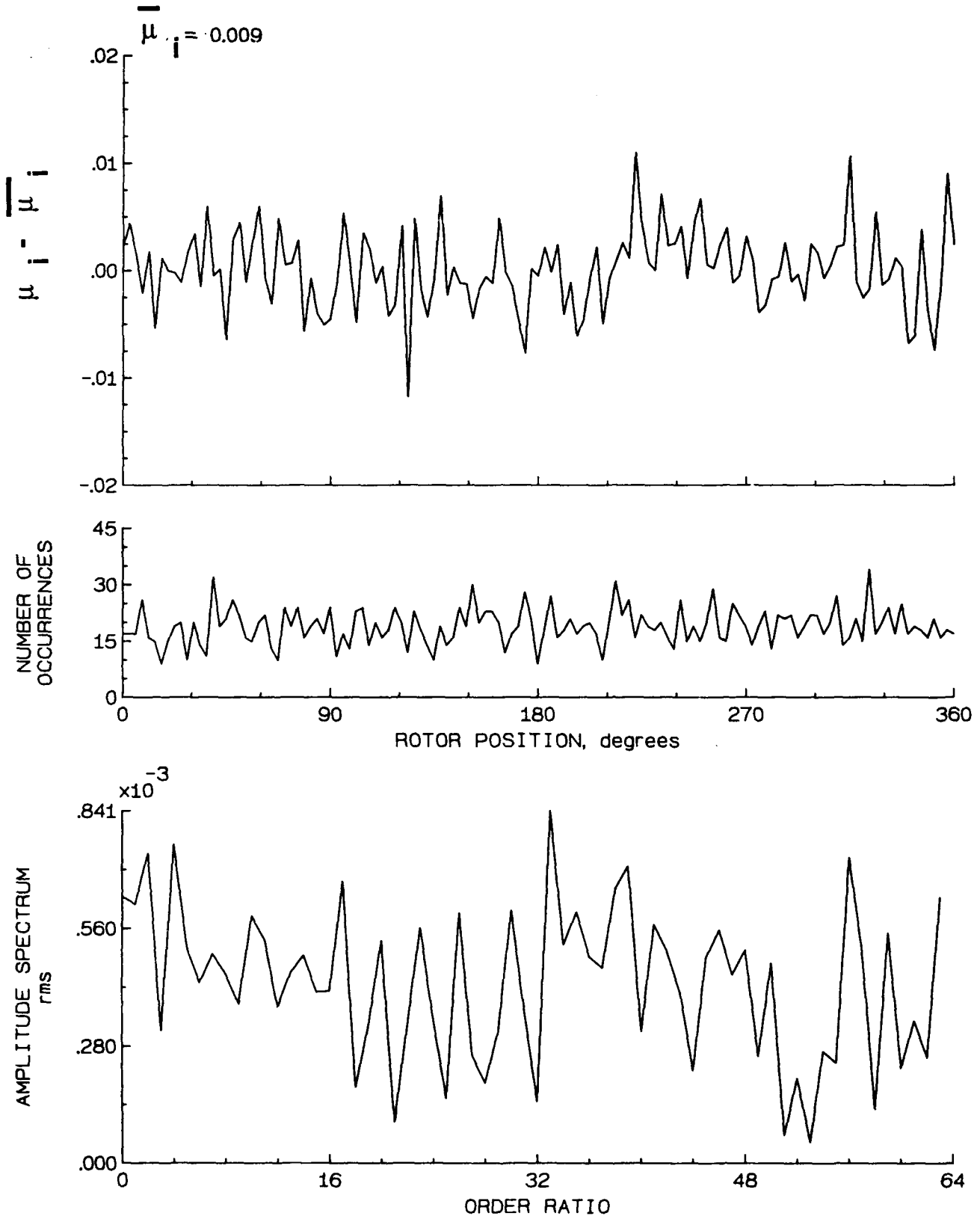

Figure 30.- Induced inflow velocity measured at 30 degrees and r/R of 0.60.

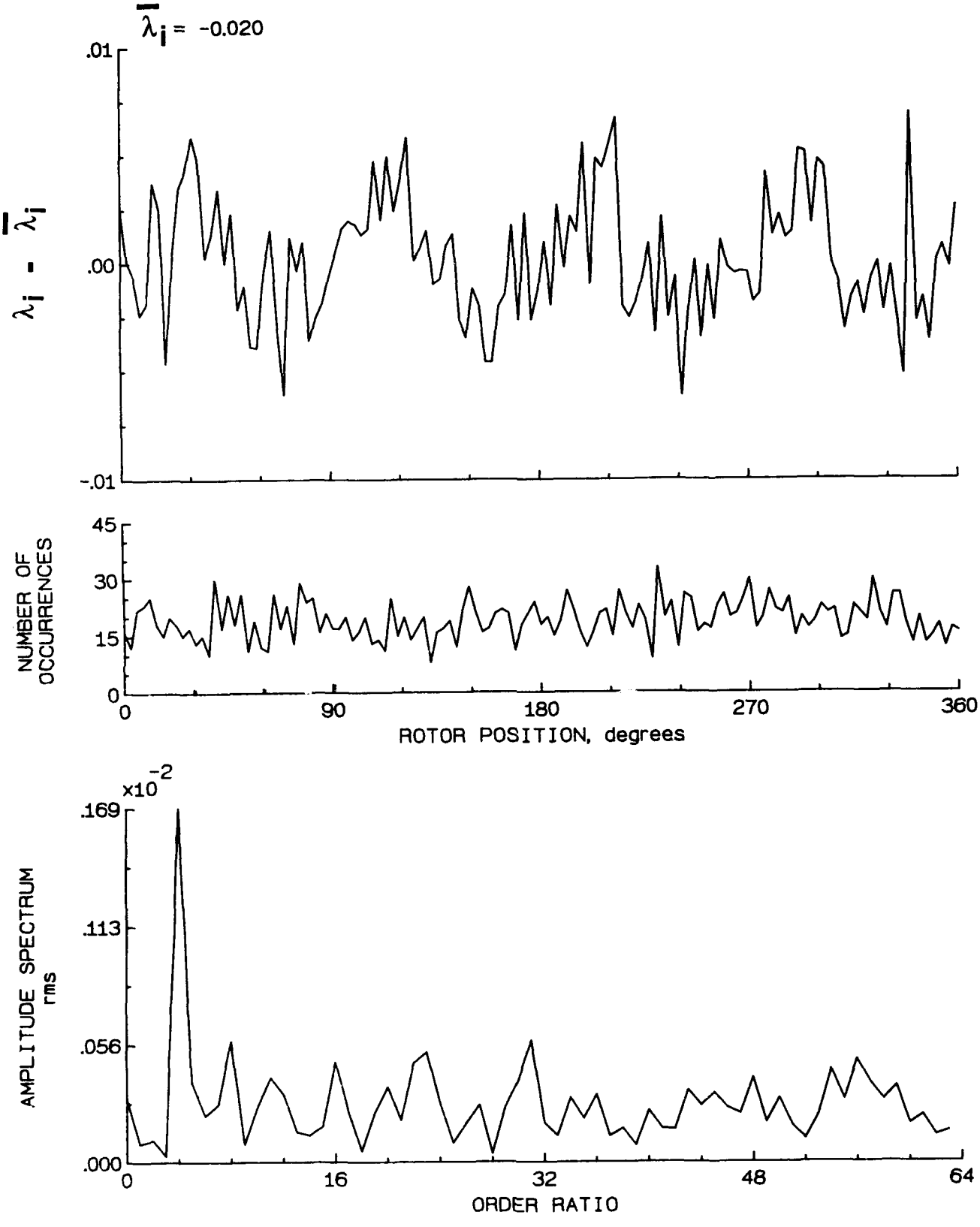

Figure 30.- Concluded.

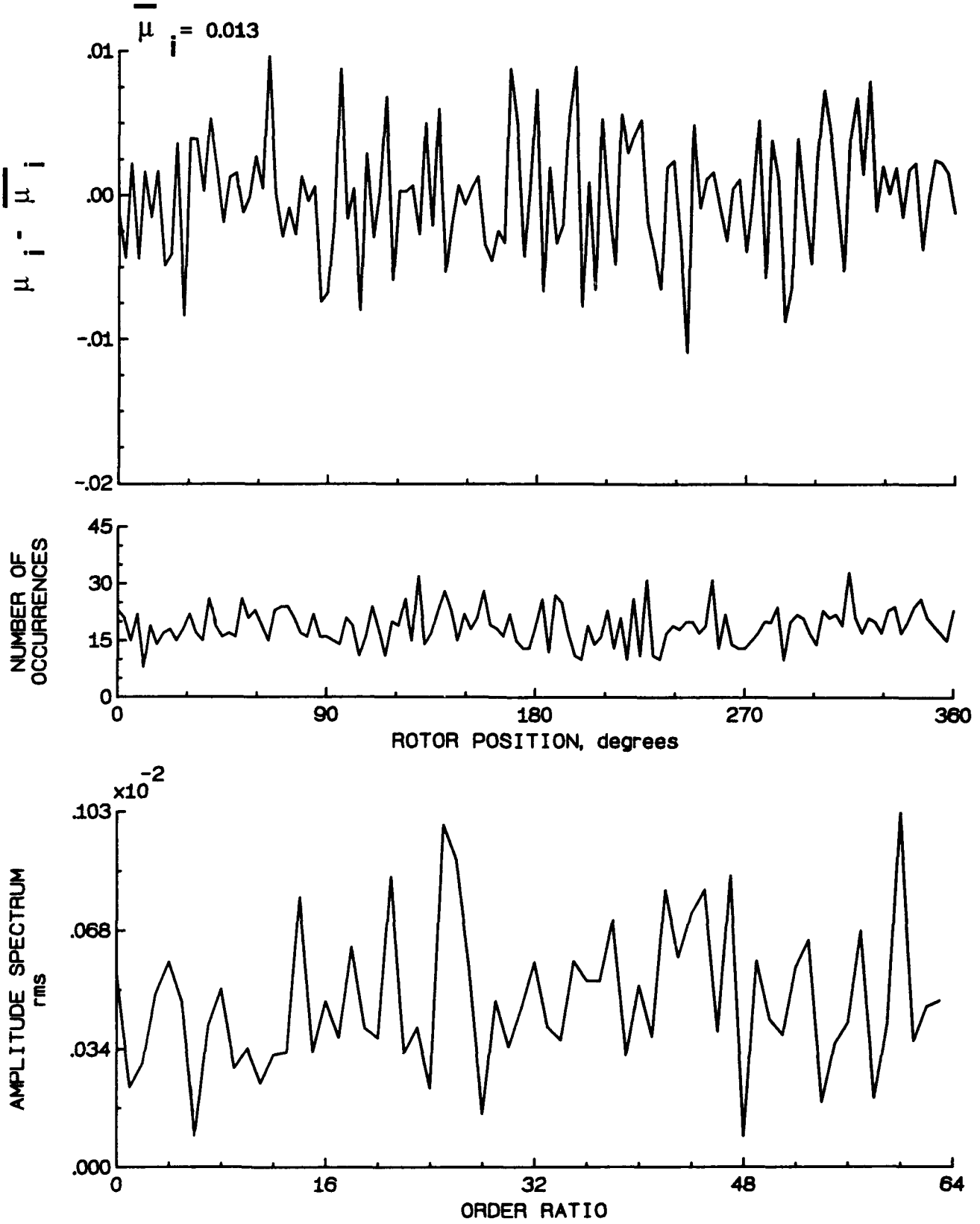

Figure 31.- Induced inflow velocity measured at 30 degrees and r/R of 0.70.

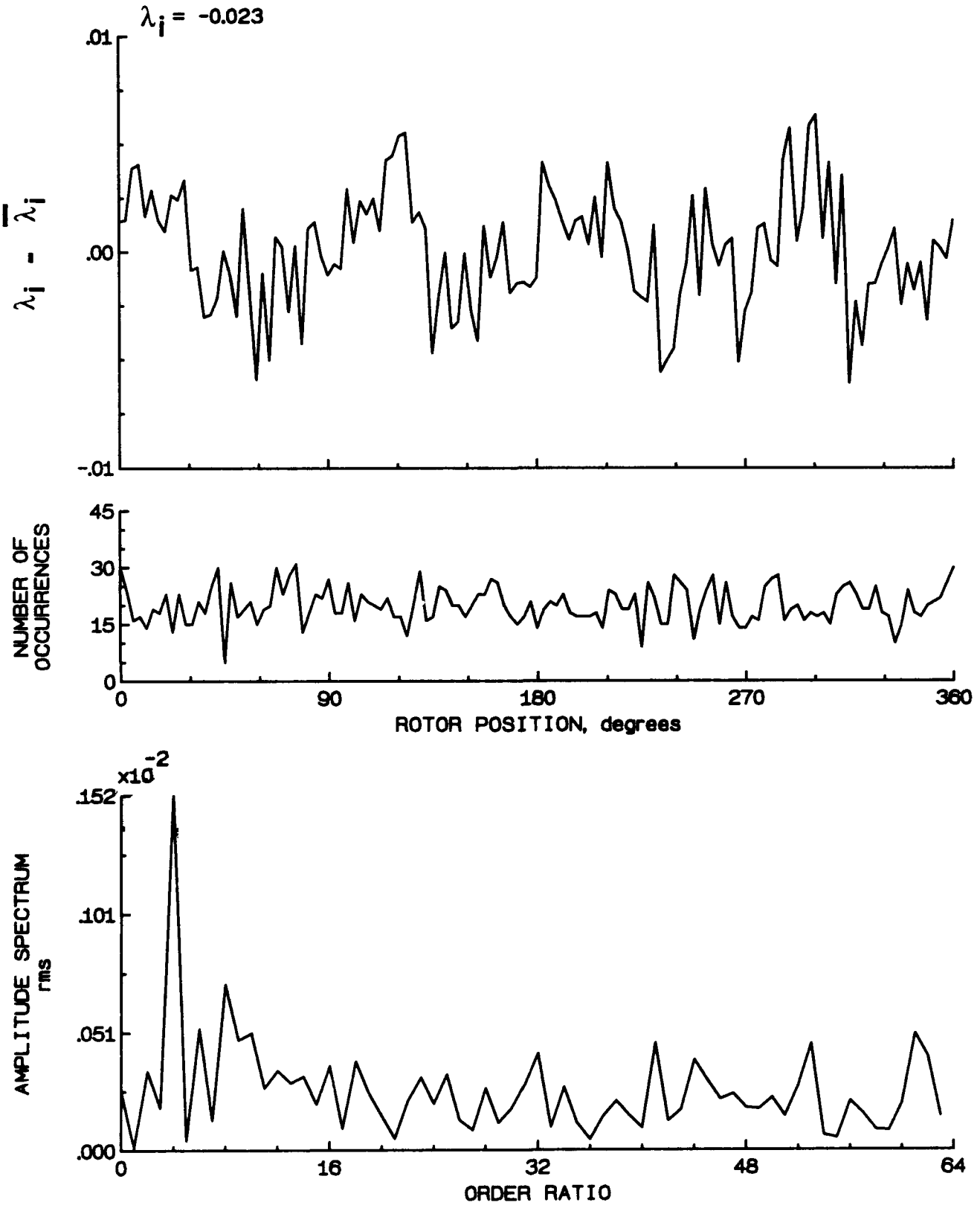

Figure 31.- Concluded.

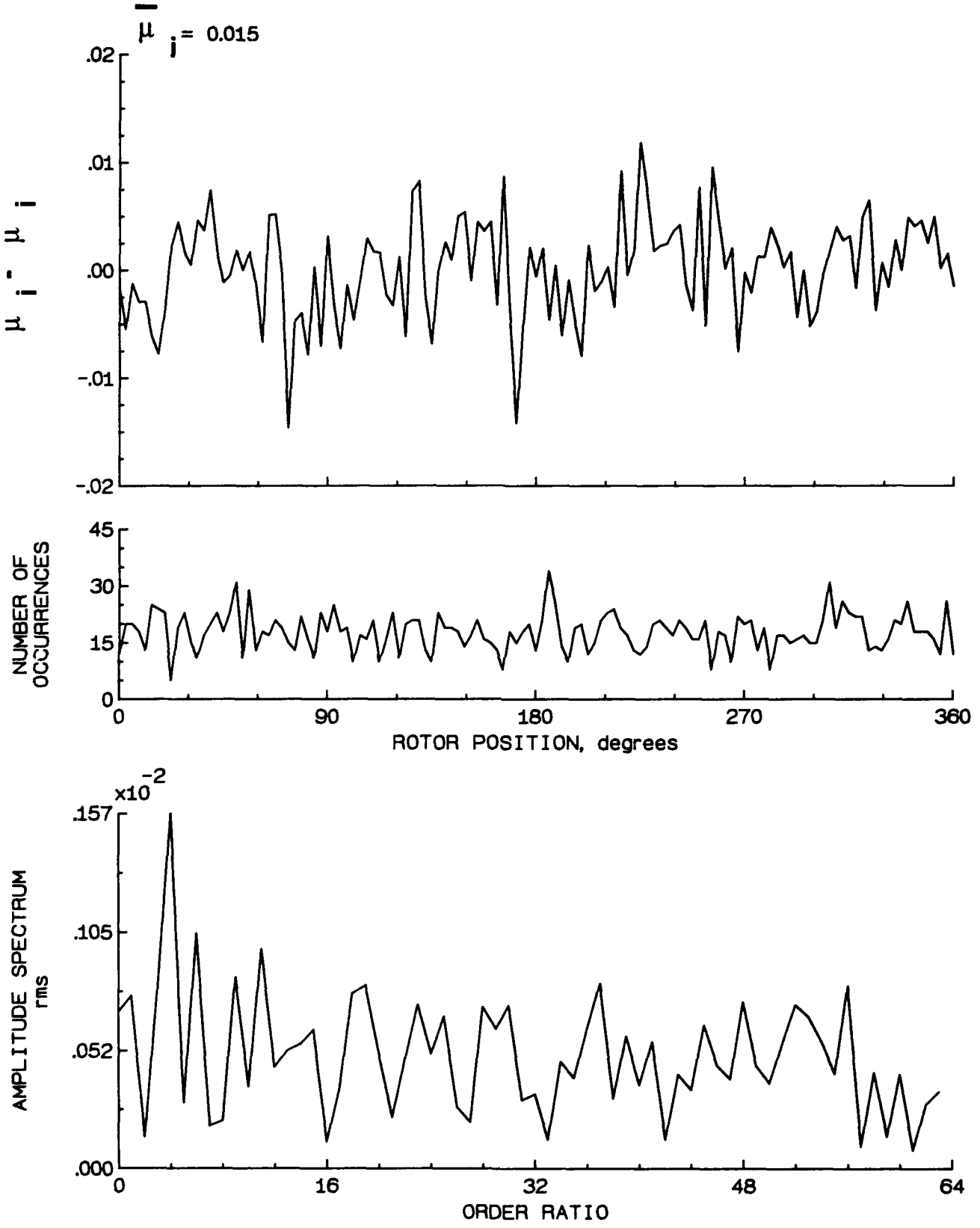

Figure 32.- Induced inflow velocity measured at 30 degrees and r/R of 0.74.

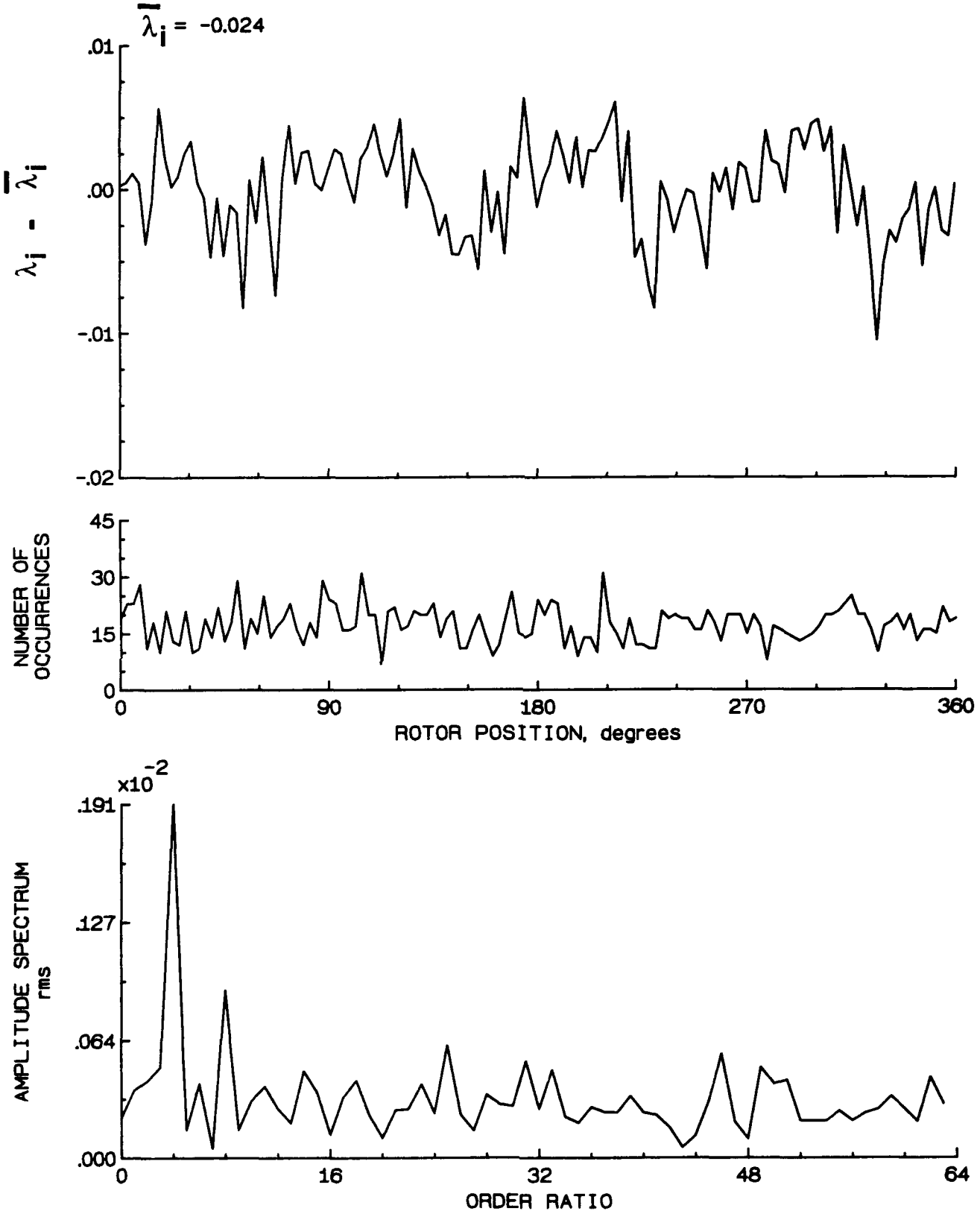

Figure 32.- Concluded.

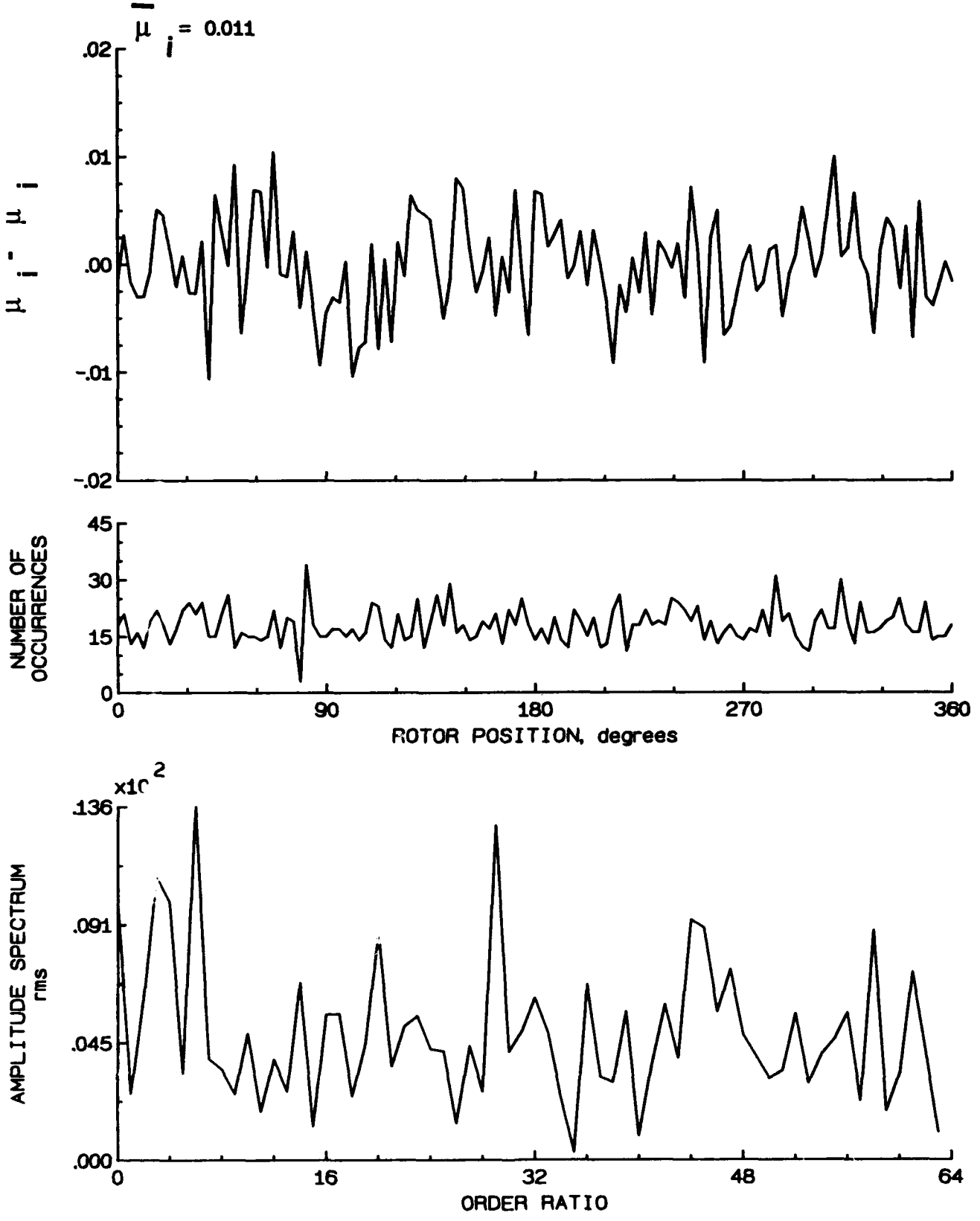

Figure 33.- Induced inflow velocity measured at 30 degrees and r/R of 0.78.

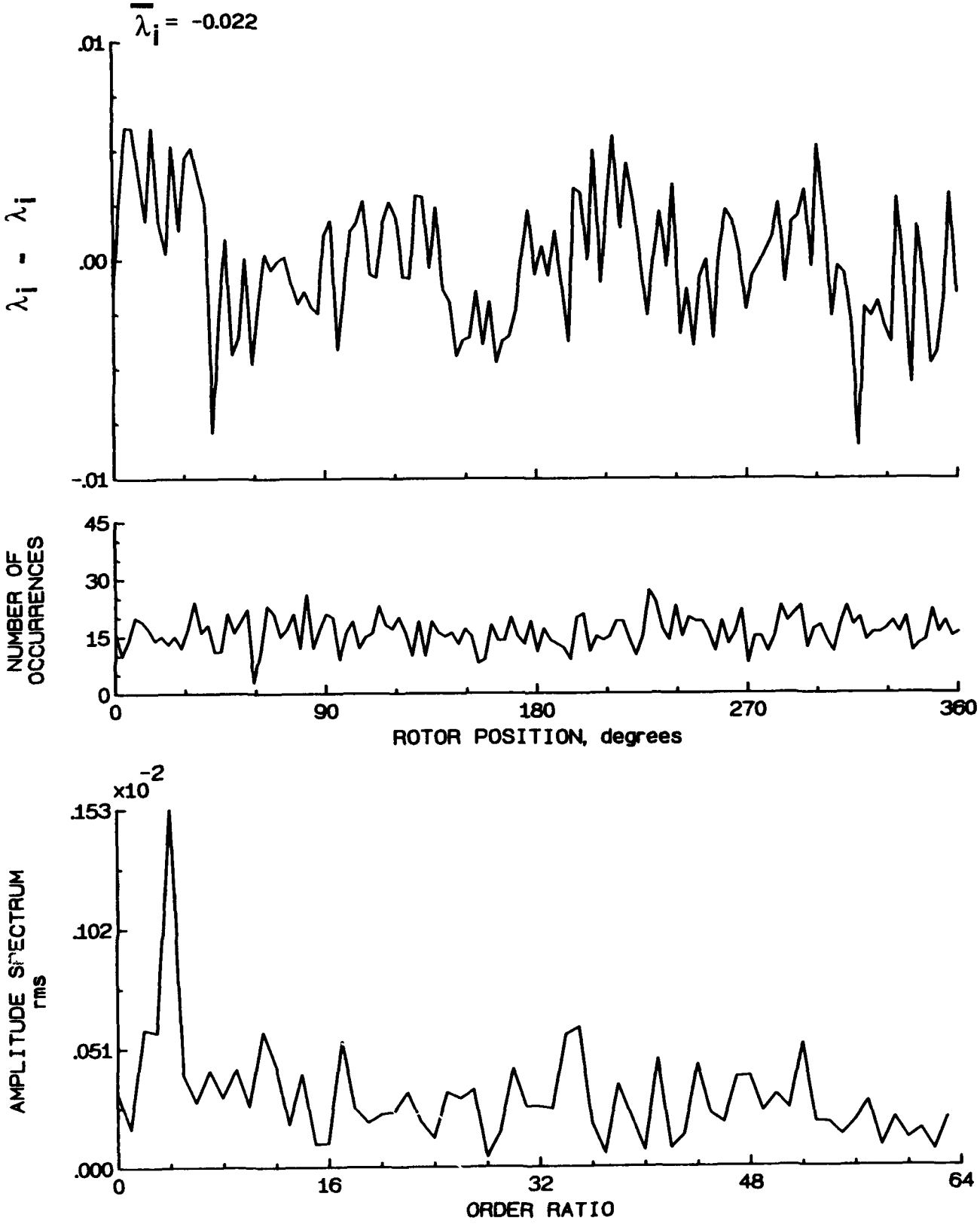

Figure 33.- Concluded.

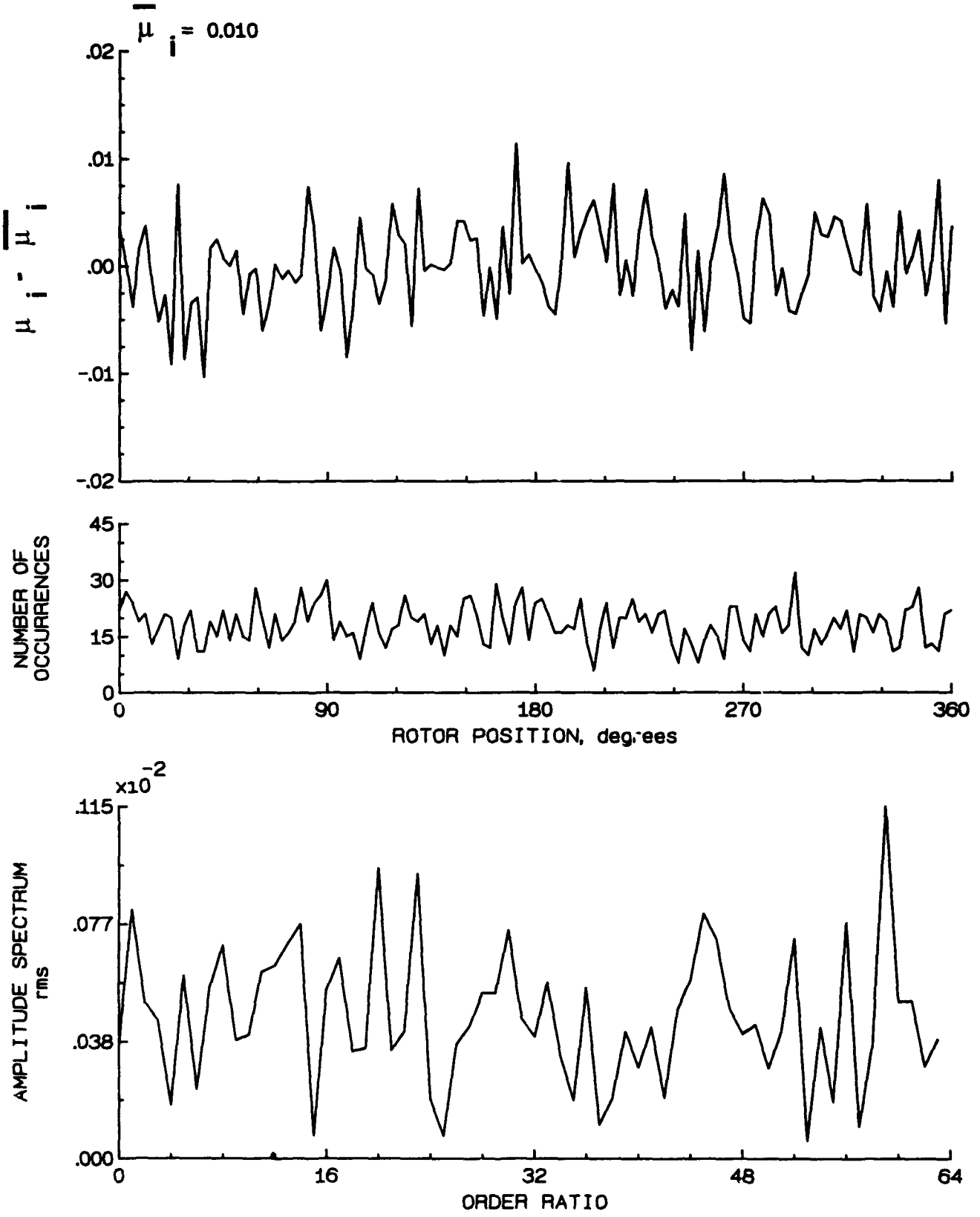

Figure 34.- Induced inflow velocity measured at 30 degrees and r/R of 0.82.

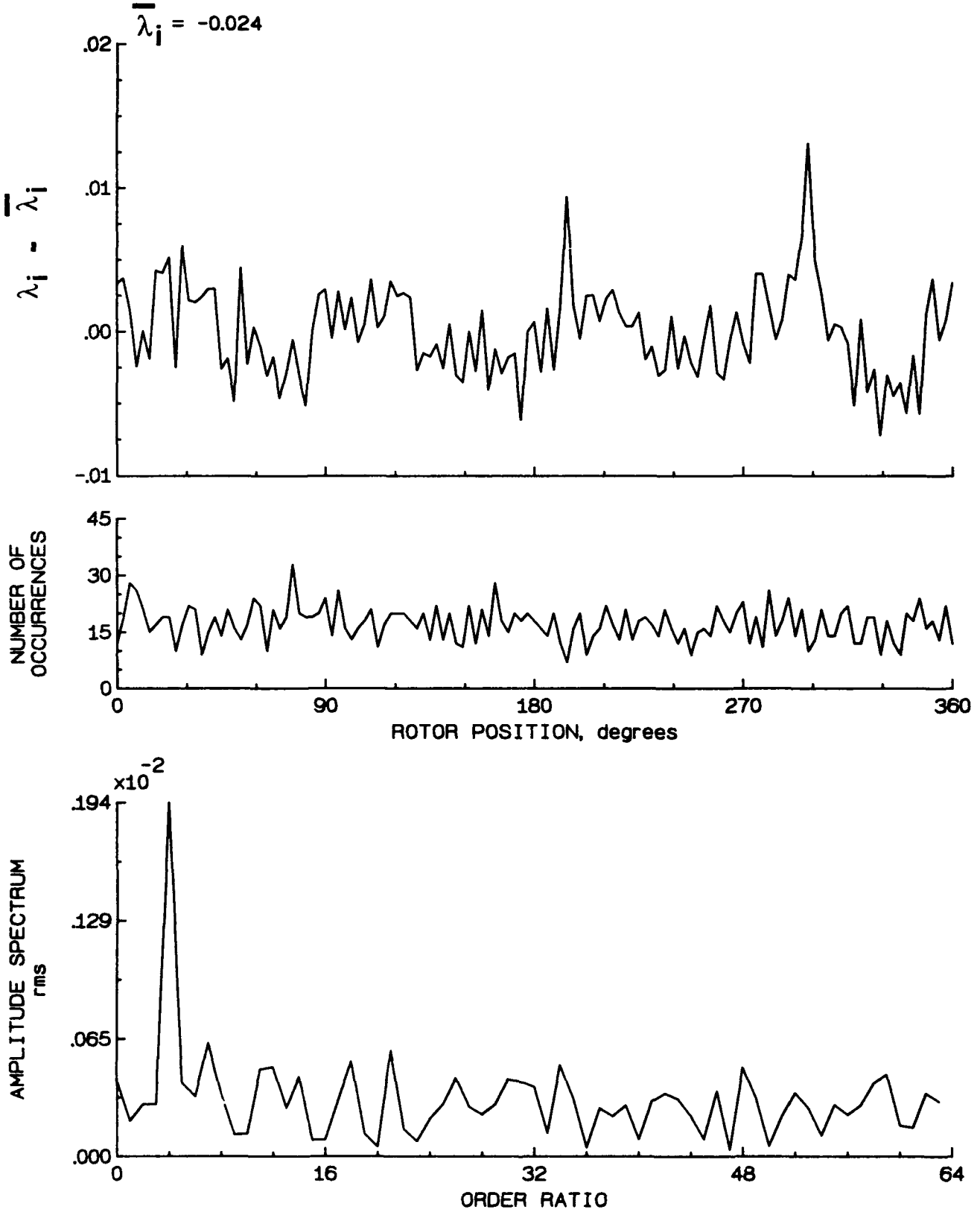

Figure 34.- Concluded.

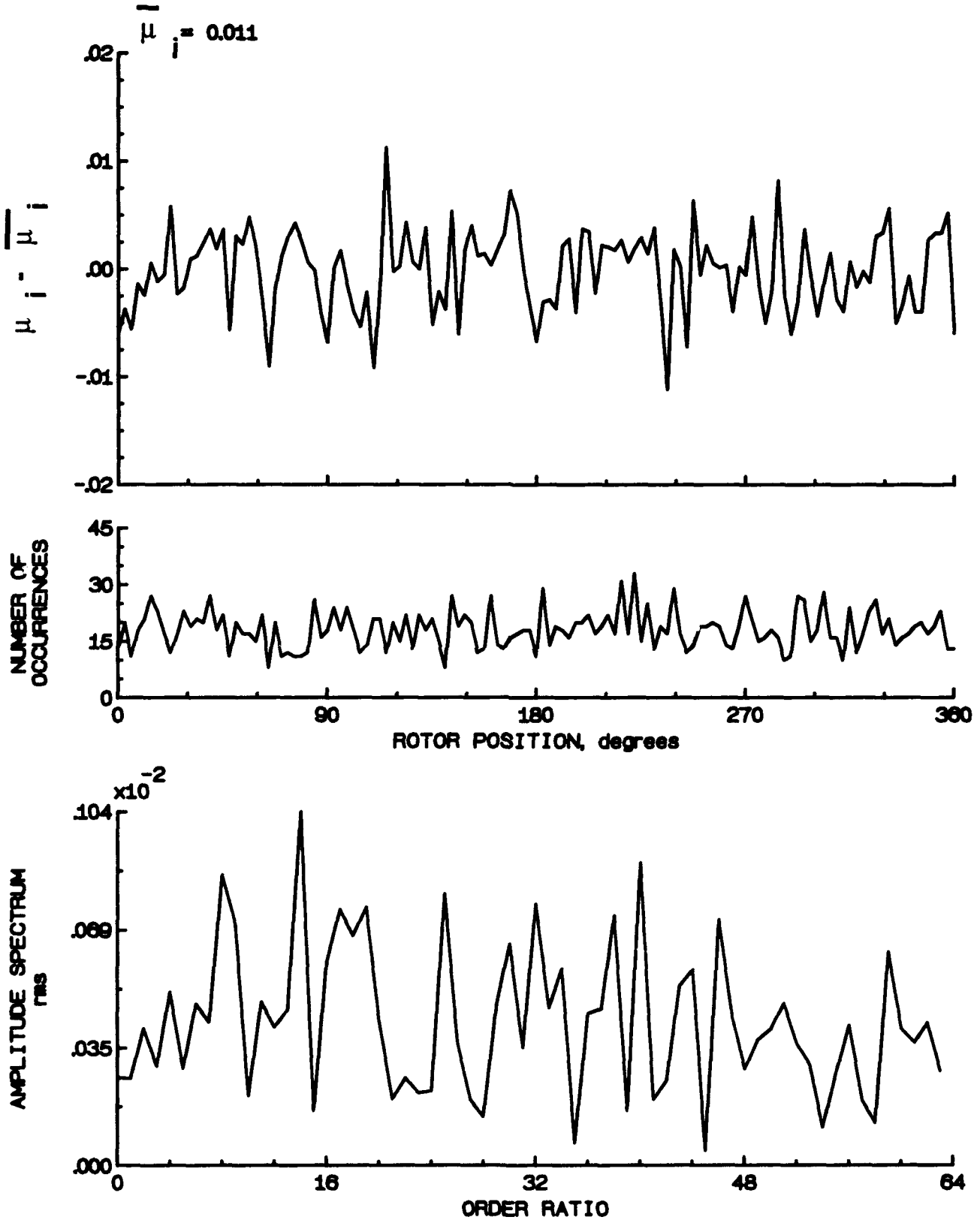

Figure 35.- Induced inflow velocity measured at 30 degrees and r/R of 0.86.

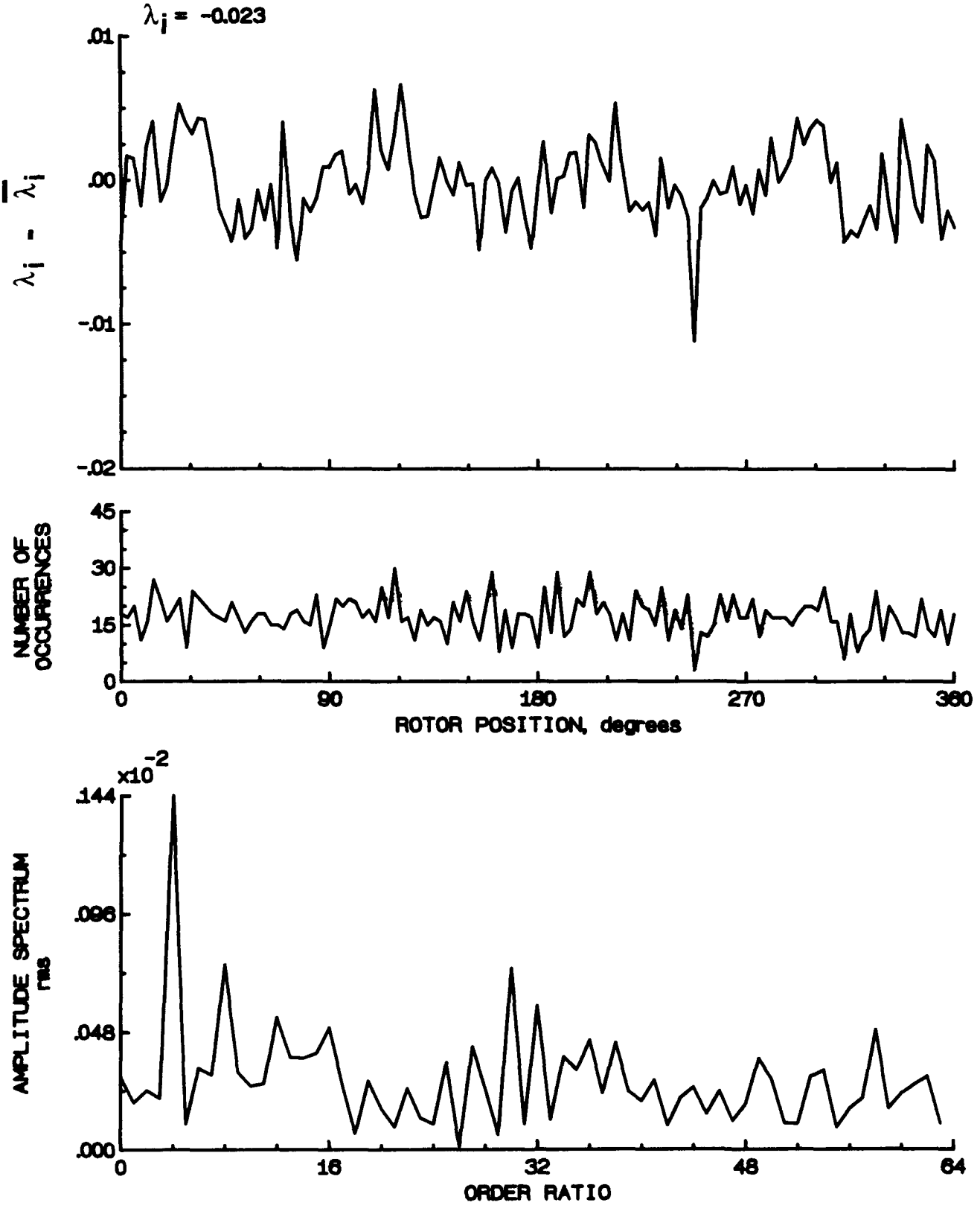

Figure 35.- Concluded.

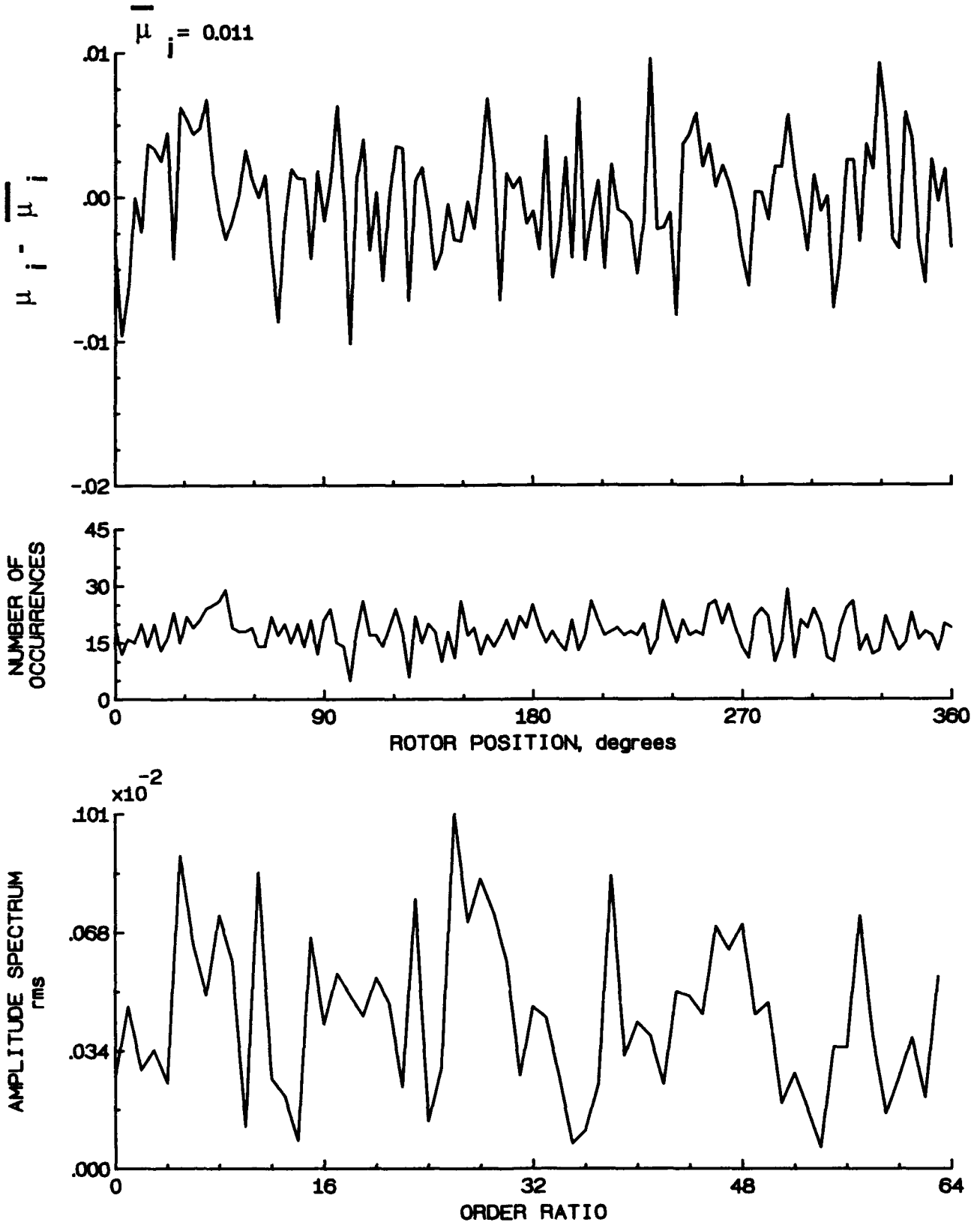

Figure 36.- Induced inflow velocity measured at 30 degrees and r/R of 0.90.

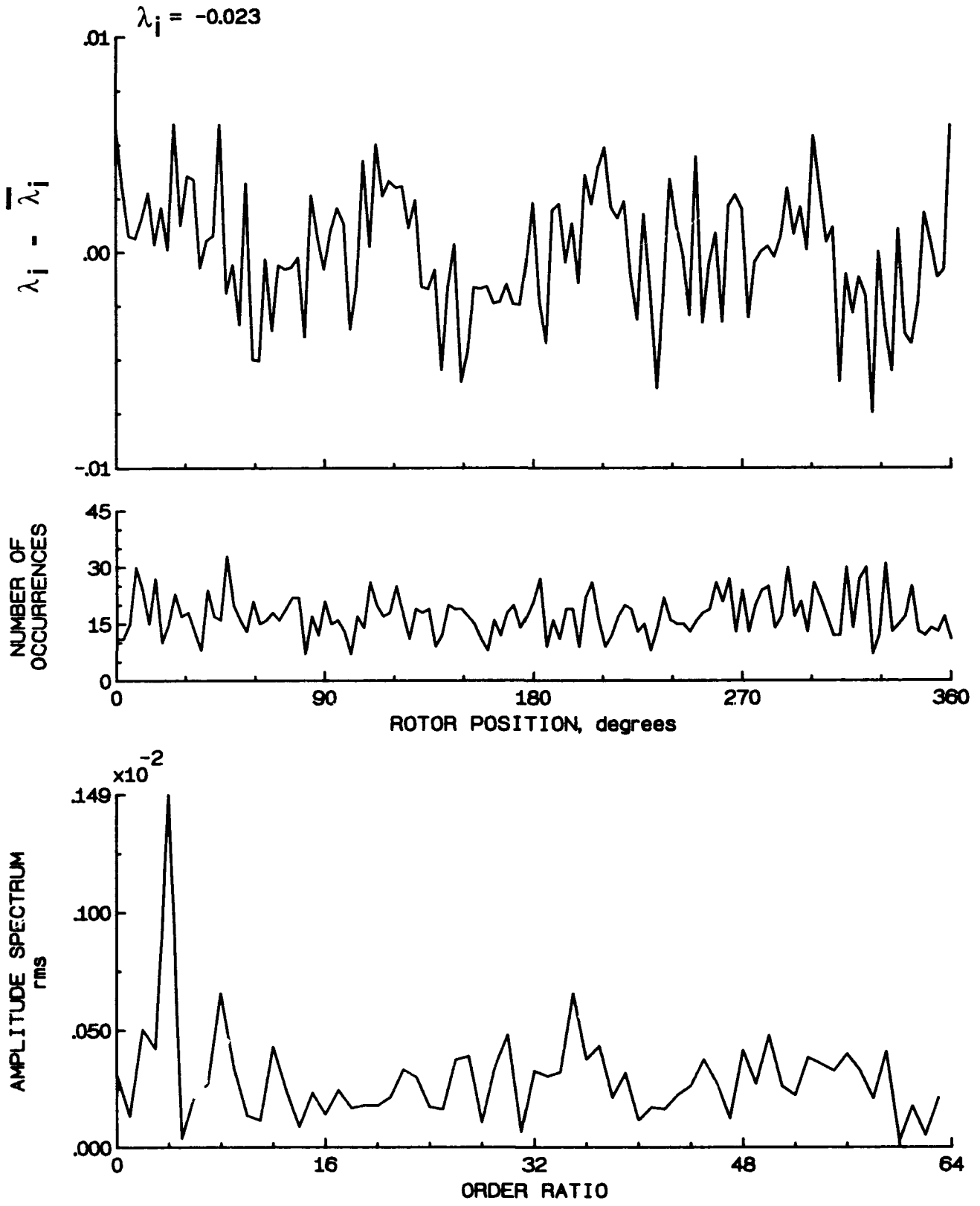

Figure 36.- Concluded.

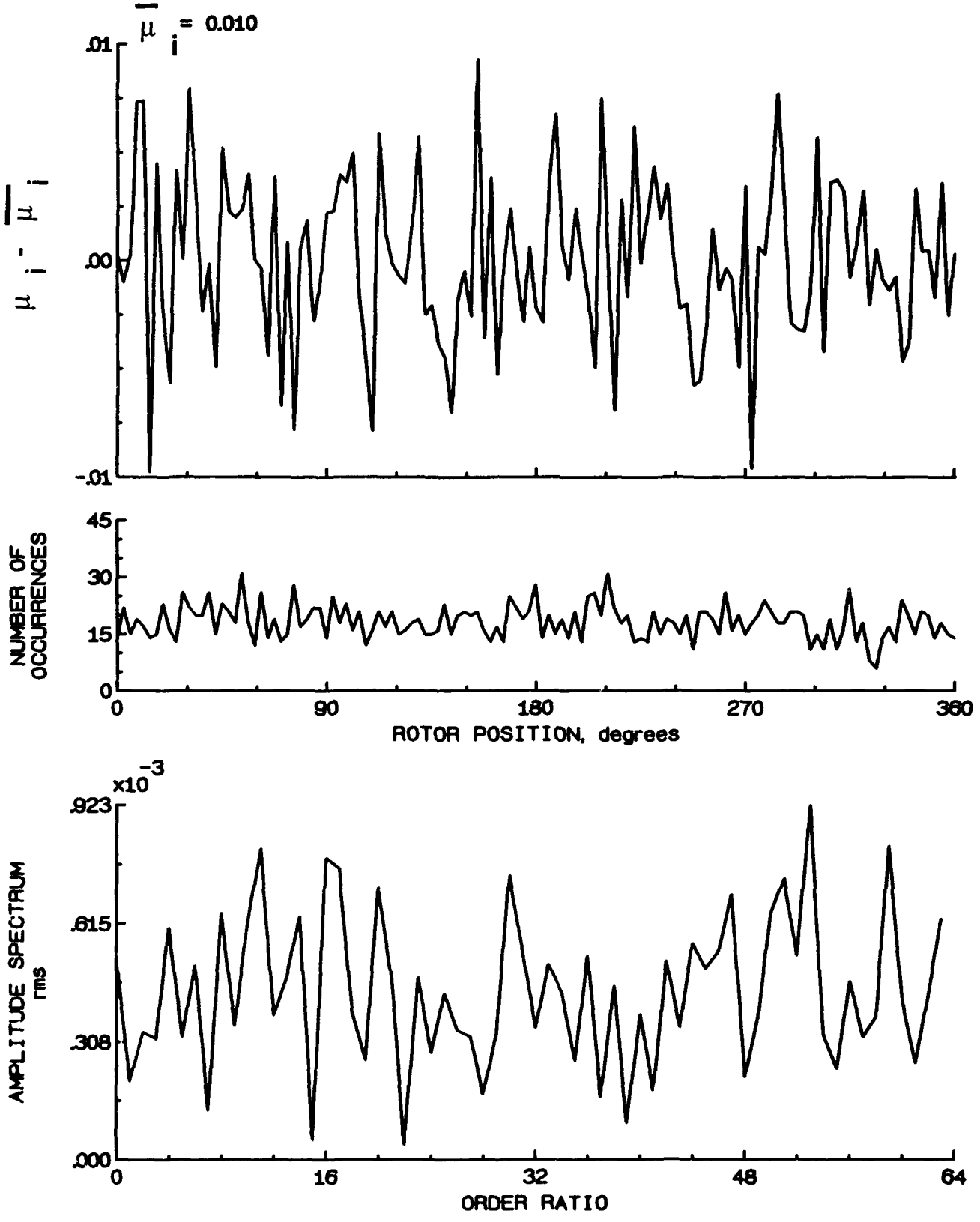

Figure 37.- Induced inflow velocity measured at 30 degrees and r/R of 0.94.

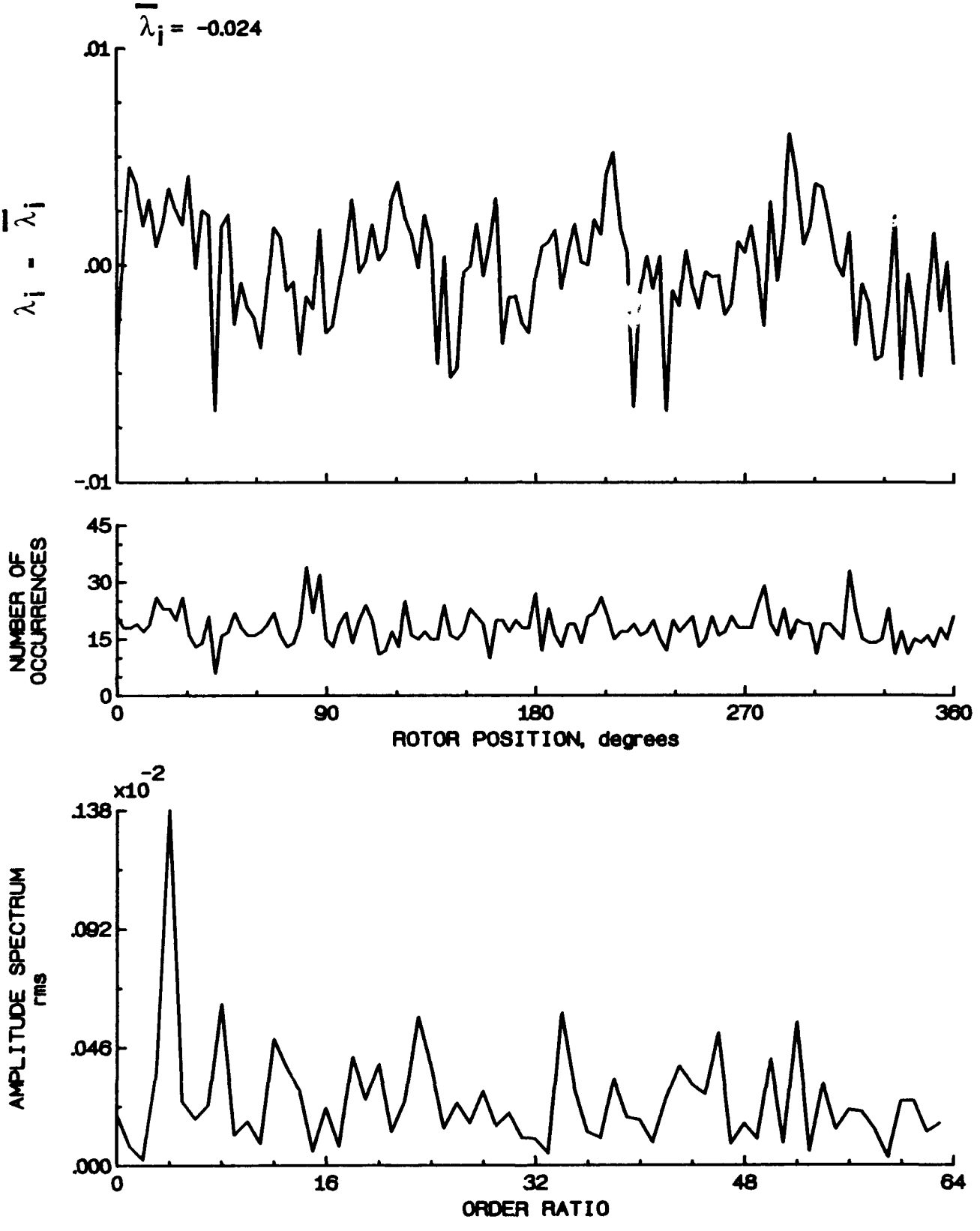

Figure 37.- Concluded.

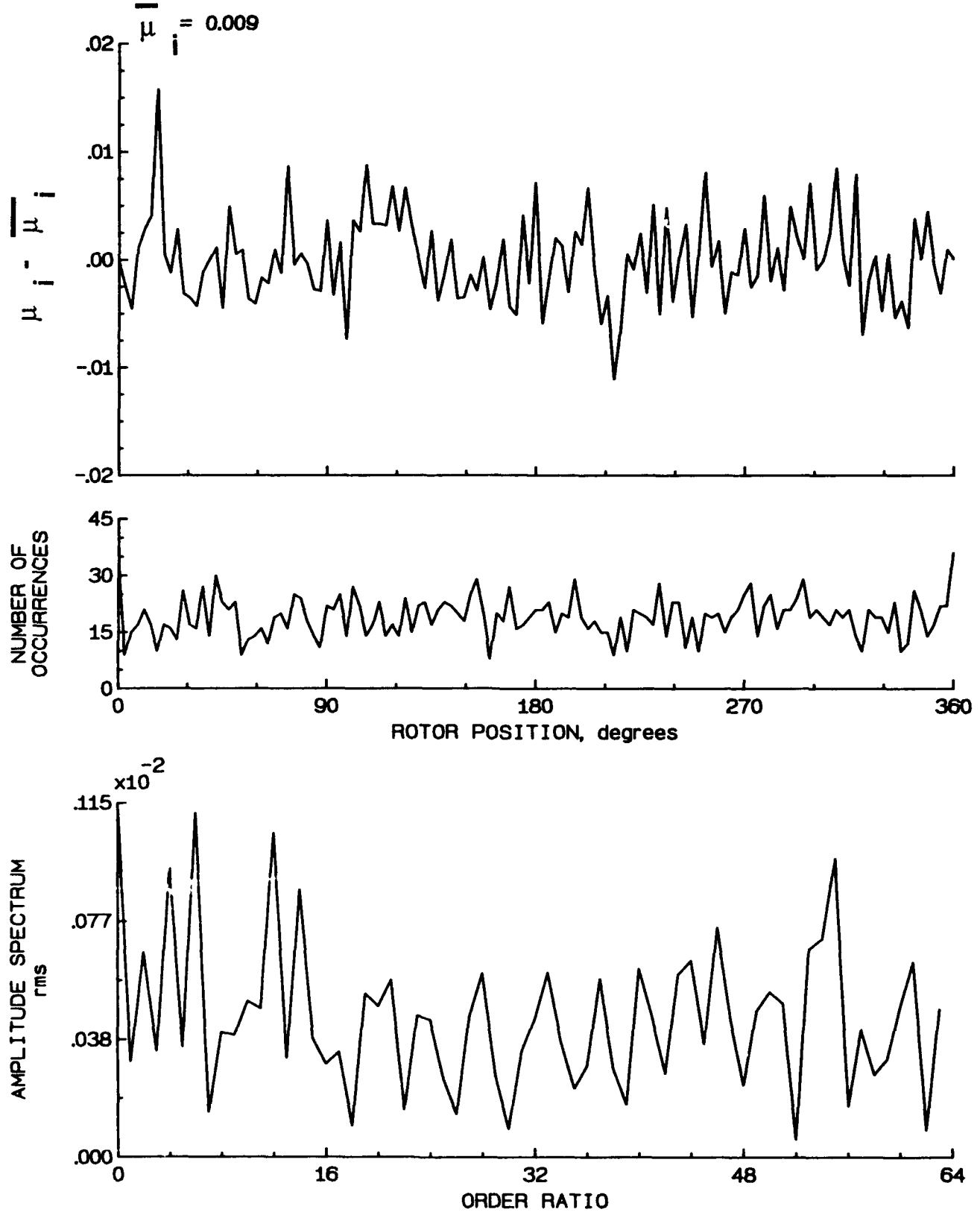

Figure 38.- Induced inflow velocity measured at 30 degrees and r/R of 0.98.

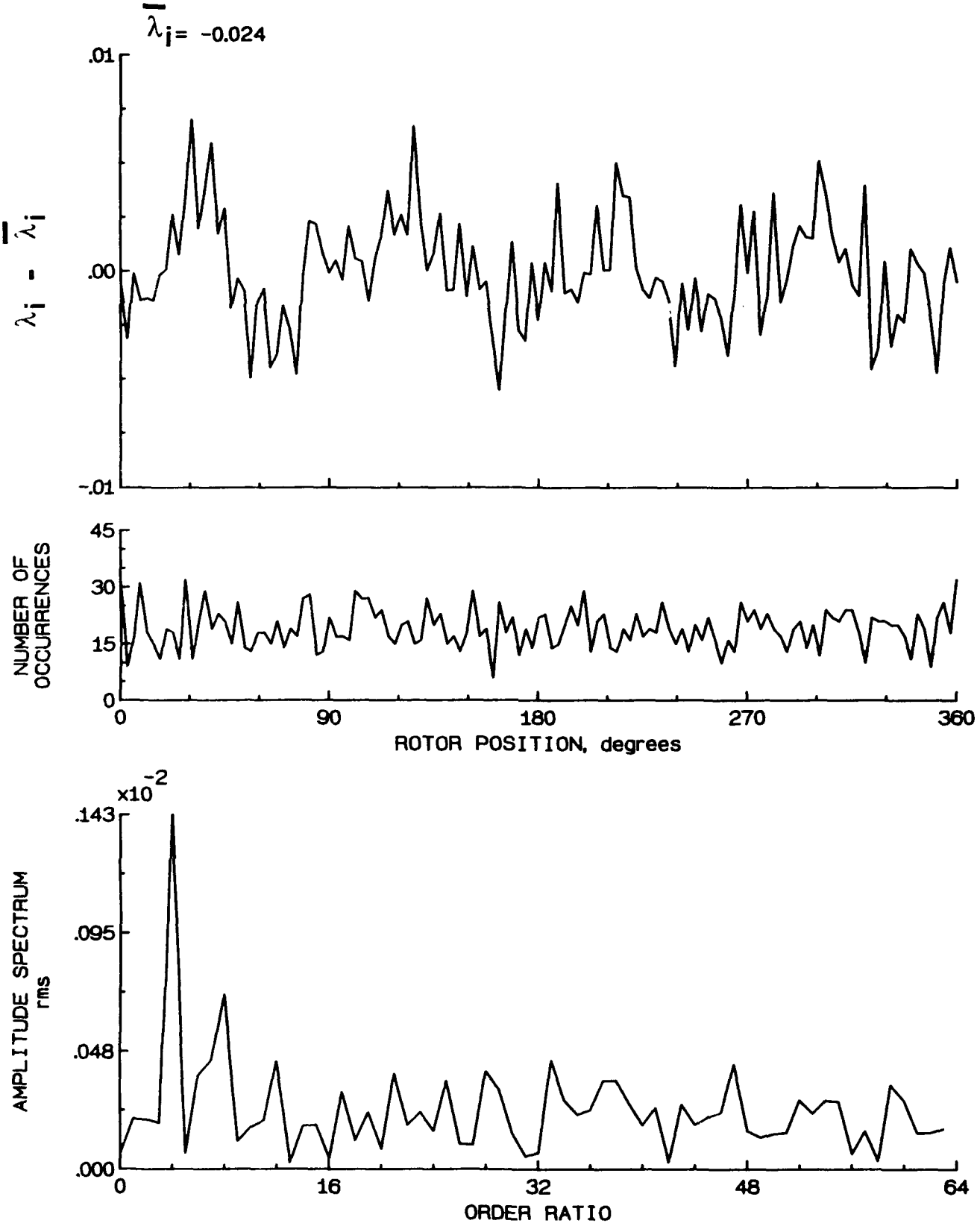

Figure 38.- Concluded.

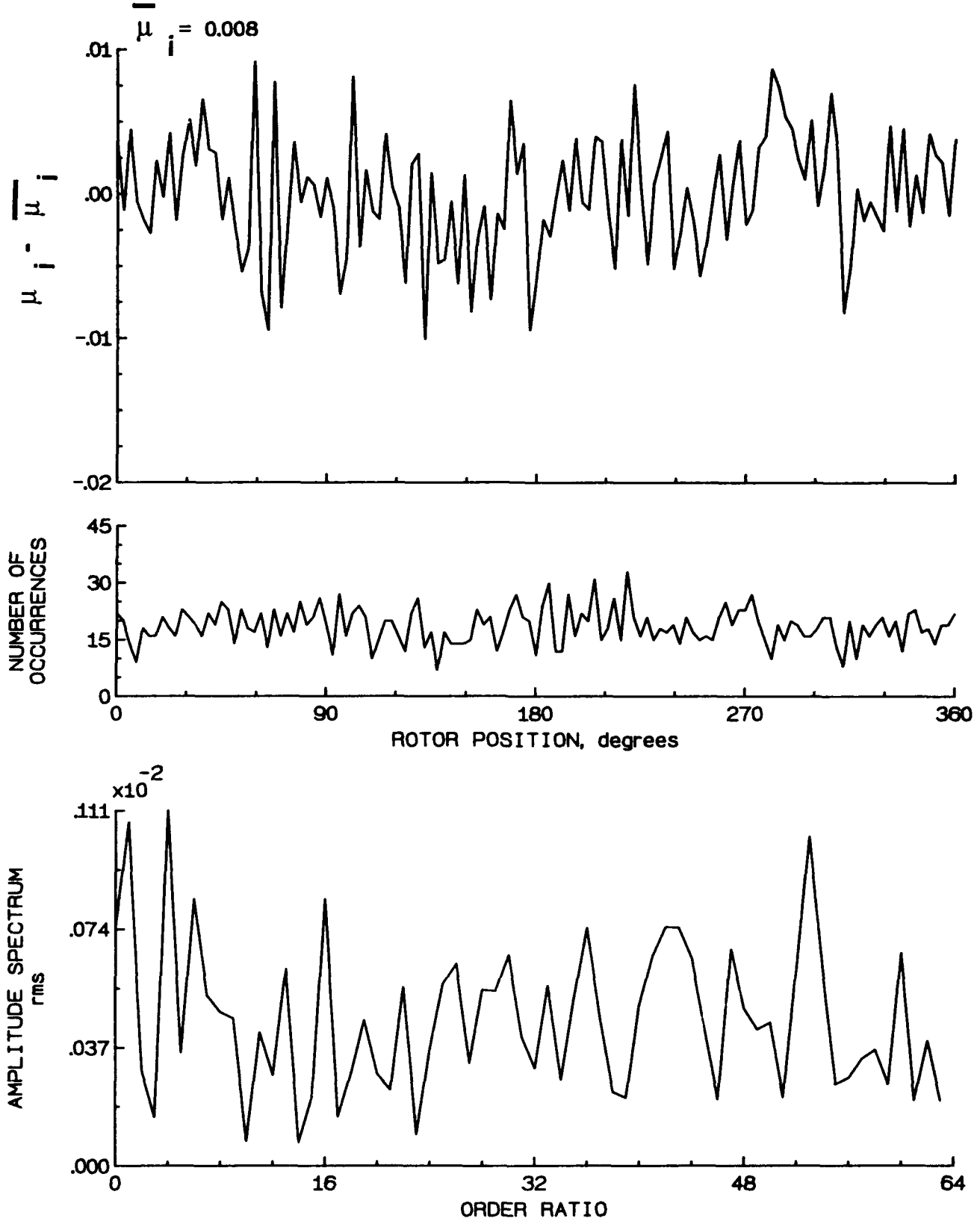

Figure 39.- Induced inflow velocity measured at 30 degrees and r/R of 1.02.

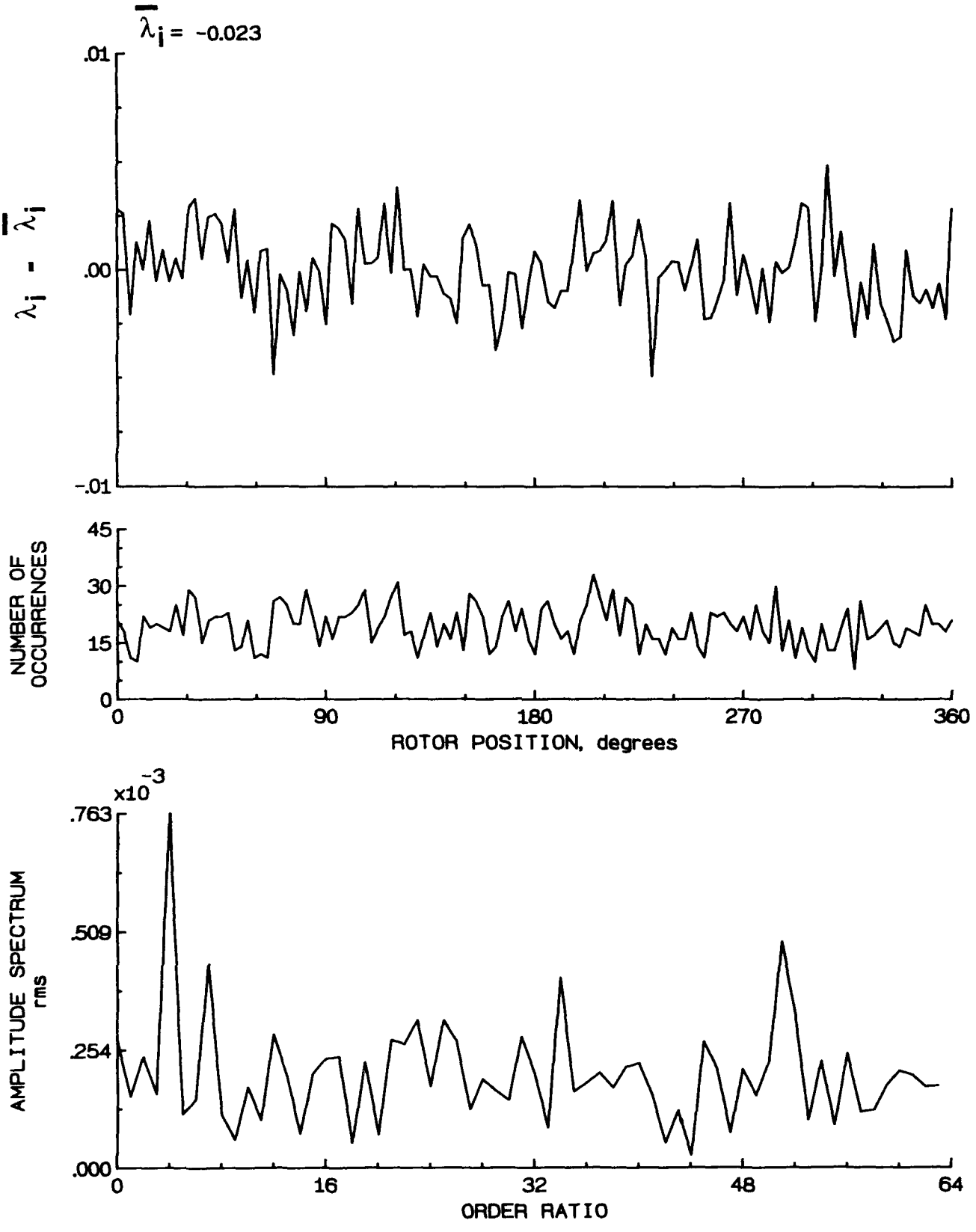

Figure 39.- Concluded.

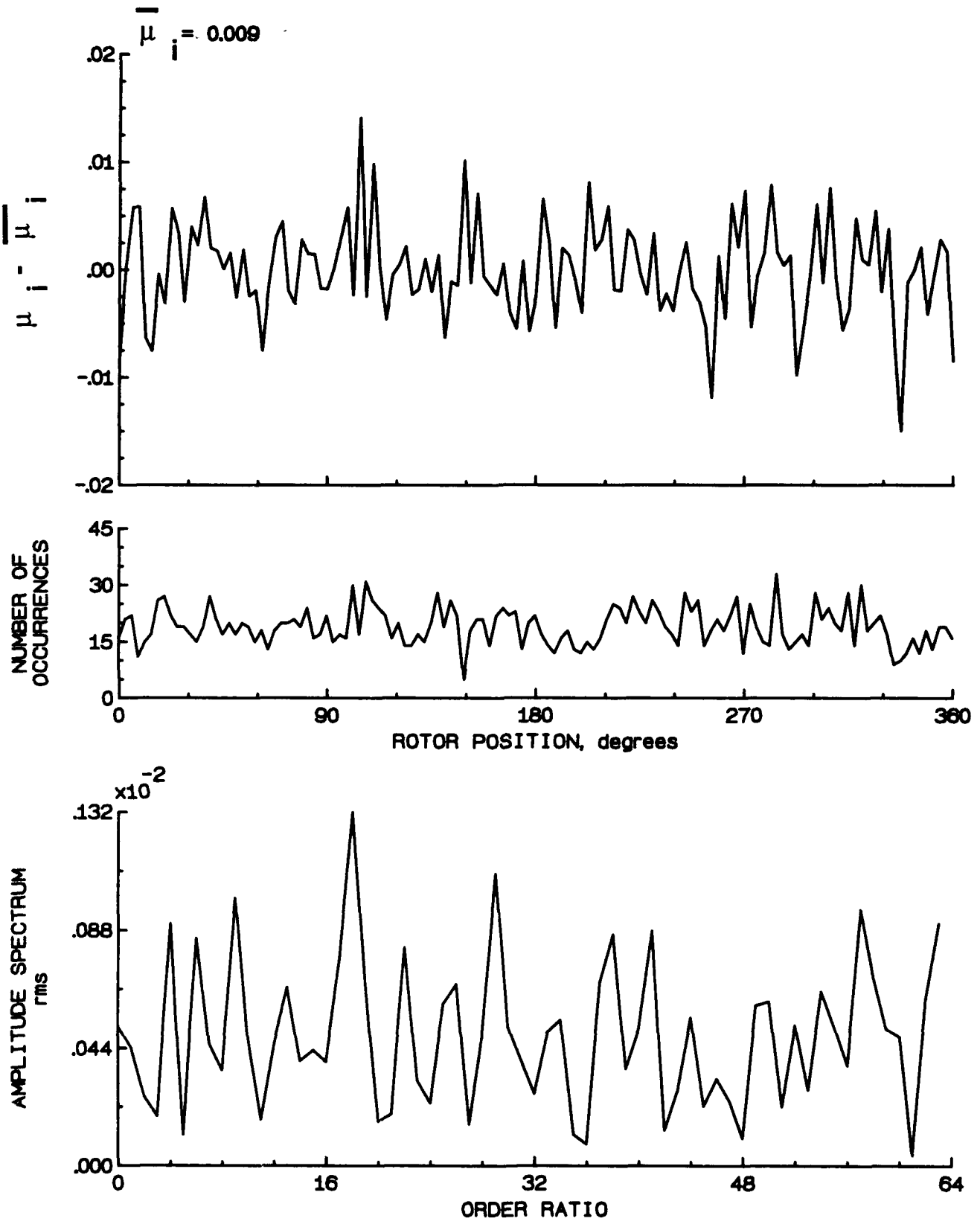

Figure 40.- Induced inflow velocity measured at 30 degrees and r/R of 1.04.

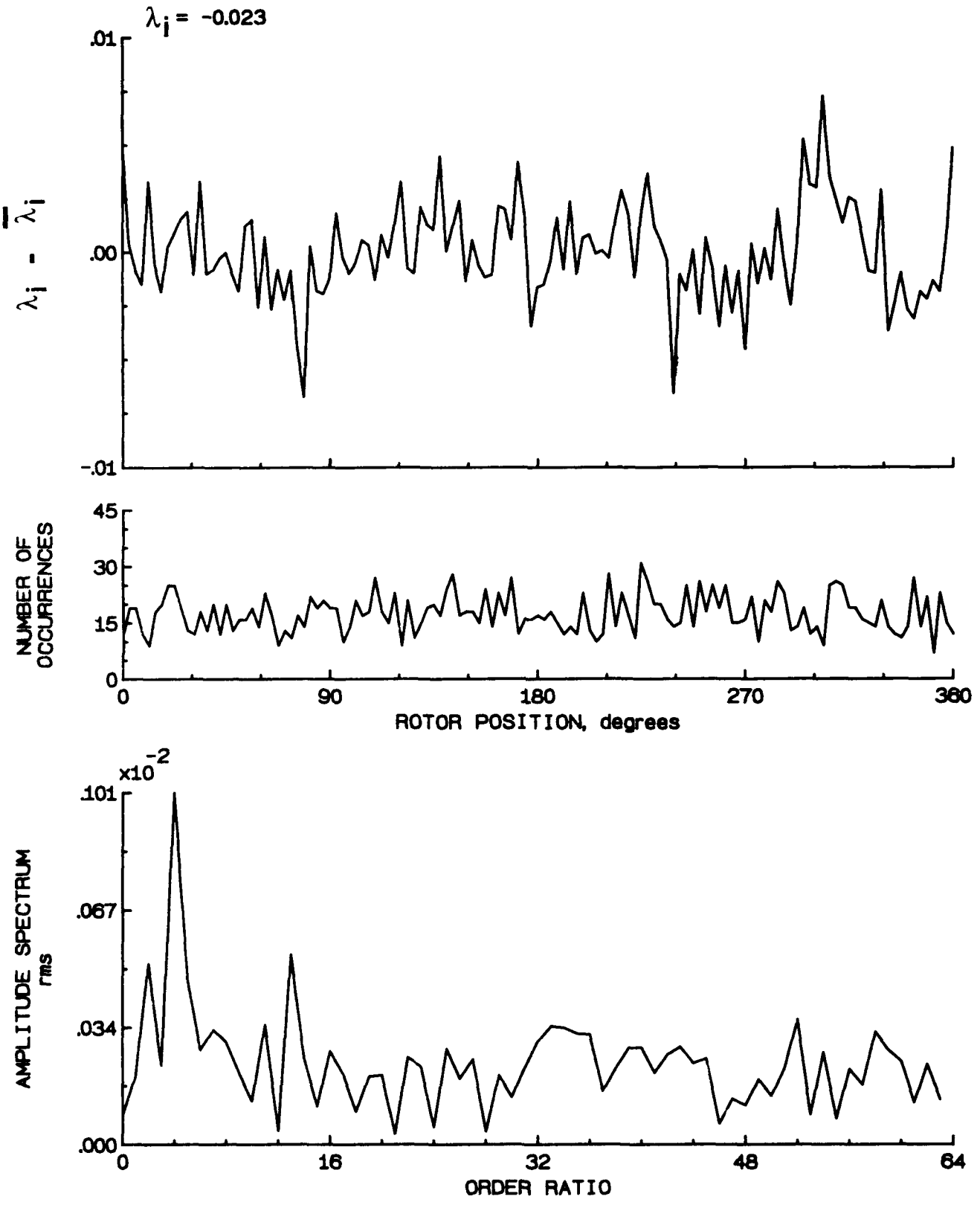

Figure 40.- Concluded.

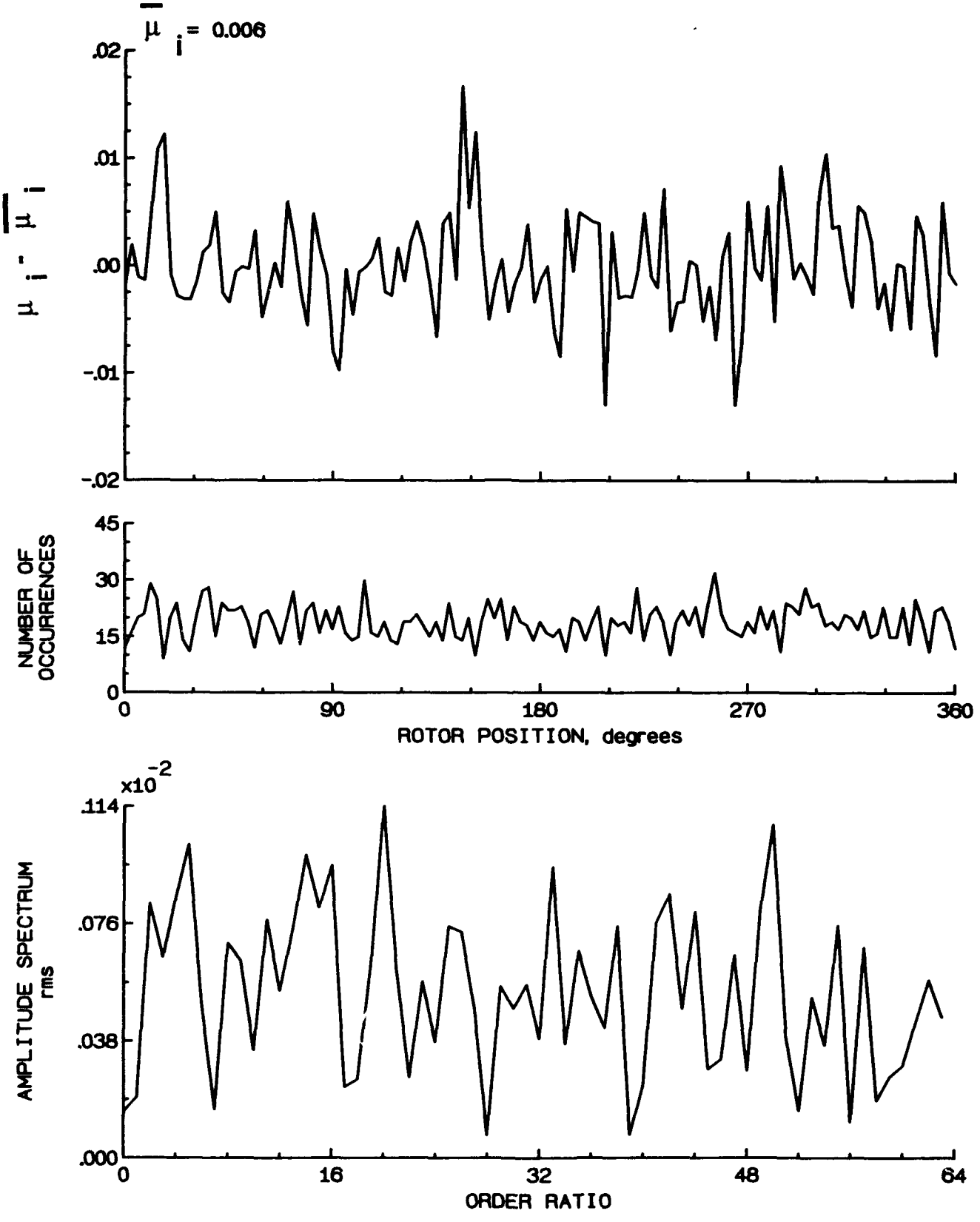

Figure 41.- Induced inflow velocity measured at 30 degrees and r/R of 1.10.

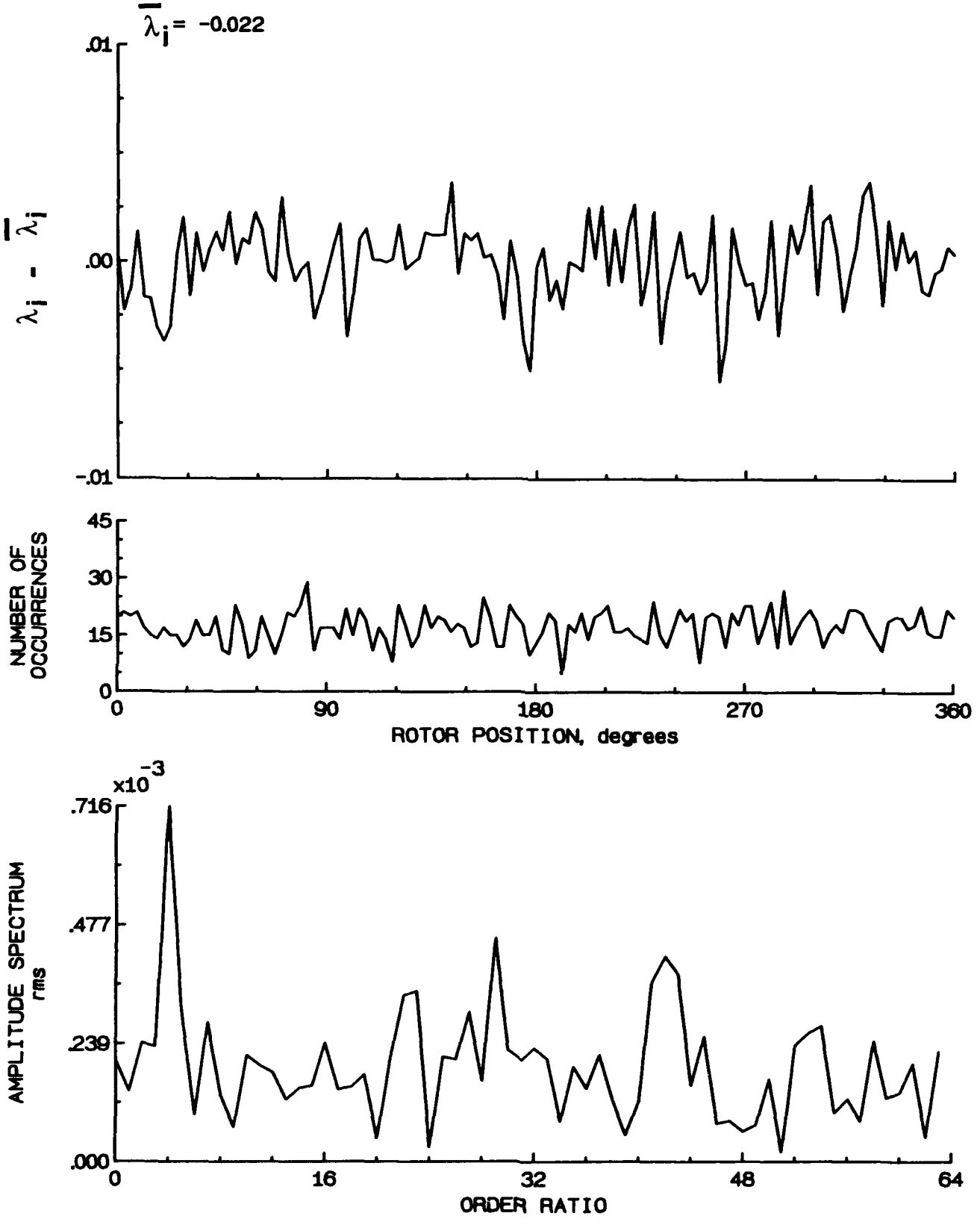

Figure 41.- Concluded.

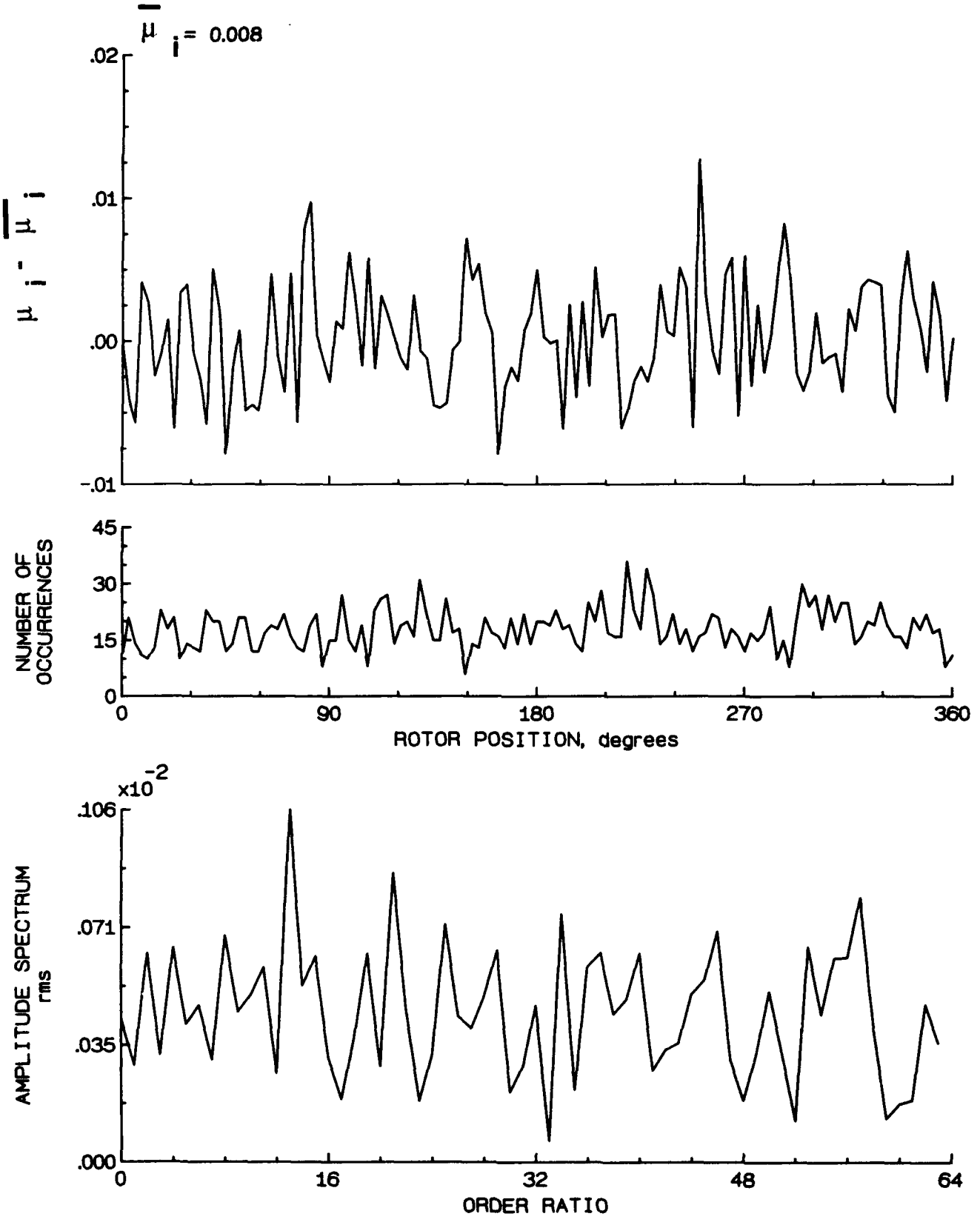

Figure 42.- Induced inflow velocity measured at 60 degrees and r/R of 0.20.

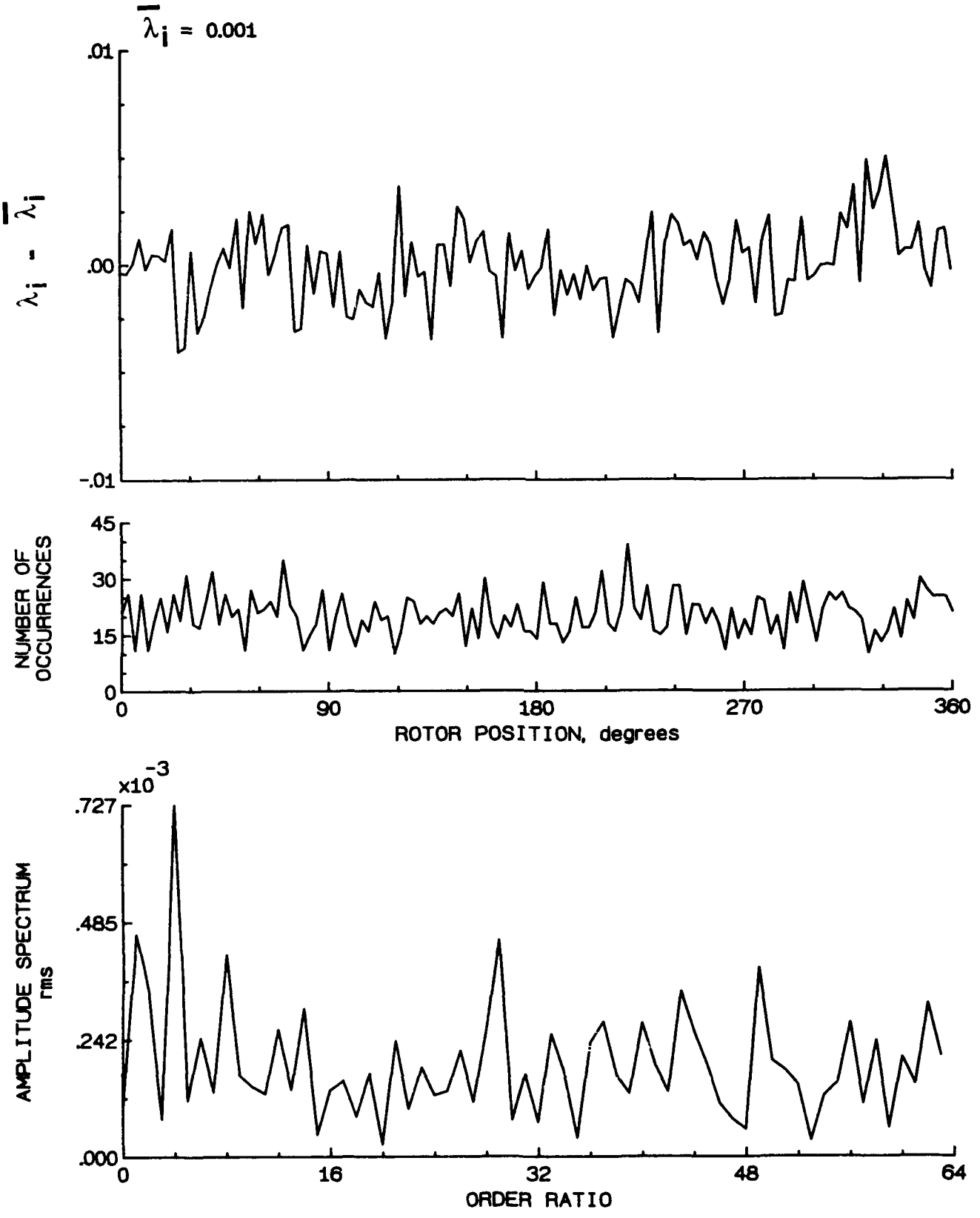

Figure 42.- Concluded.

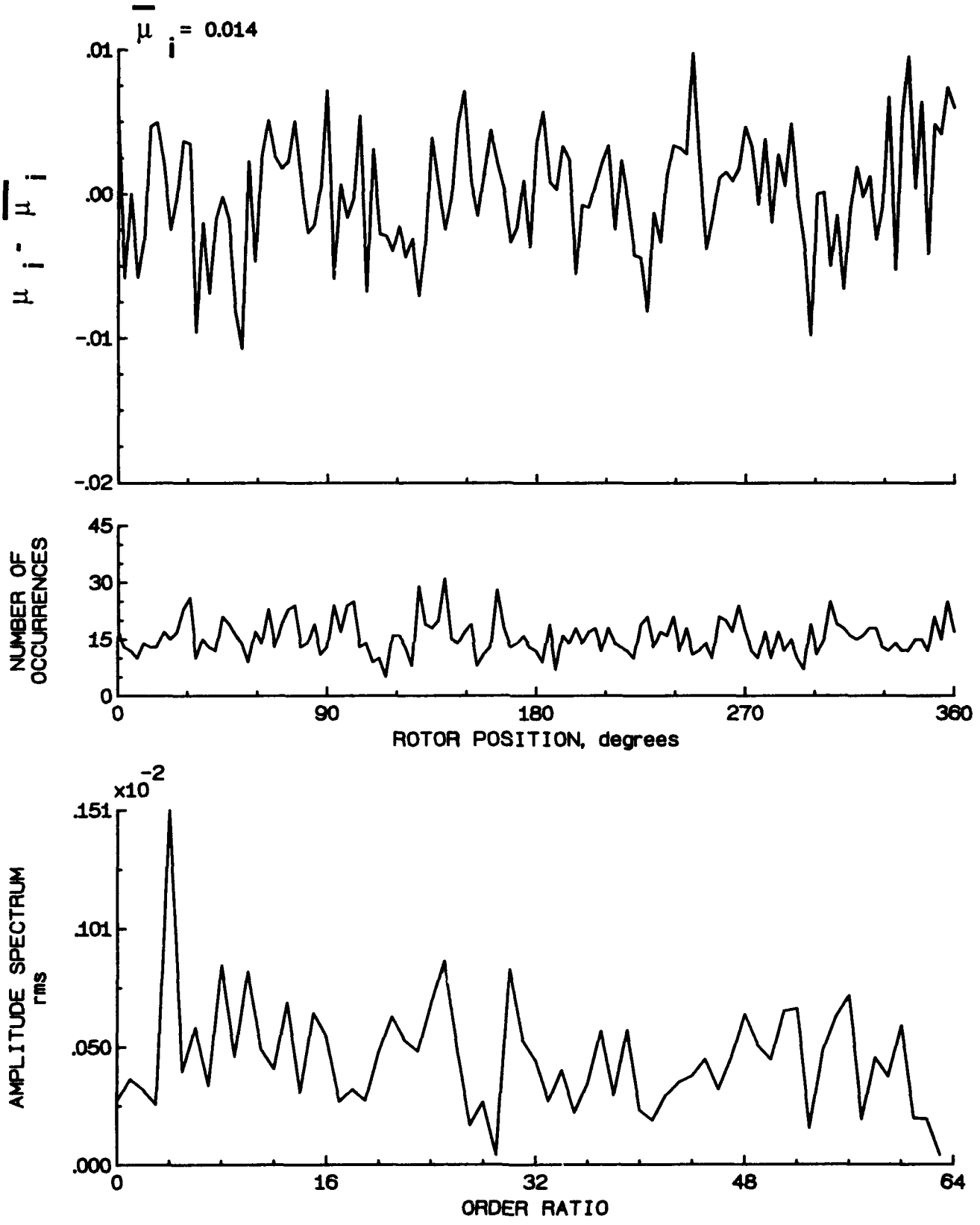

Figure 43.- Induced inflow velocity measured at 60 degrees and r/R of 0.40.

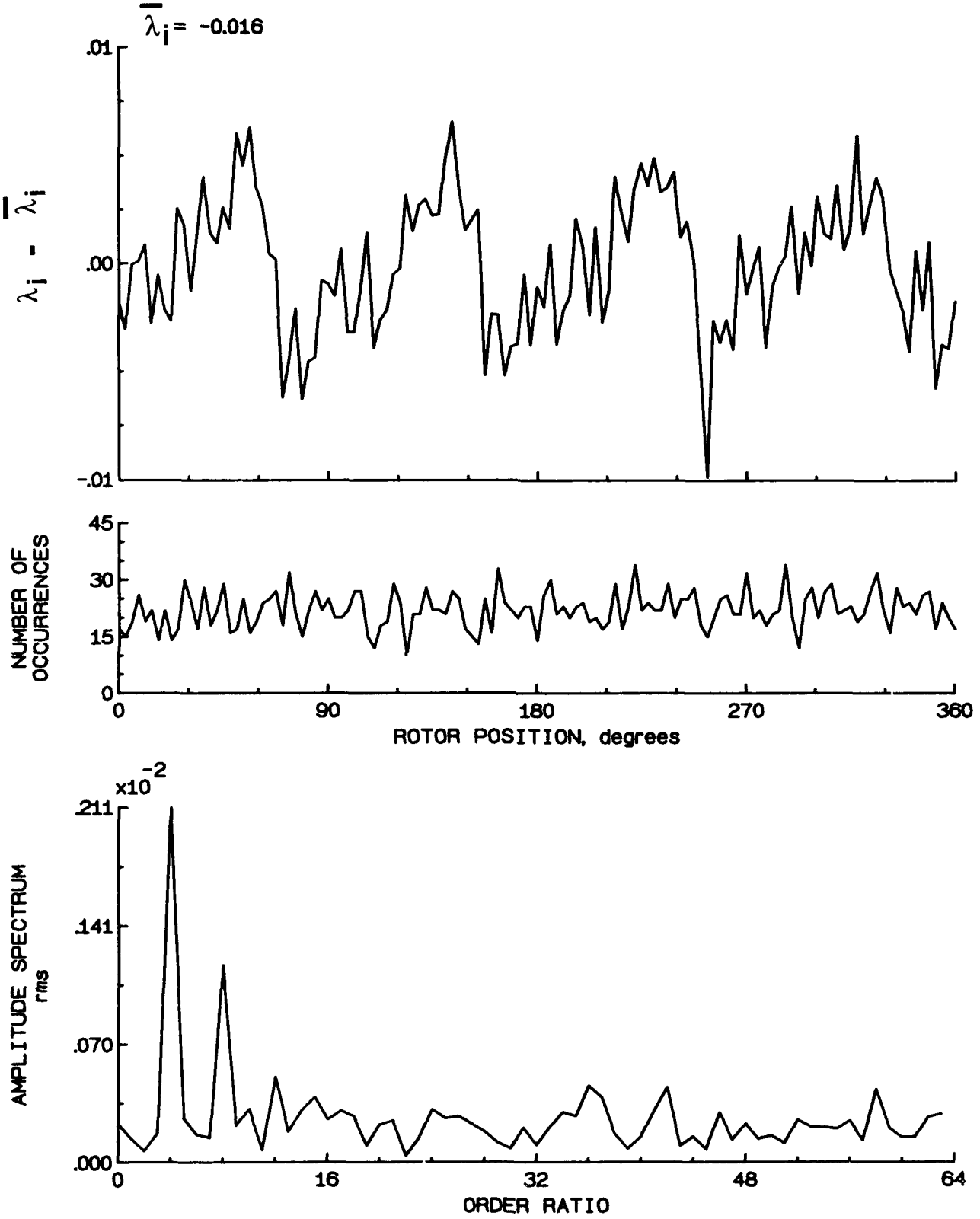

Figure 43.- Concluded.

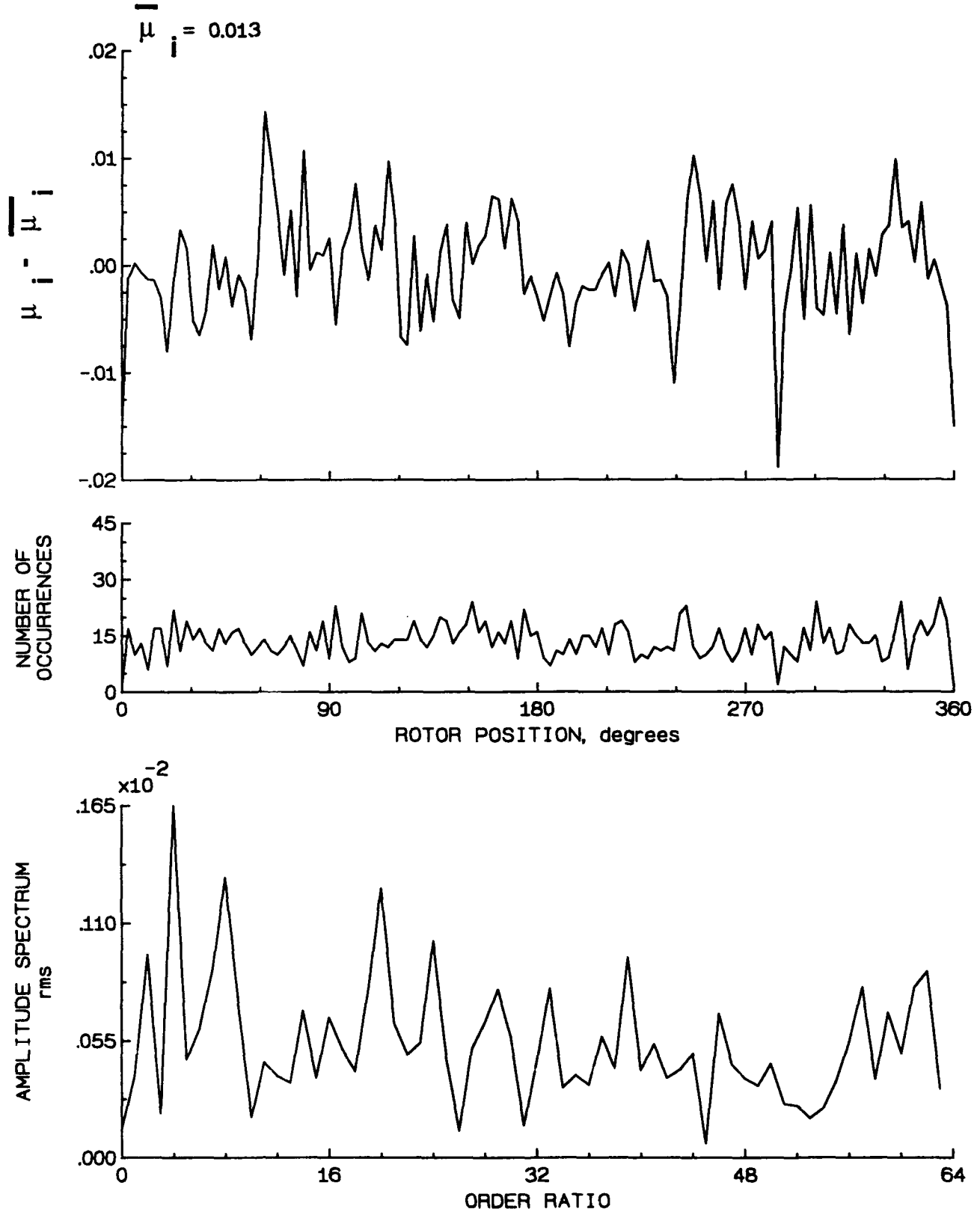

Figure 44.- Induced inflow velocity measured at 60 degrees and r/R of 0.50.

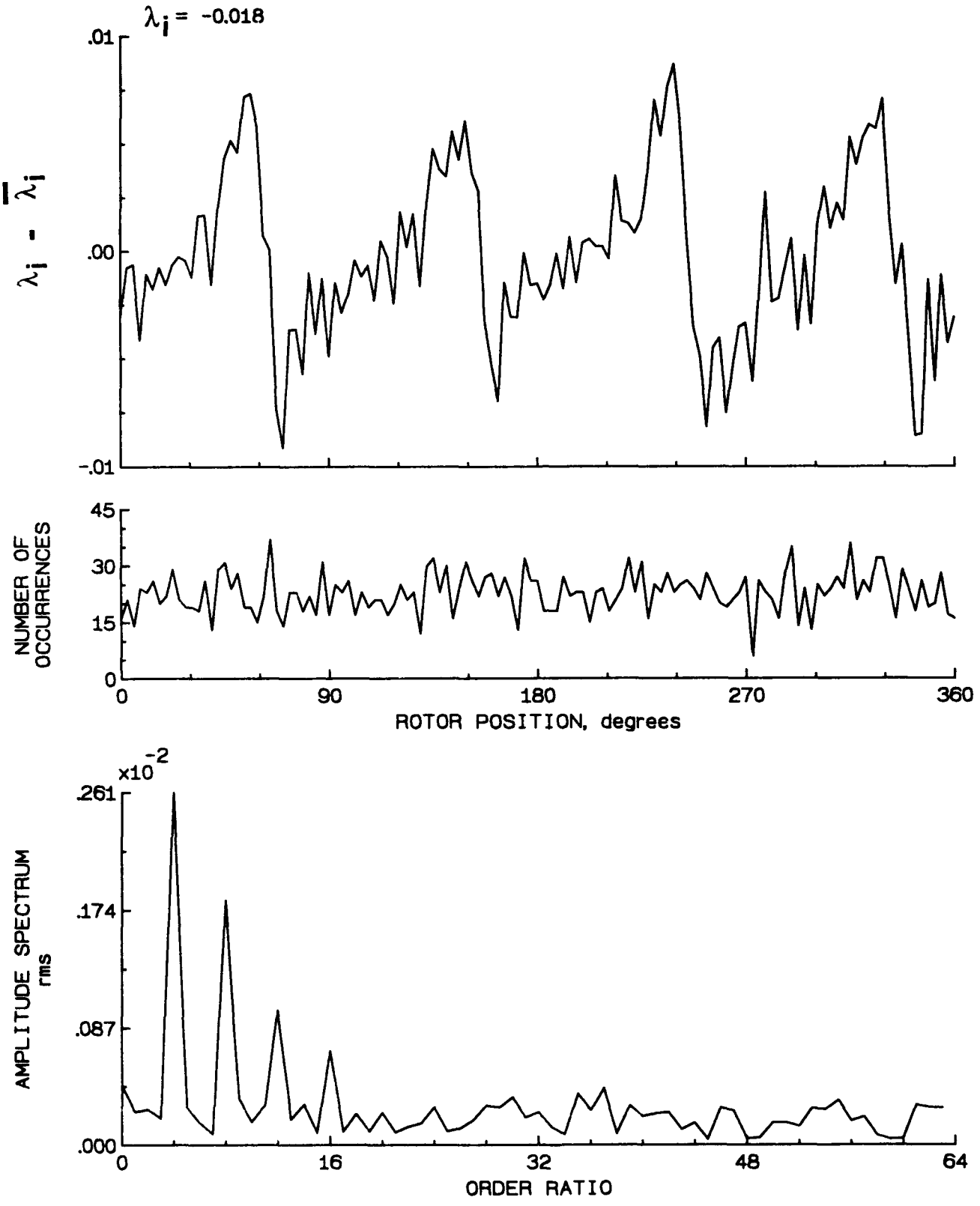

Figure 44.- Concluded.

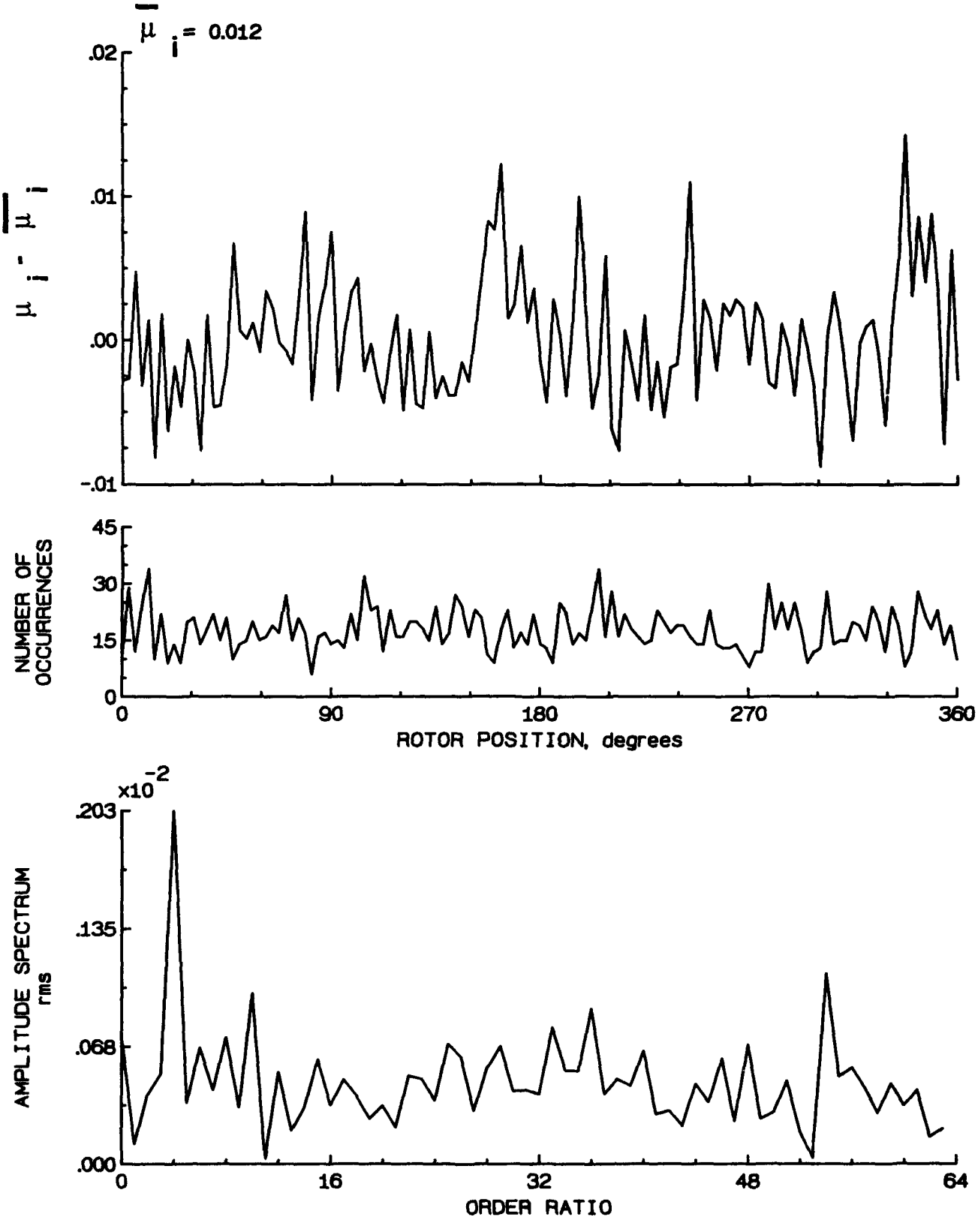

Figure 45.- Induced inflow velocity measured at 60 degrees and r/R of 0.60.

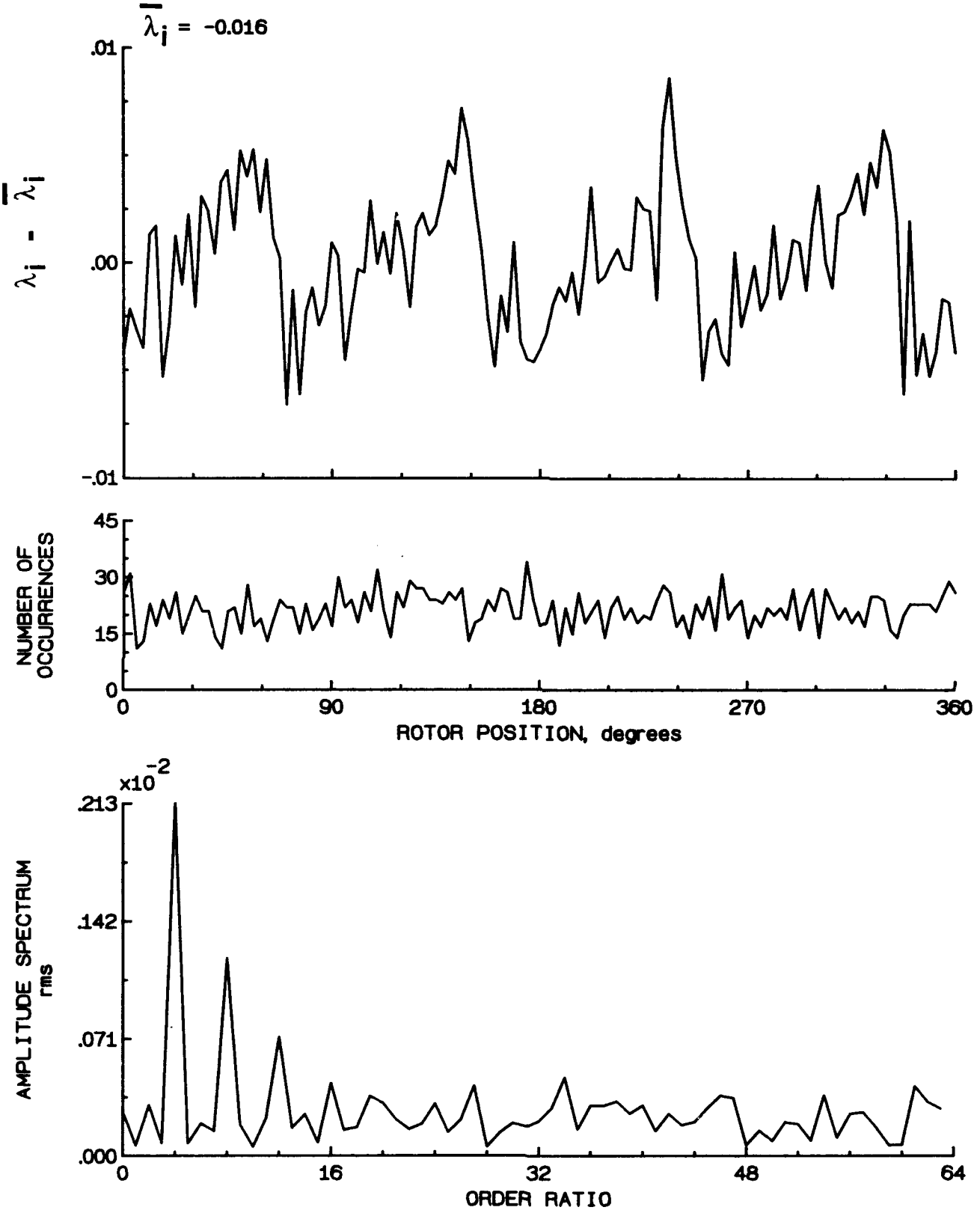

Figure 45.- Concluded.

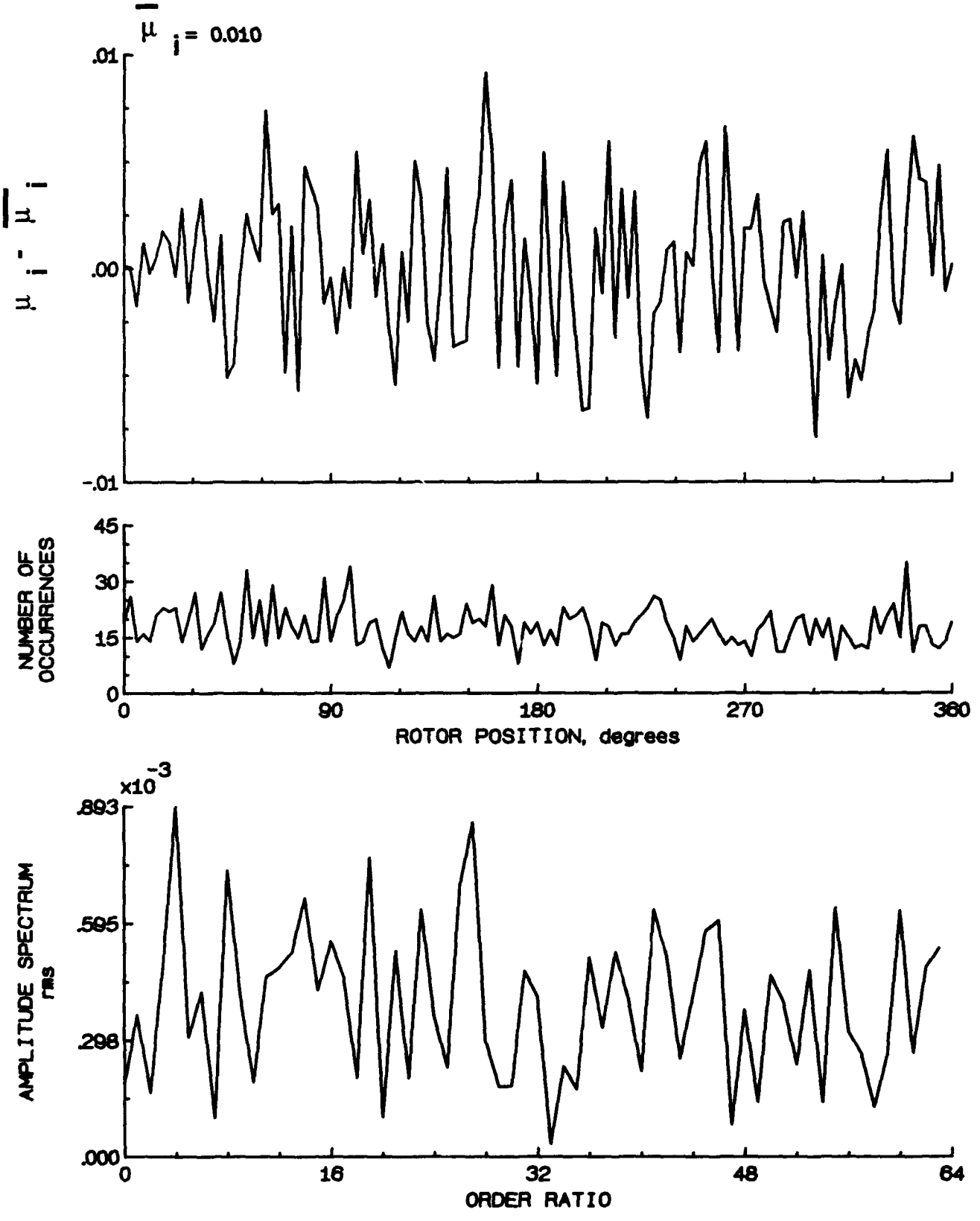

Figure 46.- Induced inflow velocity measured at 60 degrees and r/R of 0.70.

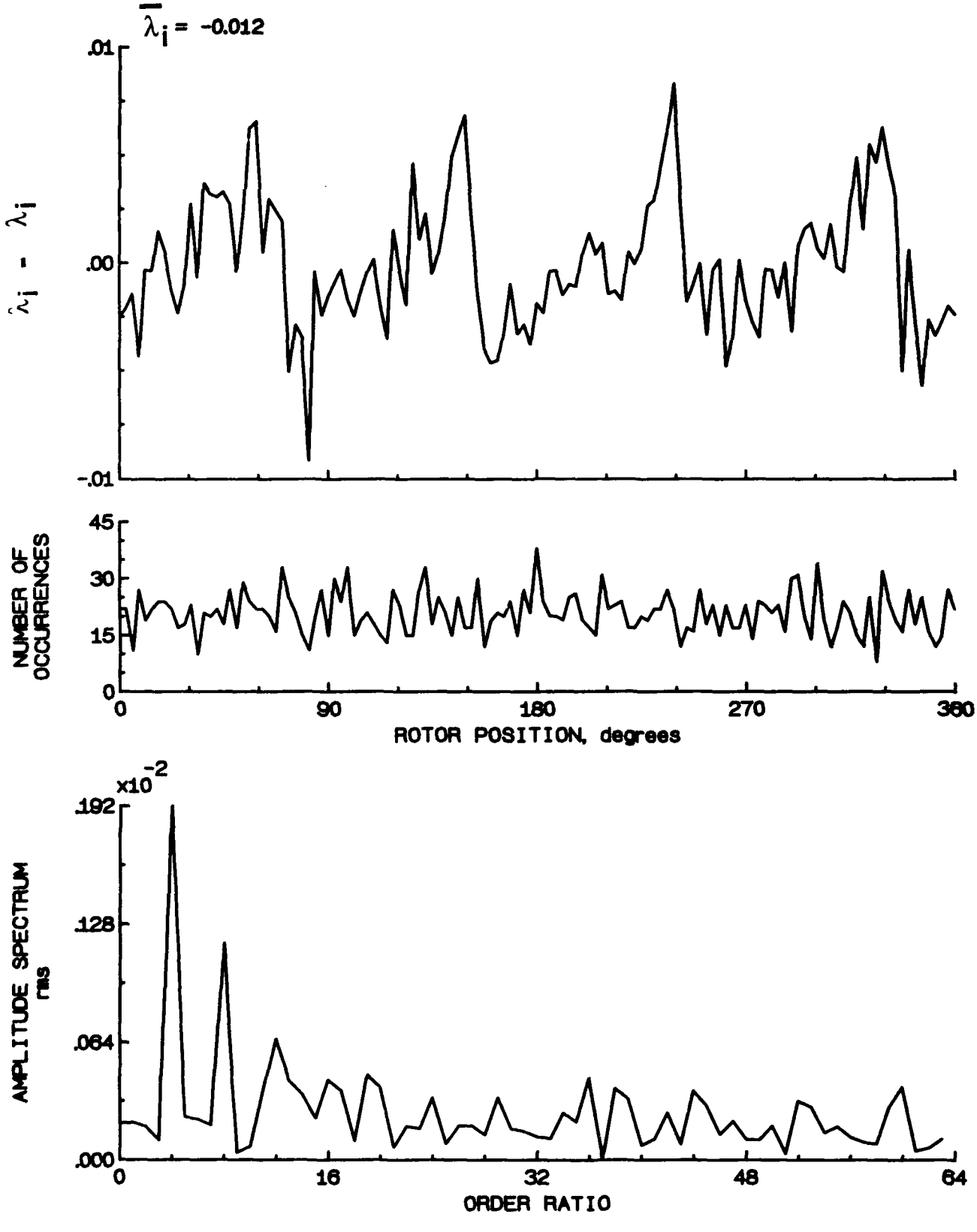

Figure 46.- Concluded.

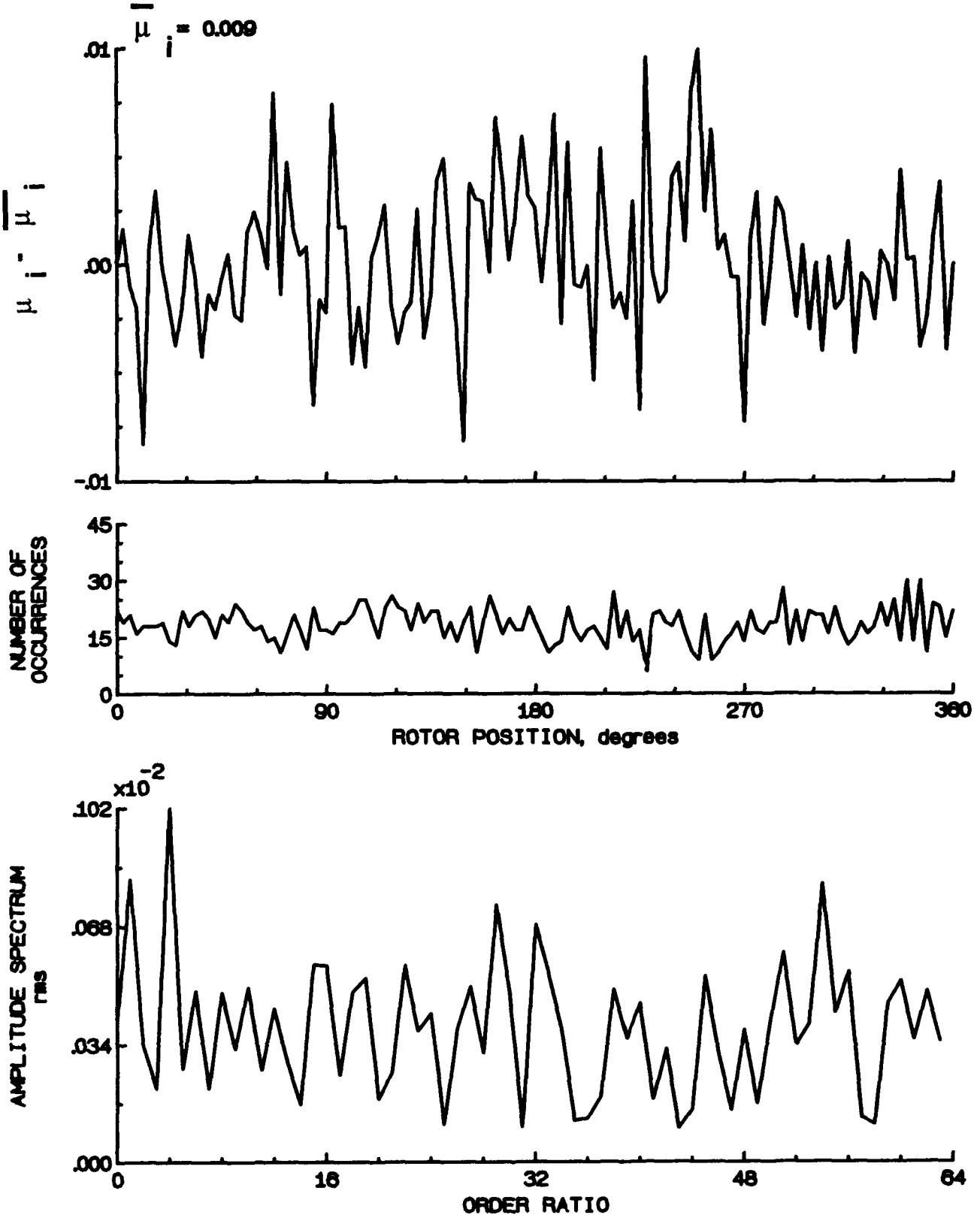

Figure 47.- Induced inflow velocity measured at 60 degrees and r/R of 0.74.

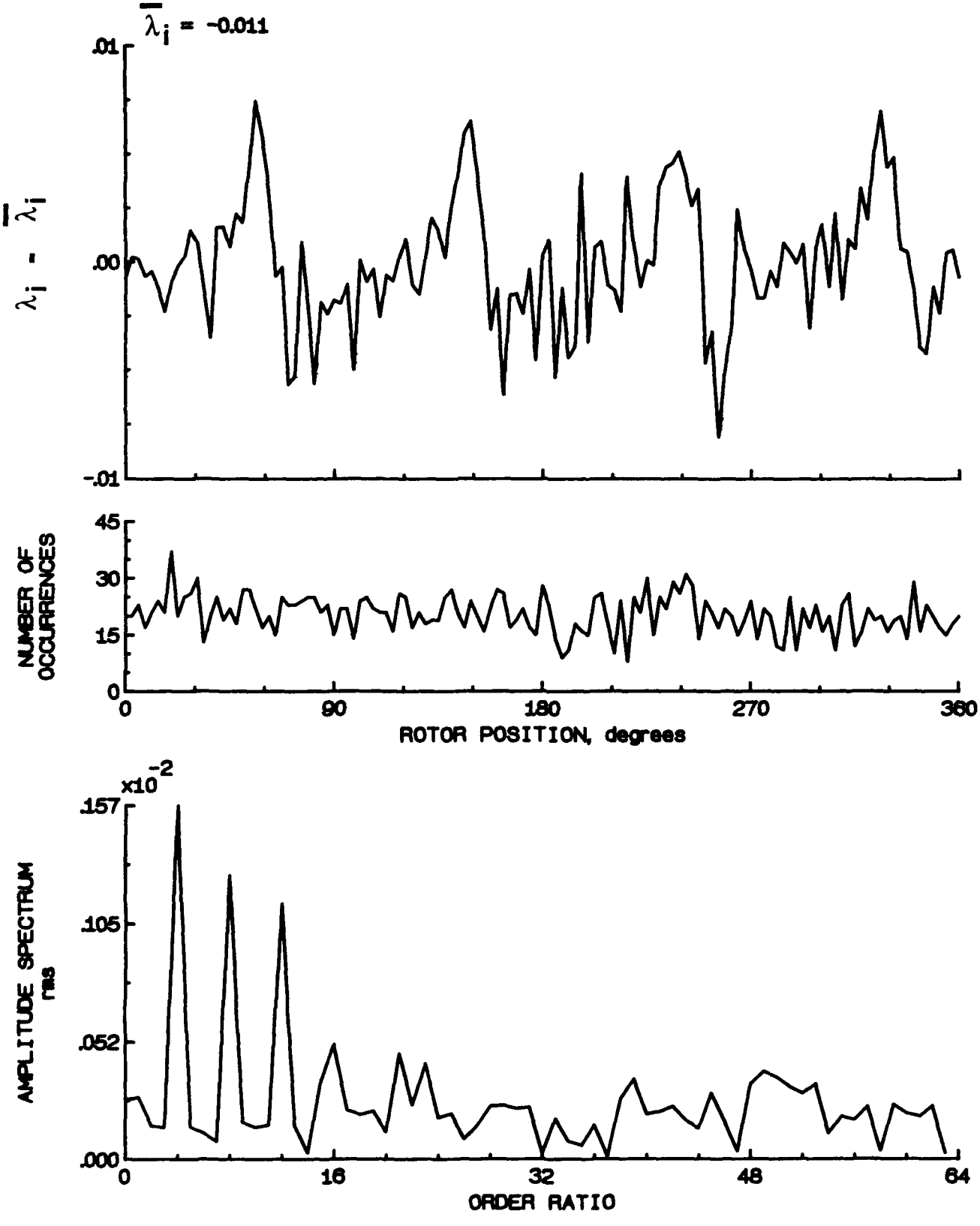

Figure 47.- Concluded.

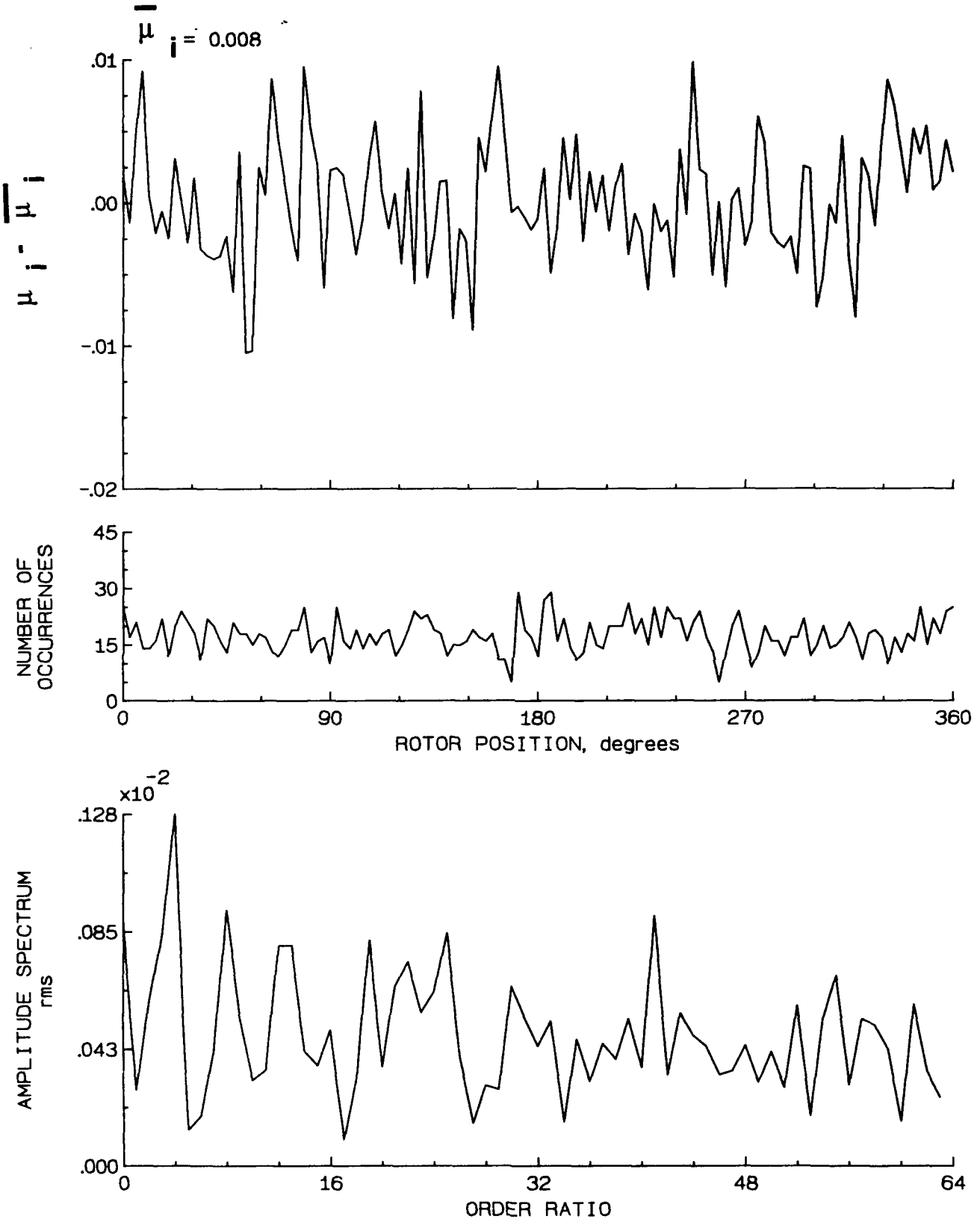

Figure 48.- Induced inflow velocity measured at 60 degrees and r/R of 0.78.

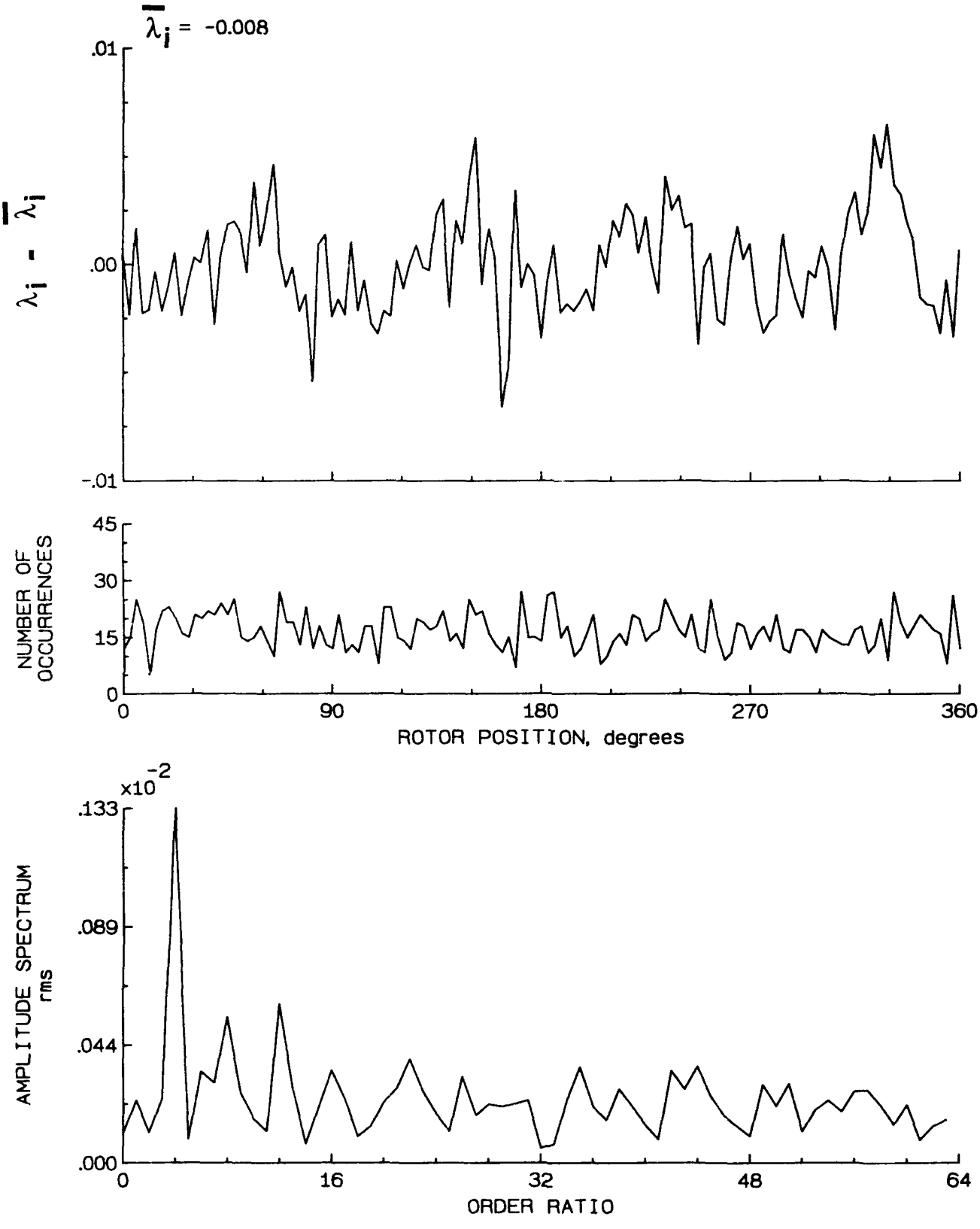

Figure 48.- Concluded.

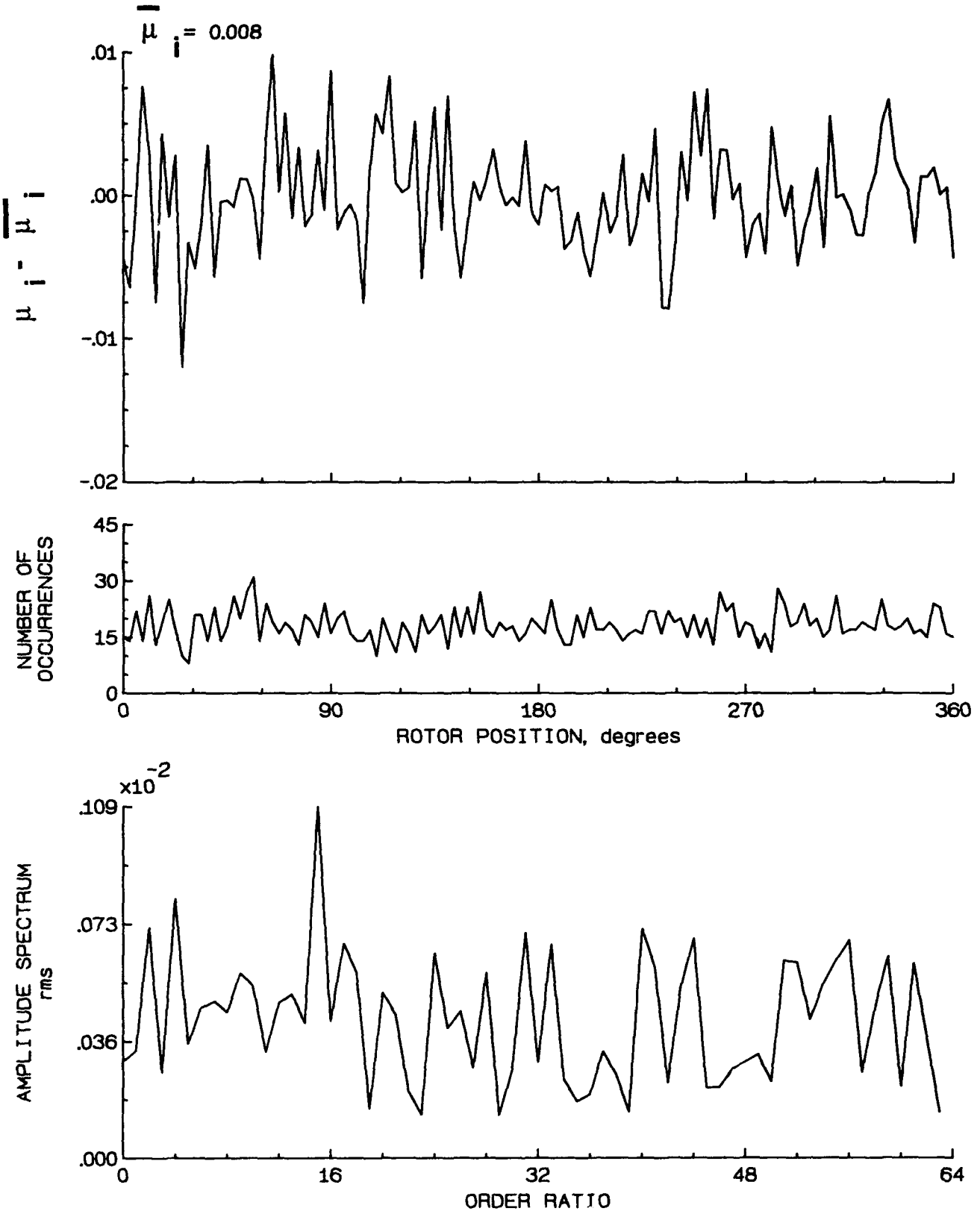

Figure 49.- Induced inflow velocity measured at 60 degrees and r/R of 0.82.

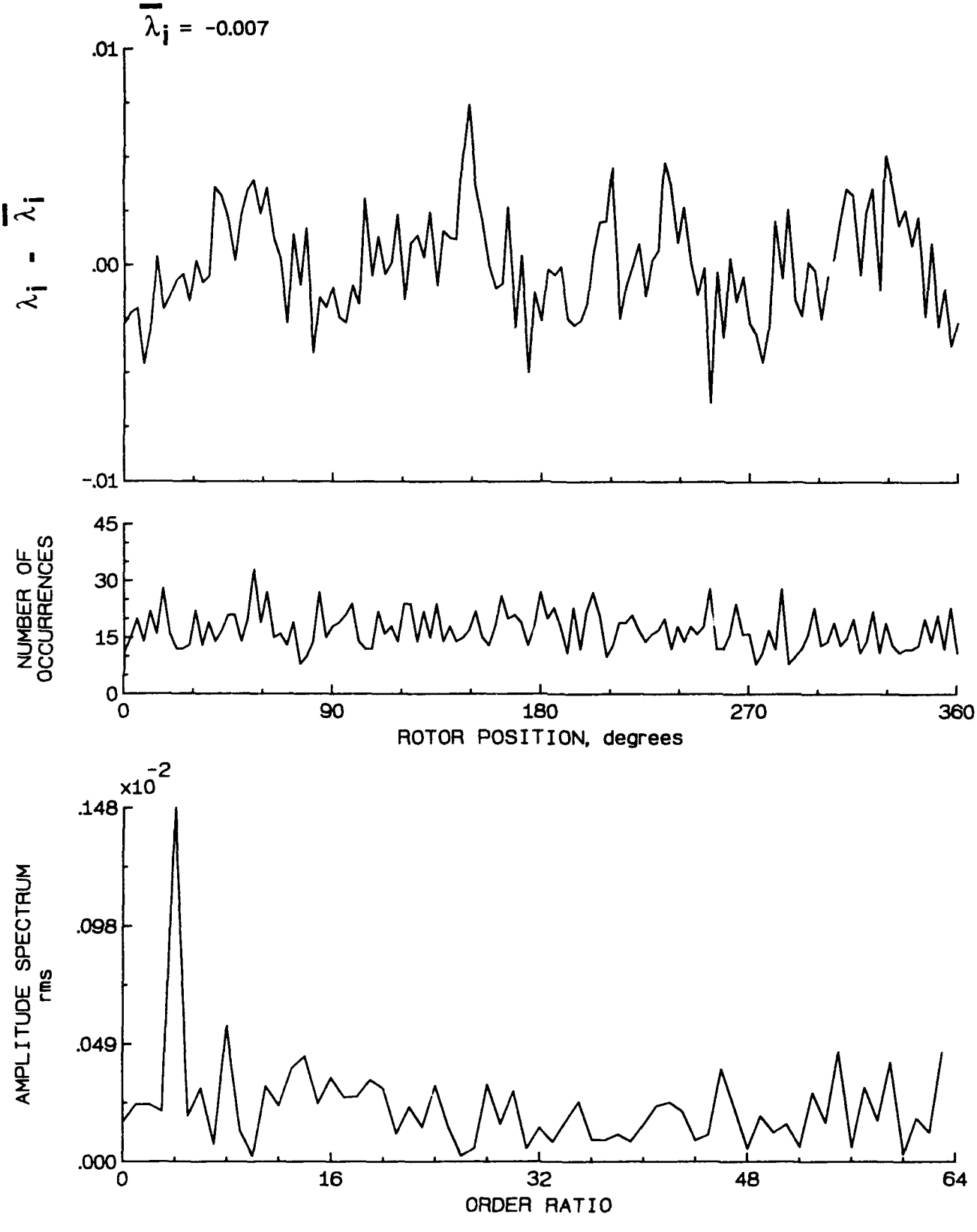

Figure 49.- Concluded.

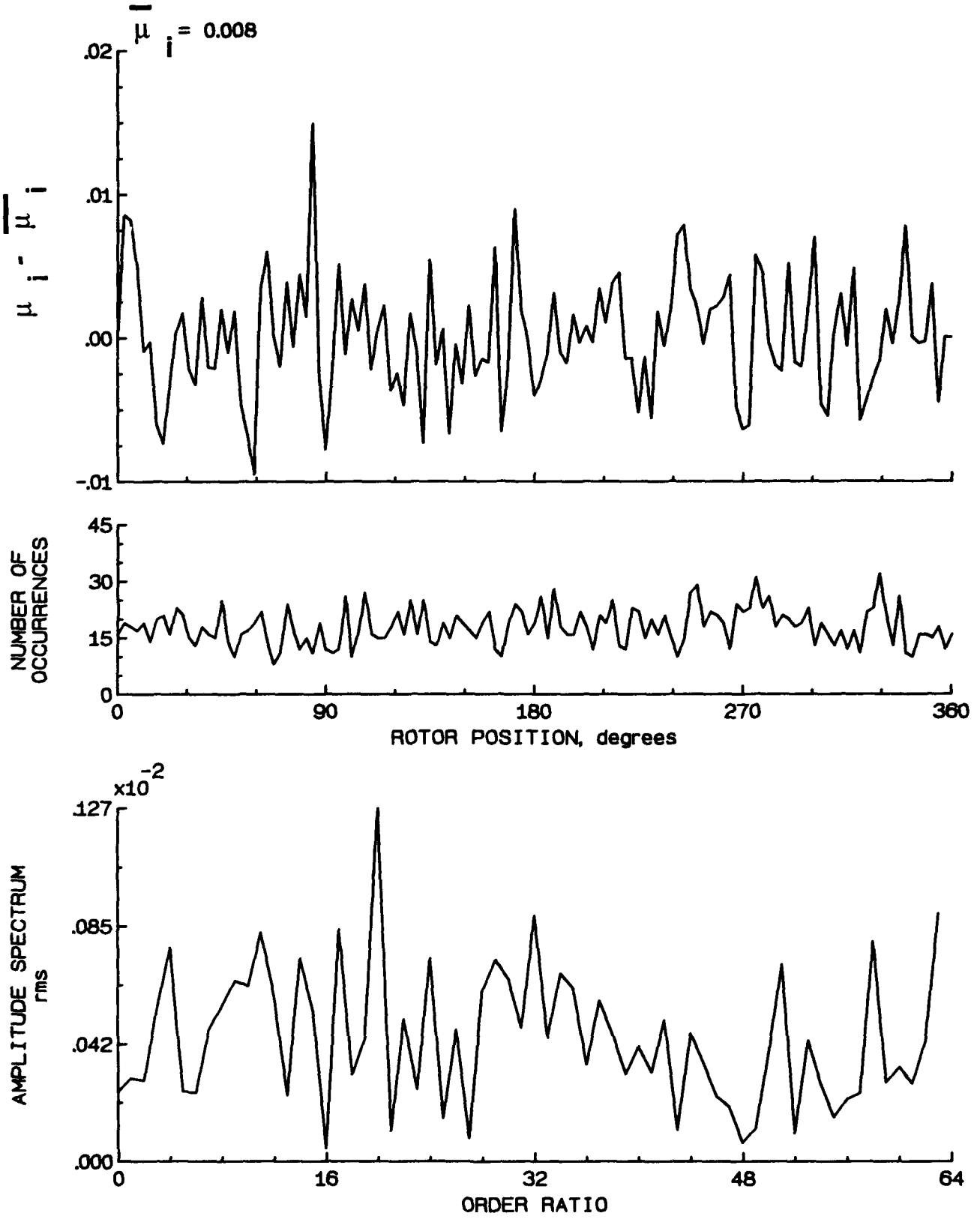

Figure 50.- Induced inflow velocity measured at 60 degrees and r/R of 0.86.

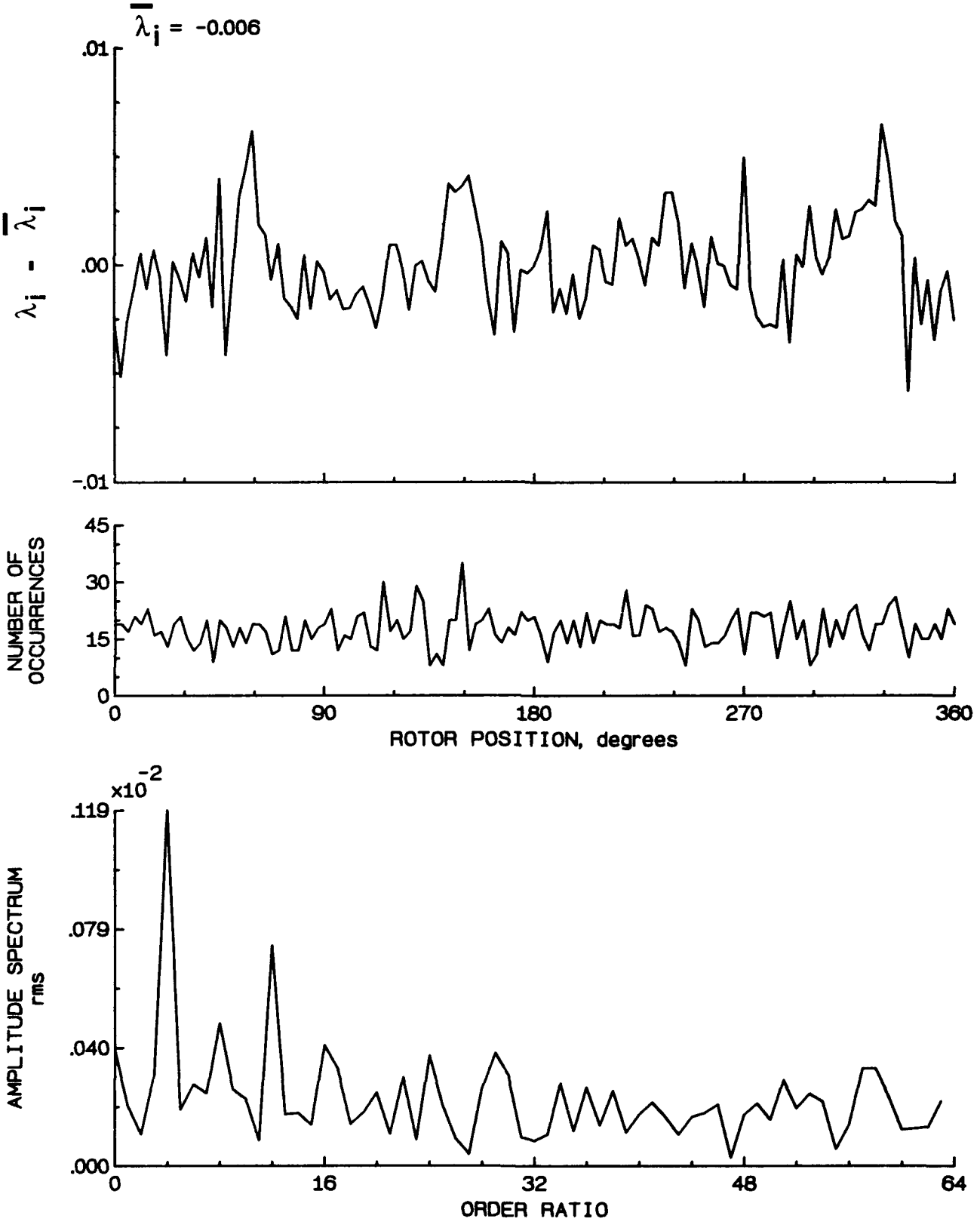

Figure 50.- Concluded.

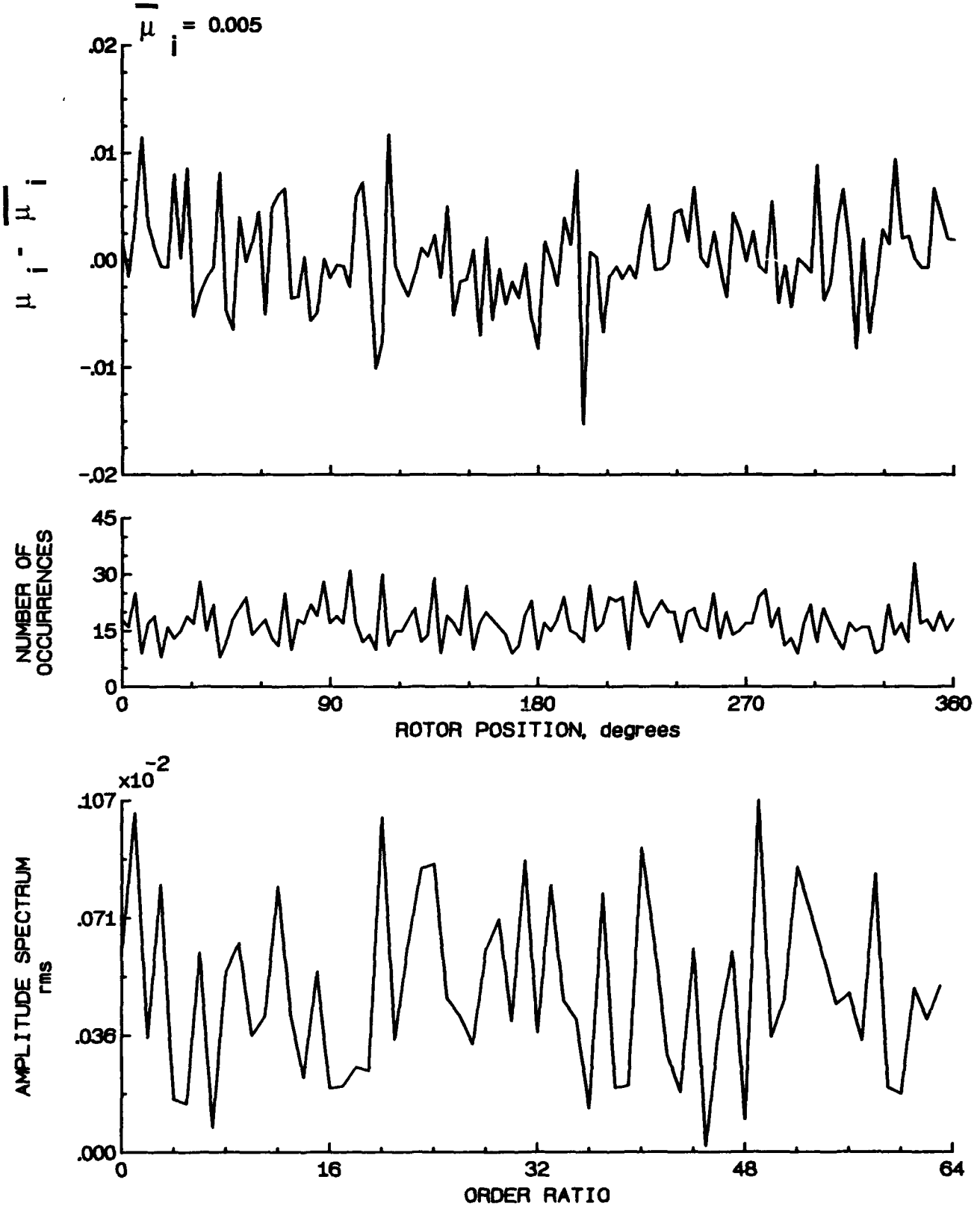

Figure 51.- Induced inflow velocity measured at 60 degrees and r/R of 0.90.

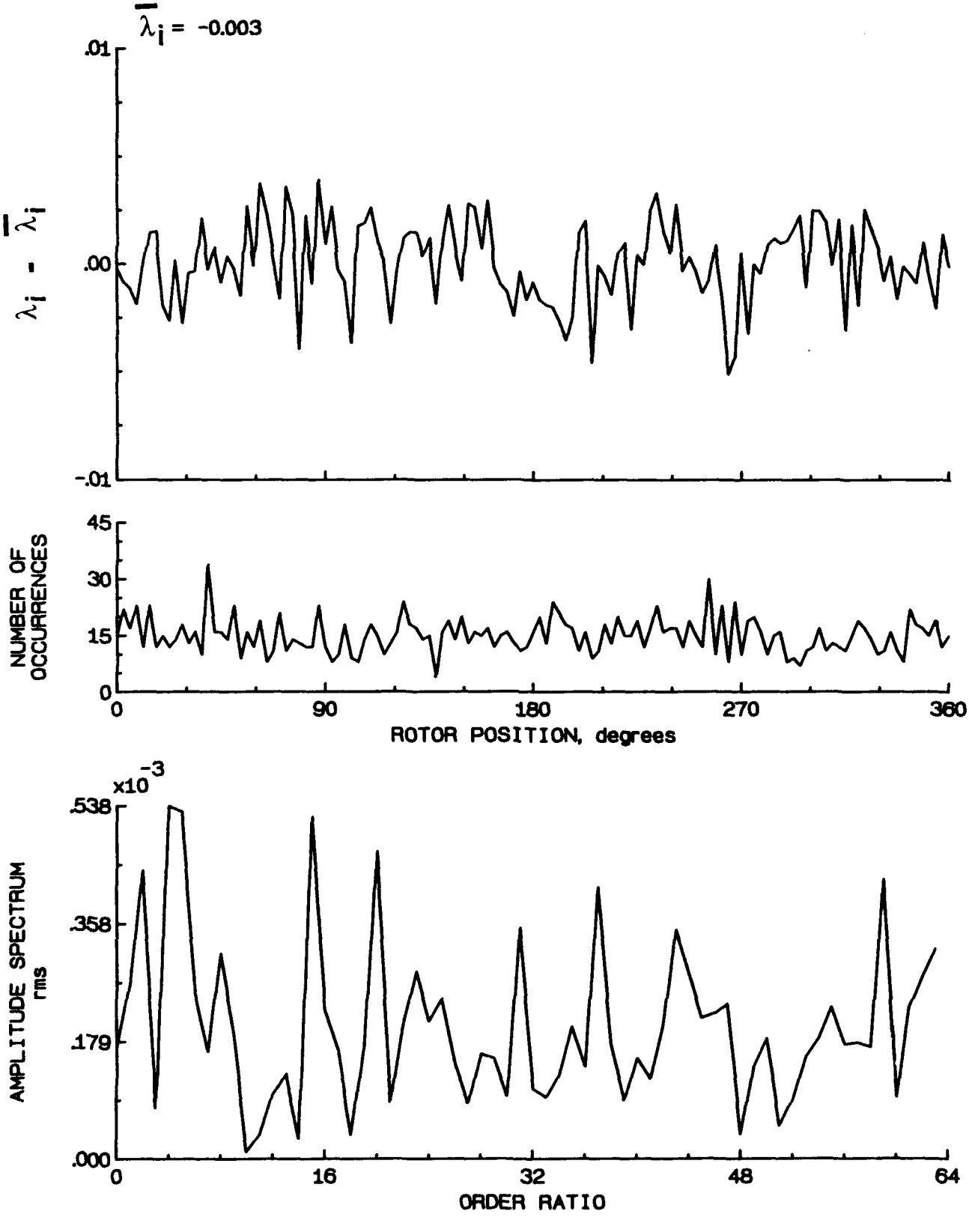

Figure 51.- Concluded.

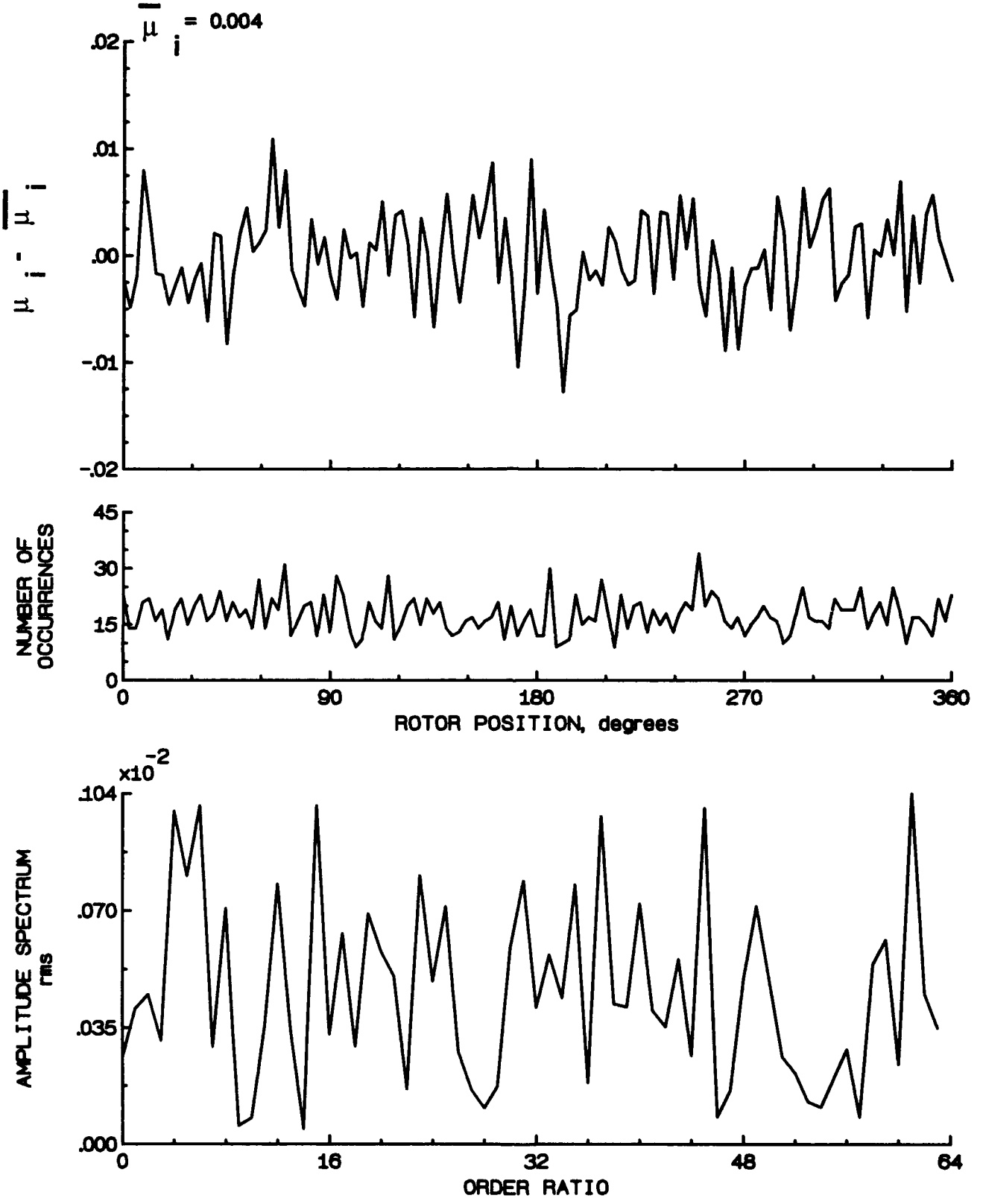

Figure 52.- Induced inflow velocity measured at 60 degrees and r/R of 0.94.

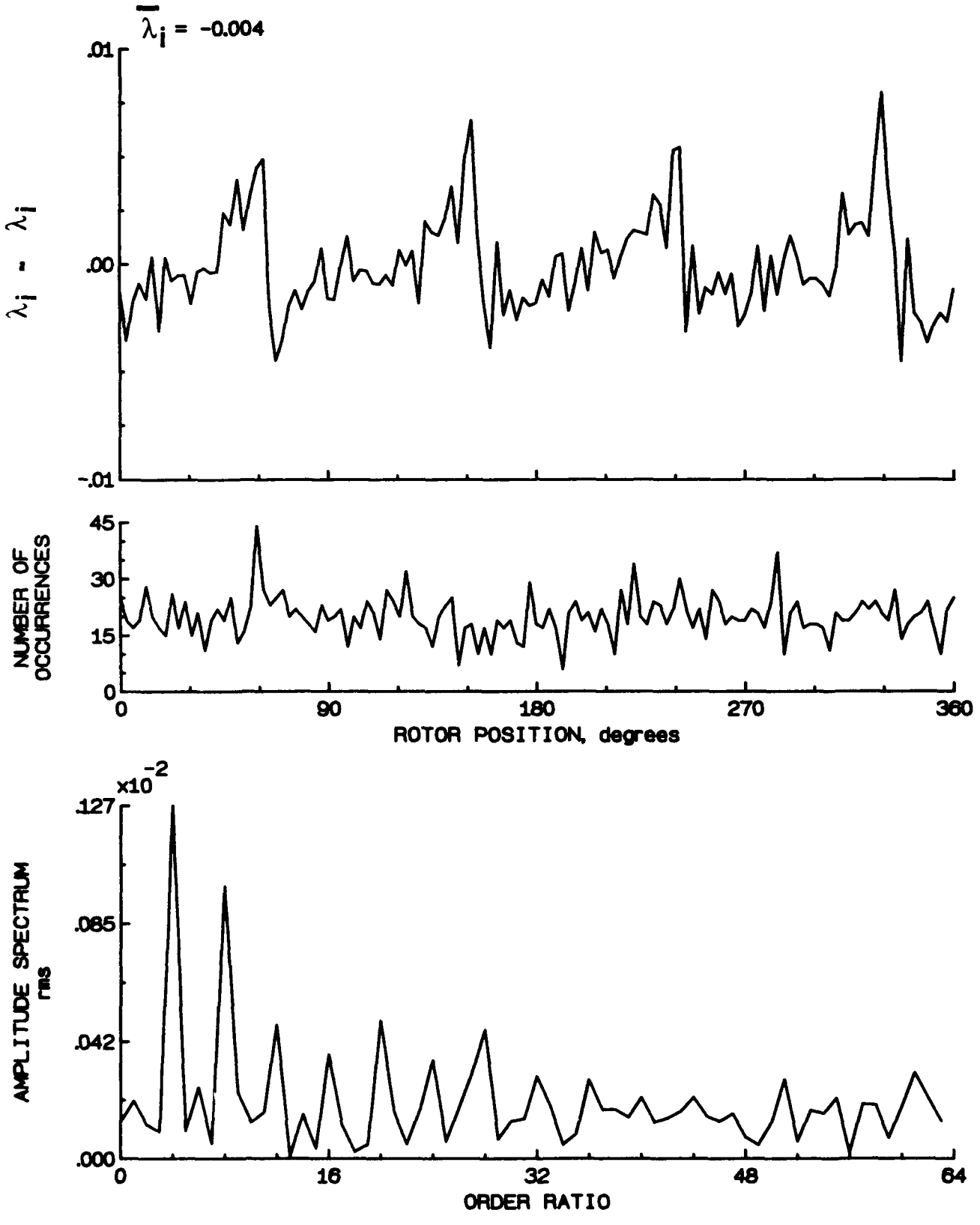

Figure 52.- Concluded.

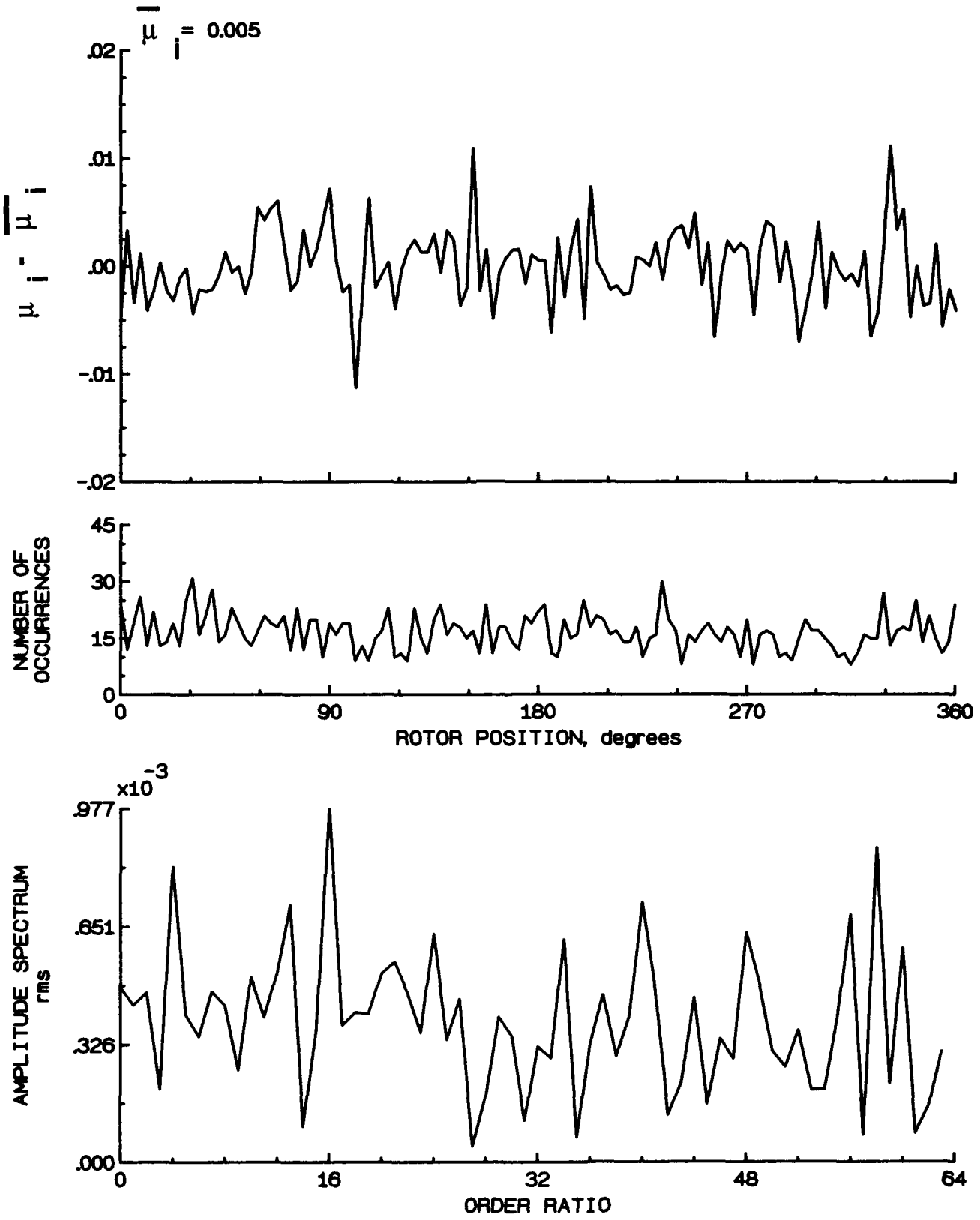

Figure 53.- Induced inflow velocity measured at 60 degrees and r/R of 0.98.

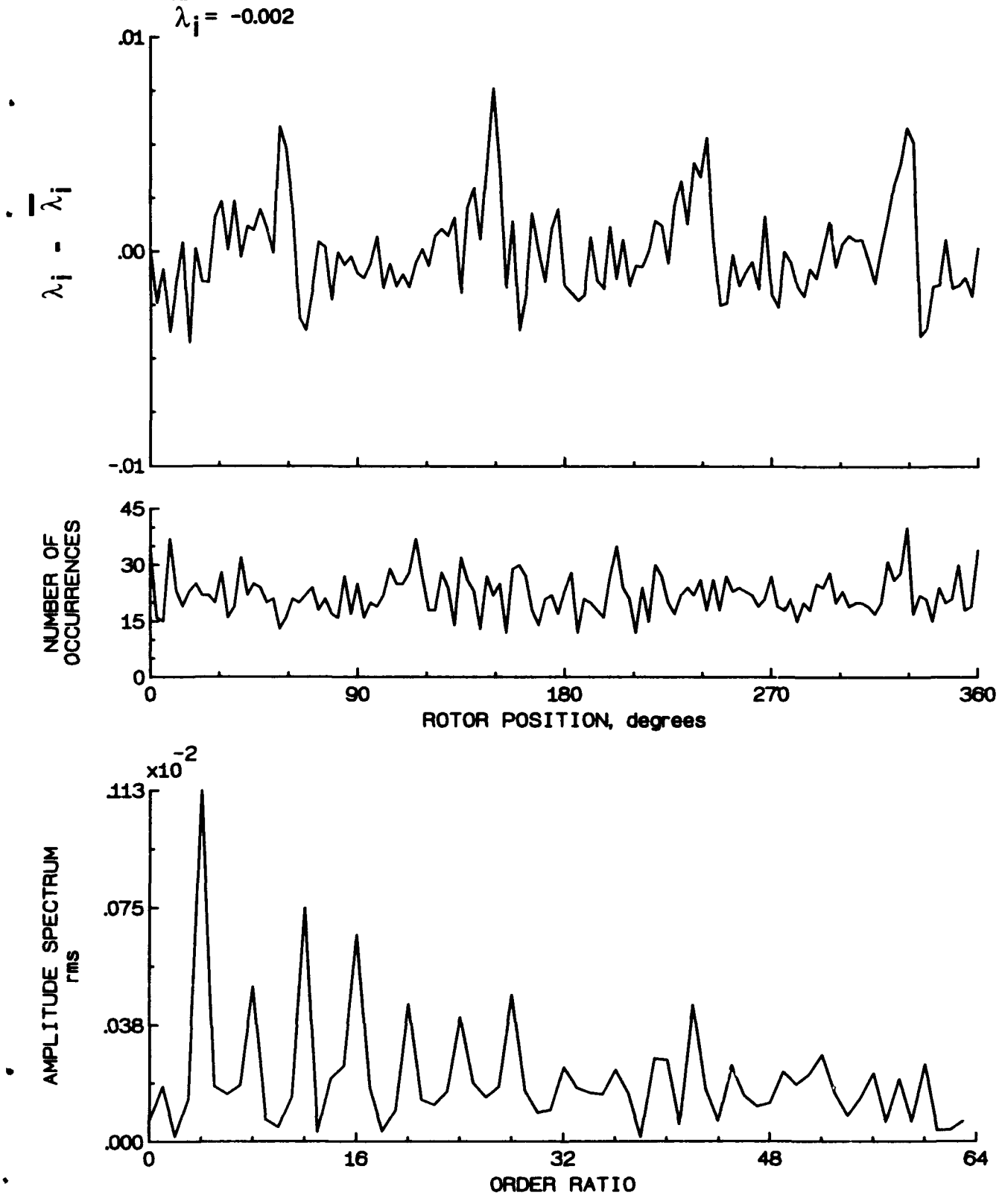

Figure 53.- Concluded.

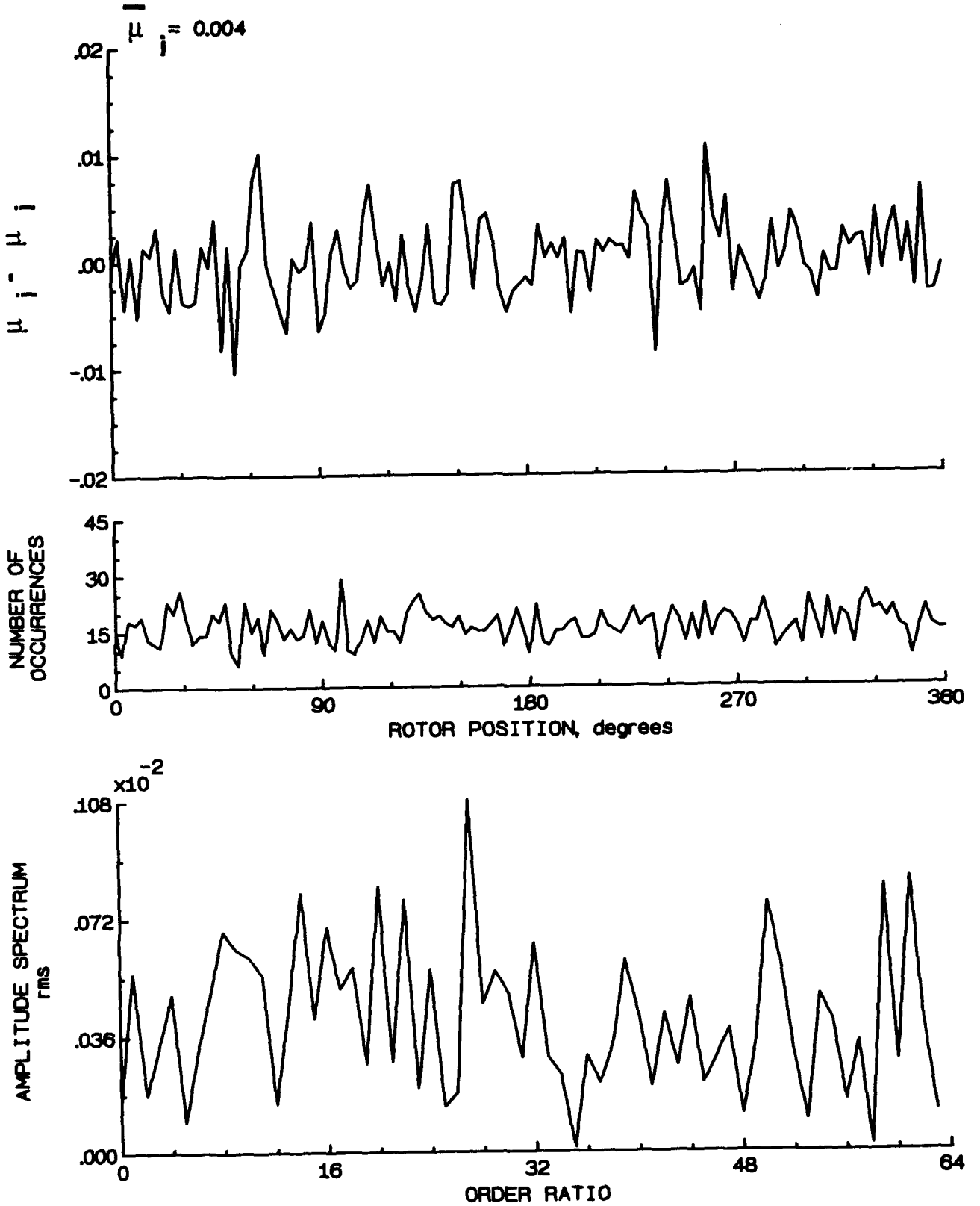

Figure 54.- Induced inflow velocity measured at 60 degrees and r/R of 1.02.

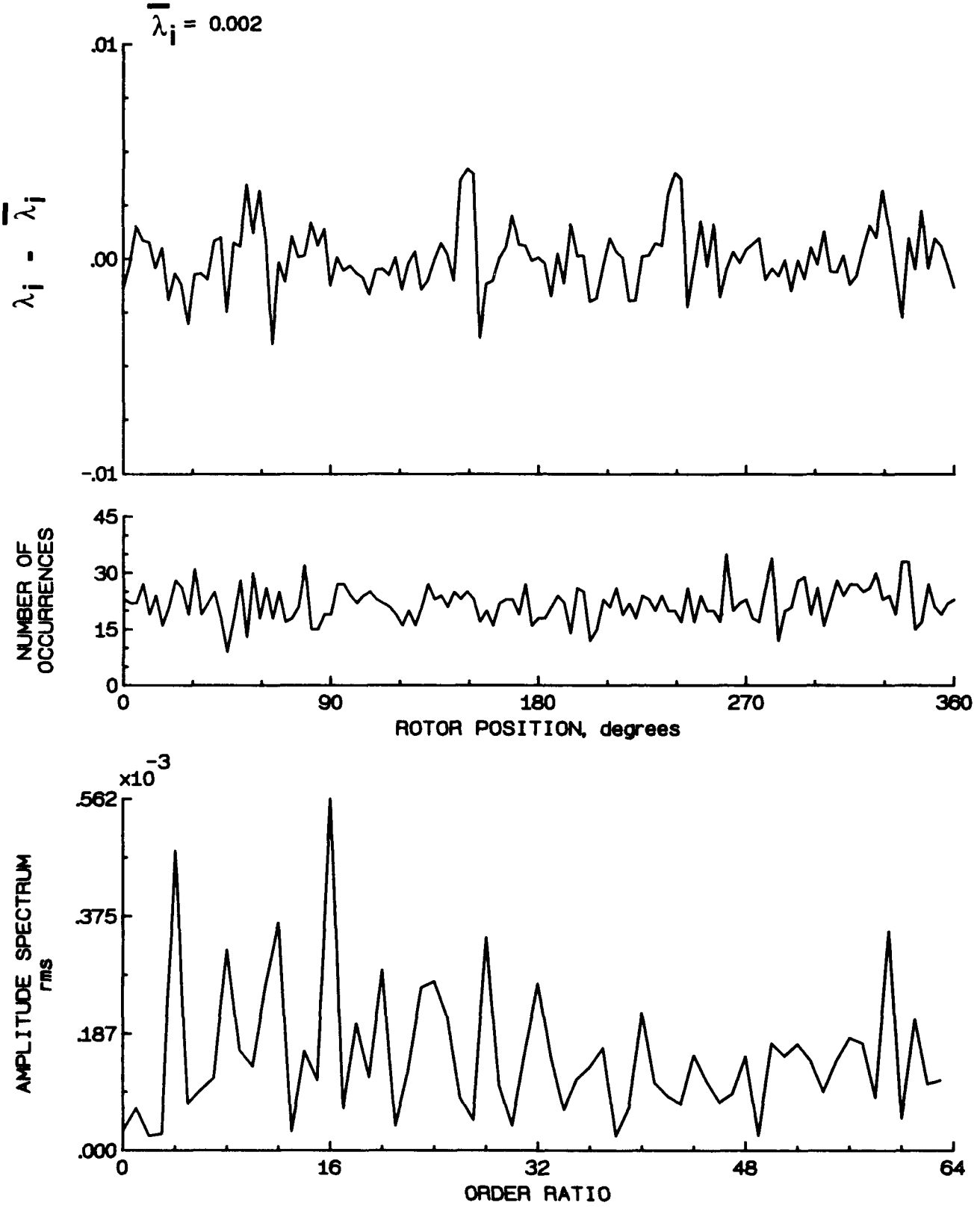

Figure 54.- Concluded.

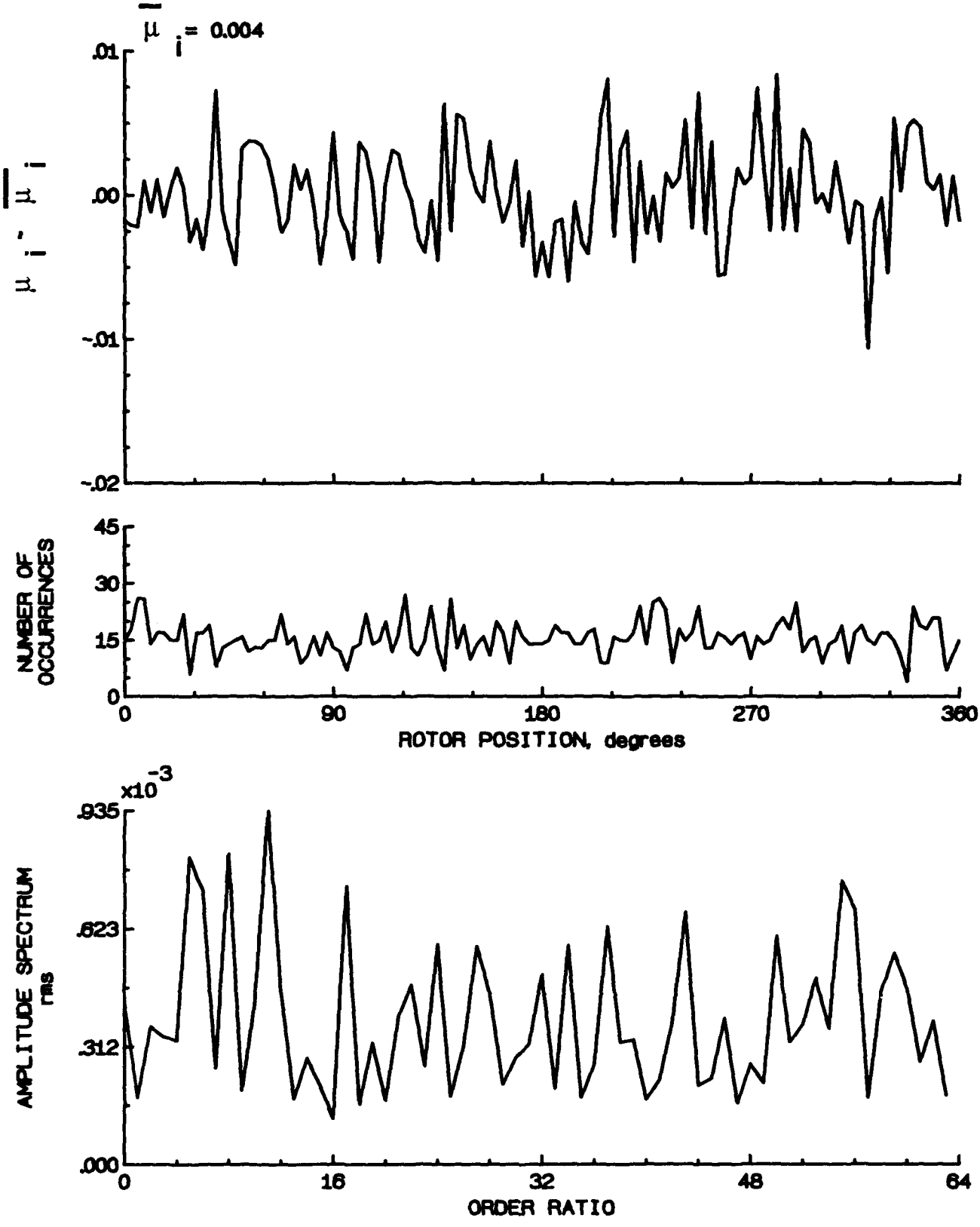

Figure 55.- Induced inflow velocity measured at 60 degrees and r/R of 1.04.

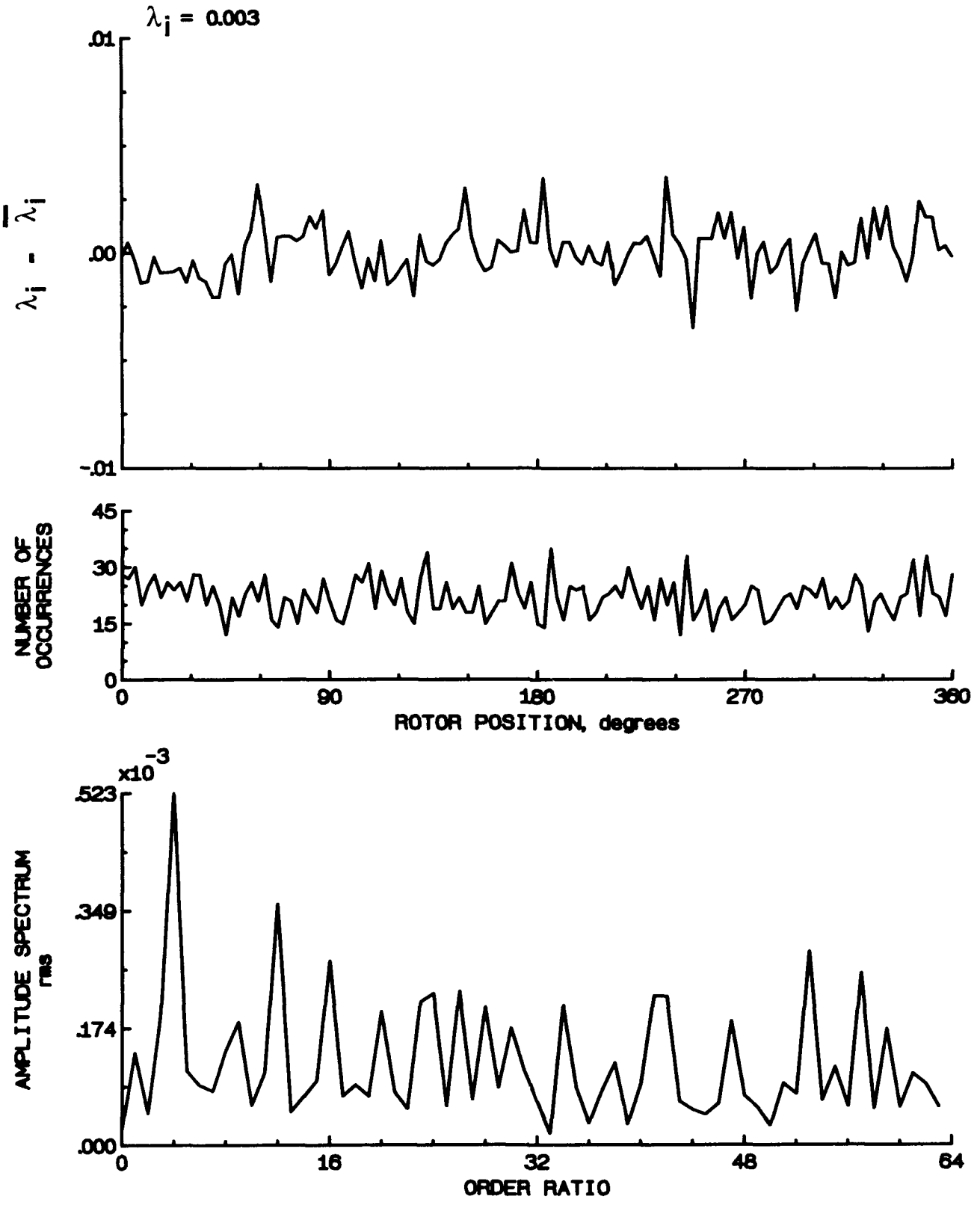

Figure 55.- Concluded.

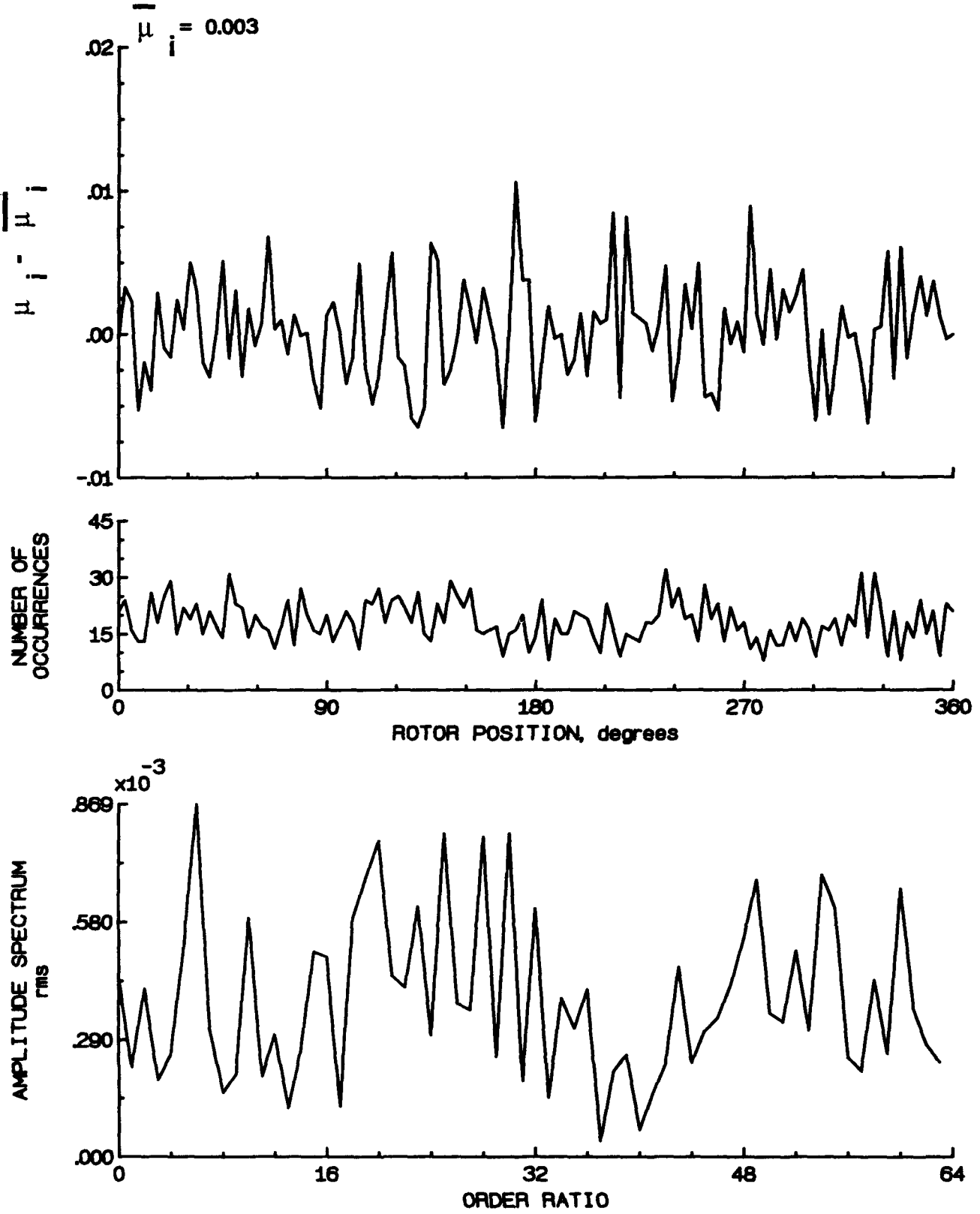

Figure 56.- Induced inflow velocity measured at 60 degrees and r/R of 1.10.

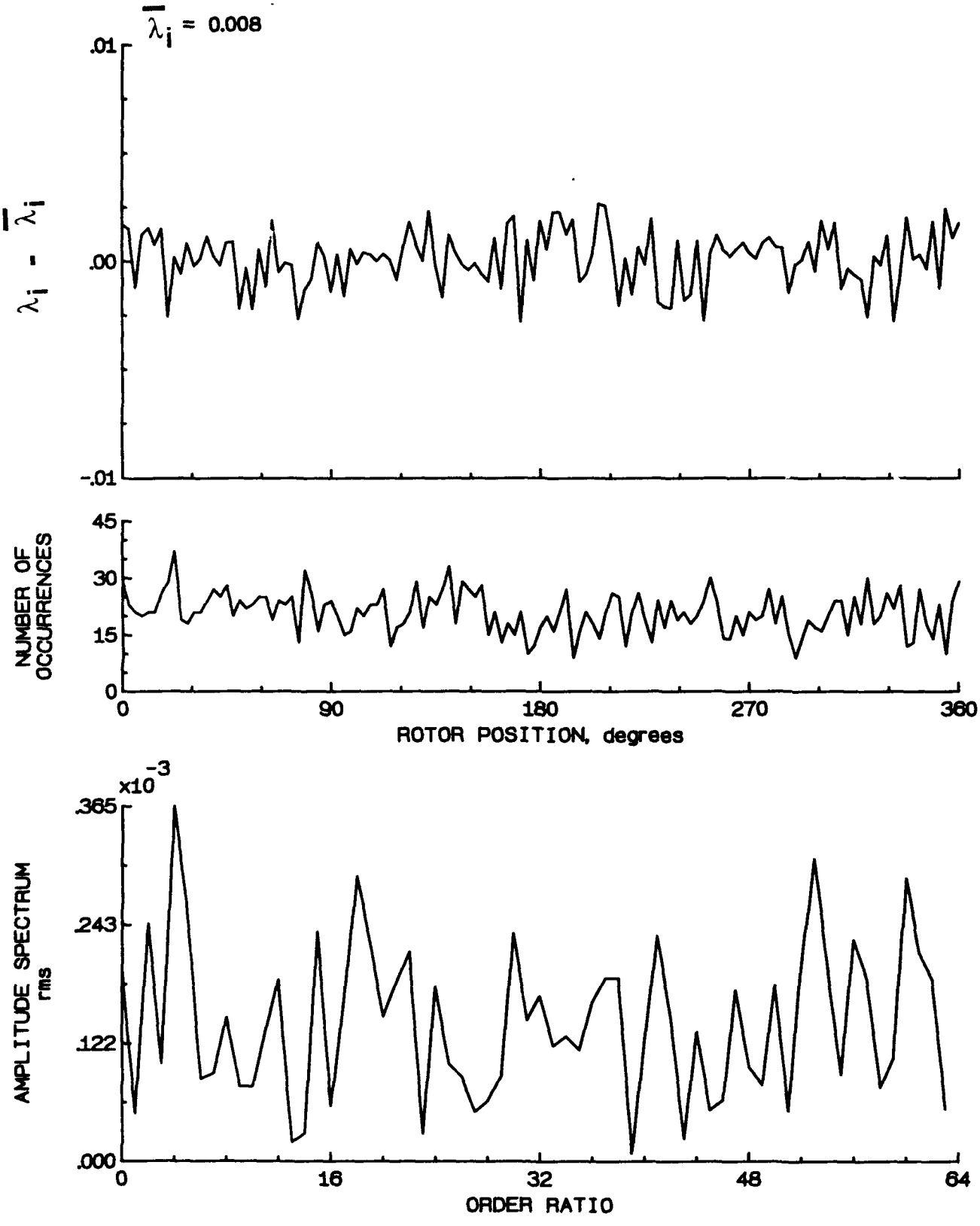

Figure 56.- Concluded.

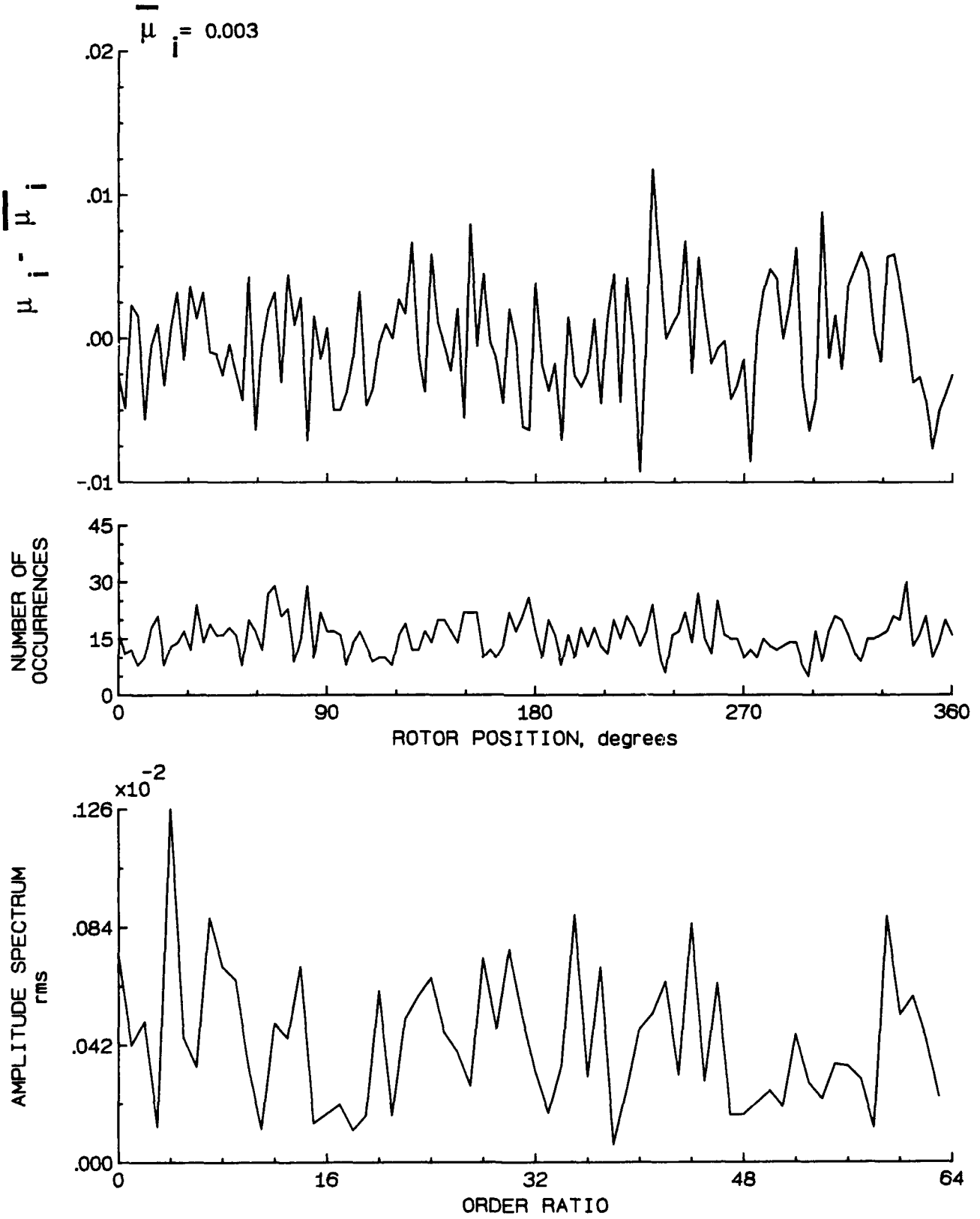

Figure 57.- Induced inflow velocity measured at 90 degrees and r/R of 0.20.

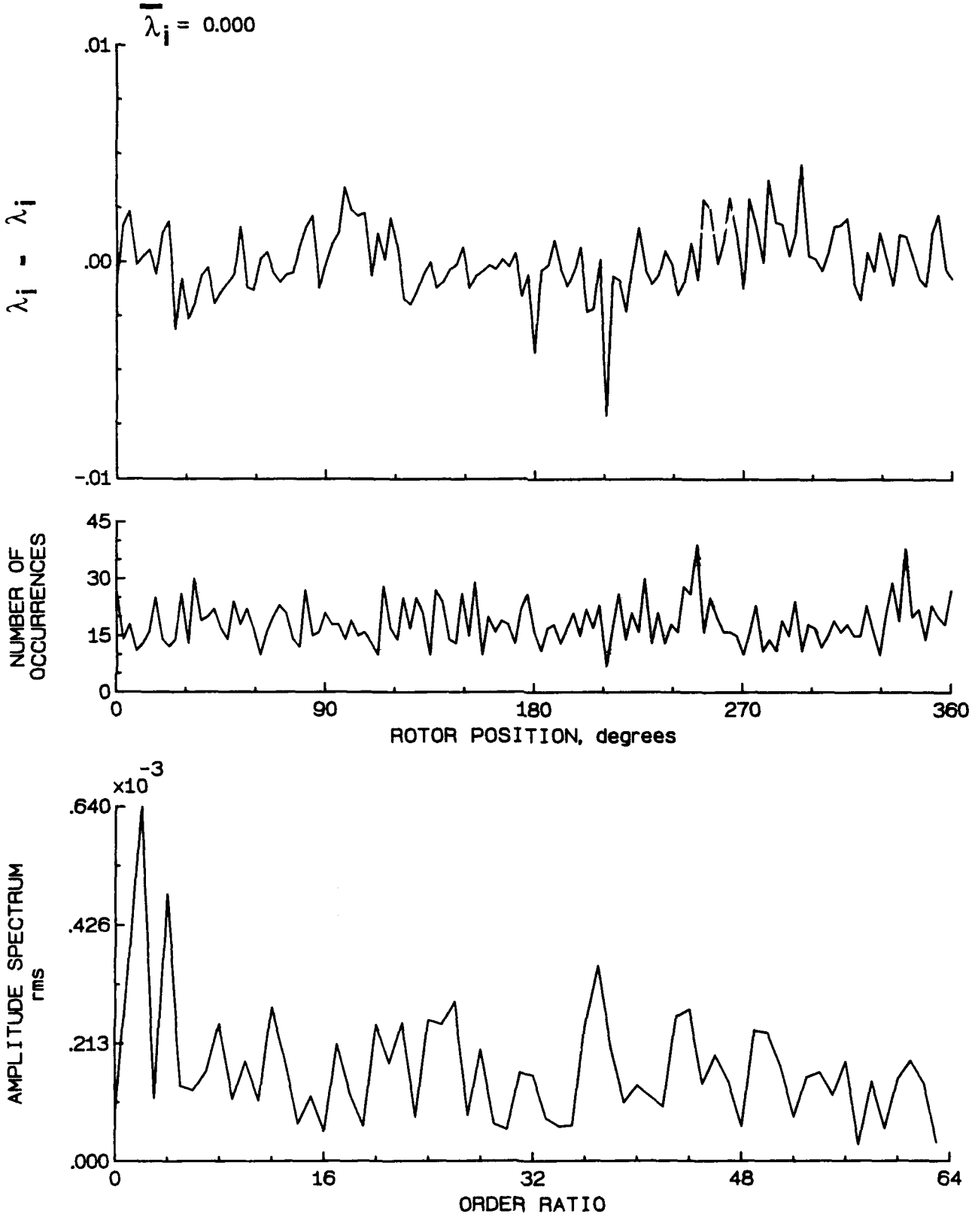

Figure 57.- Concluded.

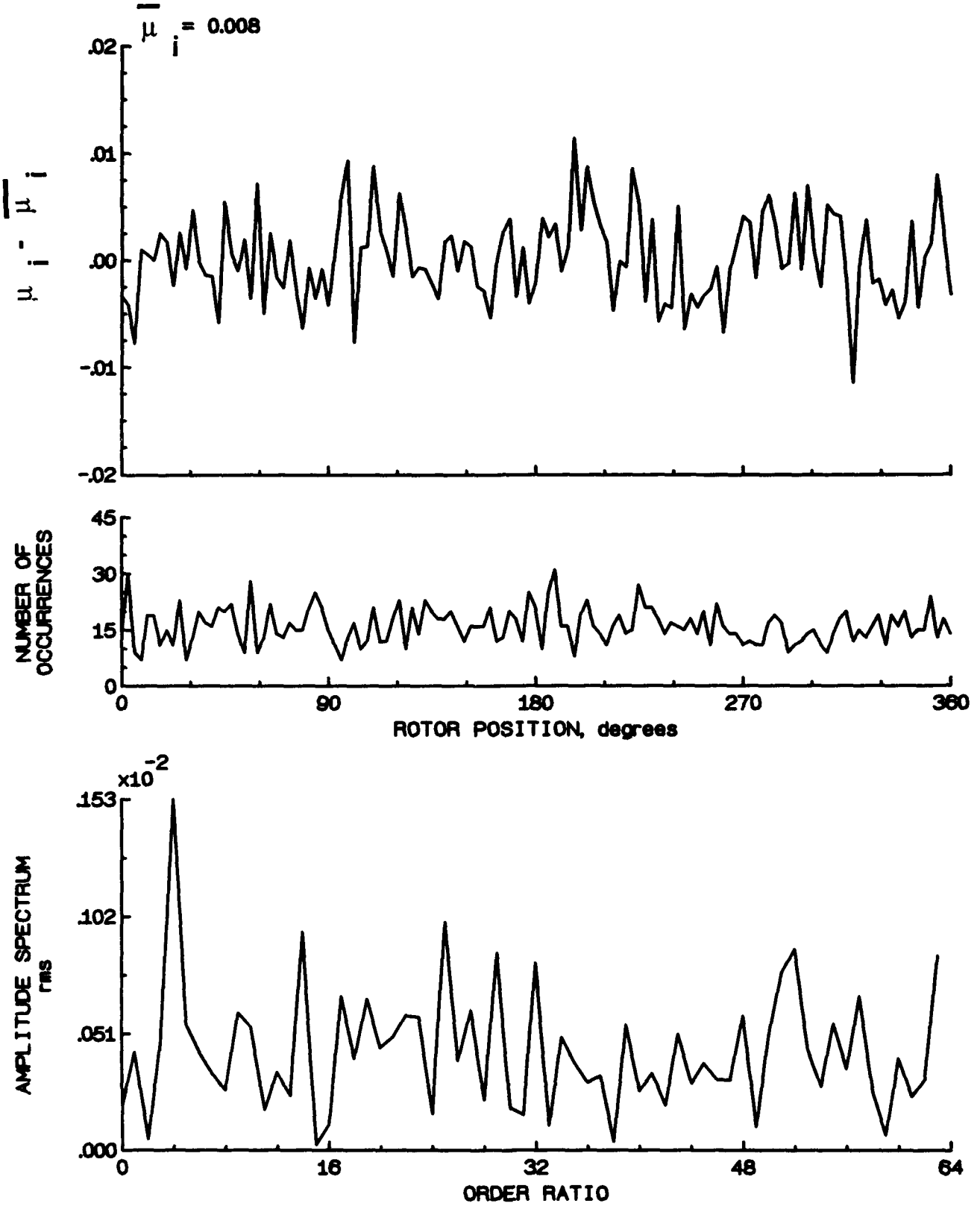

Figure 58.- Induced inflow velocity measured at 90 degrees and r/R of 0.40.

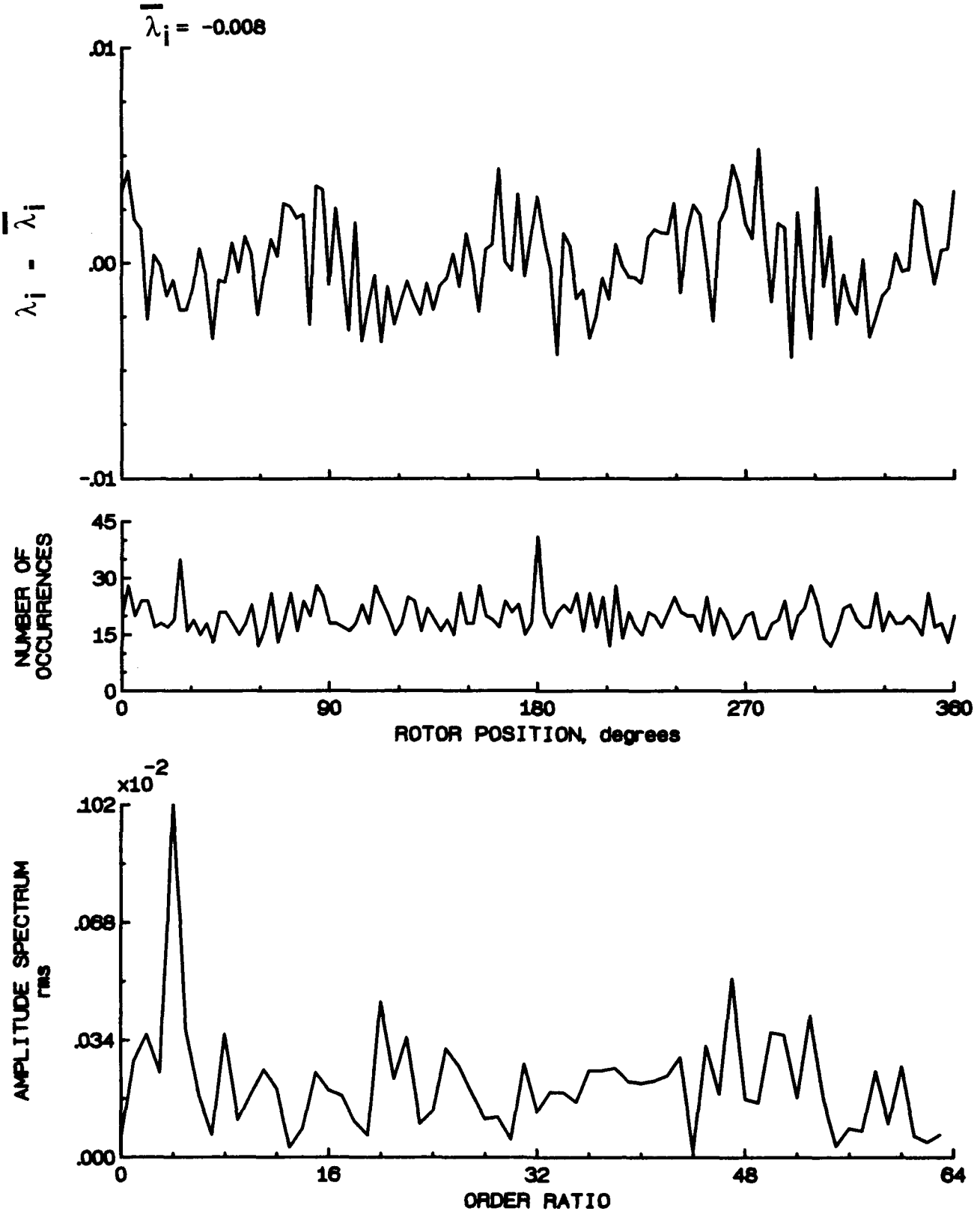

Figure 58.- Concluded.

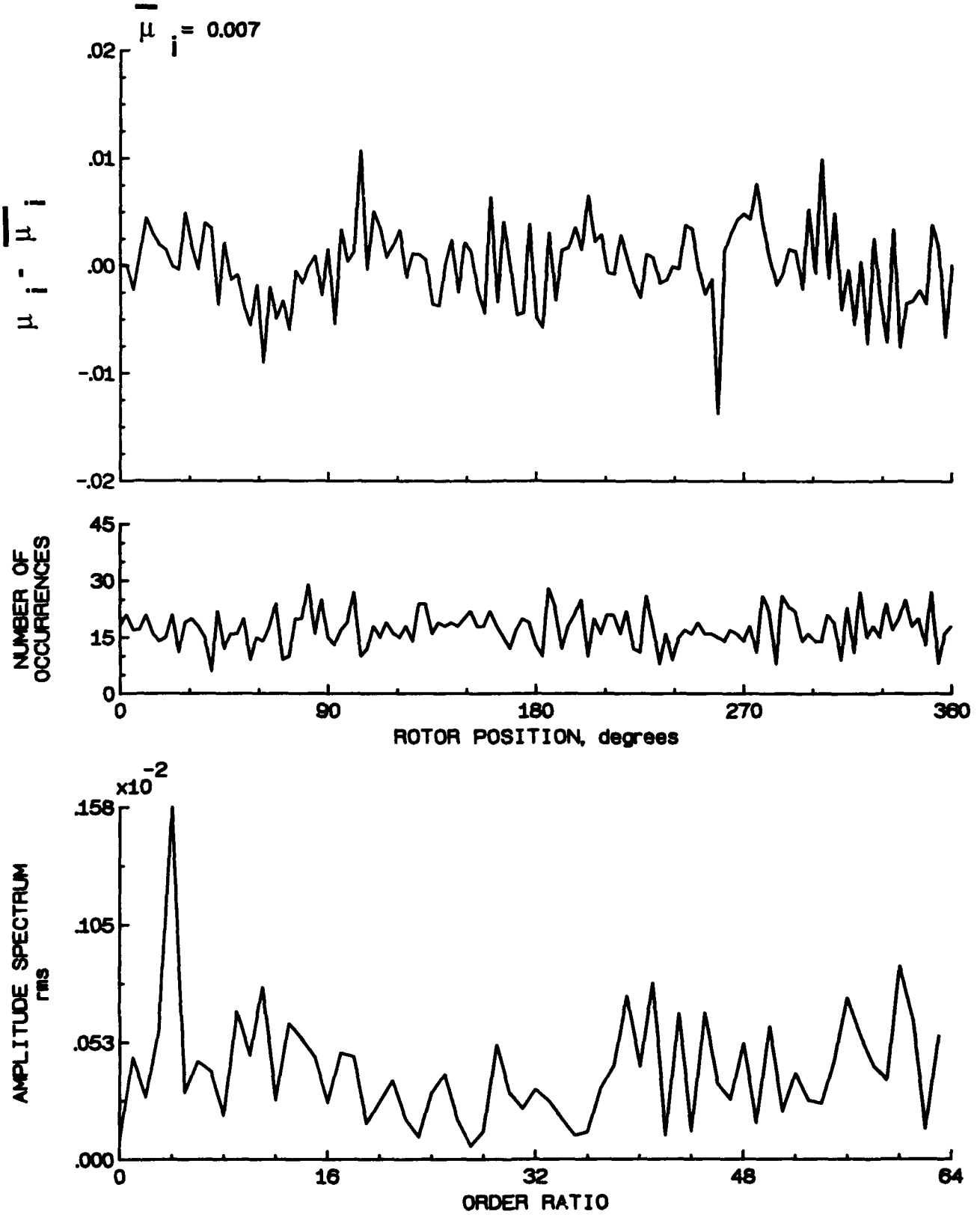

Figure 59.- Induced inflow velocity measured at 90 degrees and r/R of 0.50.

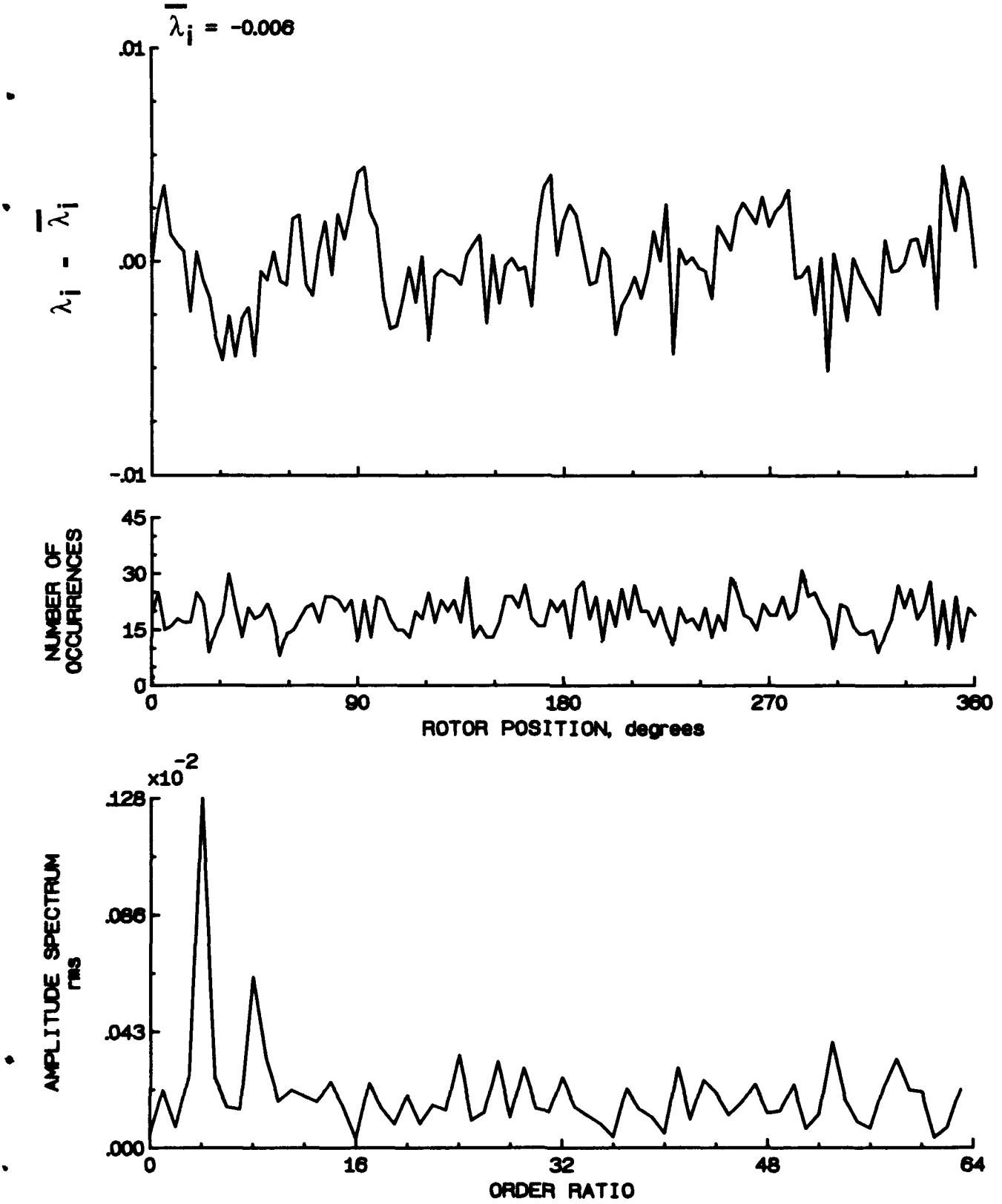

Figure 59.- Concluded.

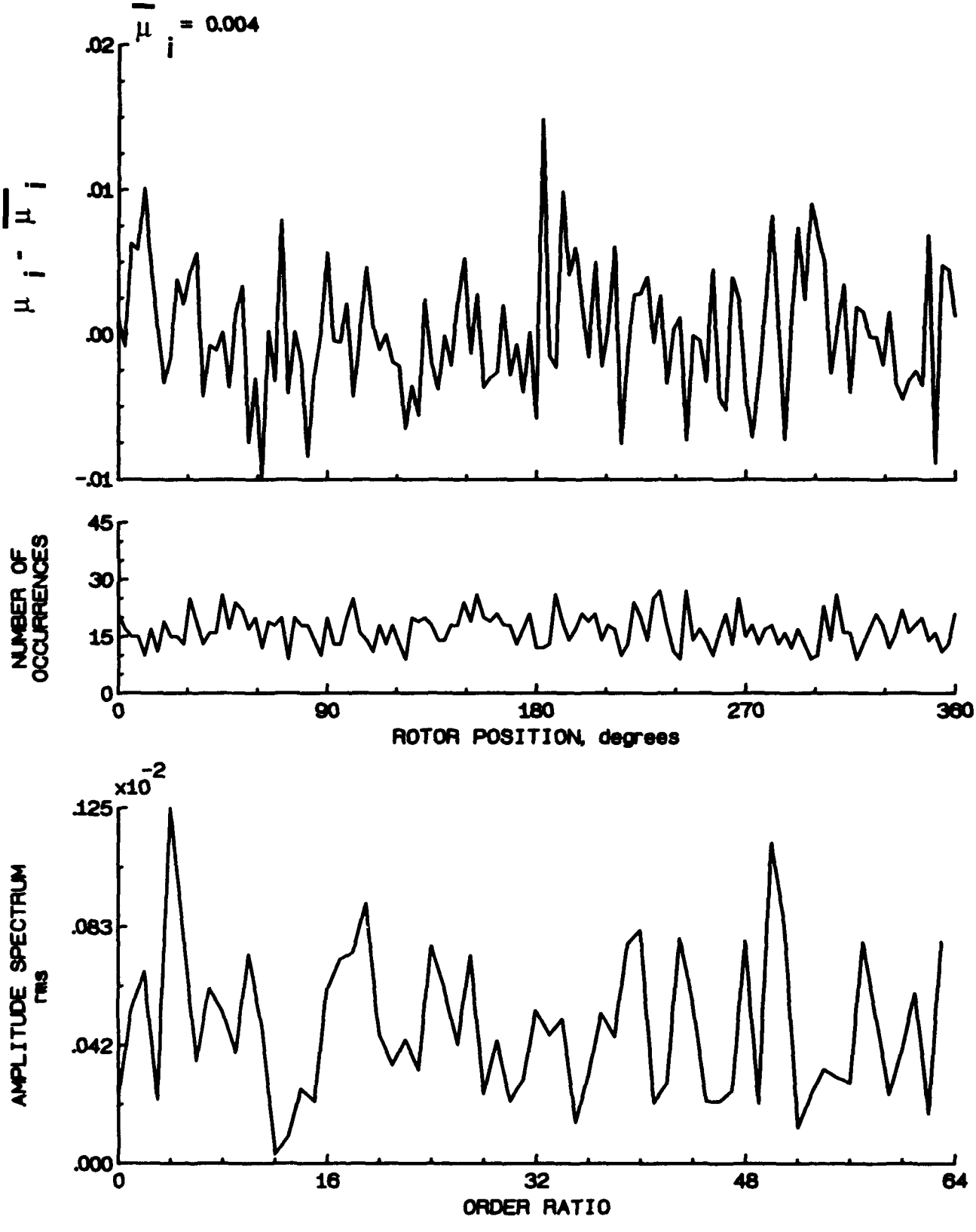

Figure 60.- Induced inflow velocity measured at 90 degrees and r/R of 0.60.

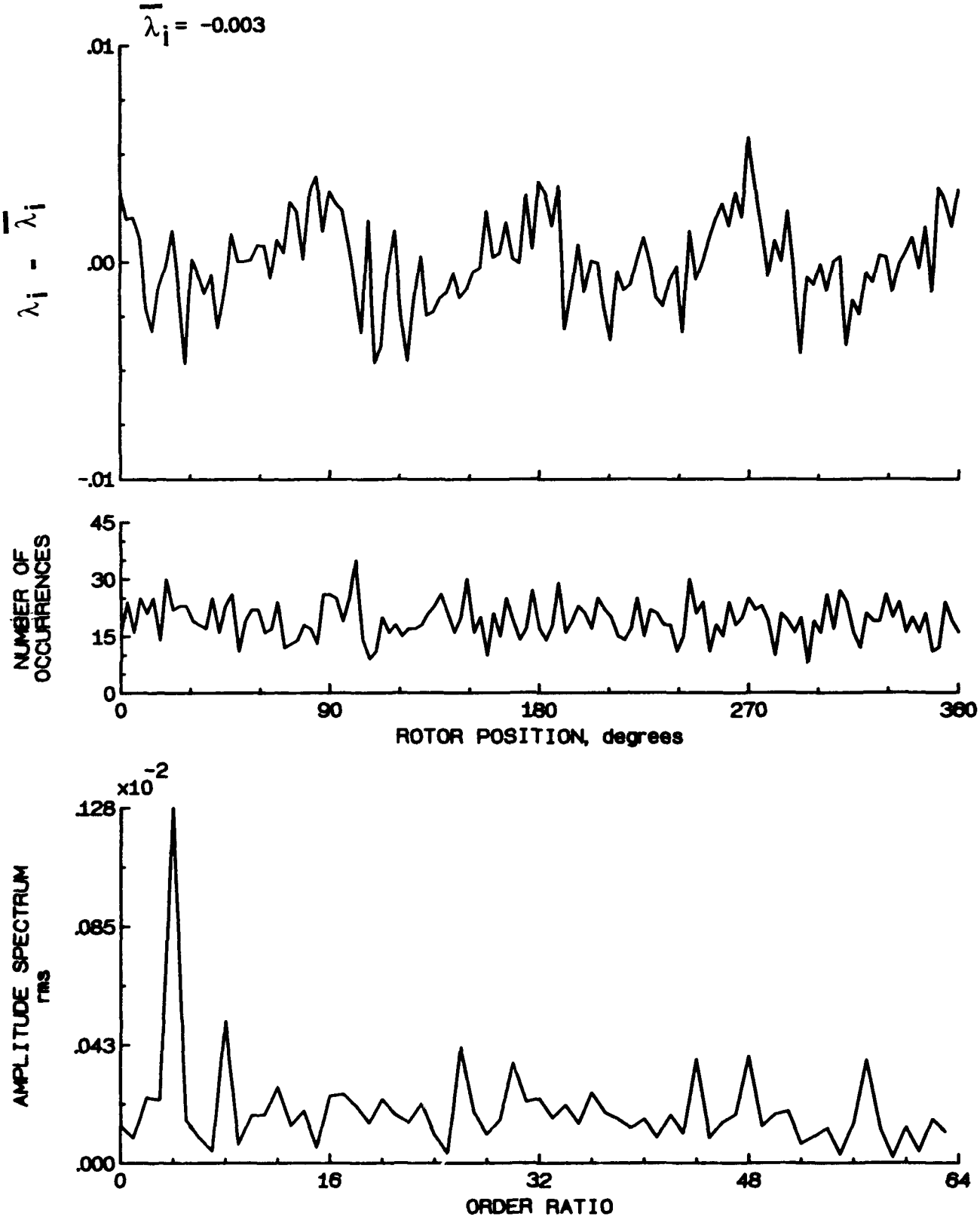

Figure 60.- Concluded.

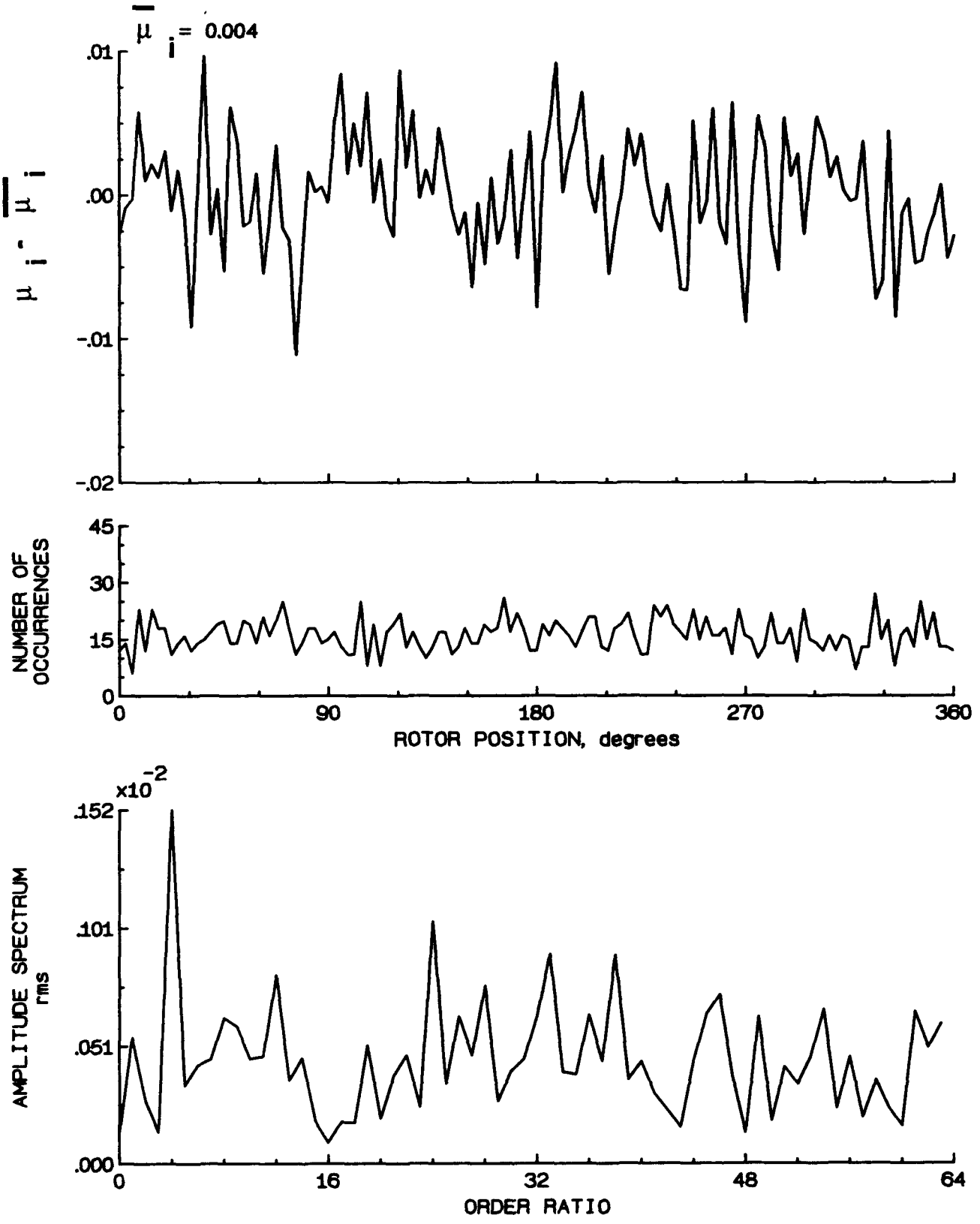

Figure 61.- Induced inflow velocity measured at 90 degrees and r/R of 0.70.

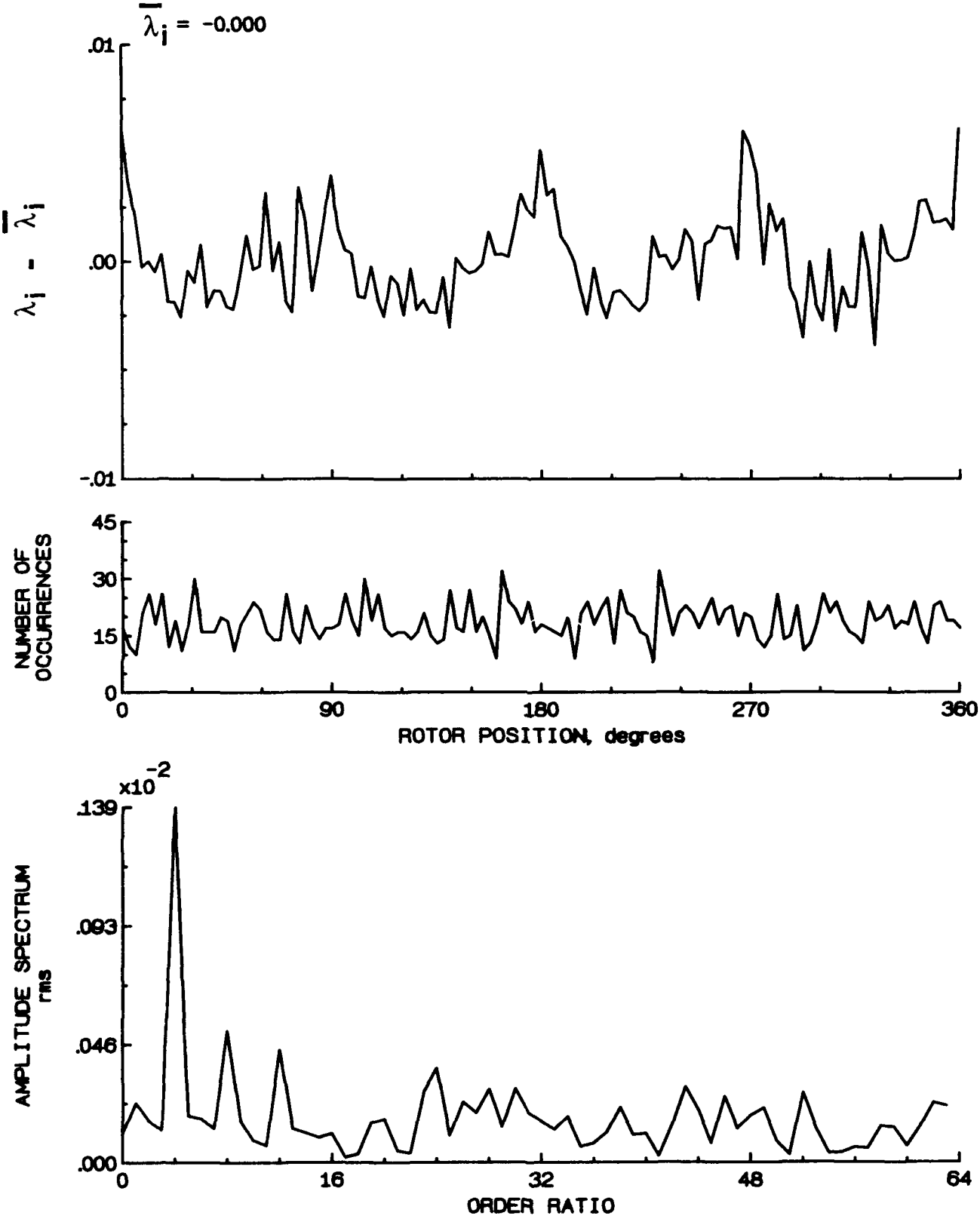

Figure 61.- Concluded.

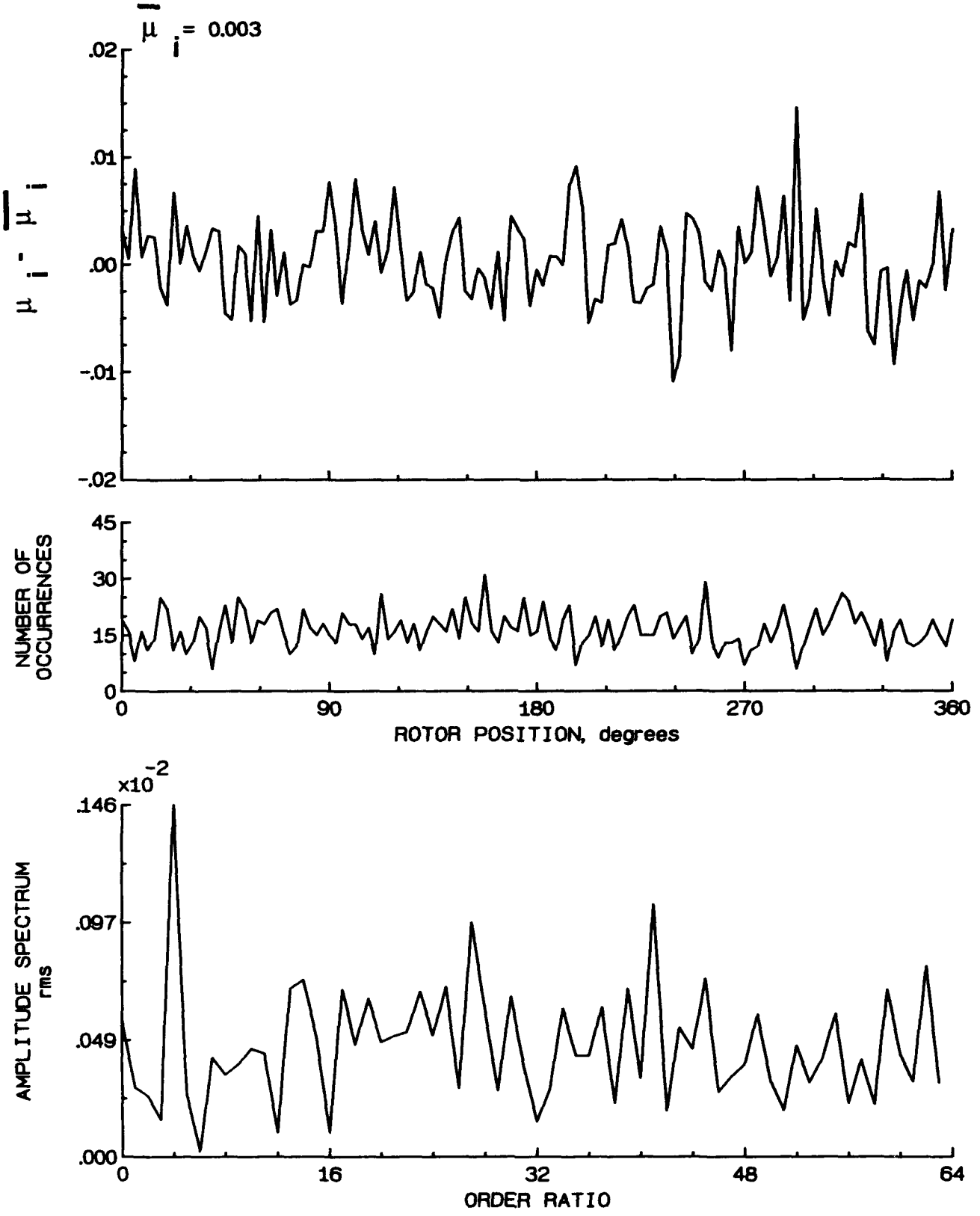

Figure 62.- Induced inflow velocity measured at 90 degrees and r/R of 0.74.

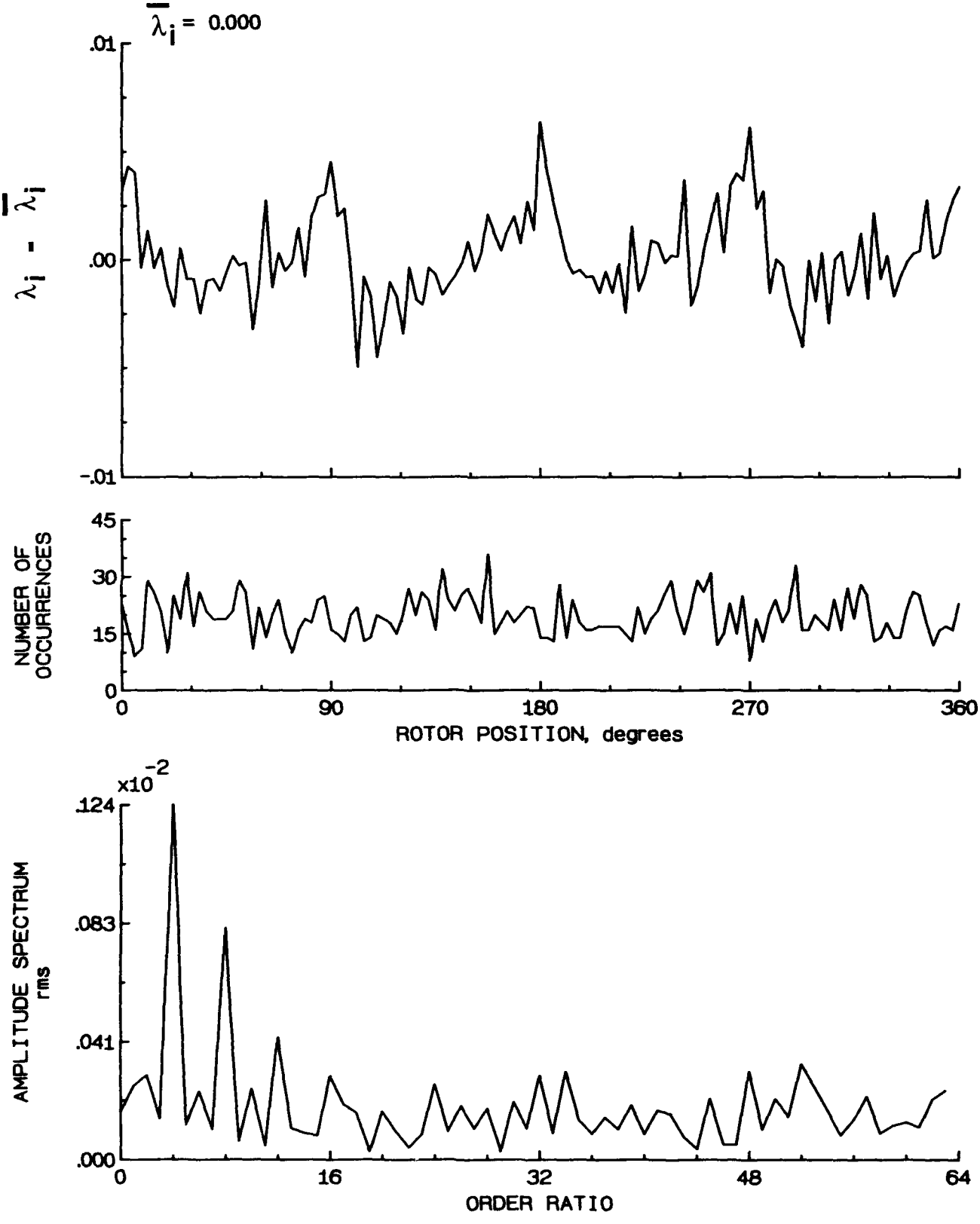

Figure 62.- Concluded.

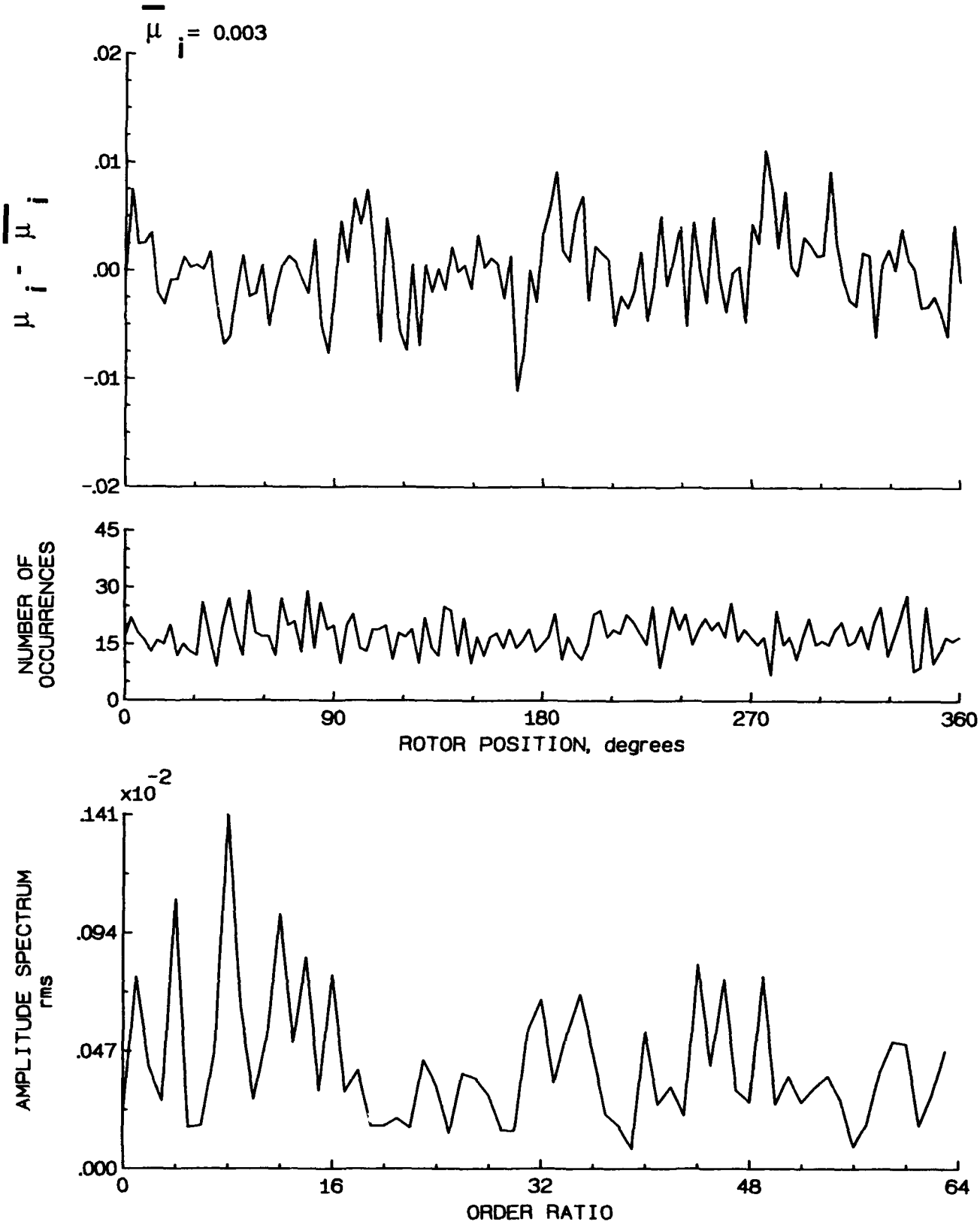

Figure 63.- Induced inflow velocity measured at 90 degrees and r/R of 0.78.

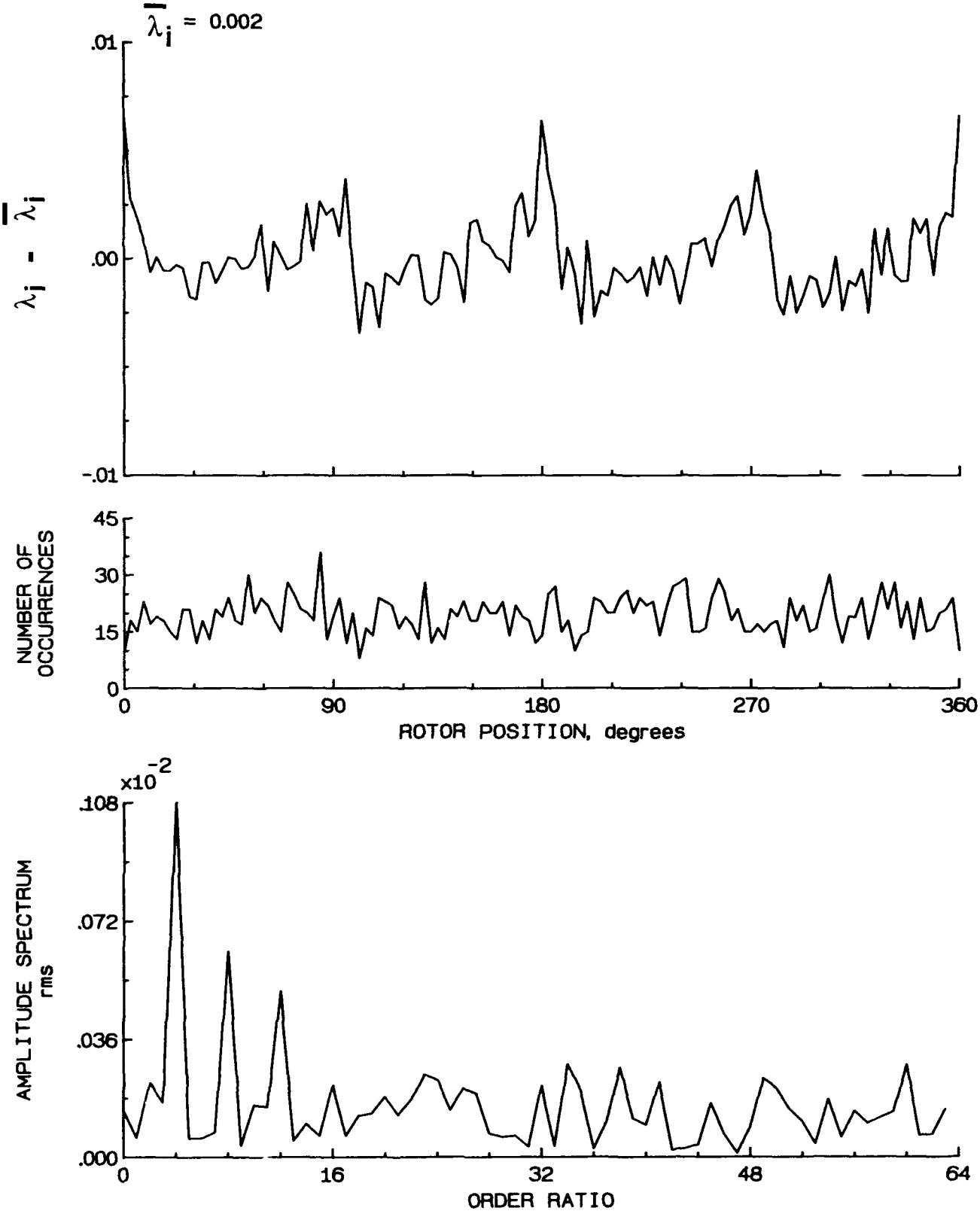

Figure 63.- Concluded.

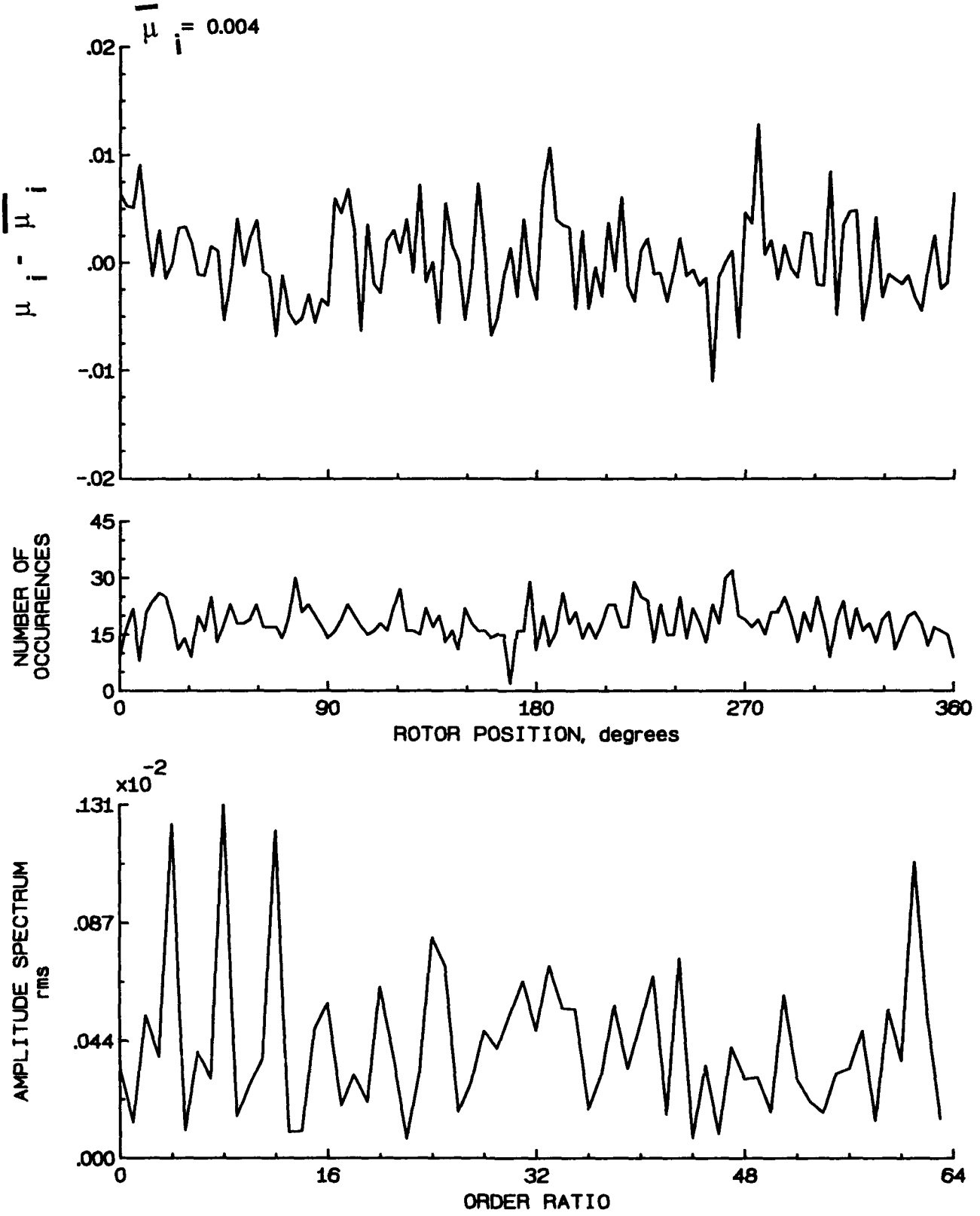

Figure 64.- Induced inflow velocity measured at 90 degrees and r/R of 0.82.

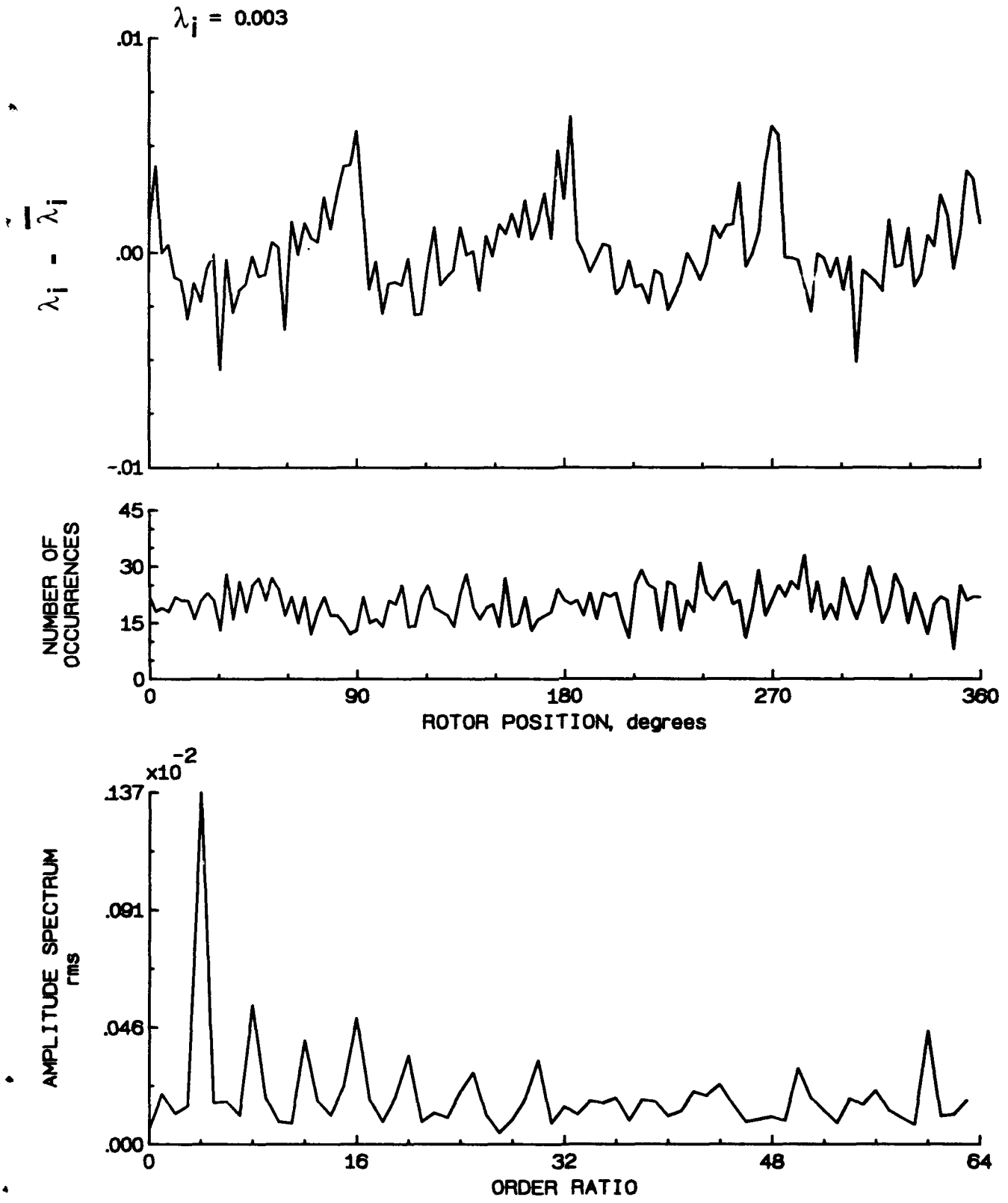

Figure 64.- Concluded.

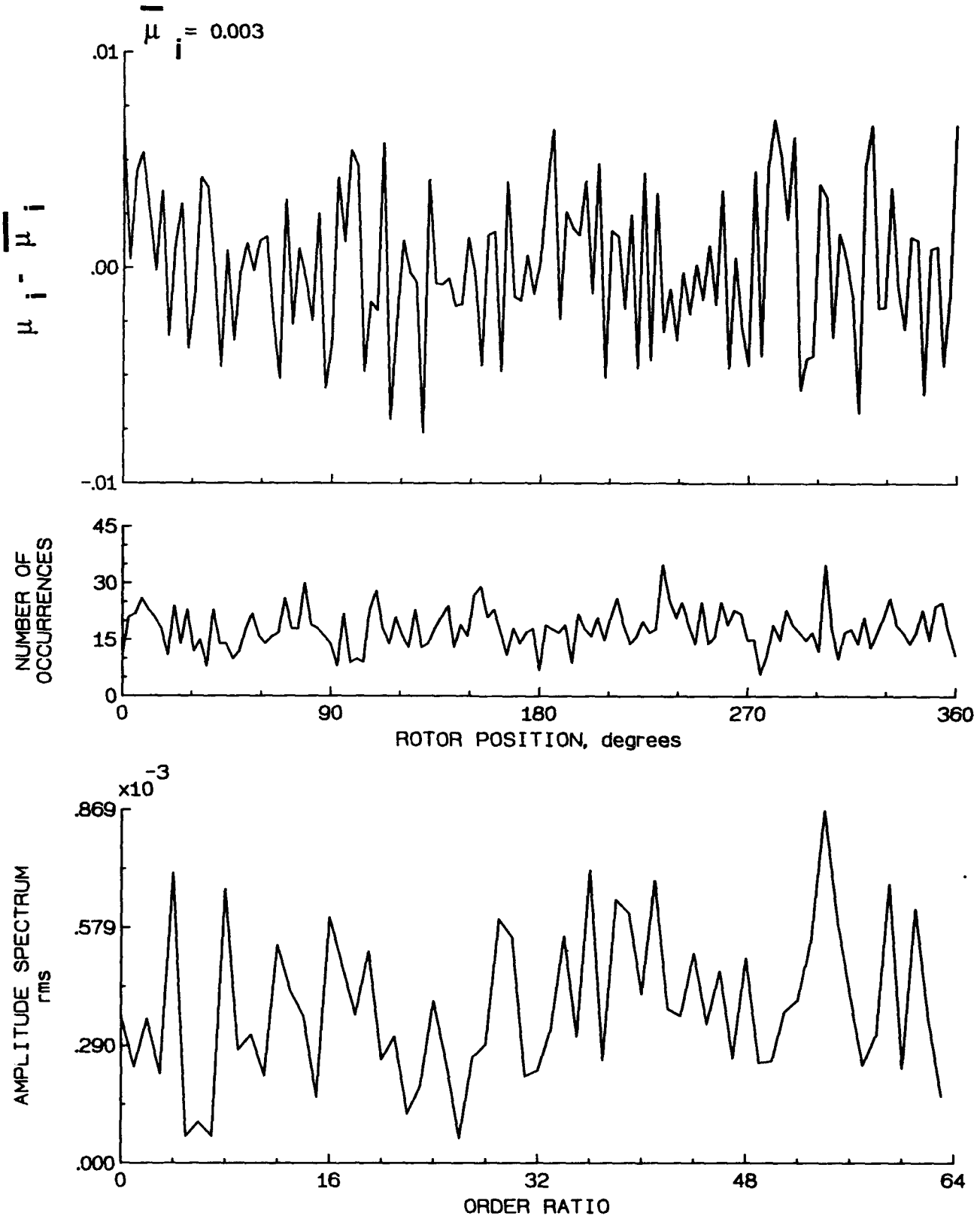

Figure 65.- Induced inflow velocity measured at 90 degrees and r/R of 0.86.

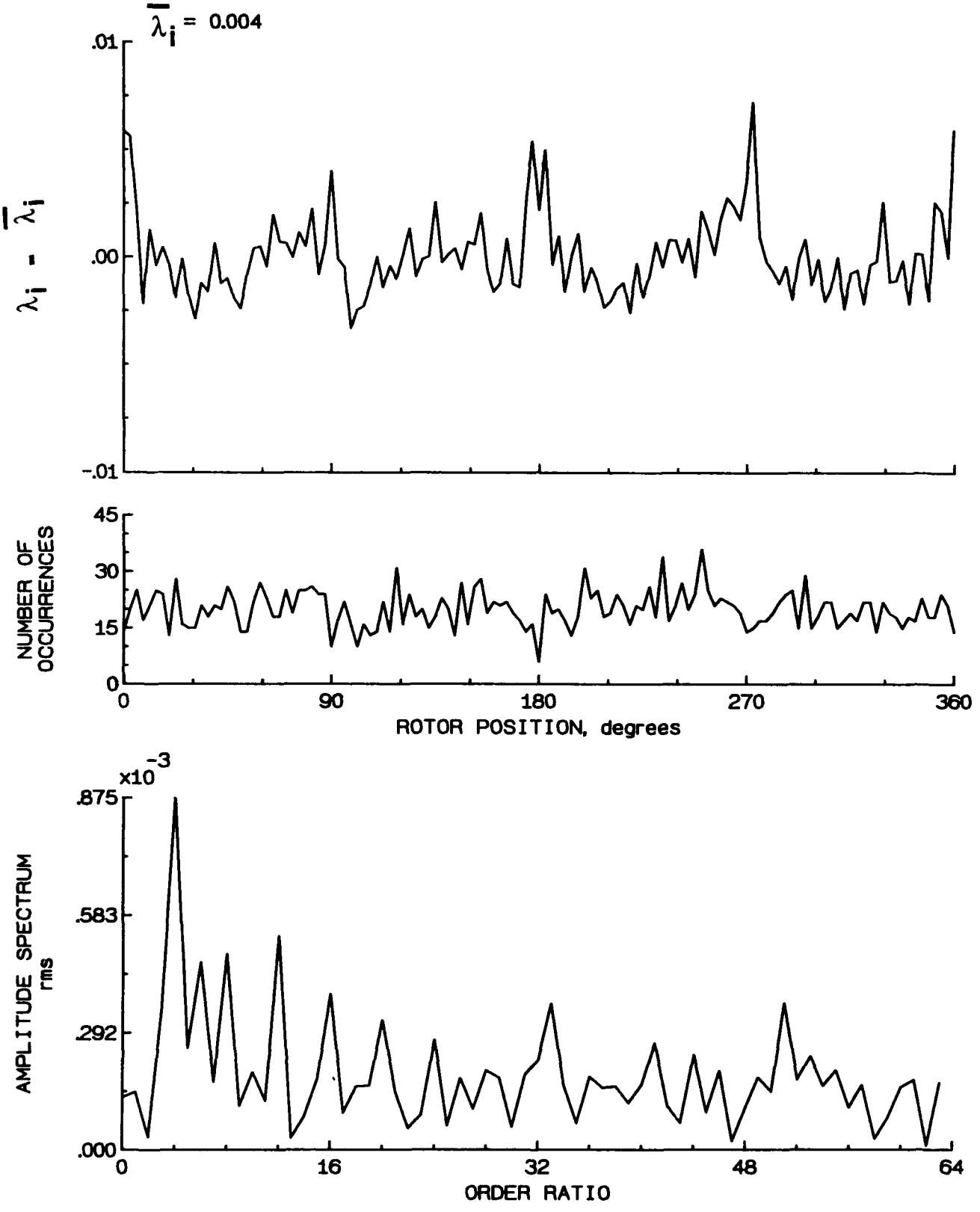

Figure 65.- Concluded.

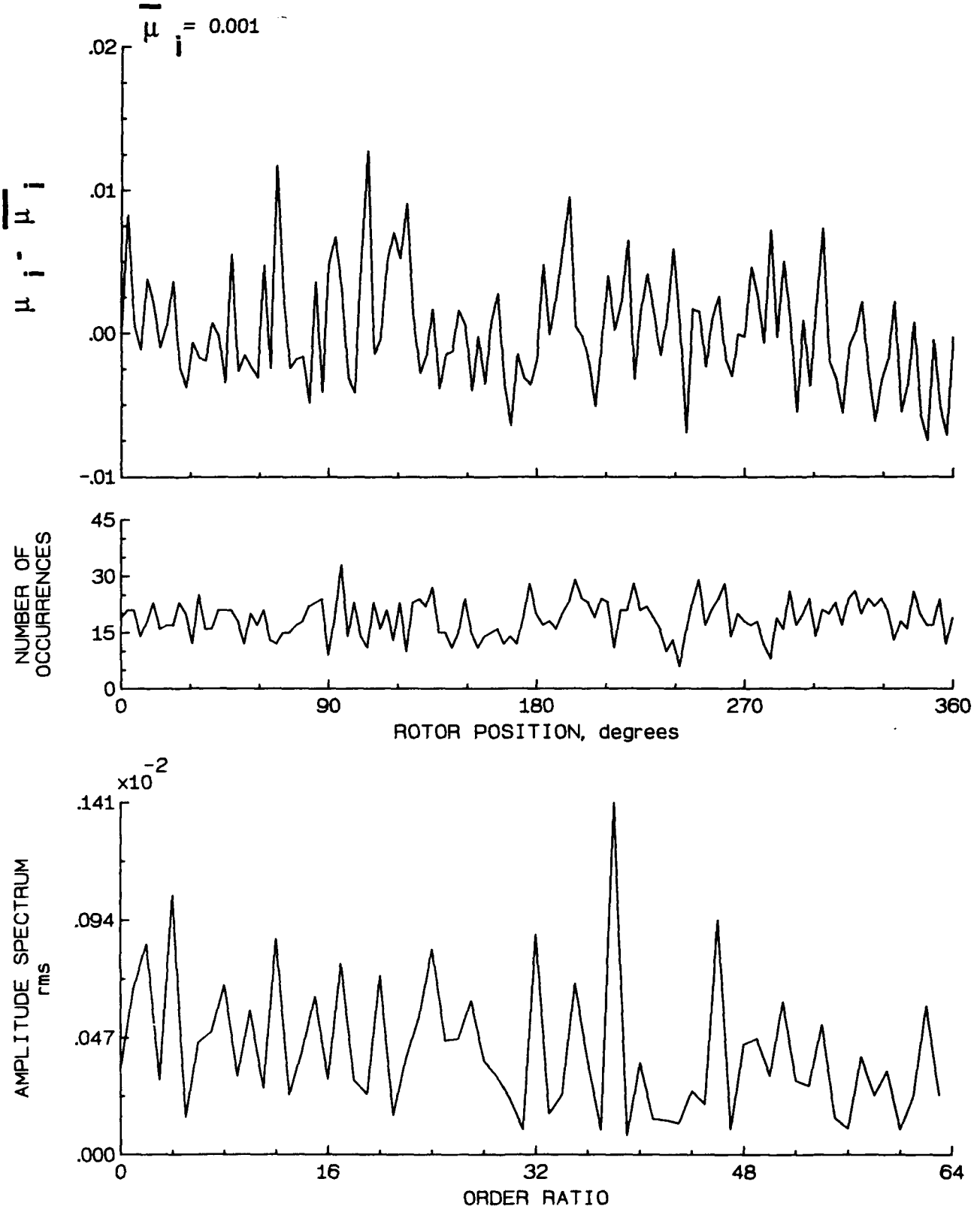

Figure 66.- Induced inflow velocity measured at 90 degrees and r/R of 0.90.

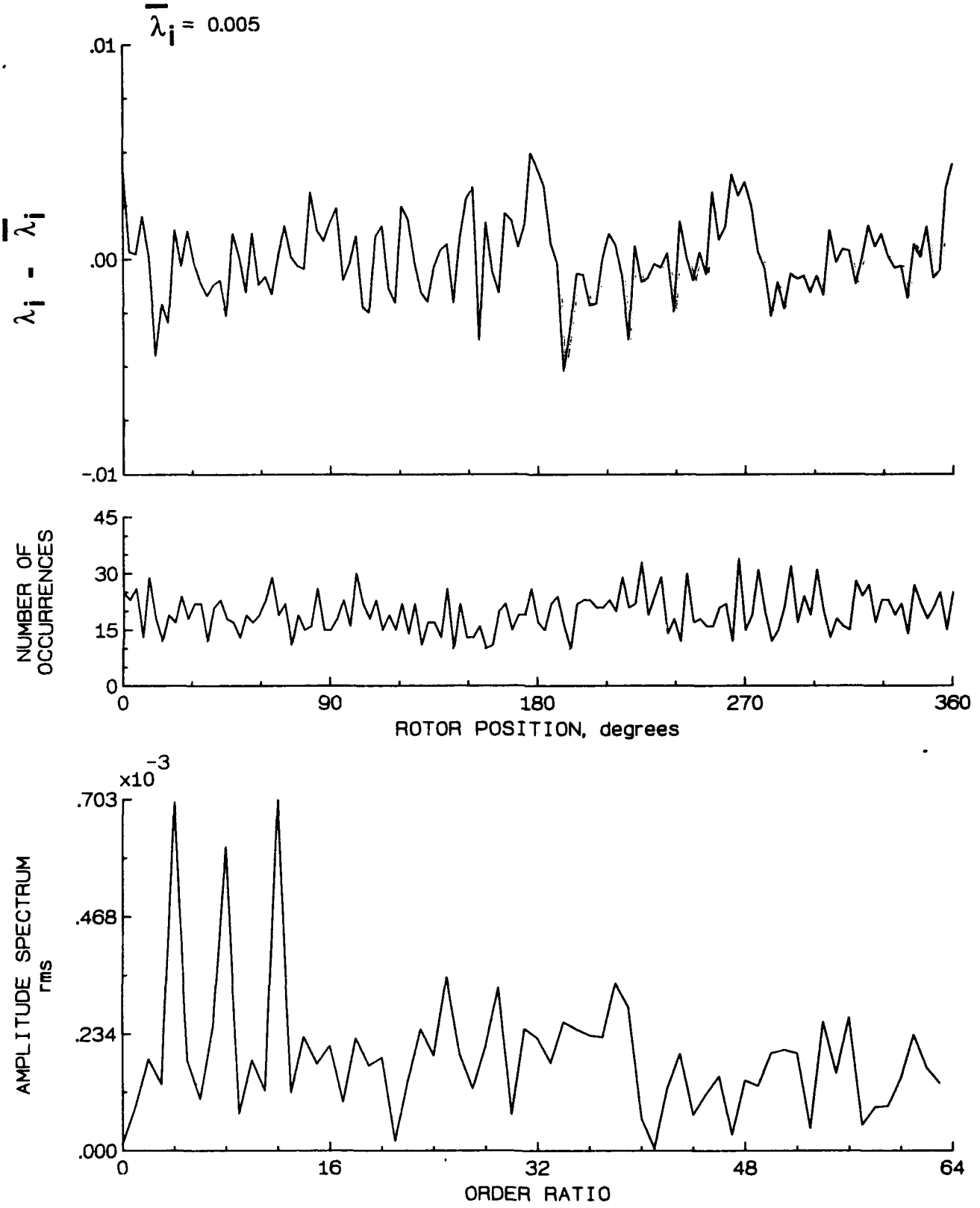

Figure 66.- Concluded.

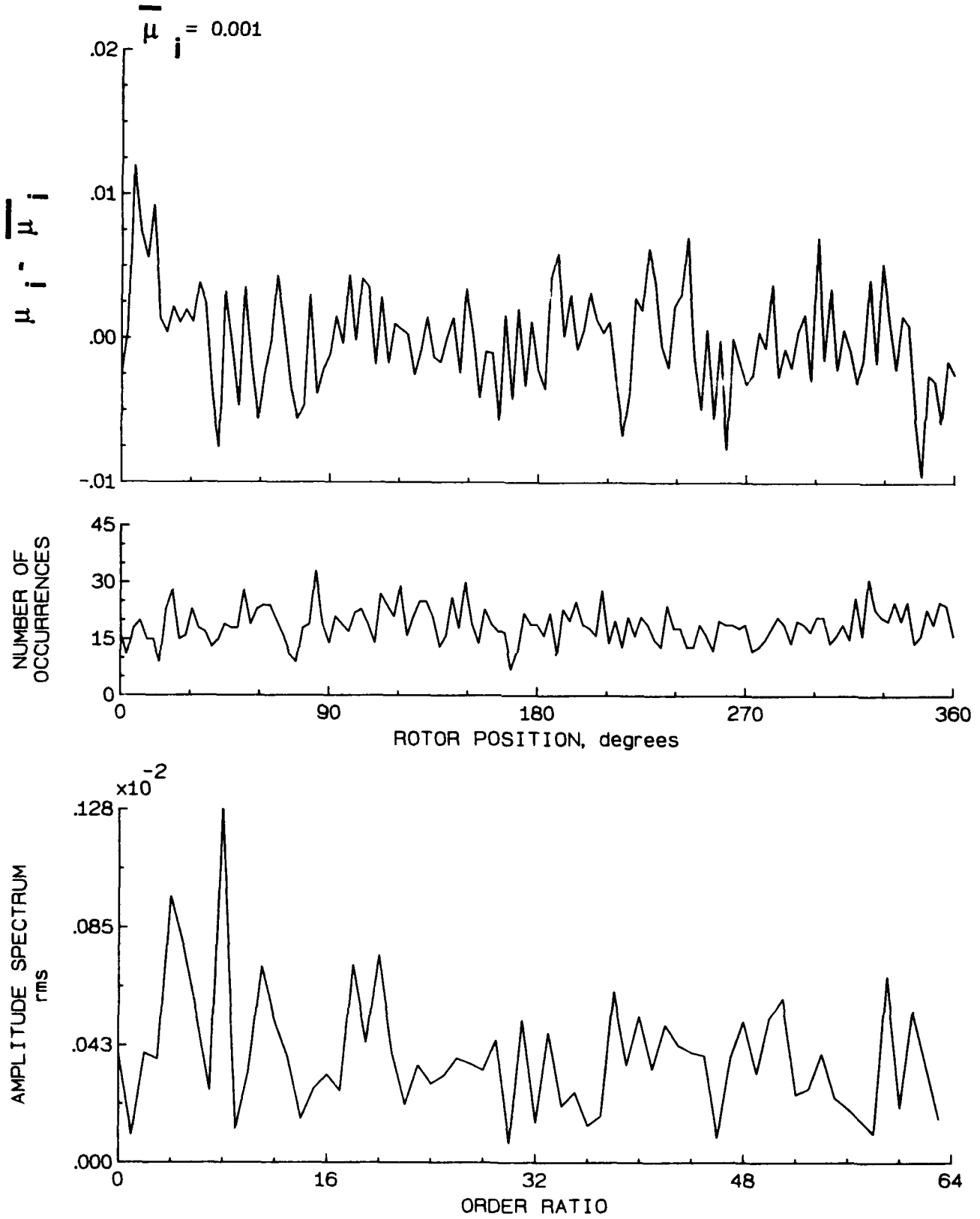

Figure 67.- Induced inflow velocity measured at 90 degrees and r/R of 0.94.

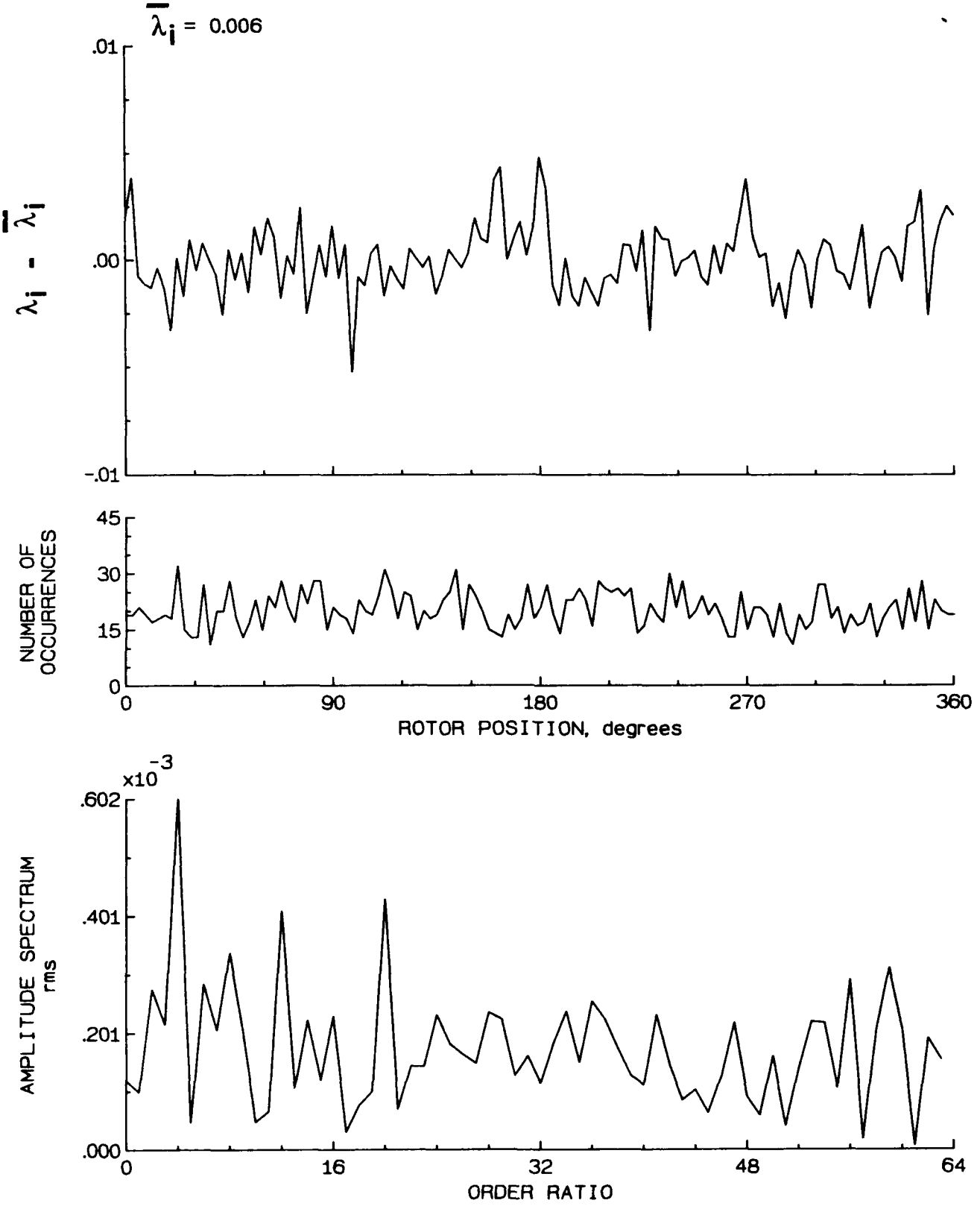

Figure 67.- Concluded.

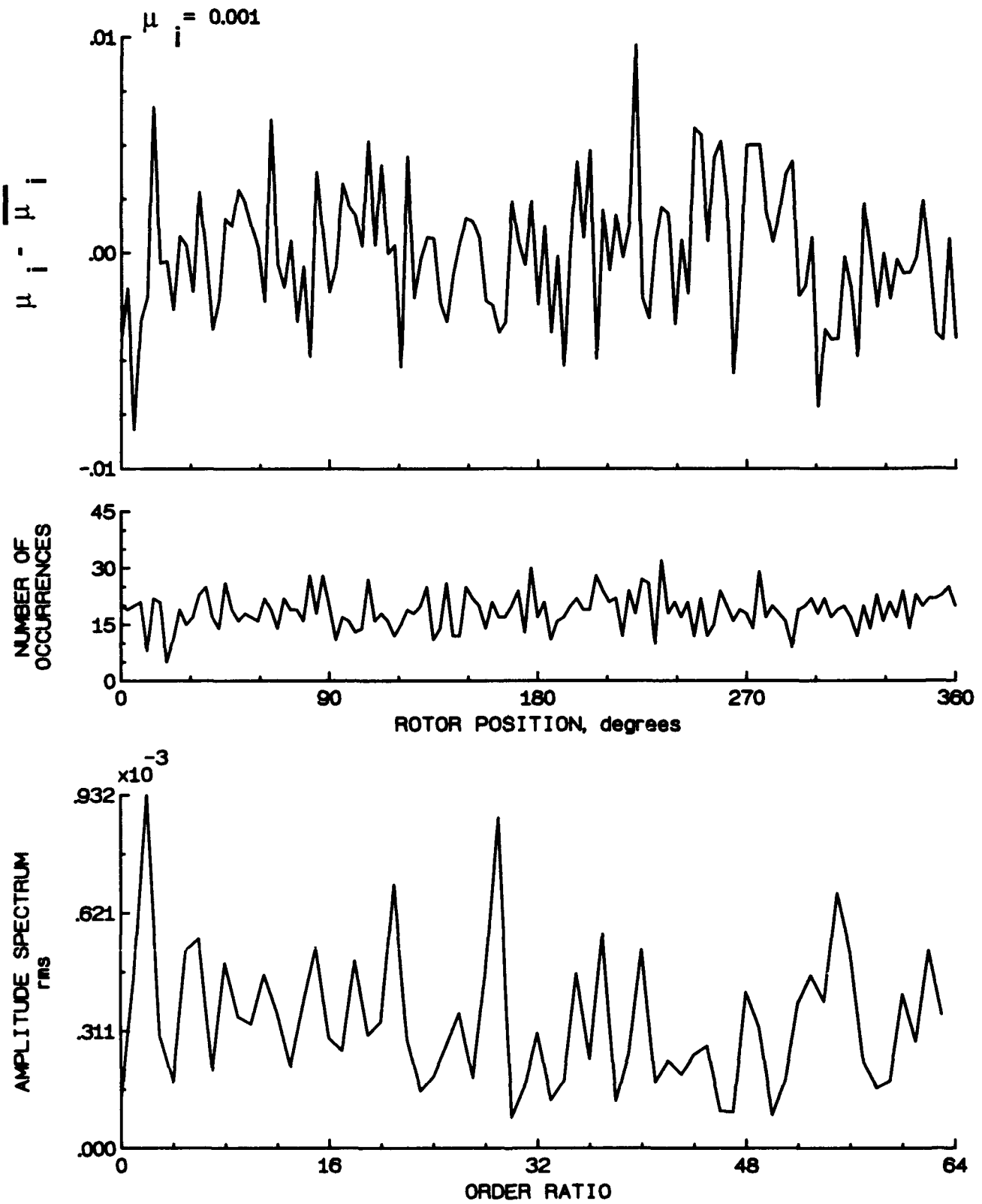

Figure 68.- Induced inflow velocity measured at 90 degrees and r/R of 0.98.

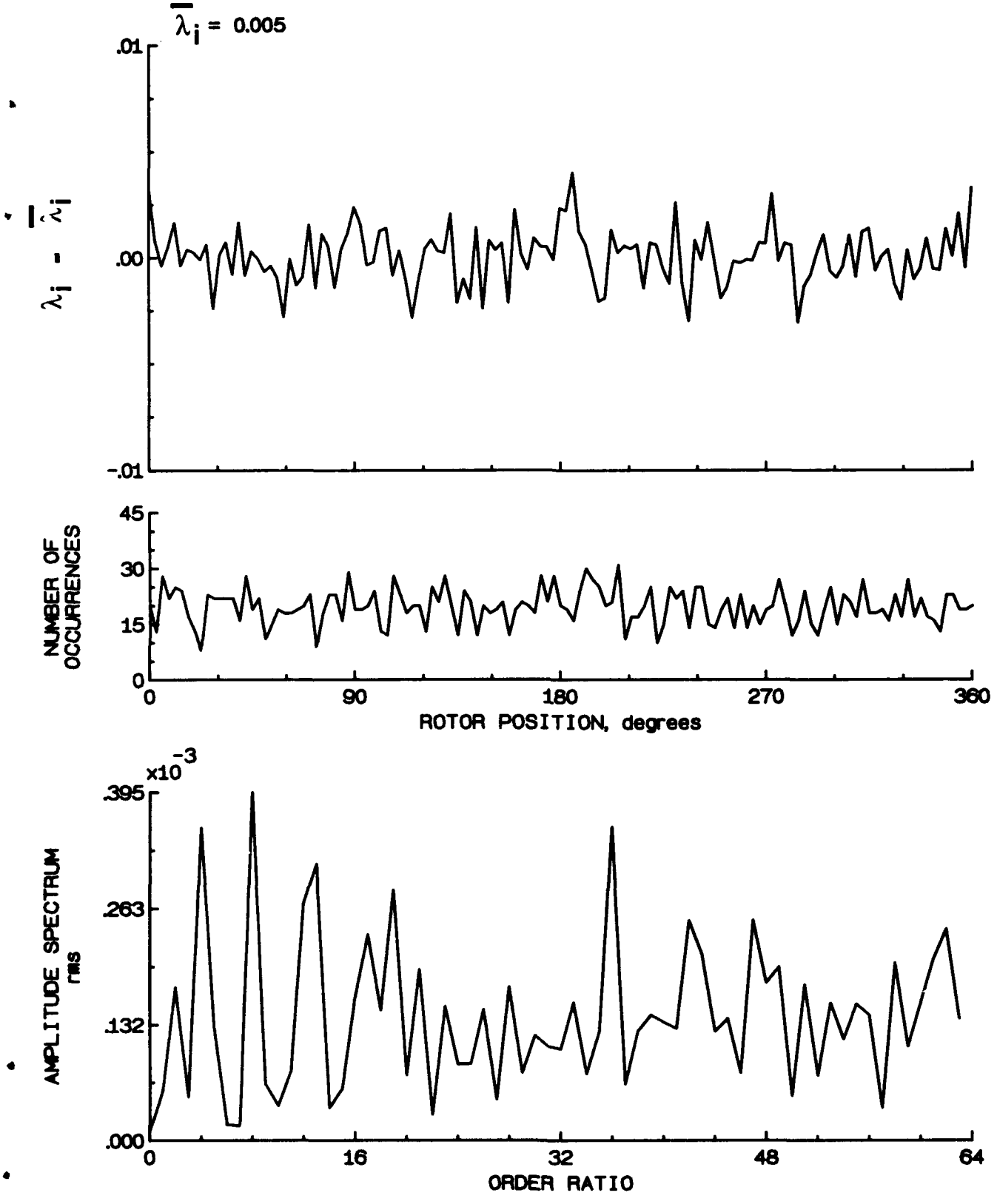

Figure 68.- Concluded.

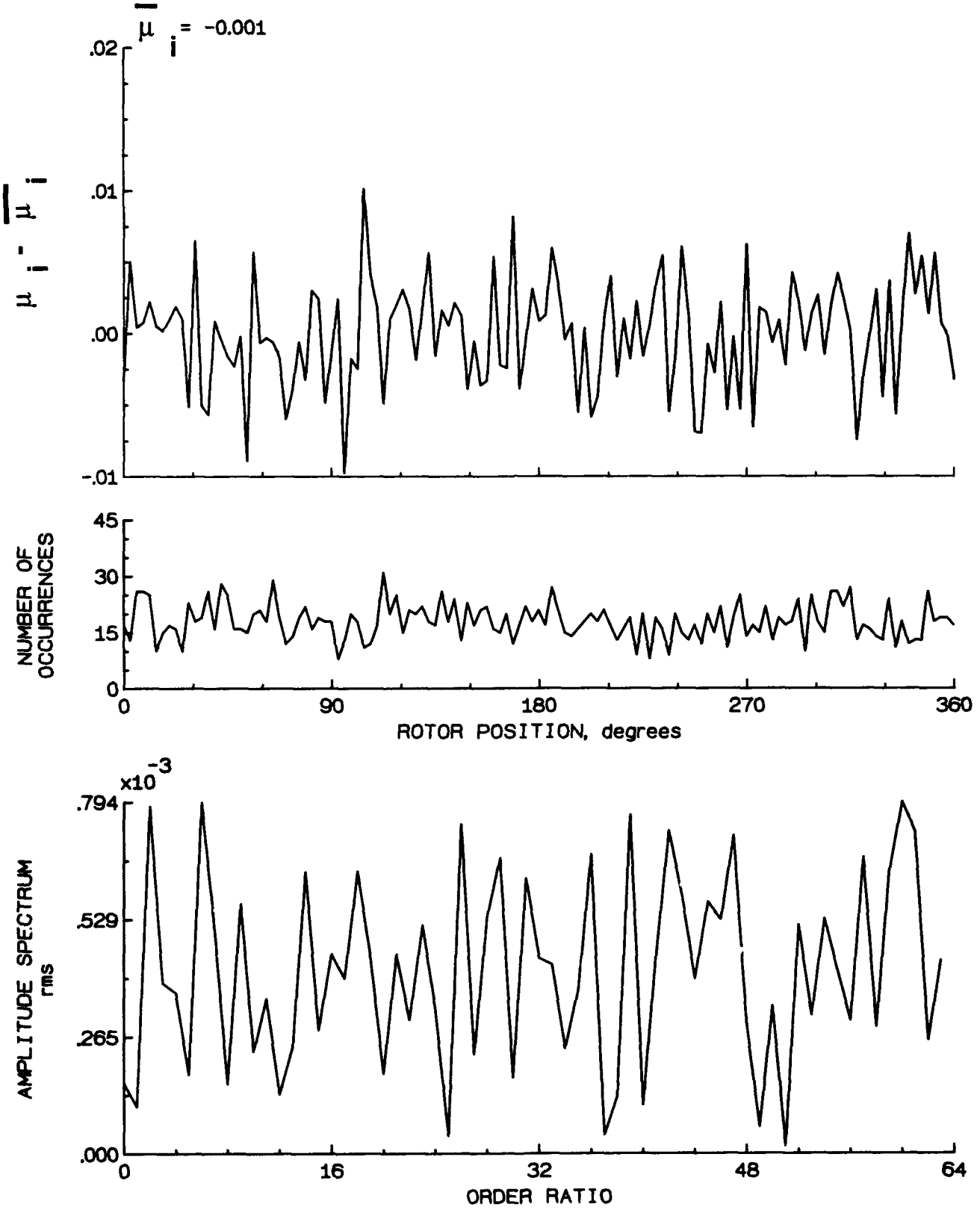

Figure 69.- Induced inflow velocity measured at 90 degrees and r/R of 1.02.

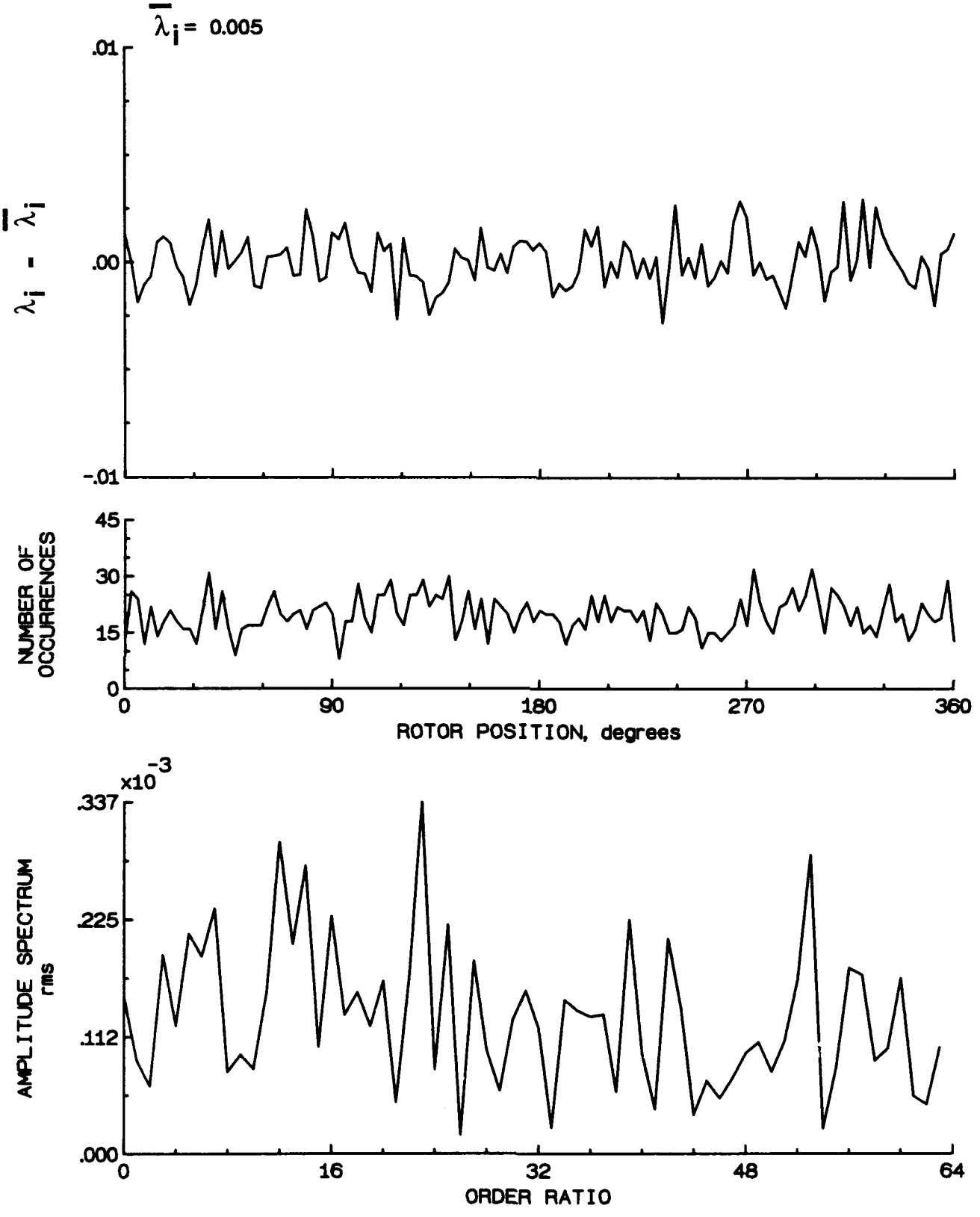

Figure 69.- Concluded.

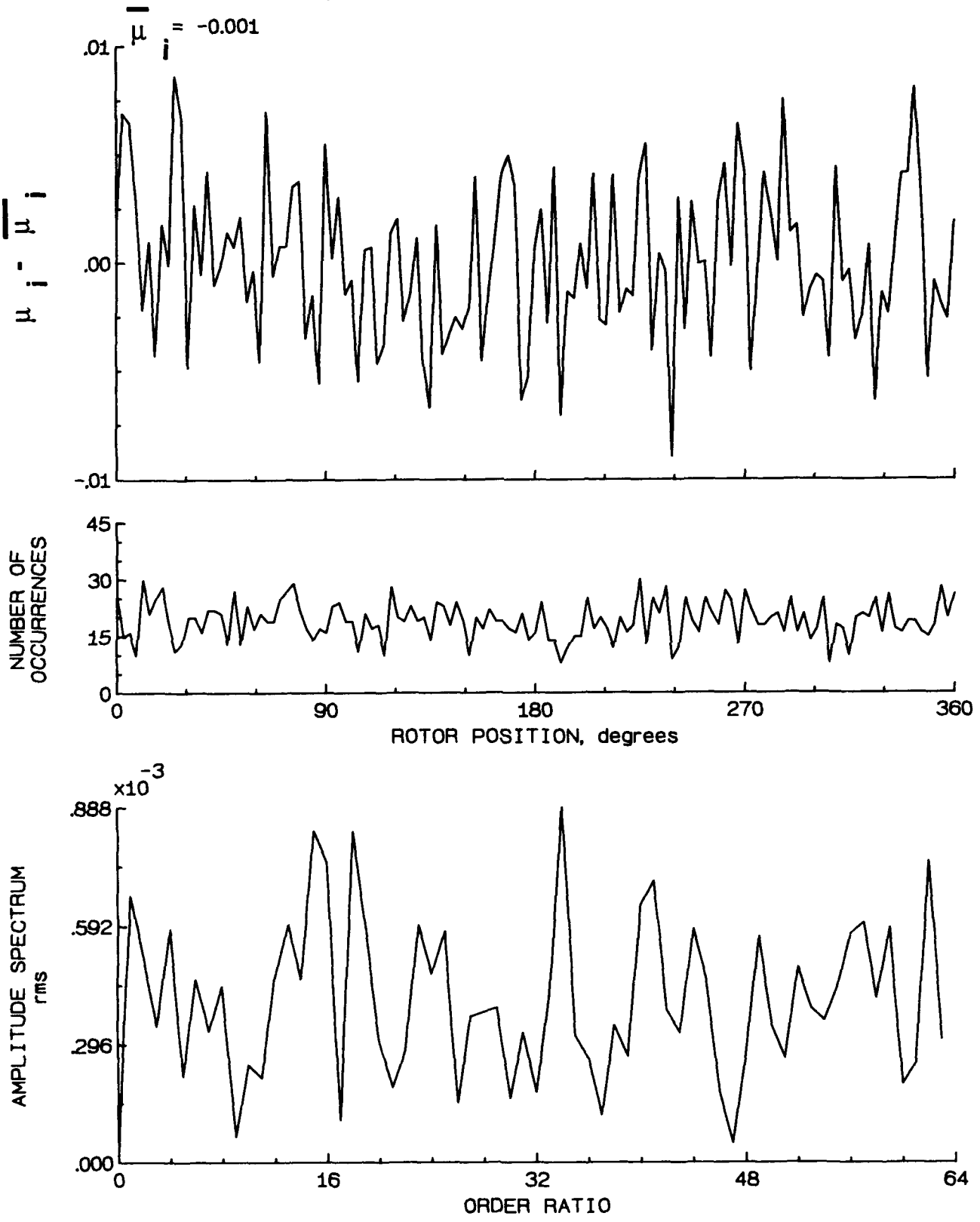

Figure 70.- Induced inflow velocity measured at 90 degrees and r/R of 1.04.

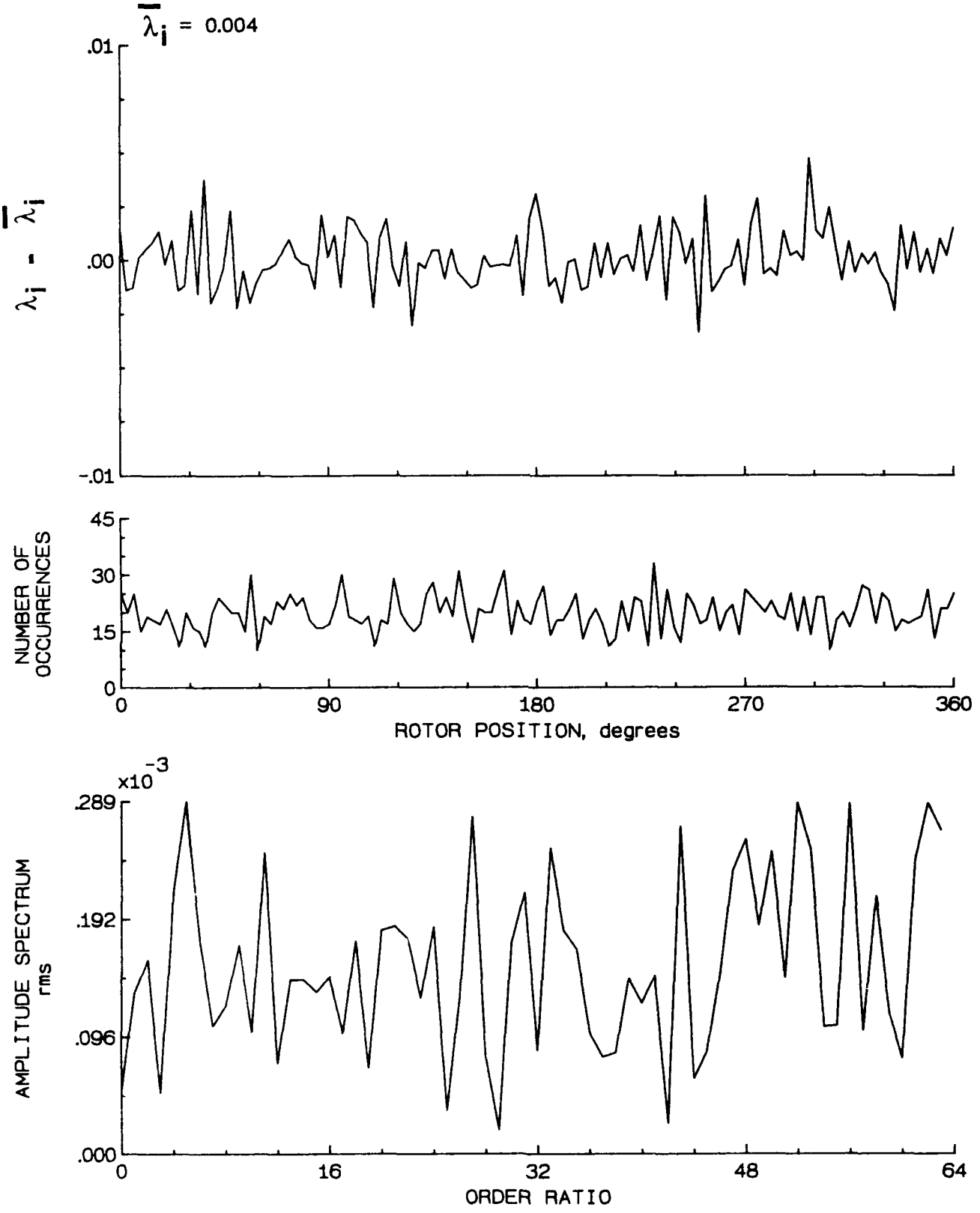

Figure 70.- Concluded.

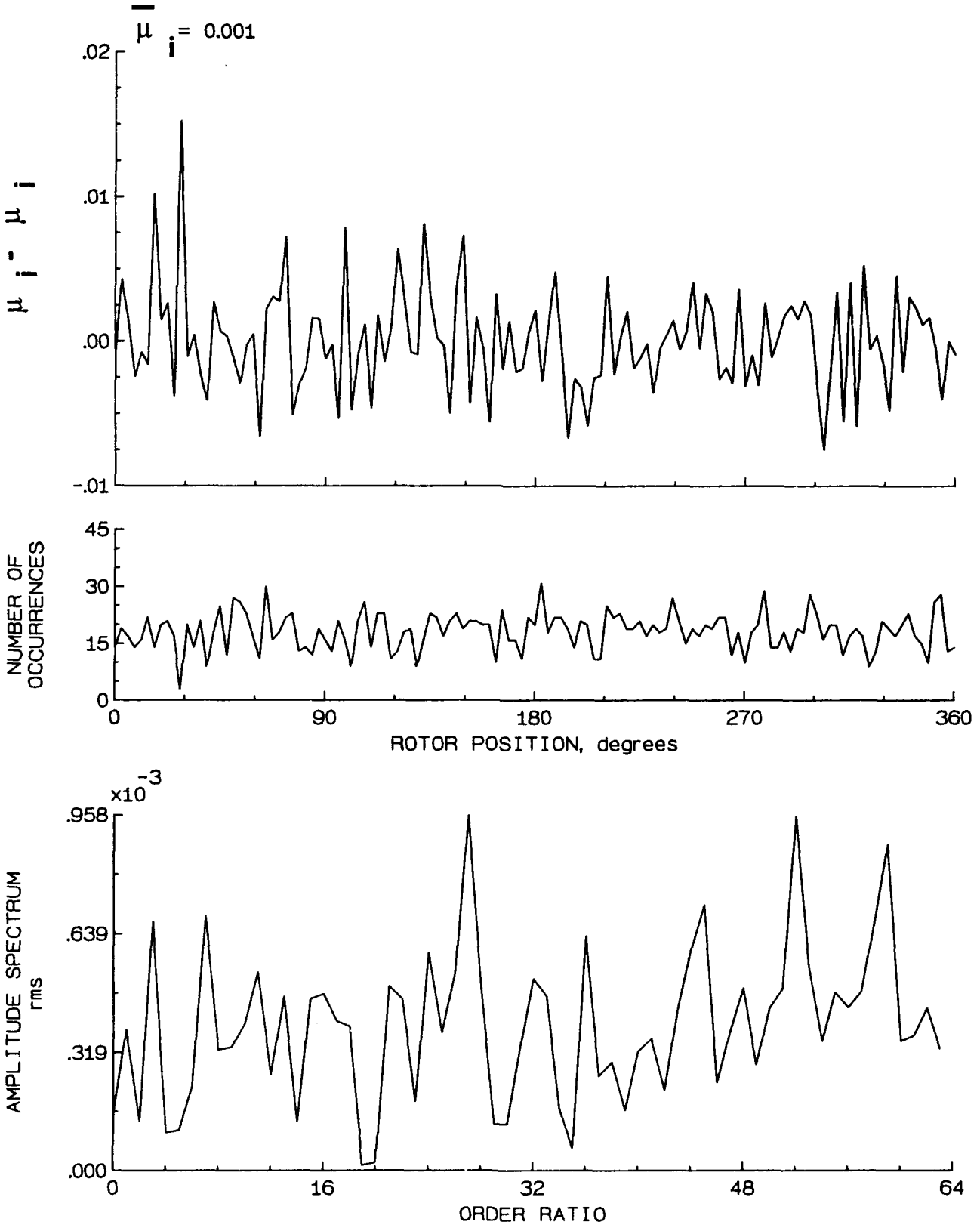

Figure 71.- Induced inflow velocity measured at 90 degrees and r/R of 1.10.

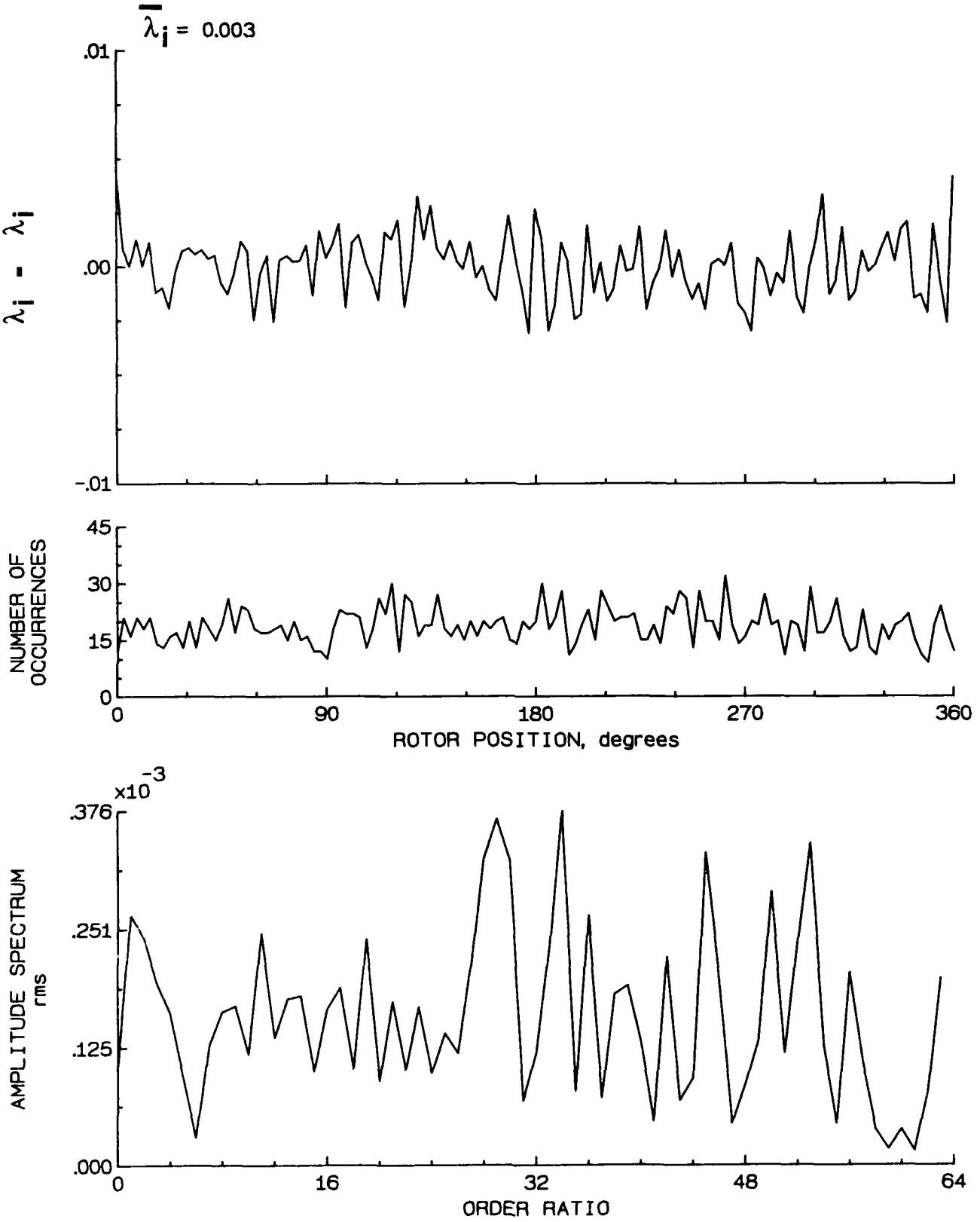

Figure 71.- Concluded.

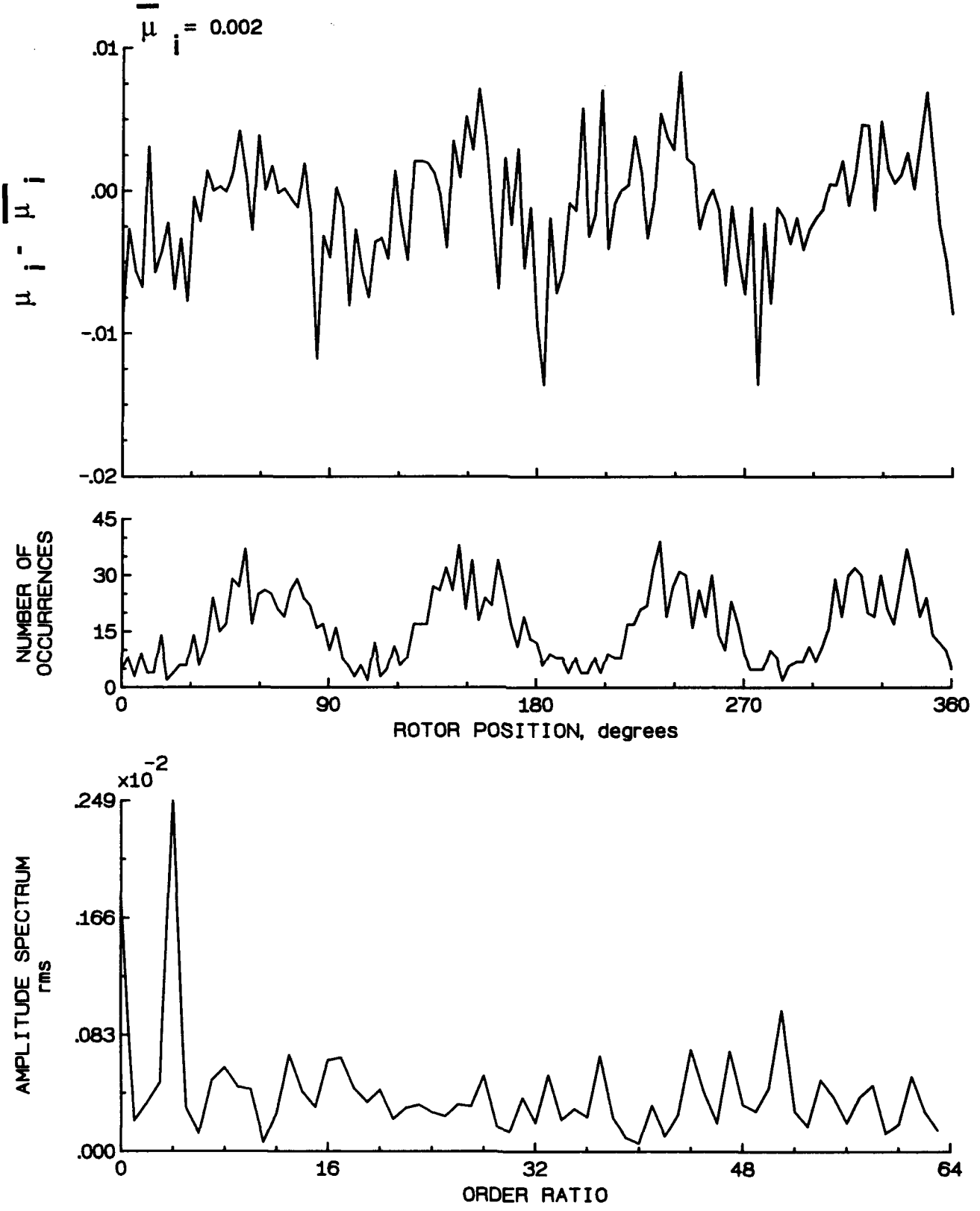

Figure 72.- Induced inflow velocity measured at 120 degrees and r/R of 0.20.

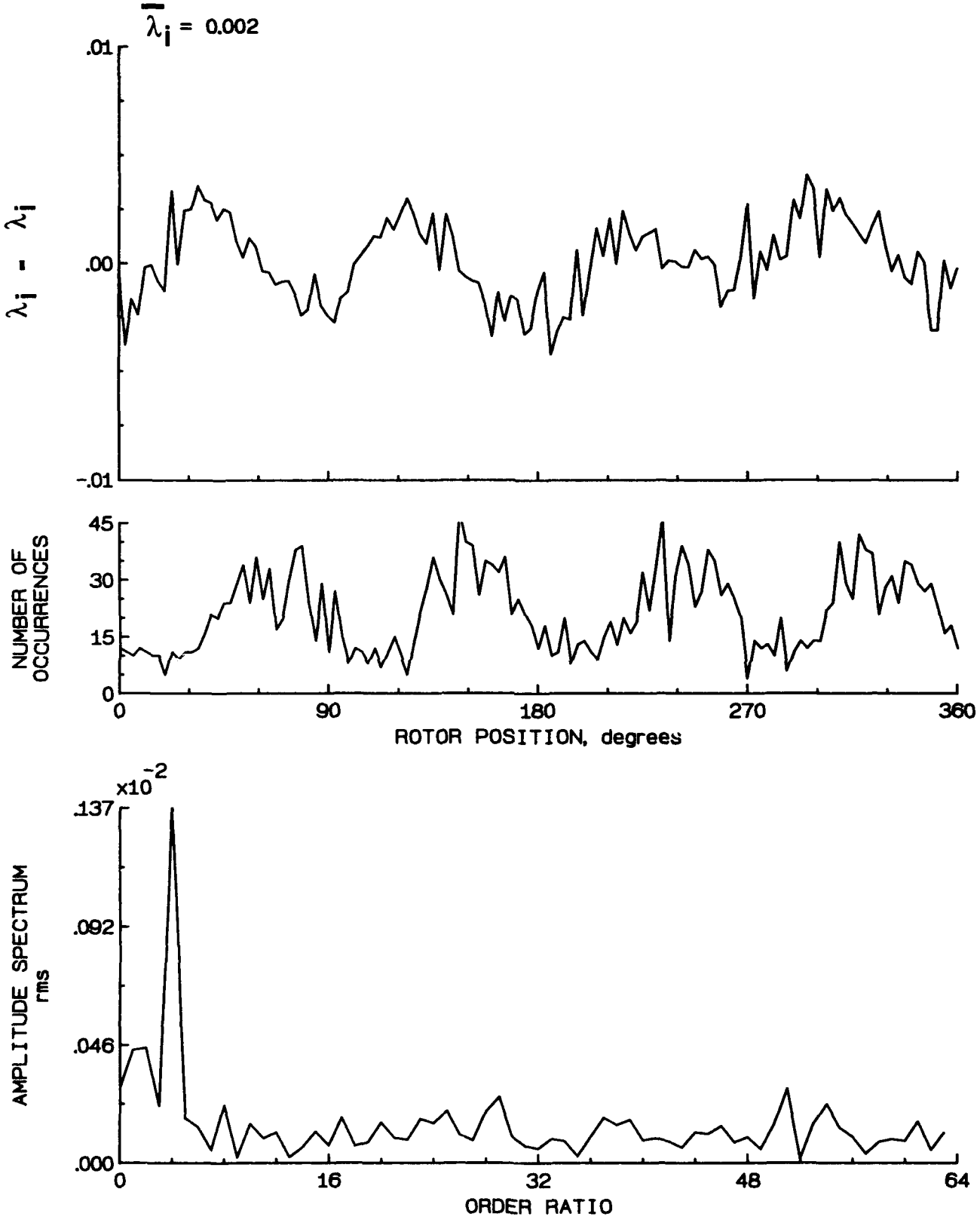

Figure 72.- Concluded.

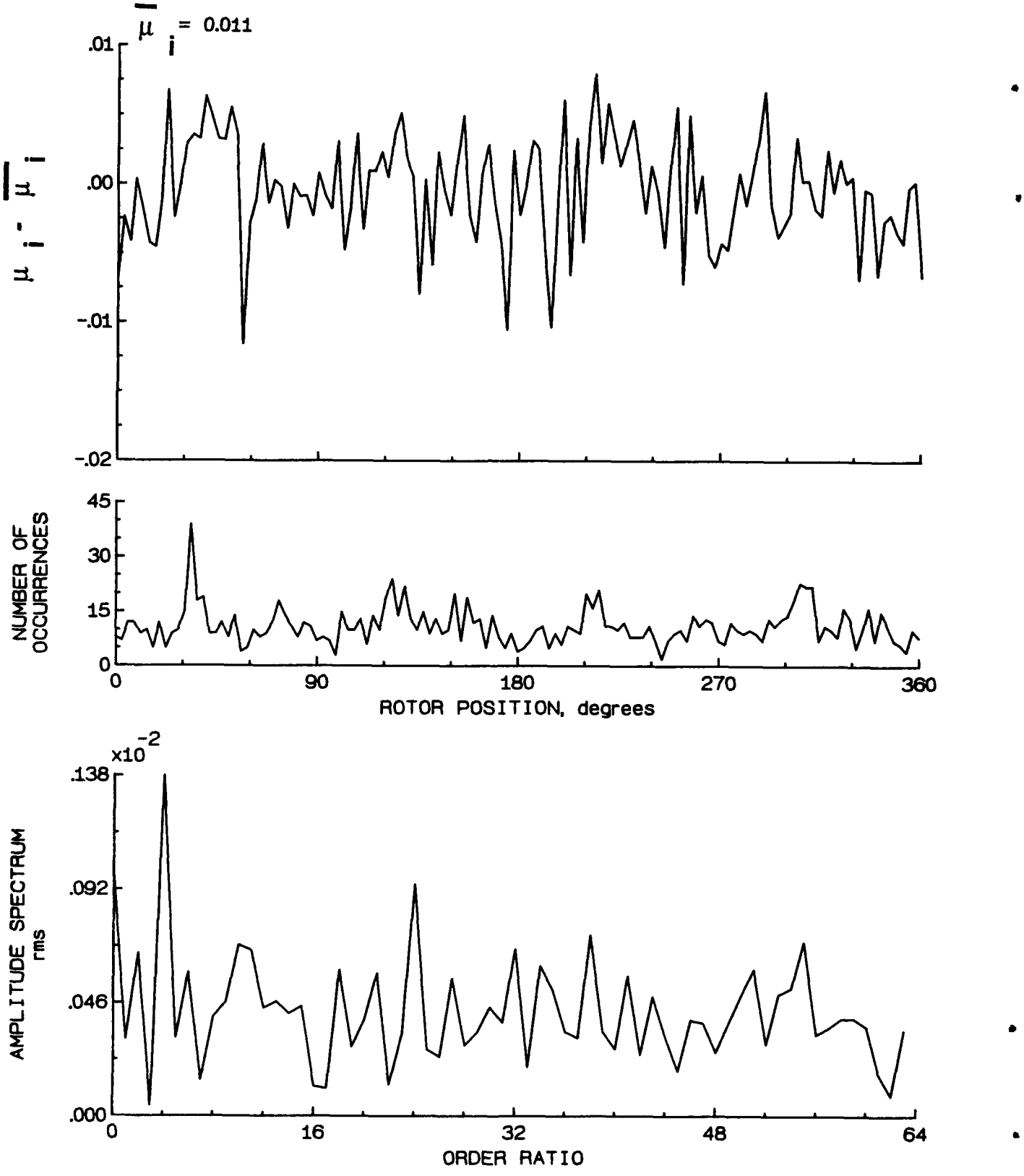

Figure 73.- Induced inflow velocity measured at 120 degrees and r/R of 0.40.

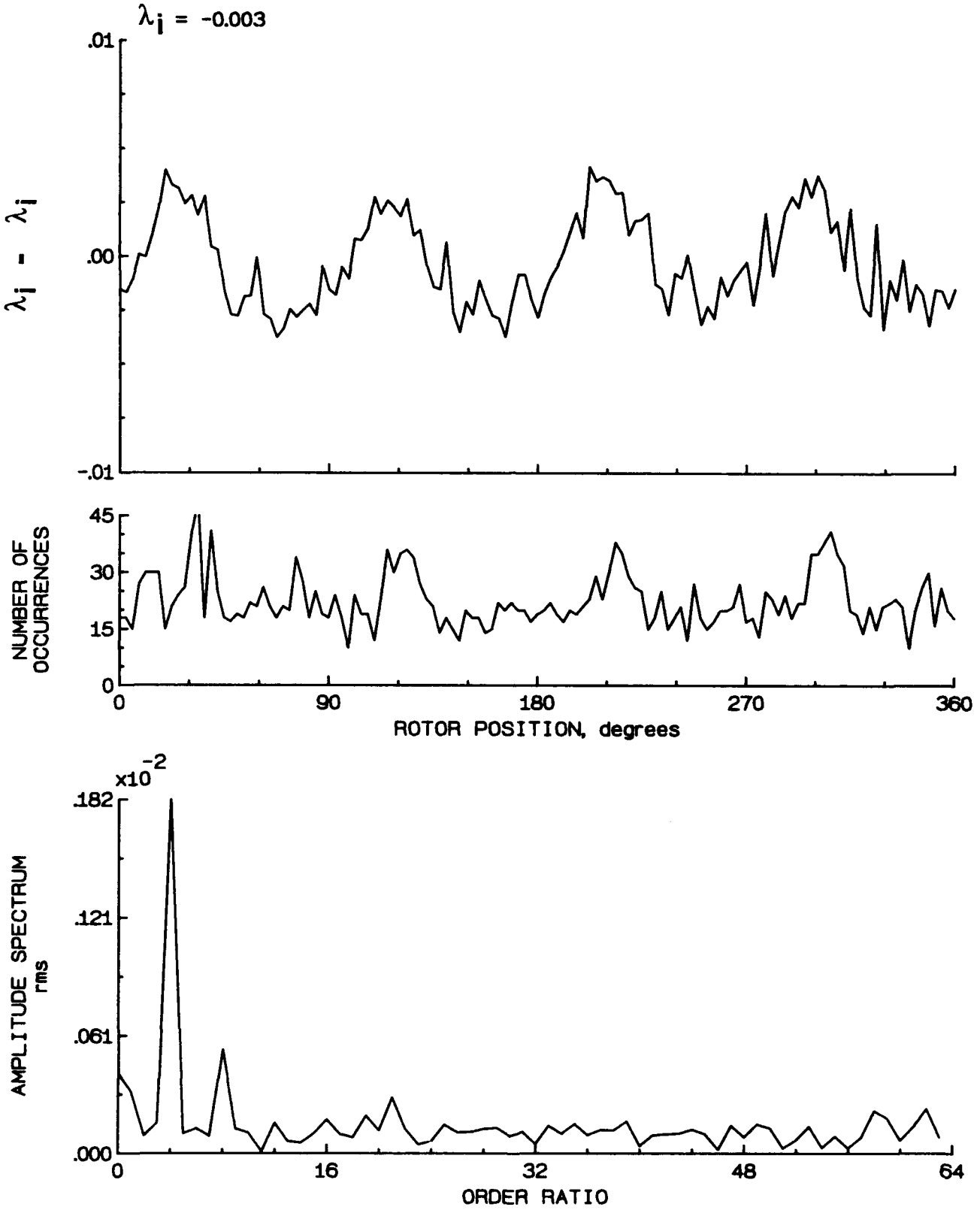

Figure 73.- Concluded.

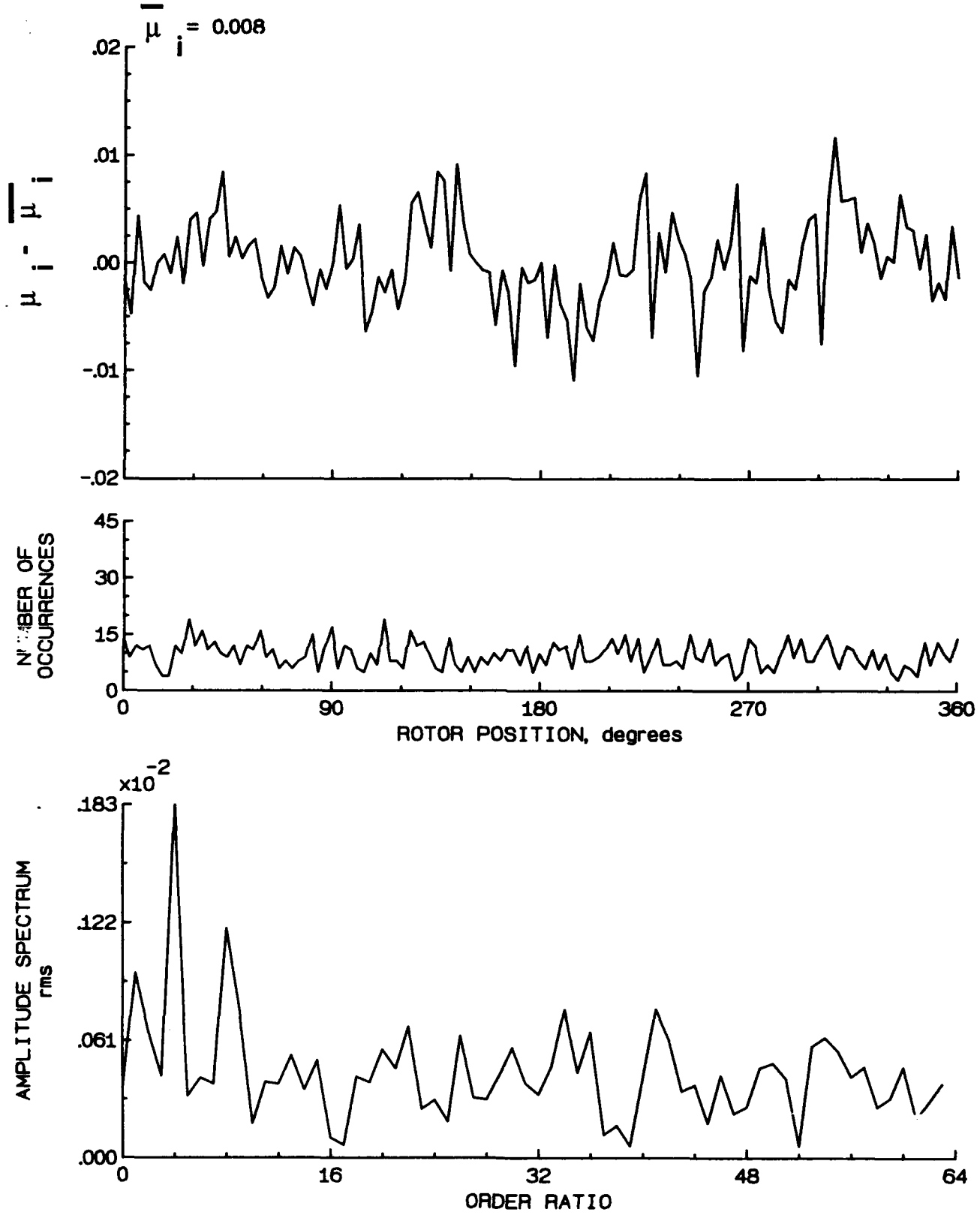

Figure 74.- Induced inflow velocity measured at 120 degrees and r/R of 0.50.

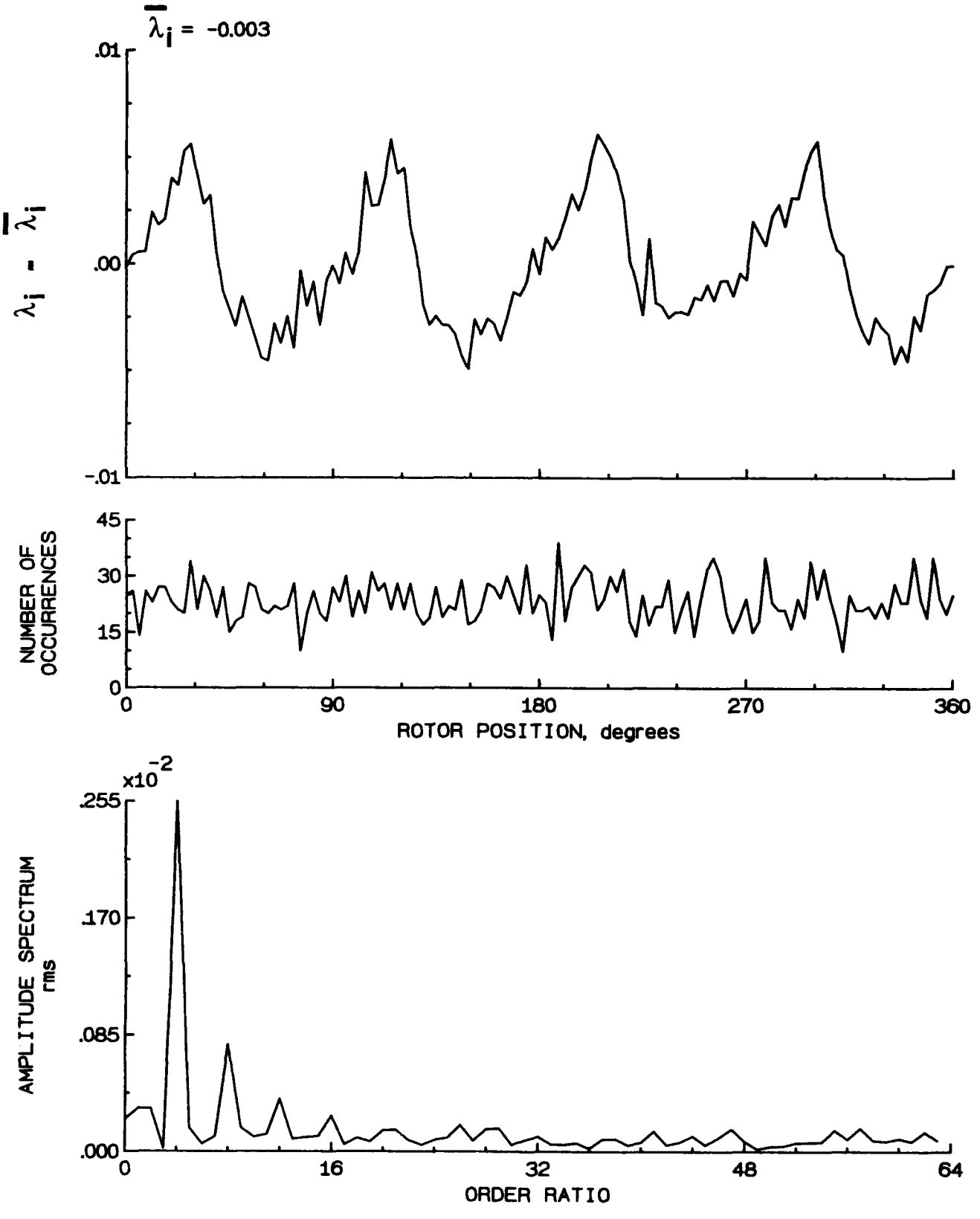

Figure 74.- Concluded.

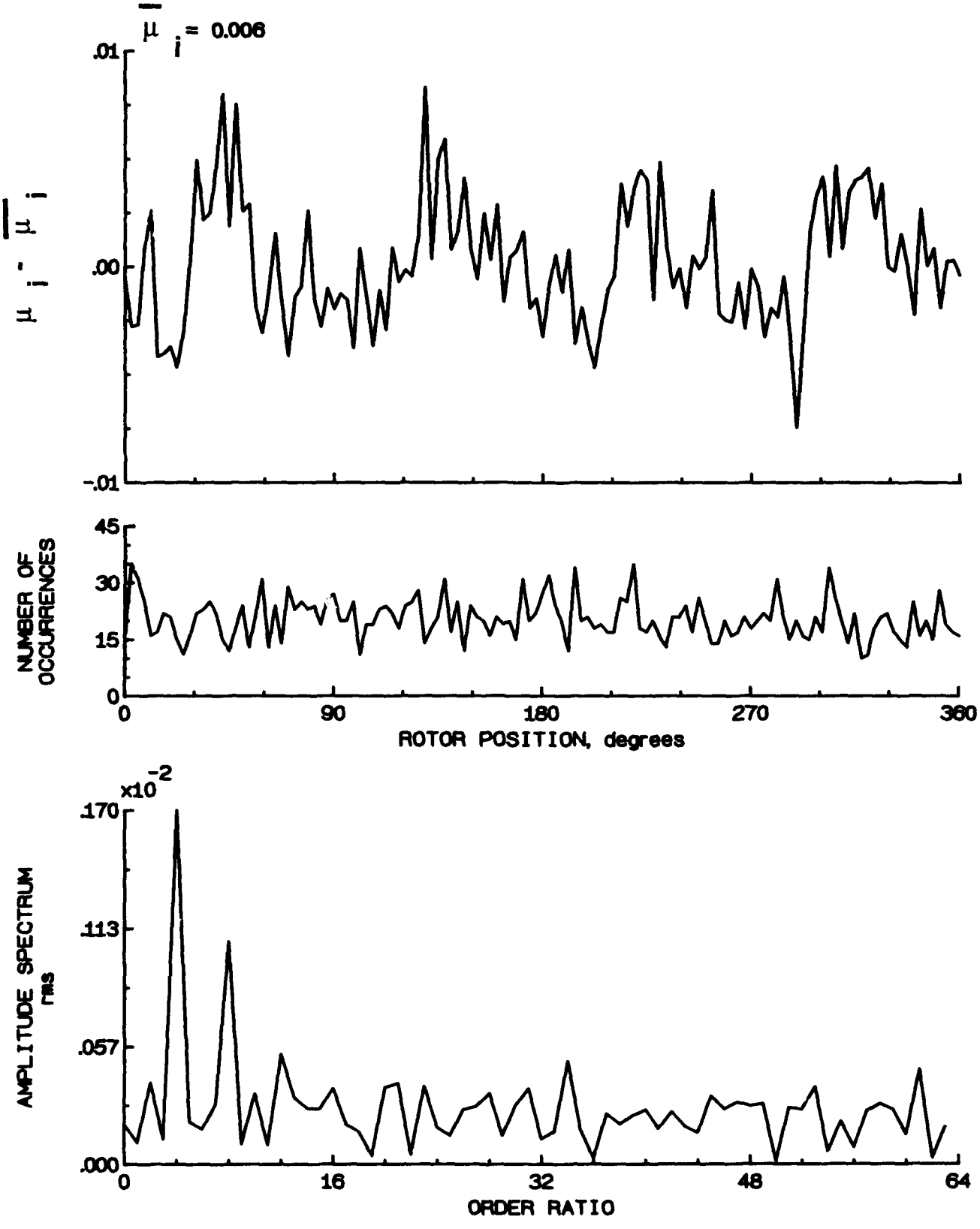

Figure 75.- Induced inflow velocity measured at 120 degrees and r/R of 0.60.

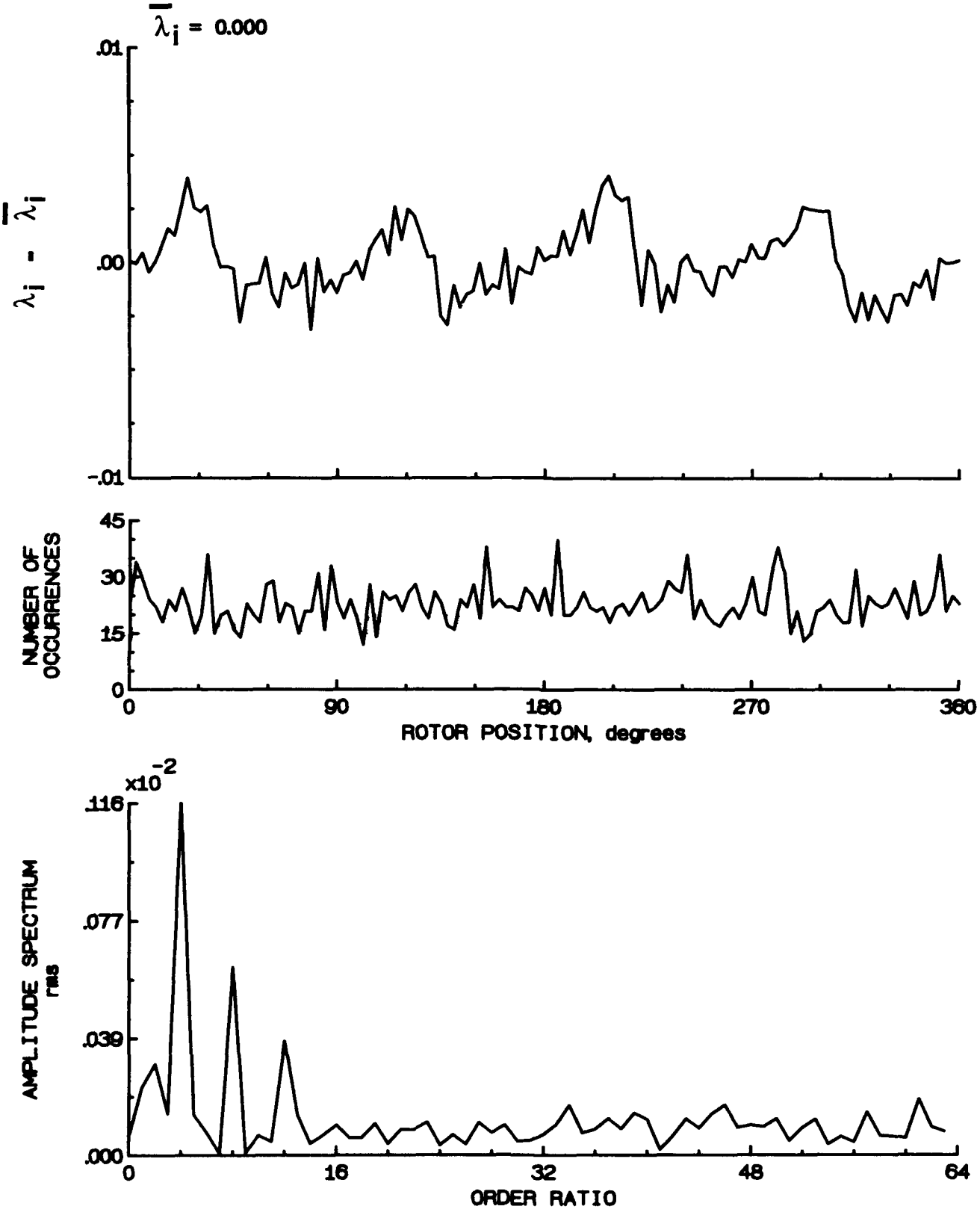

Figure 75.- Concluded.

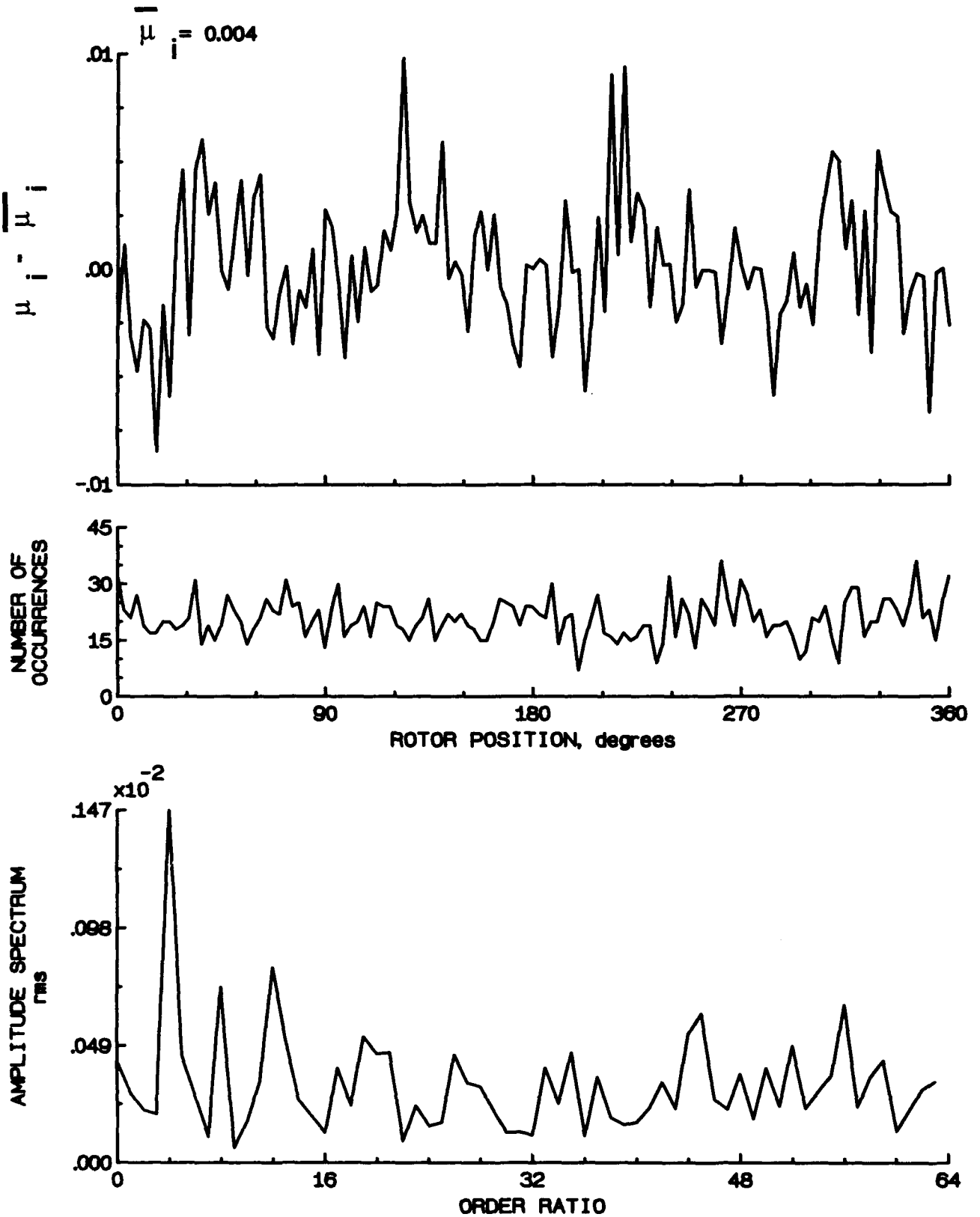

Figure 76.- Induced inflow velocity measured at 120 degrees and r/R of 0.70.

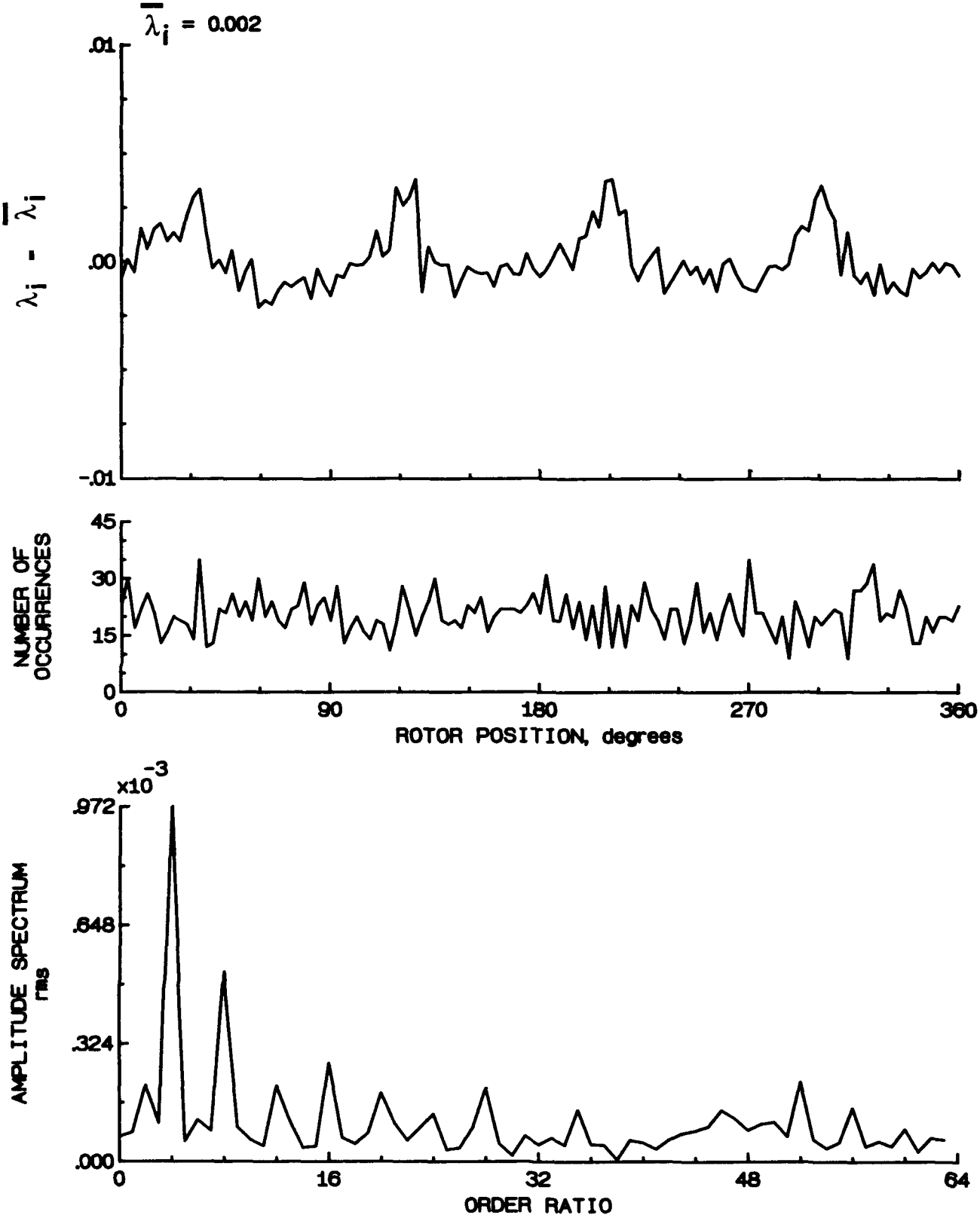

Figure 76.- Concluded.

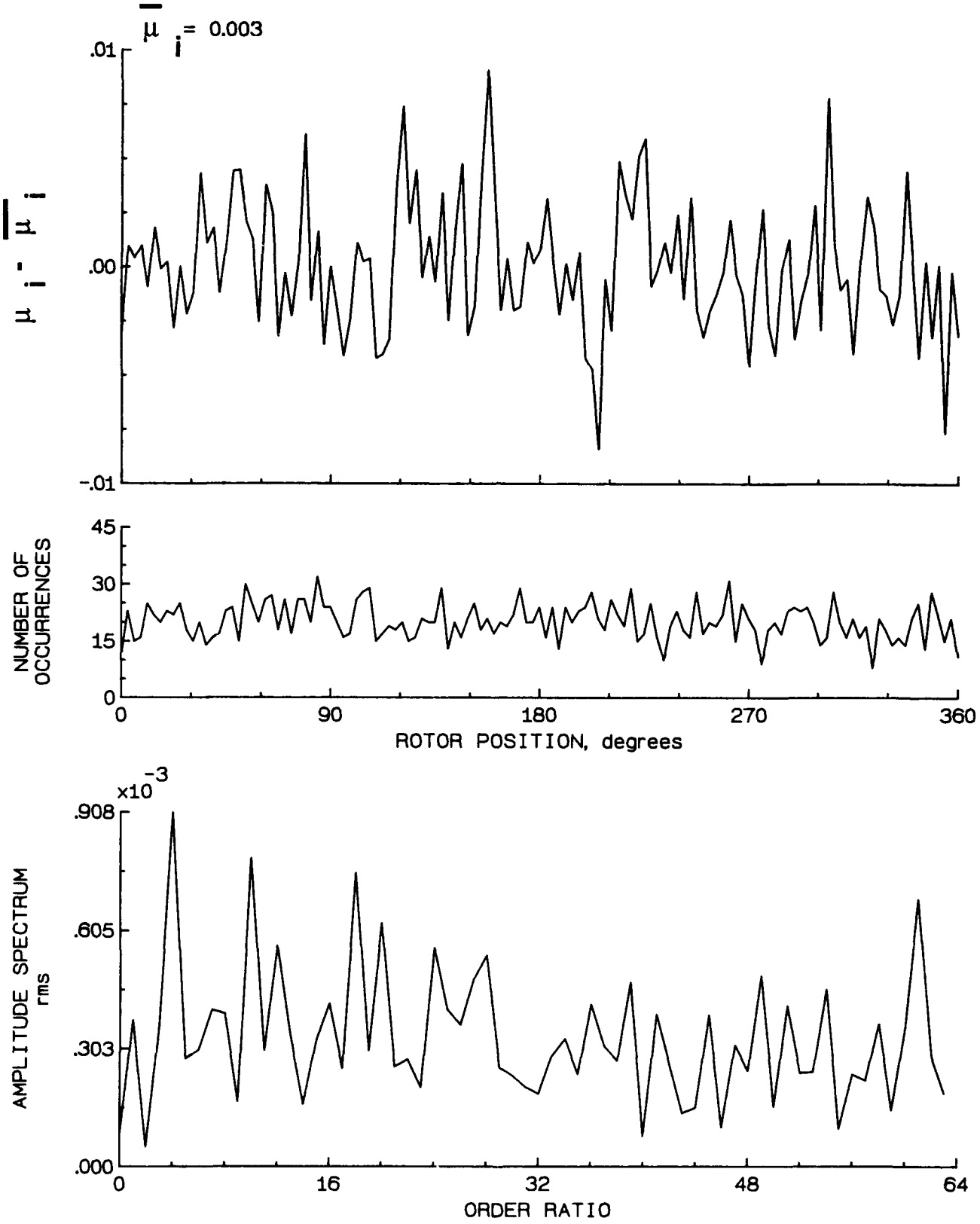

Figure 77.- Induced inflow velocity measured at 120 degrees and r/R of 0.74.

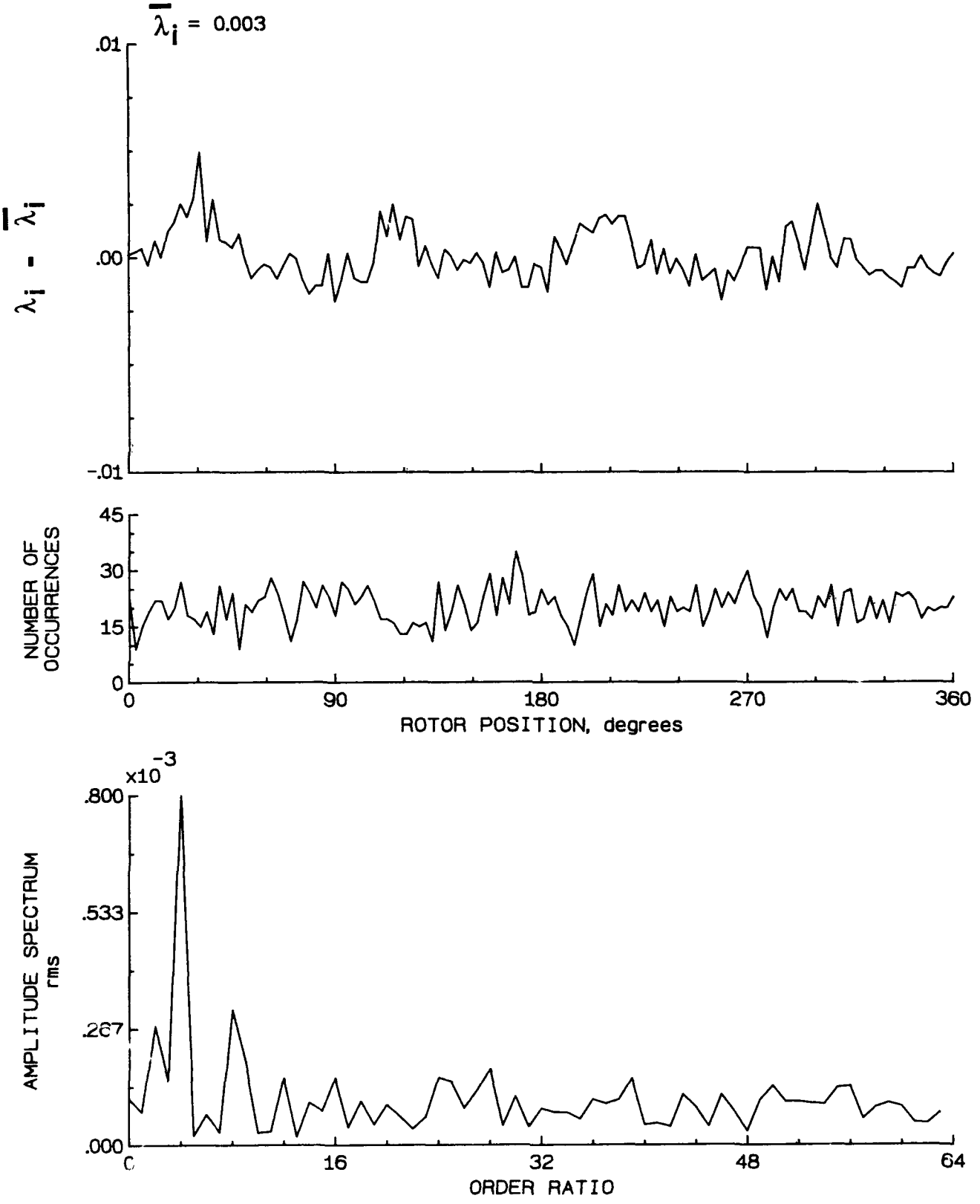

Figure 77.- Concluded.

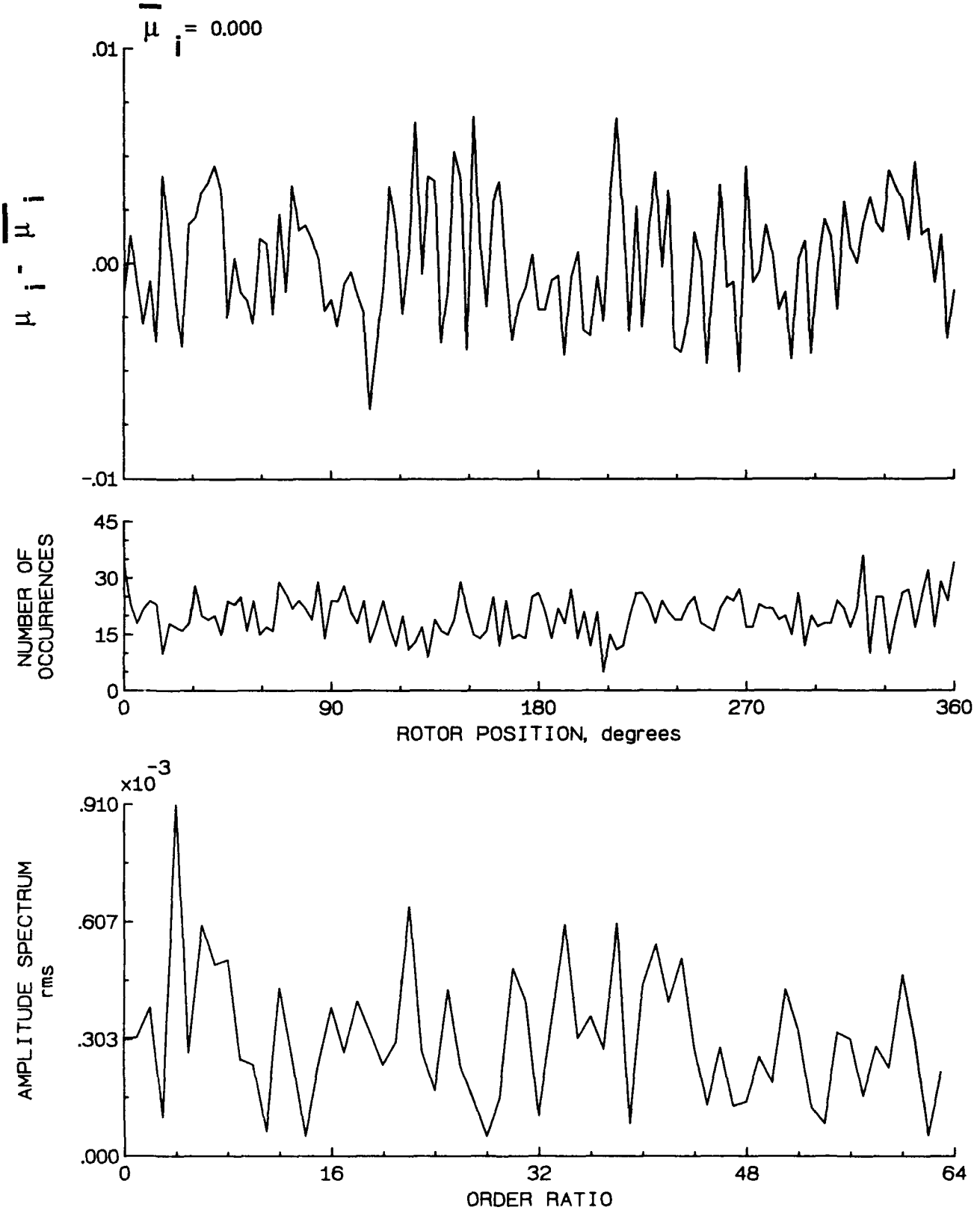

Figure 78.- Induced inflow velocity measured at 120 degrees and r/R of 0.78.

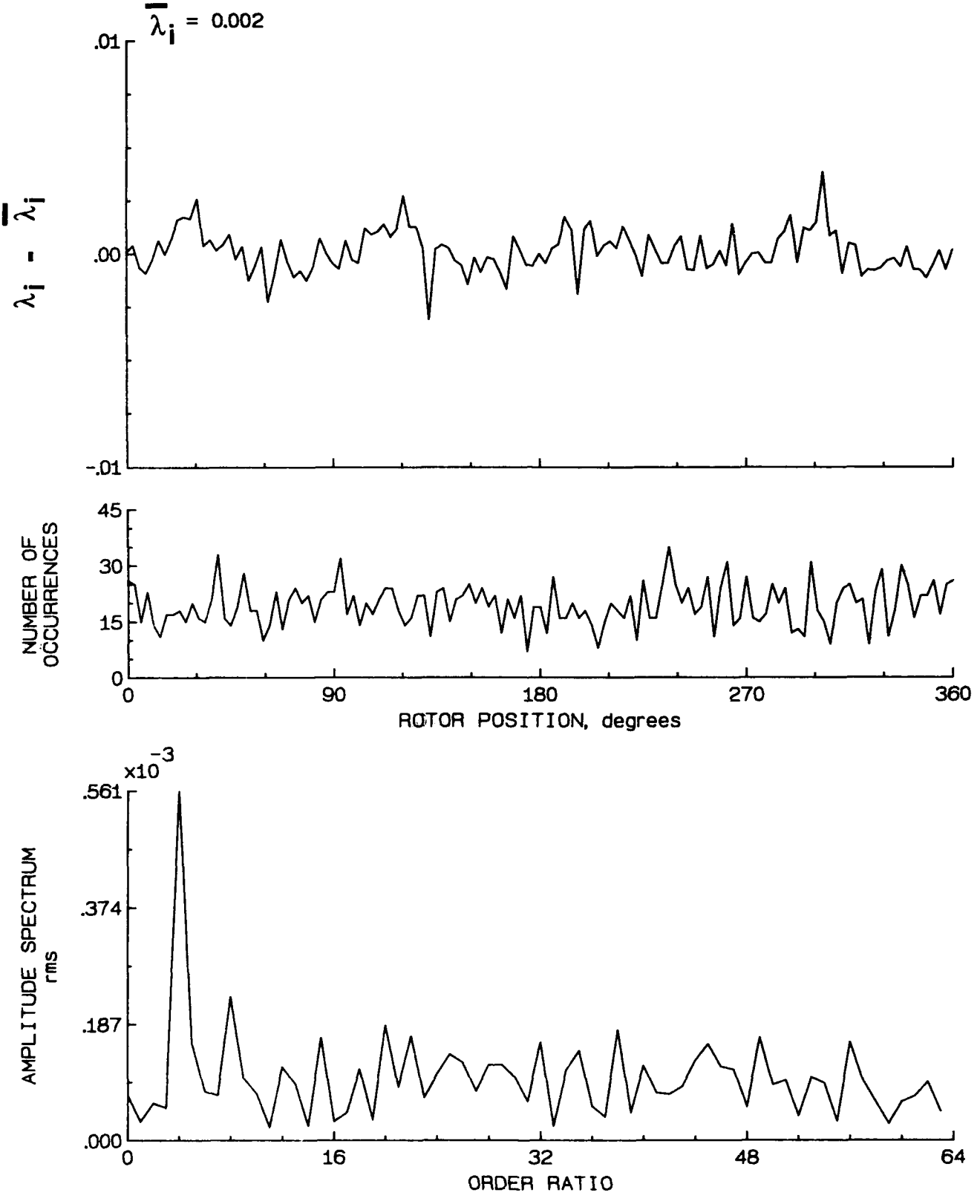

Figure 78.- Concluded.

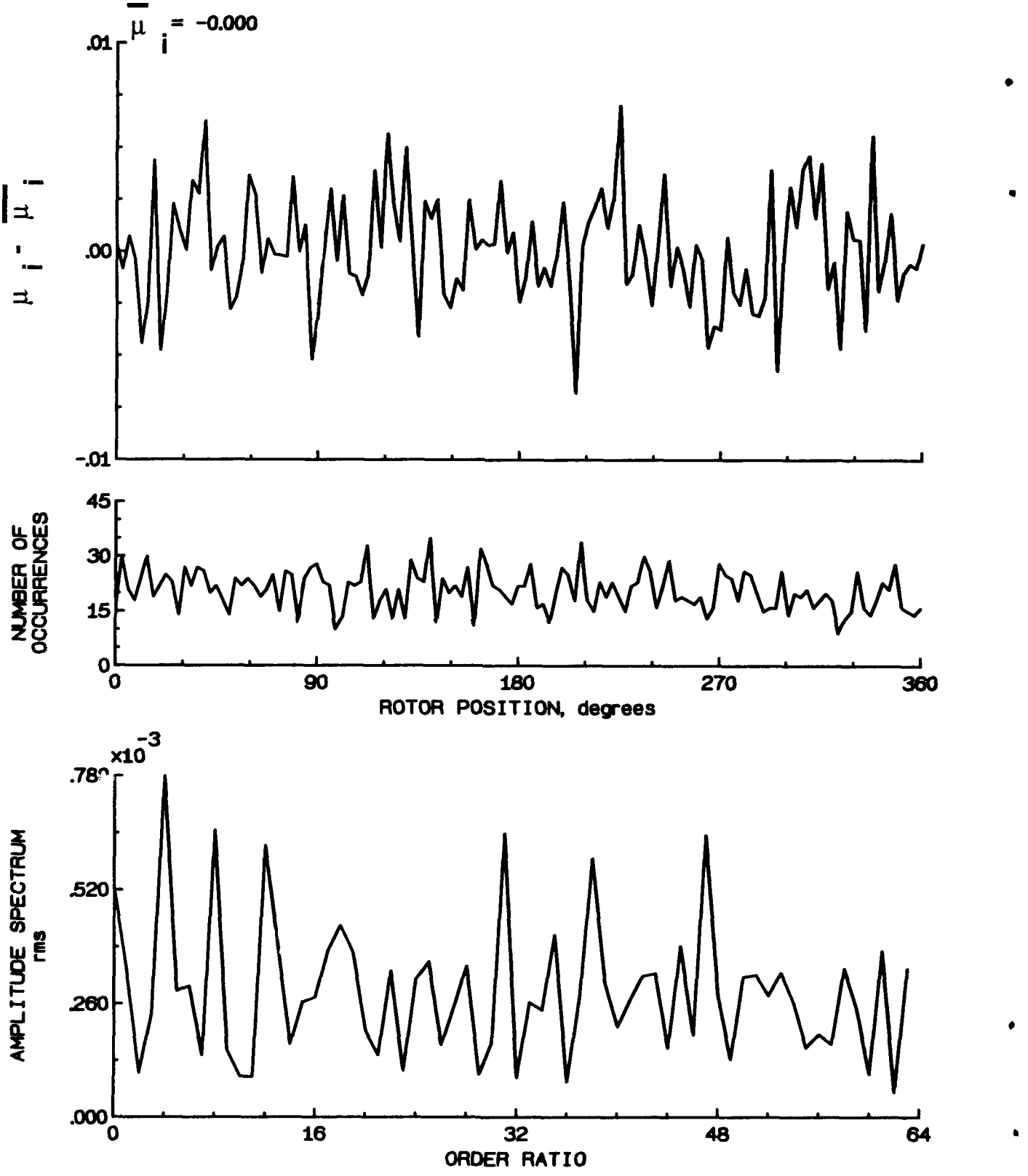

Figure 79.- Induced inflow velocity measured at 120 degrees and r/R of 0.82.

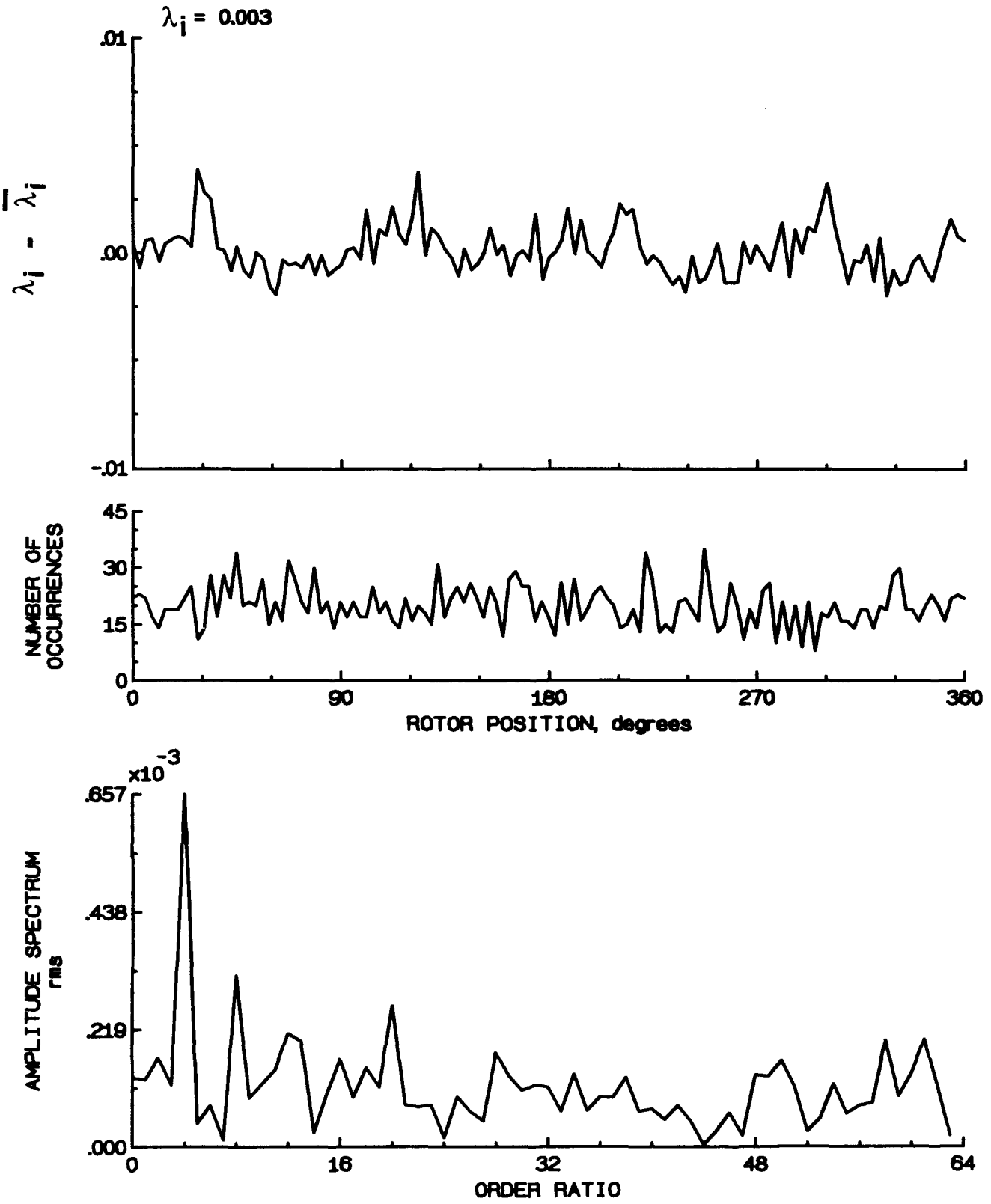

Figure 79.- Concluded.

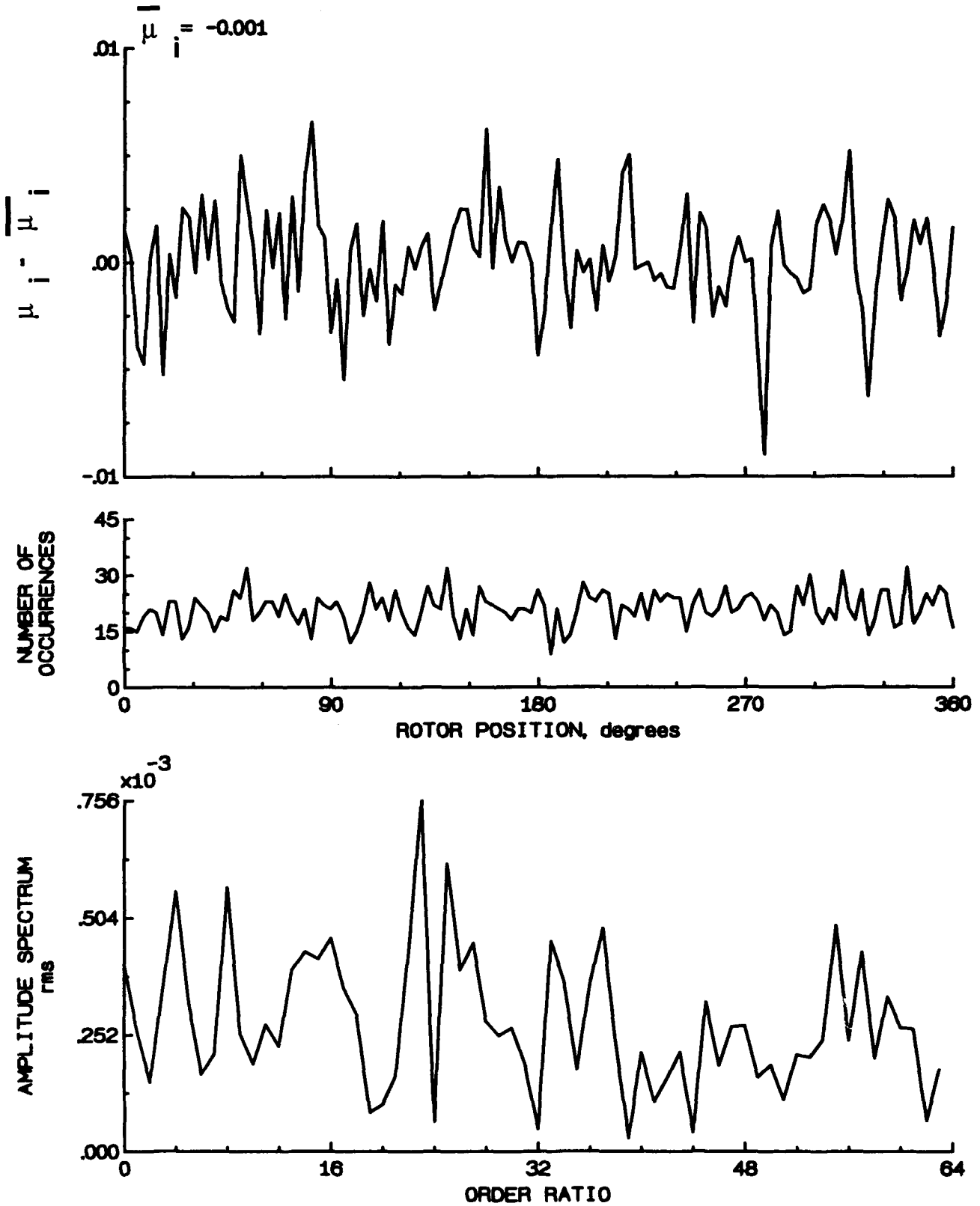

Figure 80.- Induced inflow velocity measured at 120 degrees and r/R of 0.86.

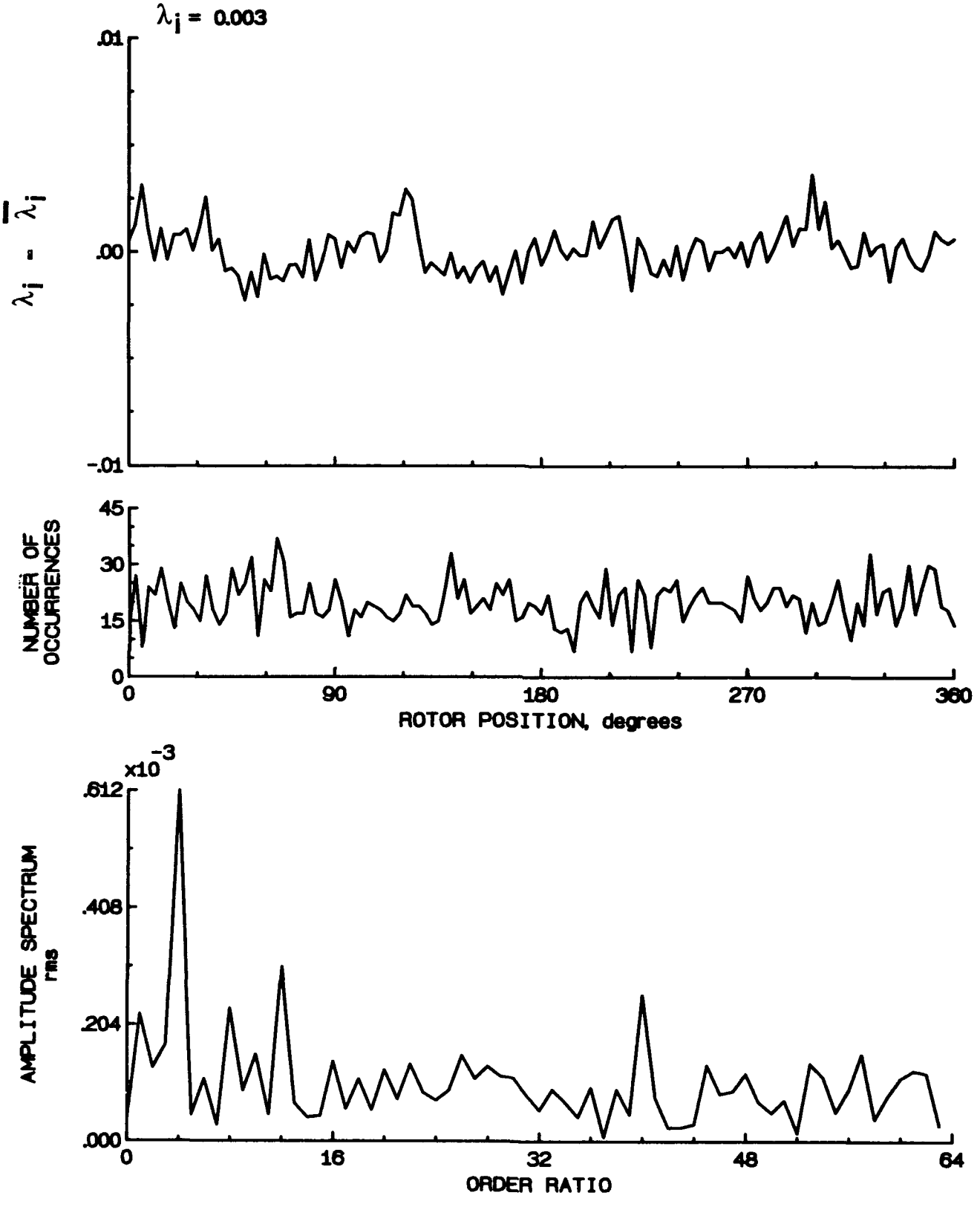

Figure 80.- Concluded.

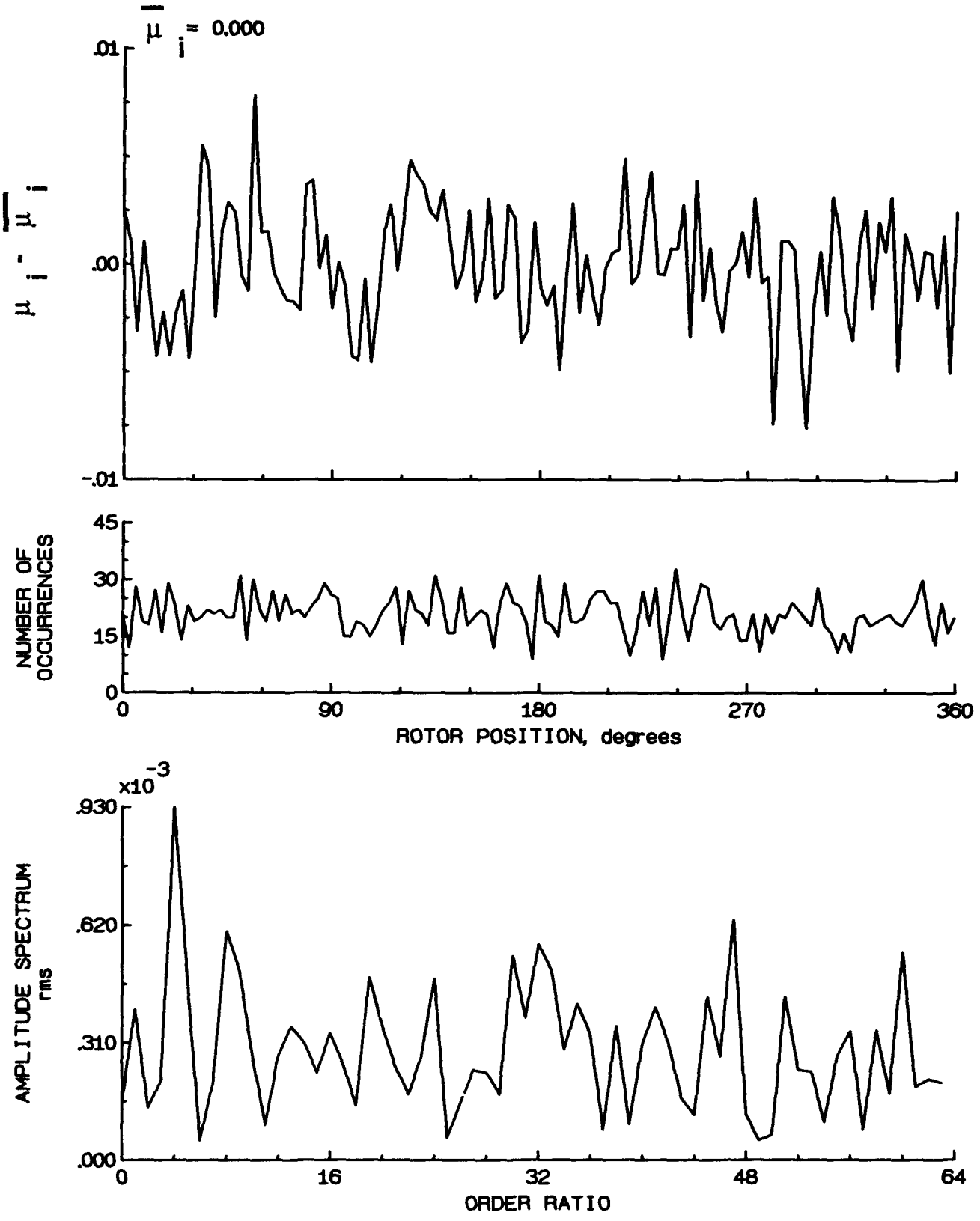

Figure 81.- Induced inflow velocity measured at 120 degrees and r/R of 0.90.

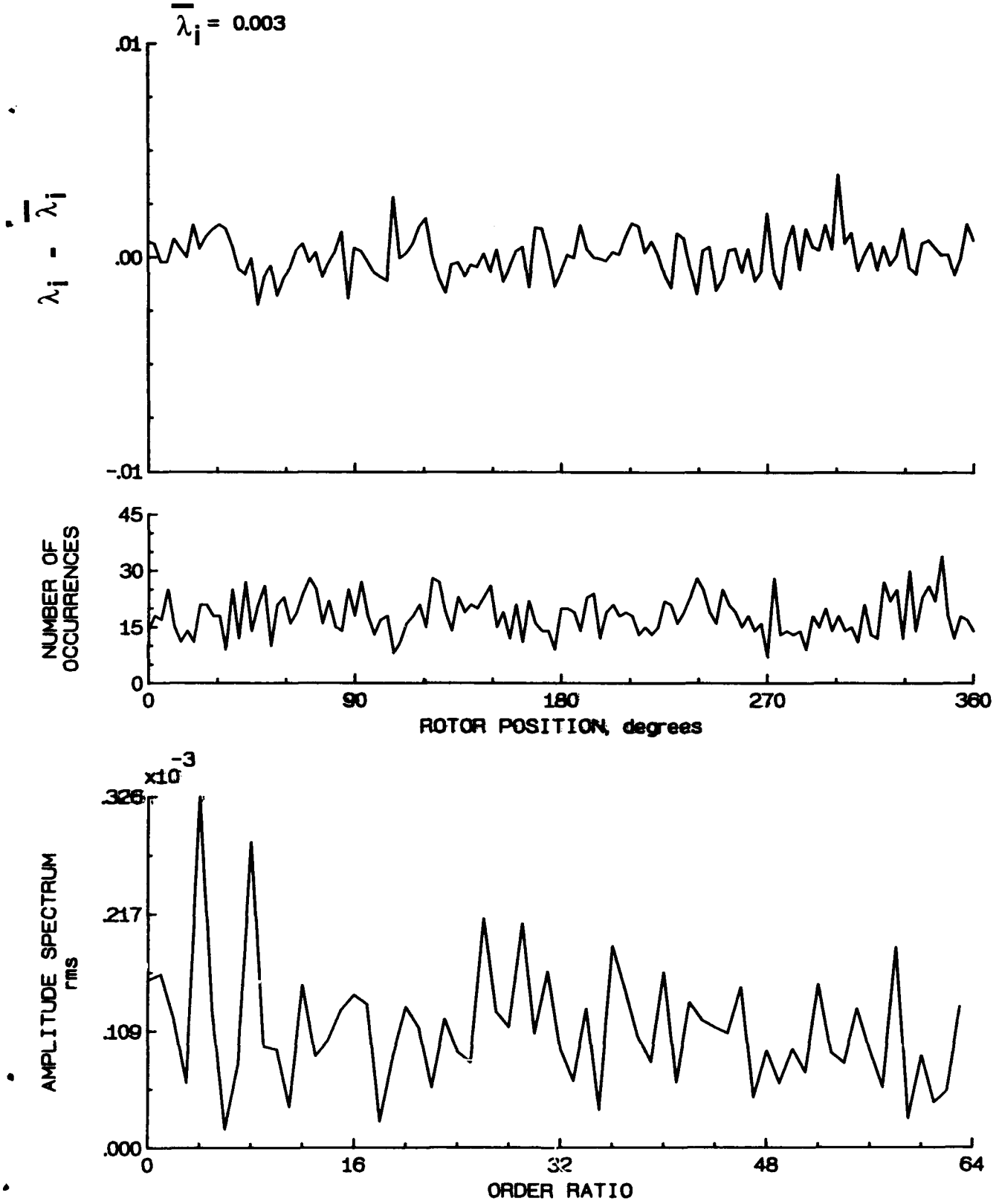

Figure 81.- Concluded.

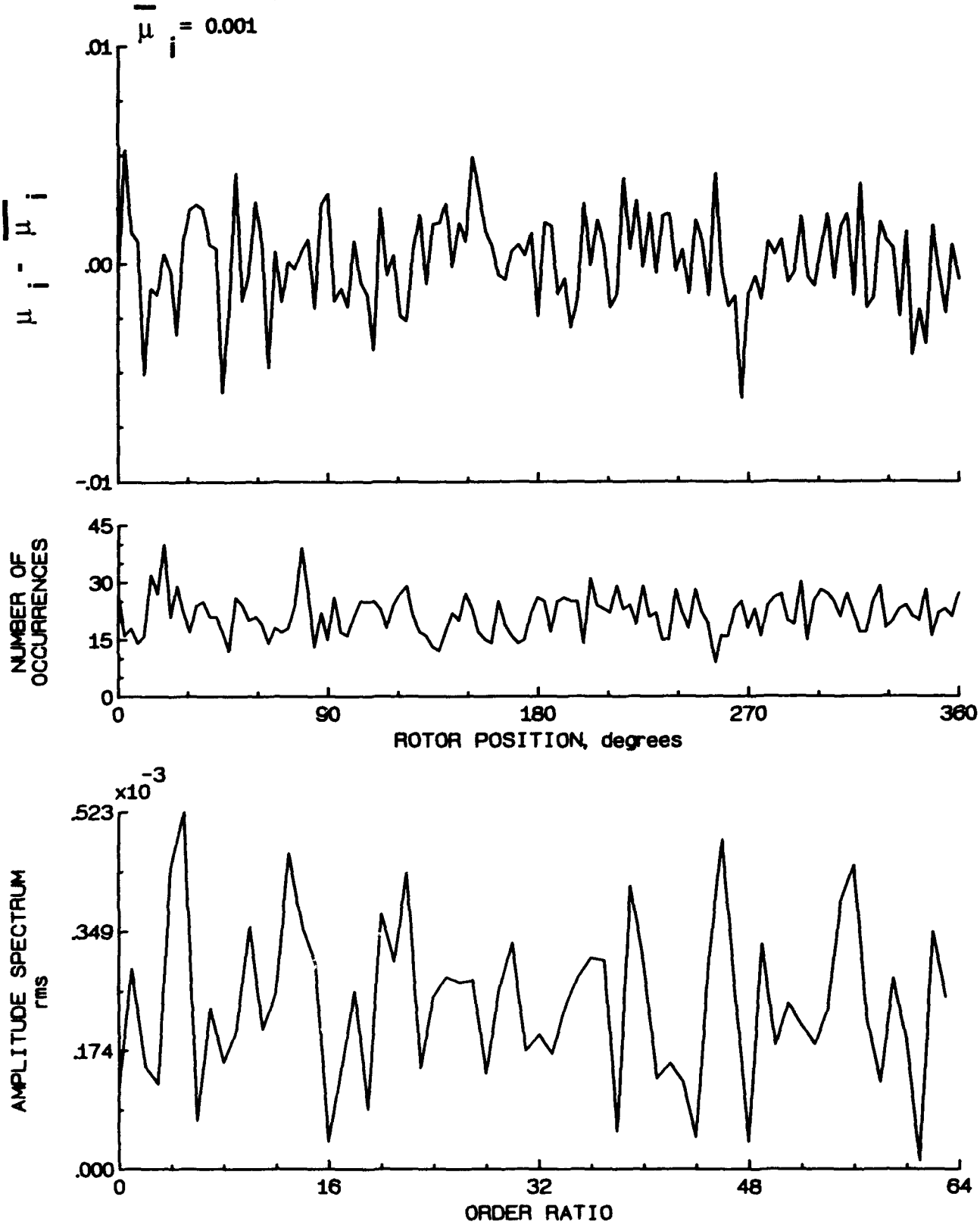

Figure 82.- Induced inflow velocity measured at 120 degrees and r/R of 0.94.

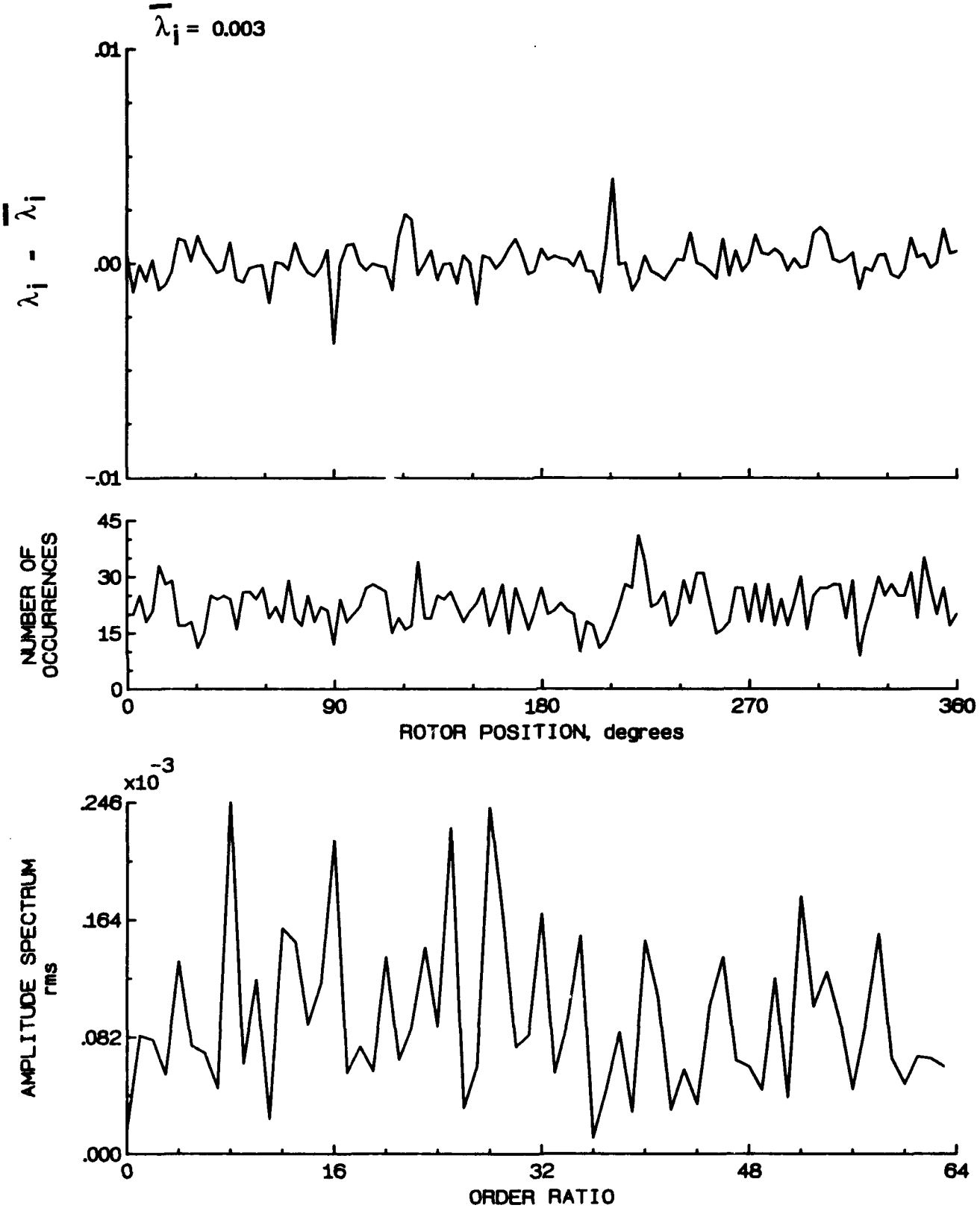

Figure 82.- Concluded.

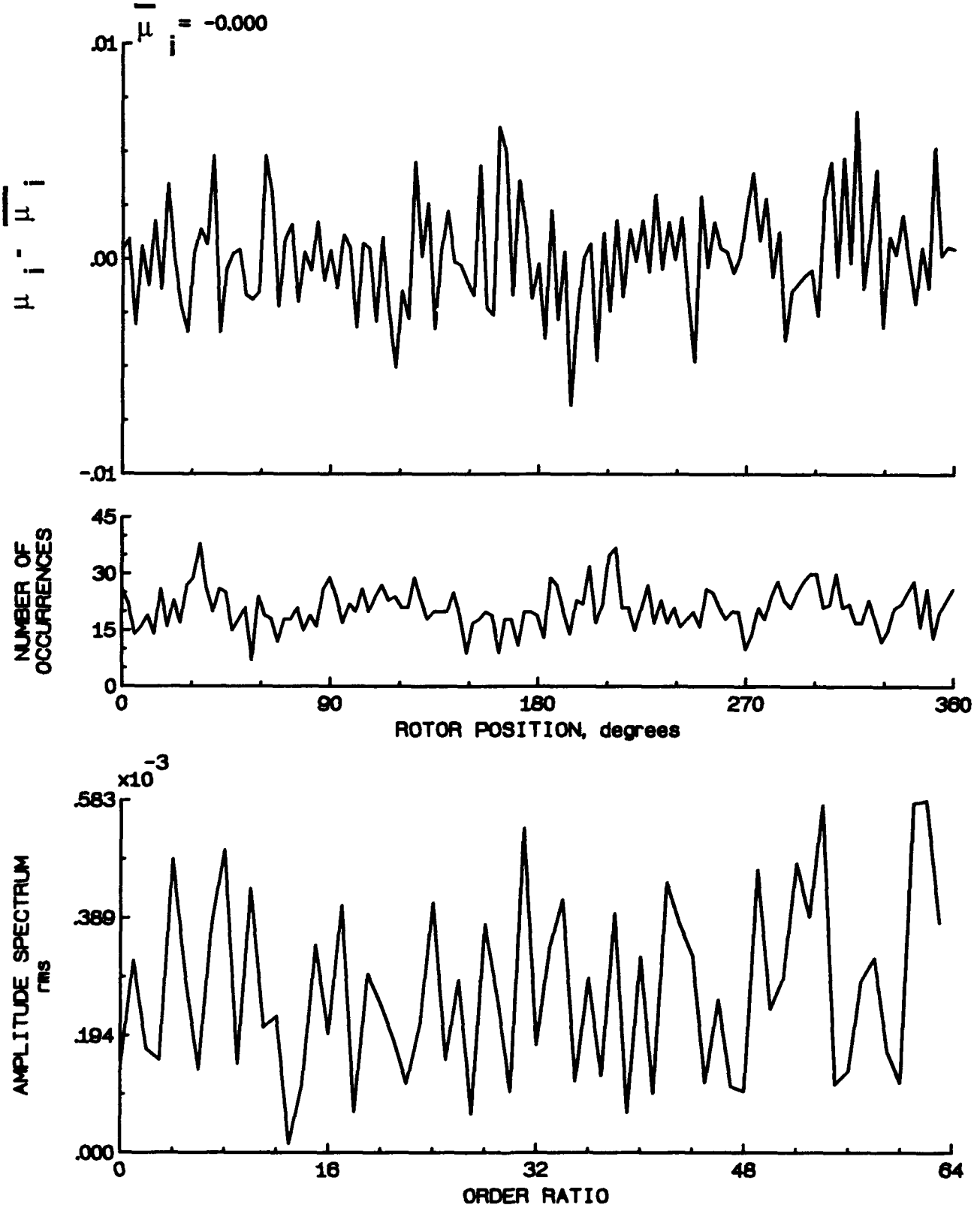

Figure 83.- Induced inflow velocity measured at 120 degrees and r/R of 0.98.

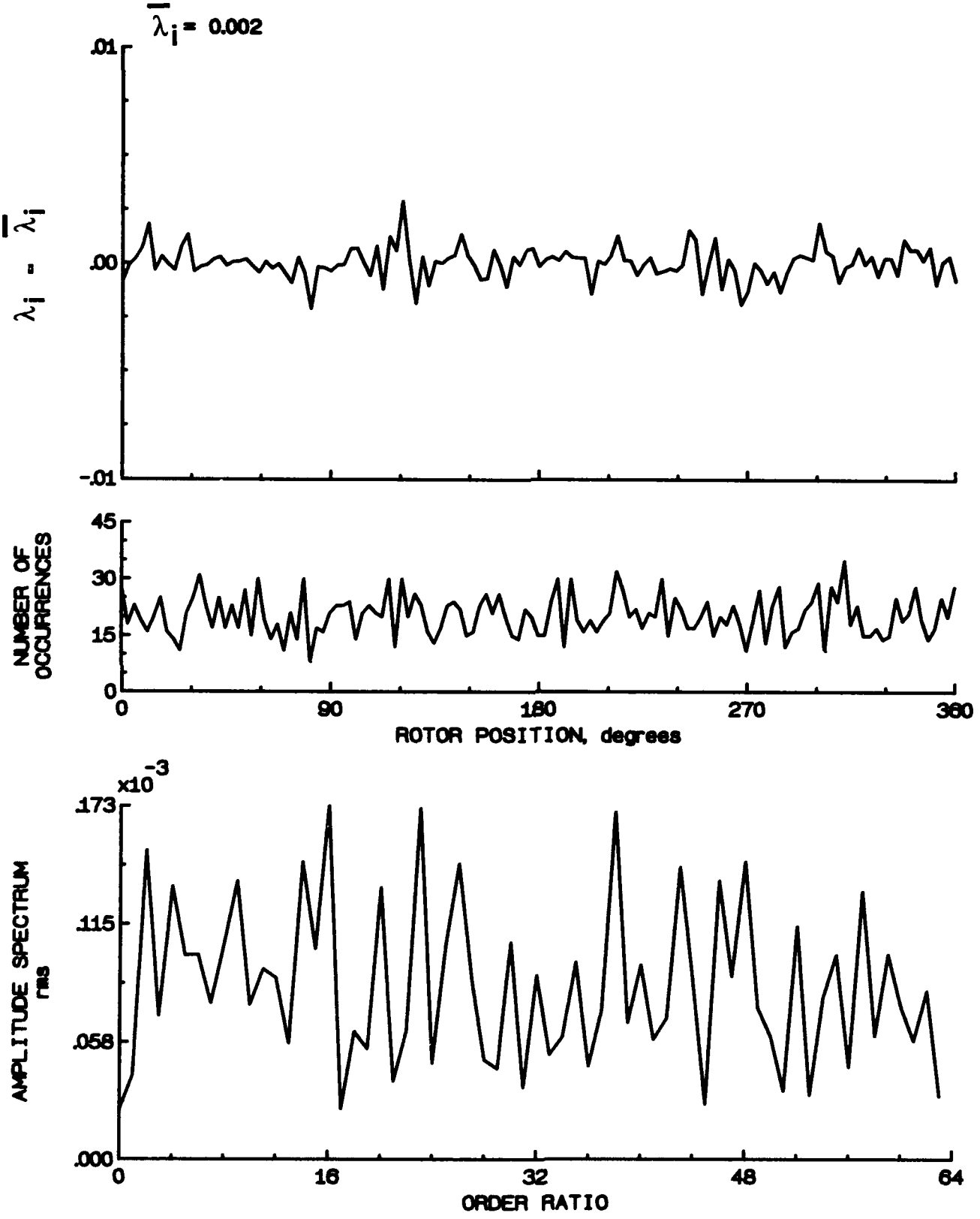

Figure 83.- Concluded.

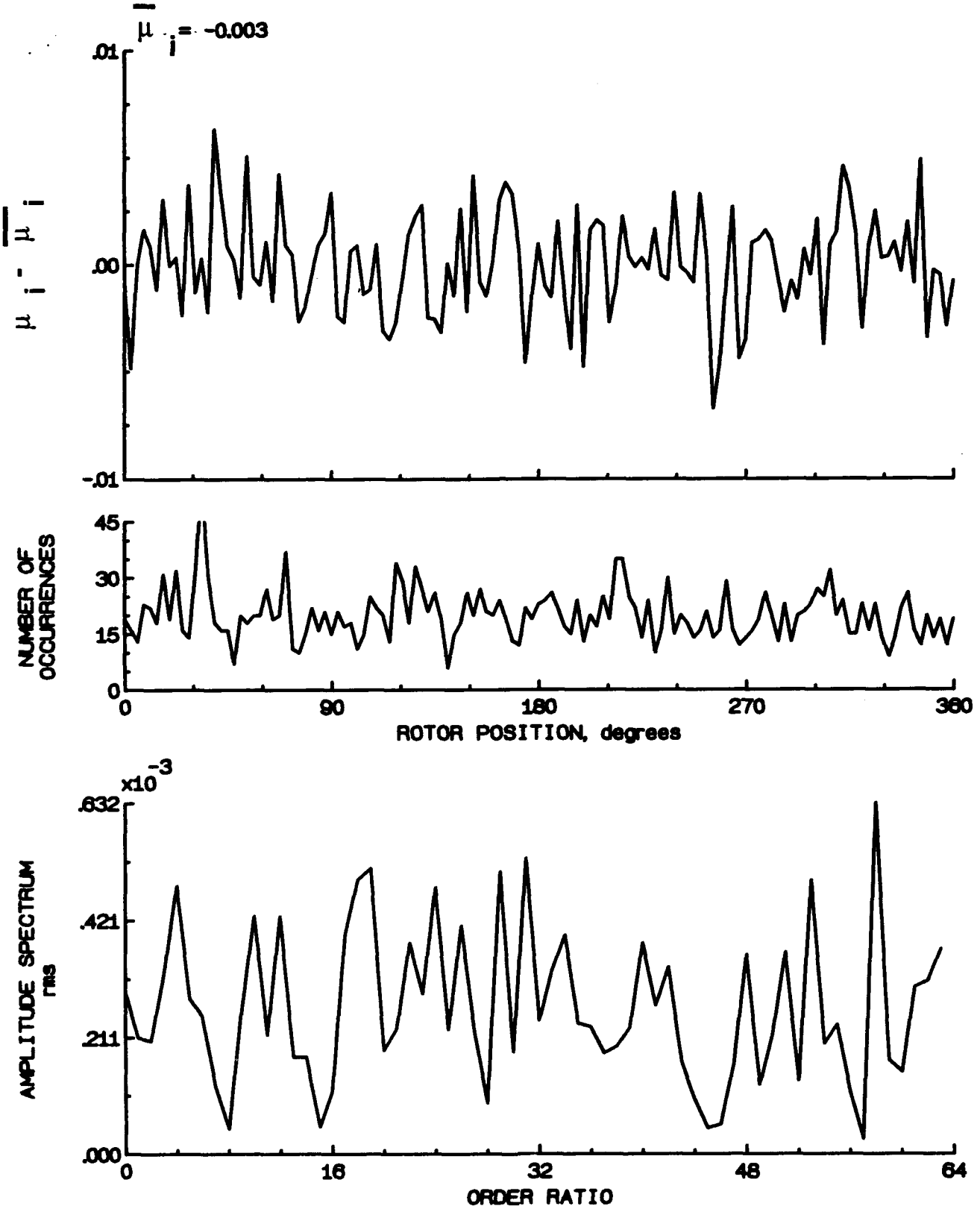

Figure 84.- Induced inflow velocity measured at 120 degrees and r/R of 1.02.

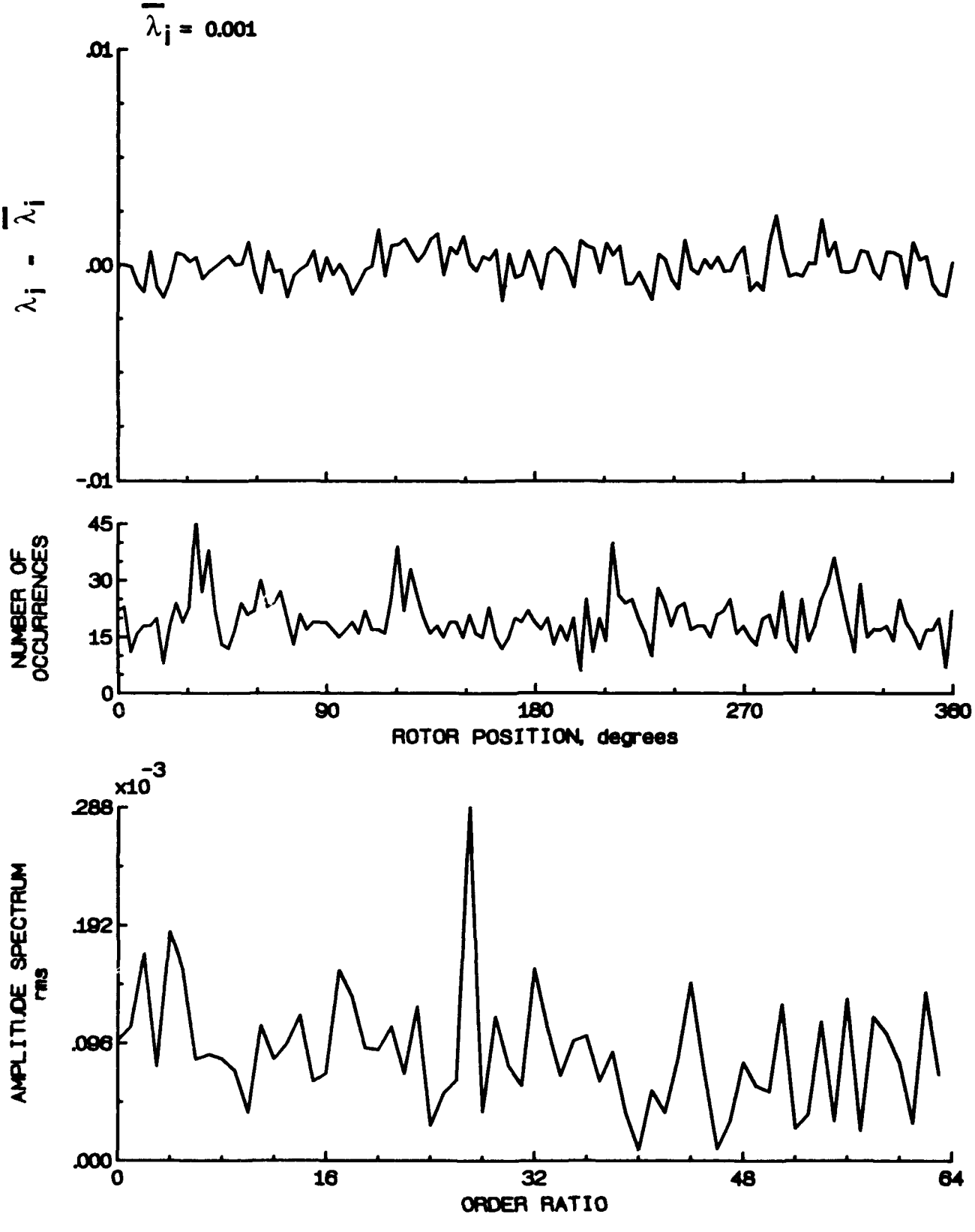

Figure 84.- Concluded.

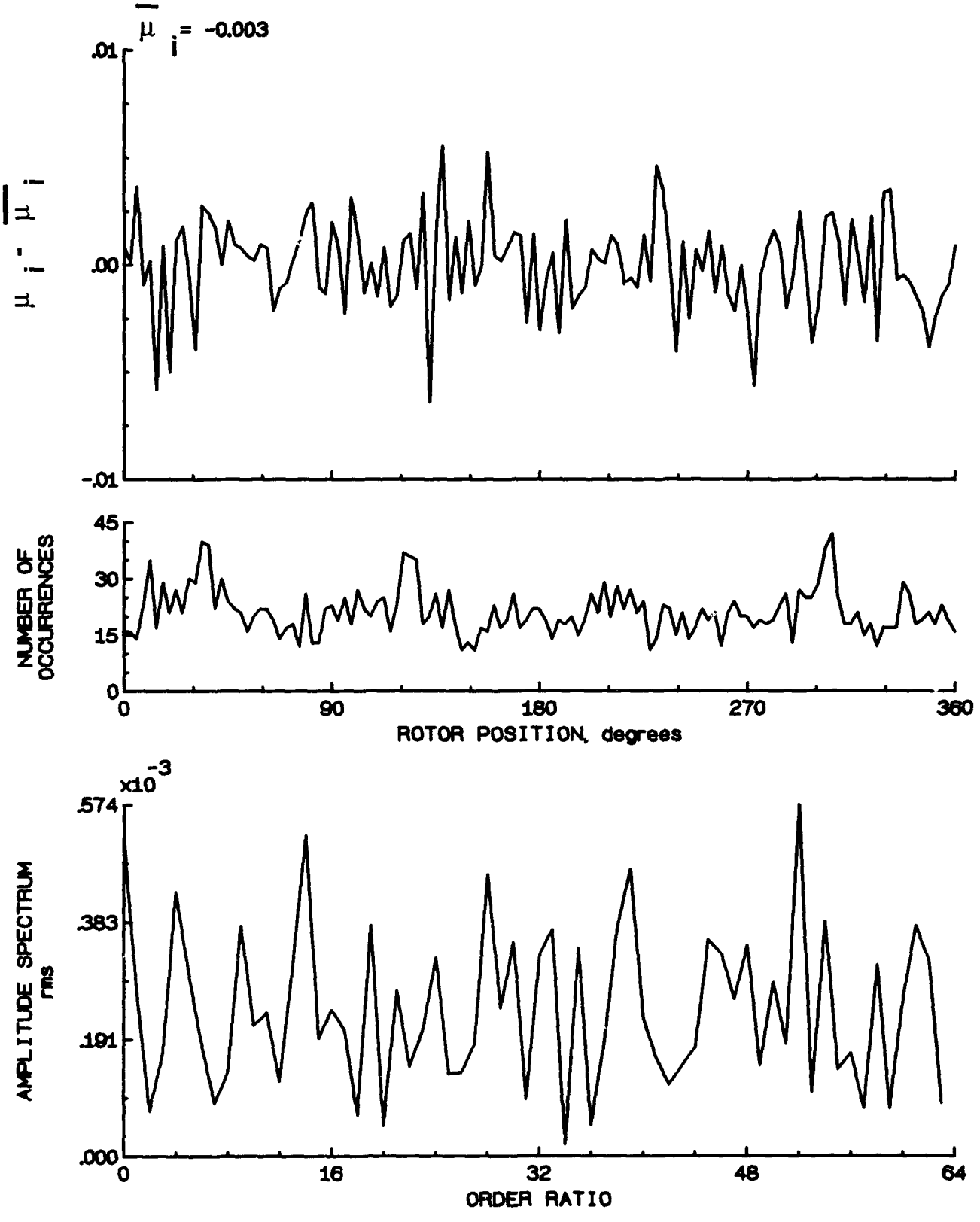

Figure 85.- Induced inflow velocity measured at 120 degrees and r/R of 1.04.

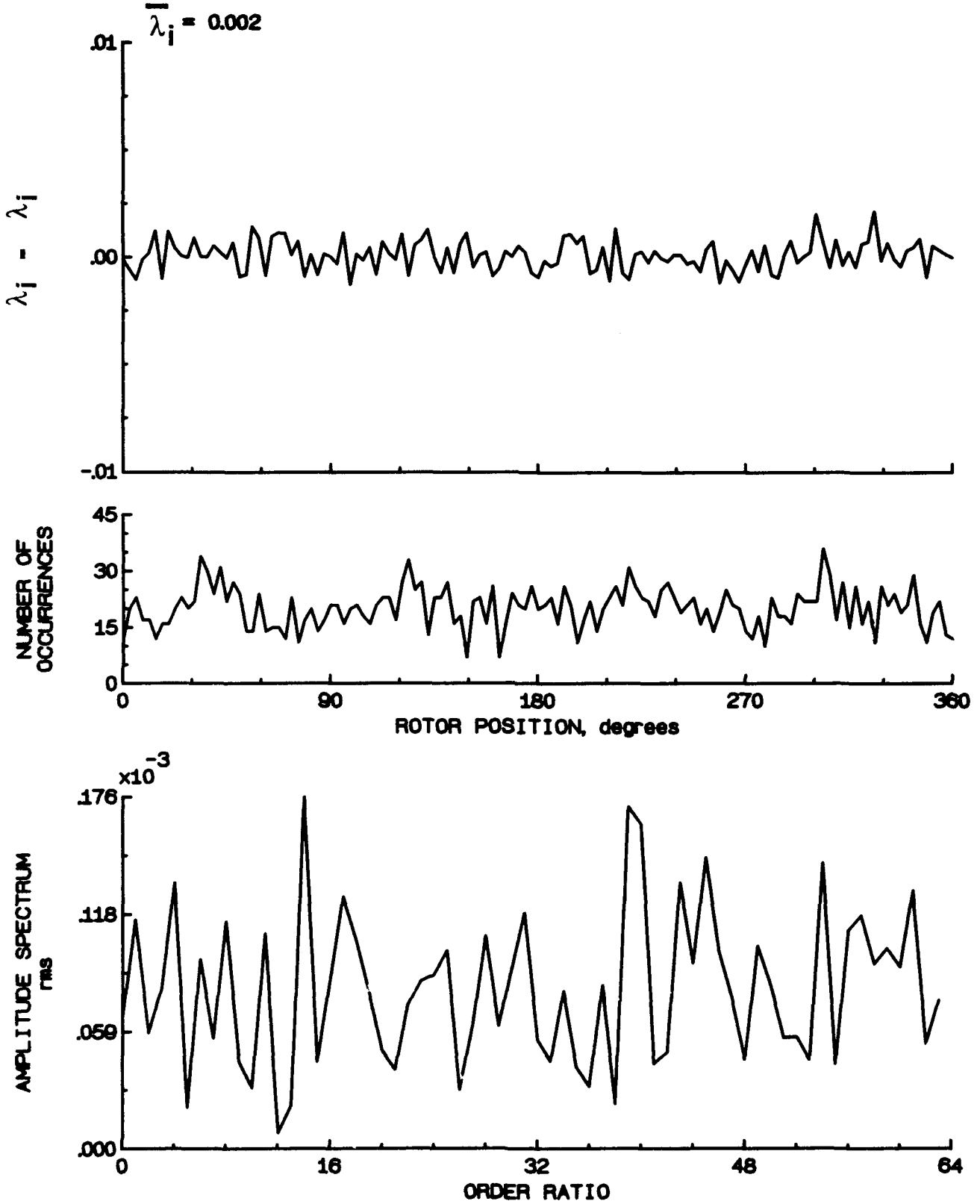

Figure 85.- Concluded.

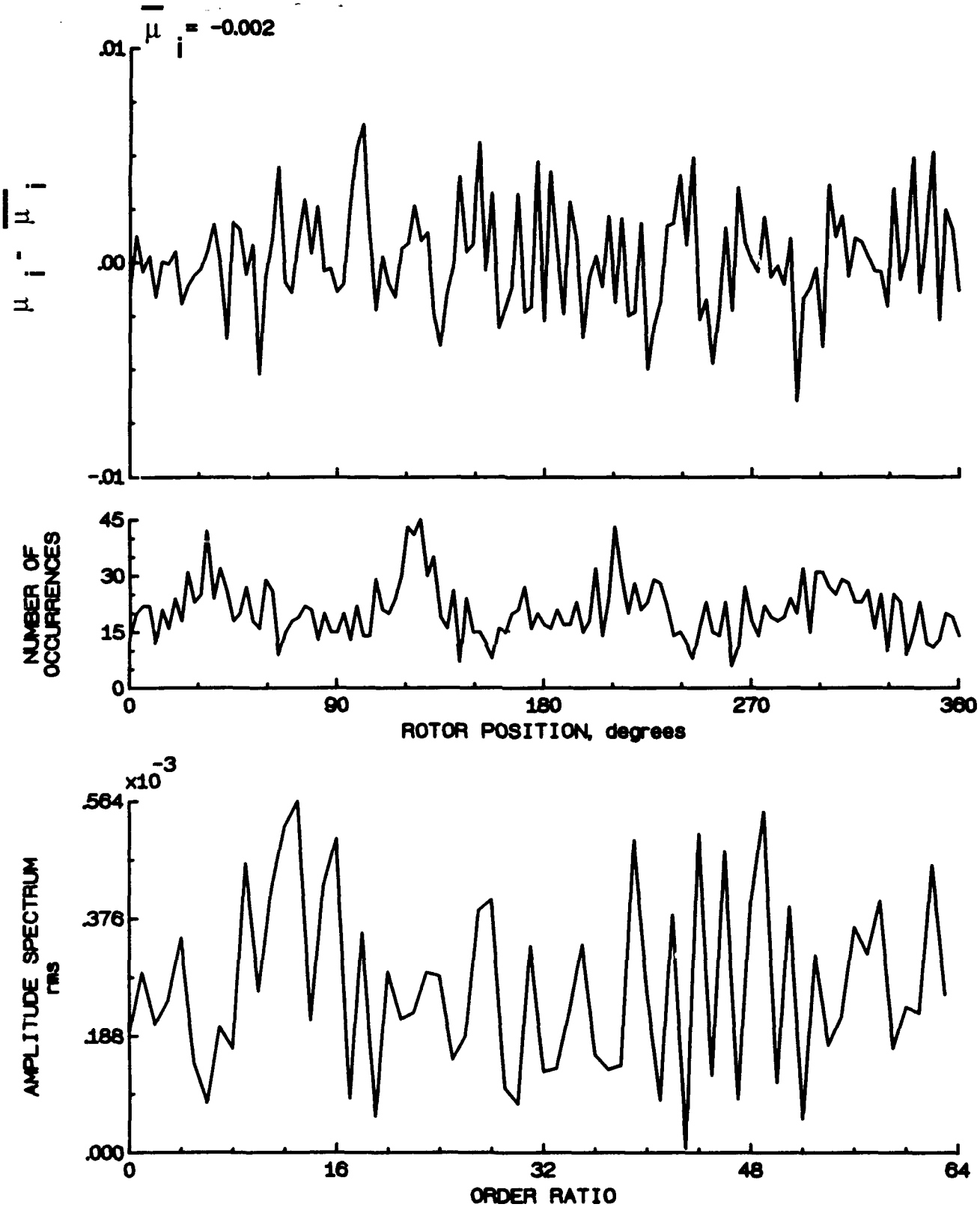

Figure 86.- Induced inflow velocity measured at 120 degrees and r/R of 1.10.

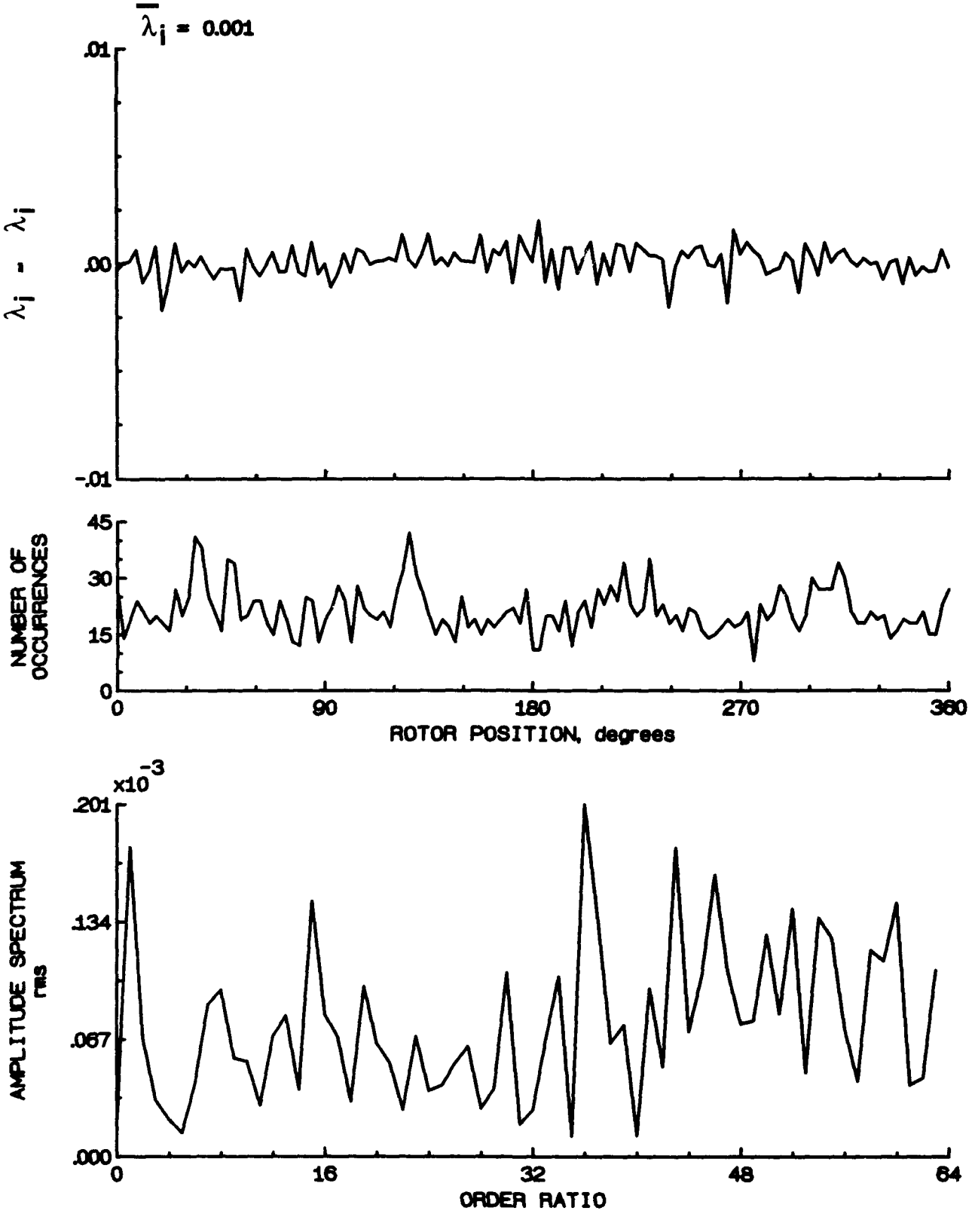

Figure 86.- Concluded.

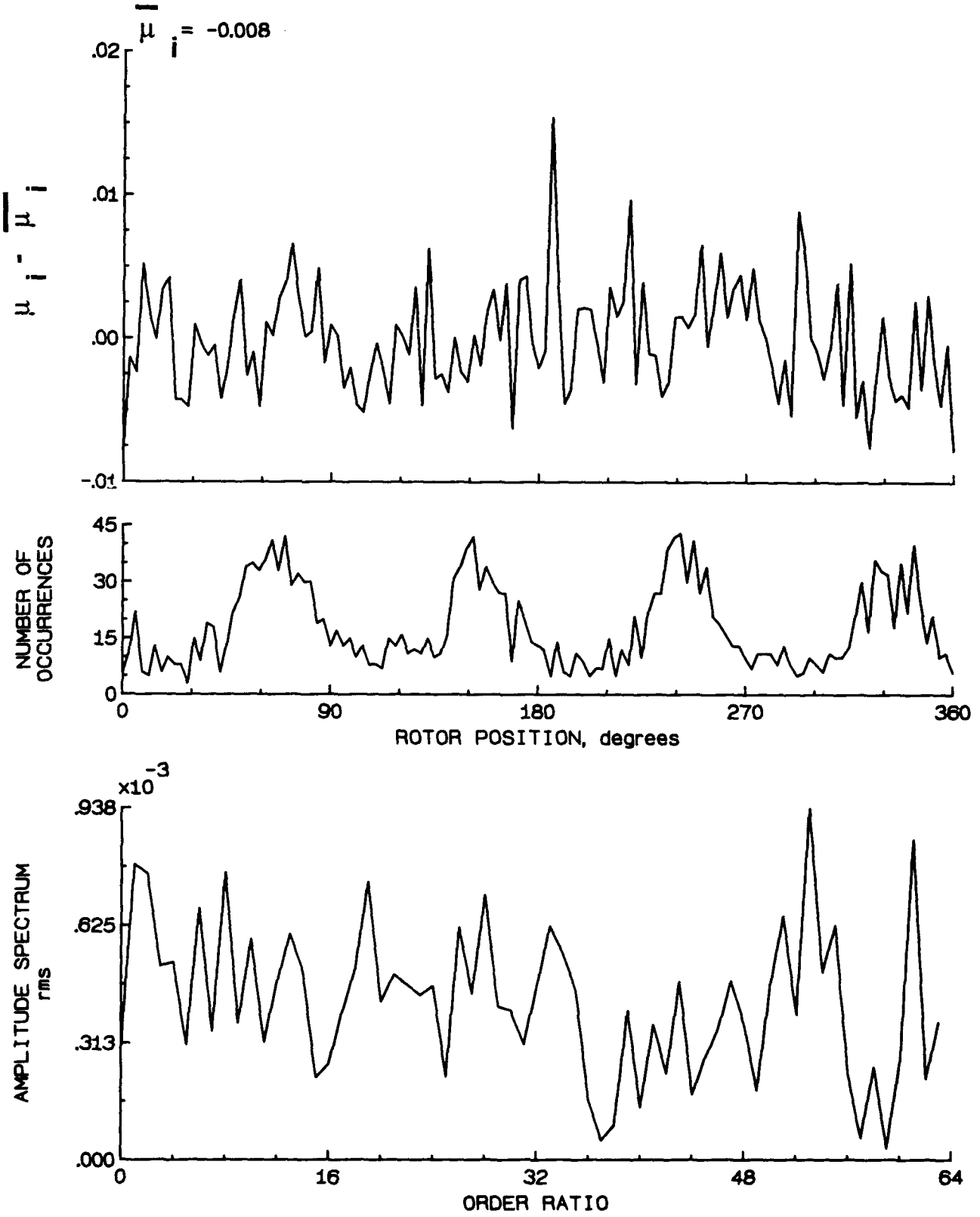

Figure 87.- Induced inflow velocity measured at 150 degrees and r/R of 0.20.

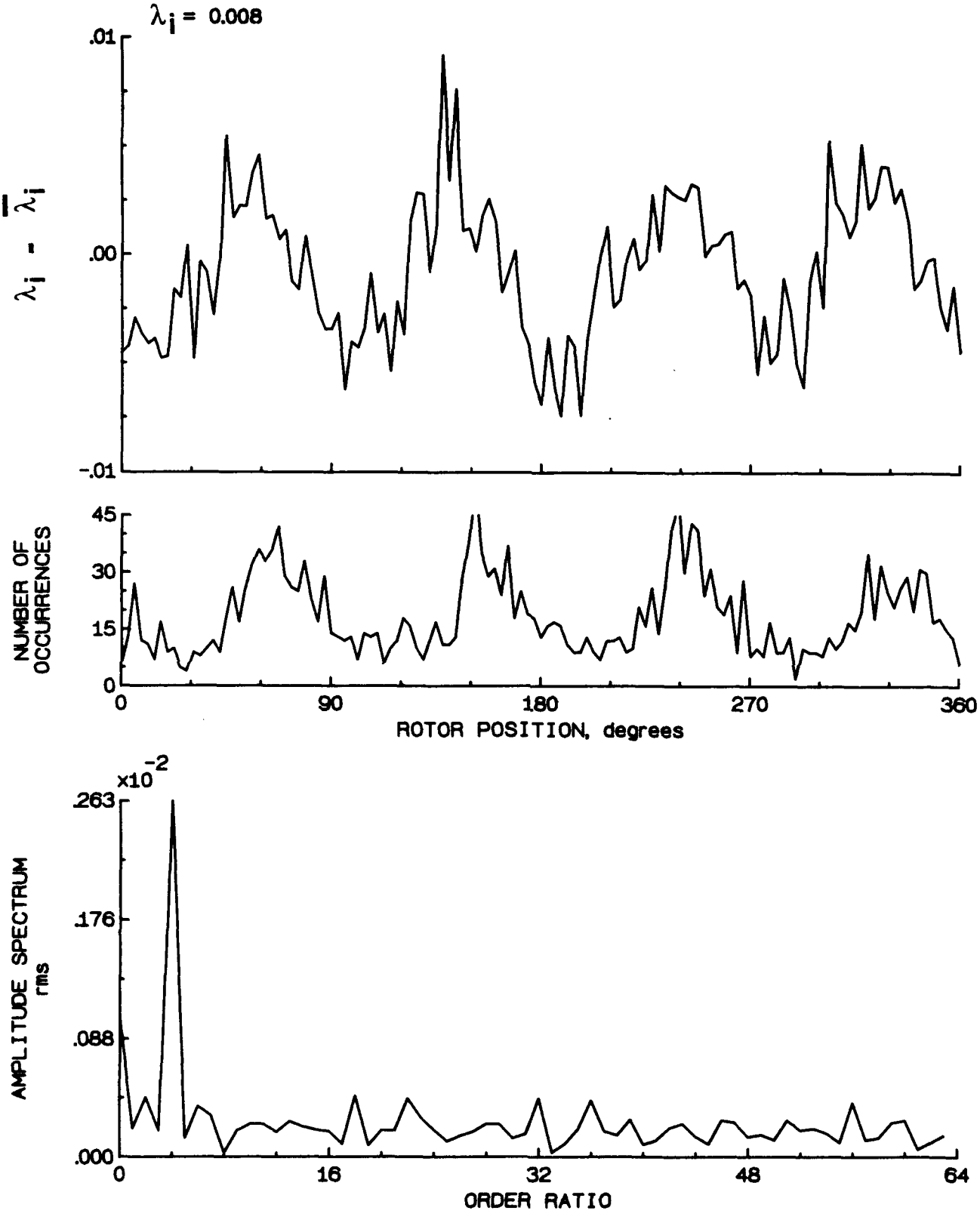

Figure 87.- Concluded.

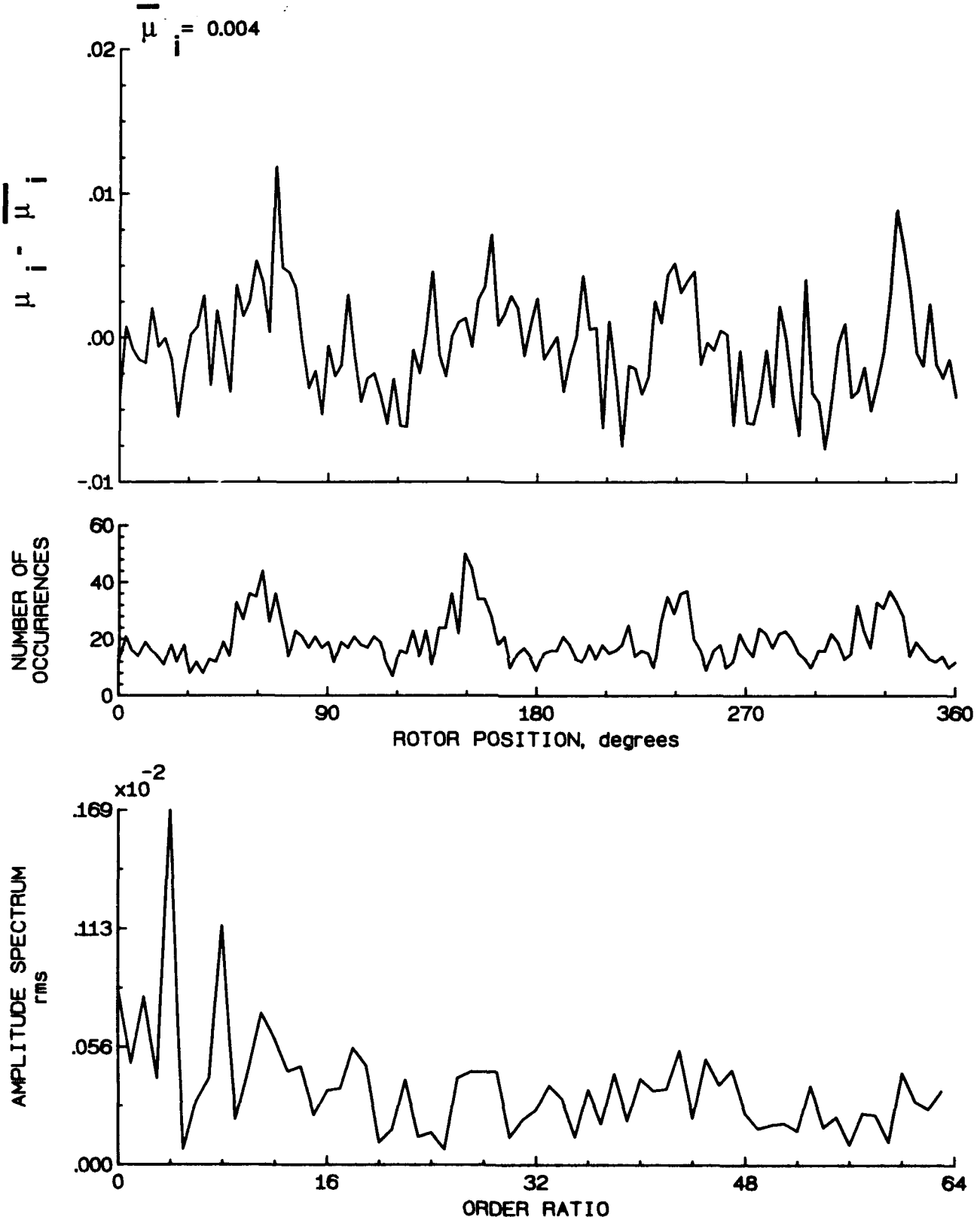

Figure 88.- Induced inflow velocity measured at 150 degrees and r/R of 0.40.

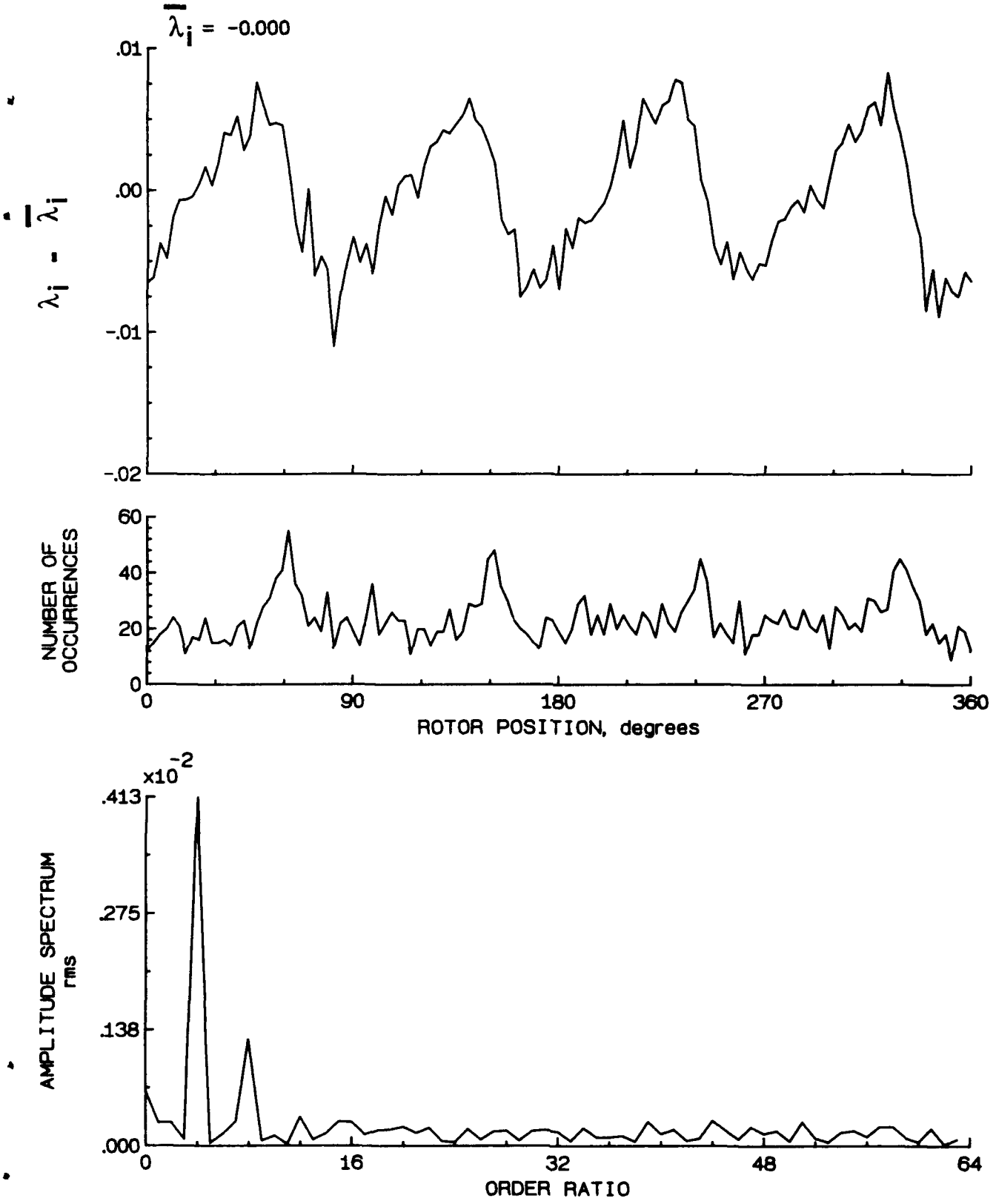

Figure 88.- Concluded.

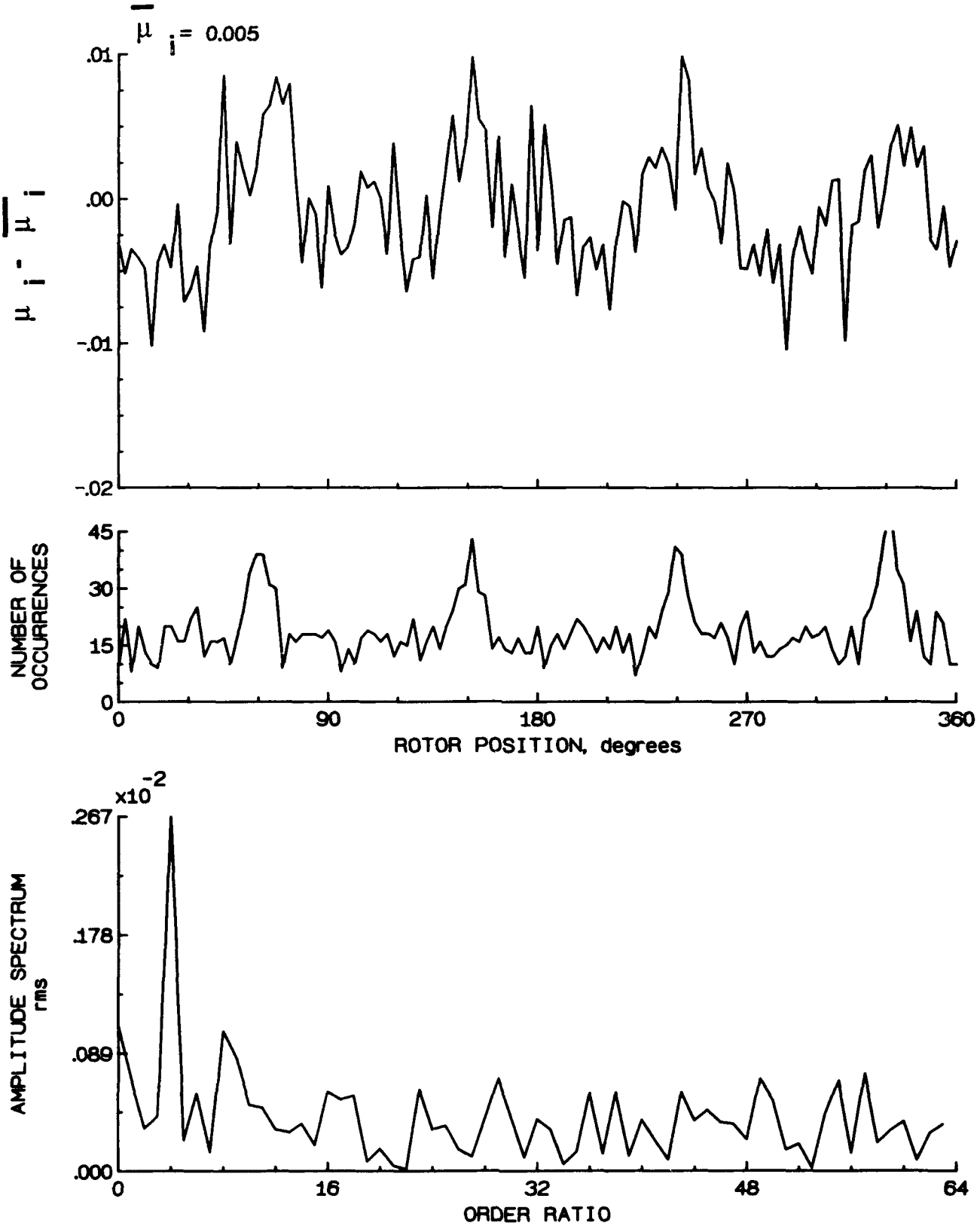

Figure 89.- Induced inflow velocity measured at 150 degrees and r/R of 0.50.

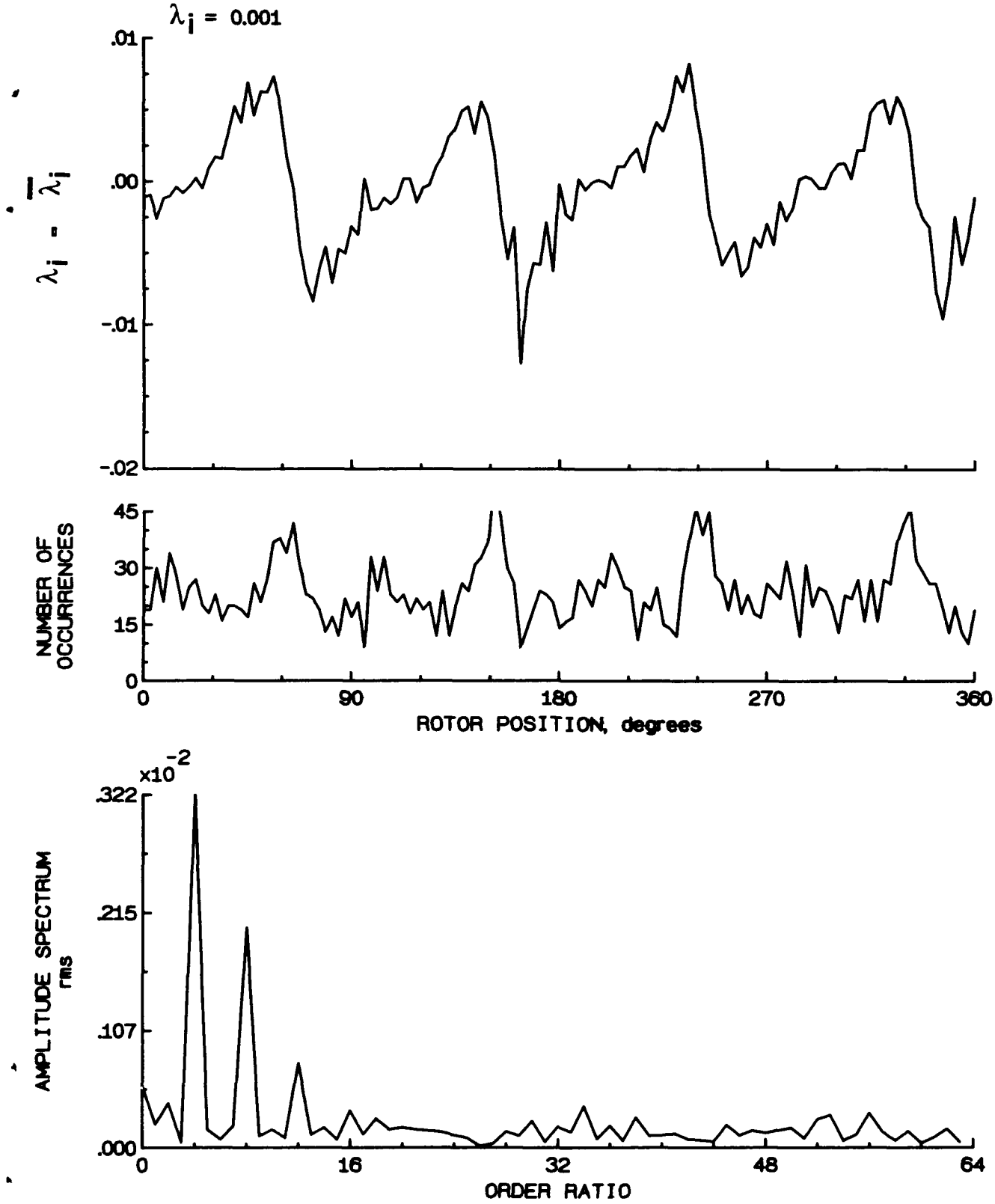

Figure 89.- Concluded.

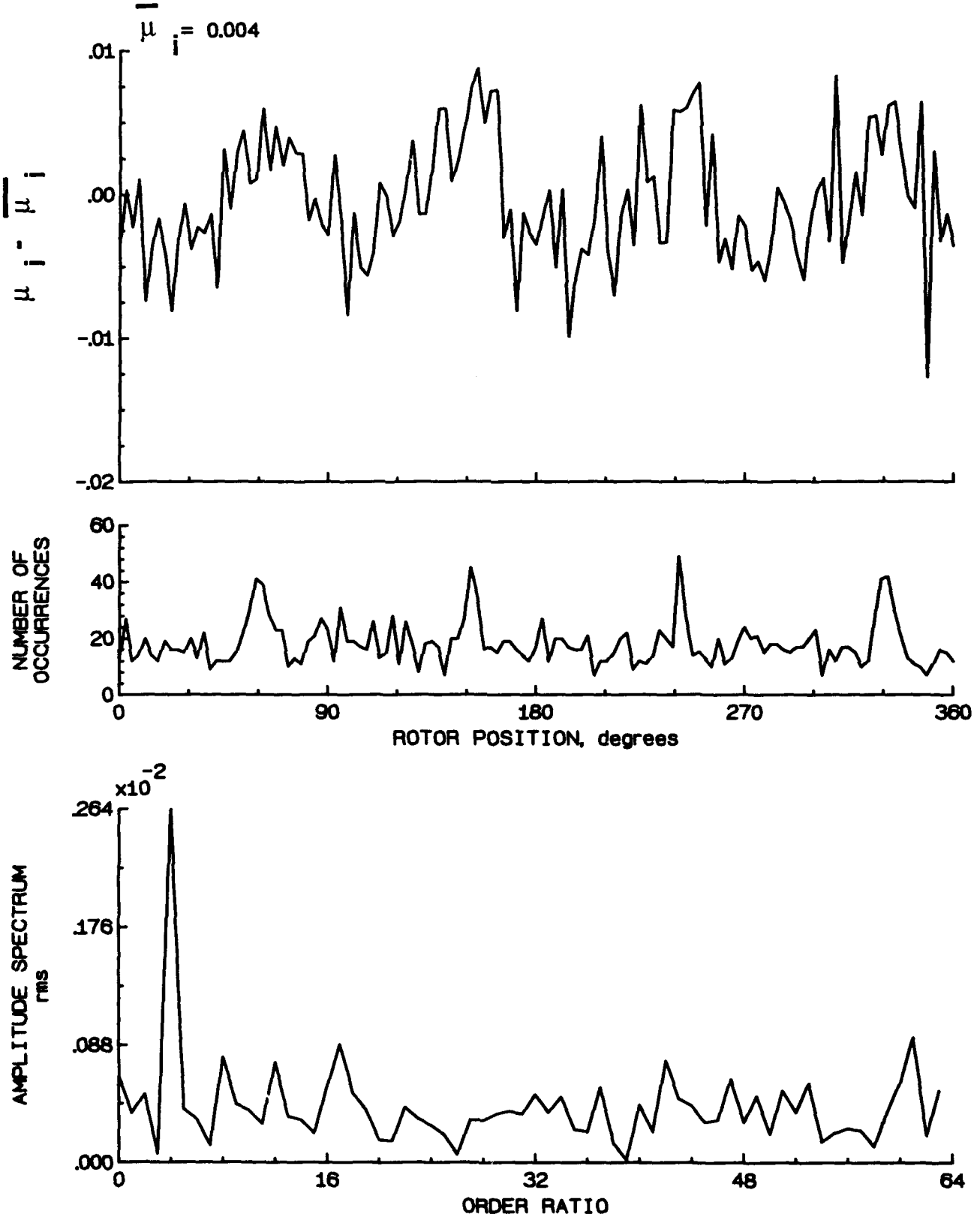

Figure 90.- Induced inflow velocity measured at 150 degrees and r/R of 0.60.

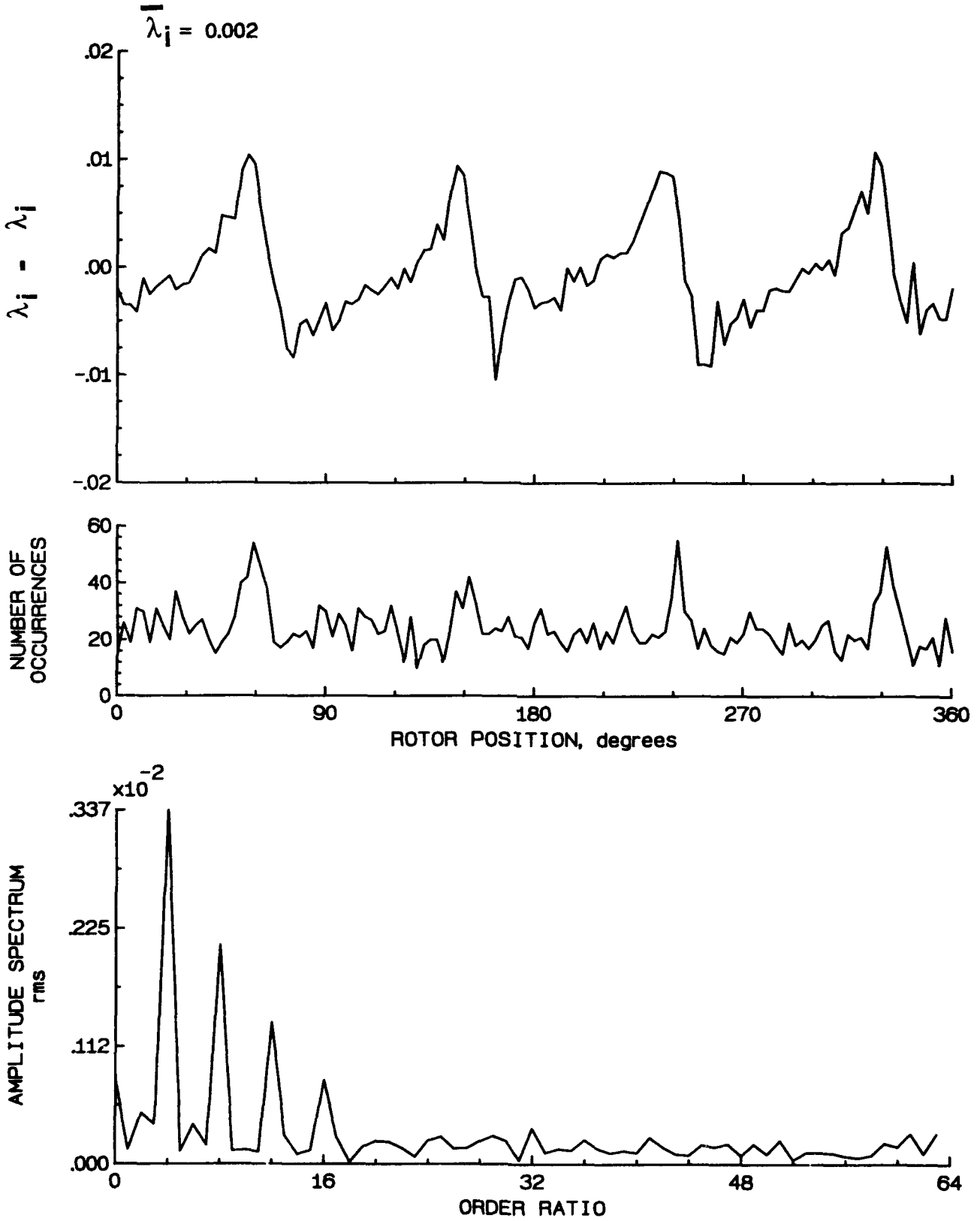

Figure 90.- Concluded.

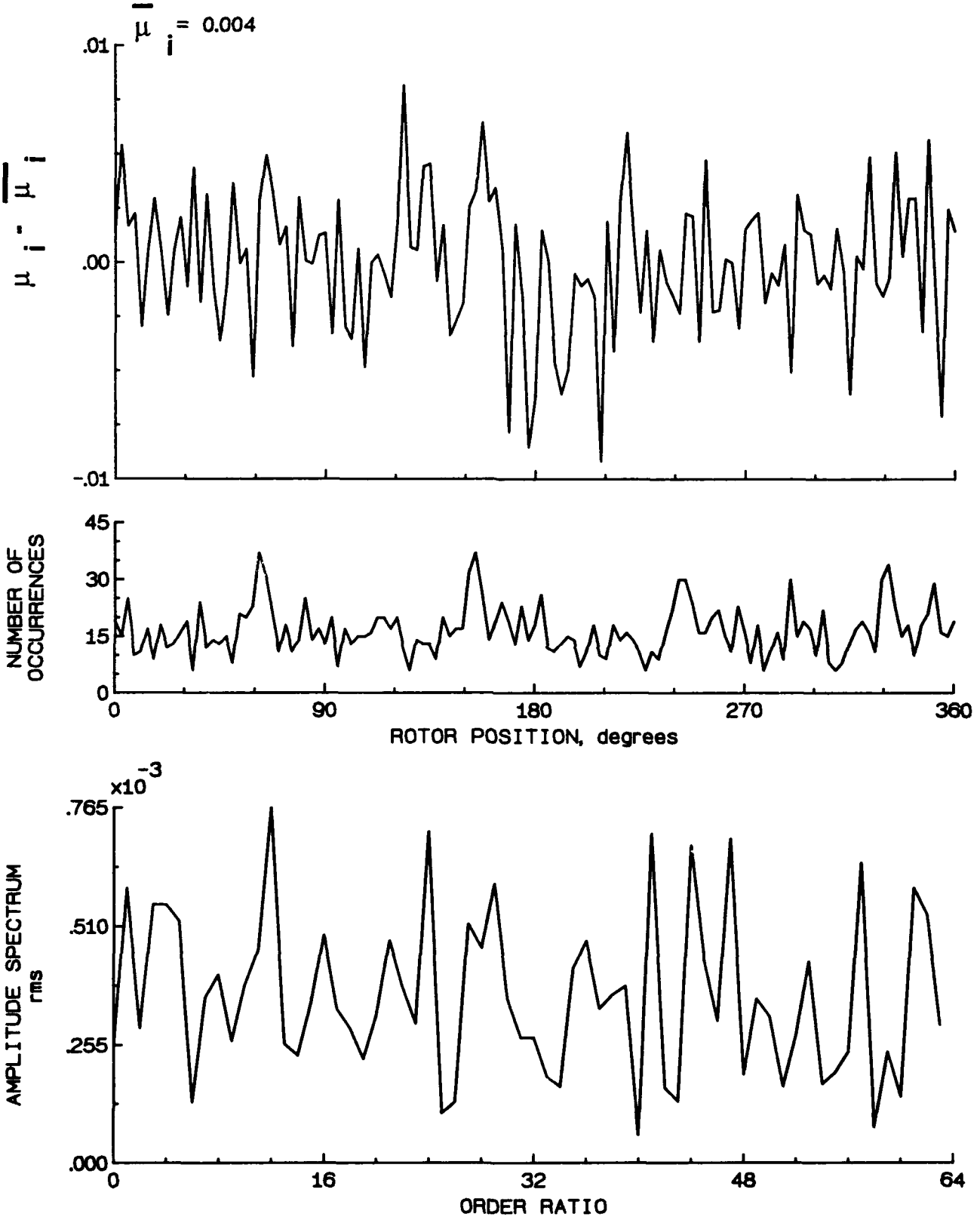

Figure 91.- Induced inflow velocity measured at 150 degrees and r/R of 0.70.

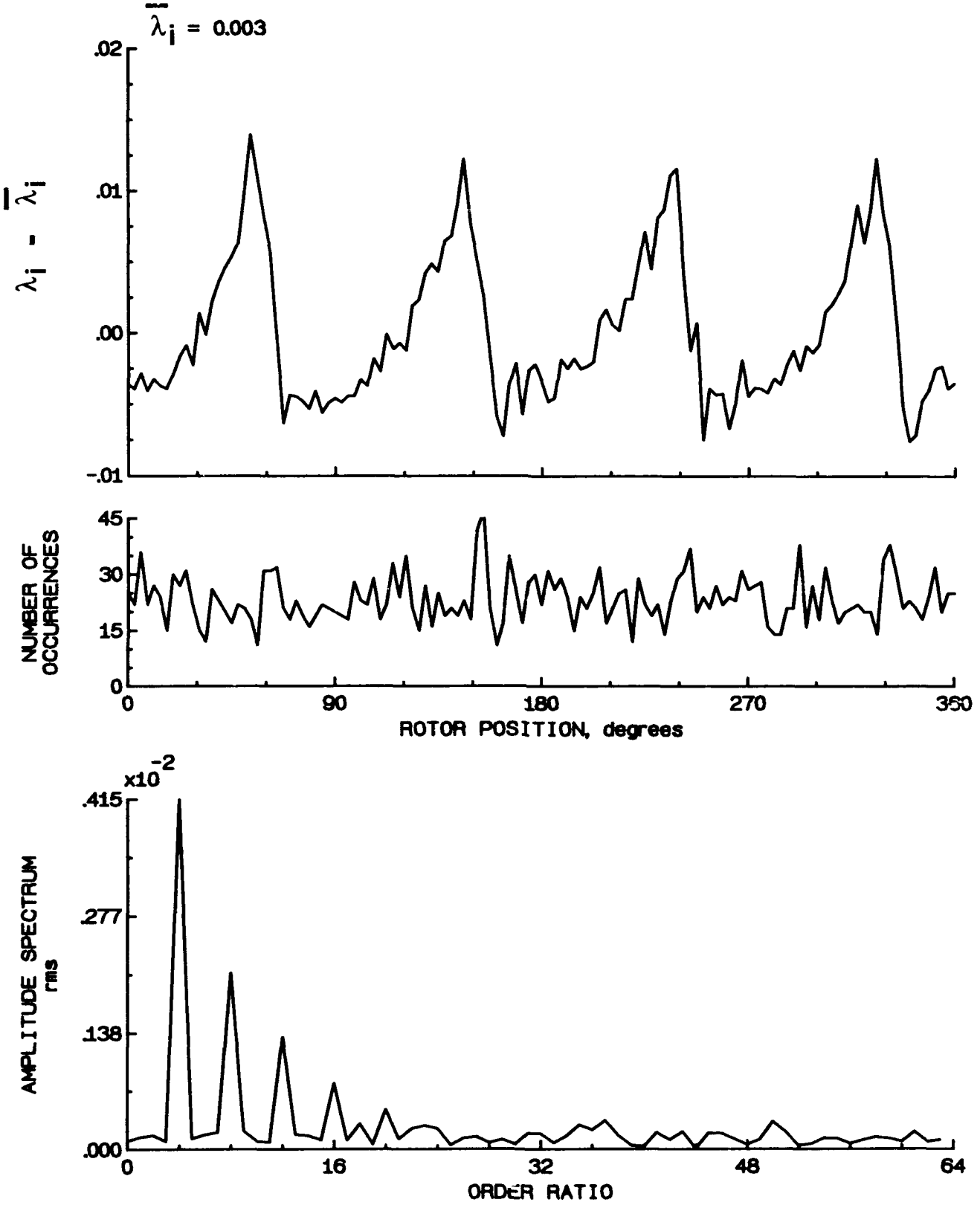

Figure 91.- Concluded.

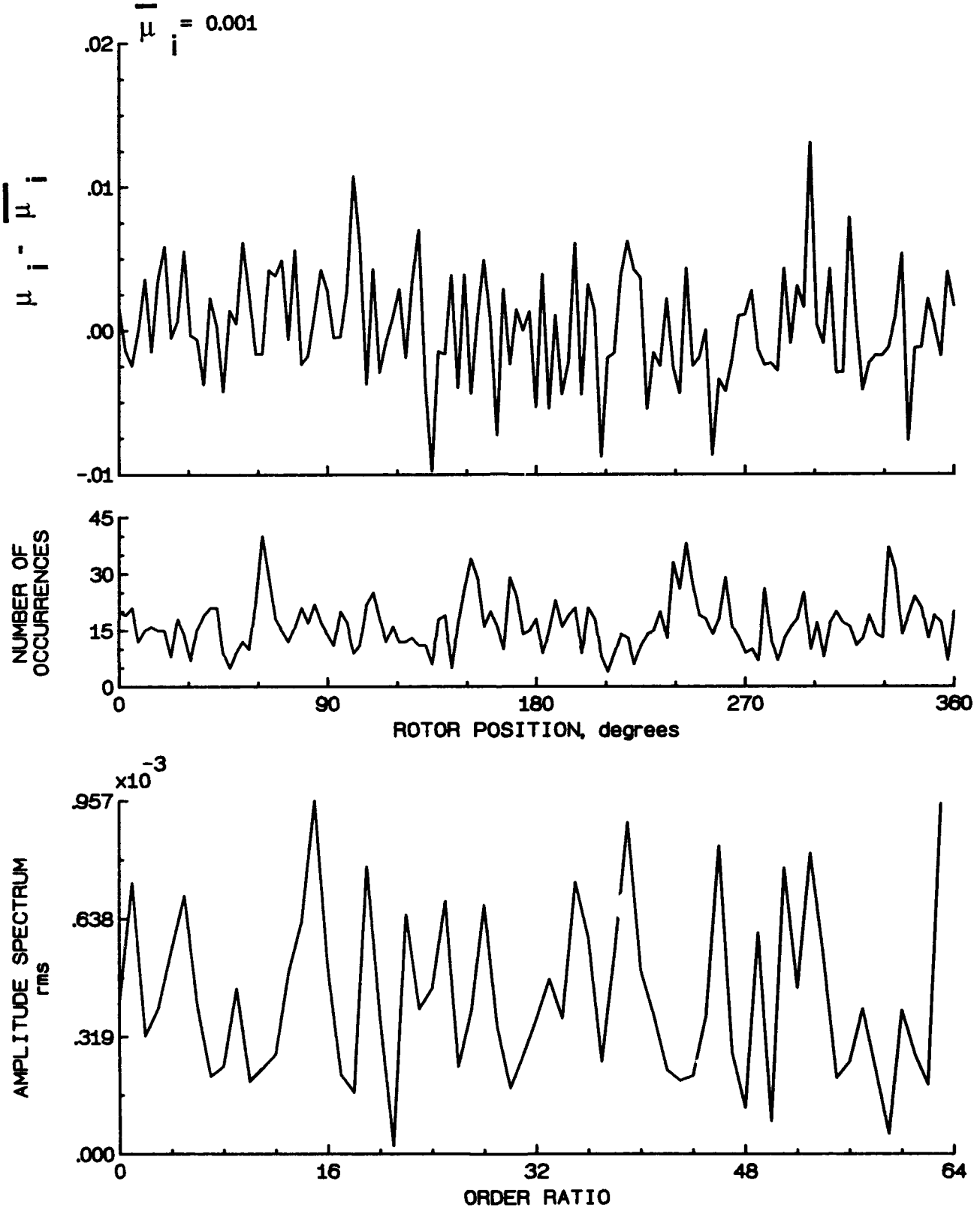

Figure 92.- Induced inflow velocity measured at 150 degrees and r/R of 0.74.

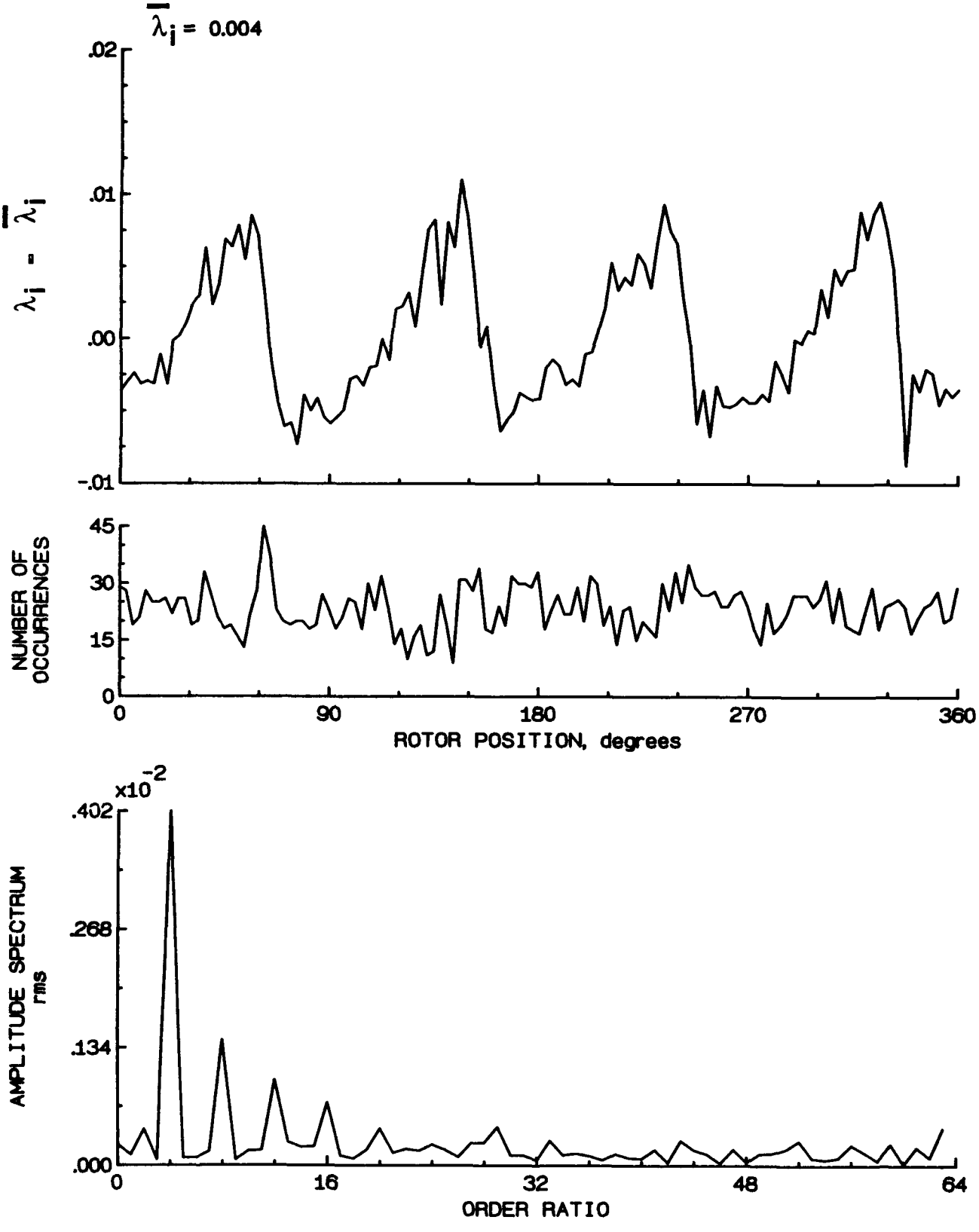

Figure 92.- Concluded.

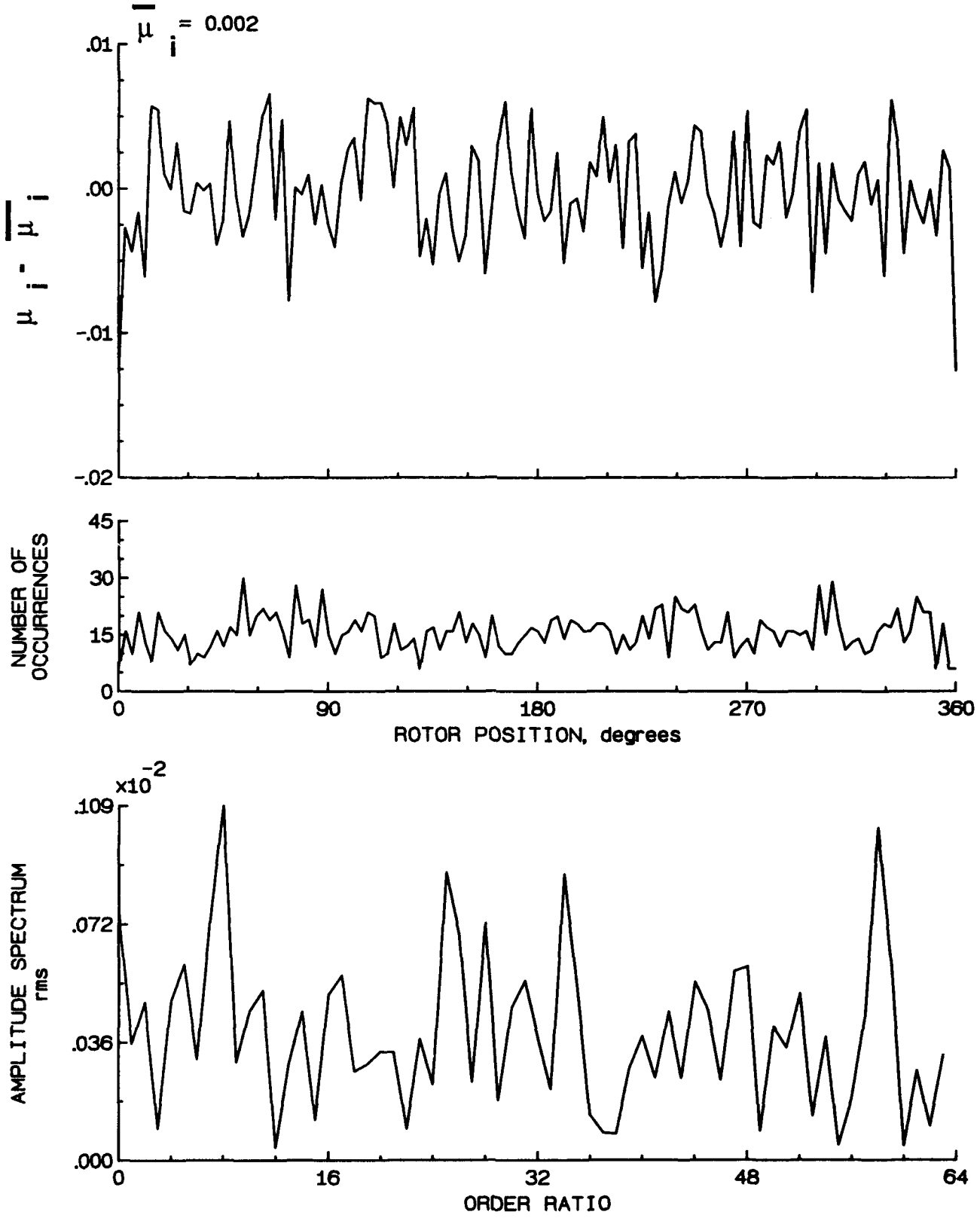

Figure 93.- Induced inflow velocity measured at 150 degrees and r/R of 0.78.

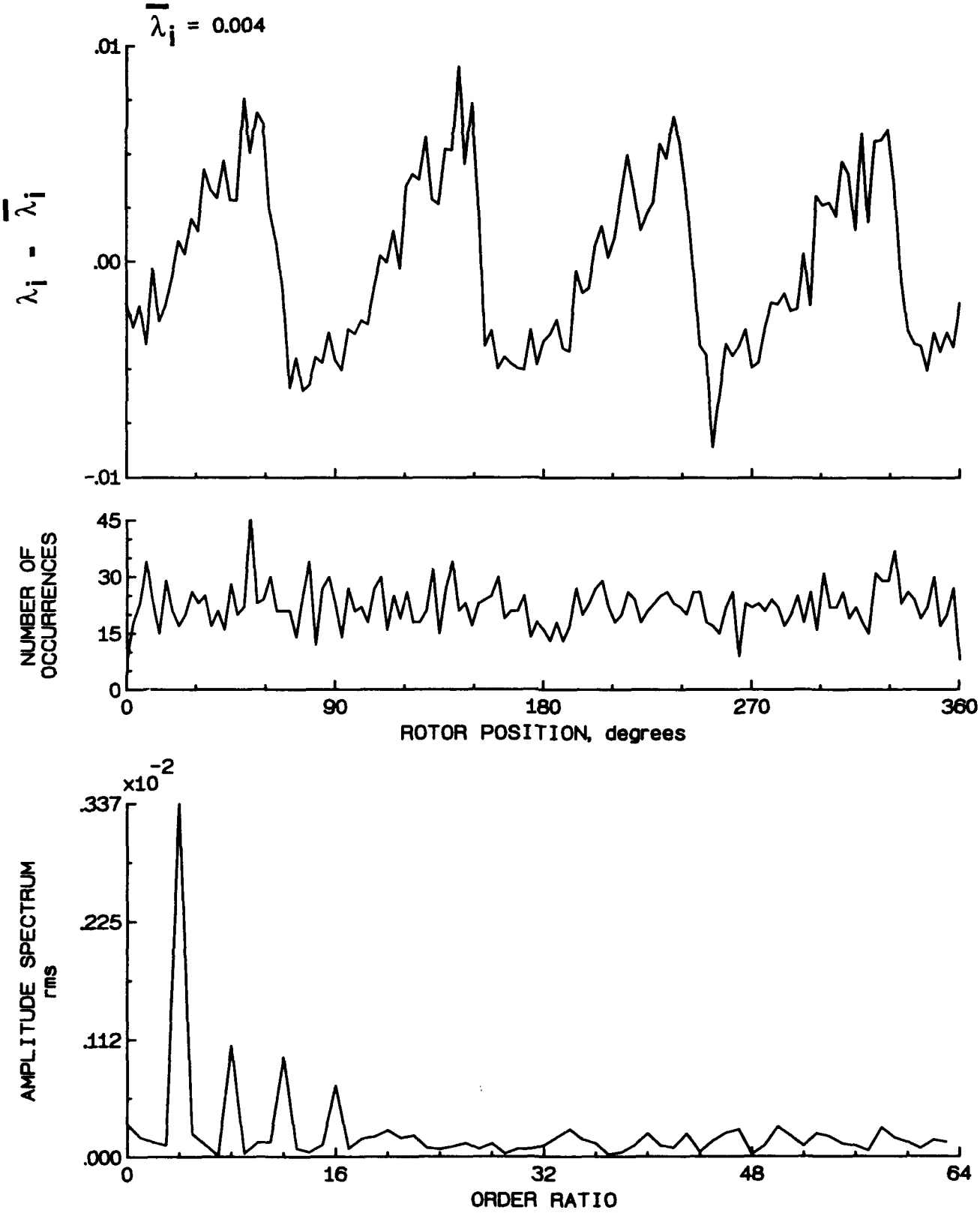

Figure 93.- Concluded.

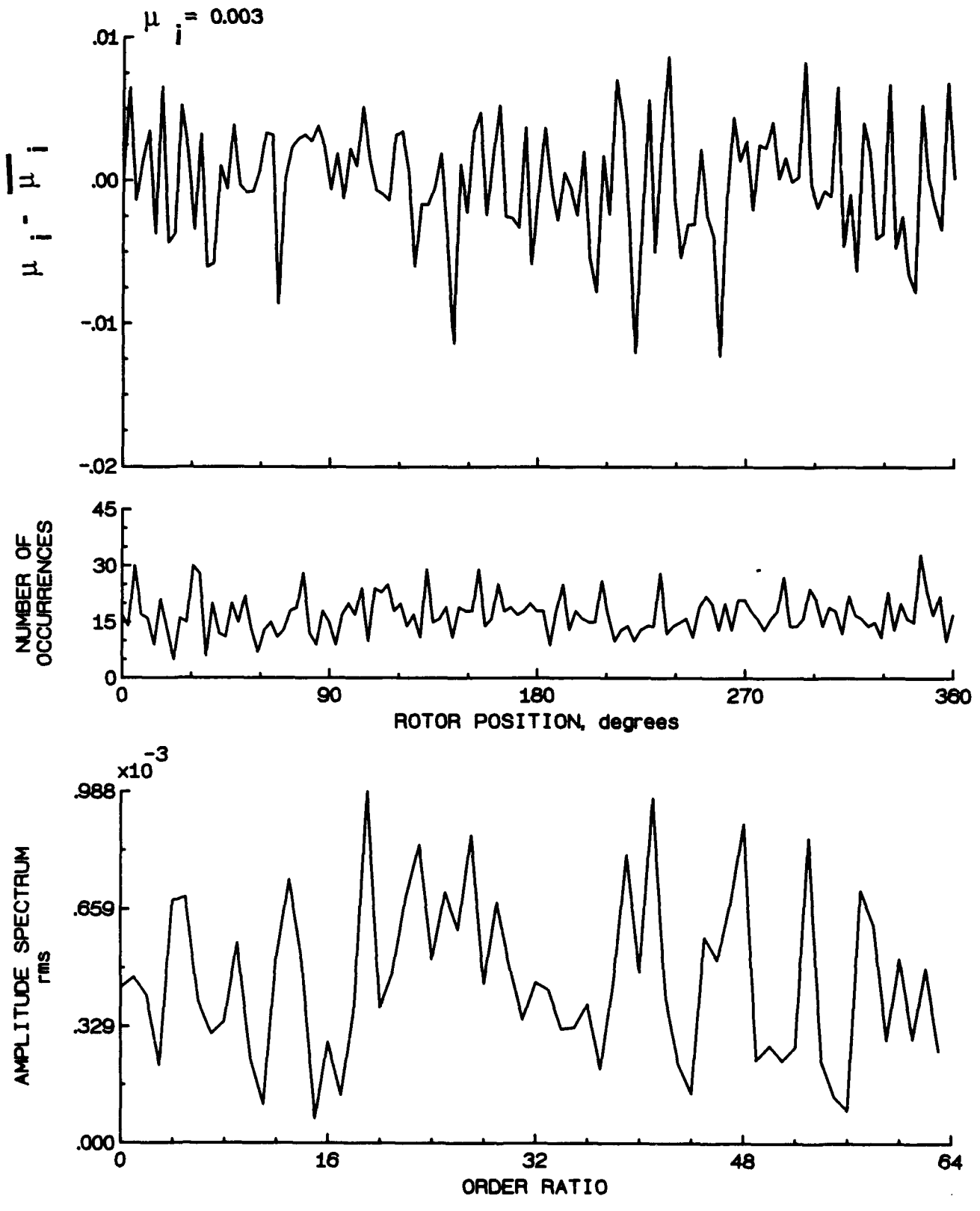

Figure 94.- Induced inflow velocity measured at 150 degrees and r/R of 0.82.

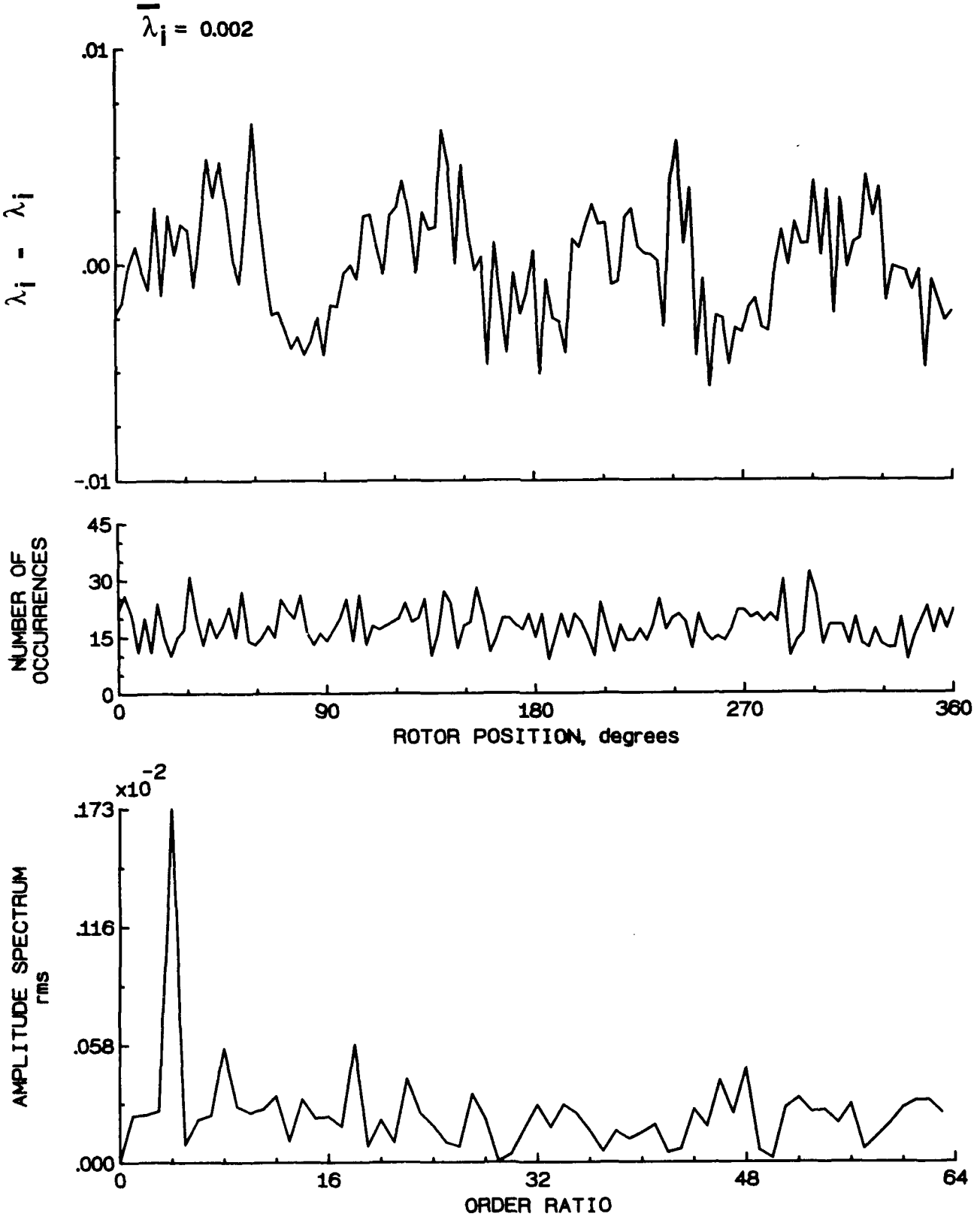

Figure 94.- Concluded.

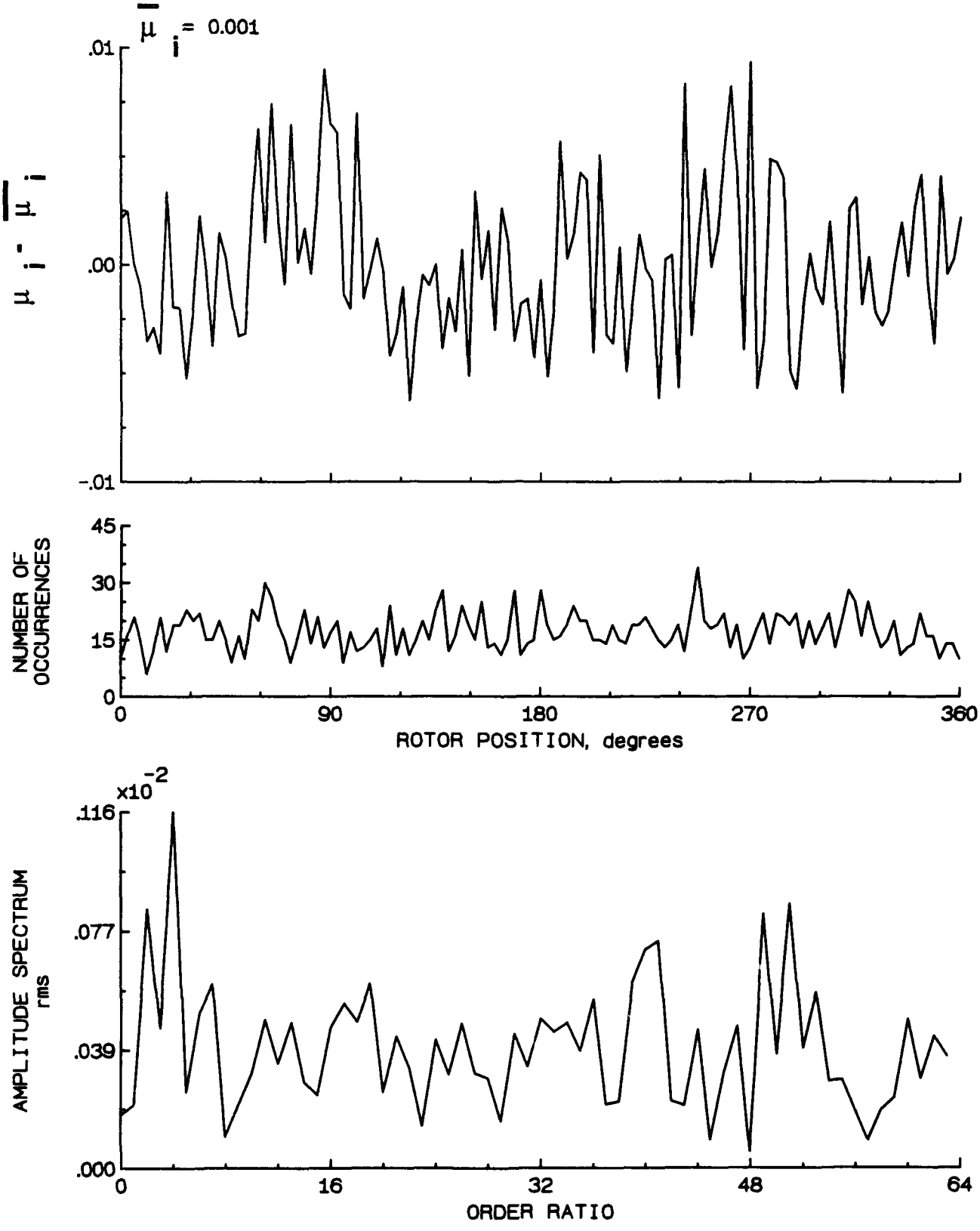

Figure 95.- Induced inflow velocity measured at 150 degrees and r/R of 0.86.

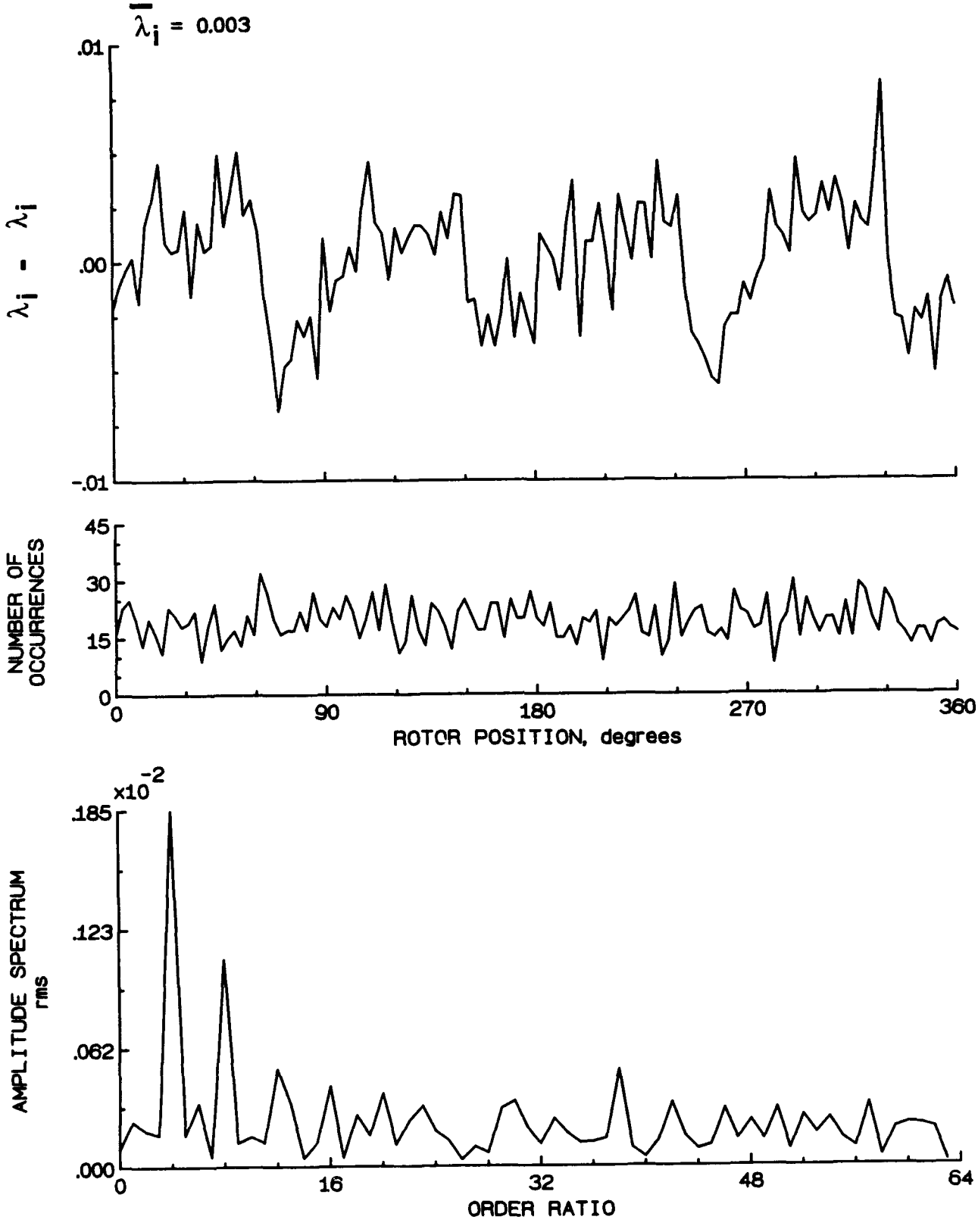

Figure 95.- Concluded.

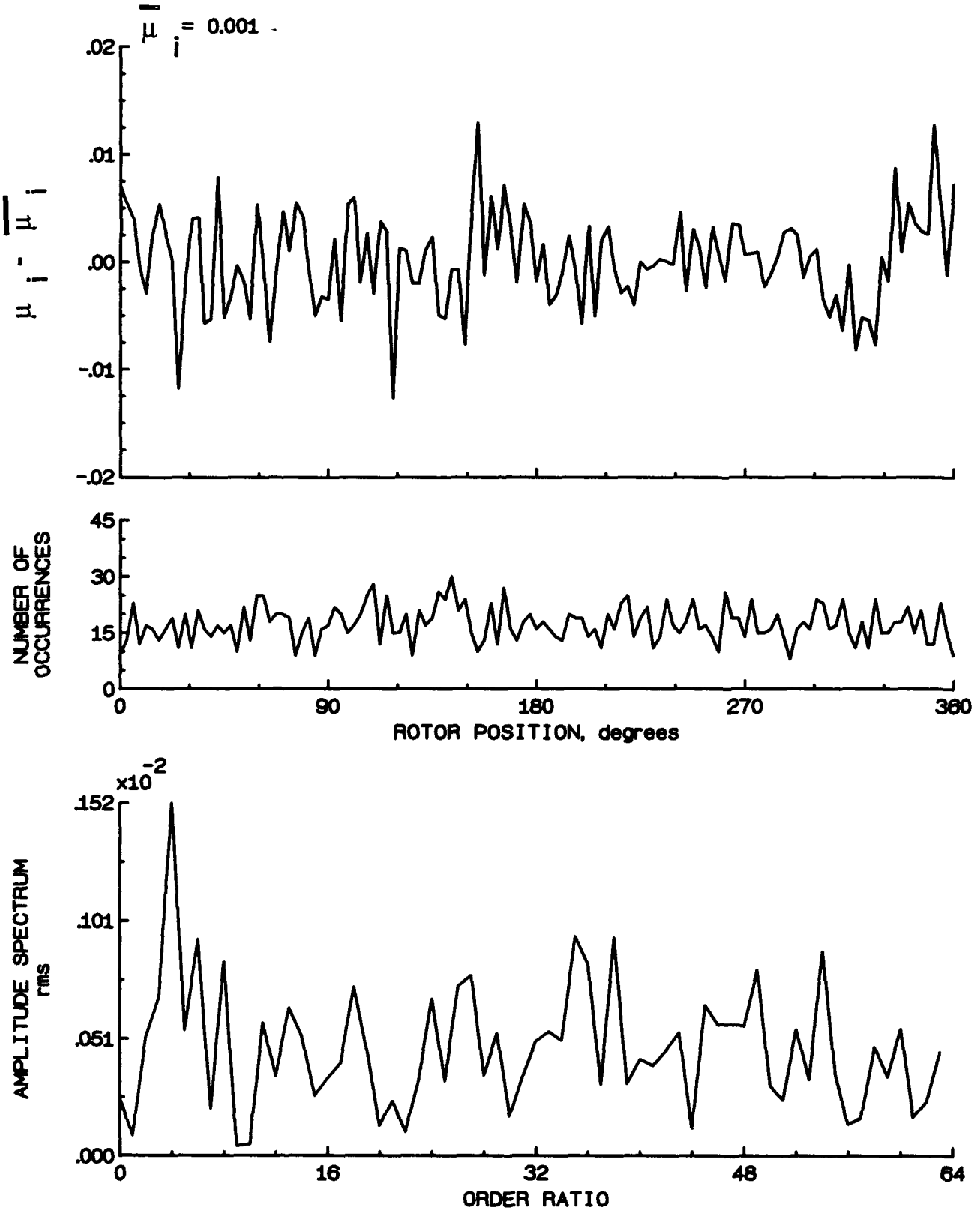

Figure 96.- Induced inflow velocity measured at 150 degrees and r/R of 0.90.

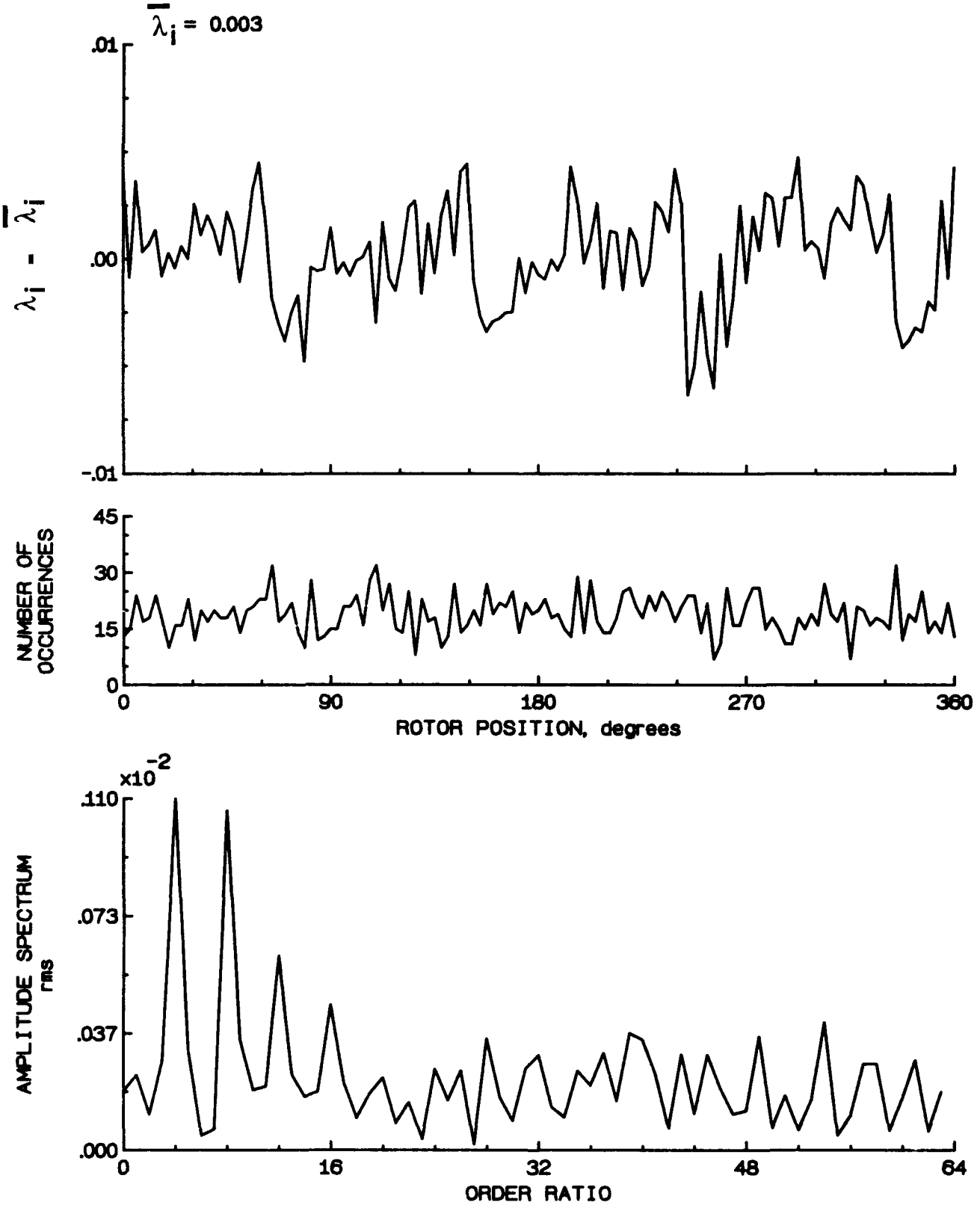

Figure 96.- Concluded.

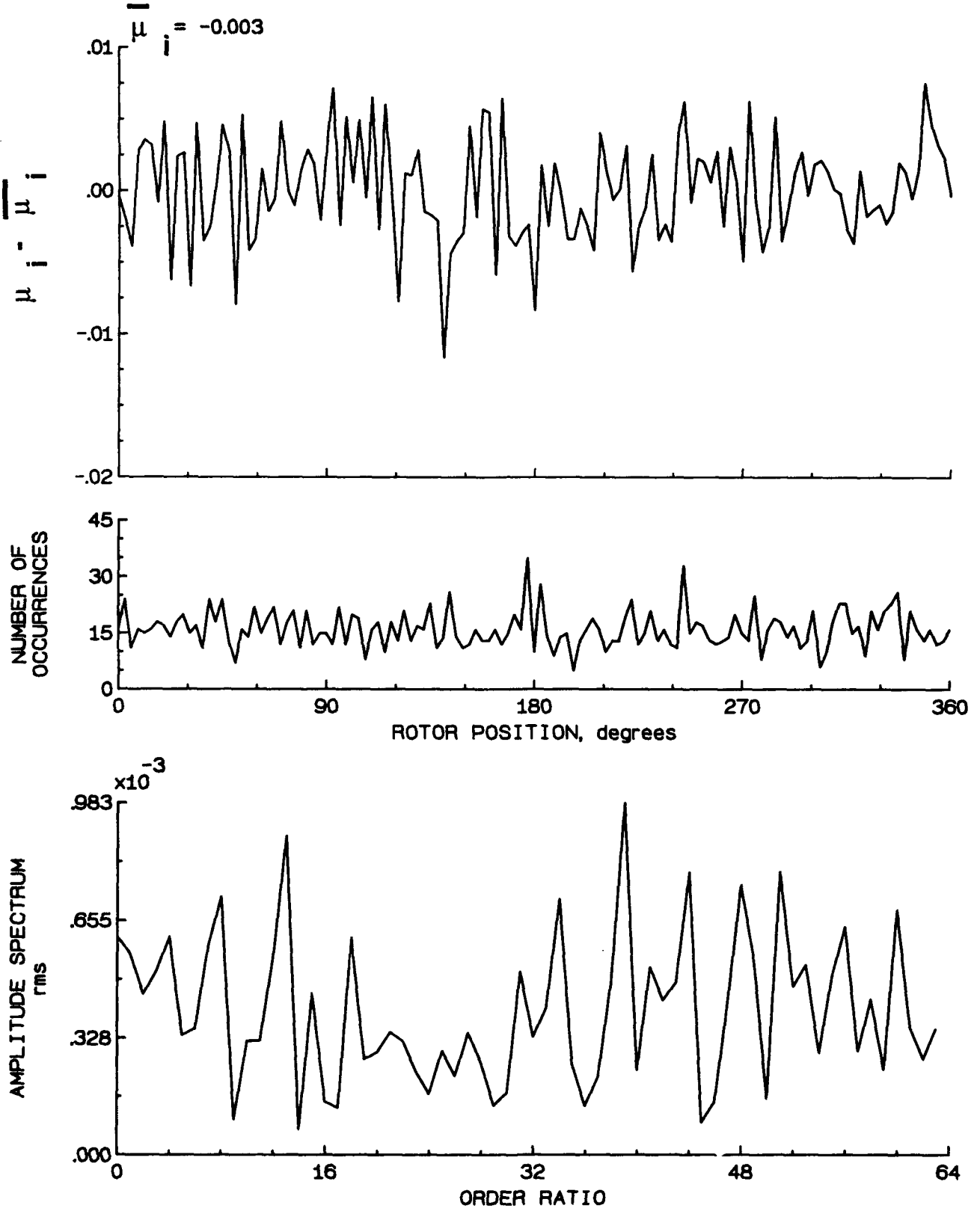

Figure 97.- Induced inflow velocity measured at 150 degrees and r/R of 0.94.

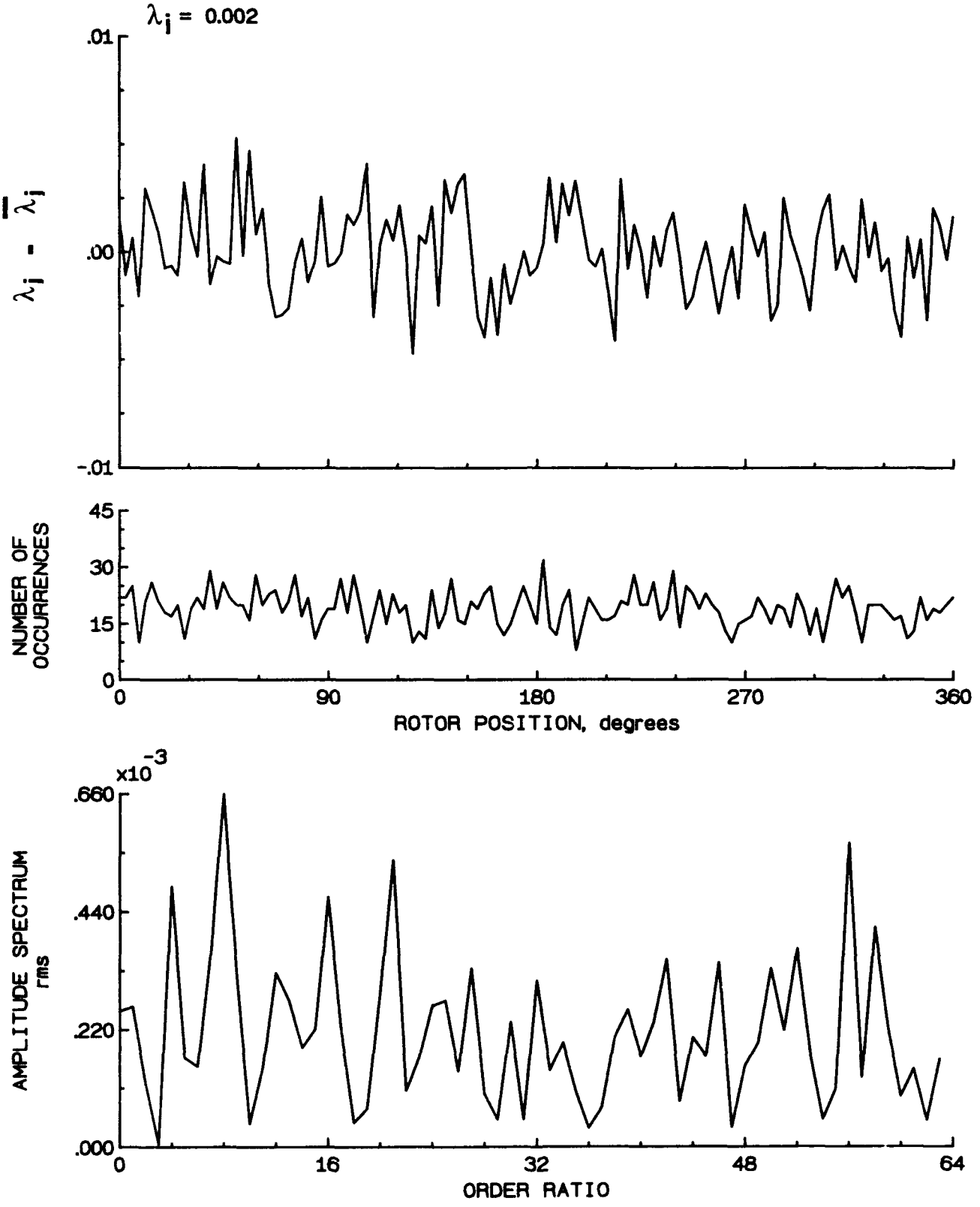

Figure 97.- Concluded.

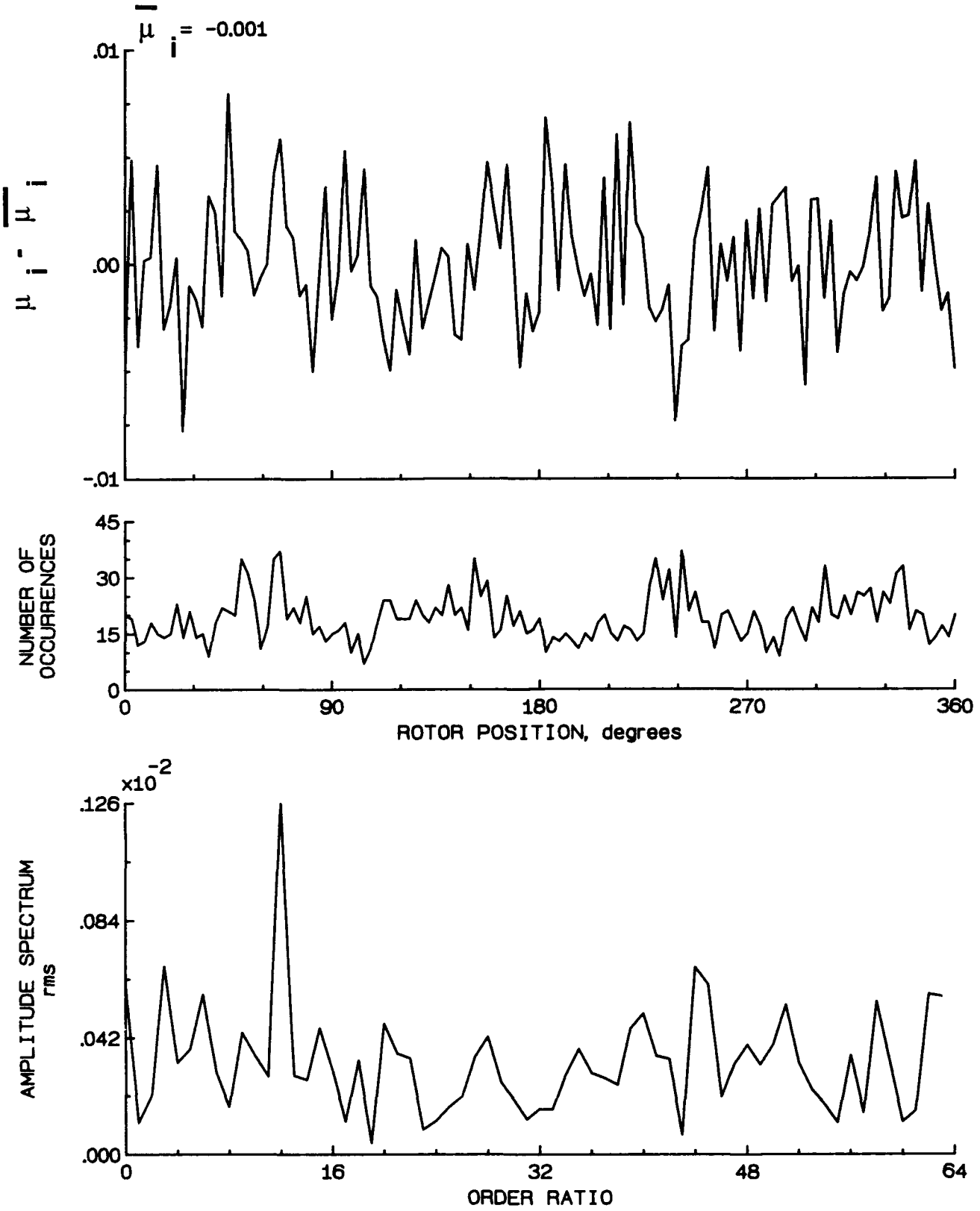

Figure 98.- Induced inflow velocity measured at 150 degrees and r/R of 0.98.

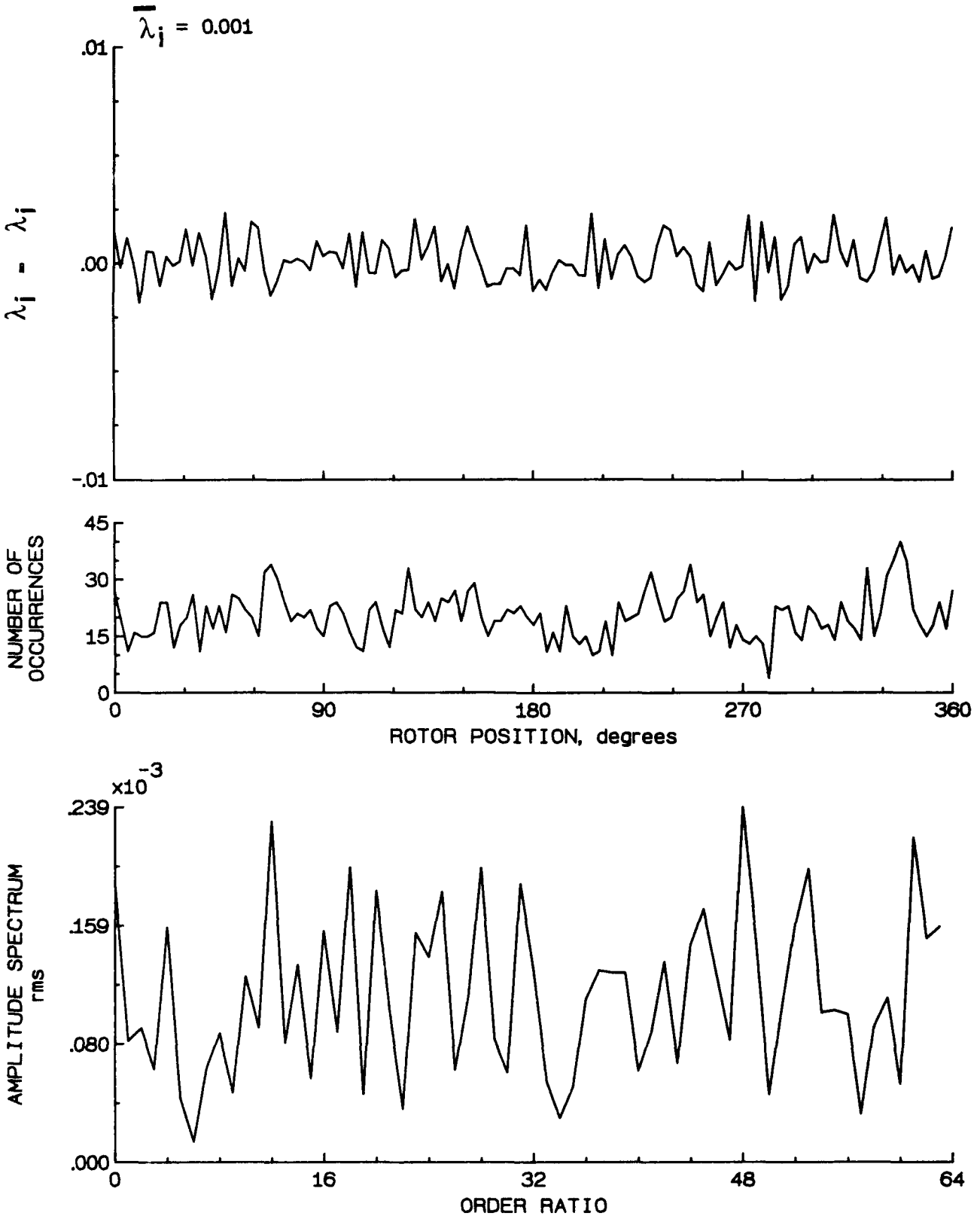

Figure 98.- Concluded.

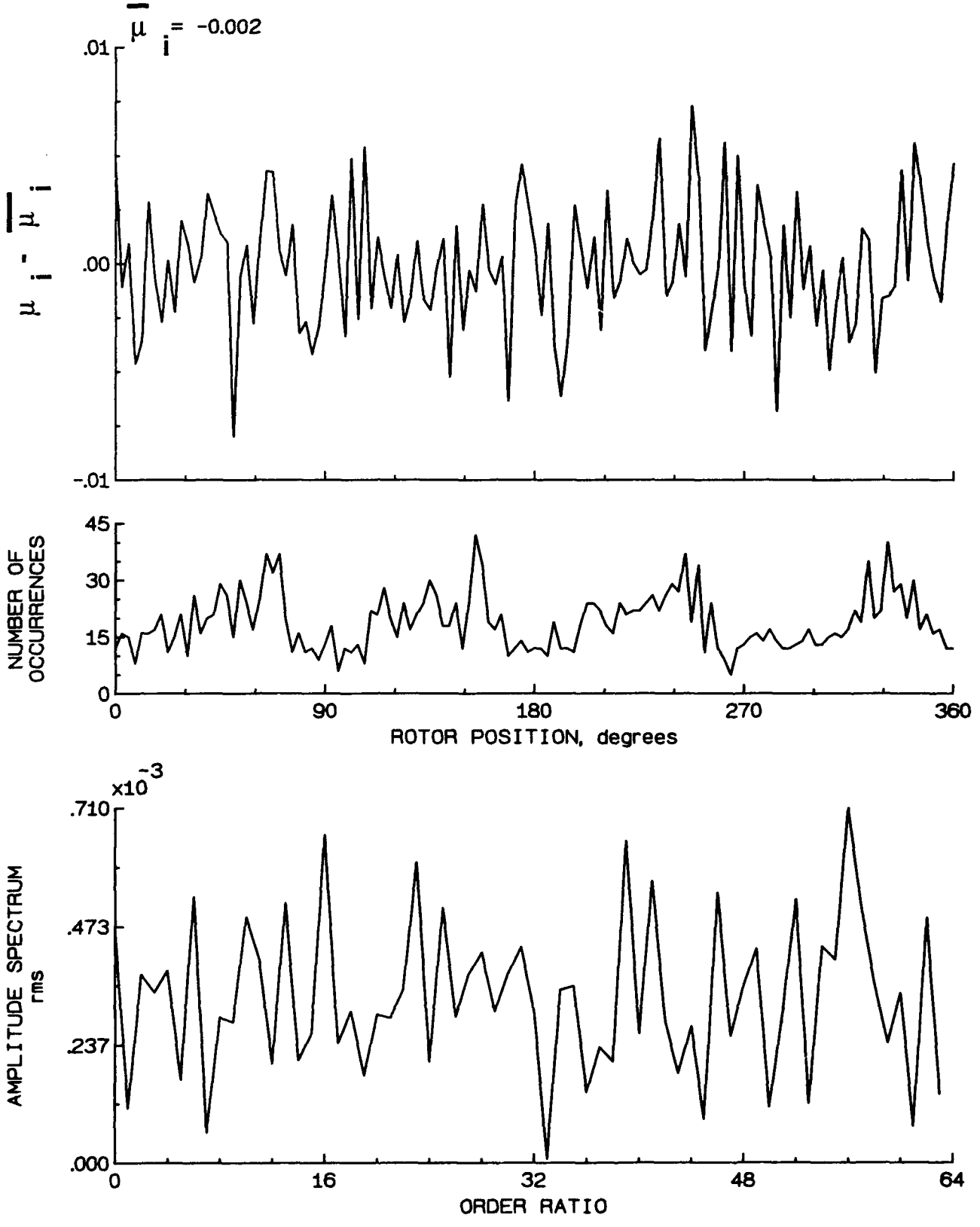

Figure 99.- Induced inflow velocity measured at 150 degrees and r/R of 1.02.

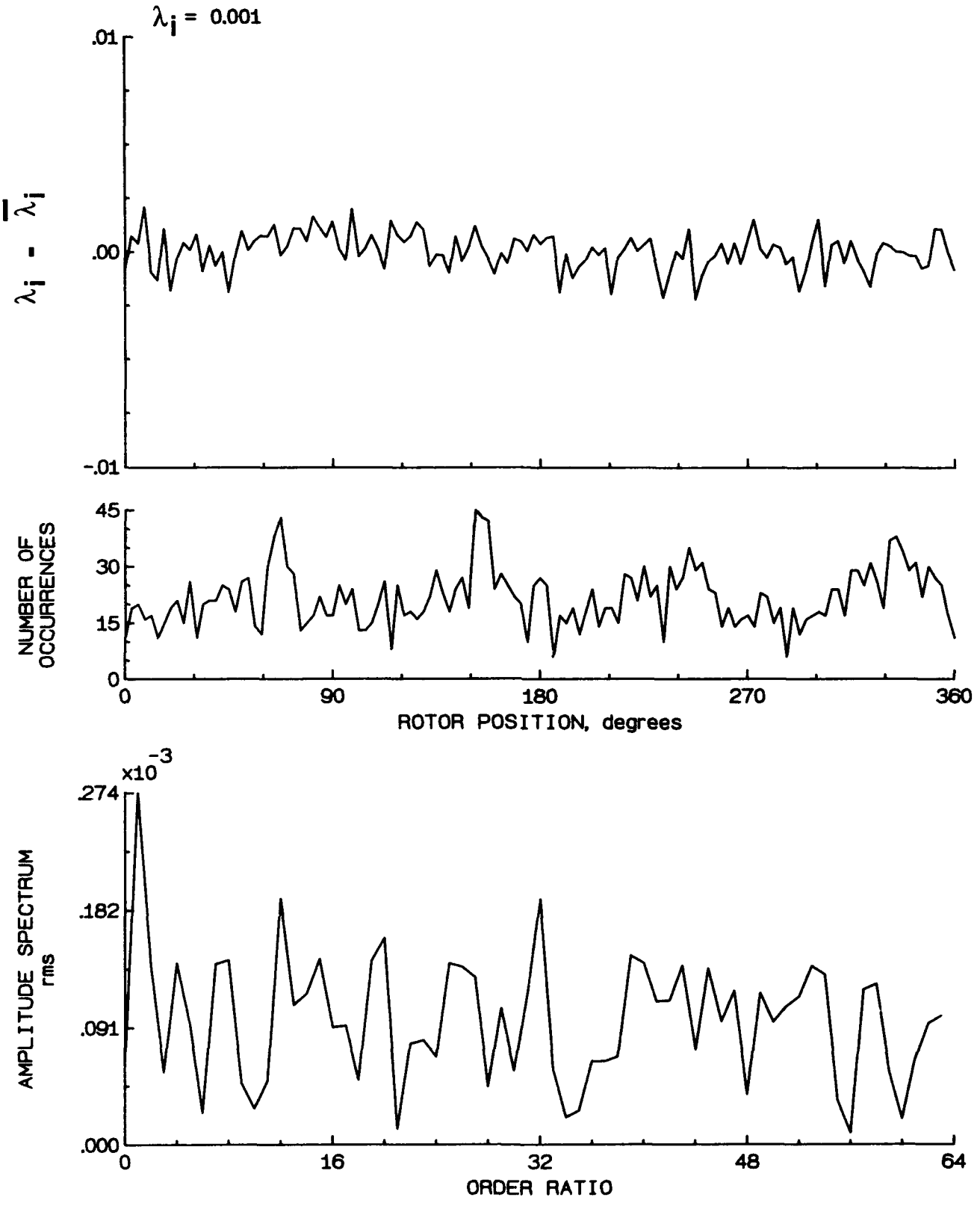

Figure 99.- Concluded.

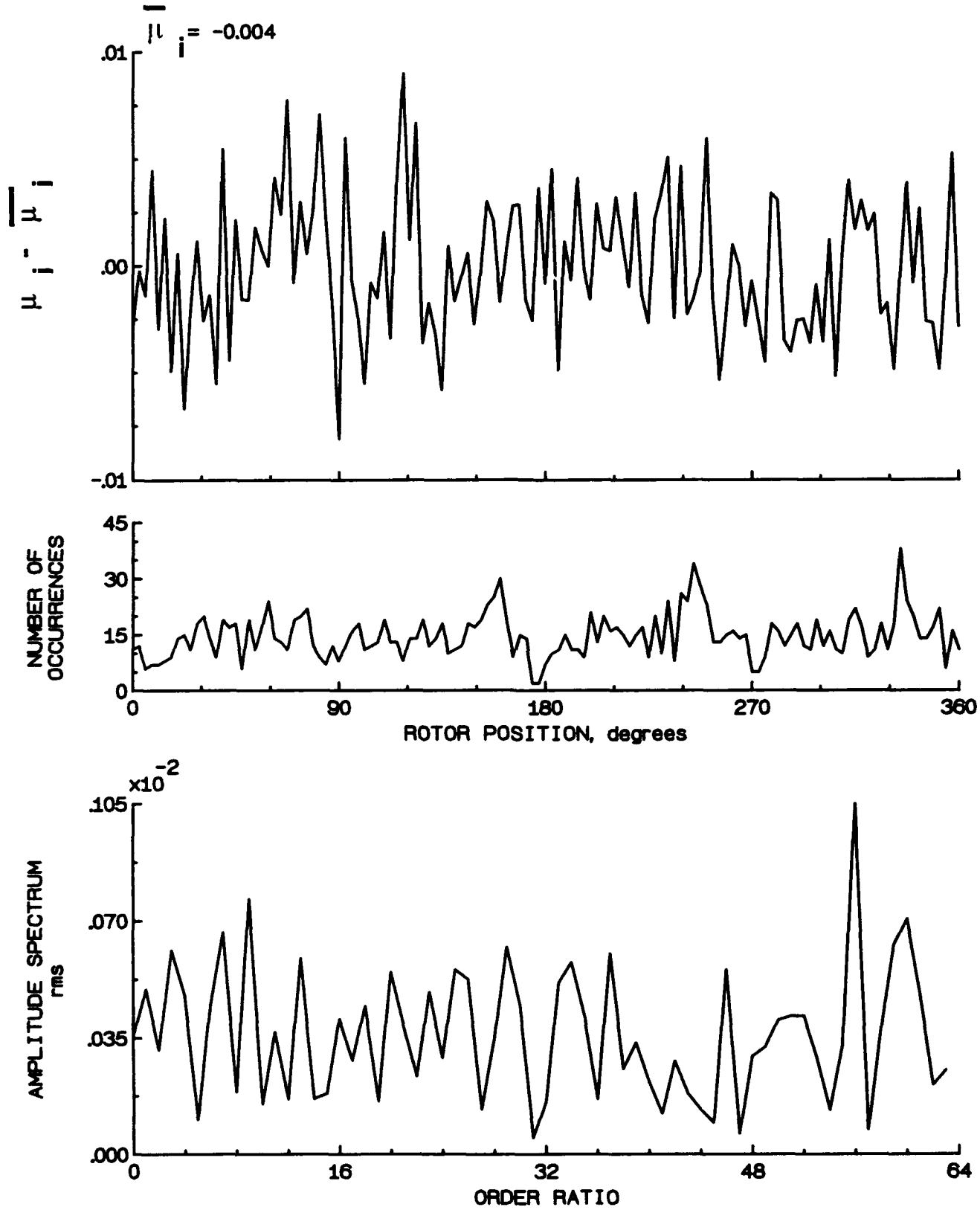

Figure 100.- Induced inflow velocity measured at 150 degrees and r/R of 1.04.

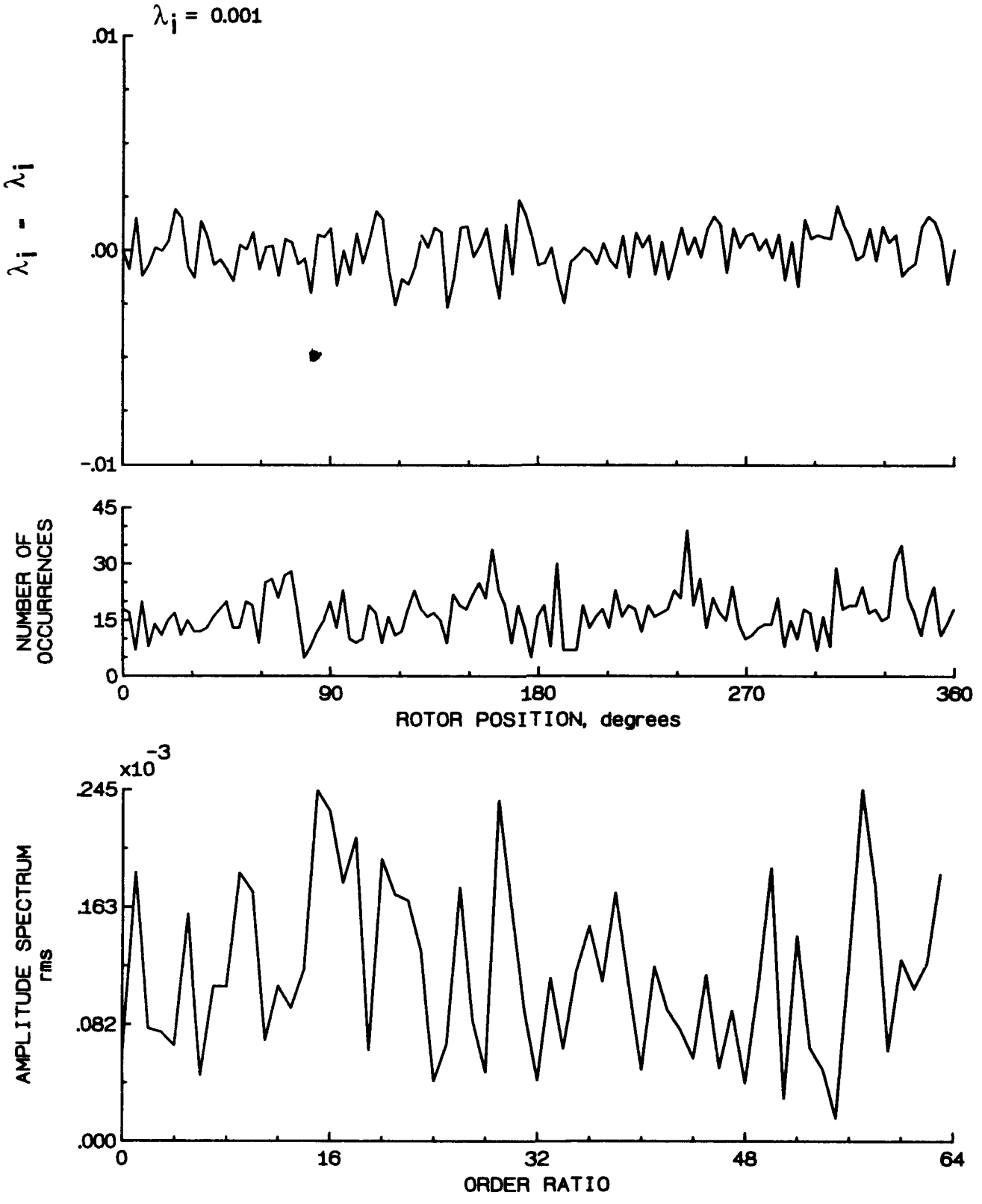

Figure 100.- Concluded.

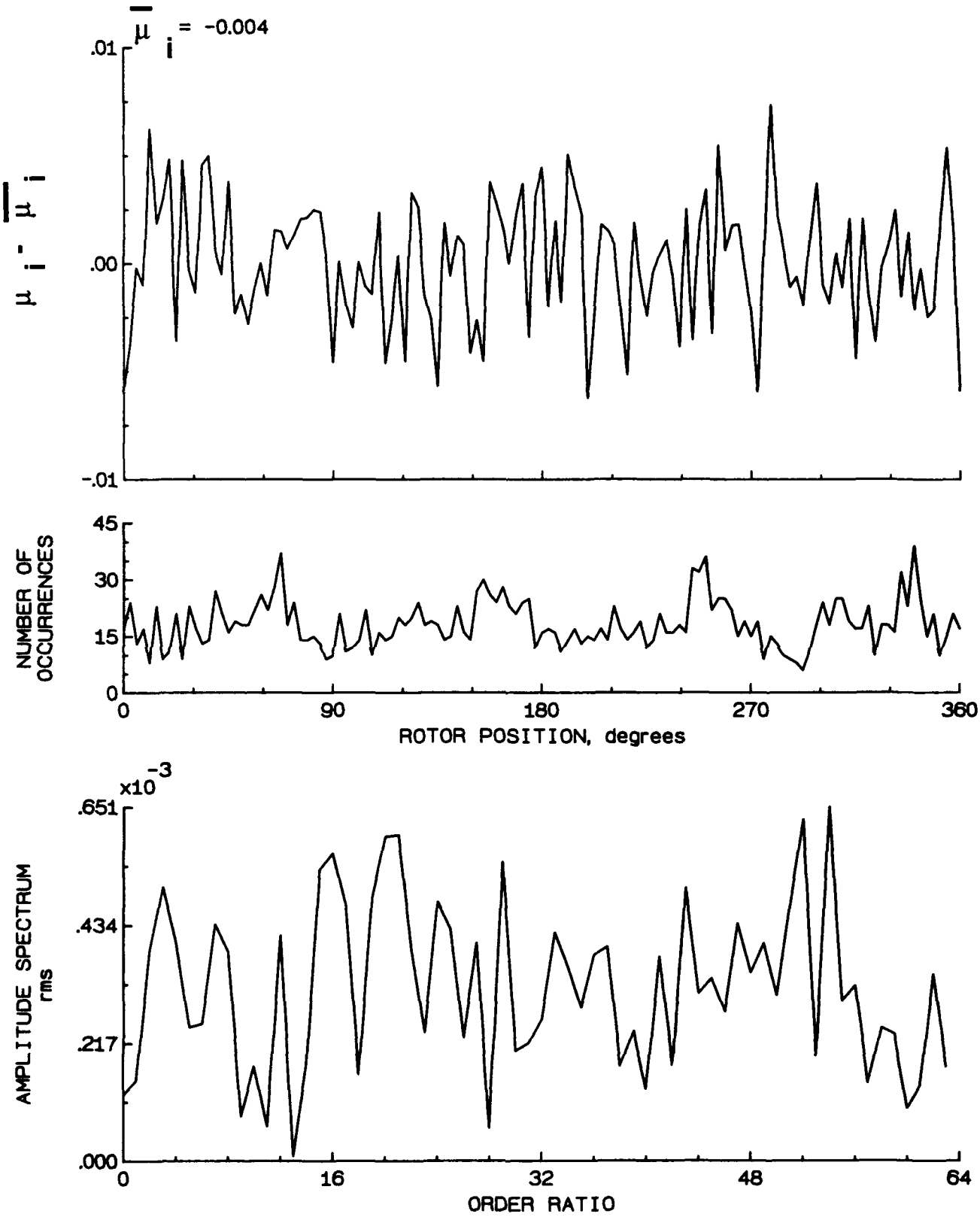

Figure 101.- Induced inflow velocity measured at 150 degrees and r/R of 1.10.

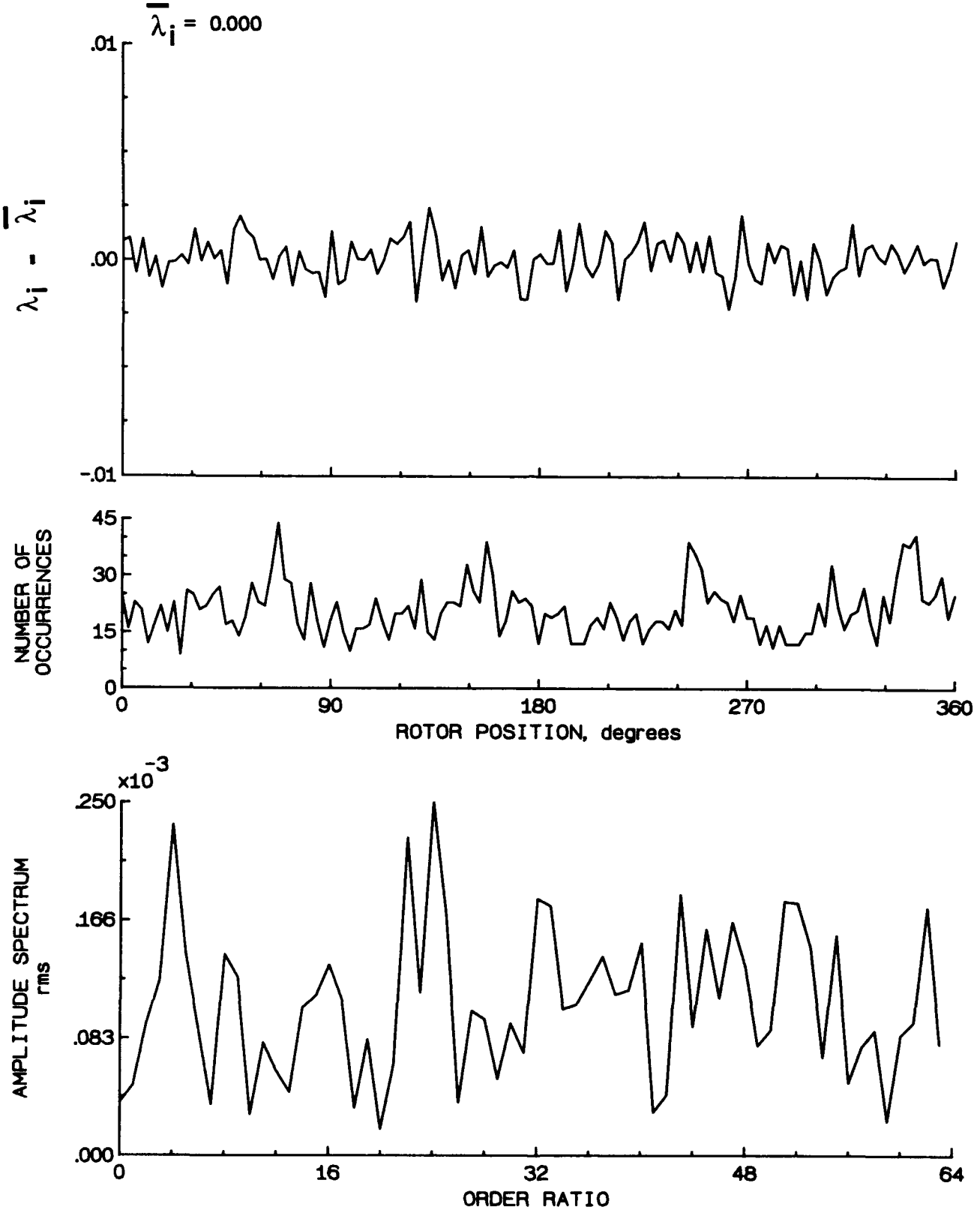

Figure 101.- Concluded.

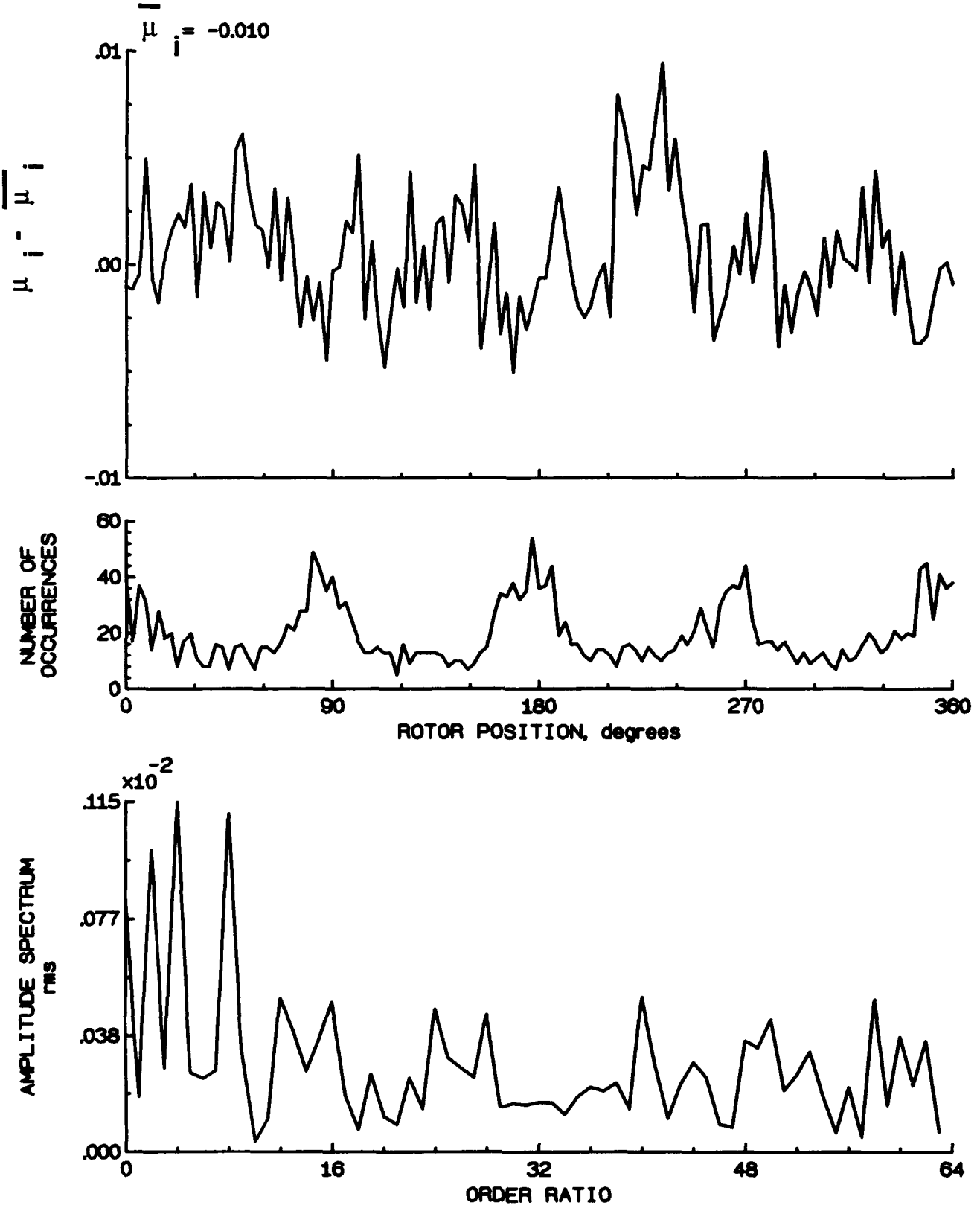

Figure 102.- Induced inflow velocity measured at 180 degrees and r/R of 0.20.

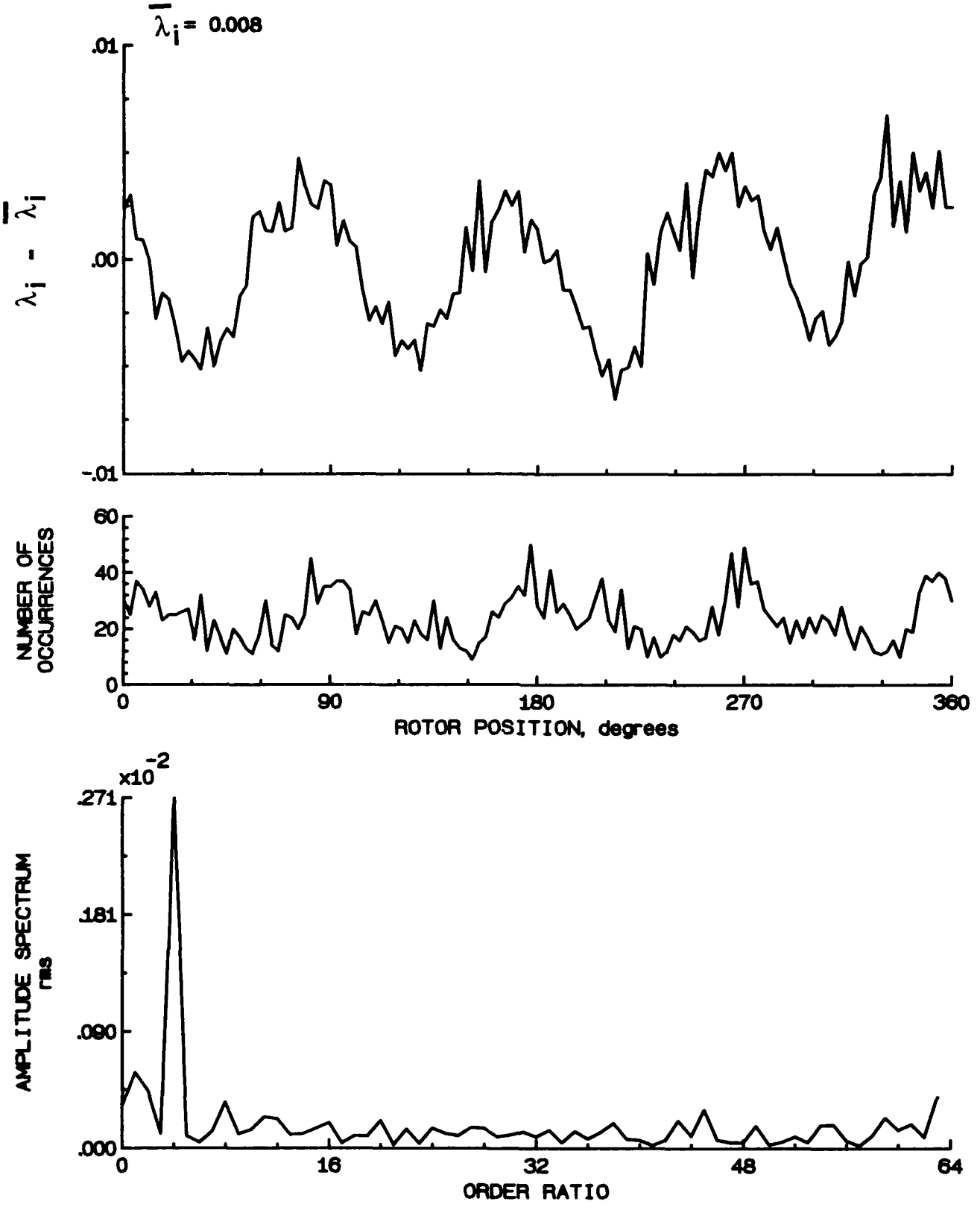

Figure 102.- Concluded.

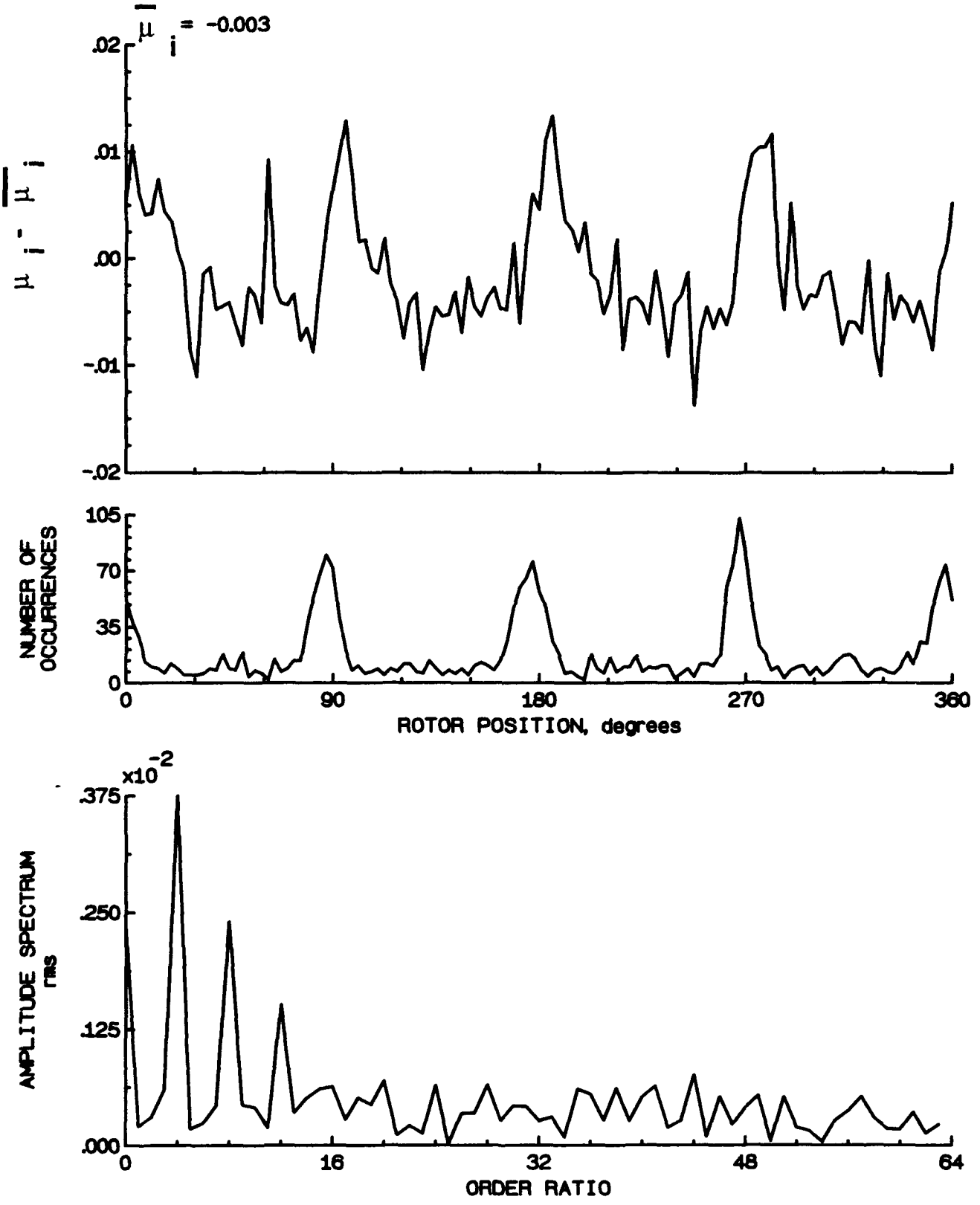

Figure 103.- Induced inflow velocity measured at 180 degrees and r/R of 0.40.

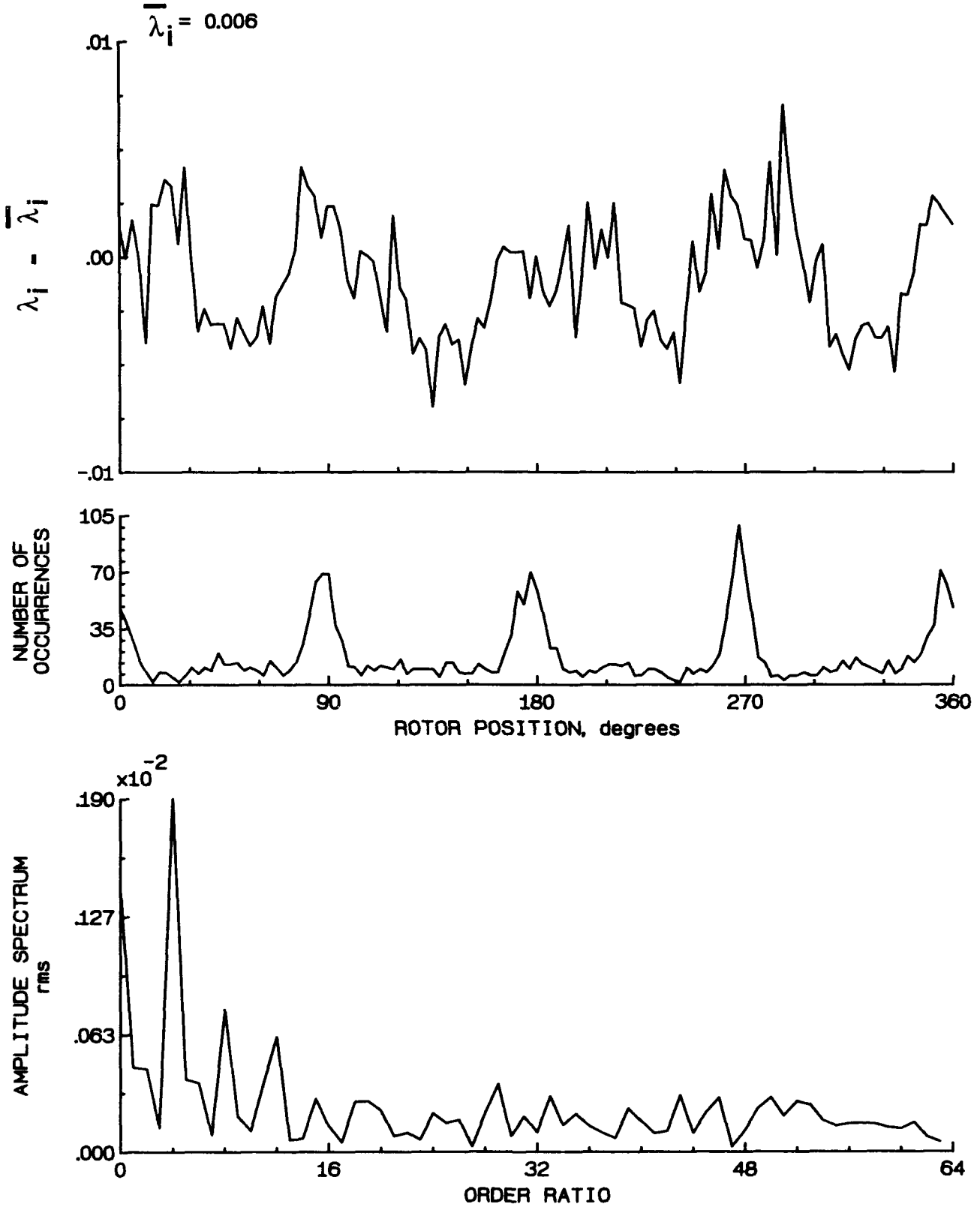

Figure 103.- Concluded.

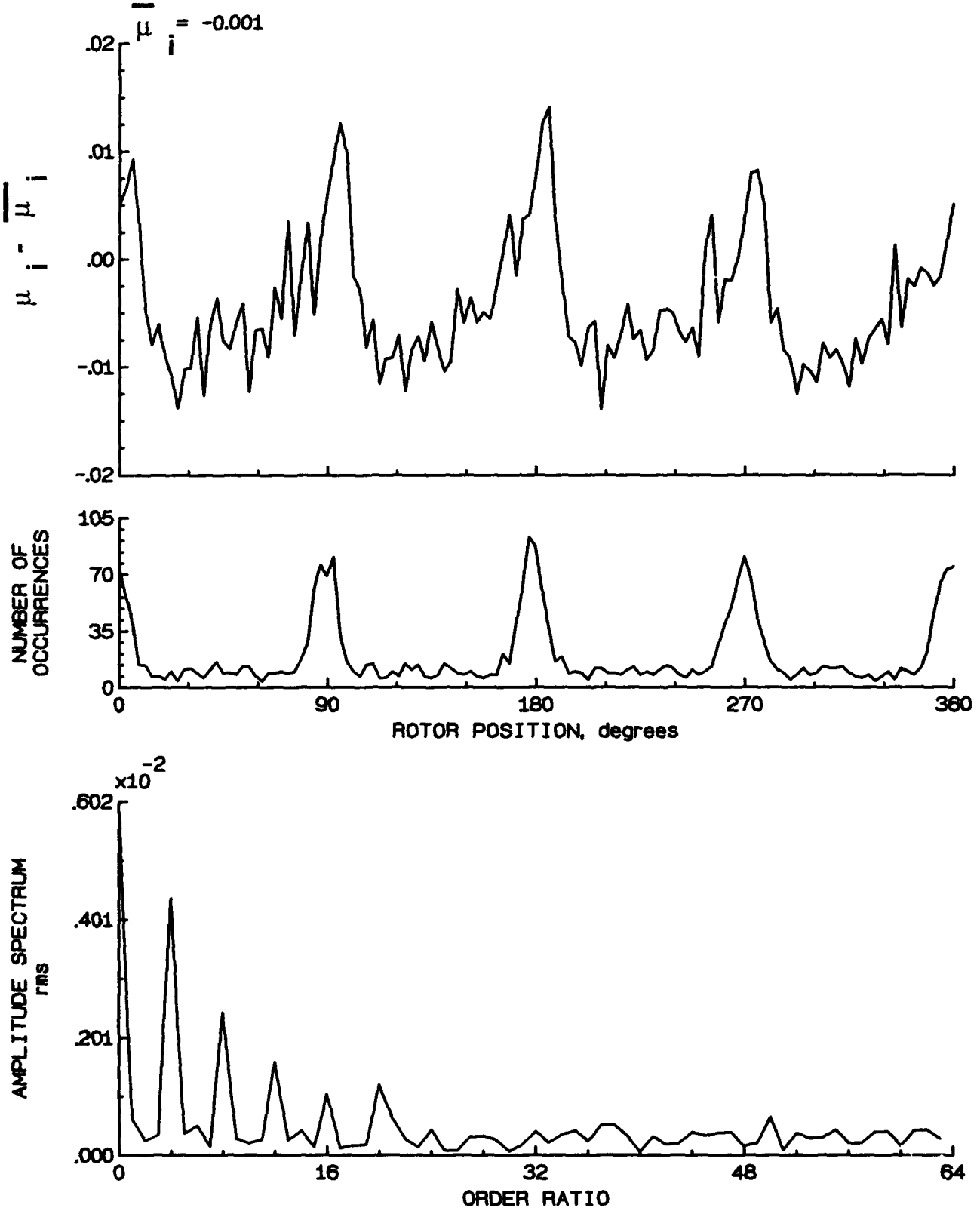

Figure 104.- Induced inflow velocity measured at 180 degrees and r/R of 0.50.

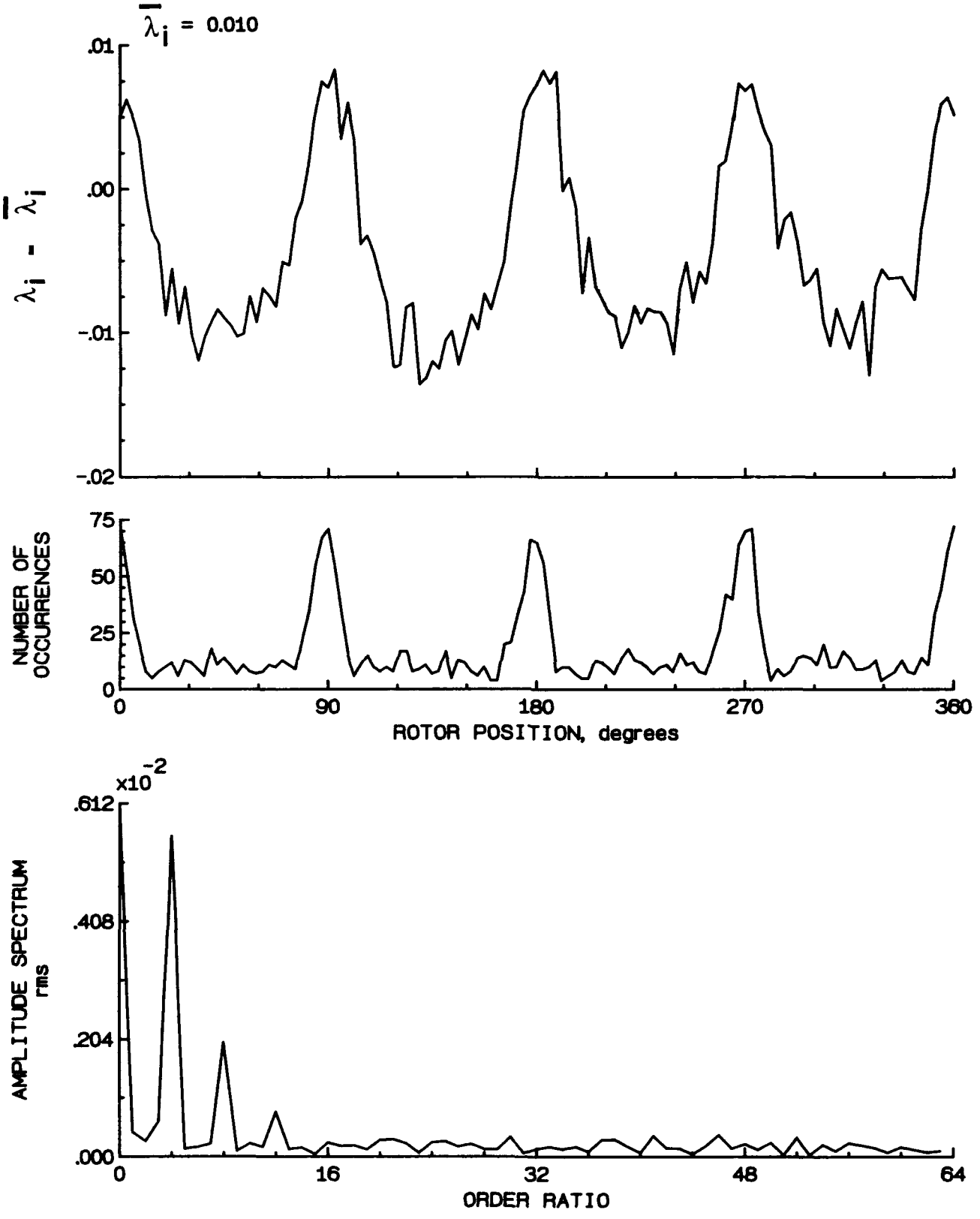

Figure 104.- Concluded.

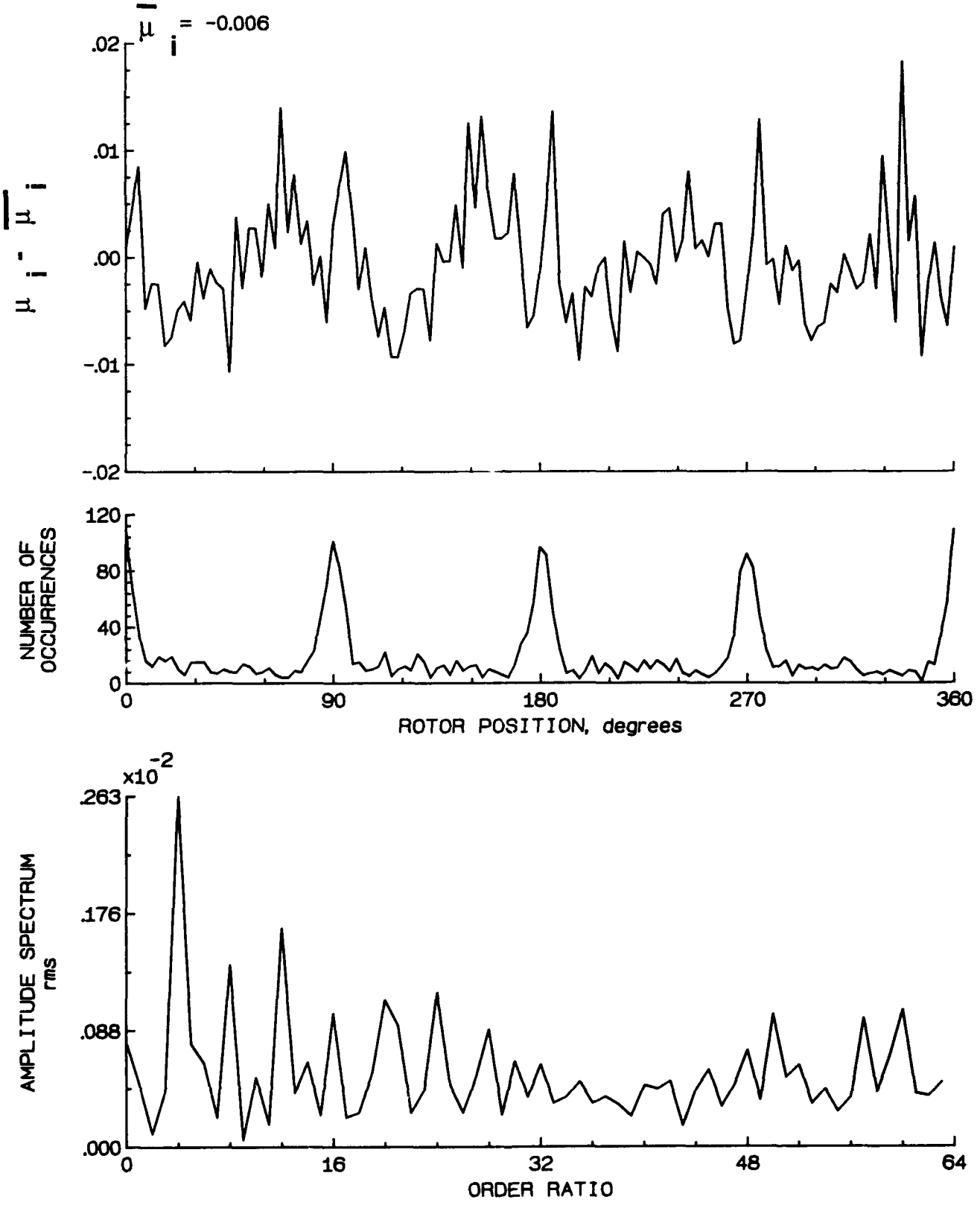

Figure 105.- Induced inflow velocity measured at 180 degrees and r/R of 0.60.

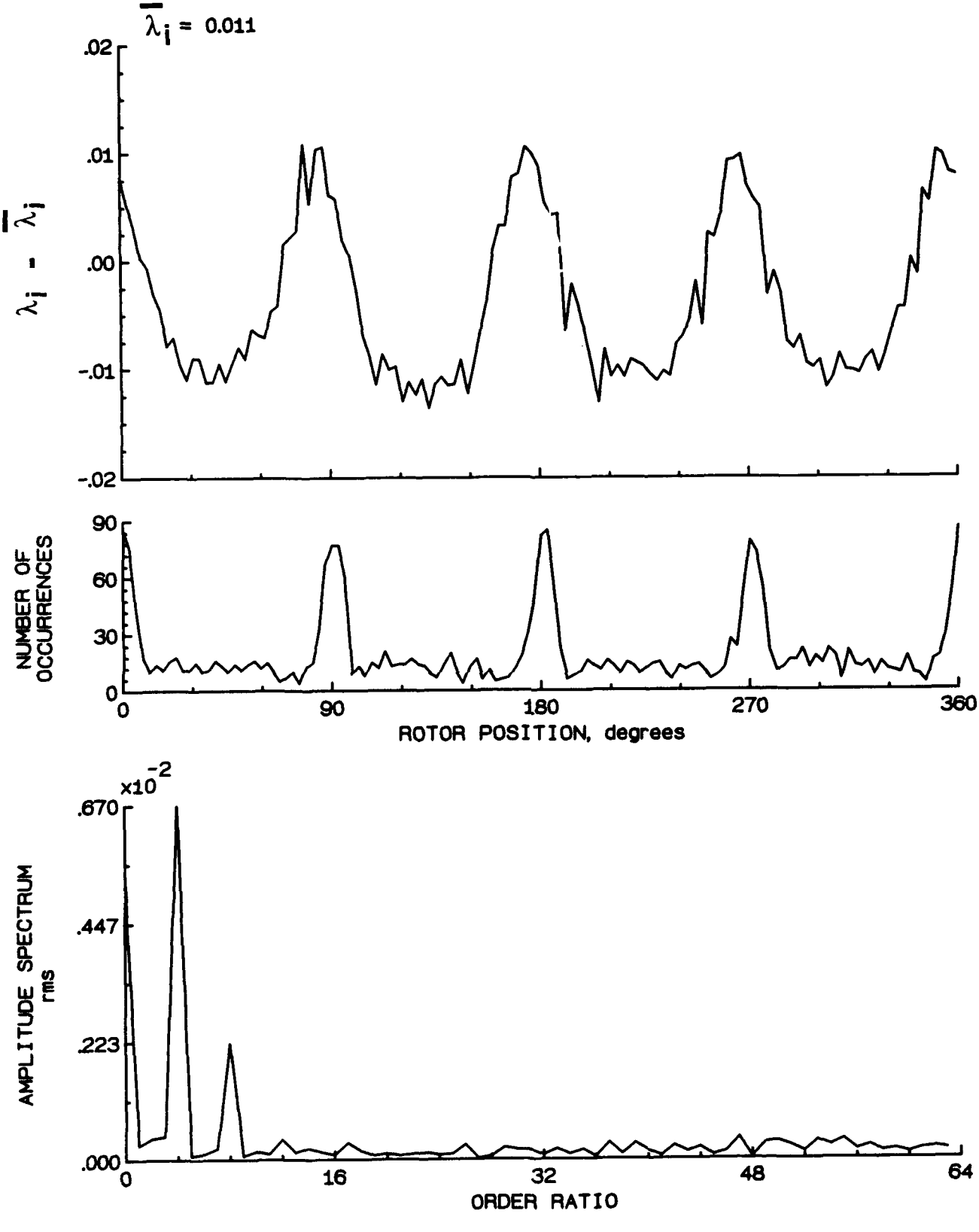

Figure 105.- Concluded.

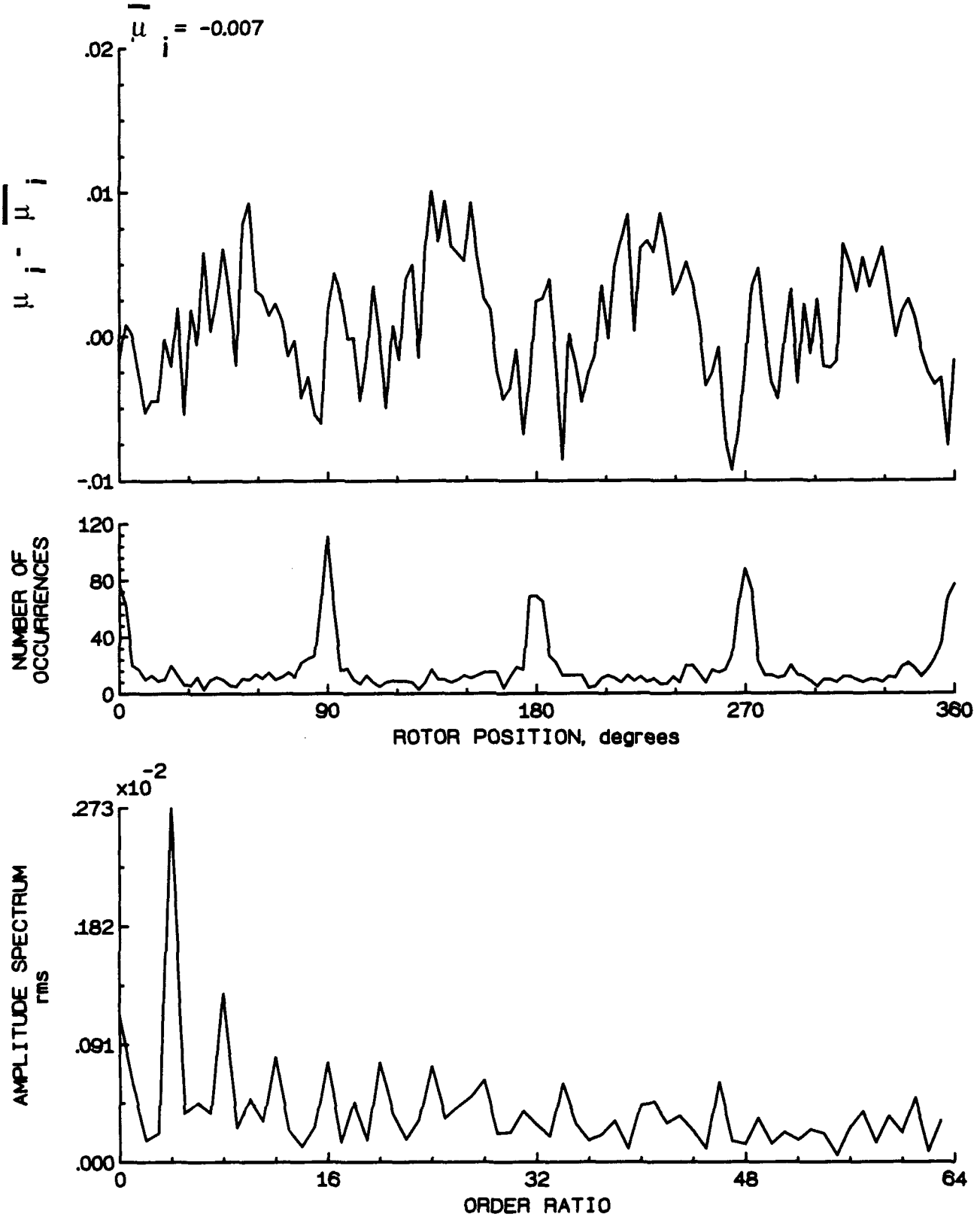

Figure 106.- Induced inflow velocity measured at 180 degrees and r/R of 0.70.

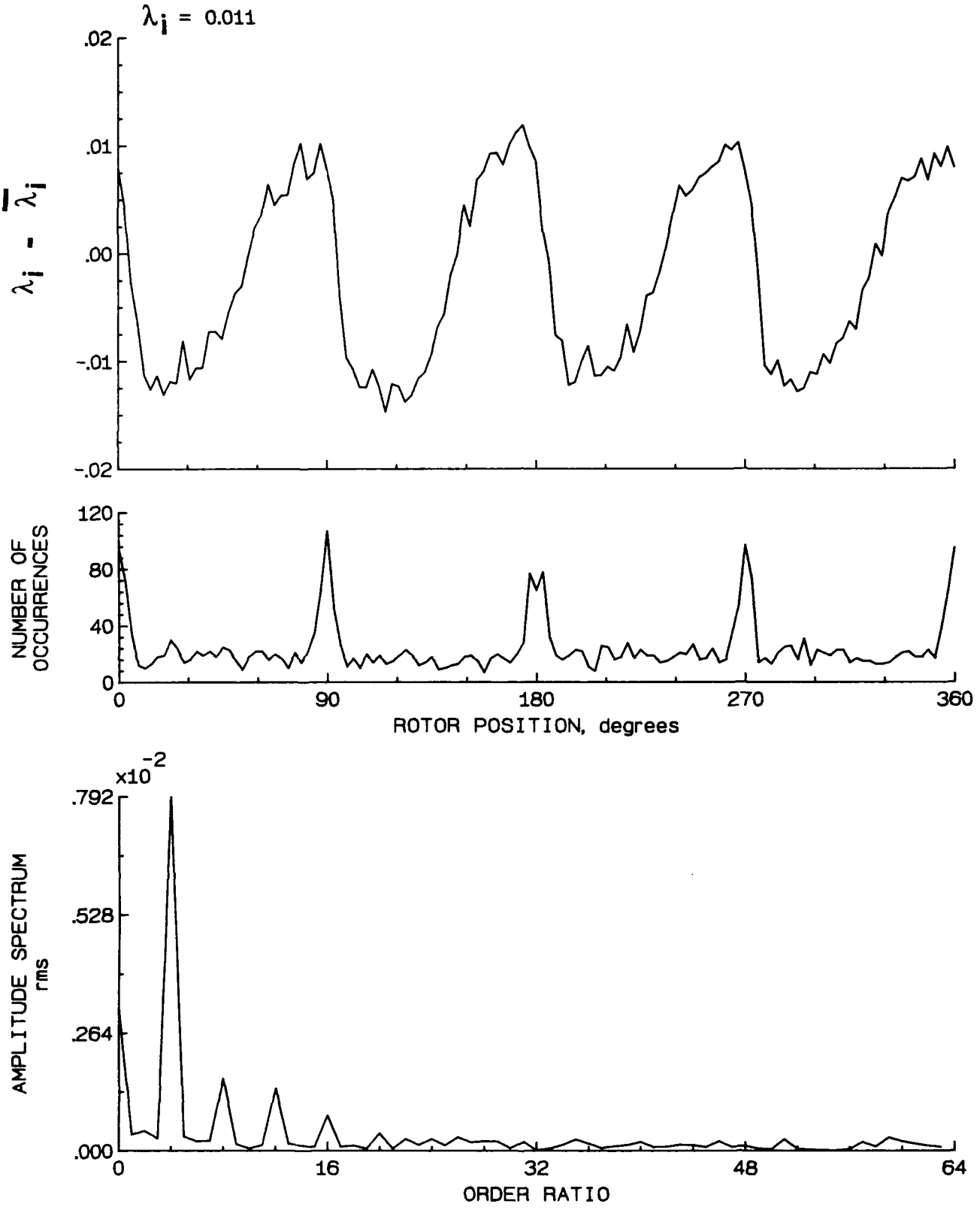

Figure 106.- Concluded.

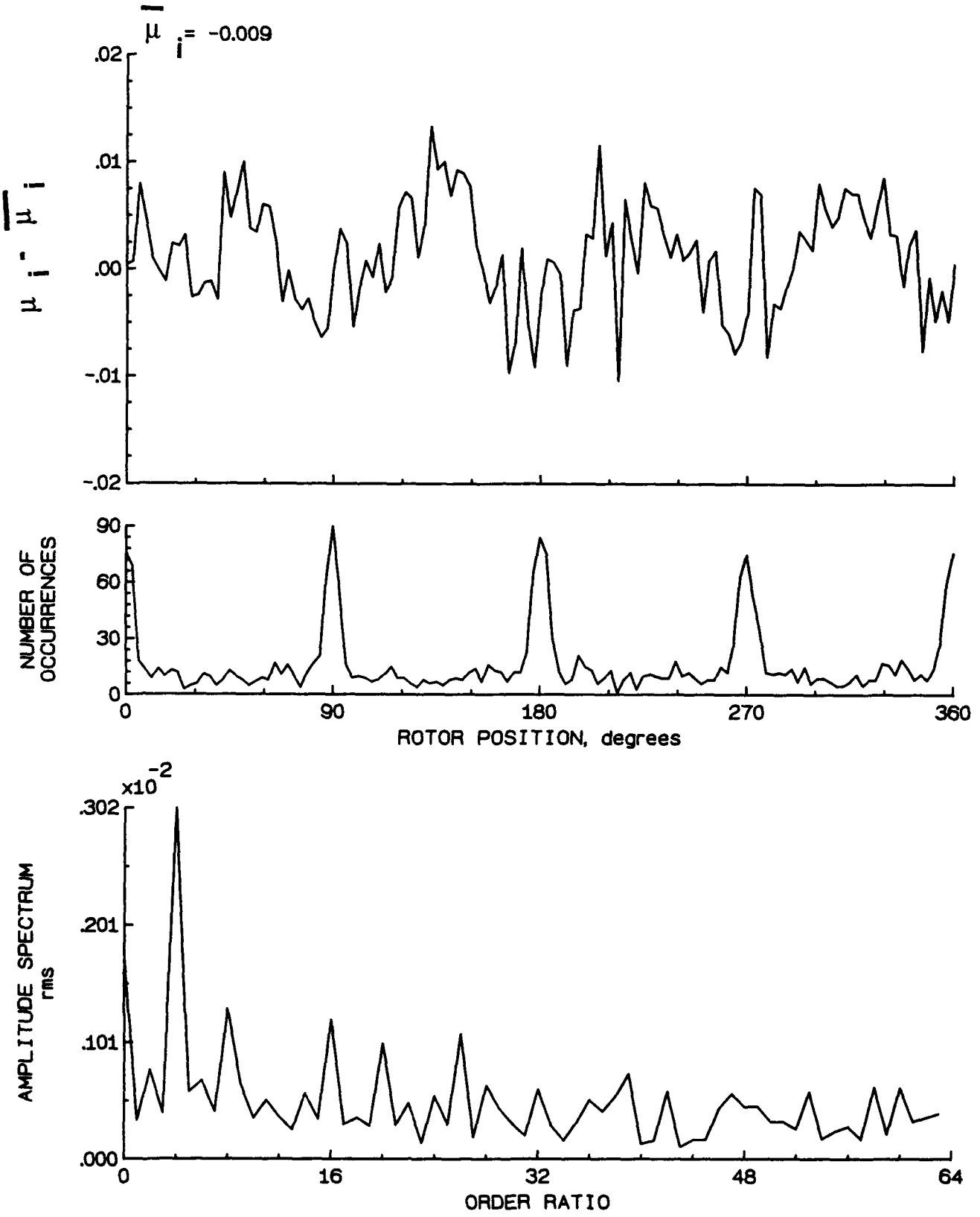

Figure 107.- Induced inflow velocity measured at 180 degrees and r/R of 0.74.

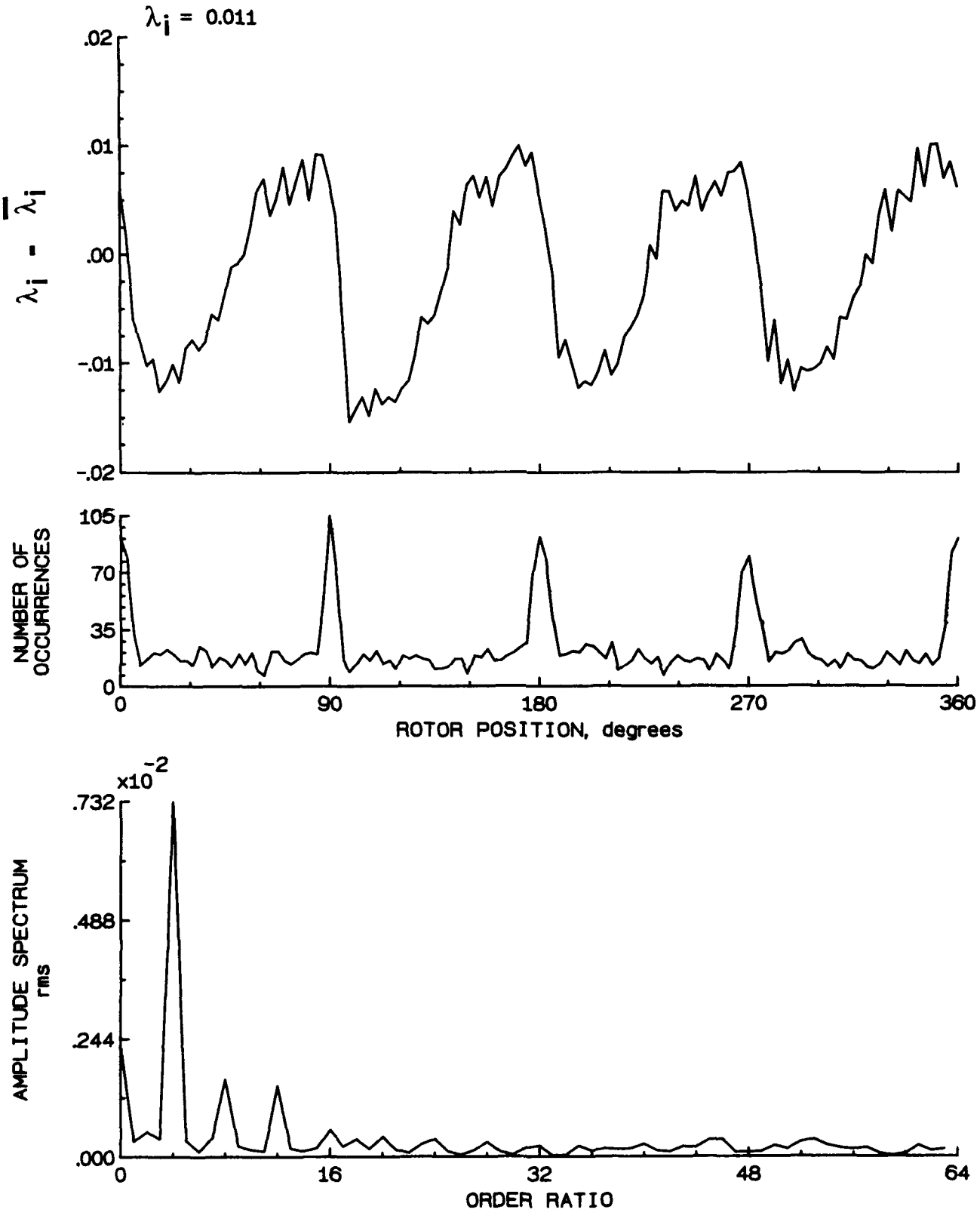

Figure 107.- Concluded.

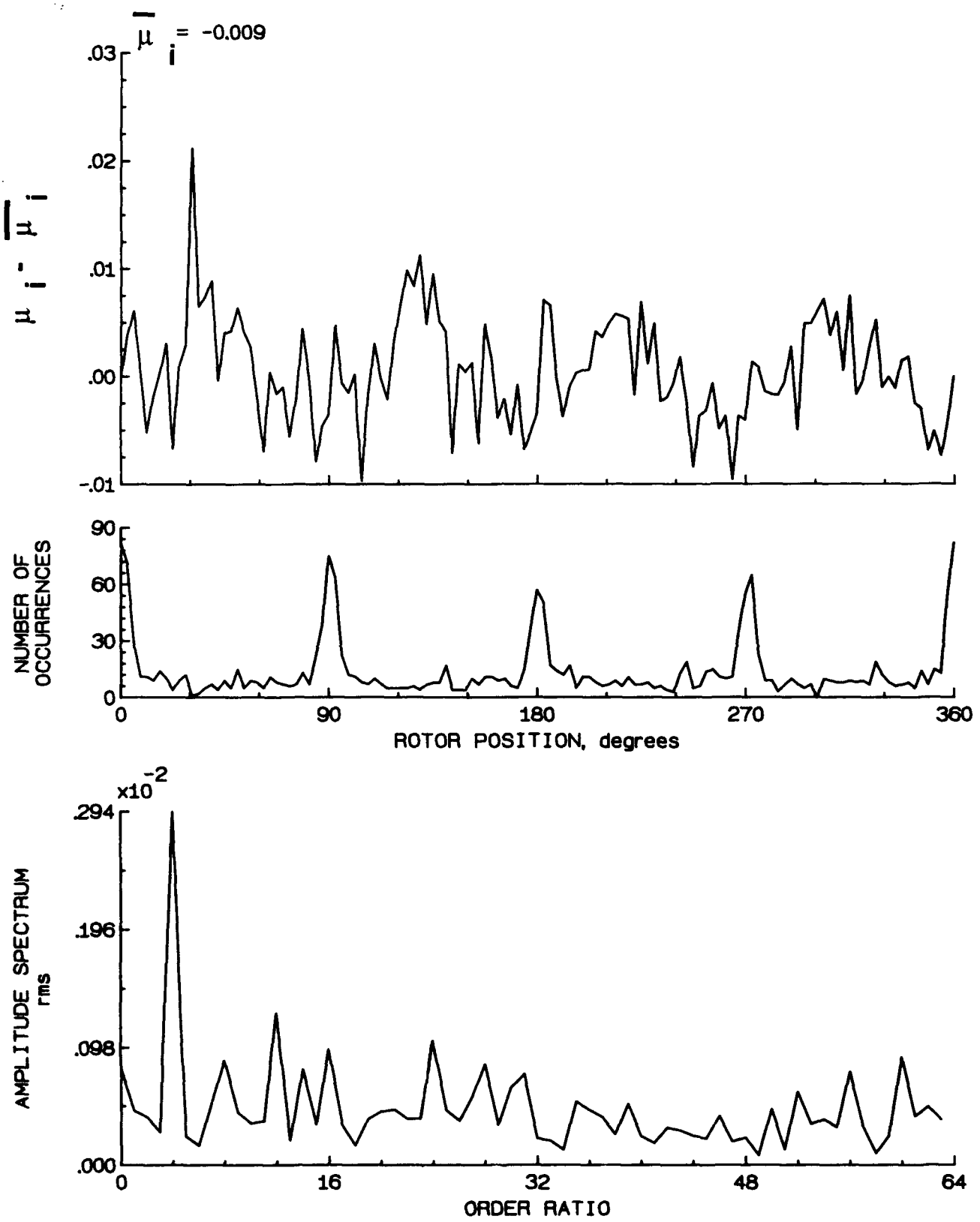

Figure 108.- Induced inflow velocity measured at 180 degrees and r/R of 0.78.

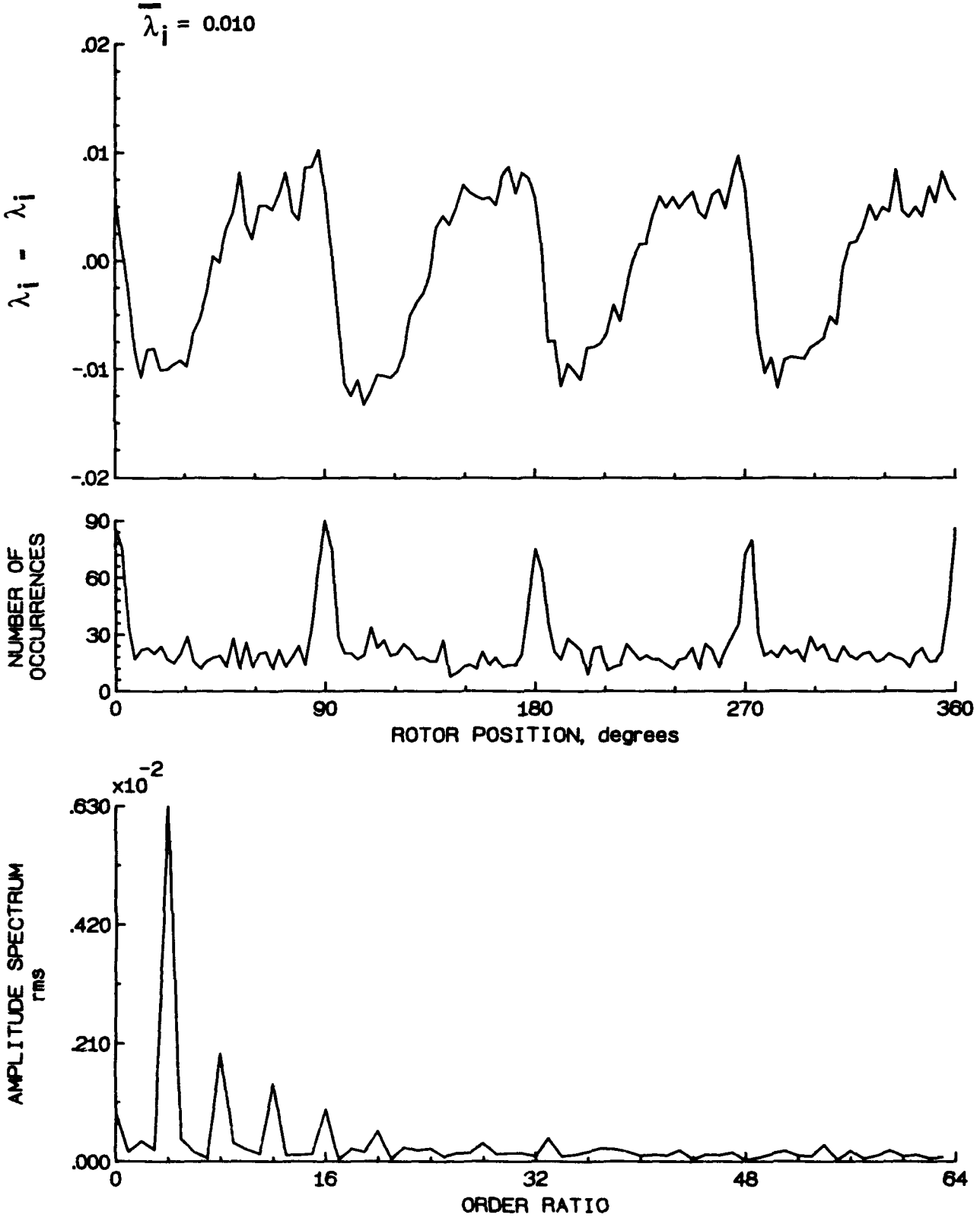

Figure 108.- Concluded.

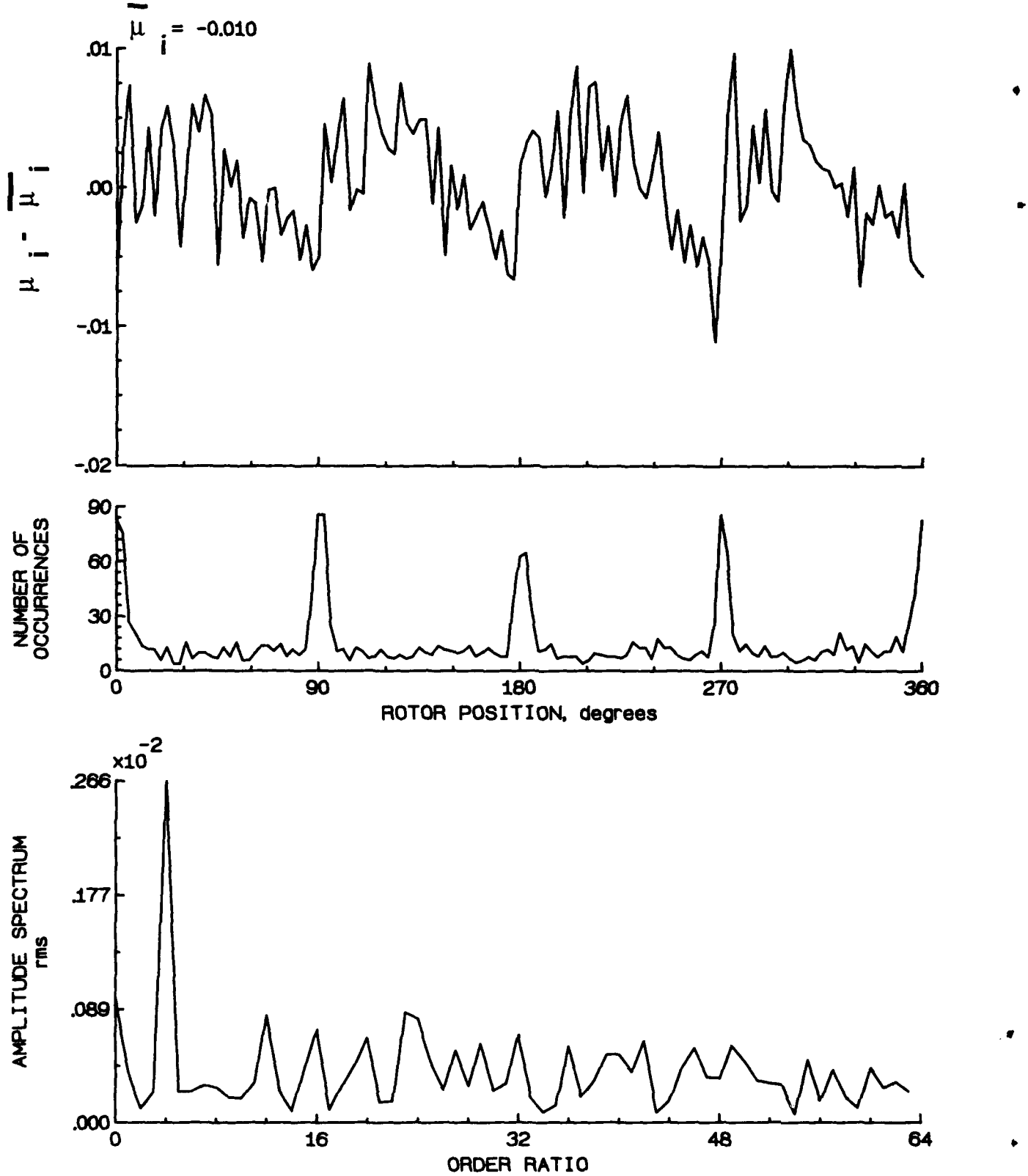

Figure 109.- Induced inflow velocity measured at 180 degrees and r/R of 0.82.

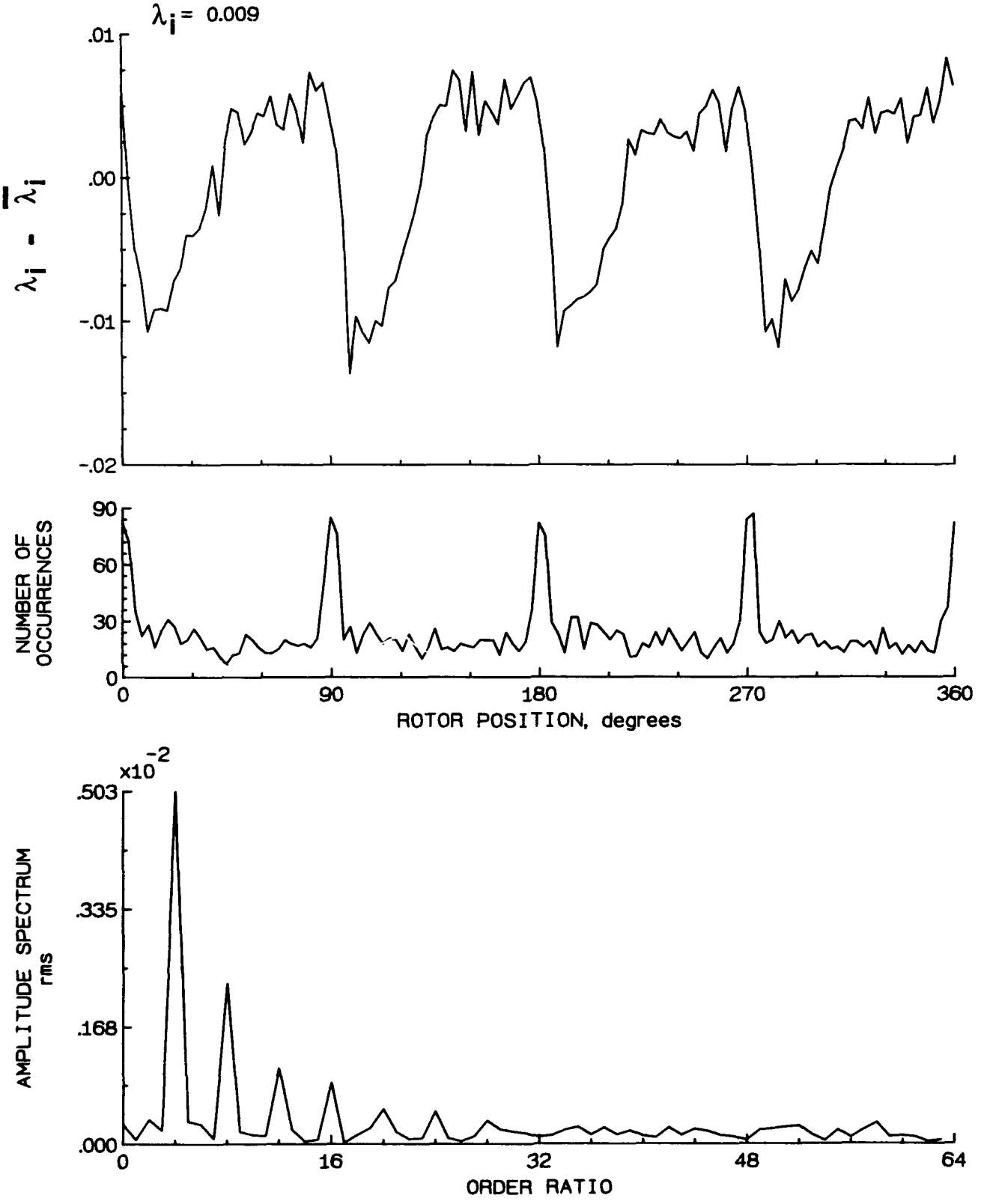

Figure 109.- Concluded.

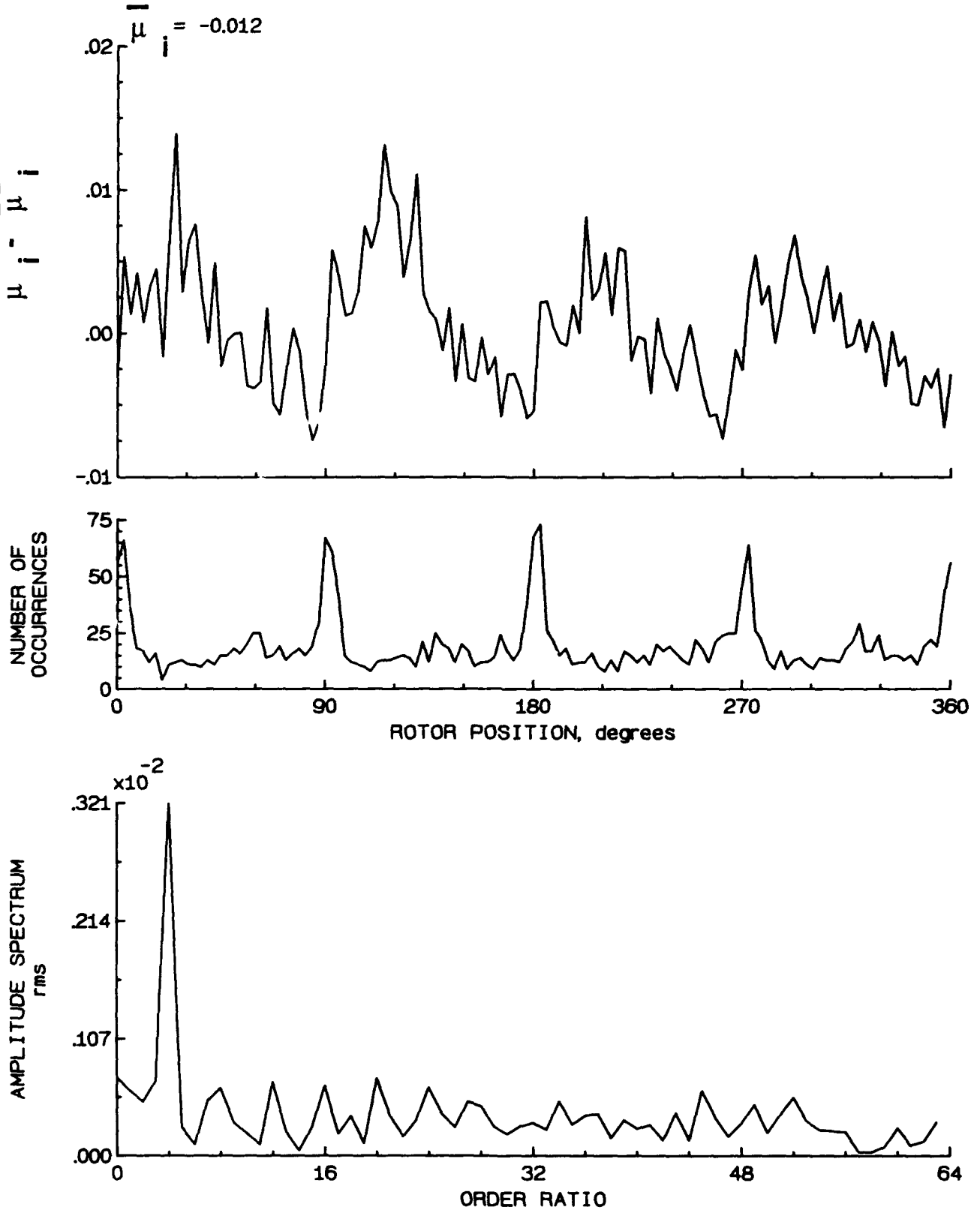

Figure 110.- Induced inflow velocity measured at 180 degrees and r/R of 0.86.

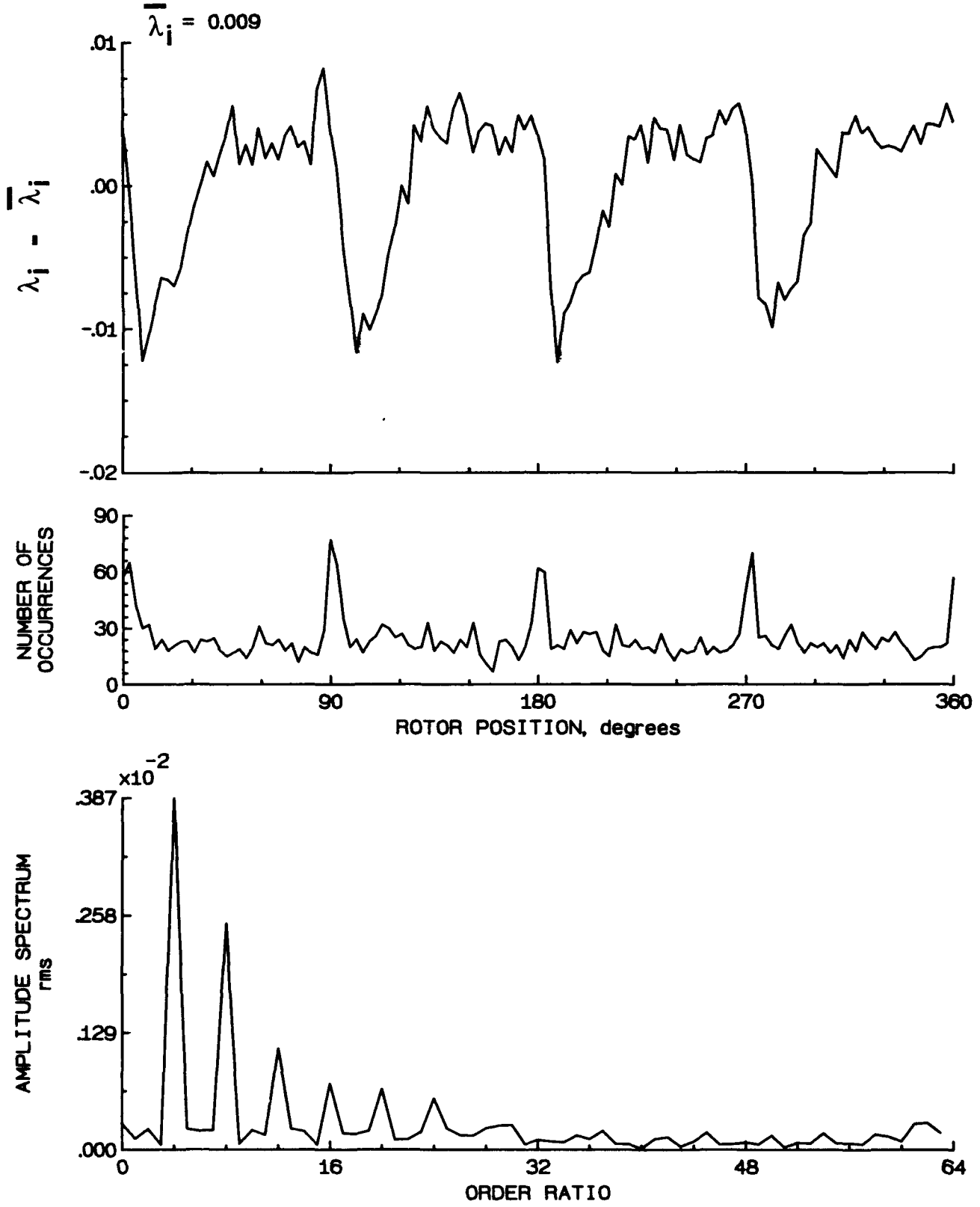

Figure 110 - Concluded.

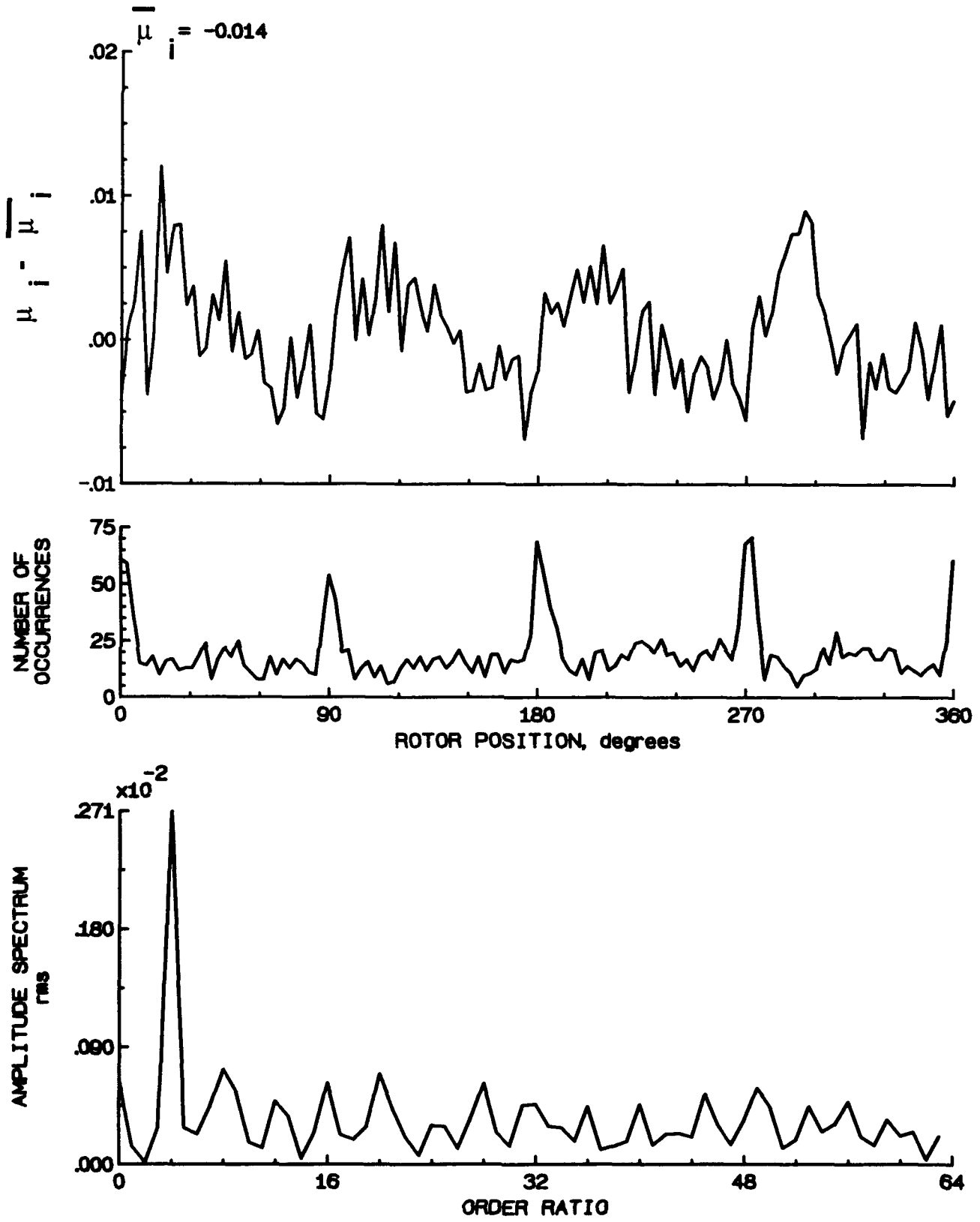

Figure 111.- Induced inflow velocity measured at 180 degrees and r/R of 0.90.

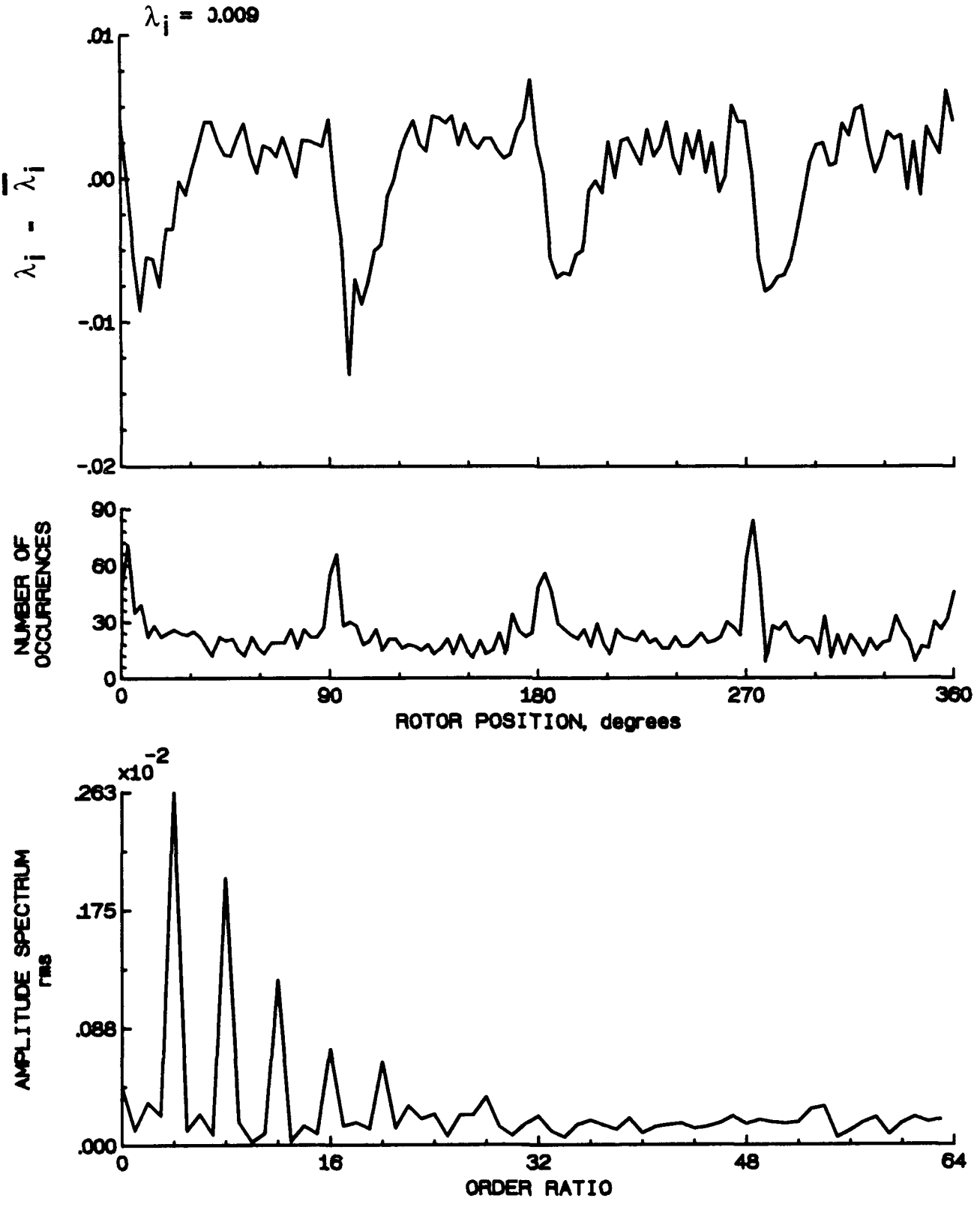

Figure 111.- Concluded.

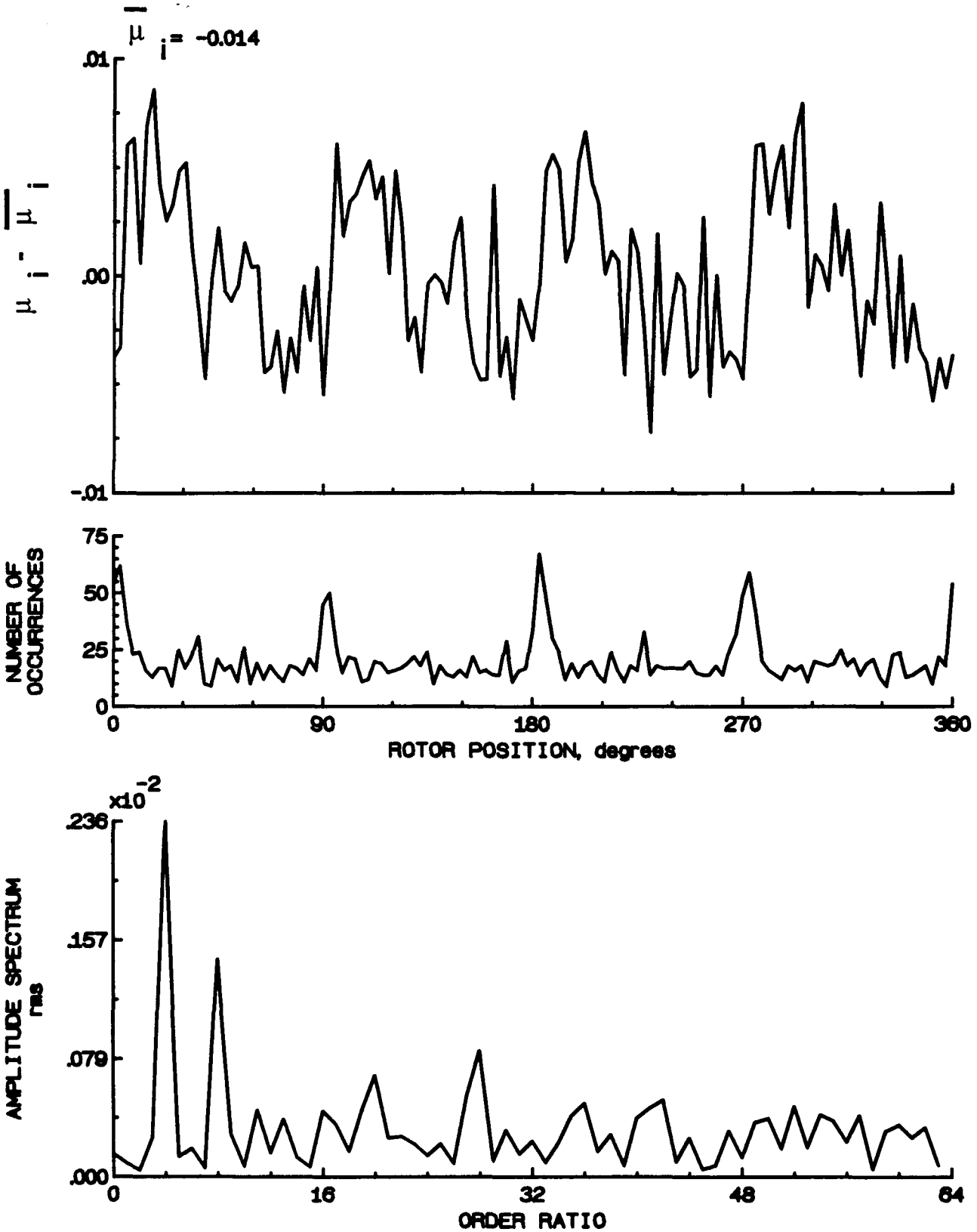

Figure 112.- Induced inflow velocity measured at 180 degrees and r/R of 0.94.

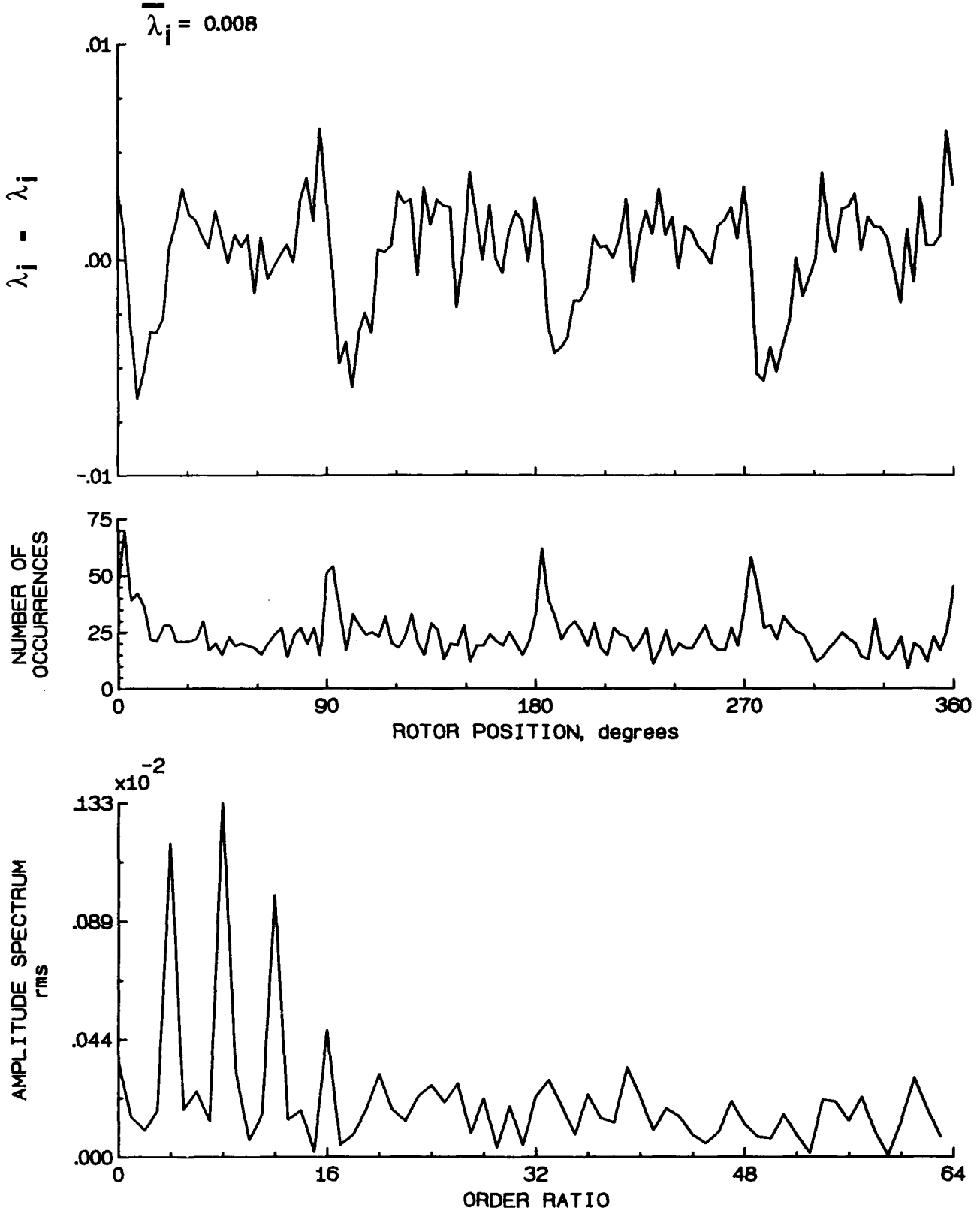

Figure 112.- Concluded.

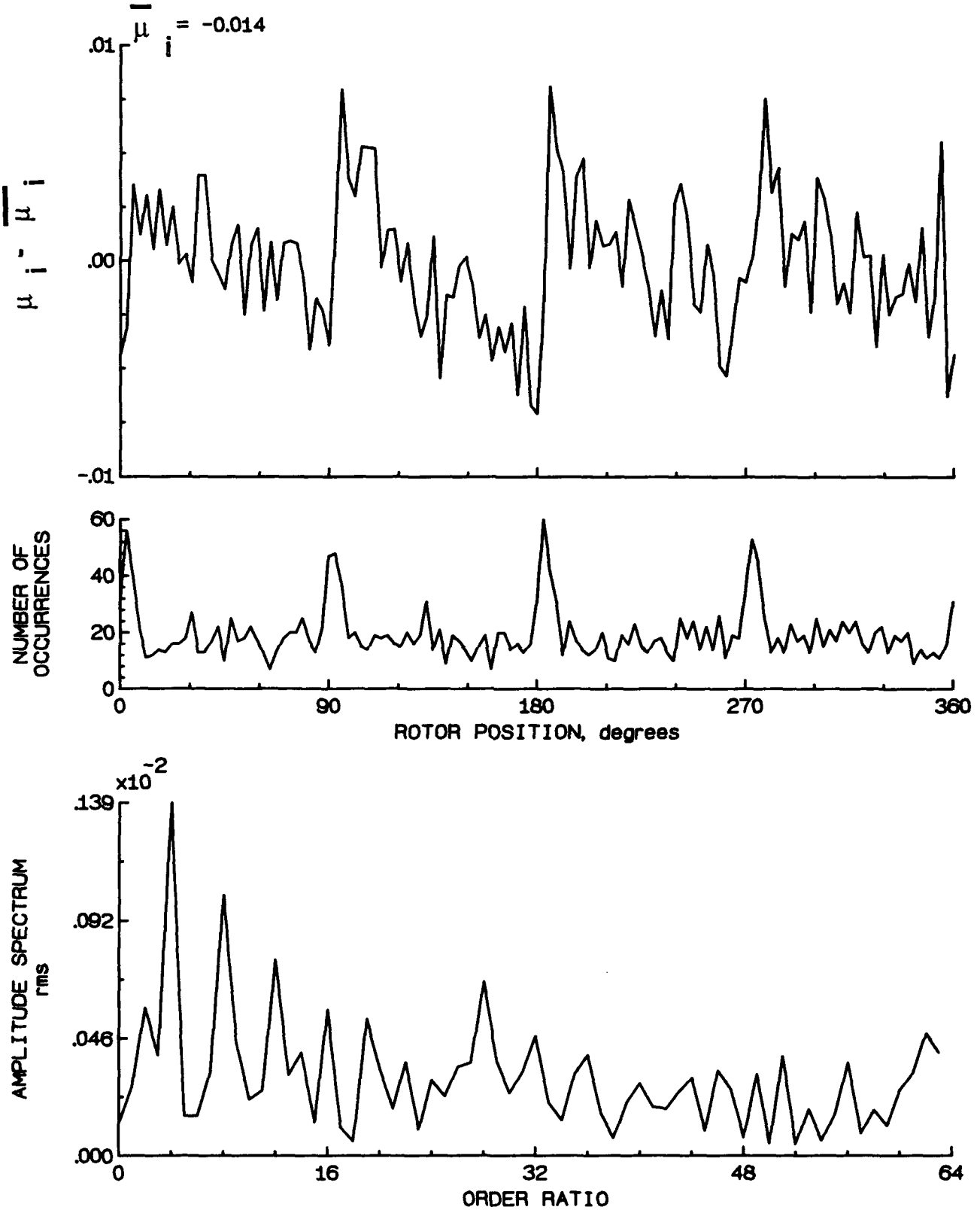

Figure 113.- Induced inflow velocity measured at 180 degrees and r/R of 0.98.

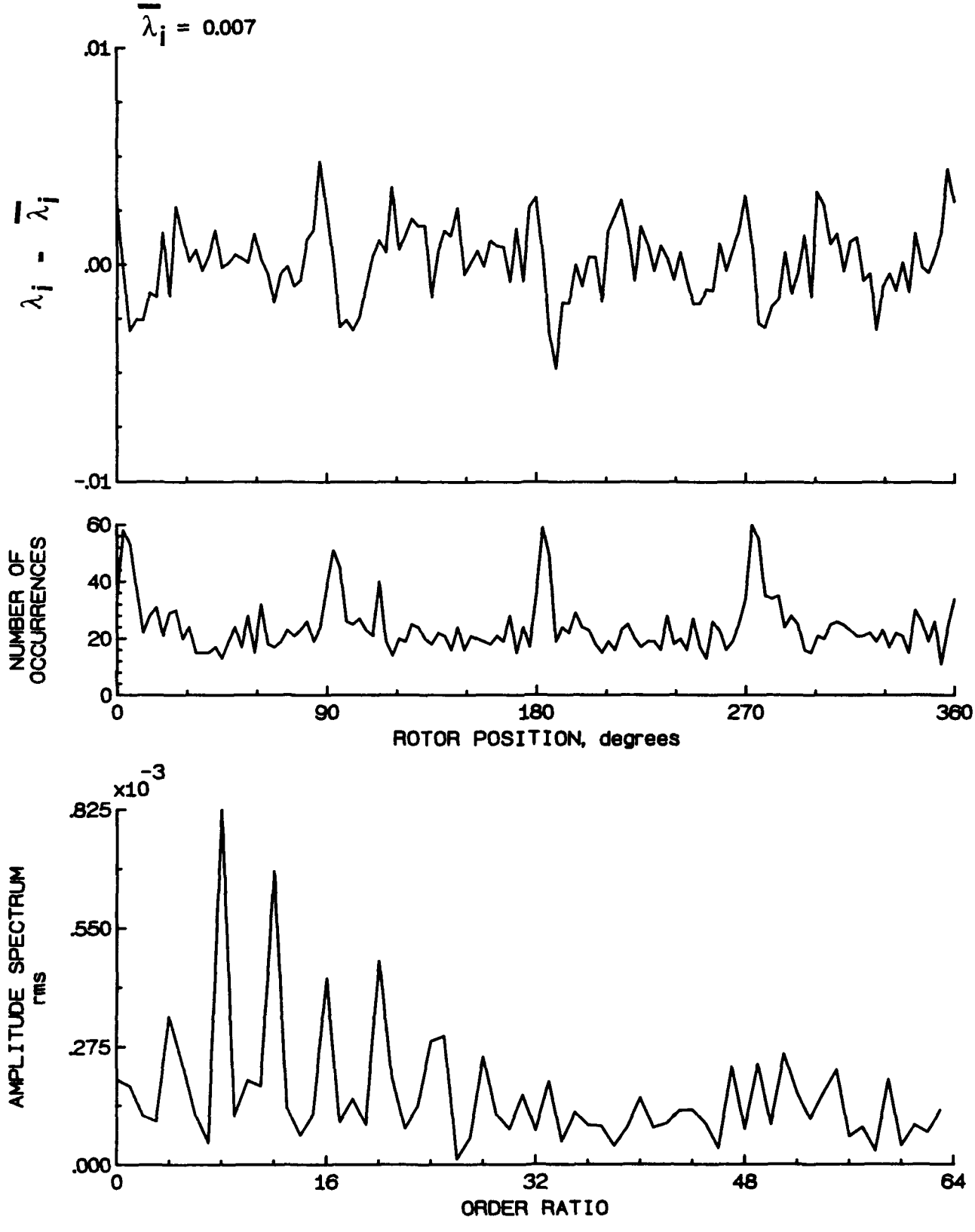

Figure 113.- Concluded.

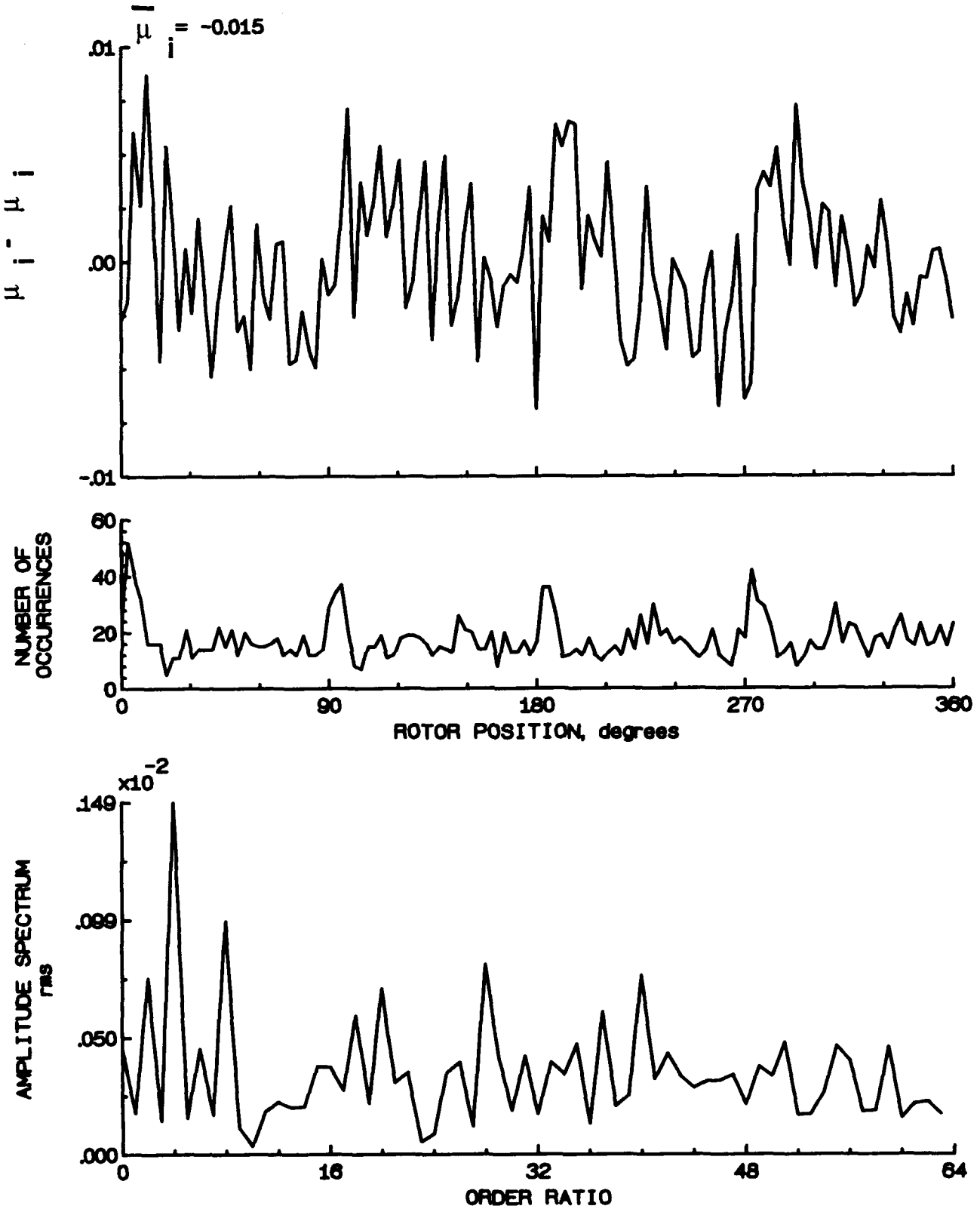

Figure 114.- Induced inflow velocity measured at 180 degrees and r/R of 1.02.

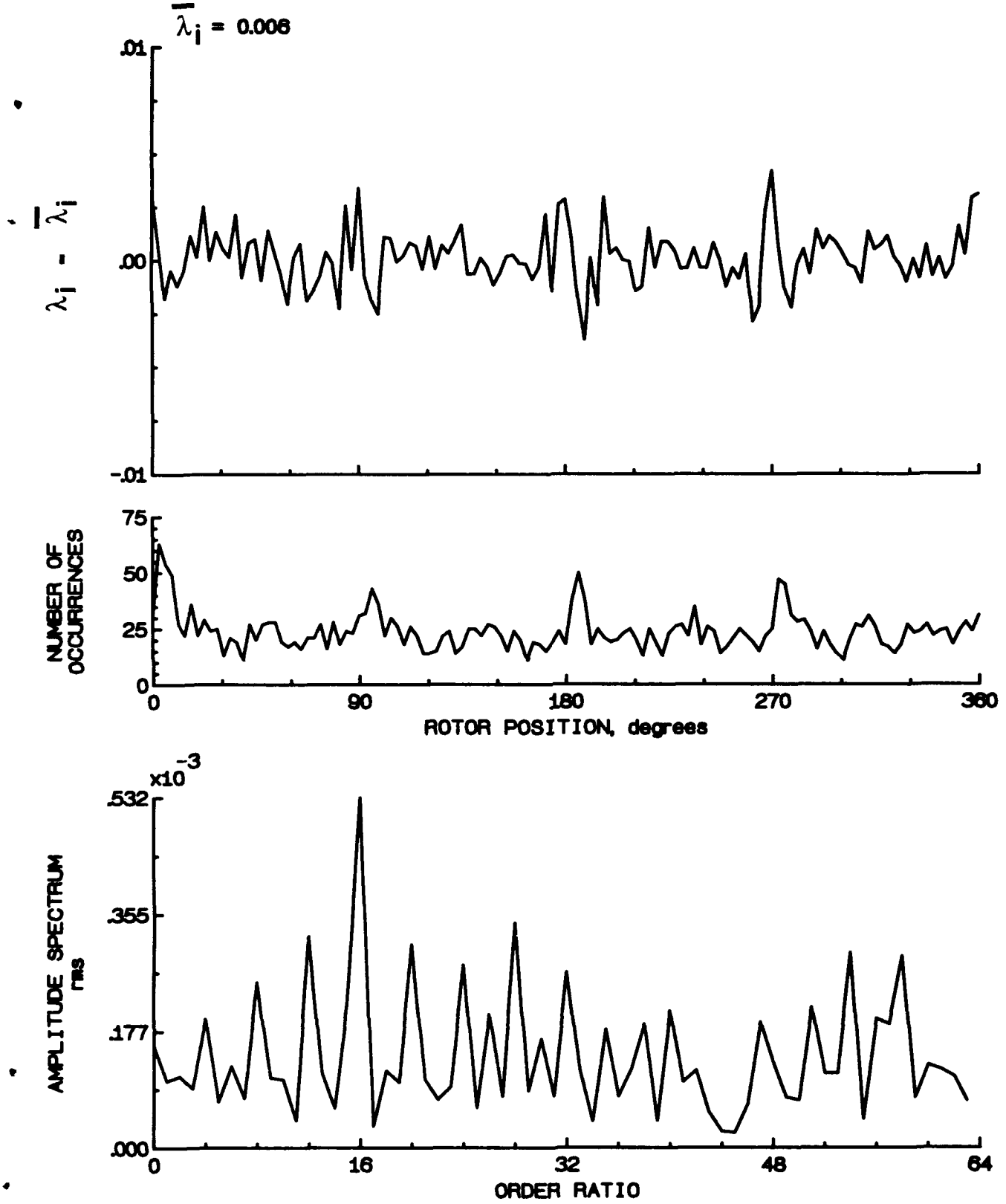

Figure 114.- Concluded.

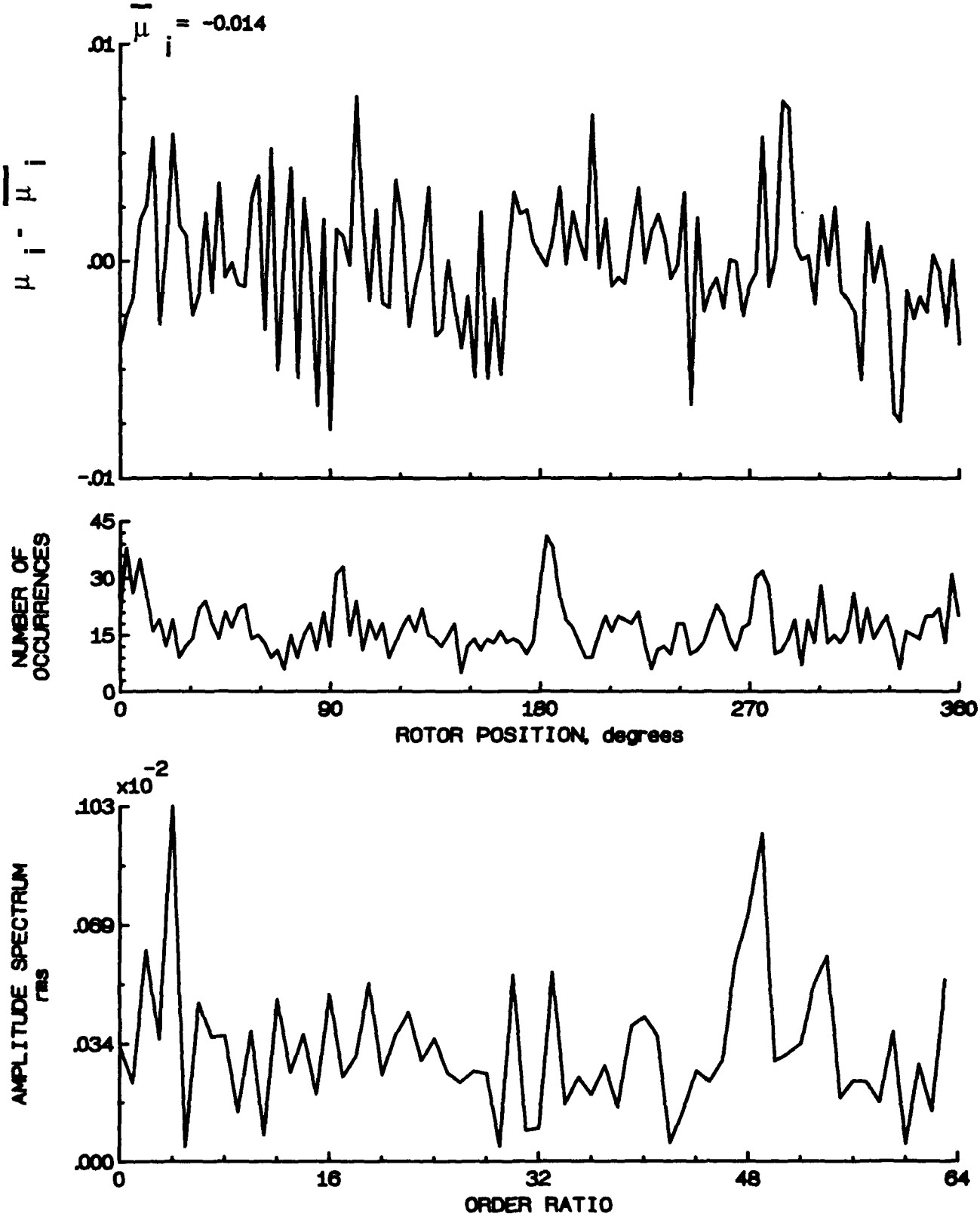

Figure 115.- Induced inflow velocity measured at 180 degrees and r/R of 1.04.

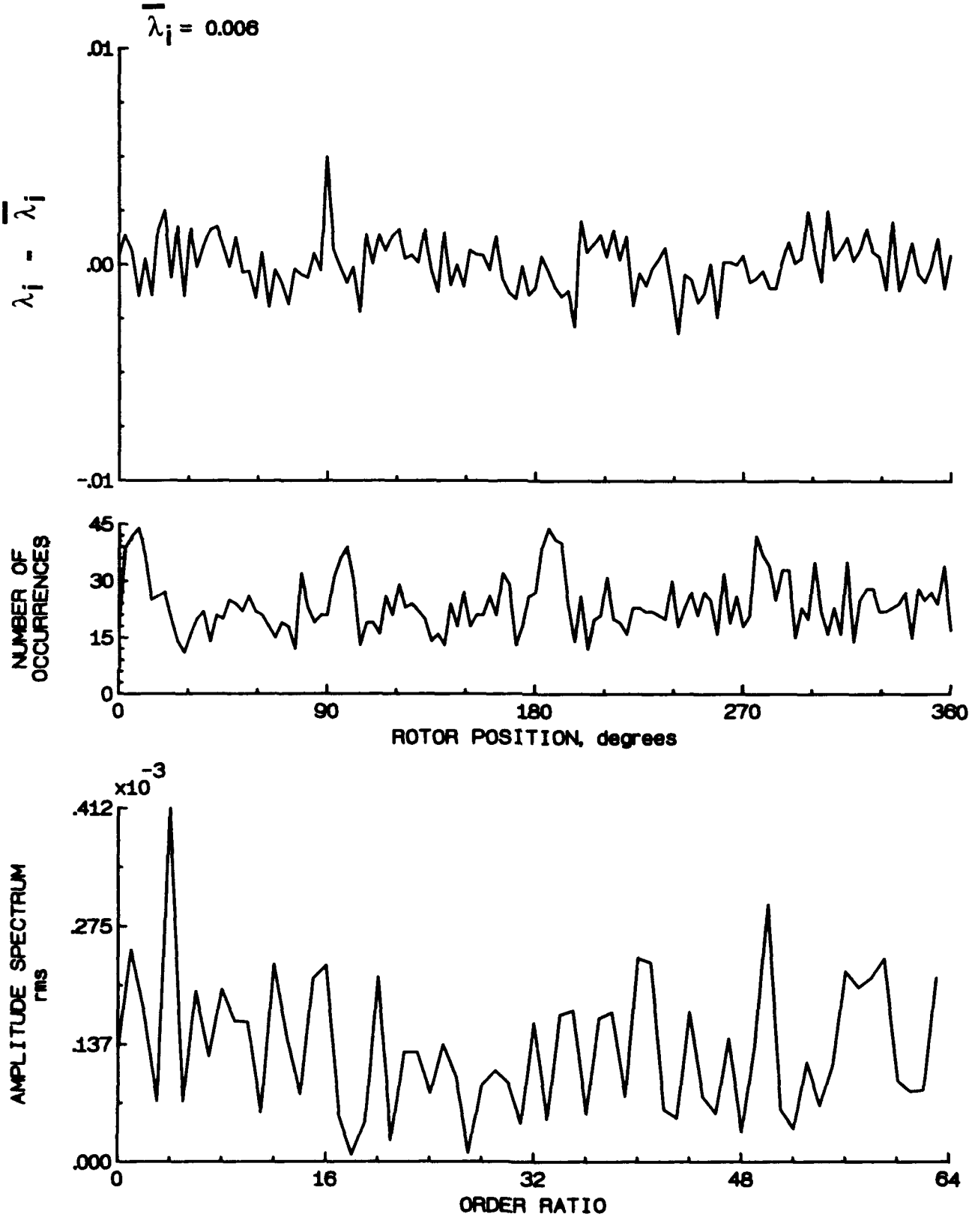

Figure 115.- Concluded.

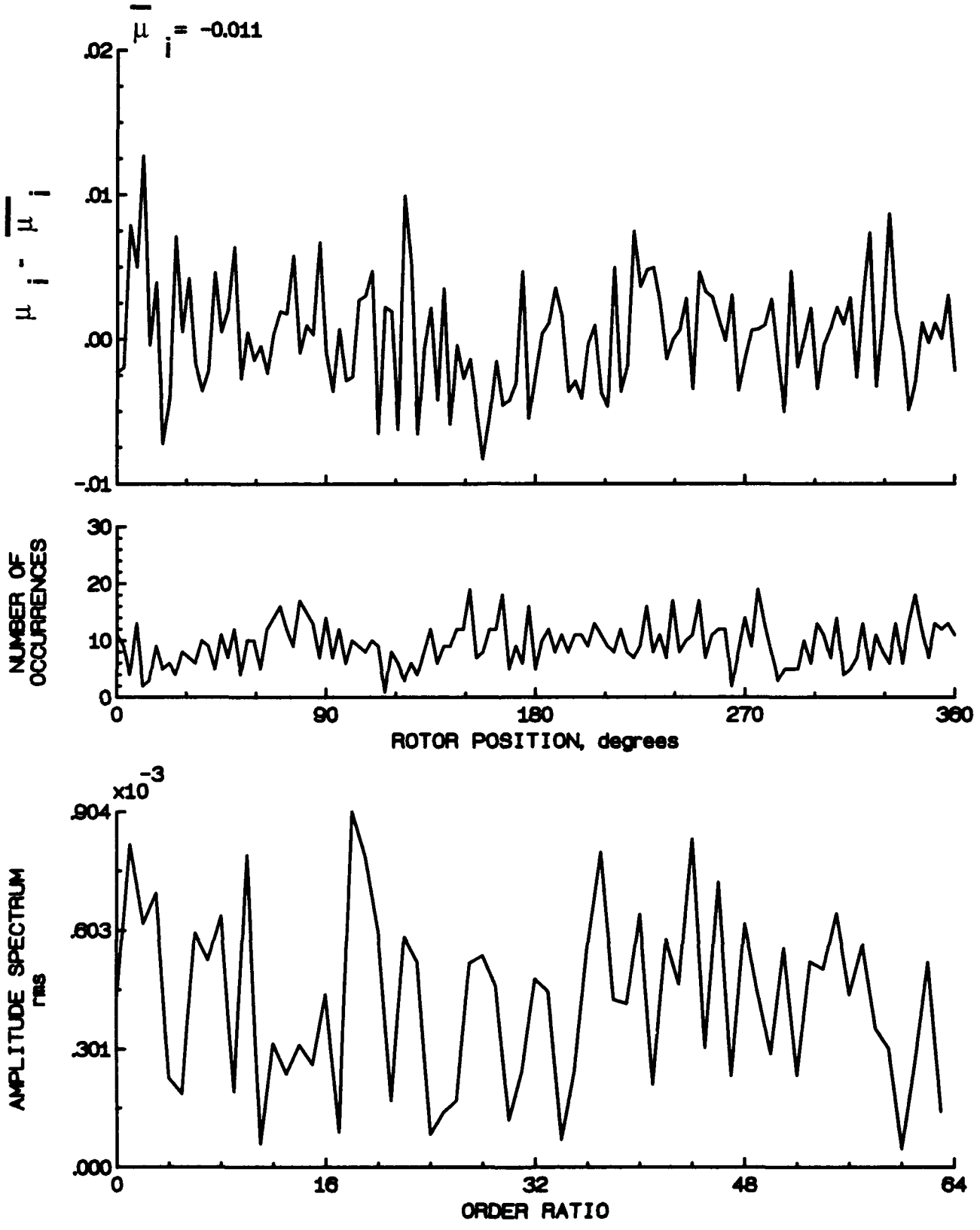

Figure 116.- Induced inflow velocity measured at 210 degrees and r/R of 0.20.

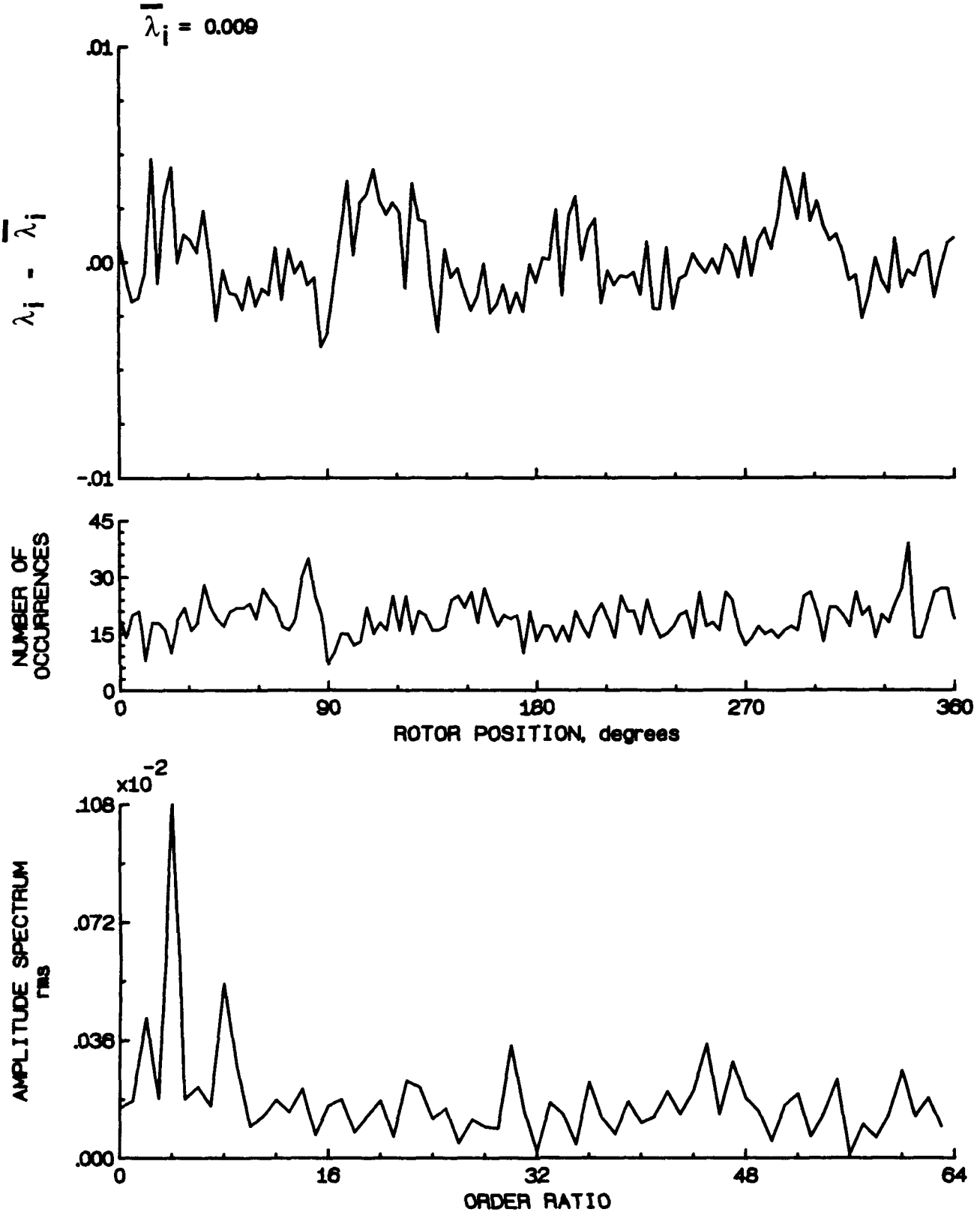

Figure 116.- Concluded.

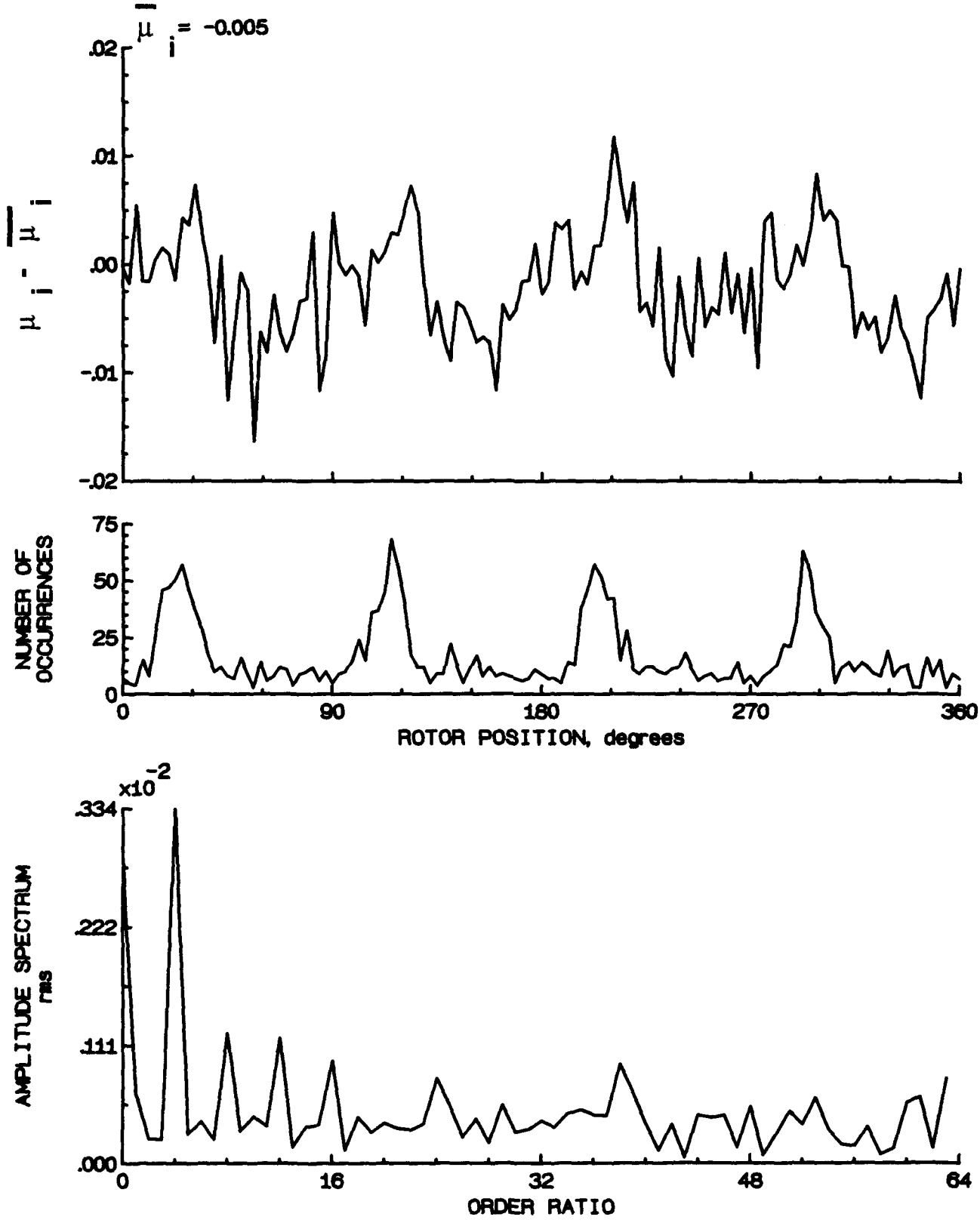

Figure 117.- Induced inflow velocity measured at 210 degrees and r/R of 0.40.

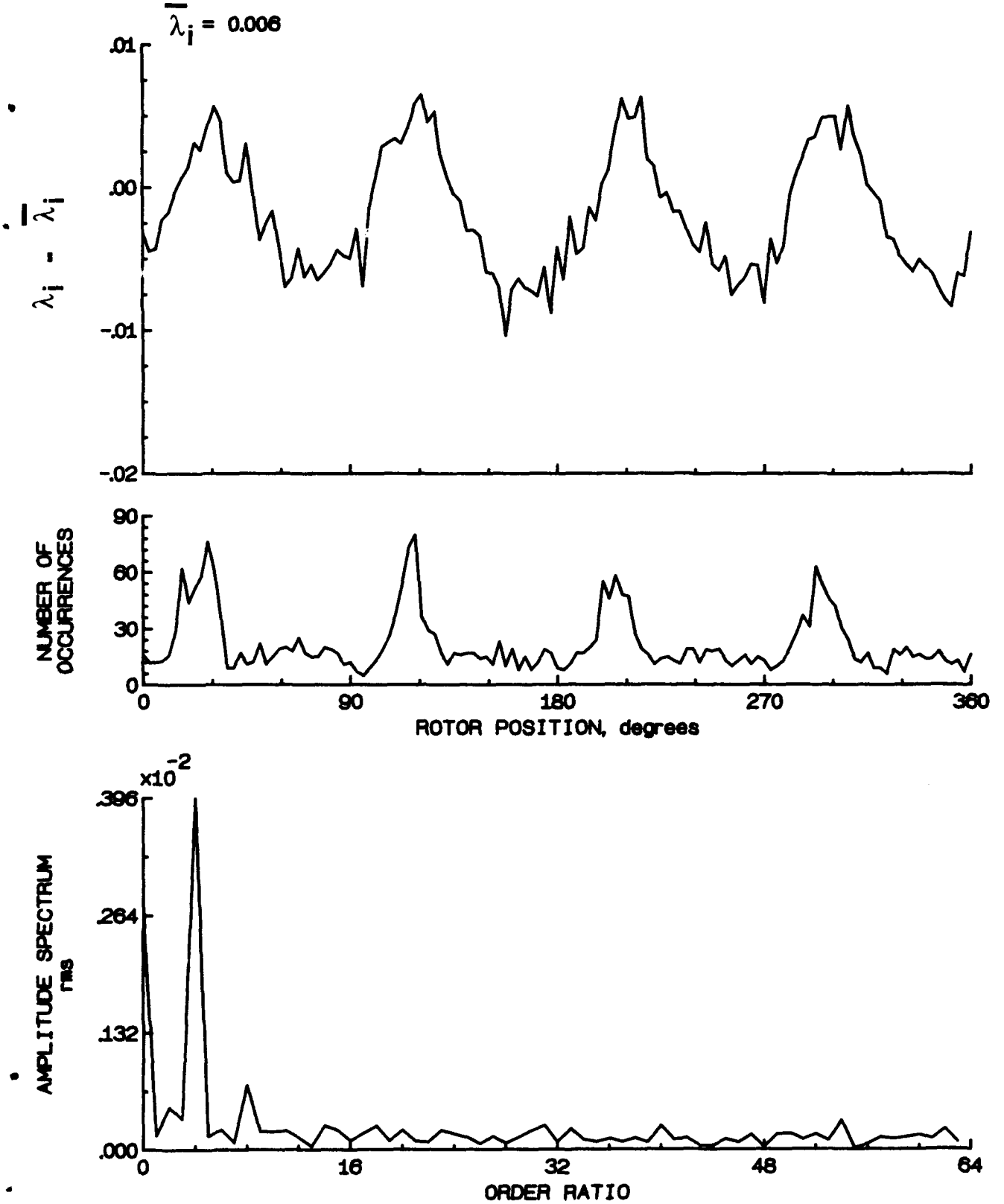

Figure 117.- Concluded.

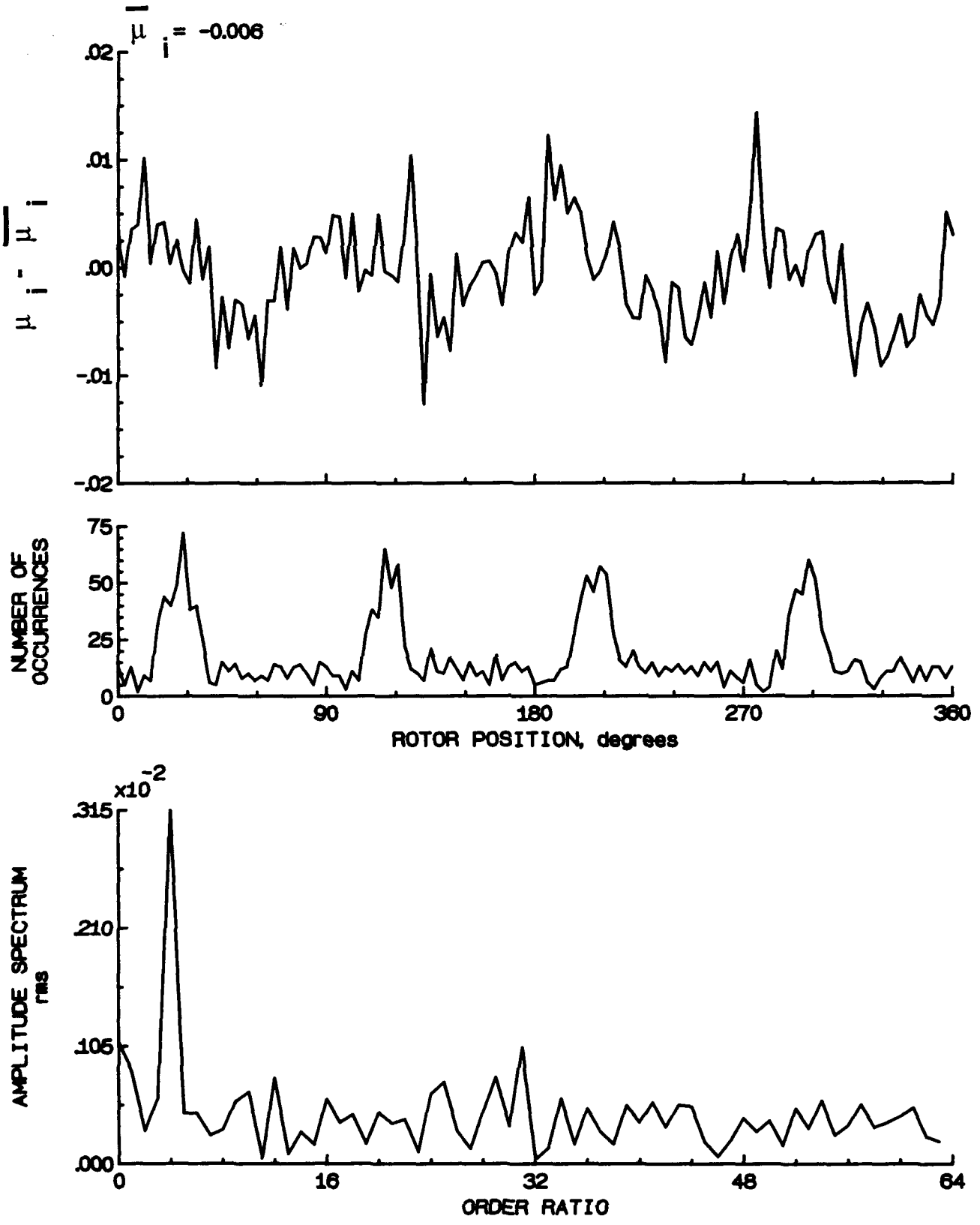

Figure 118.- Induced inflow velocity measured at 210 degrees and r/R of 0.50.

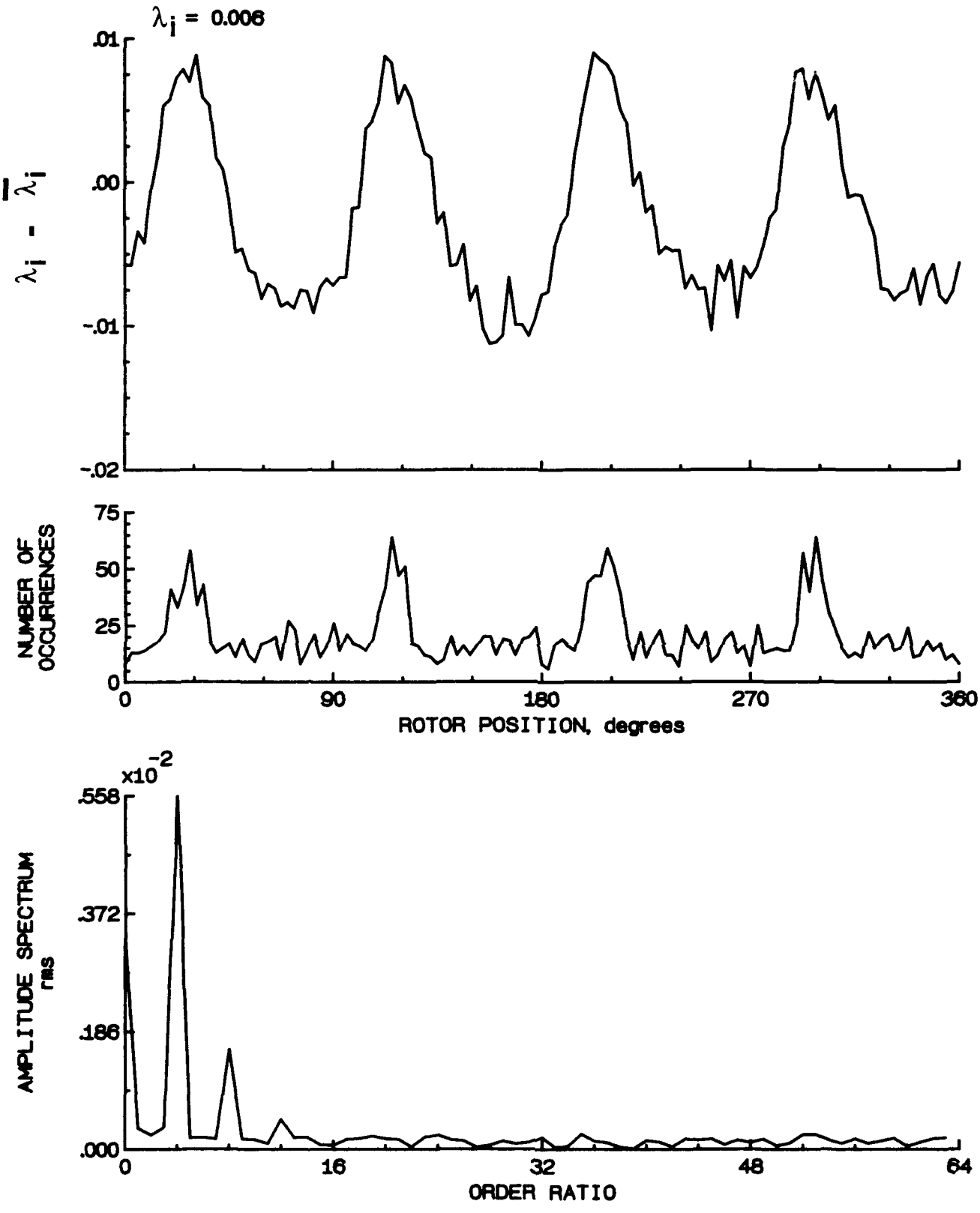

Figure 118.- Concluded.

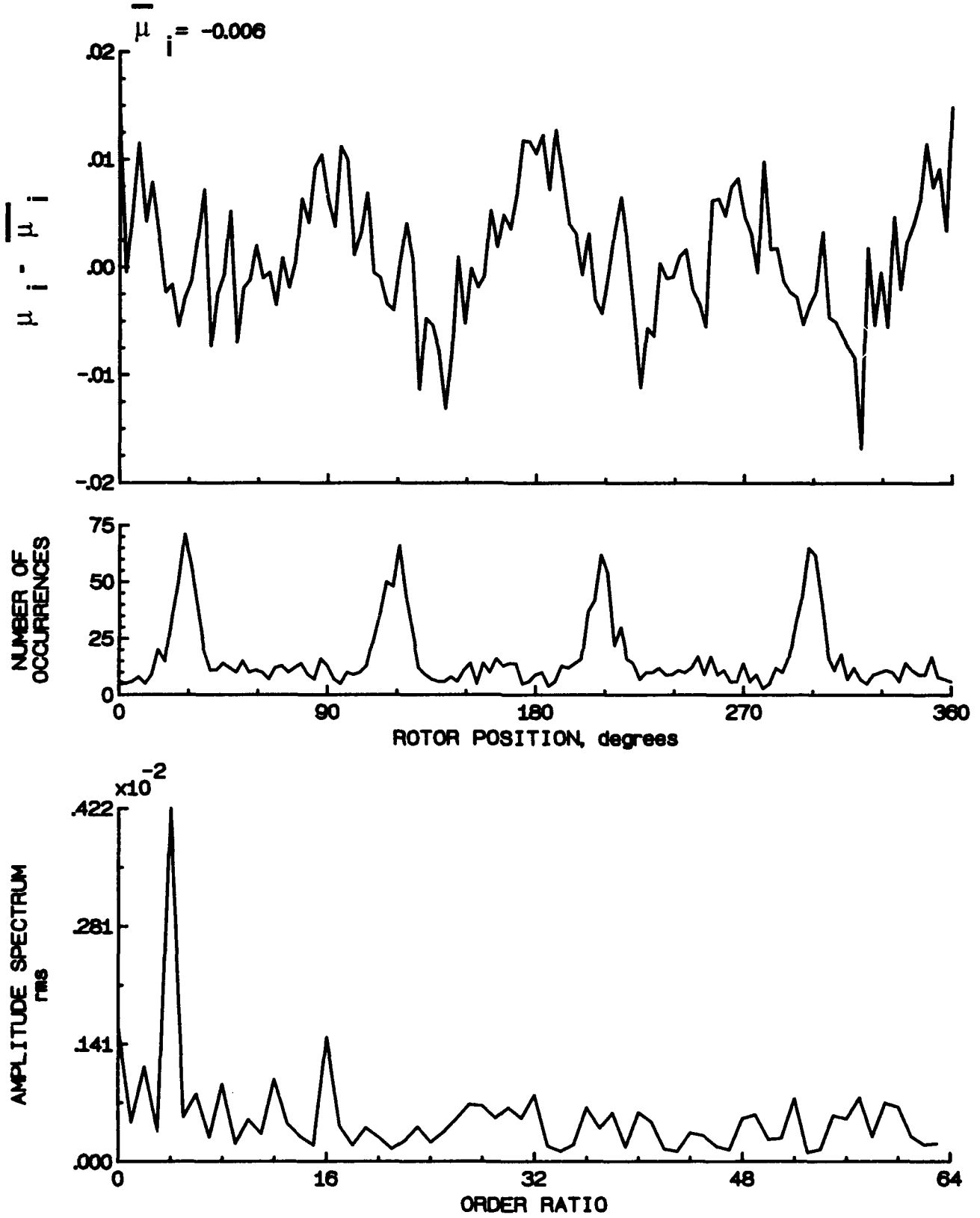

Figure 119.- Induced inflow velocity measured at 210 degrees and r/R of 0.60.

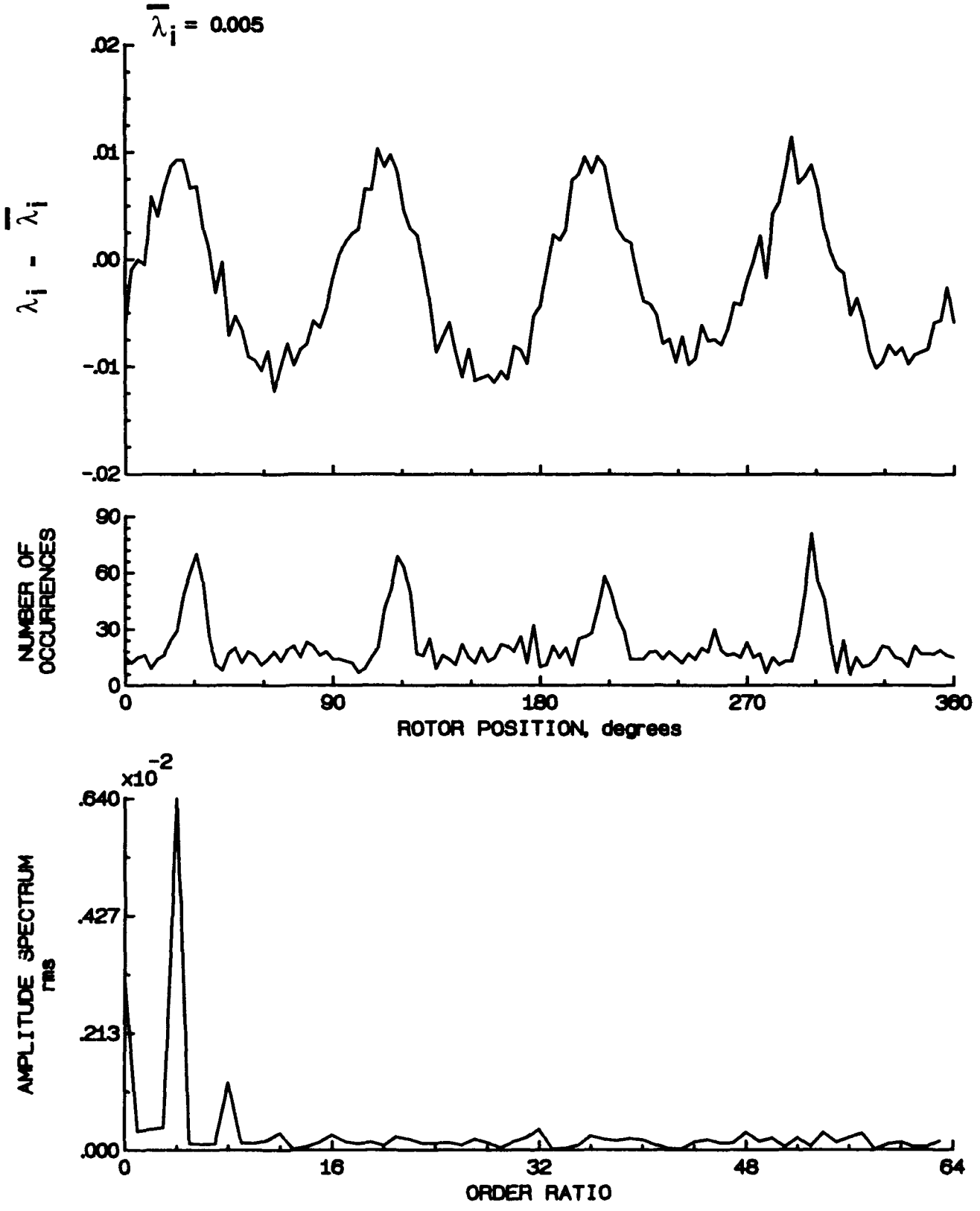

Figure 119.- Concluded.

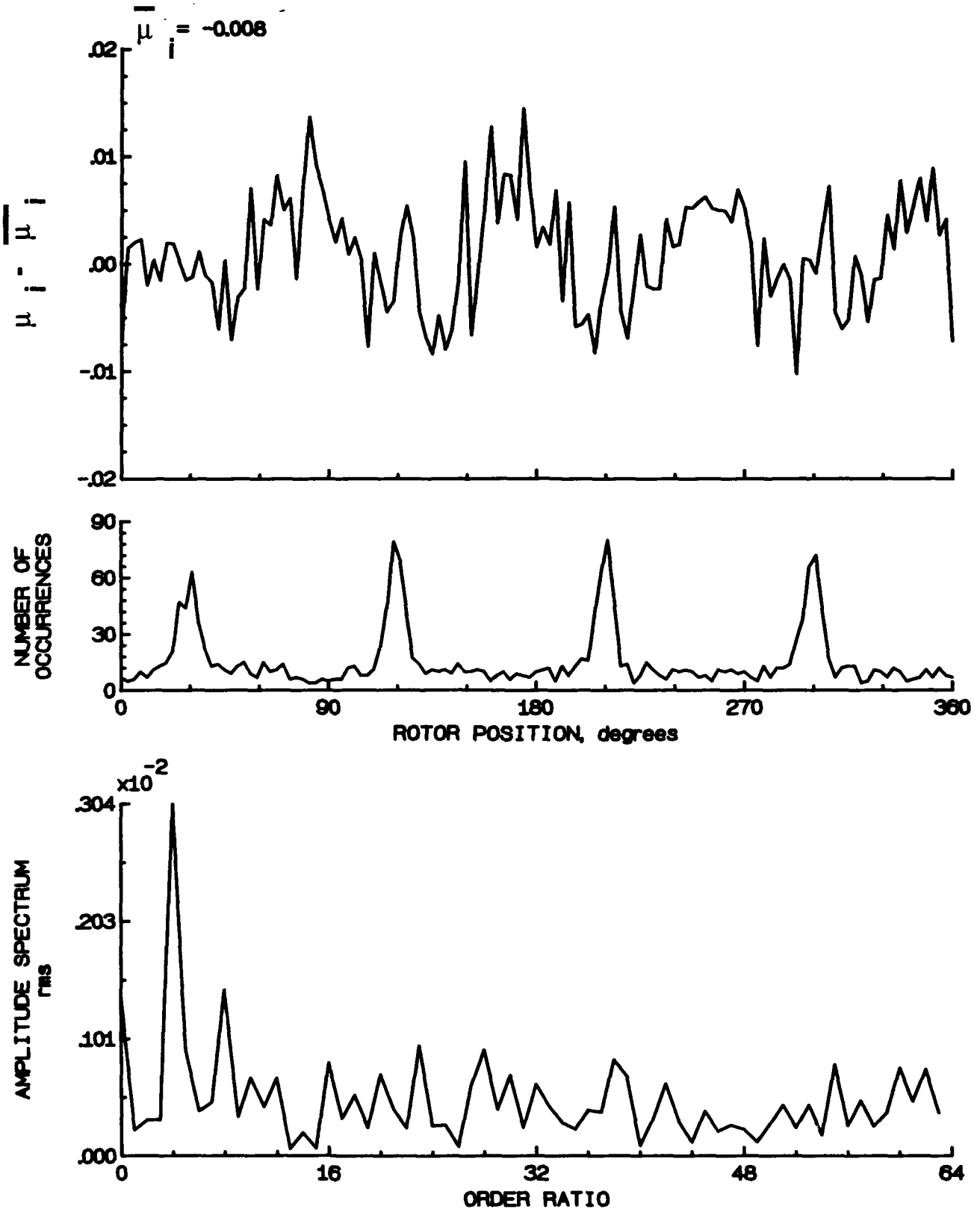

Figure 120.- Induced inflow velocity measured at 210 degrees and r/R of 0.70.

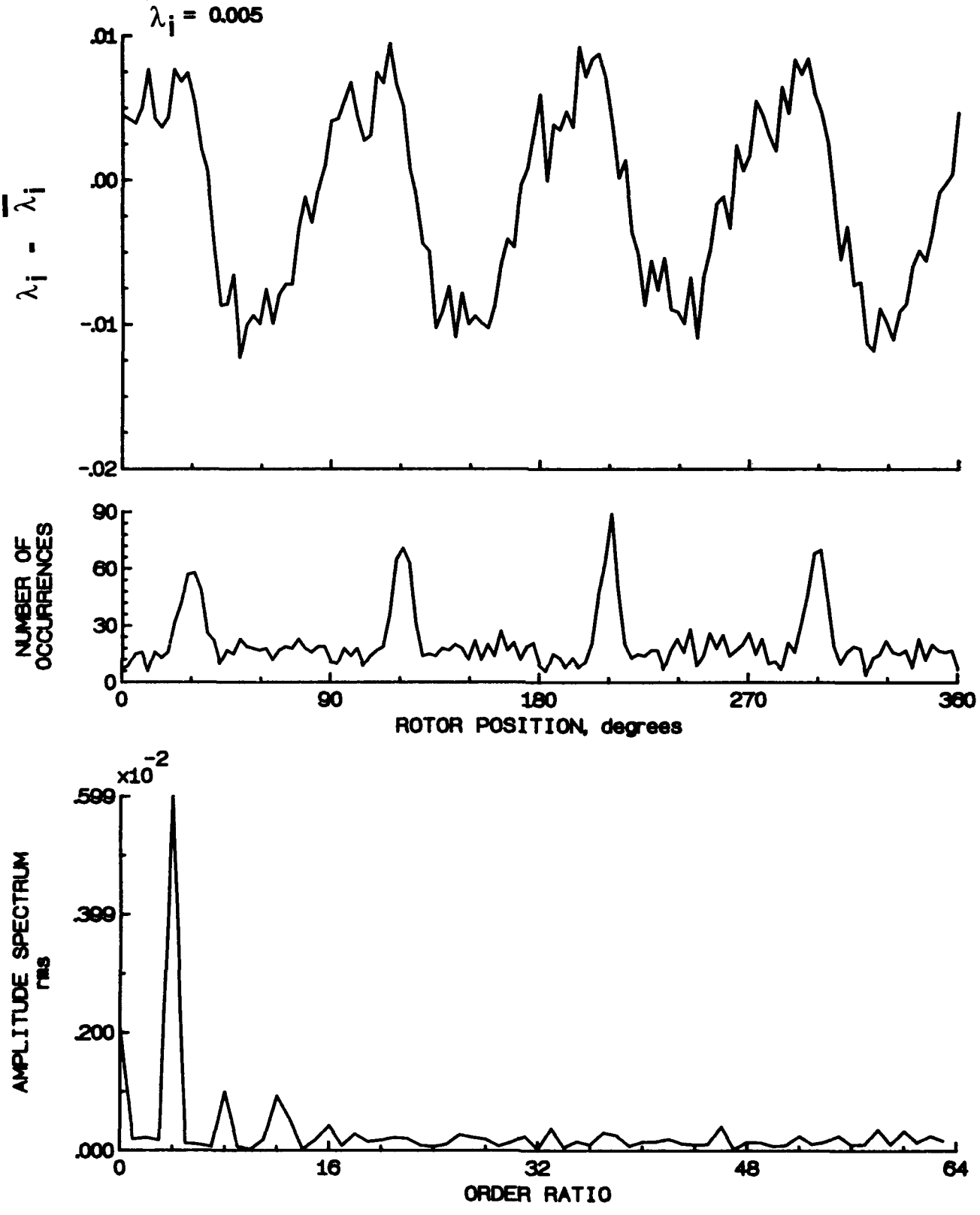

Figure 120.- Concluded.

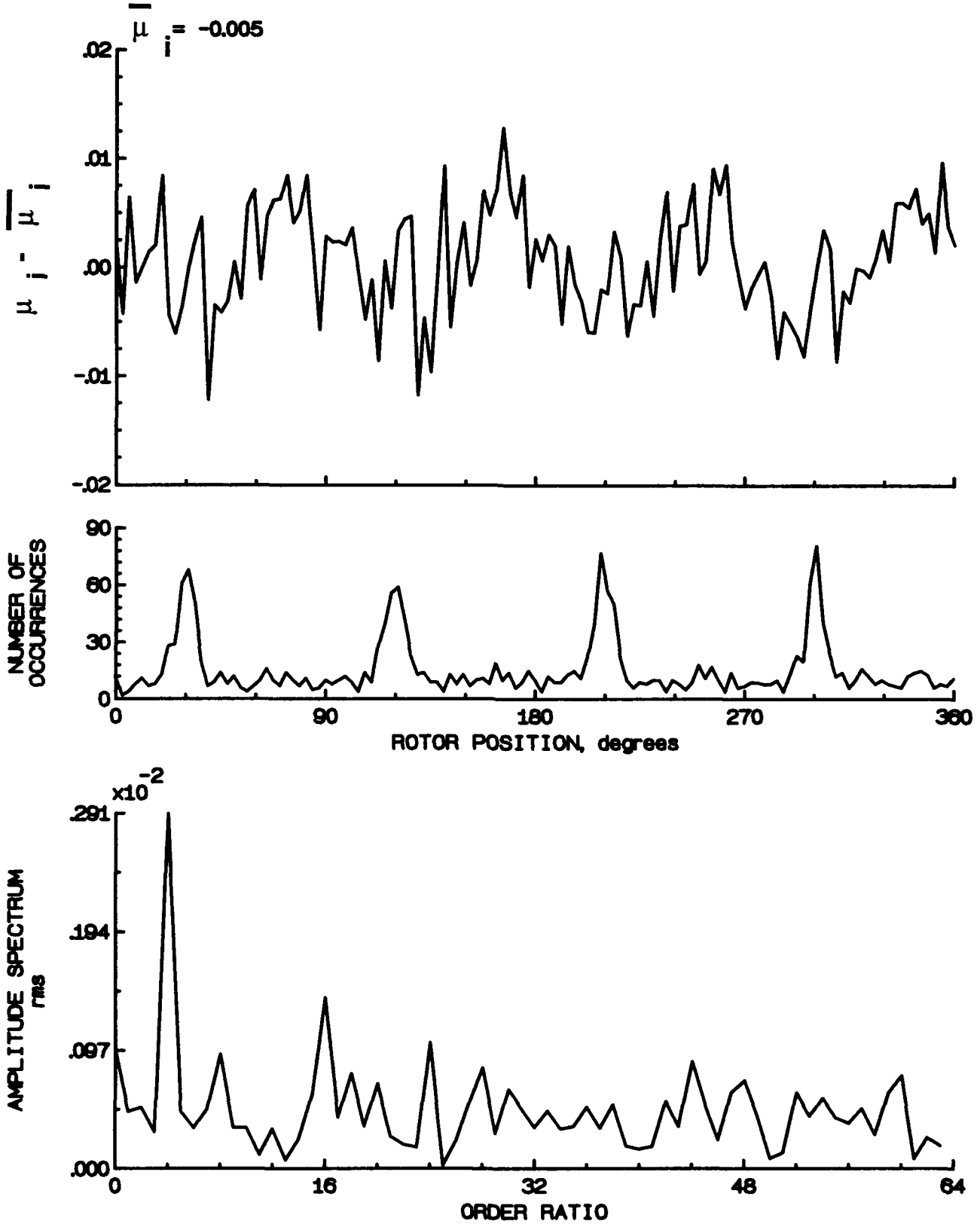

Figure 121.- Induced inflow velocity measured at 210 degrees and r/R of 0.74.

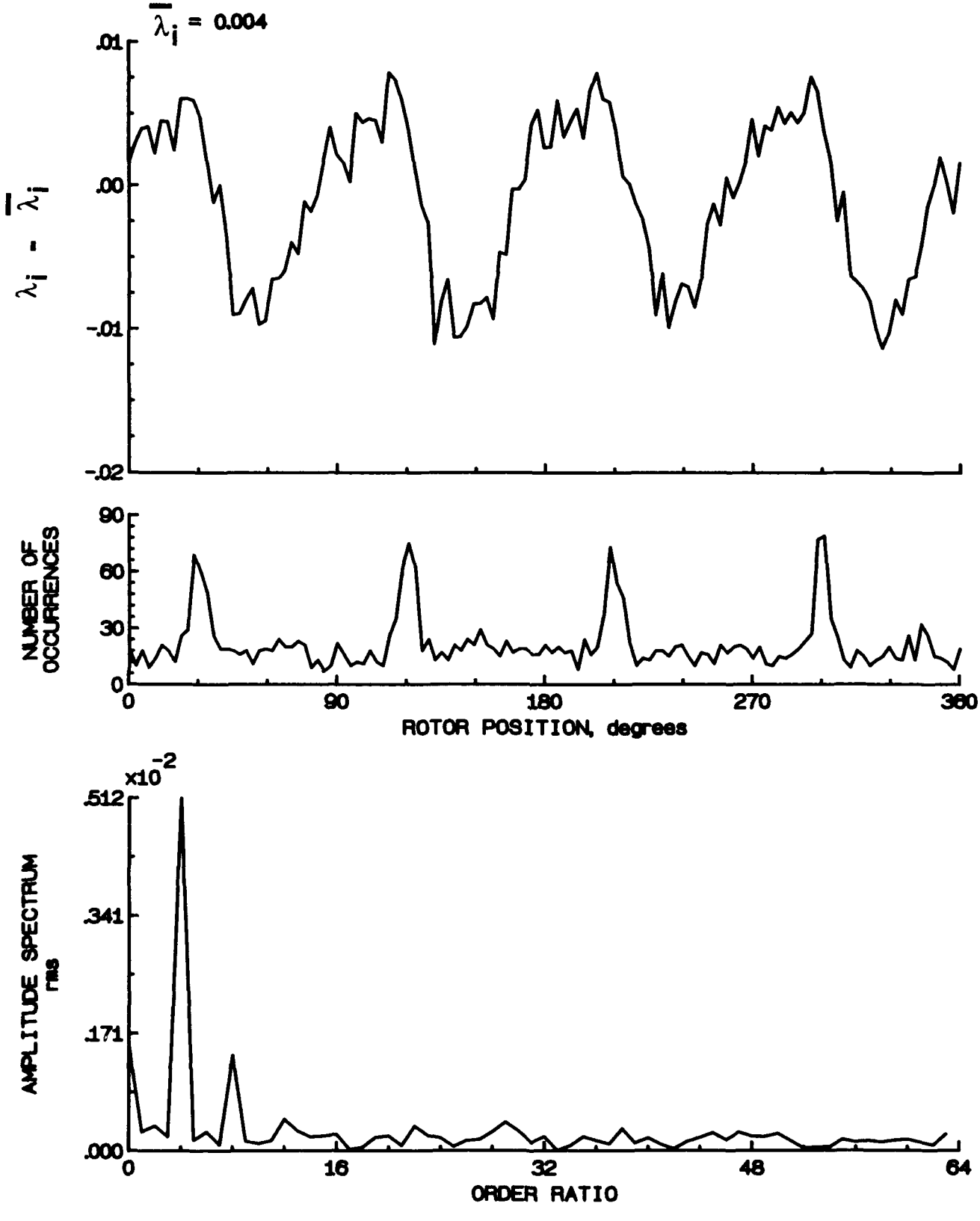

Figure 121.- Concluded.

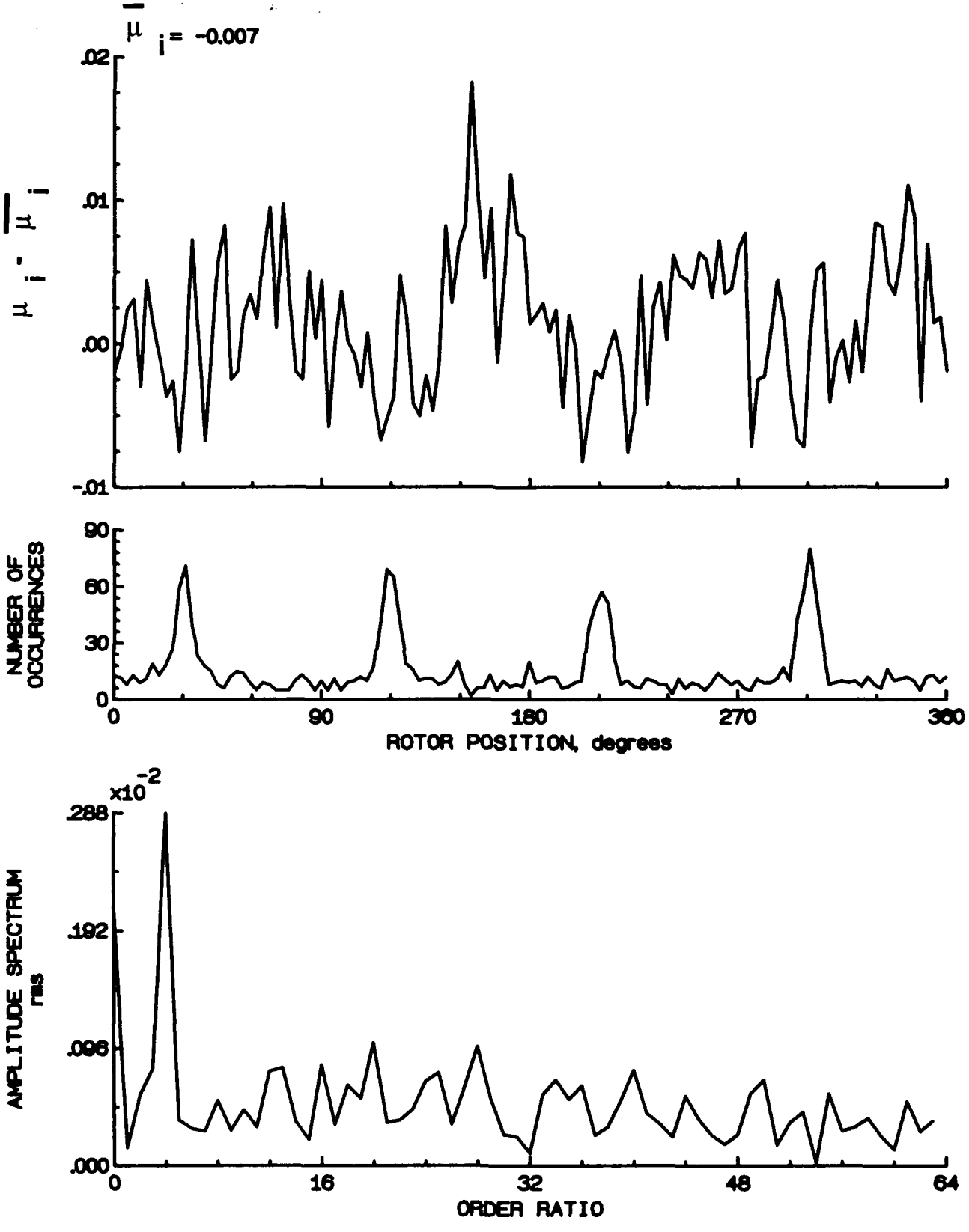

Figure 122.- Induced inflow velocity measured at 210 degrees and r/R of 0.78.

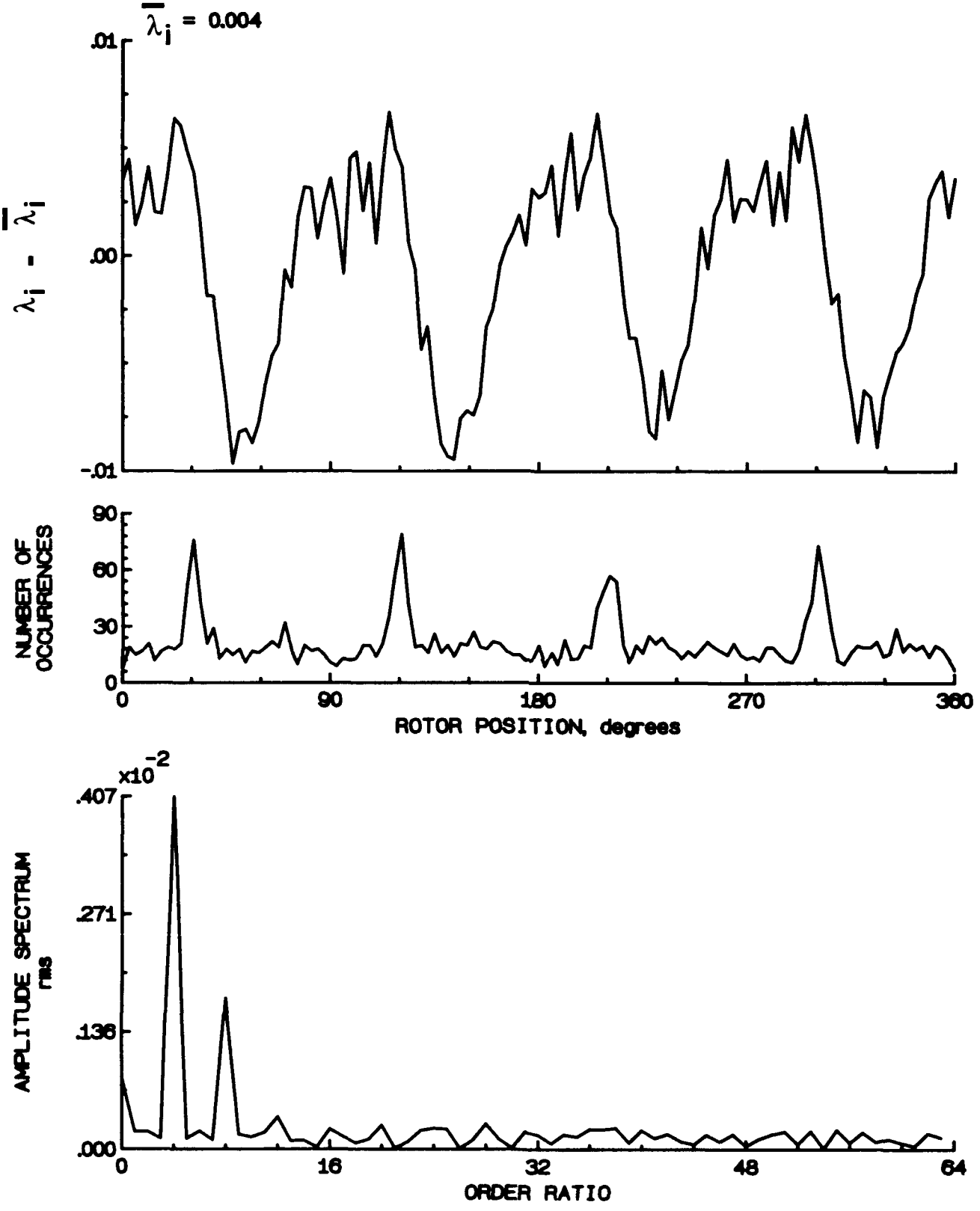

Figure 122.- Concluded.

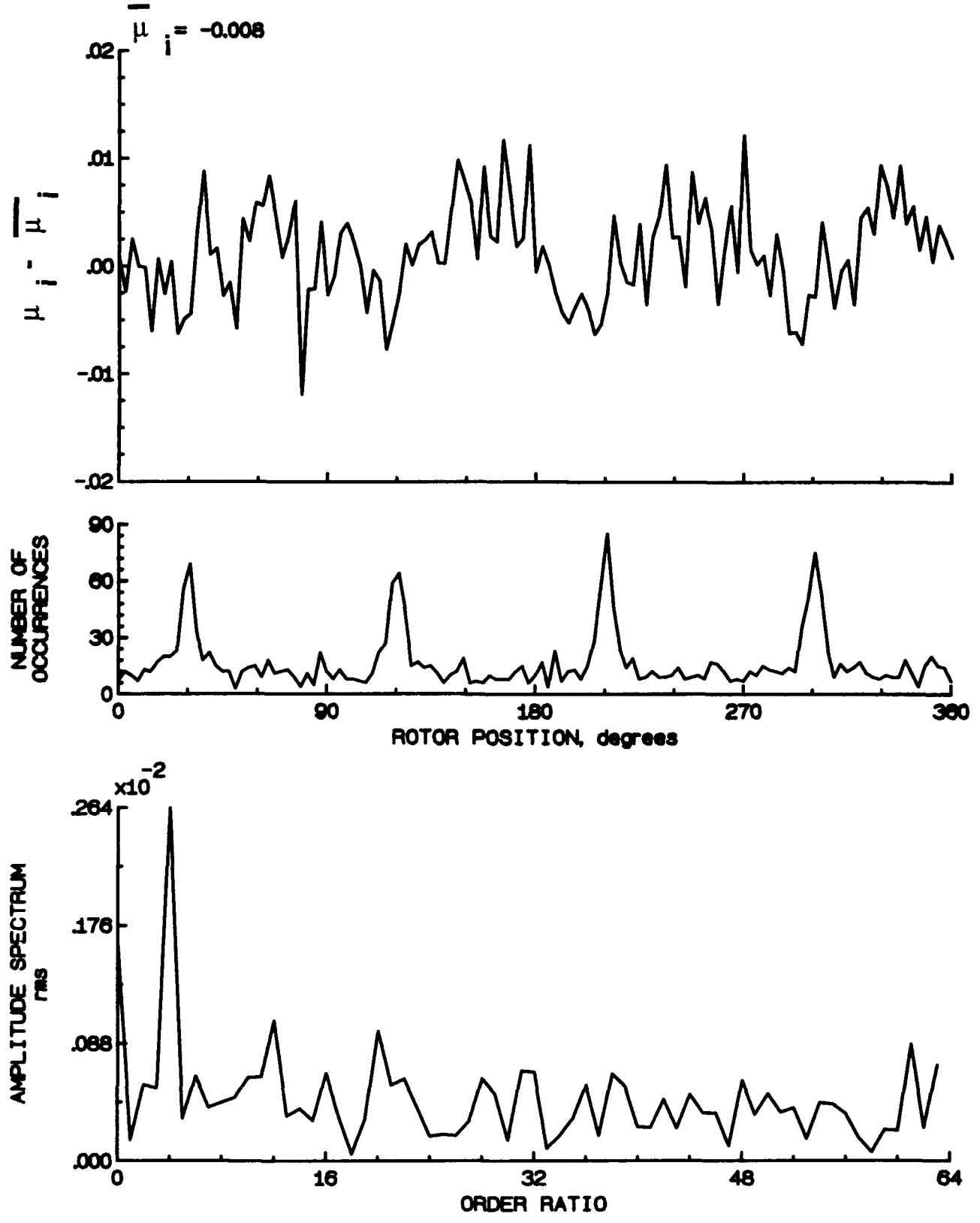

Figure 123.- Induced inflow velocity measured at 210 degrees and r/R of 0.82.

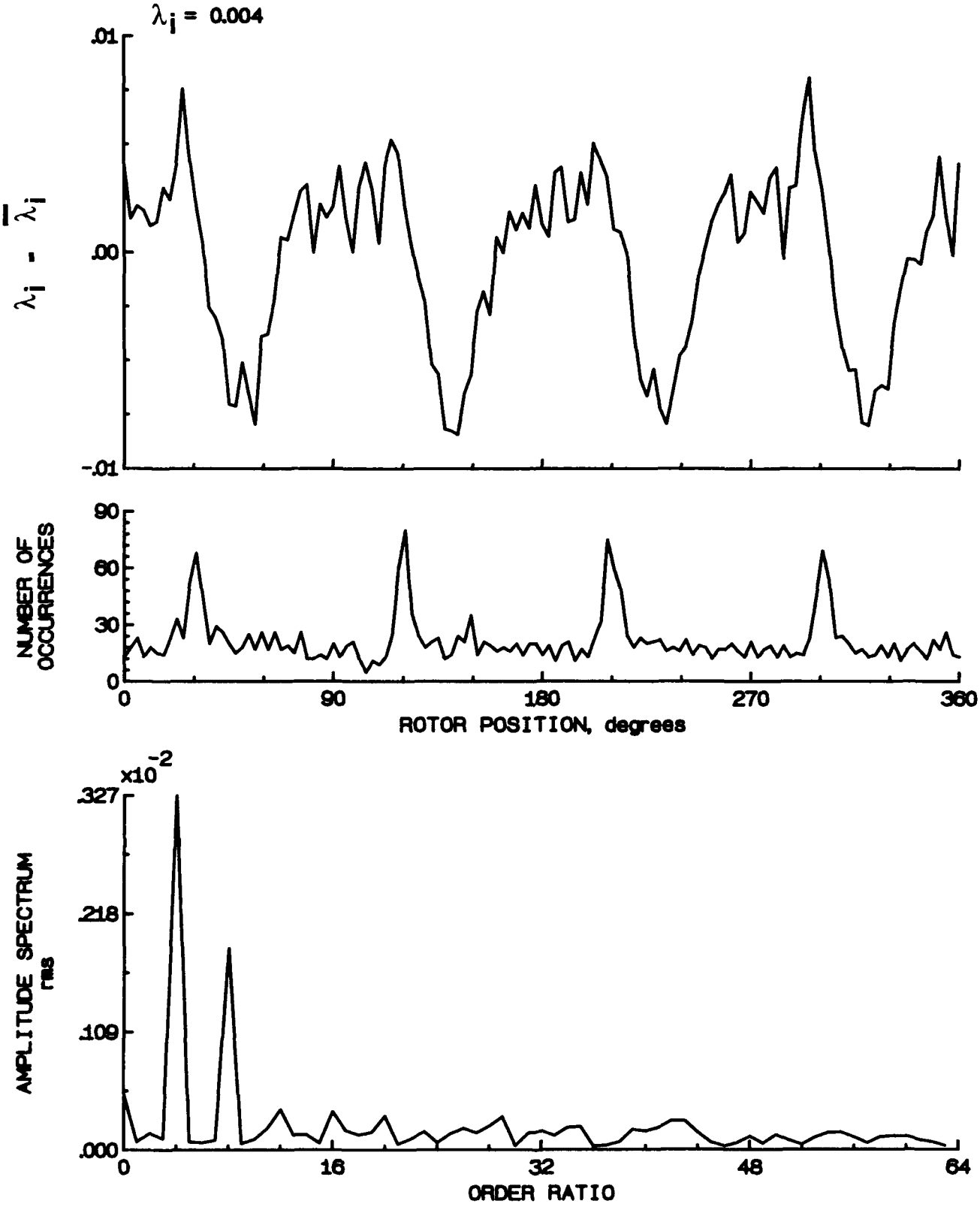

Figure 123.- Concluded.

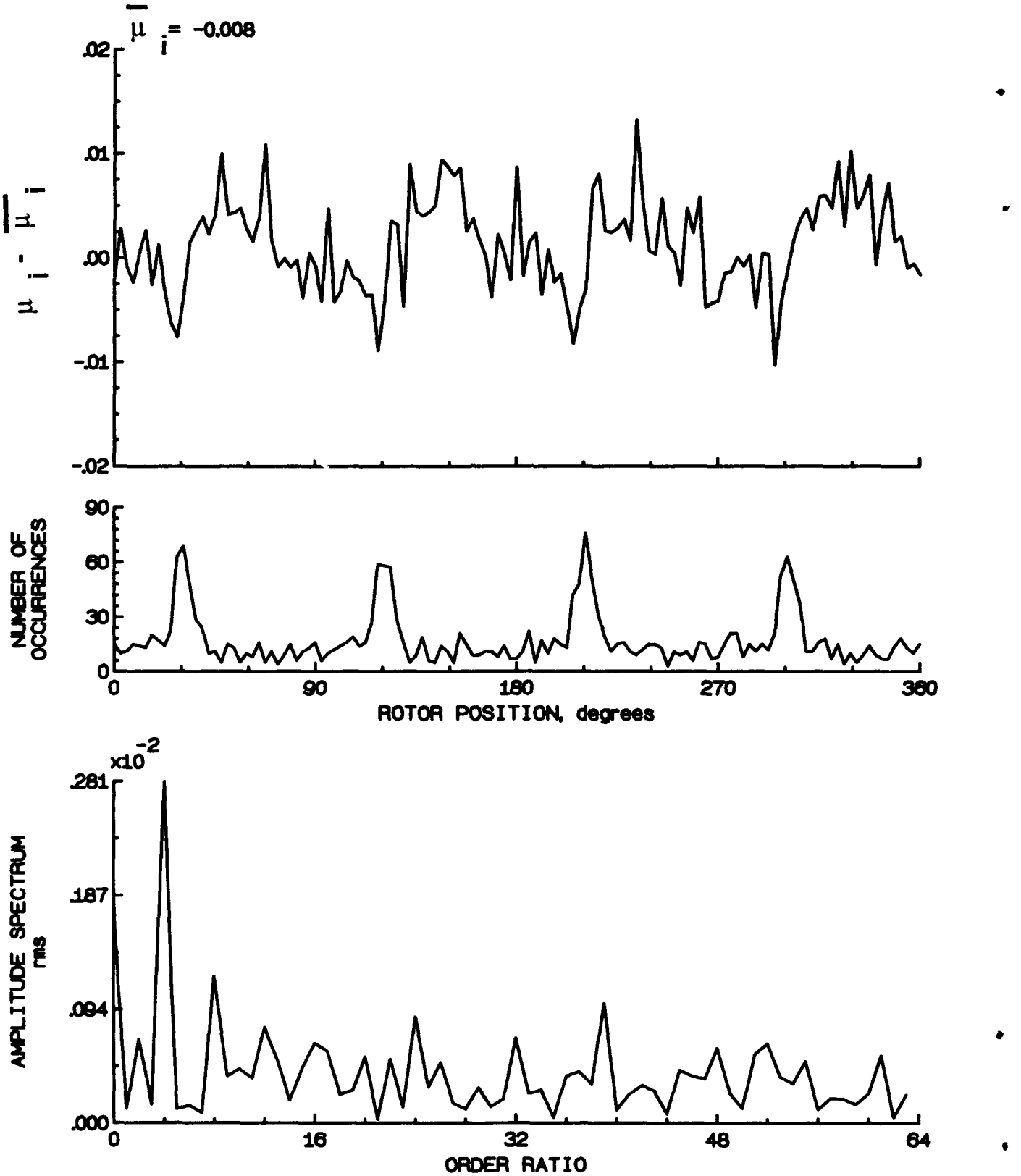

Figure 124.- Induced inflow velocity measured at 210 degrees and r/R of 0.86.

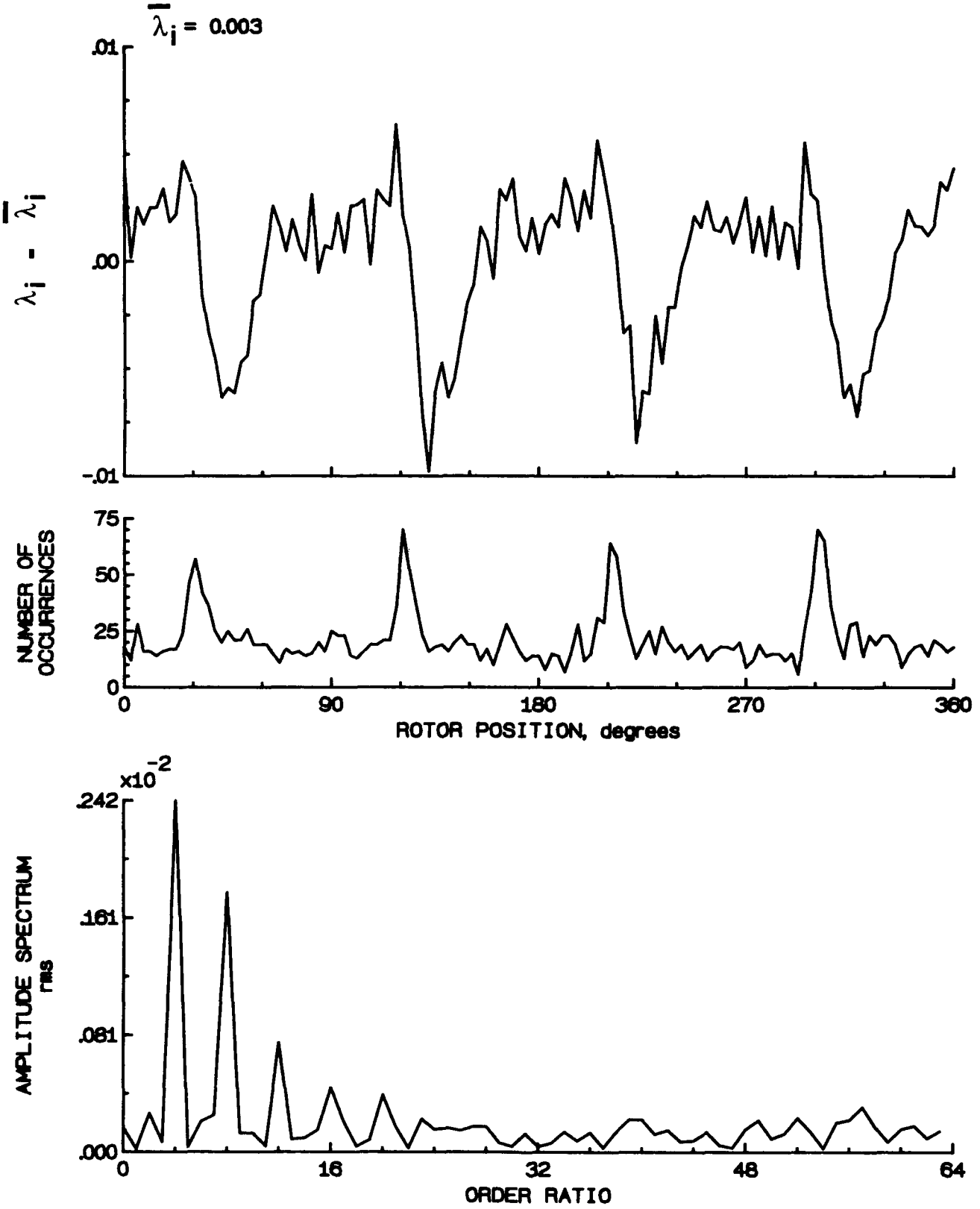

Figure 124.- Concluded.

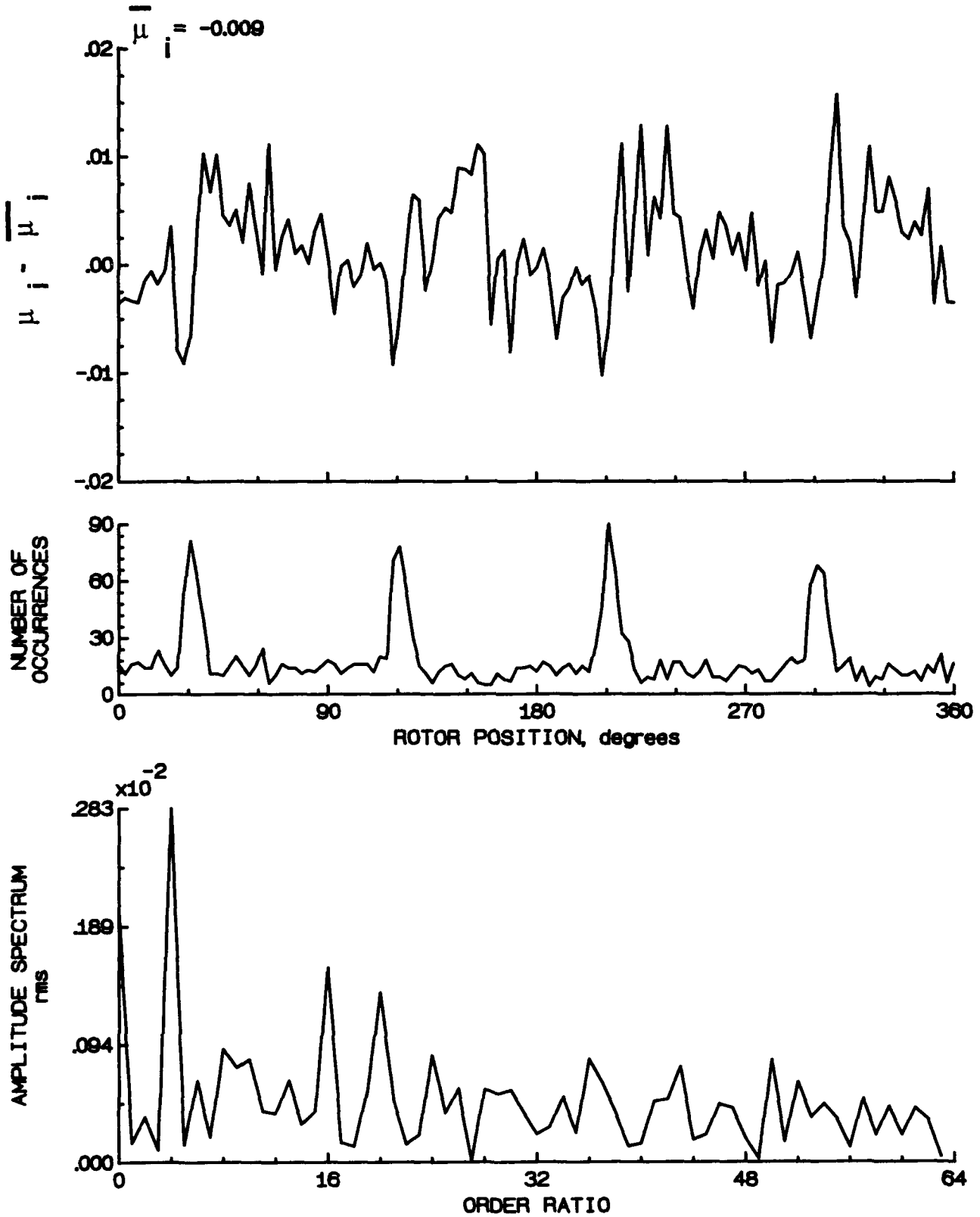

Figure 125.- Induced inflow velocity measured at 210 degrees and r/R of 0.90.

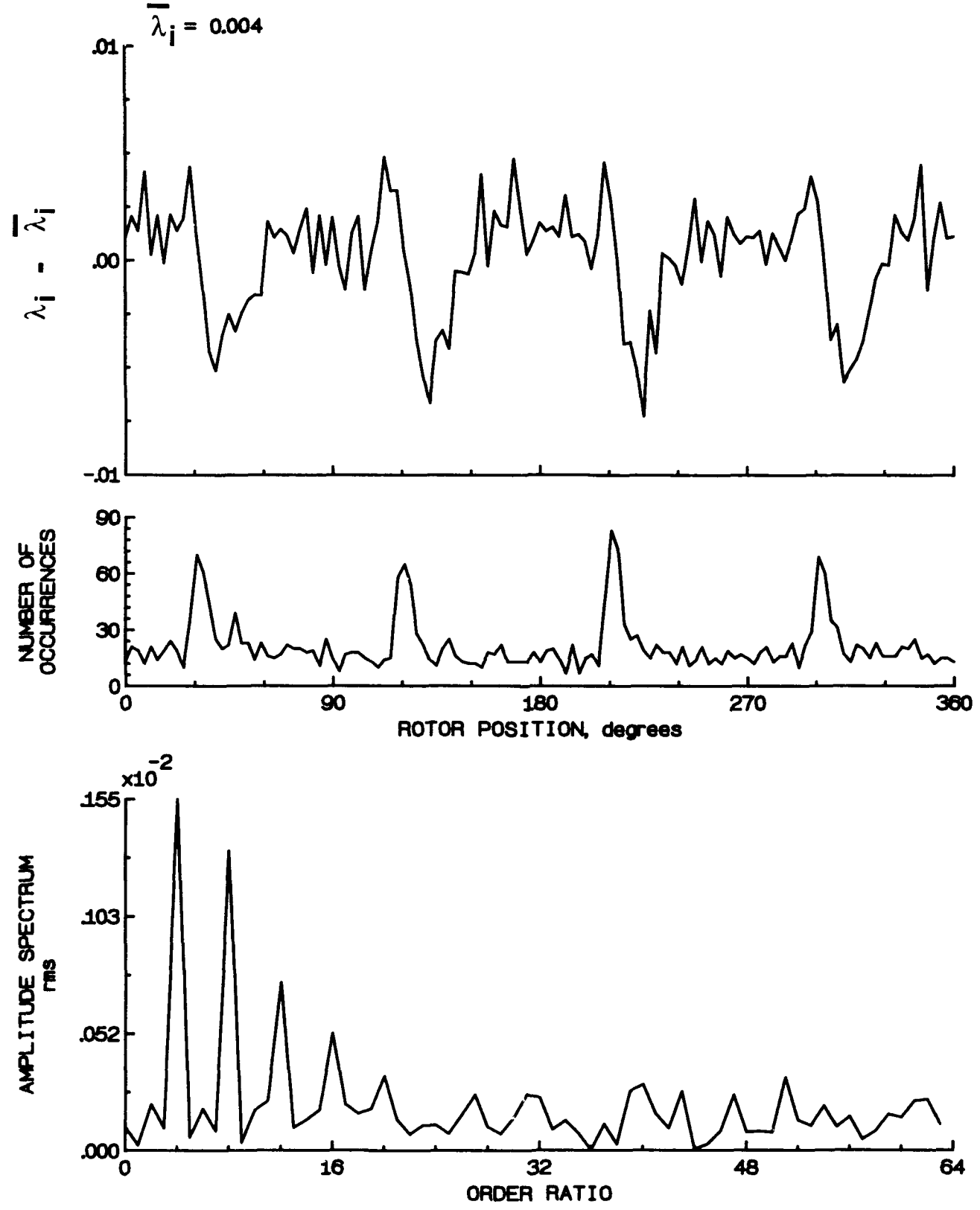

Figure 125.- Concluded.

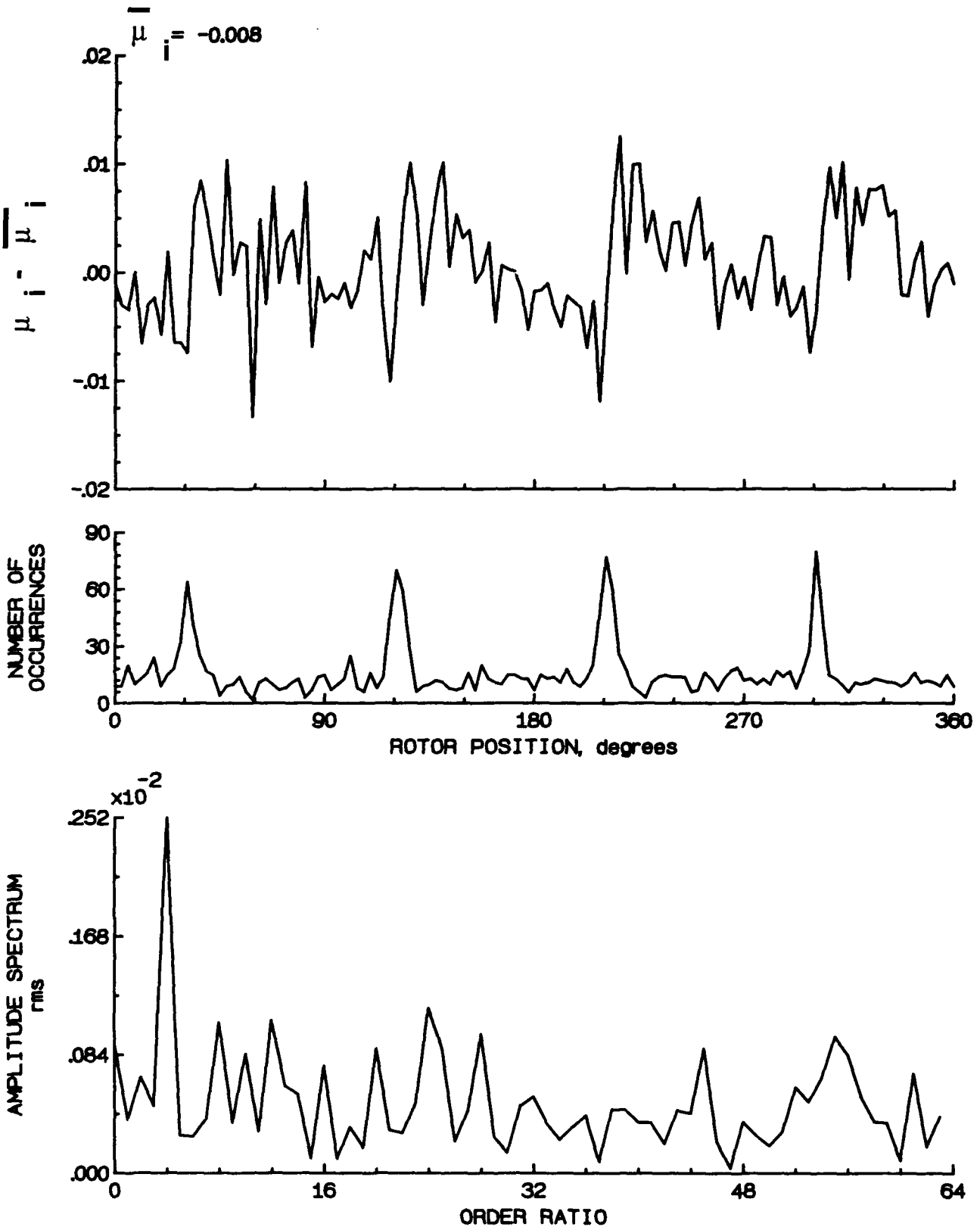

Figure 126.- Induced inflow velocity measured at 210 degrees and r/R of 0.94.

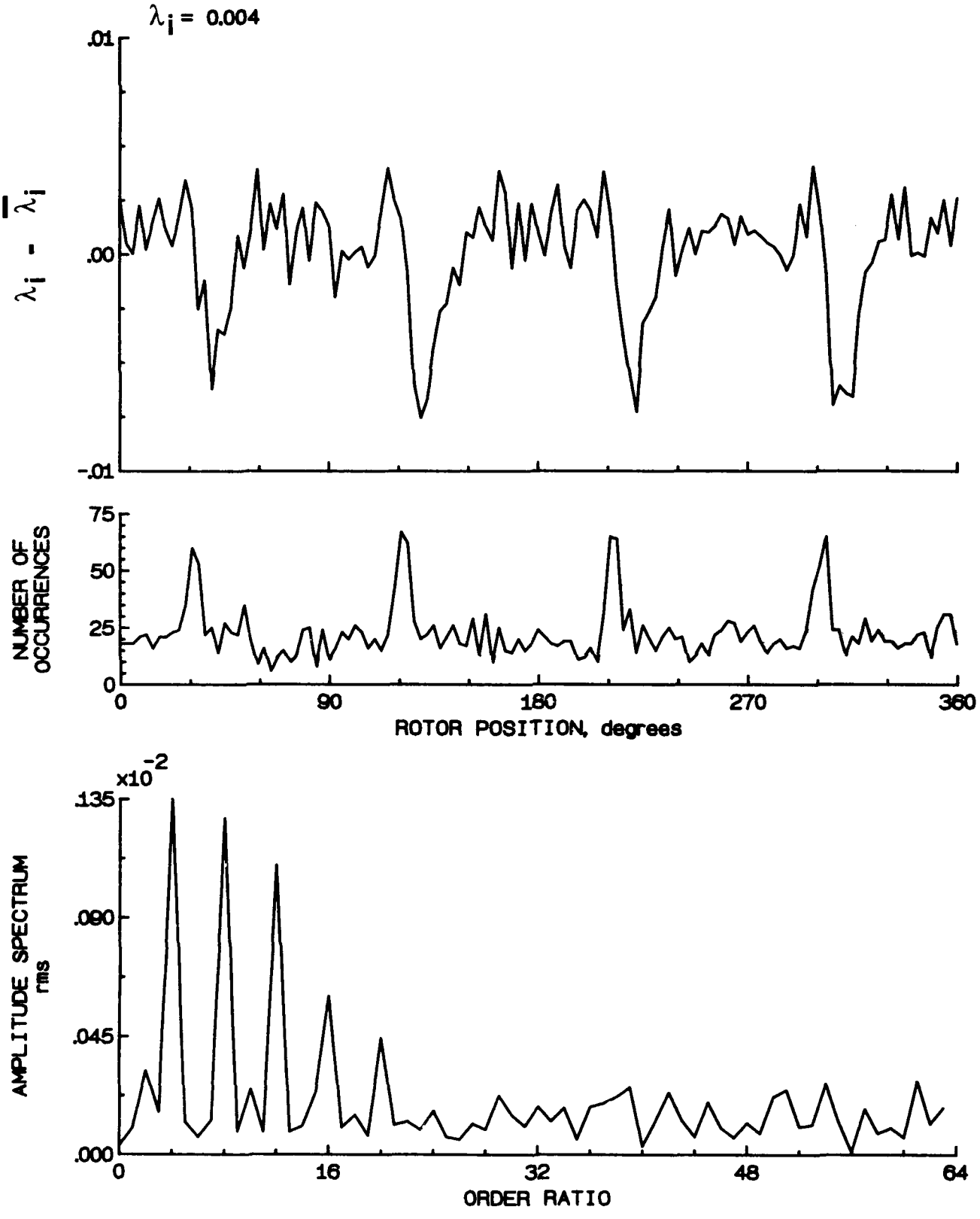

Figure 126.- Concluded.

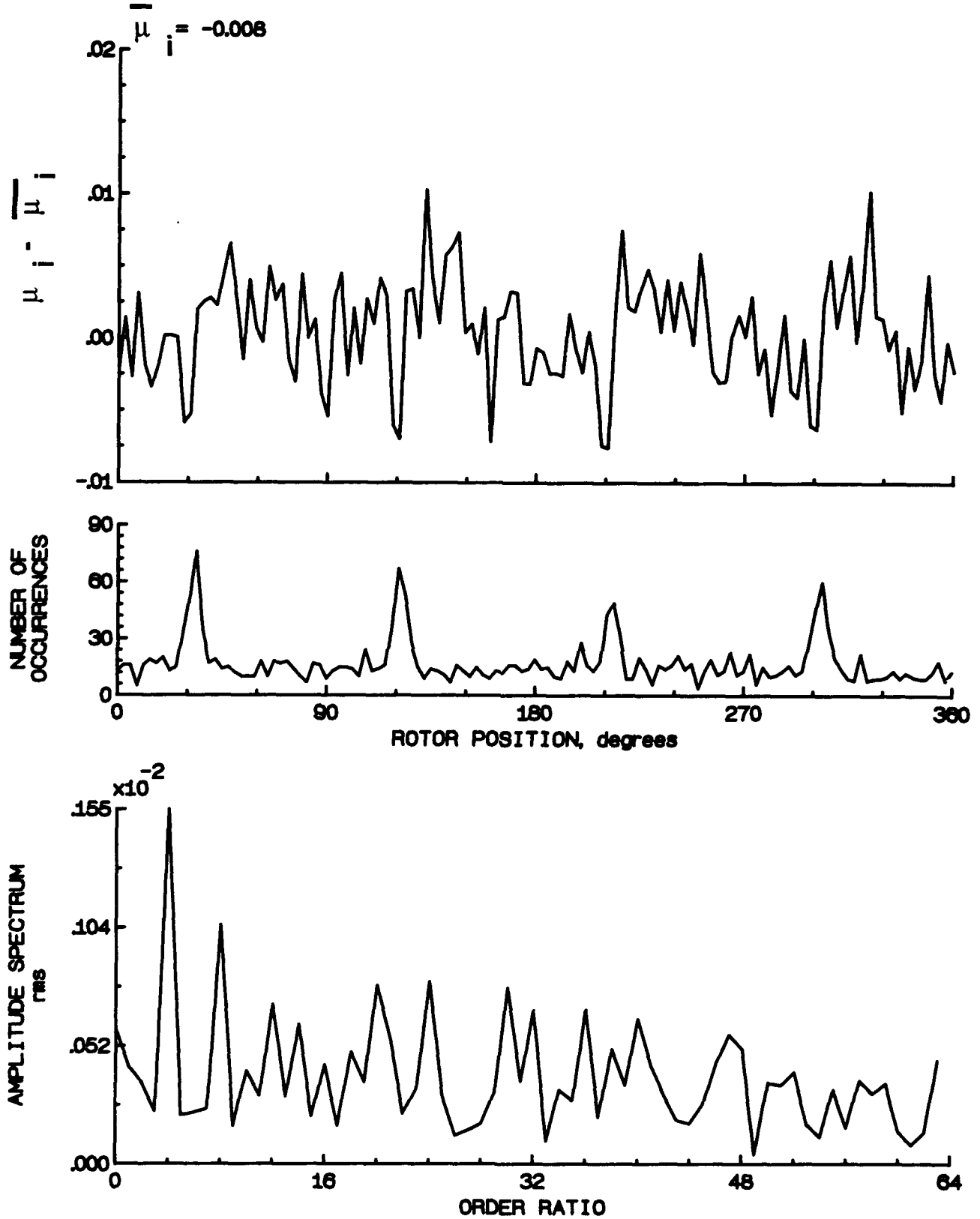

Figure 127.- Induced inflow velocity measured at 210 degrees and r/R of 0.98.

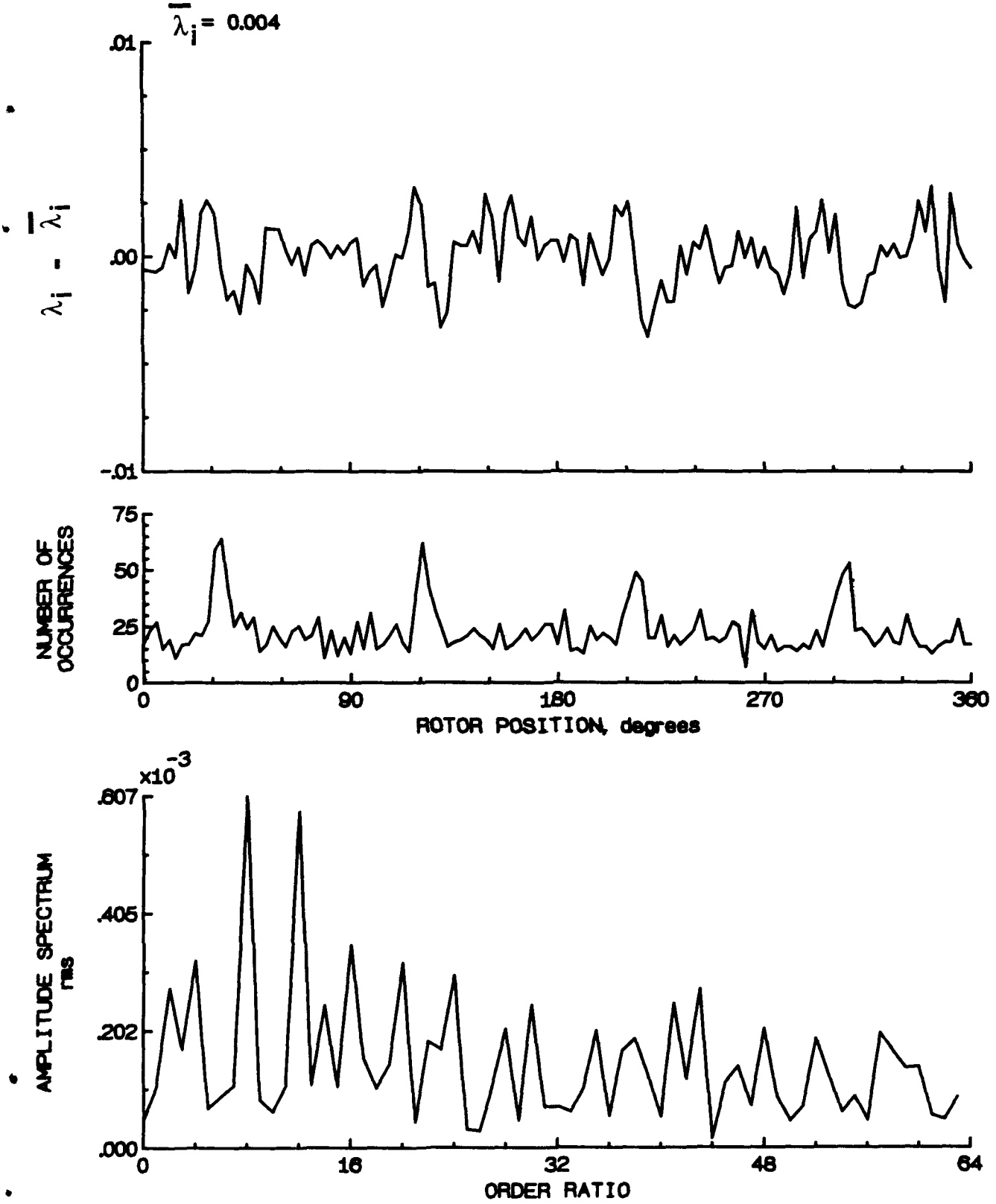

Figure 127.- Concluded.

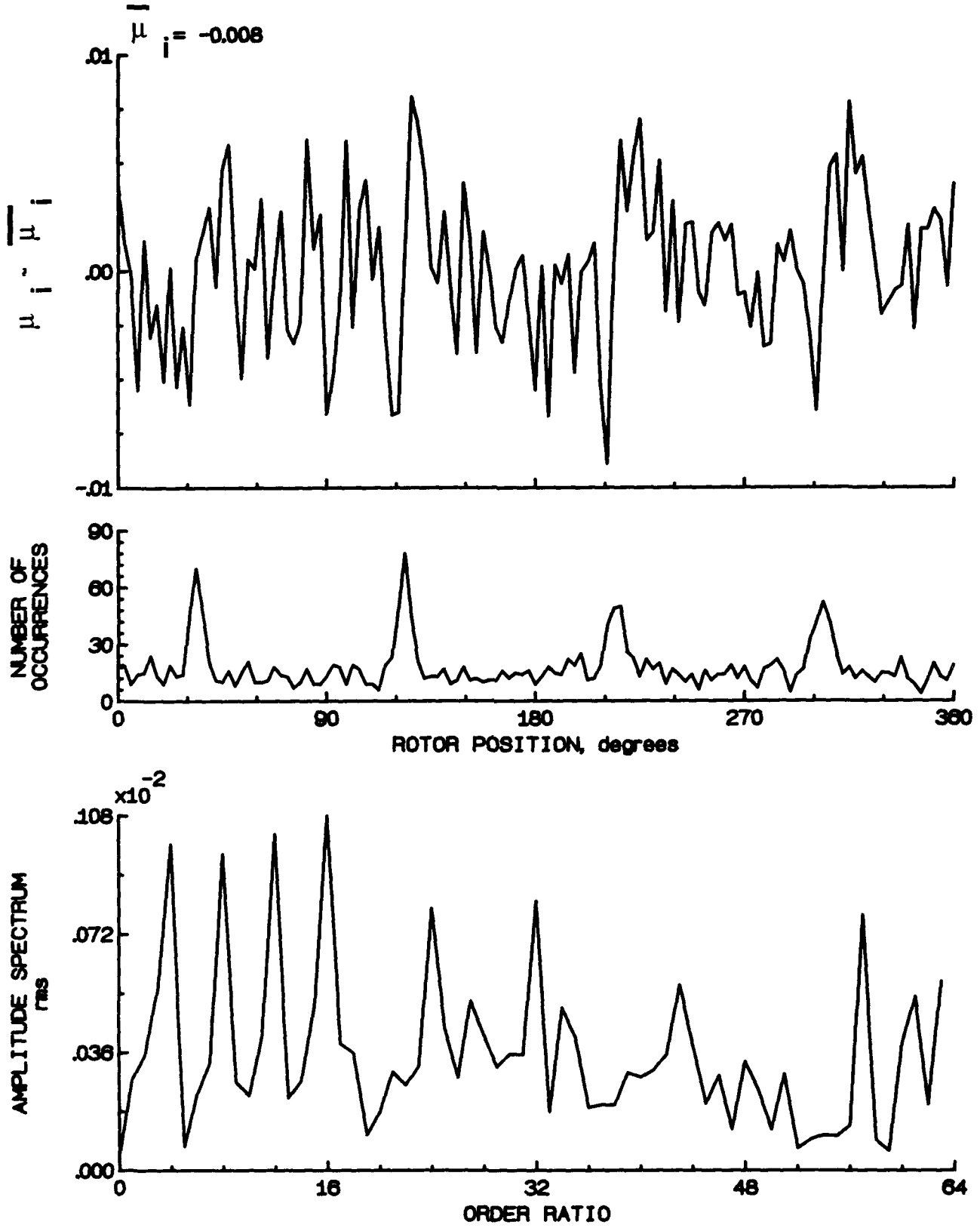

Figure 128.- Induced inflow velocity measured at 210 degrees and r/R of 1.02.

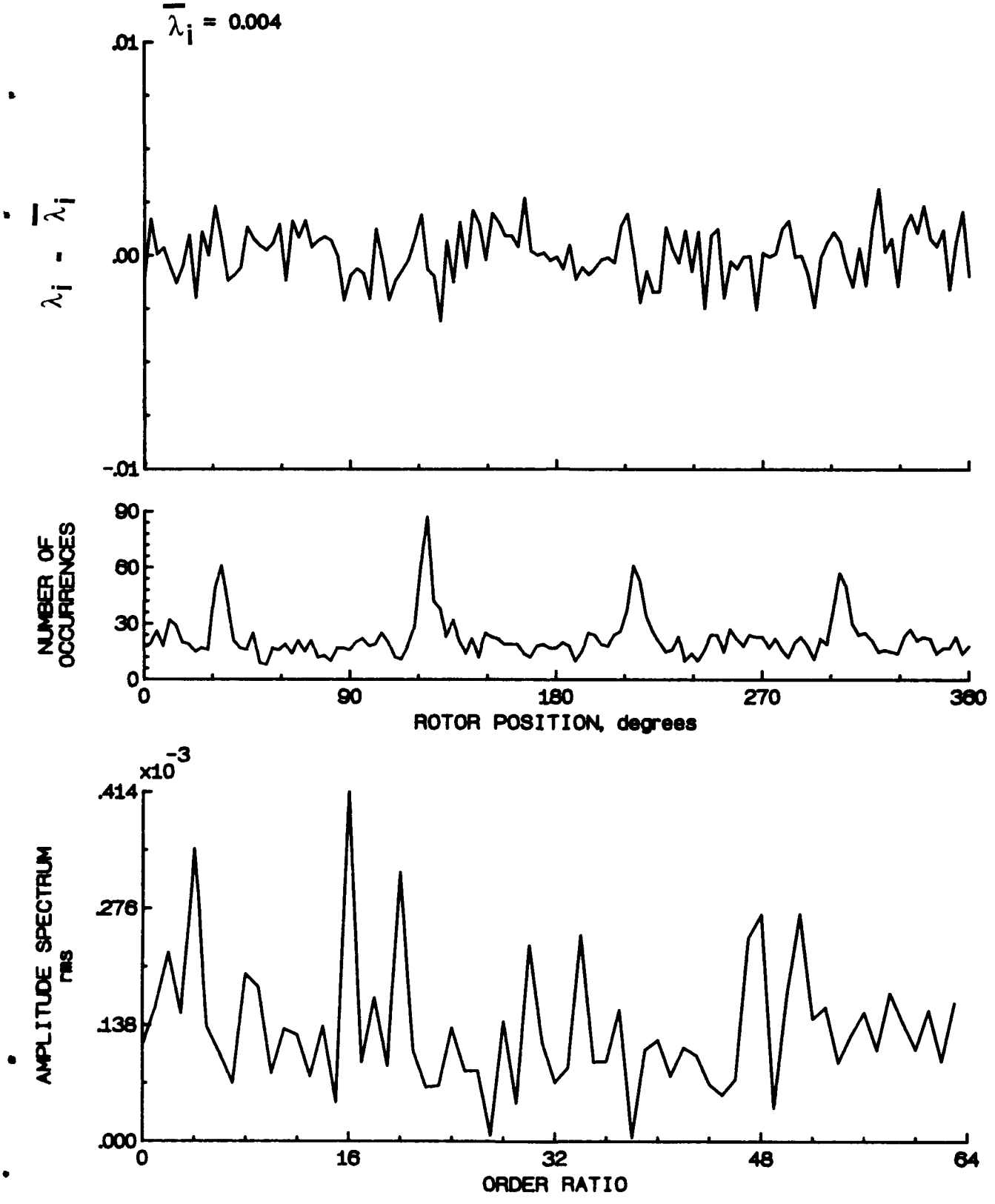

Figure 128.- Concluded.

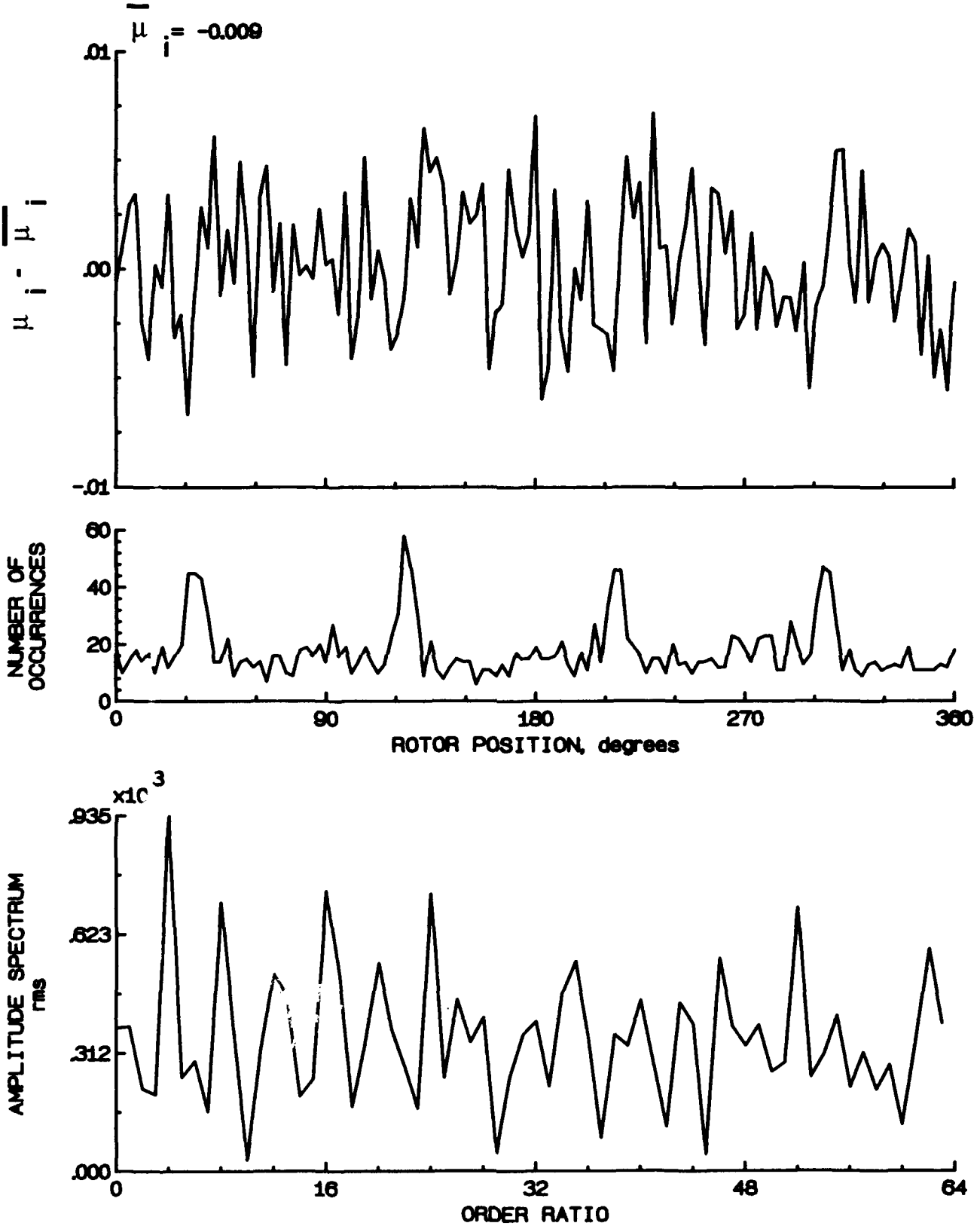

Figure 129.- Induced inflow velocity measured at 210 degrees and r/R of 1.04.

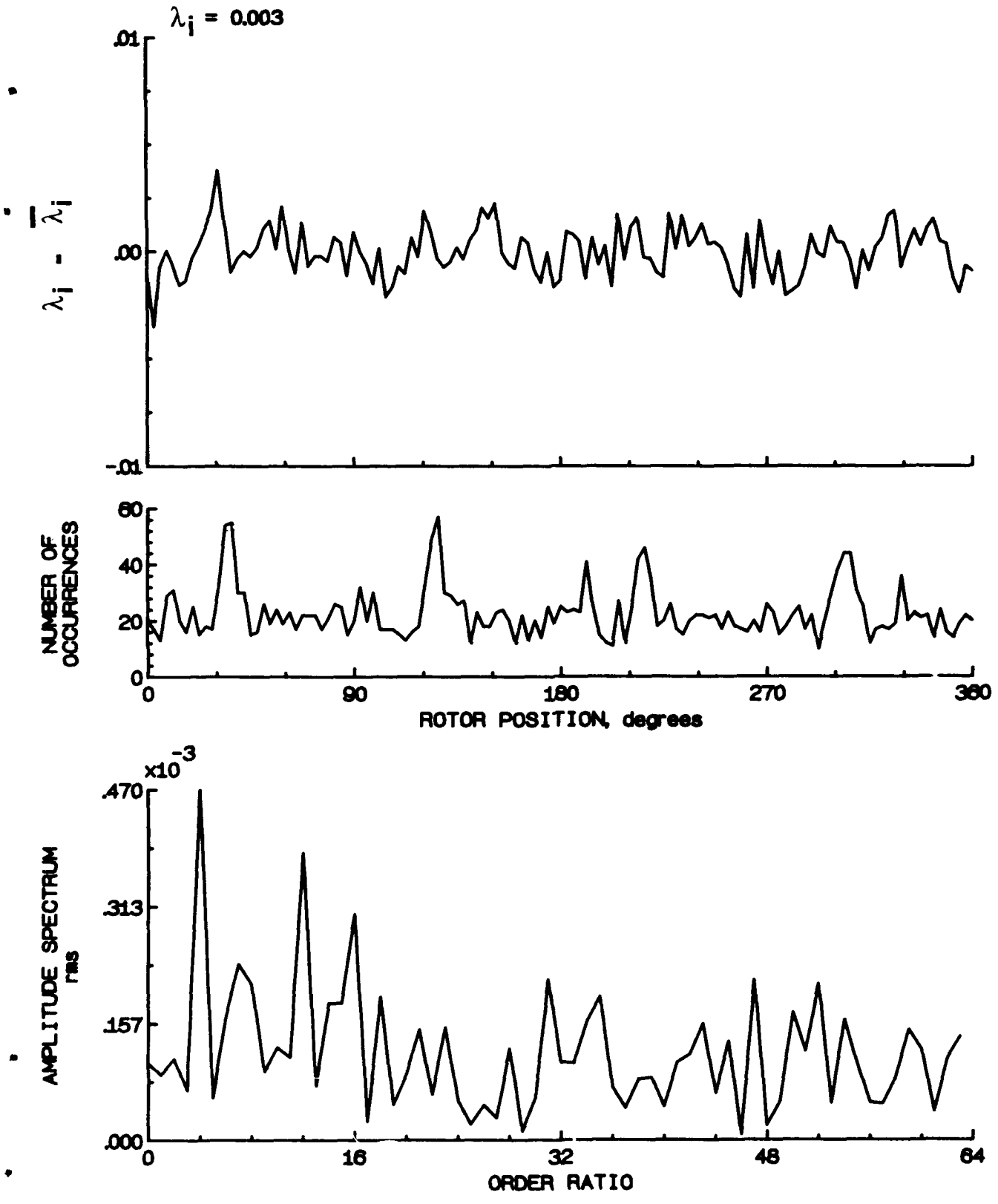

Figure 129.- Concluded.

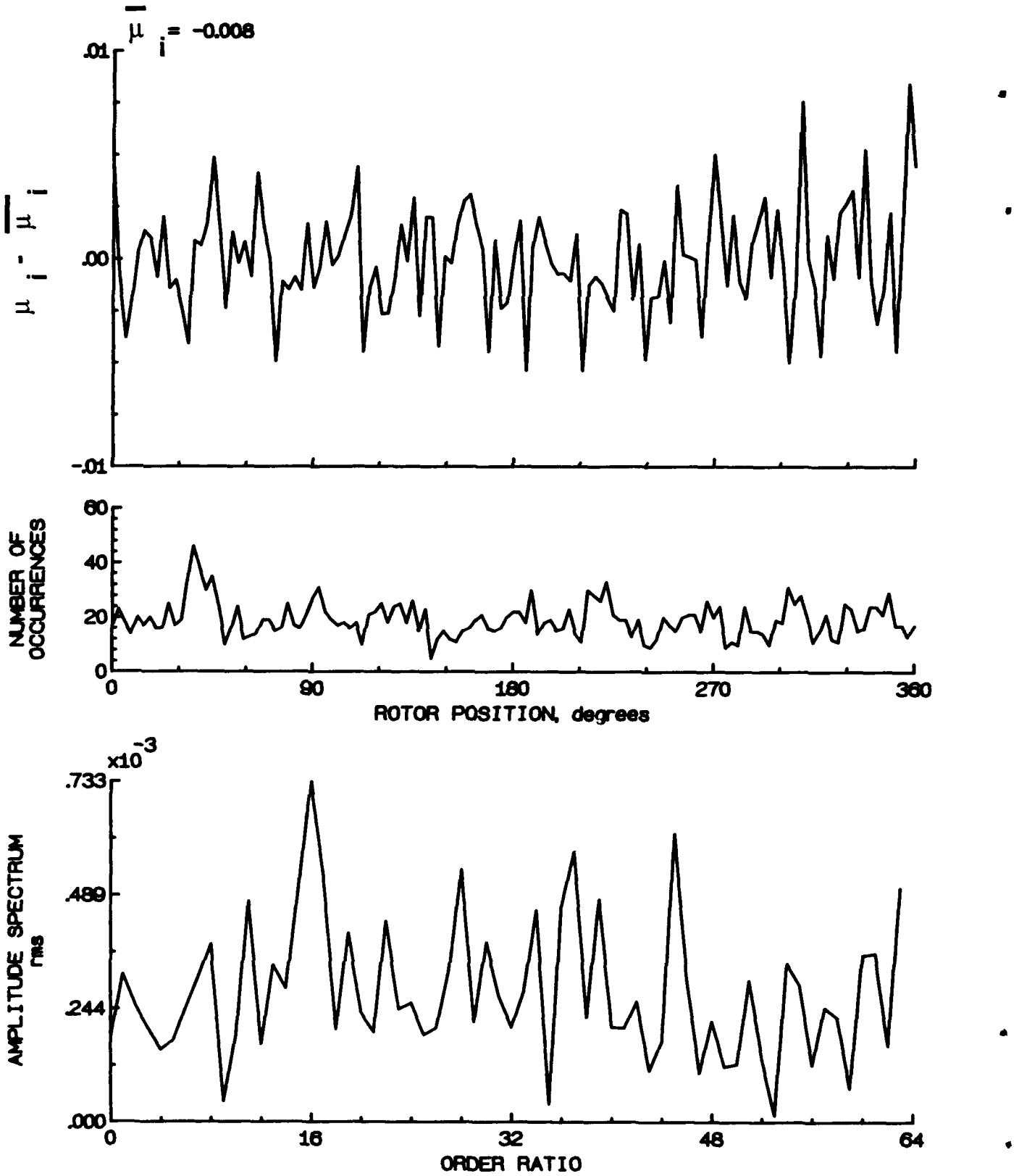

Figure 130.- Induced inflow velocity measured at 210 degrees and r/R of 1.10.

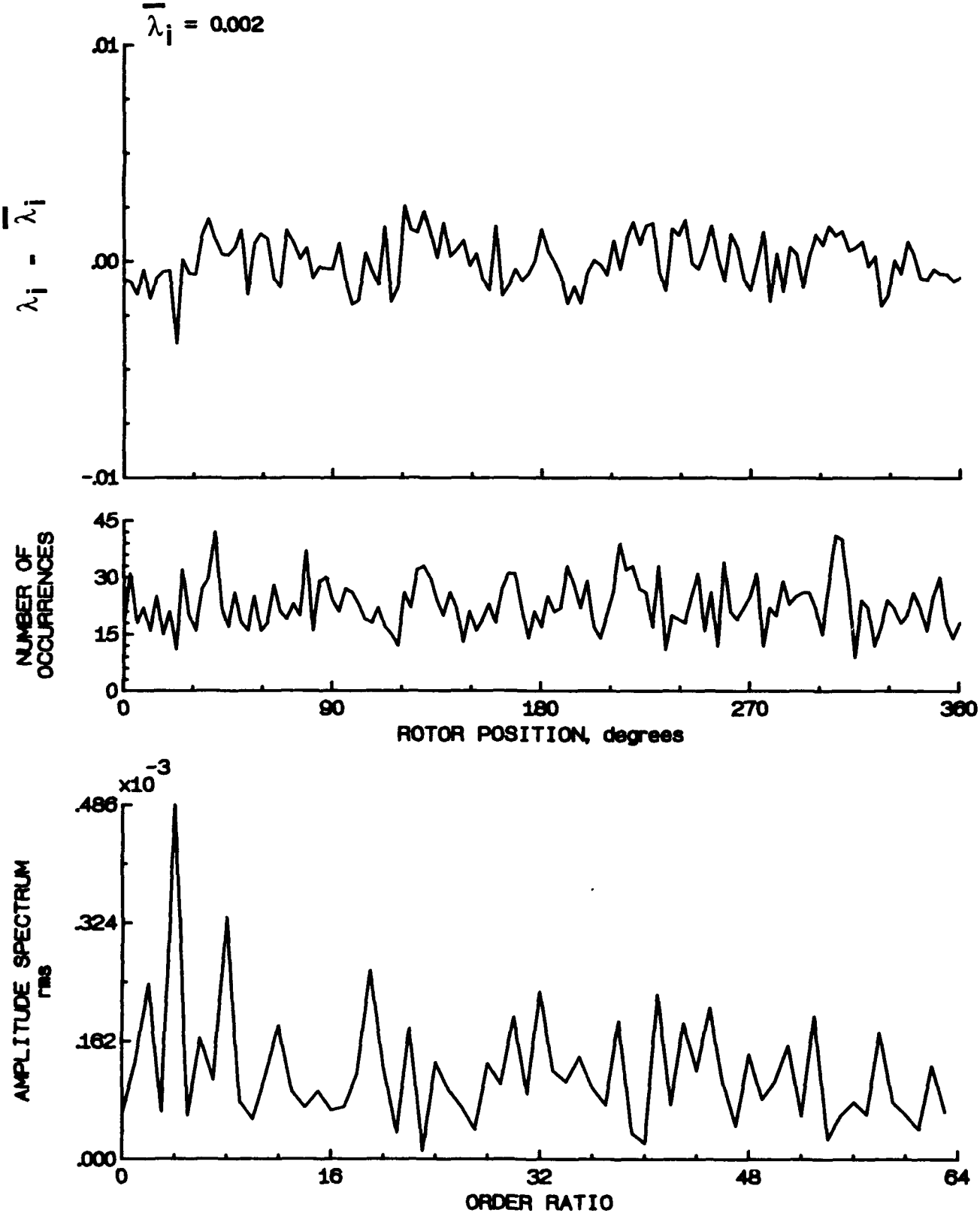

Figure 130.- Concluded.

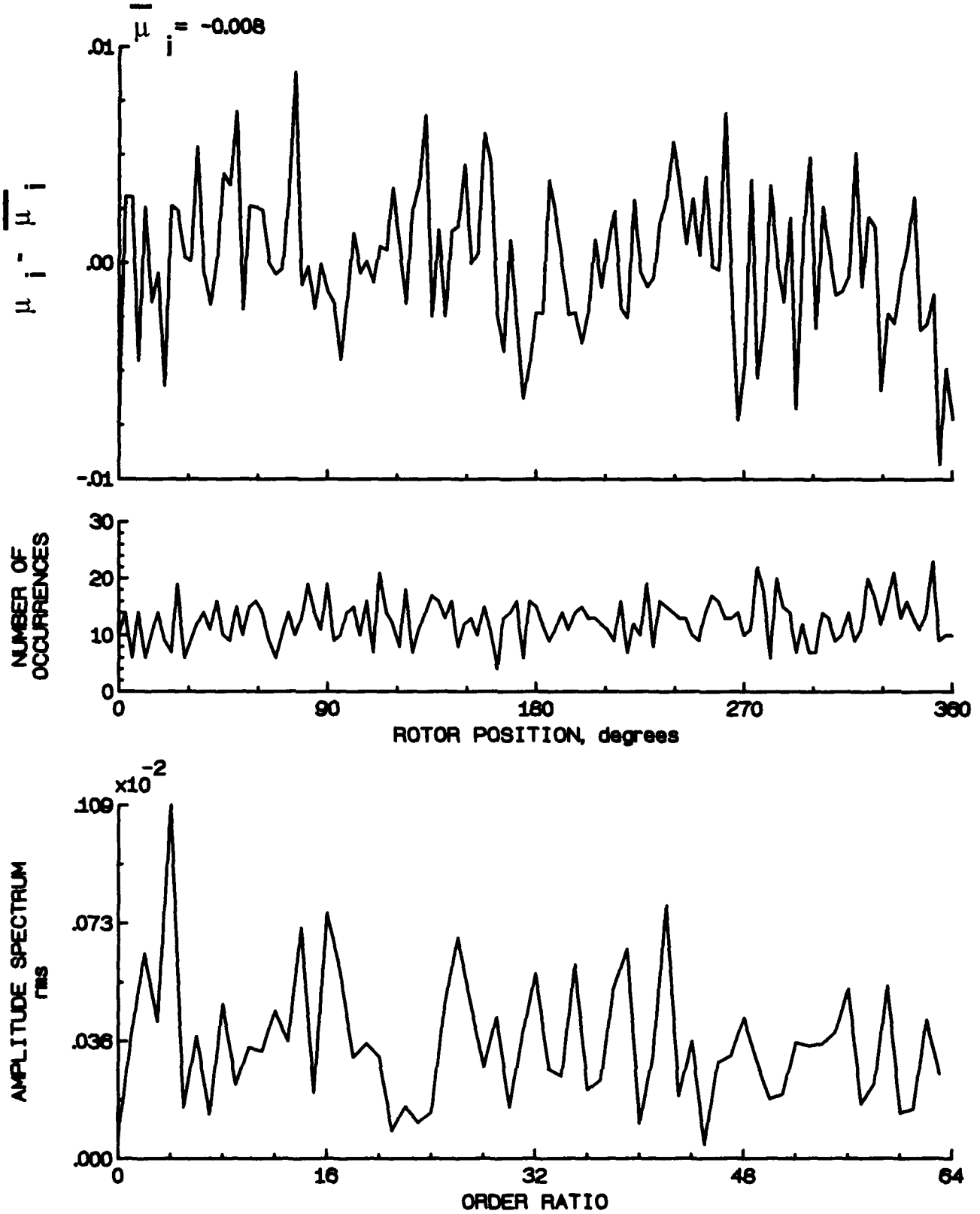

Figure 131.- Induced inflow velocity measured at 240 degrees and r/R of 0.20.

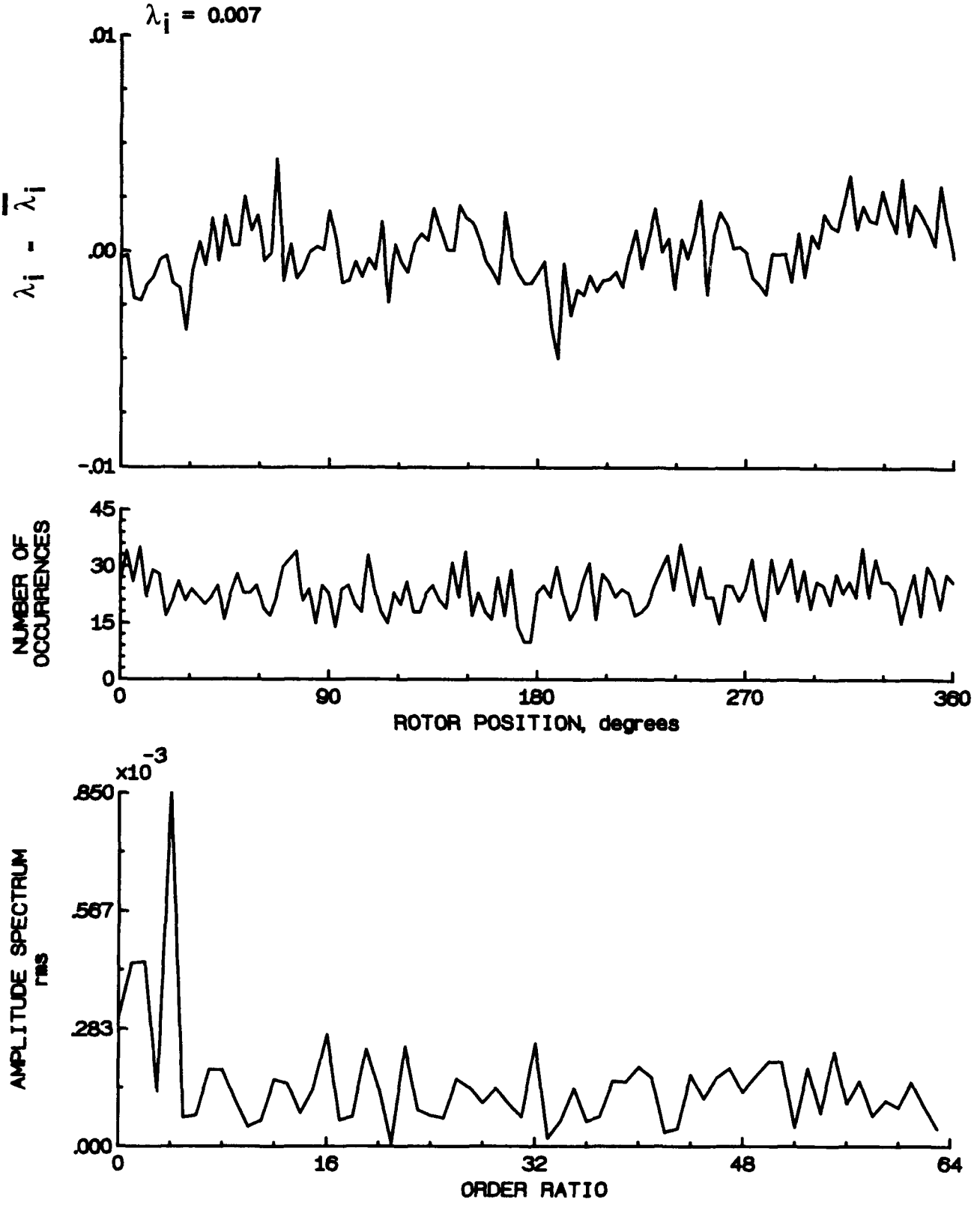

Figure 131.- Concluded.

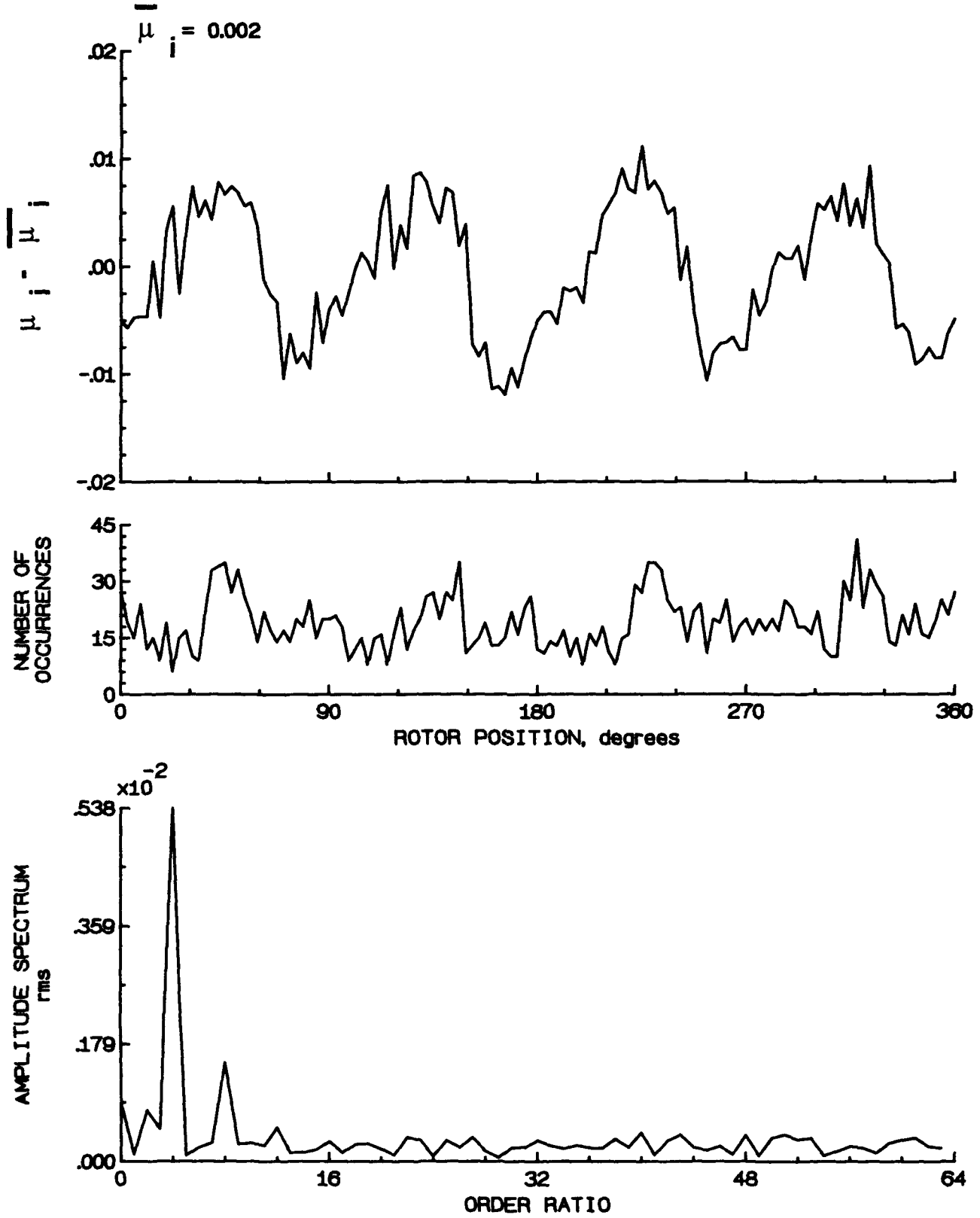

Figure 132.- Induced inflow velocity measured at 240 degrees and r/R of 0.40.

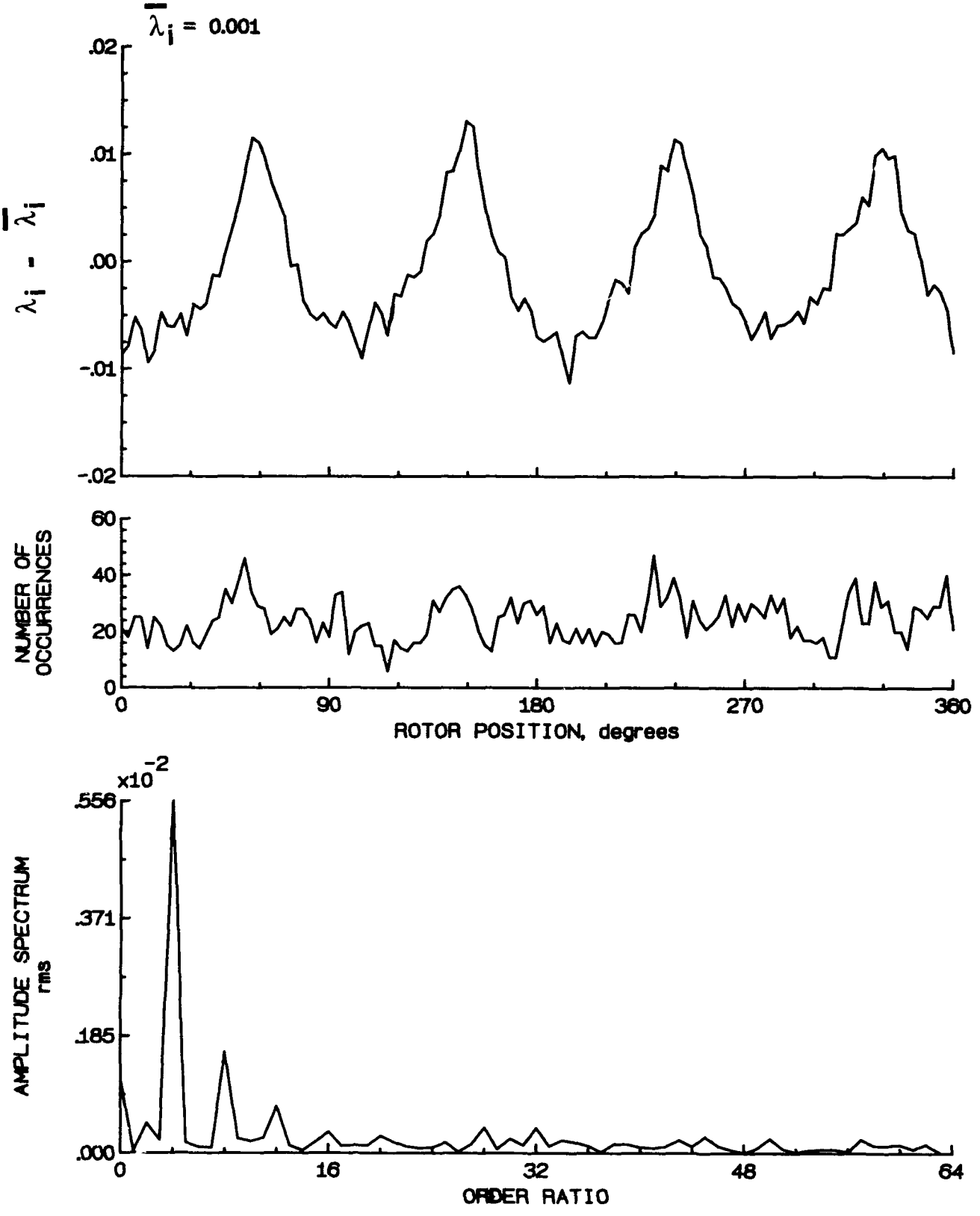

Figure 132.- Concluded.

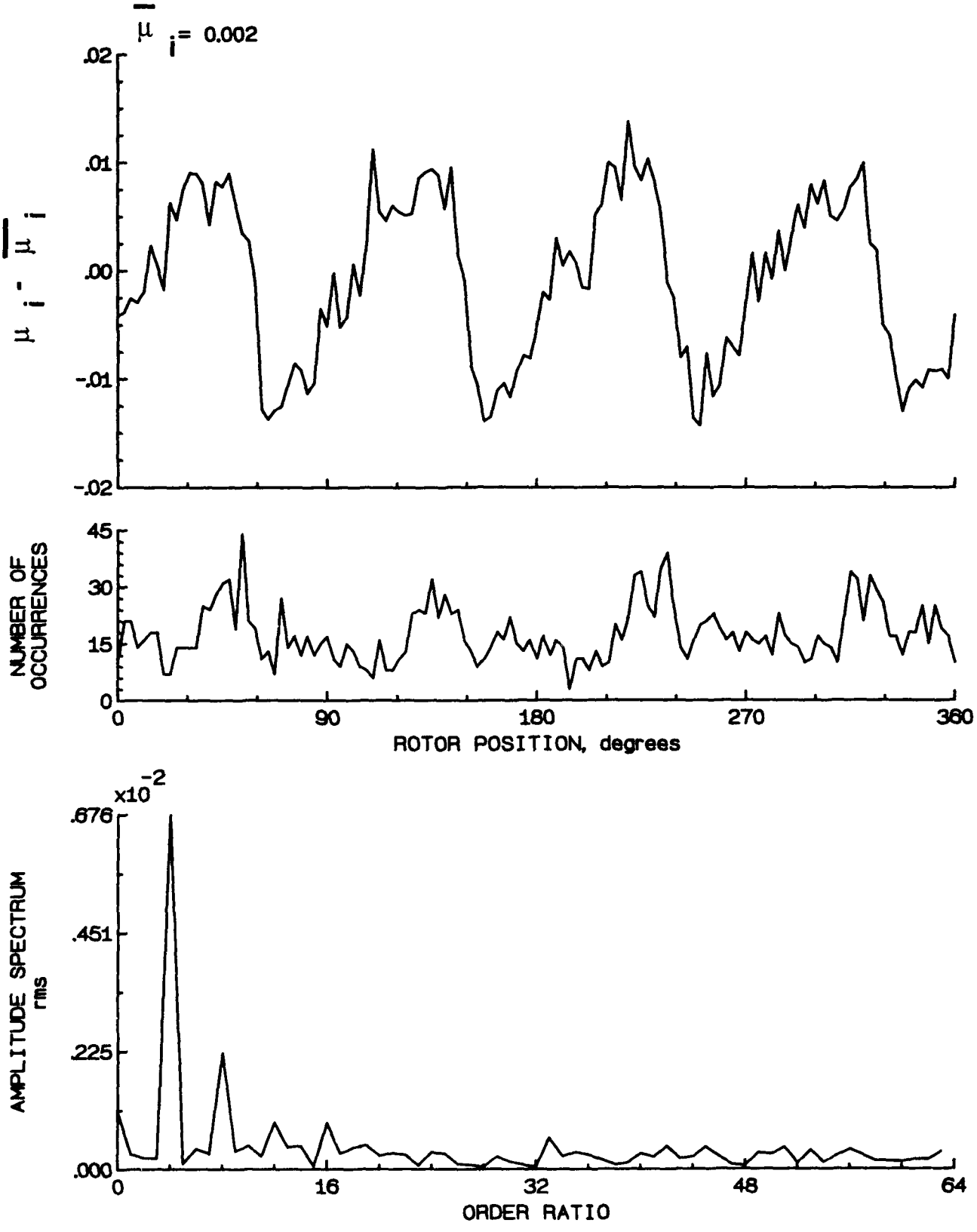

Figure 133.- Induced inflow velocity measured at 240 degrees and r/R of 0.50.

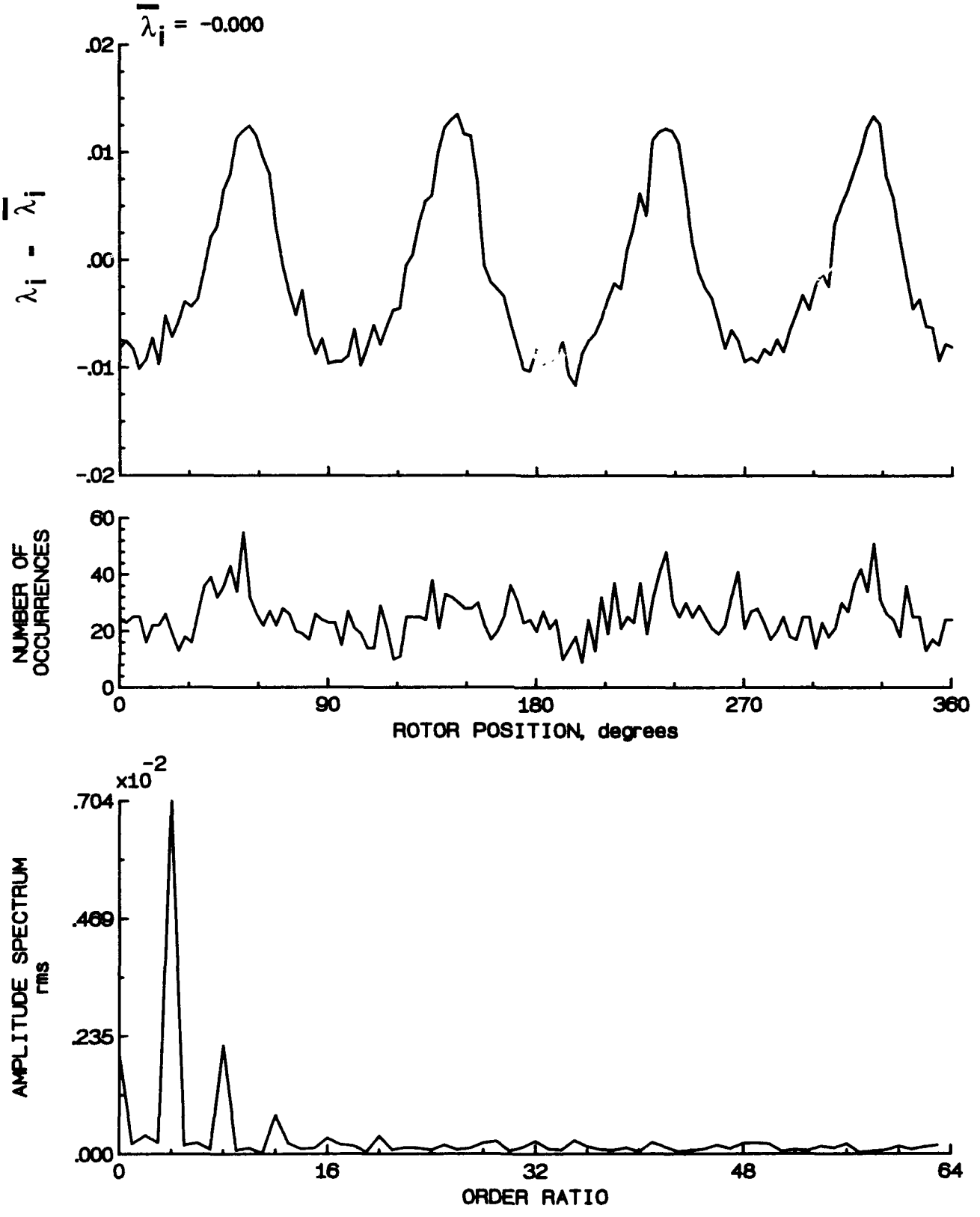

Figure 133.- Concluded.

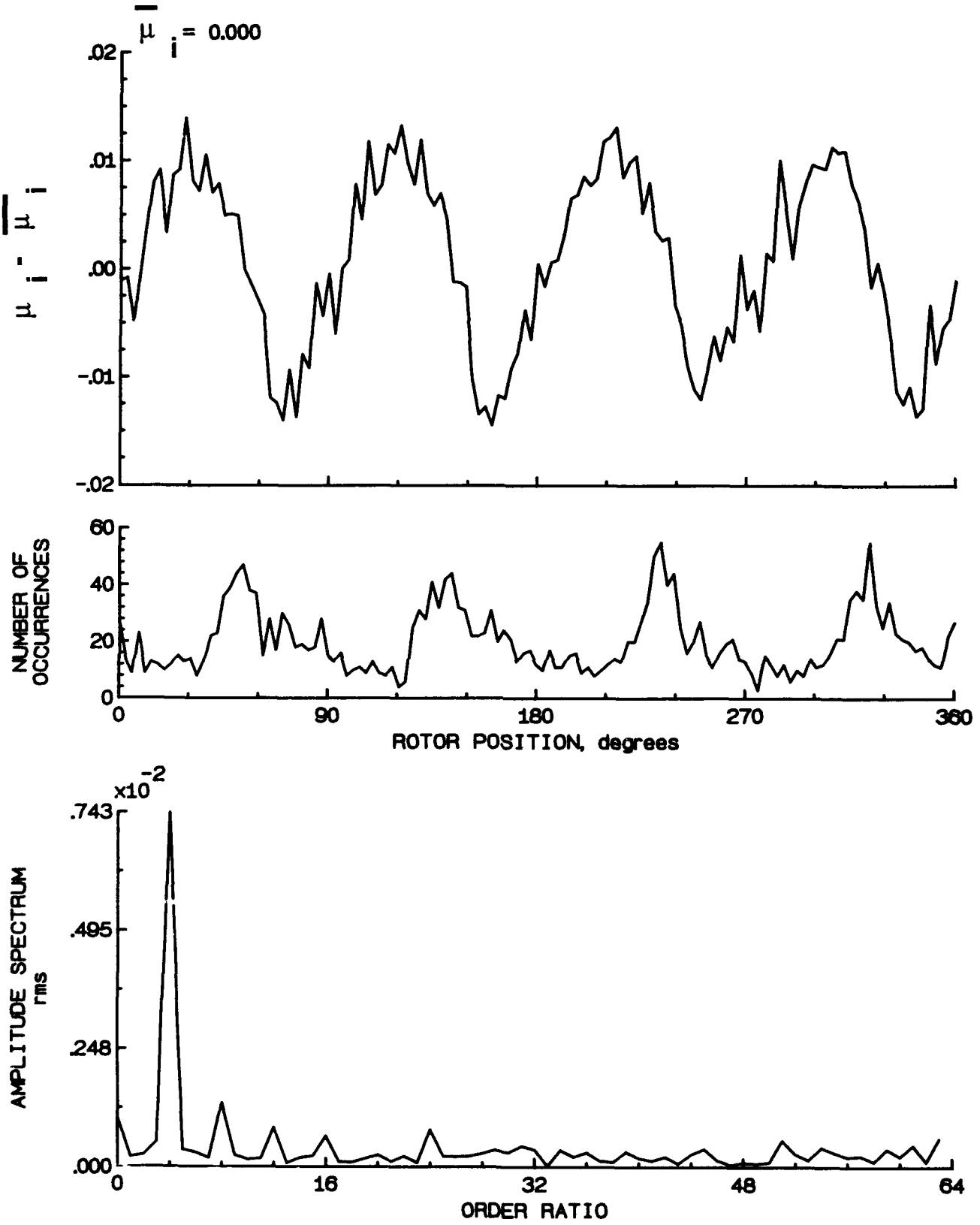

Figure 134.- Induced inflow velocity measured at 240 degrees and r/R of 0.60.

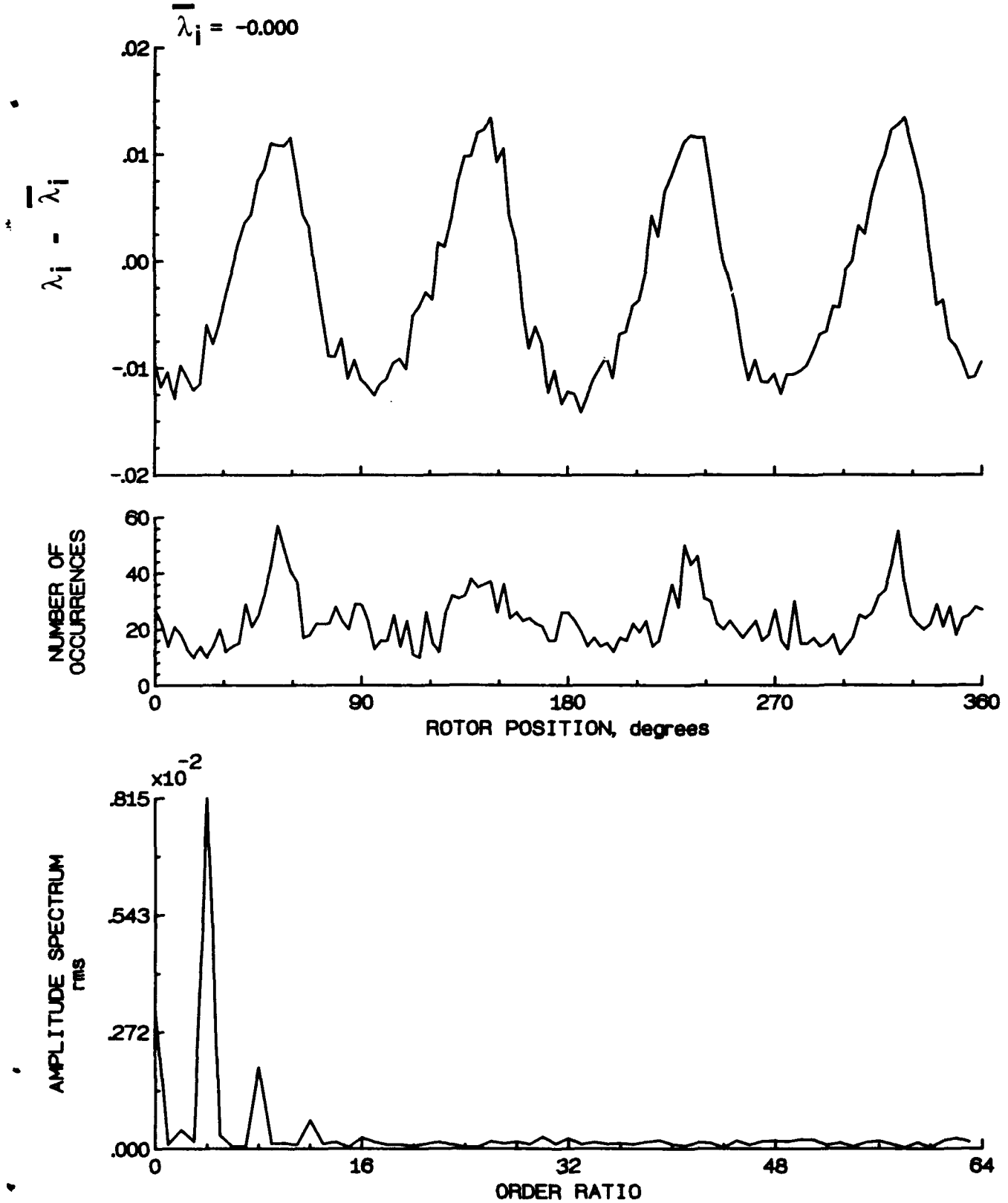

Figure 134.- Concluded.

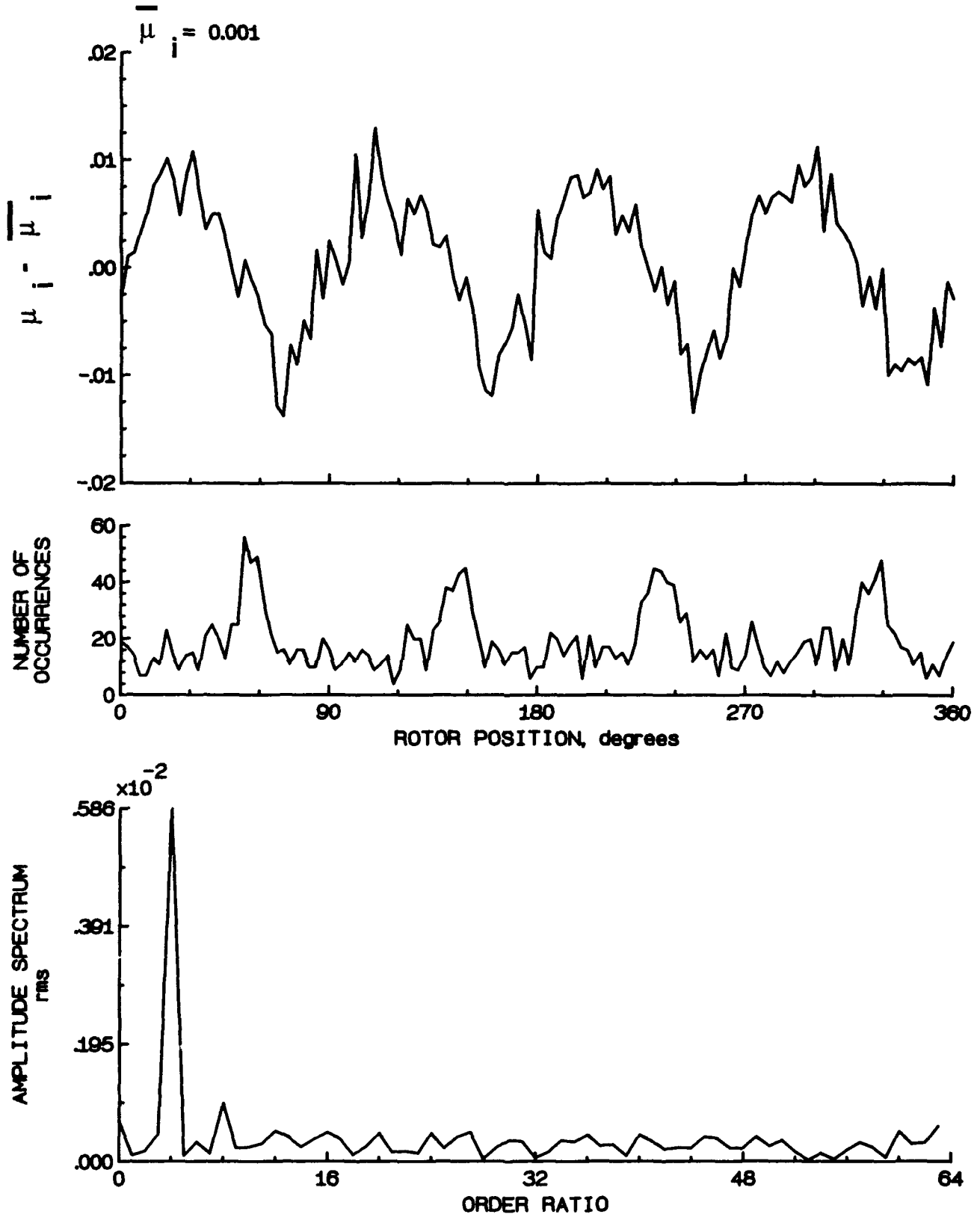

Figure 135.- Induced inflow velocity measured at 240 degrees and r/R of 0.70.

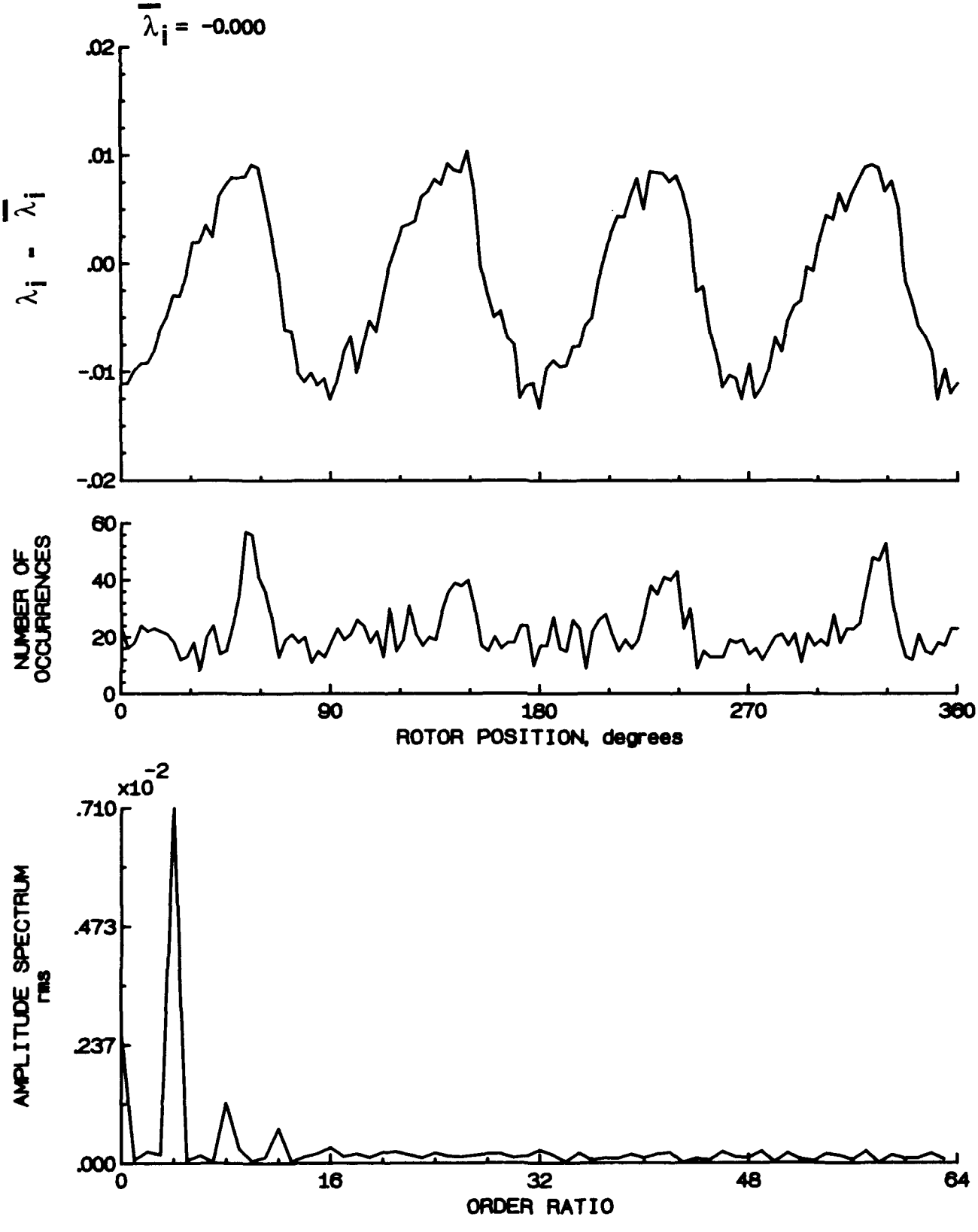

Figure 135.- Concluded.

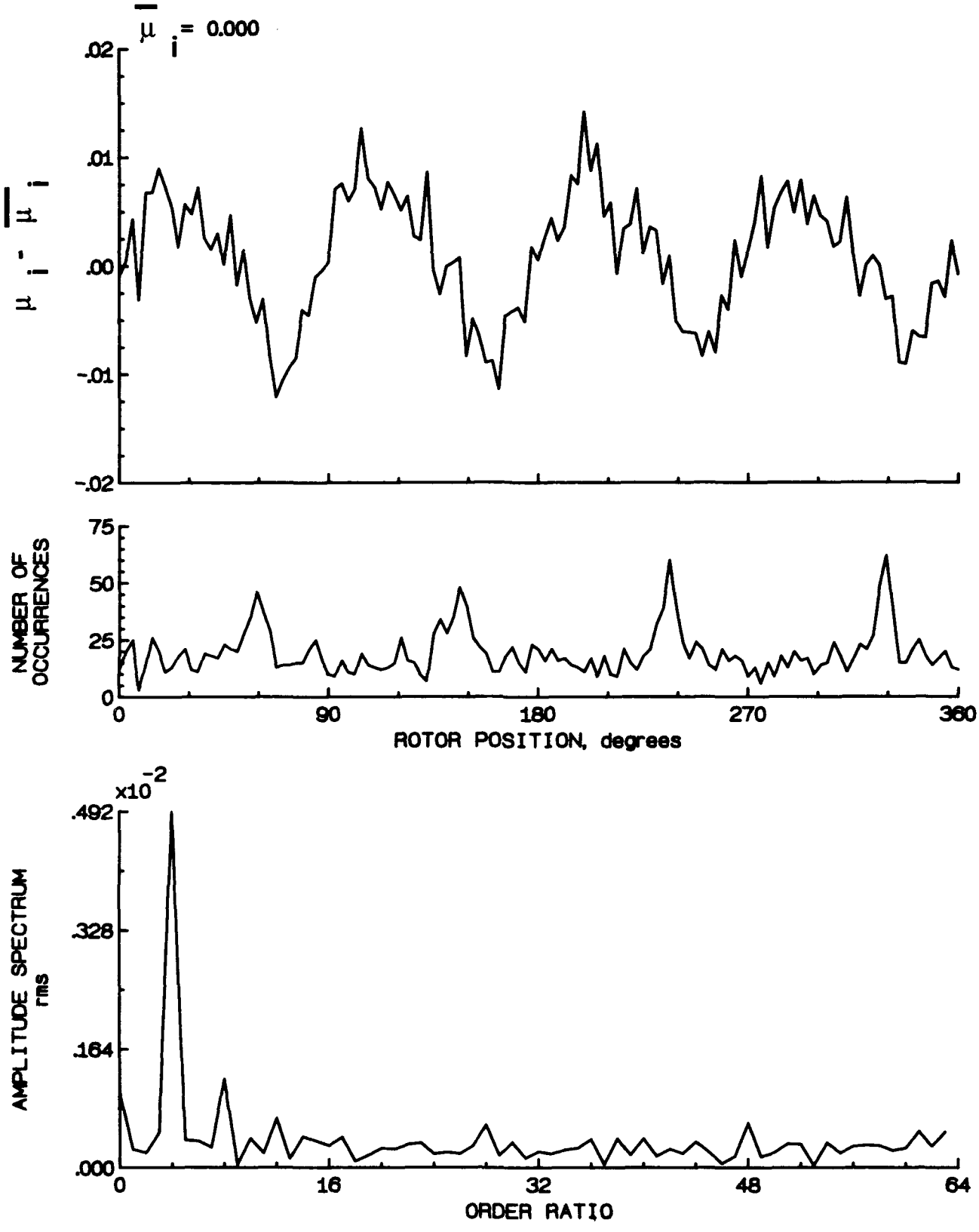

Figure 136.- Induced inflow velocity measured at 240 degrees and r/R of 0.74.

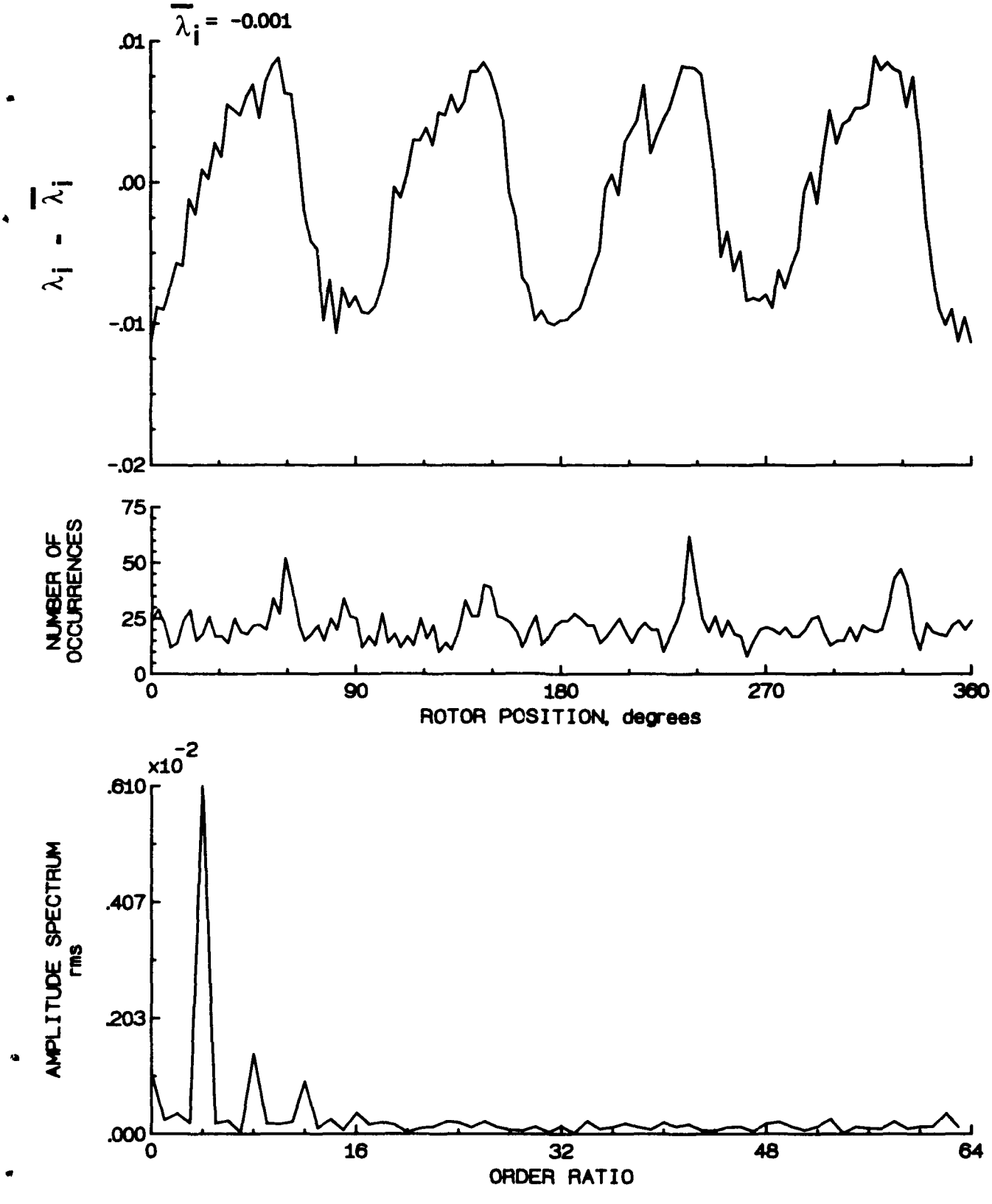

Figure 136.- Concluded.

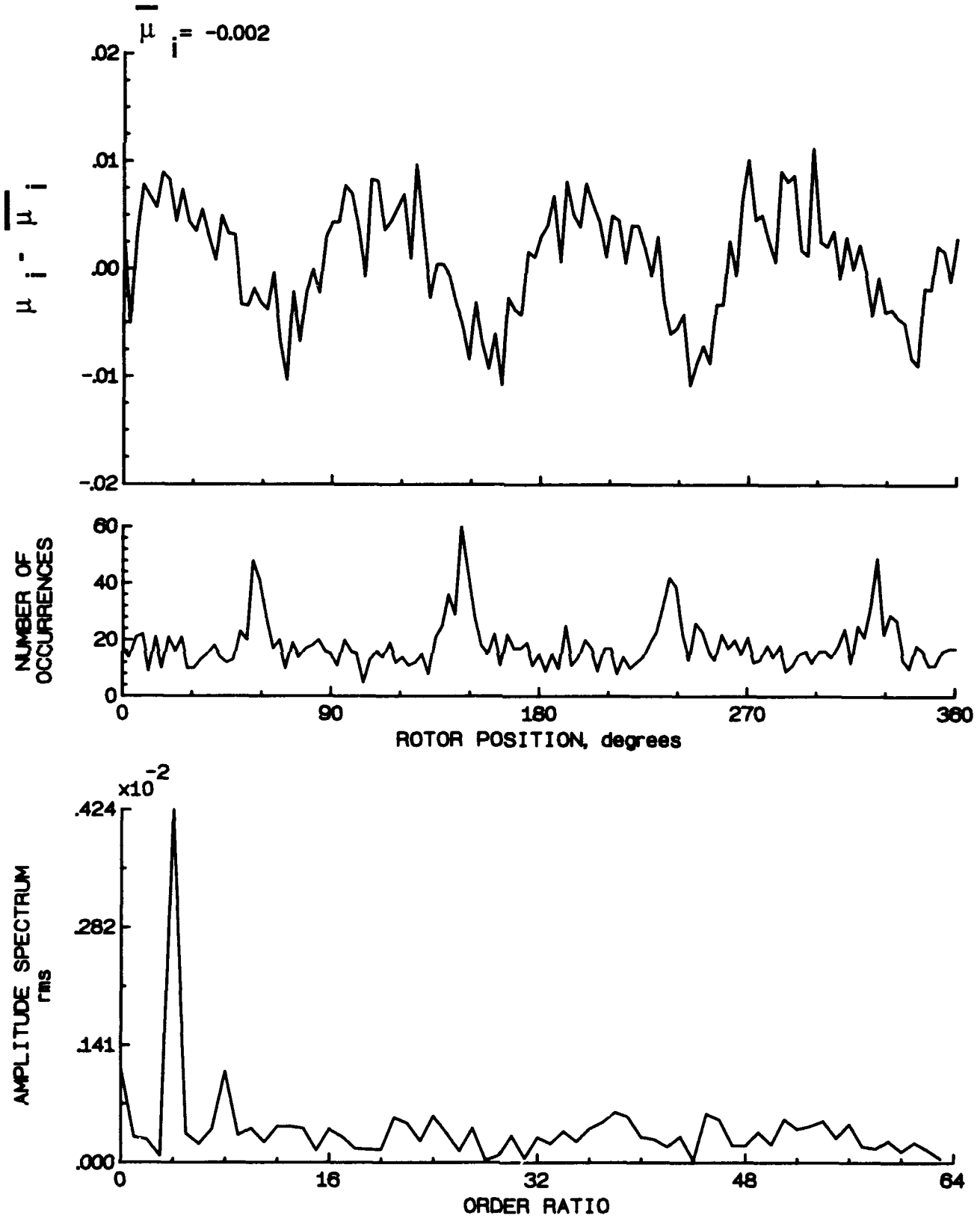

Figure 137.- Induced inflow velocity measured at 240 degrees and r/R of 0.78.

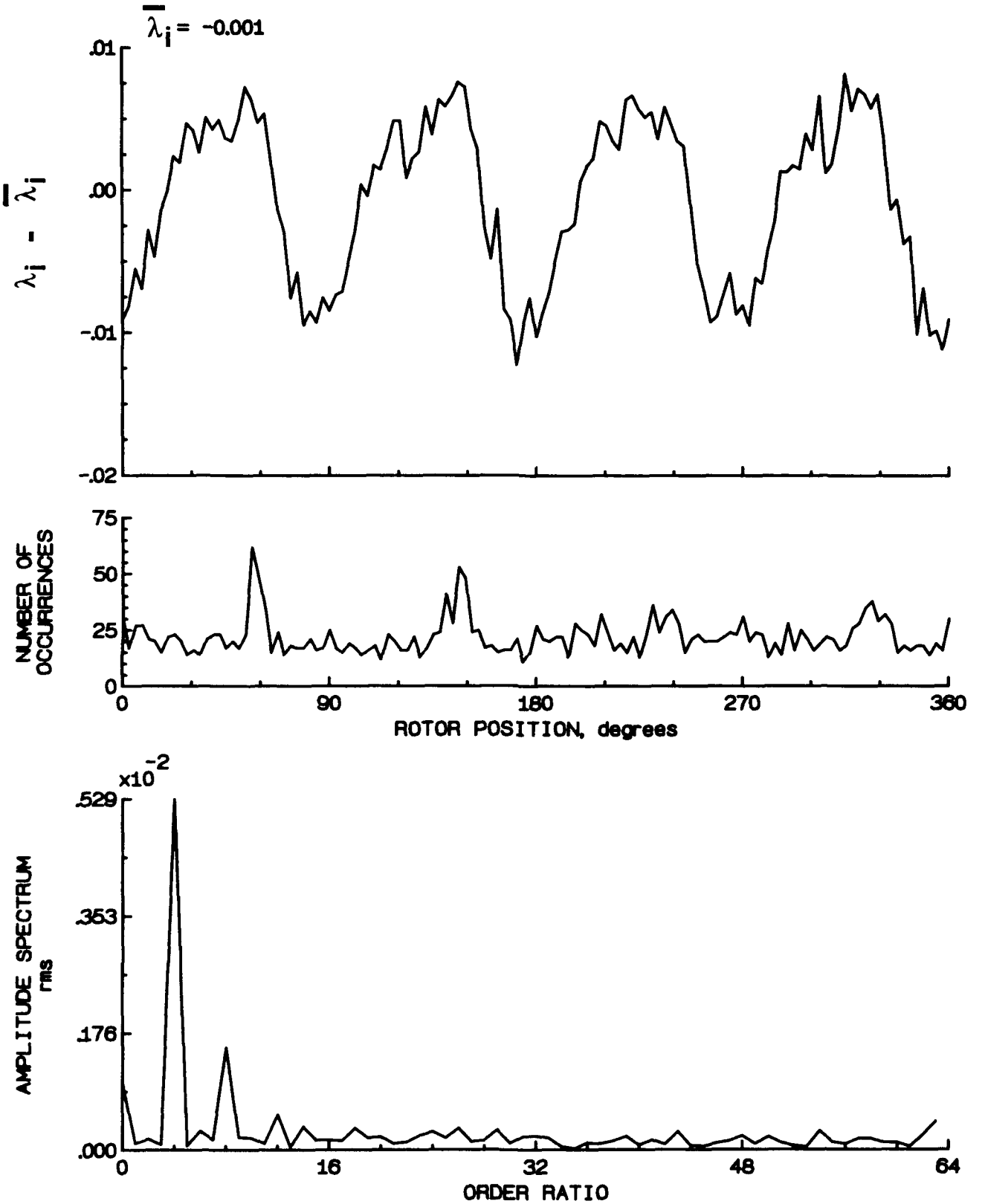

Figure 137.- Concluded.

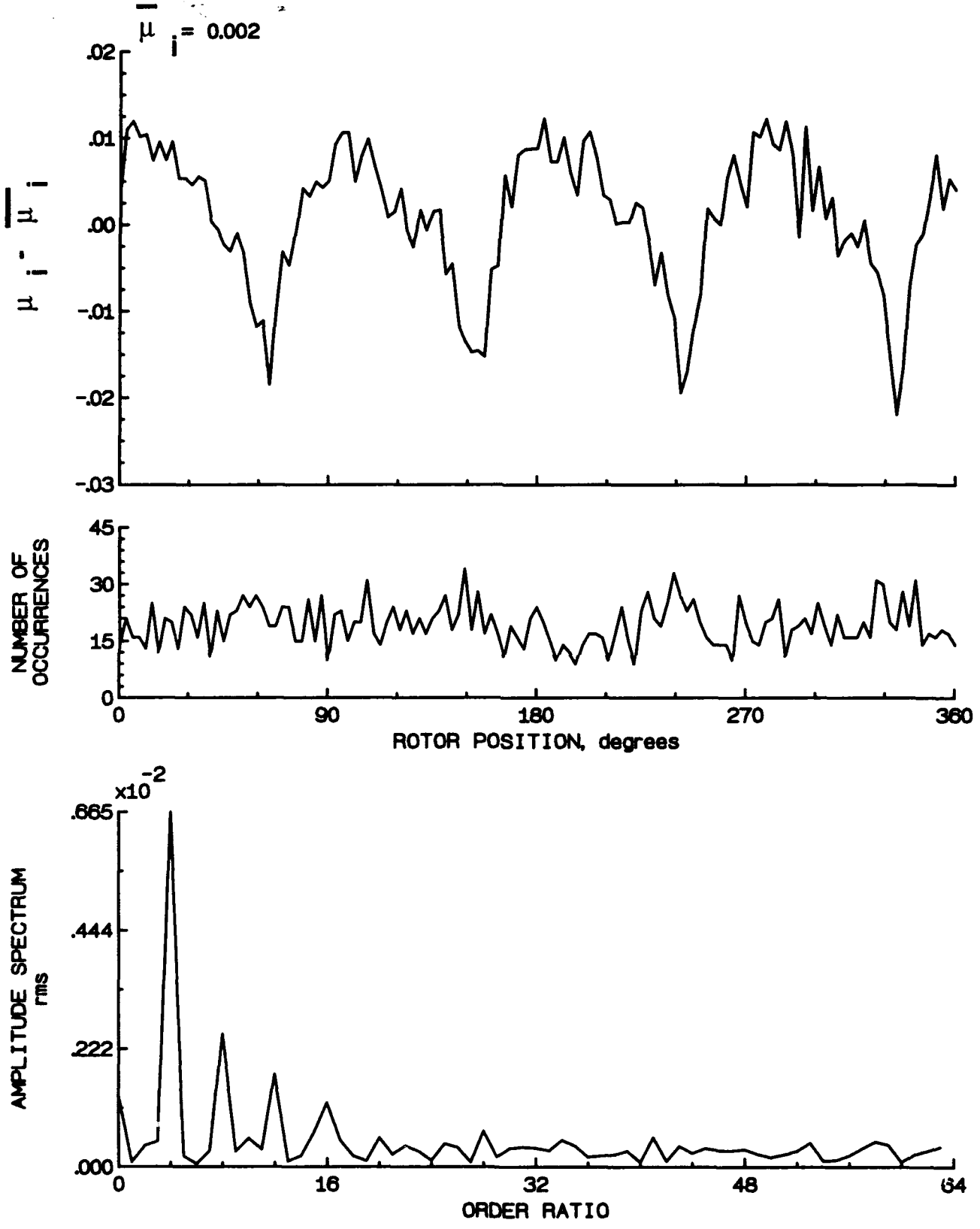

Figure 138.- Induced inflow velocity measured at 240 degrees and r/R of 0.82.

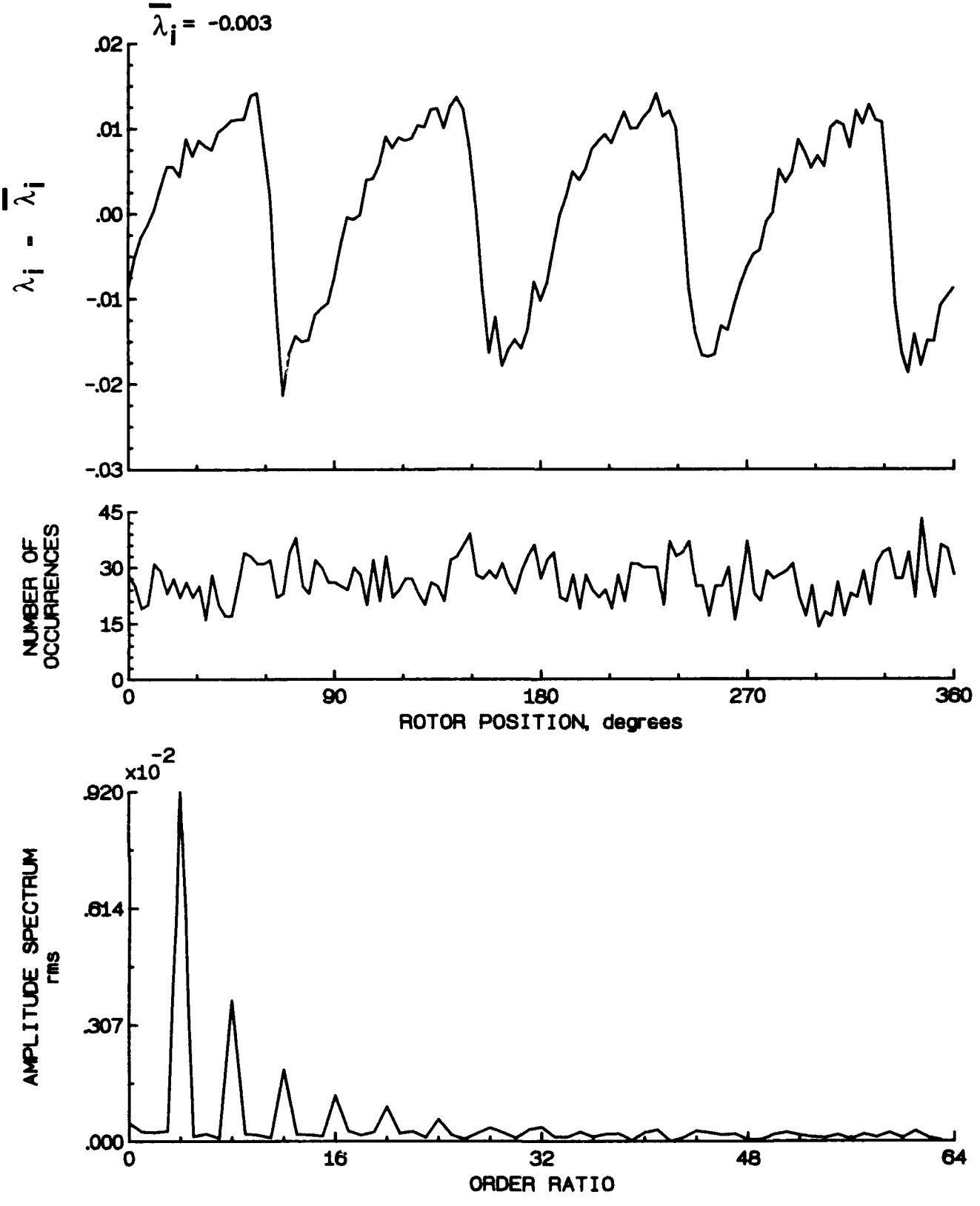

Figure 138.- Concluded.

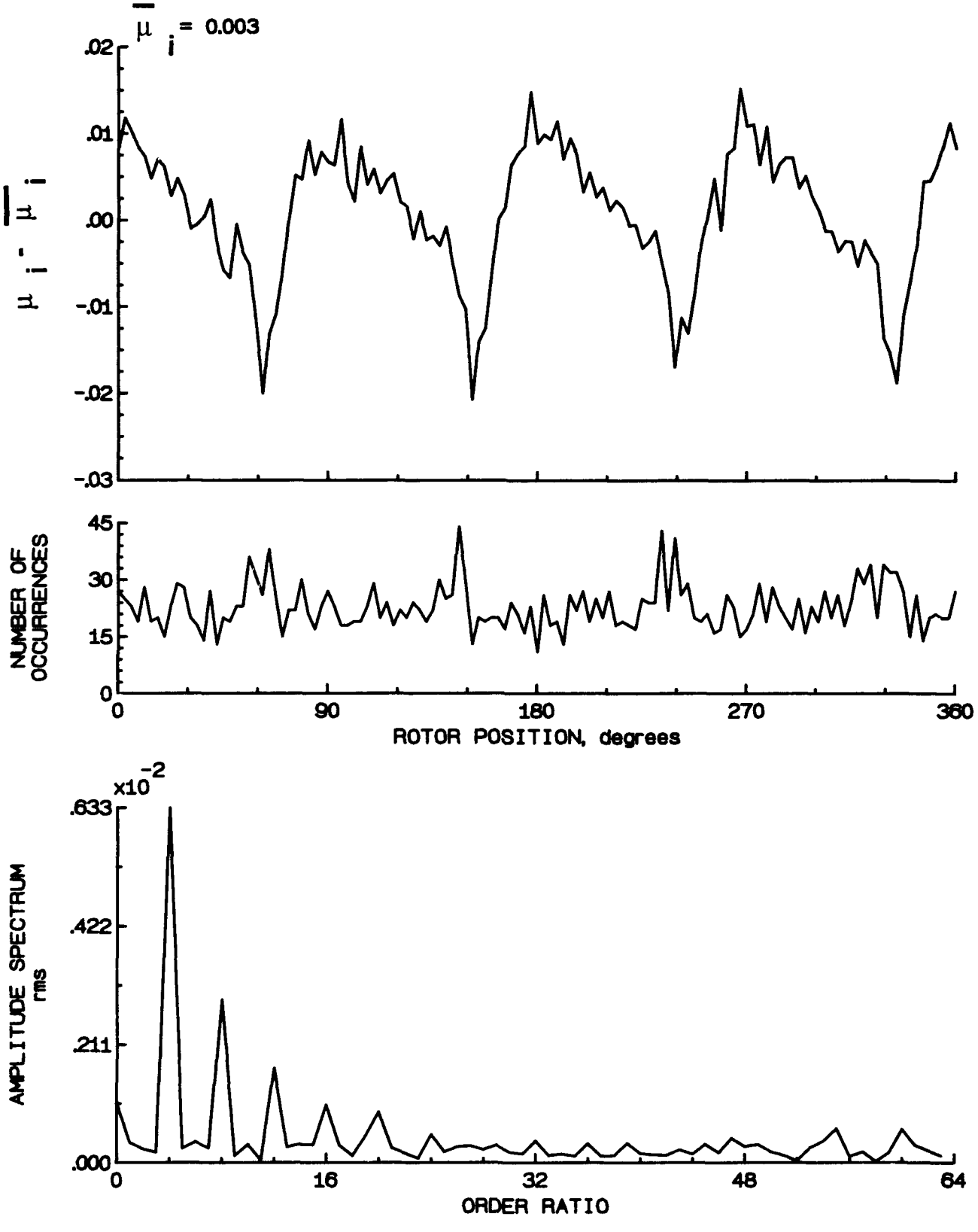

Figure 139.- Induced inflow velocity measured at 240 degrees and r/R of 0.86.

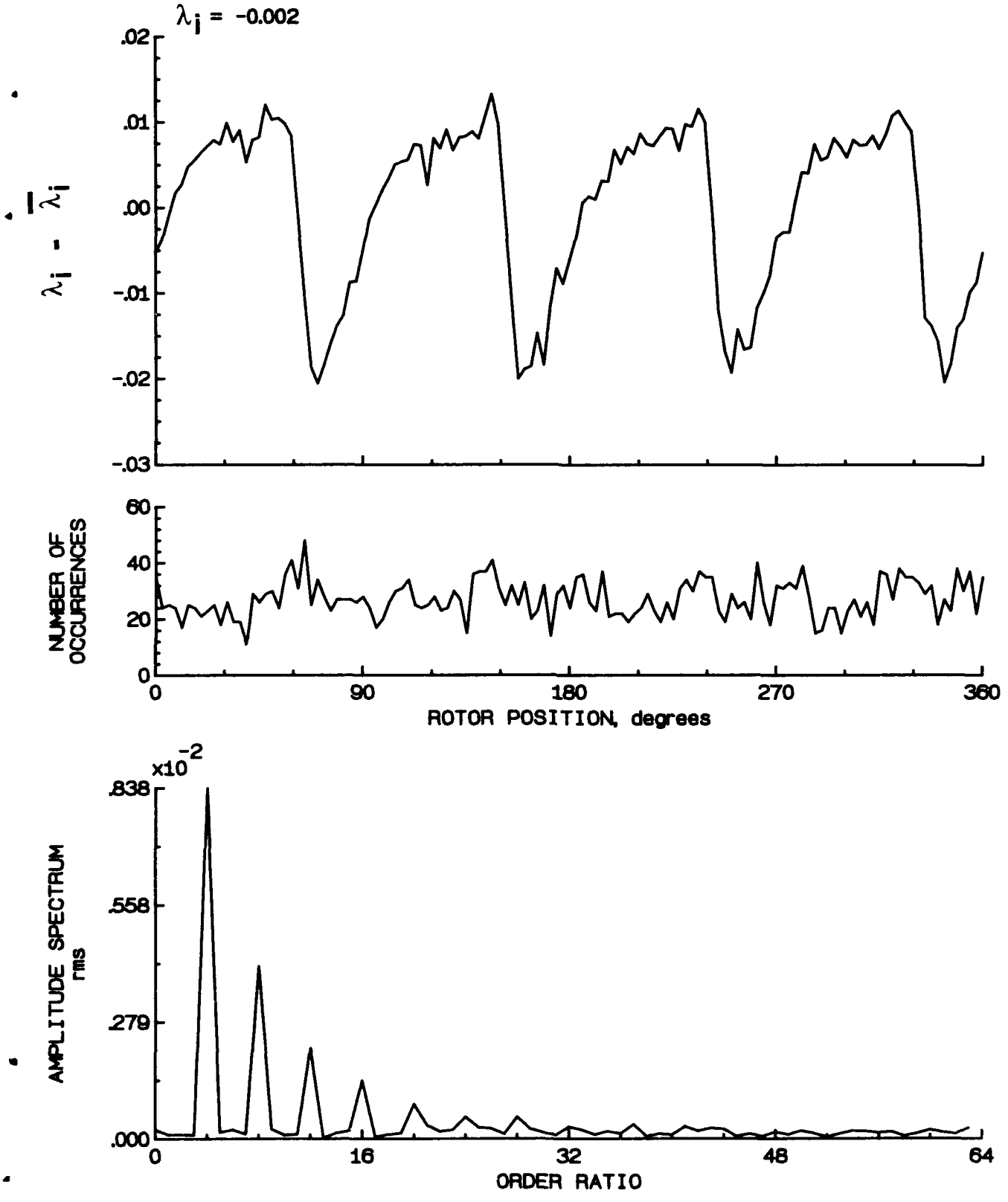

Figure 139.- Concluded.

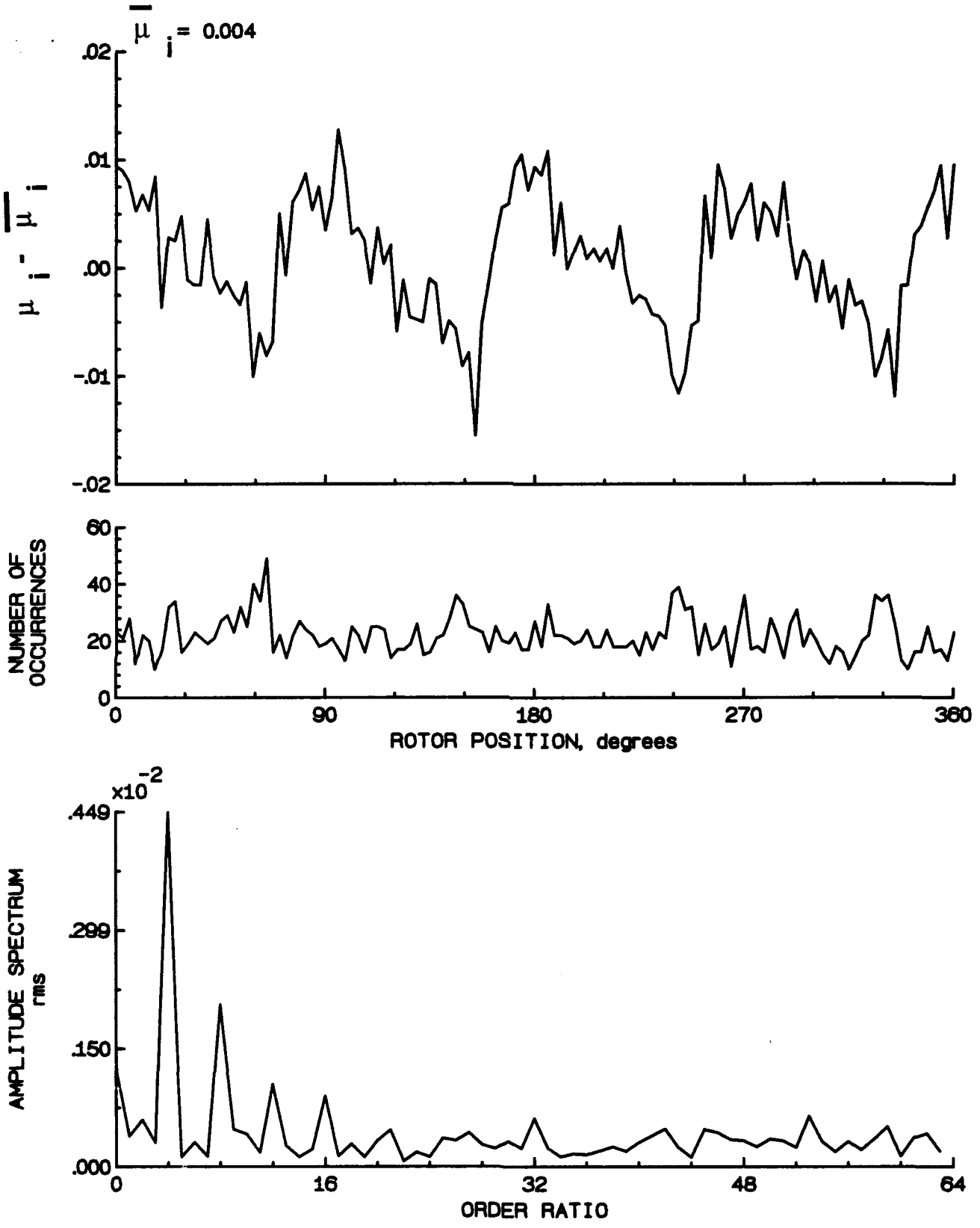

Figure 140.- Induced inflow velocity measured at 240 degrees and r/R of 0.90.

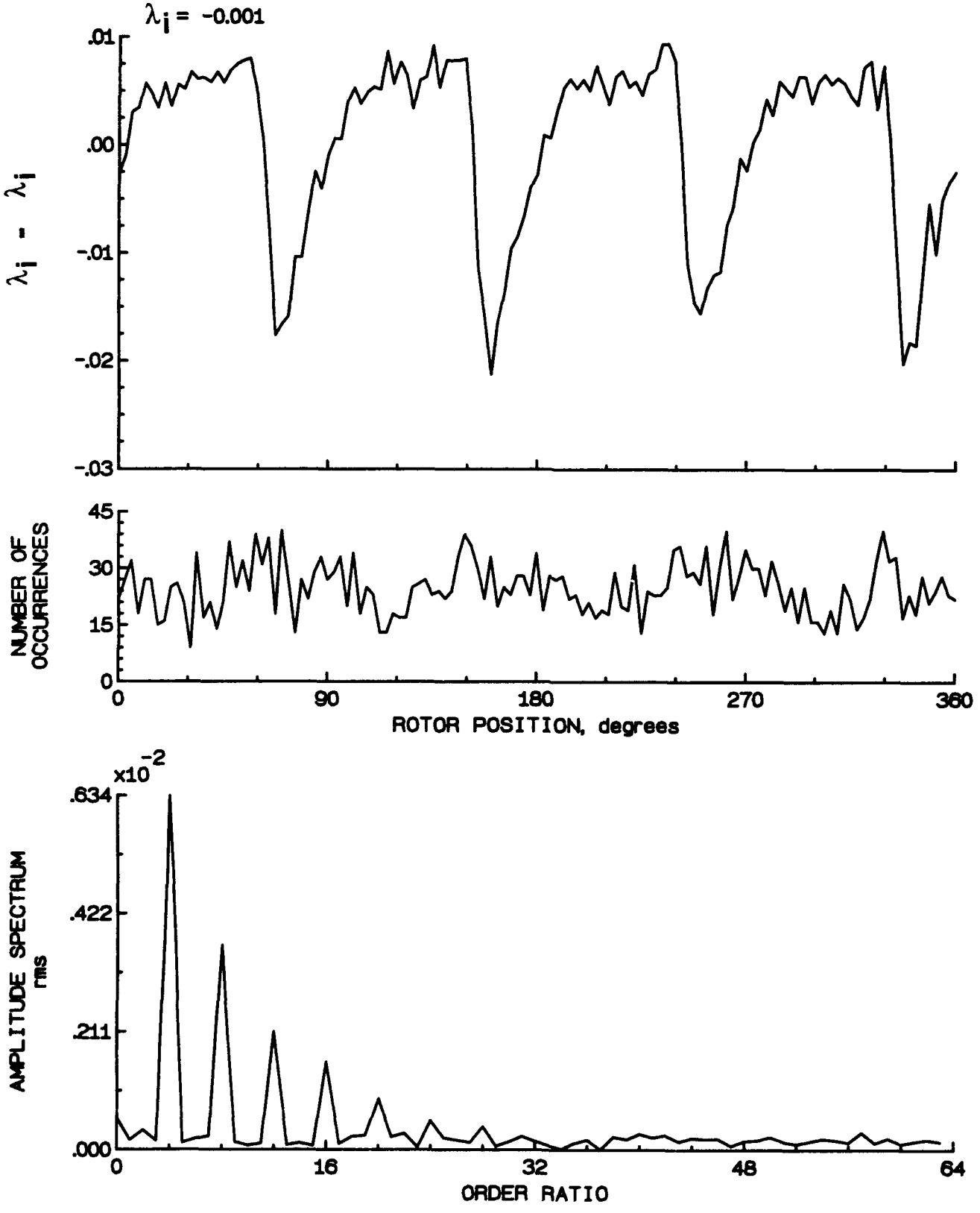

Figure 140.- Concluded.

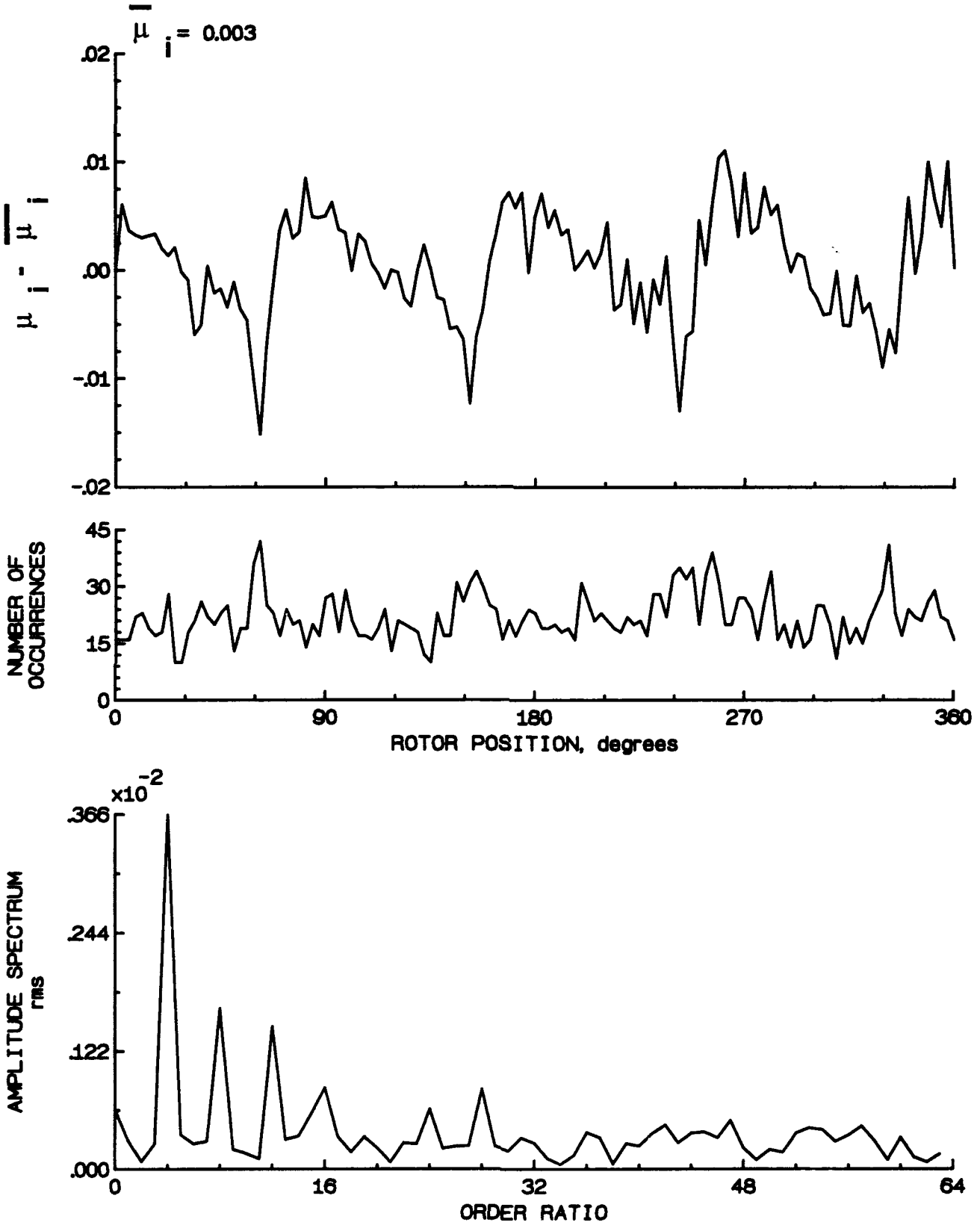

Figure 141.- Induced inflow velocity measured at 240 degrees and r/R of 0.94.

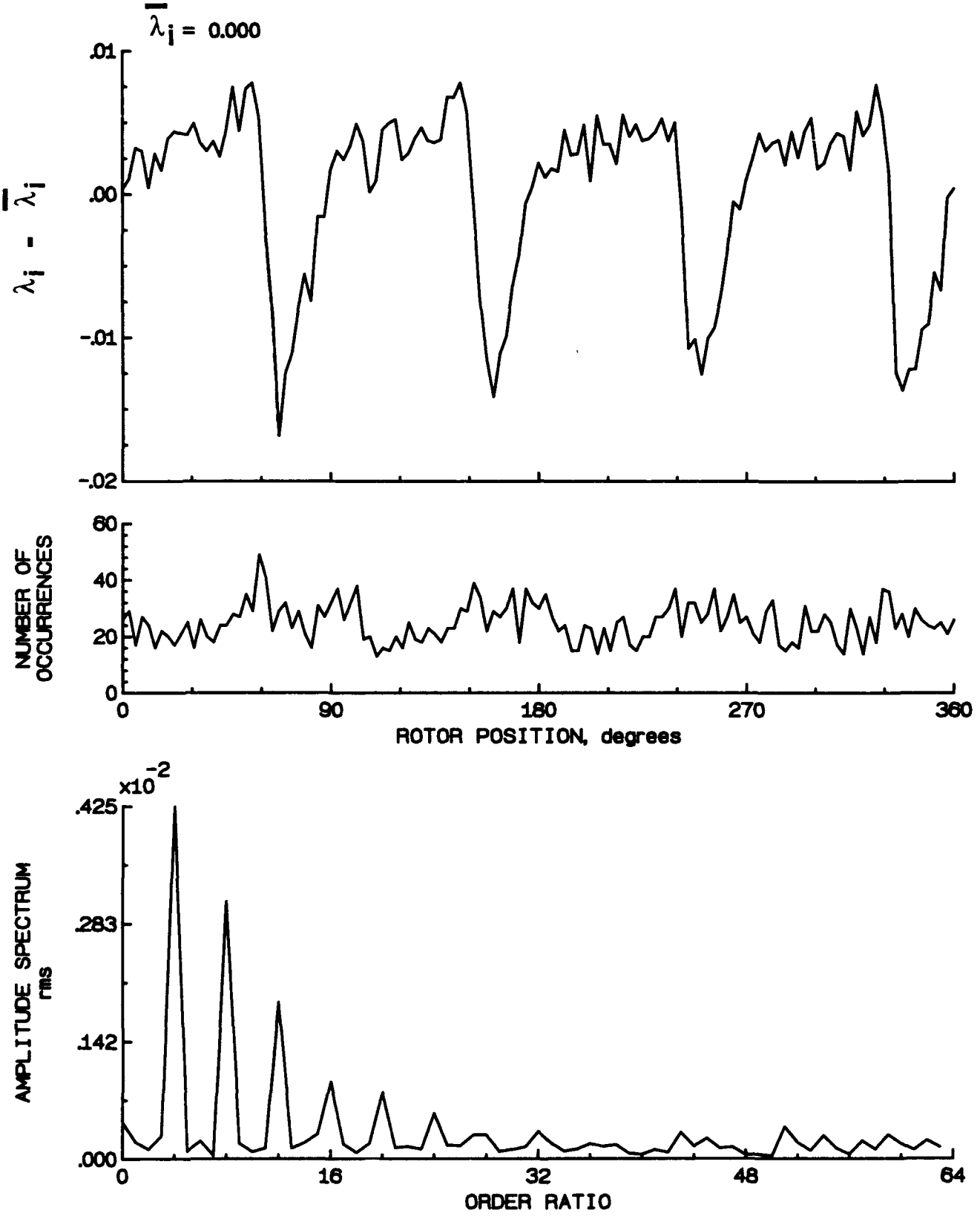

Figure 141.- Concluded.

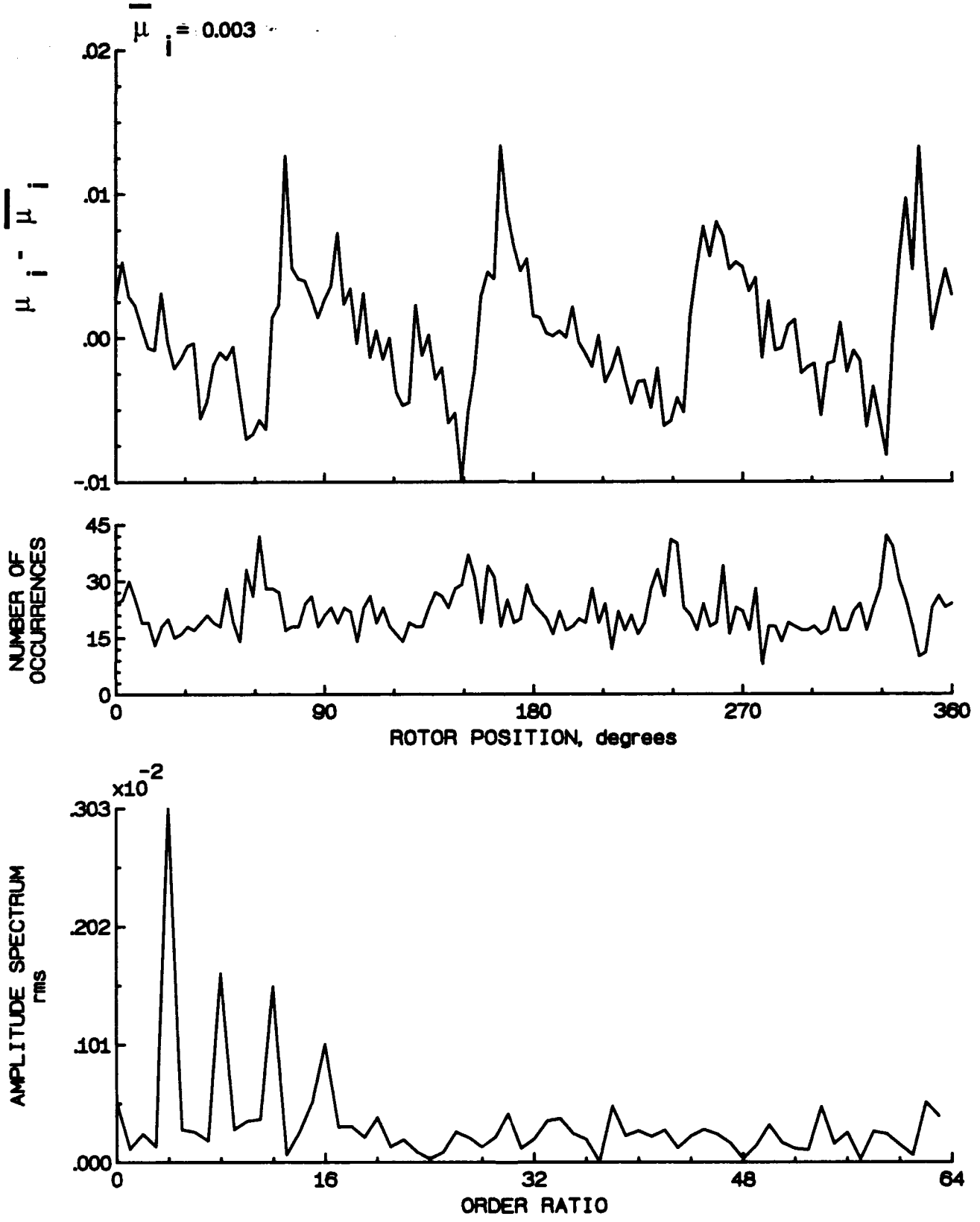

Figure 142.- Induced inflow velocity measured at 240 degrees and r/R of 0.98.

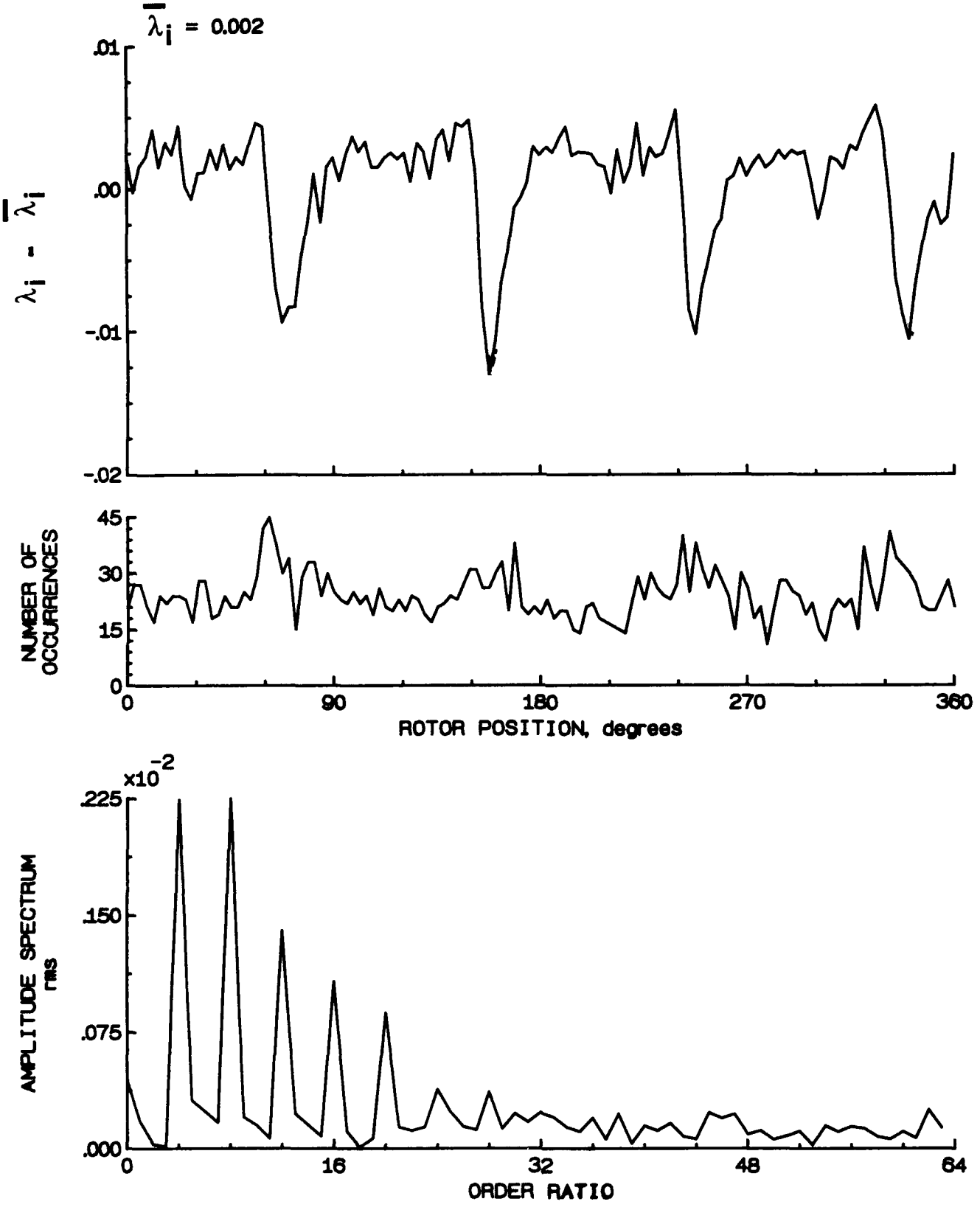

Figure 142.- Concluded.

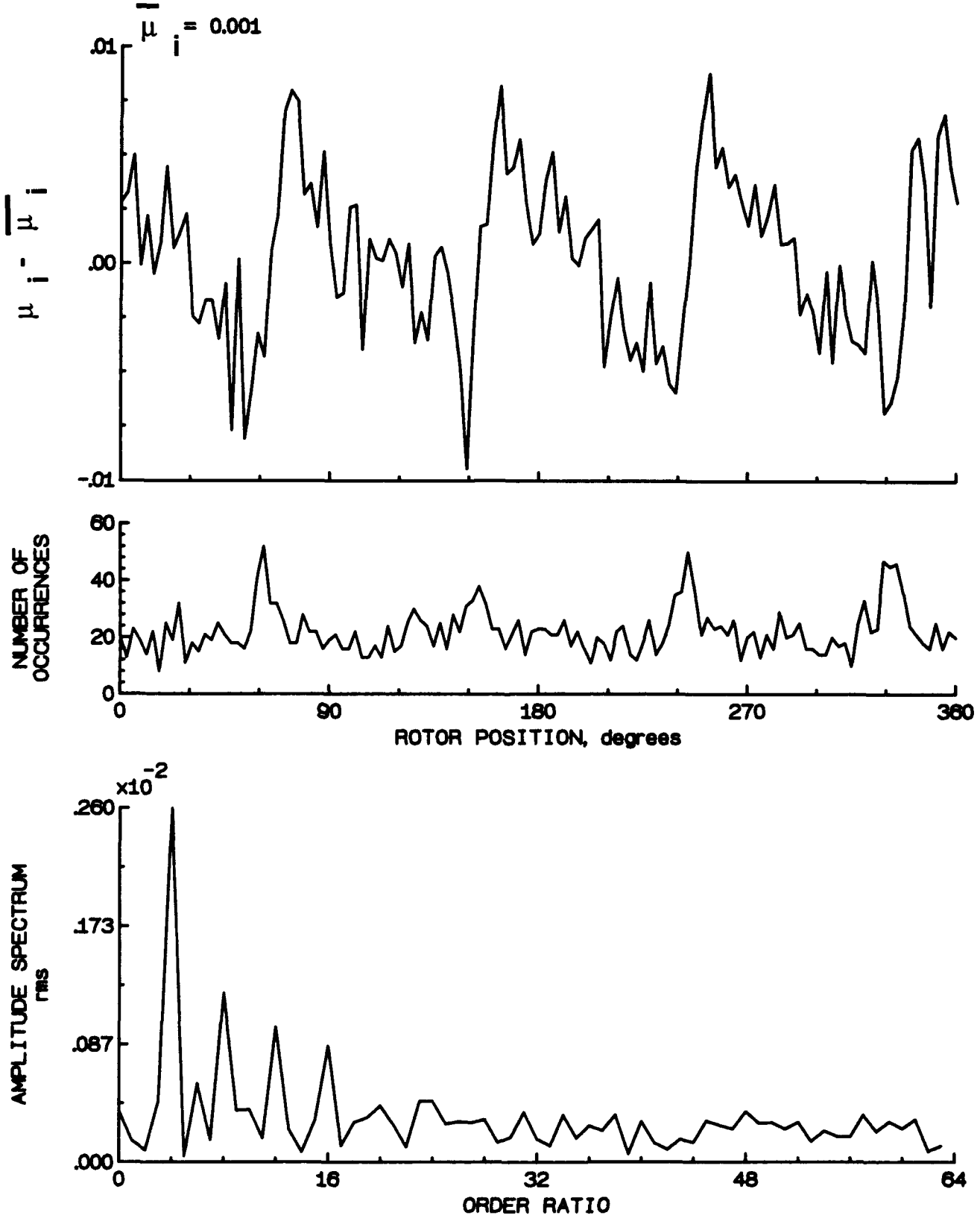

Figure 143.- Induced inflow velocity measured at 240 degrees and r/R of 1.02.

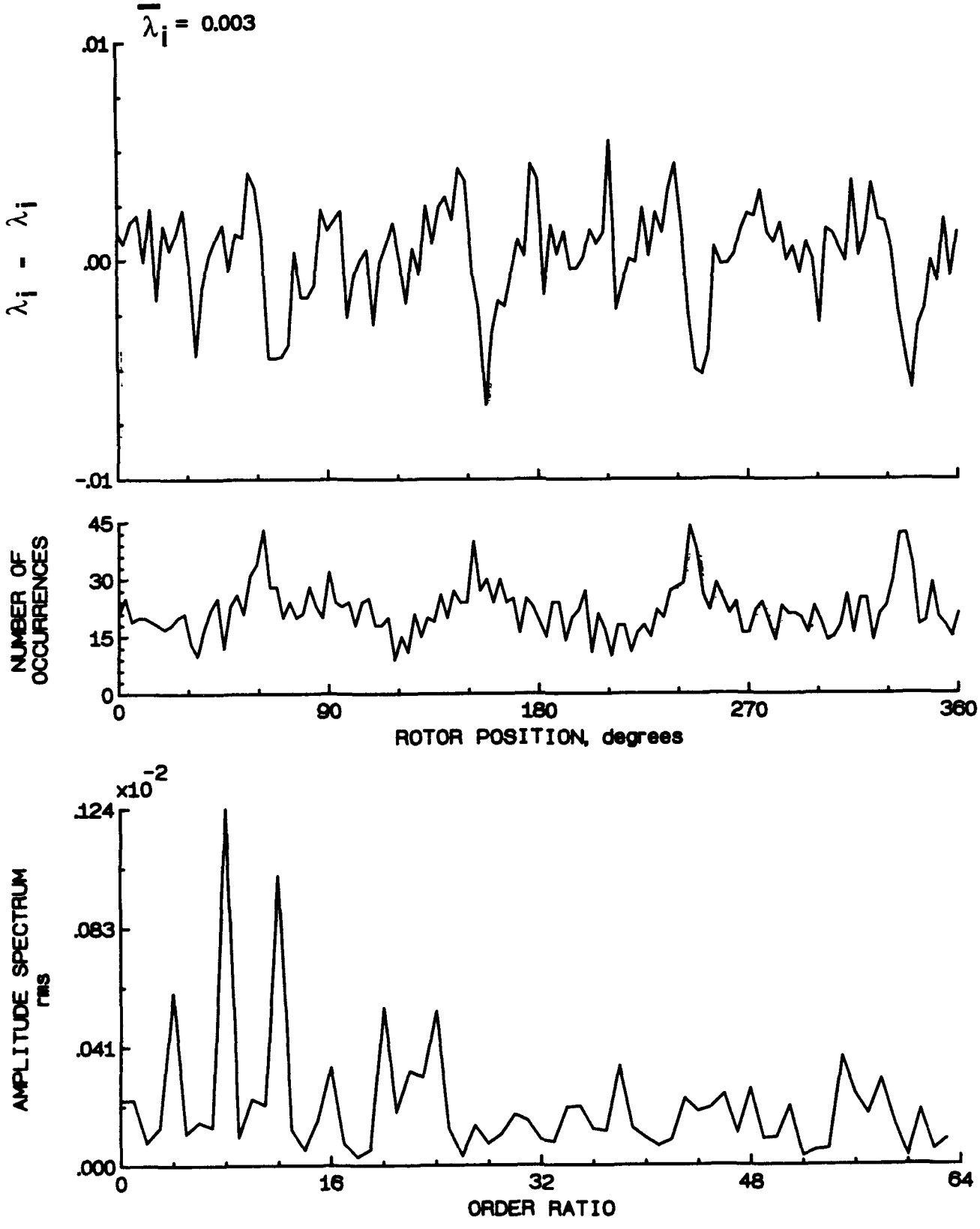

Figure 143.- Concluded.

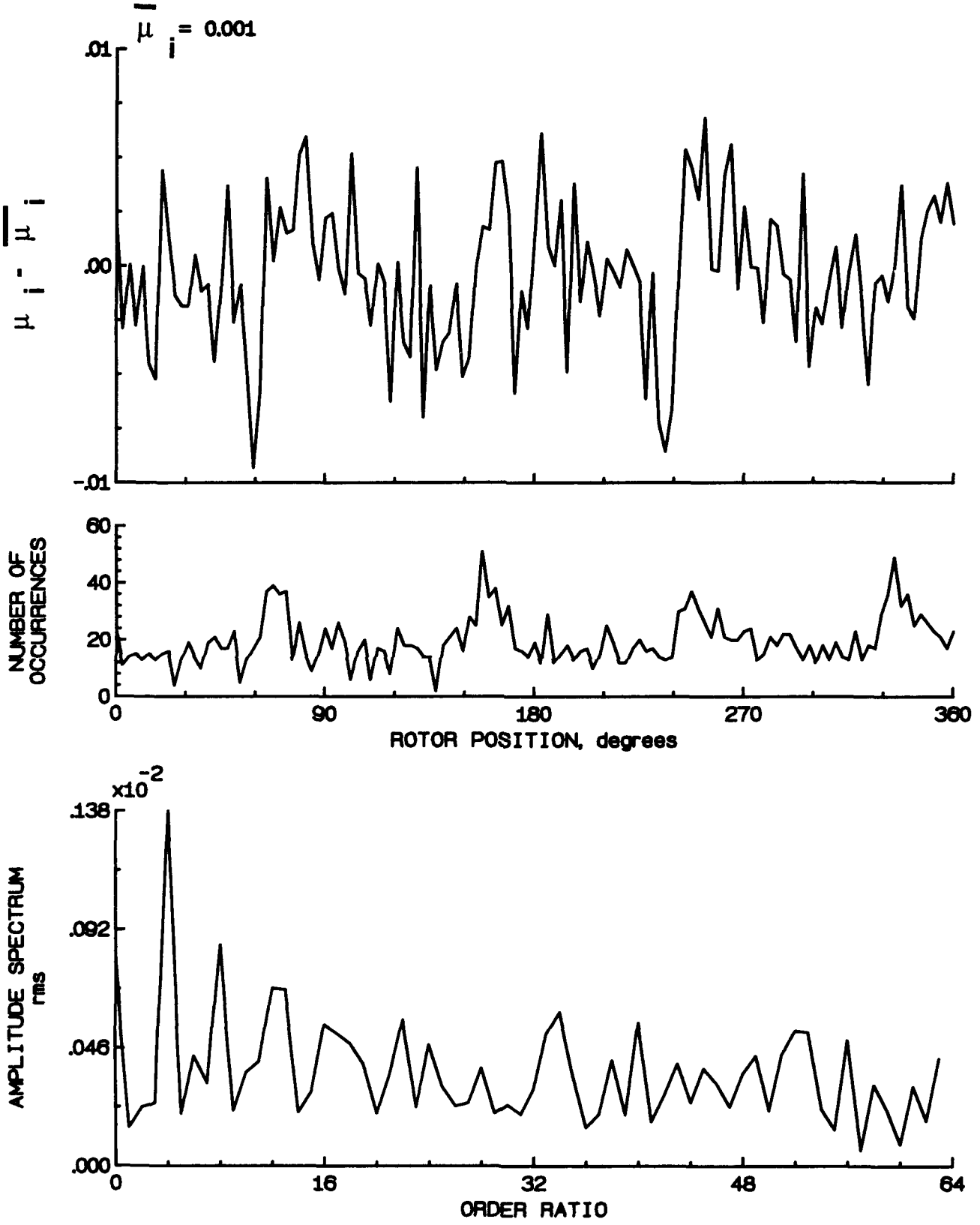

Figure 144.- Induced inflow velocity measured at 240 degrees and r/R of 1.04.

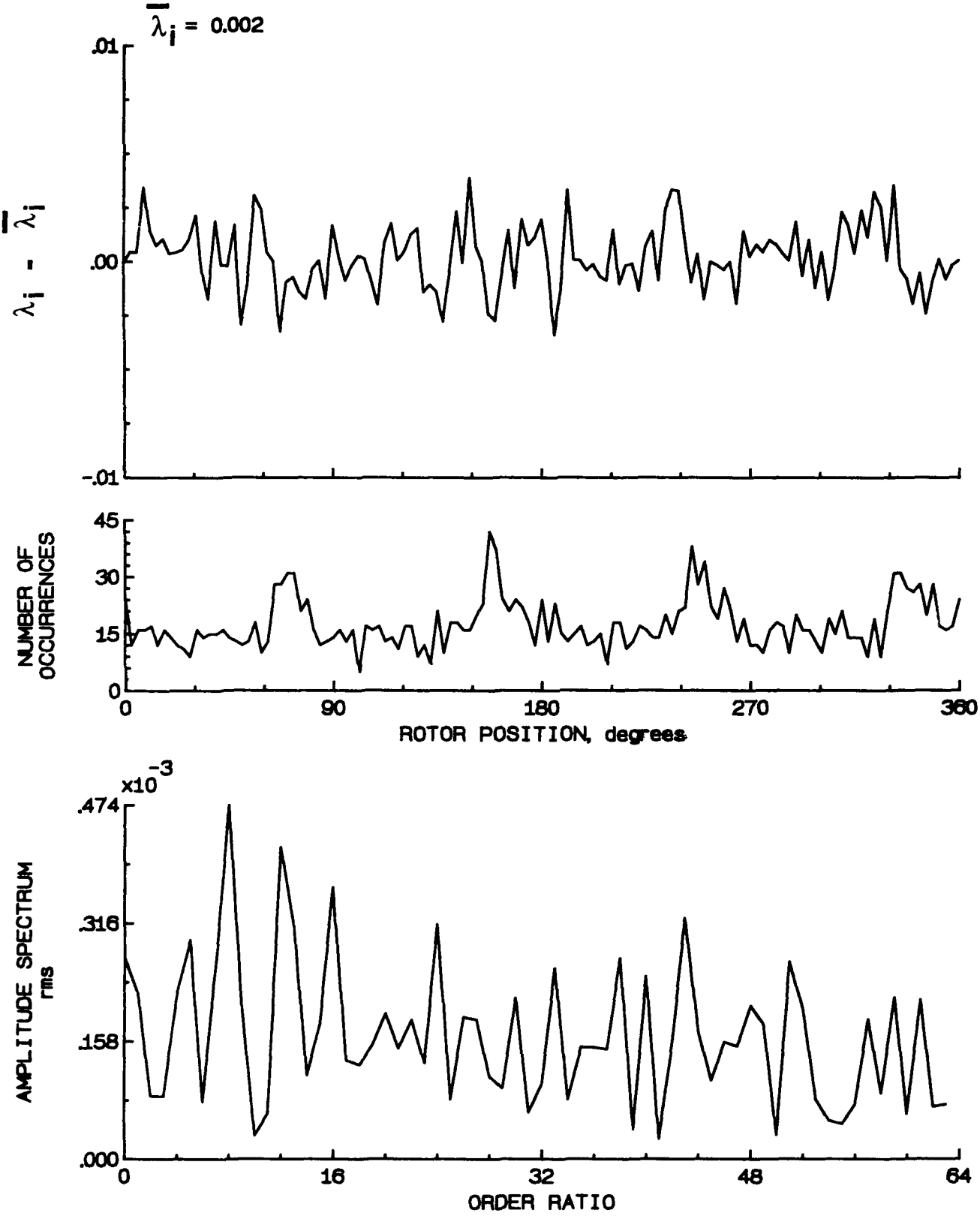

Figure 144.- Concluded.

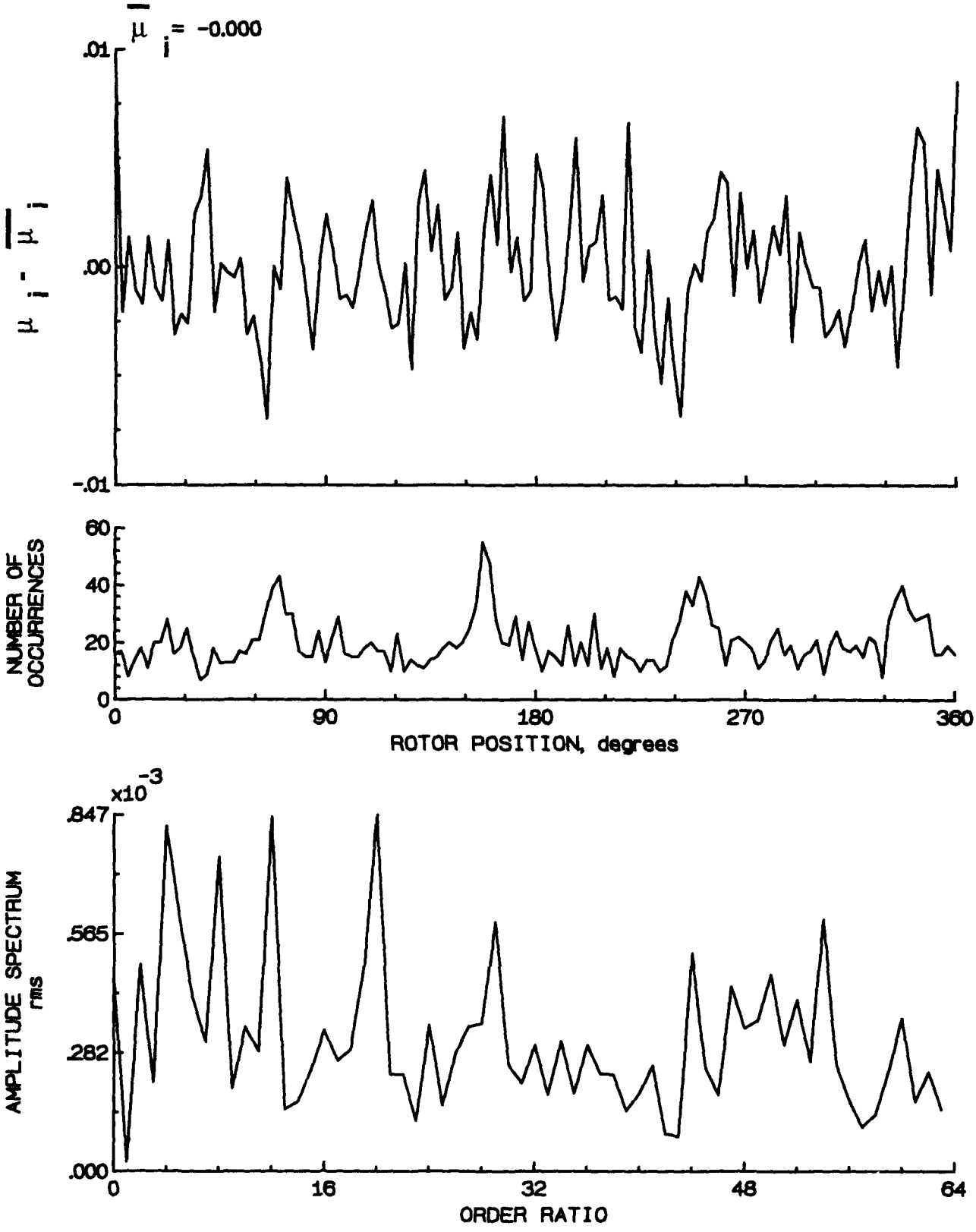

Figure 145.- Induced inflow velocity measured at 240 degrees and r/R of 1.10.

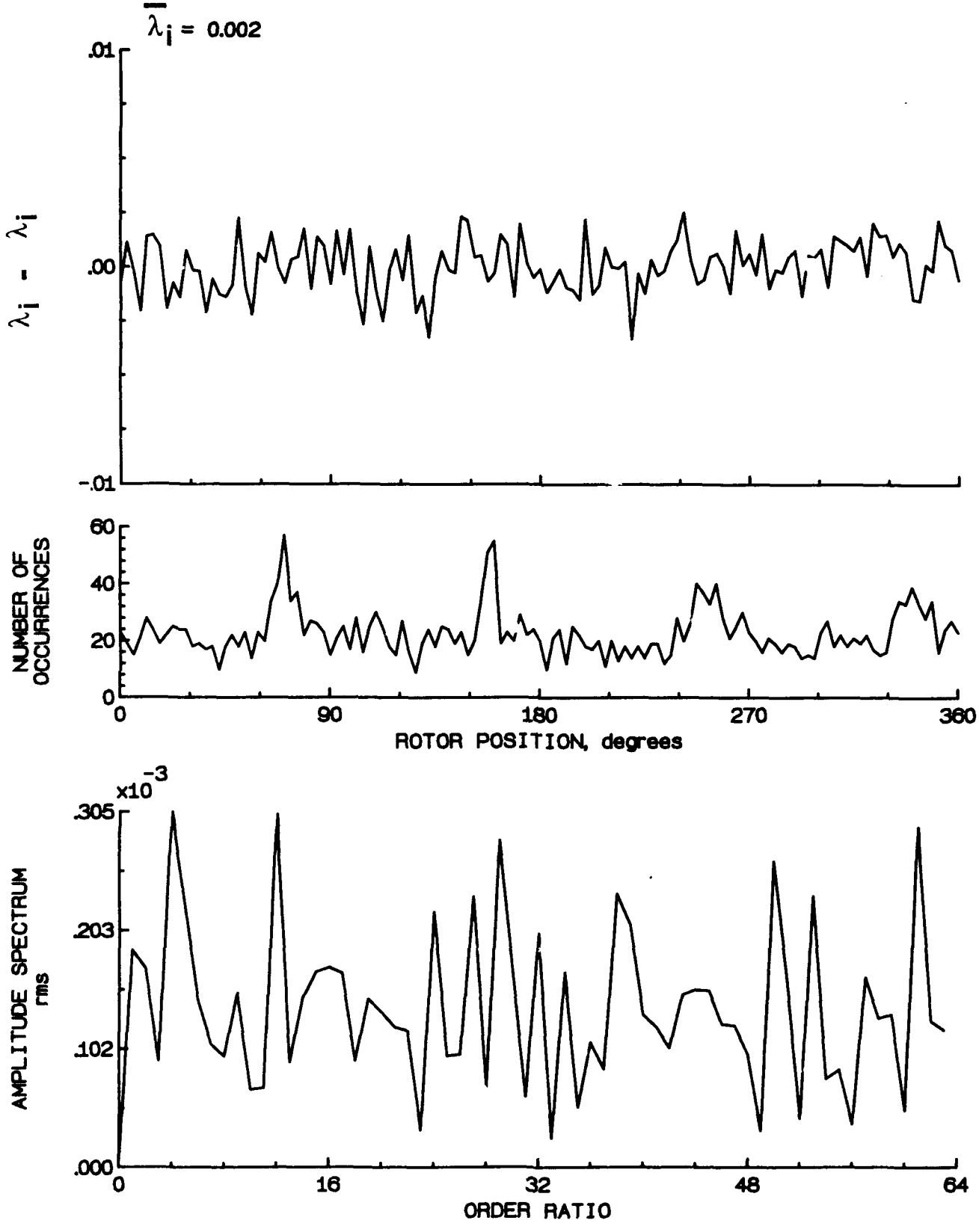

Figure 145.- Concluded.

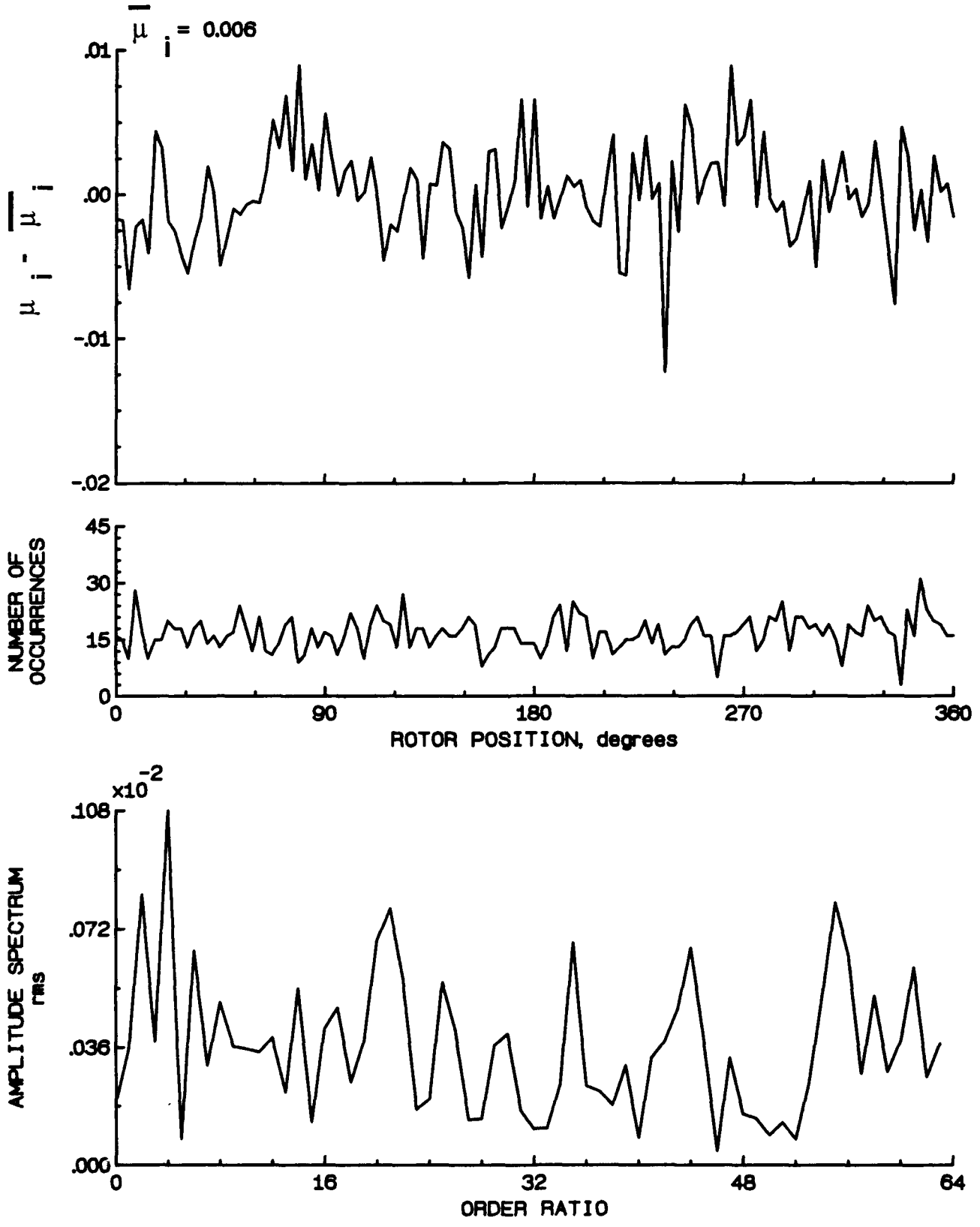

Figure 146.- Induced inflow velocity measured at 270 degrees and r/R of 0.20.

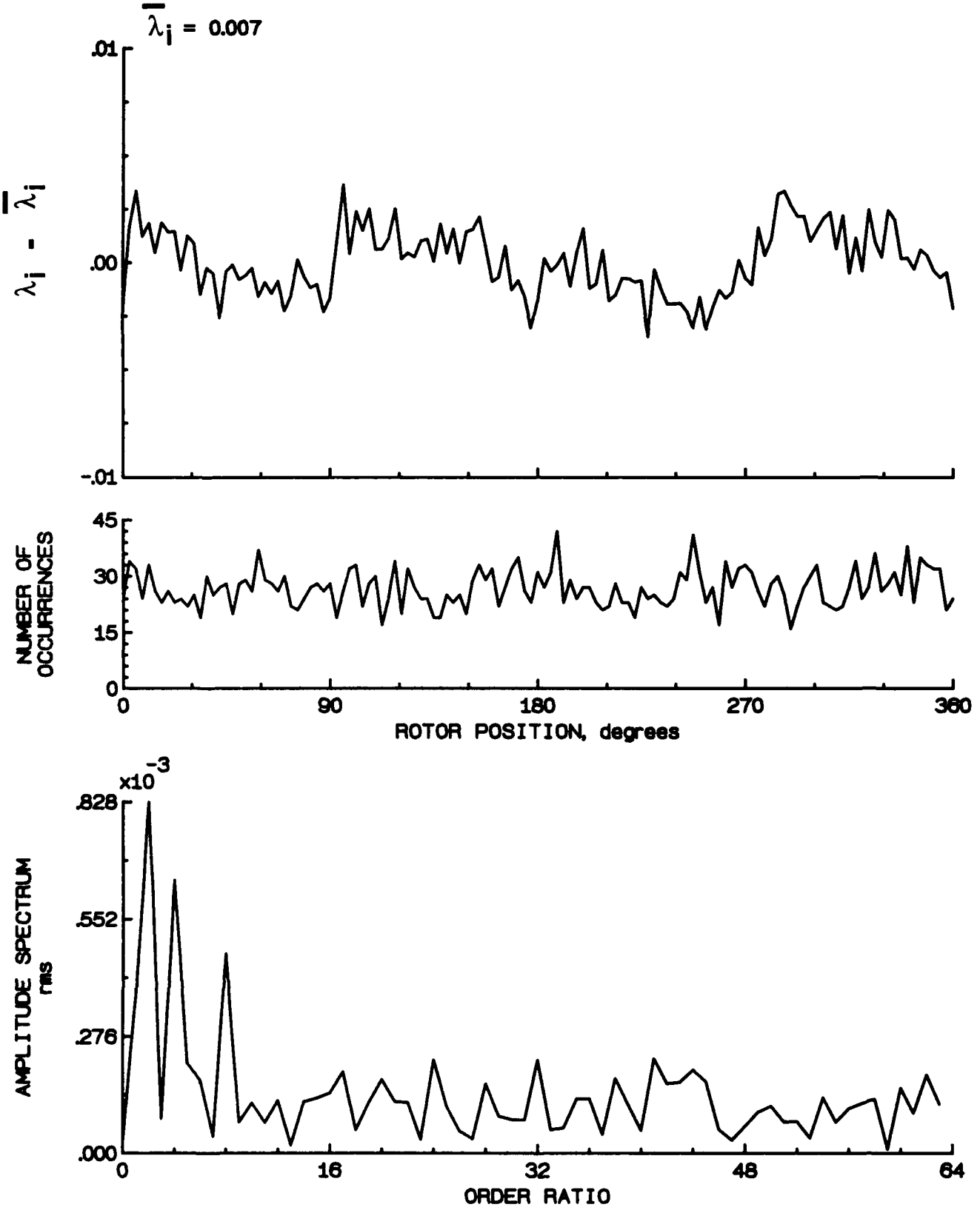

Figure 146.- Concluded.

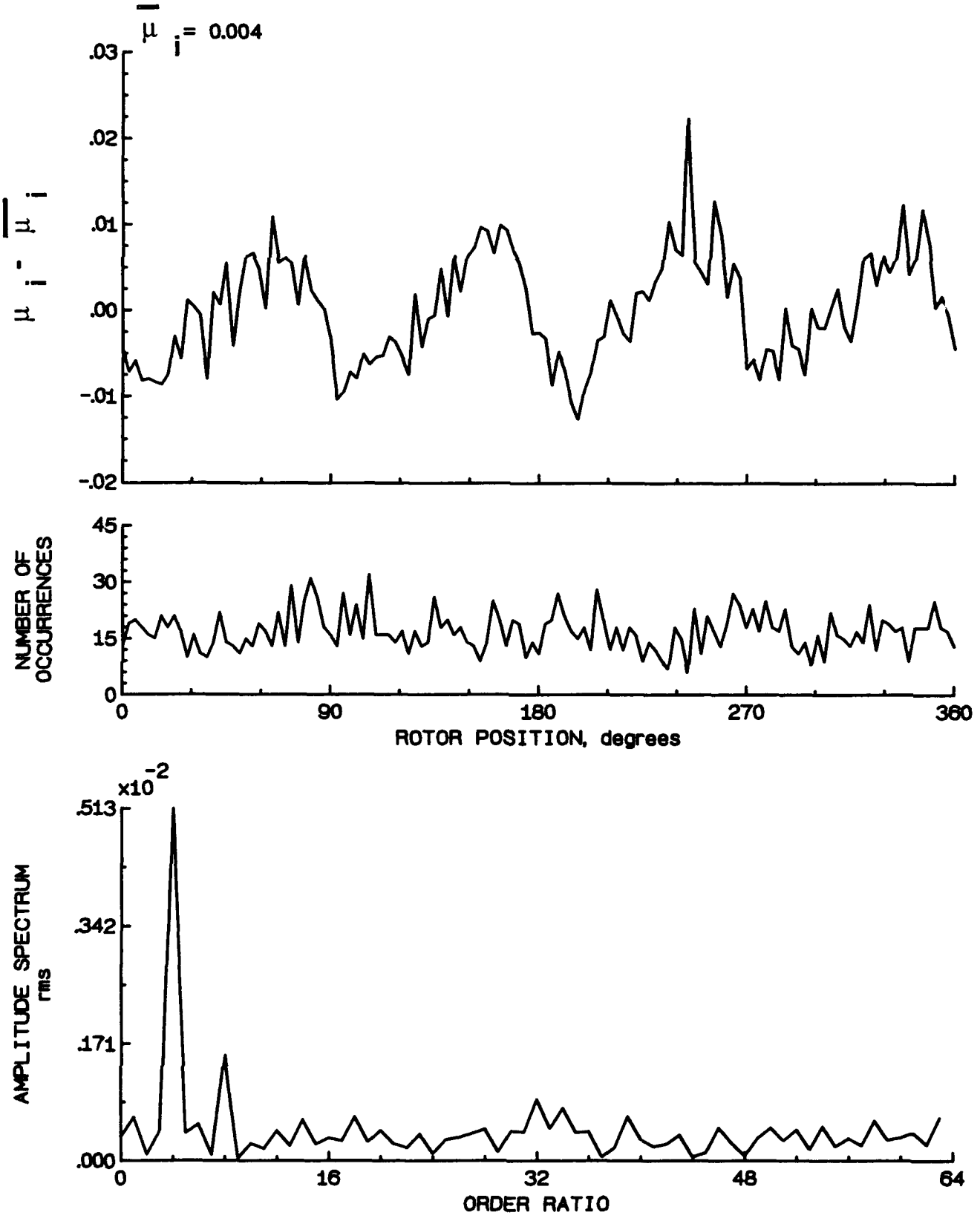

Figure 147.- Induced inflow velocity measured at 270 degrees and r/R of 0.40.

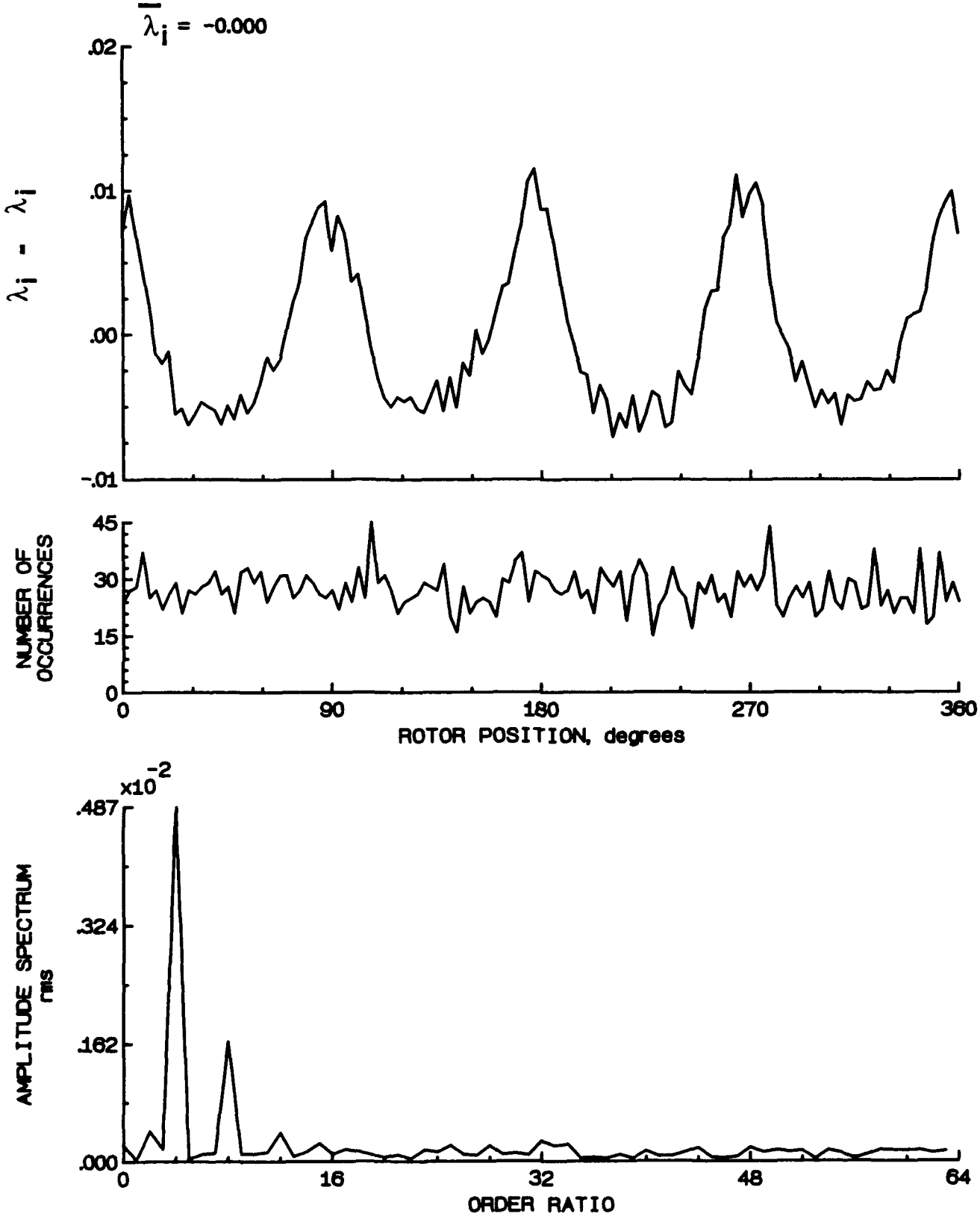

Figure 147.- Concluded.

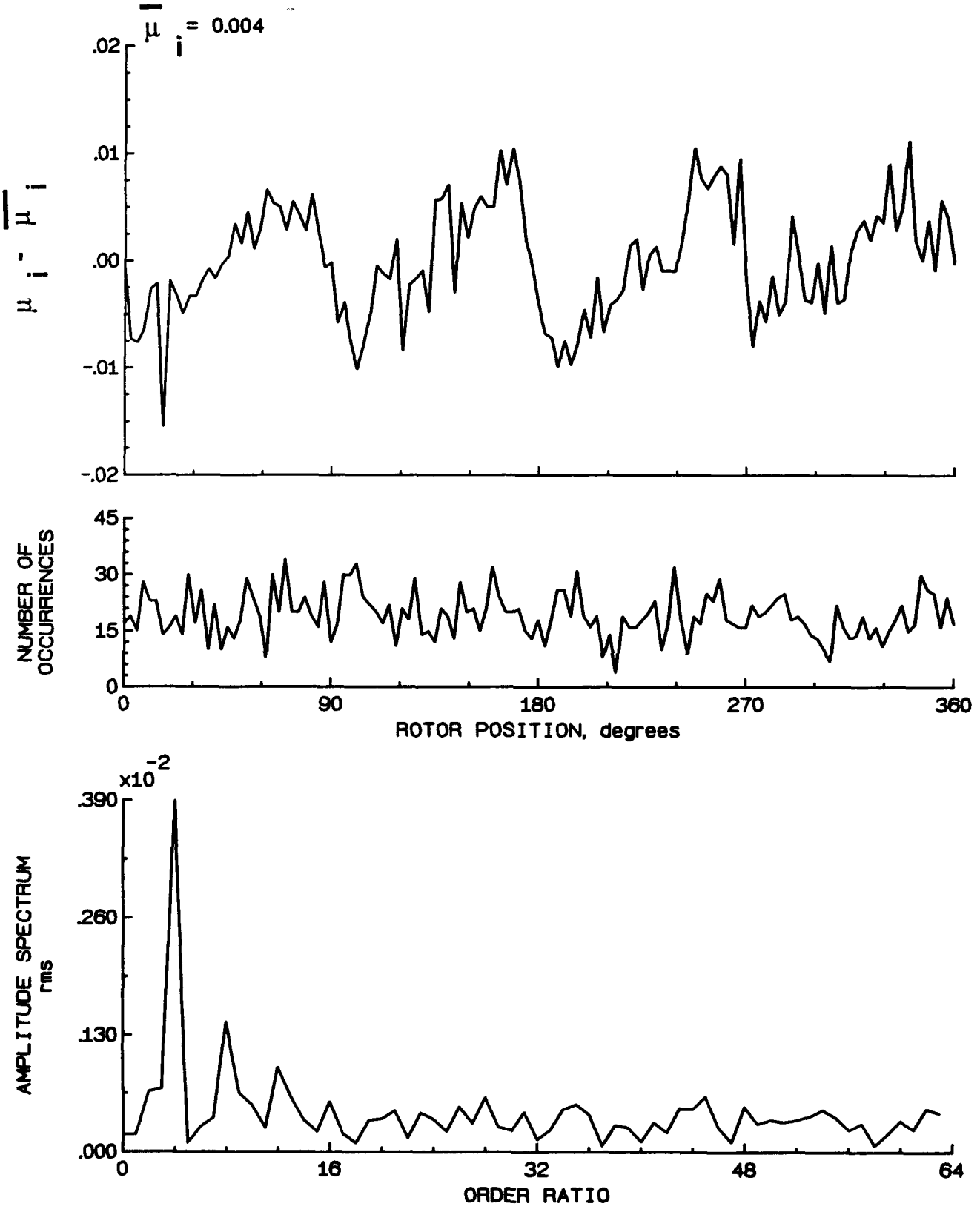

Figure 148.- Induced inflow velocity measured at 270 degrees and r/R of 0.50.

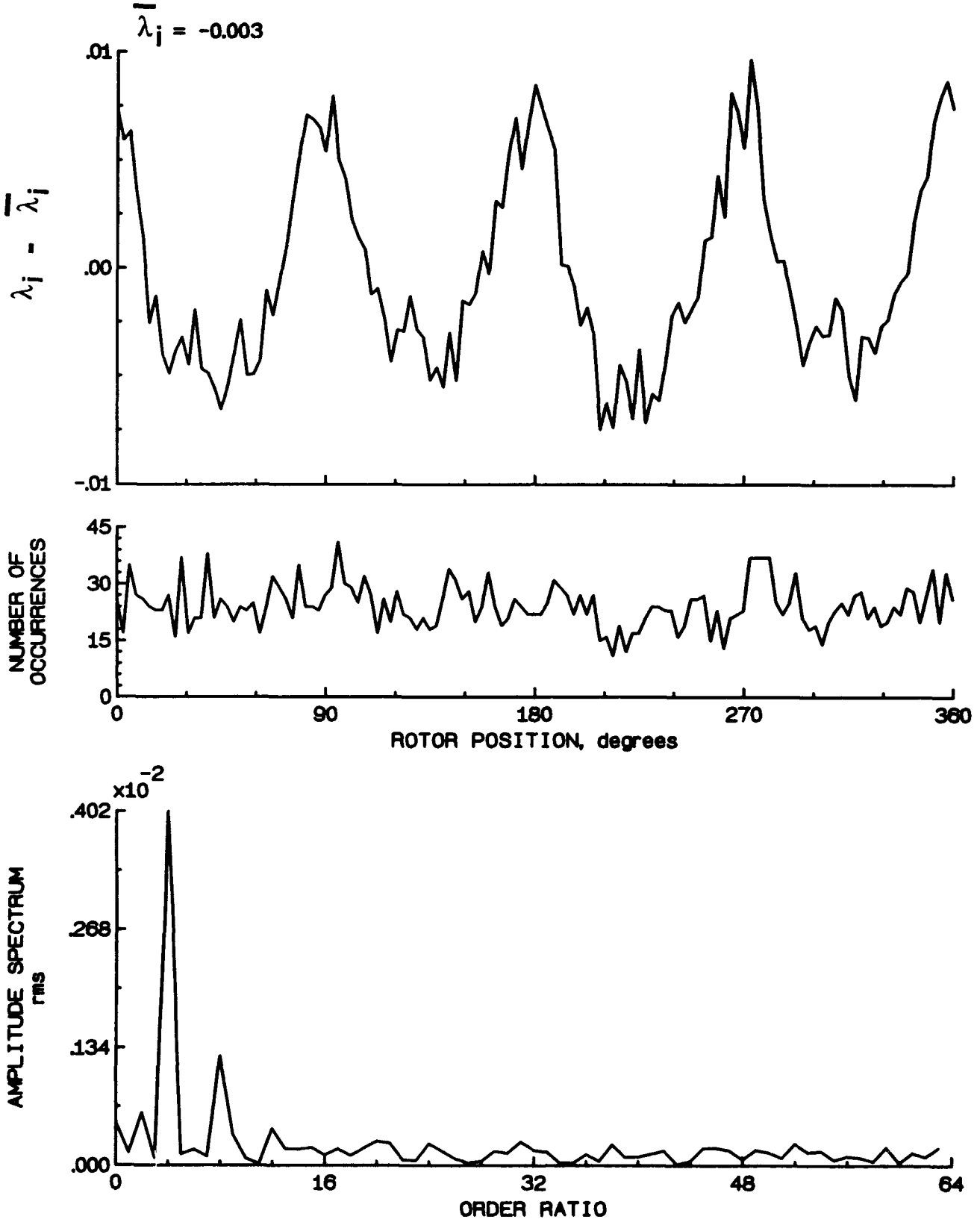

Figure 148.- Concluded.

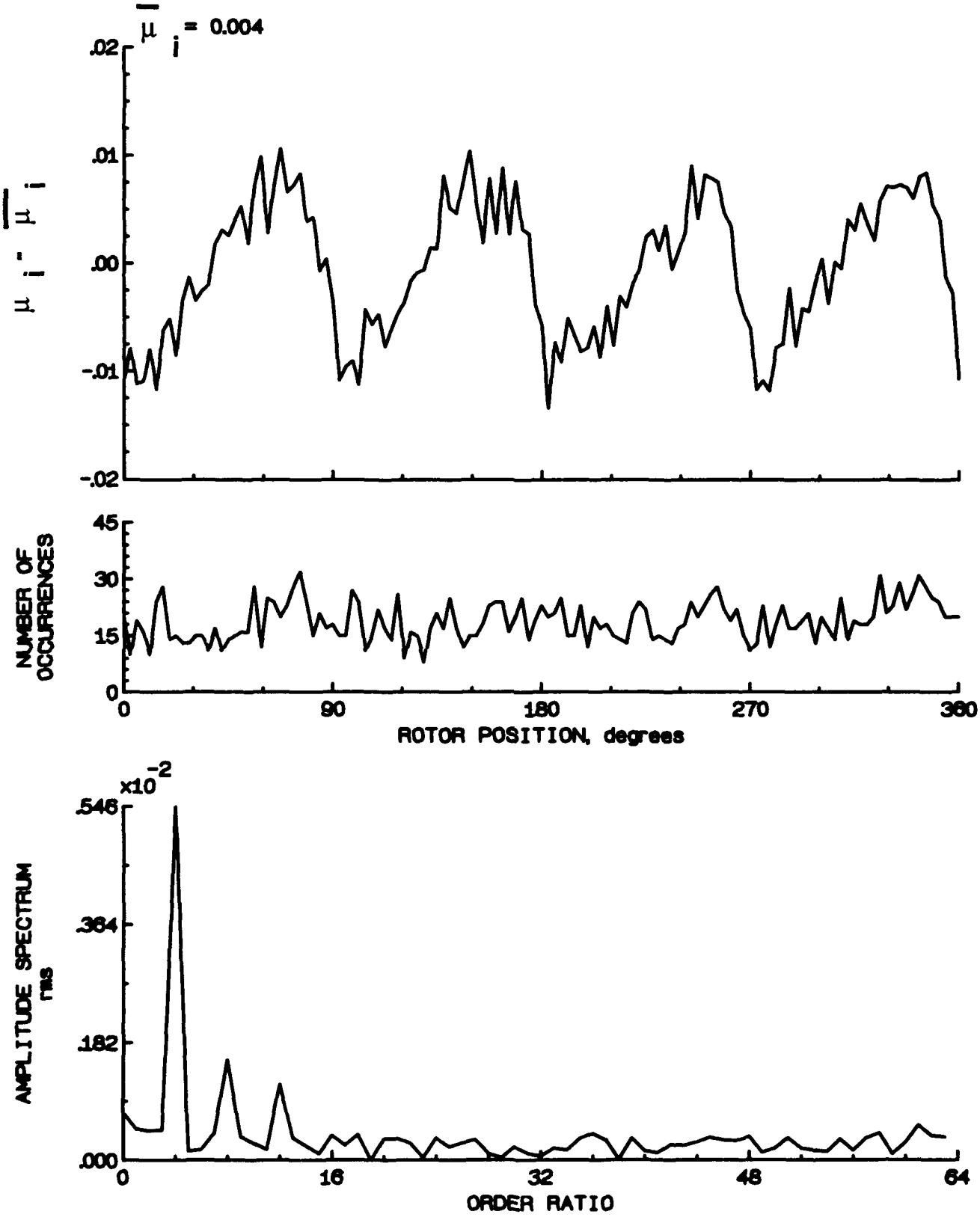

Figure 149.- Induced inflow velocity measured at 270 degrees and r/R of 0.60.

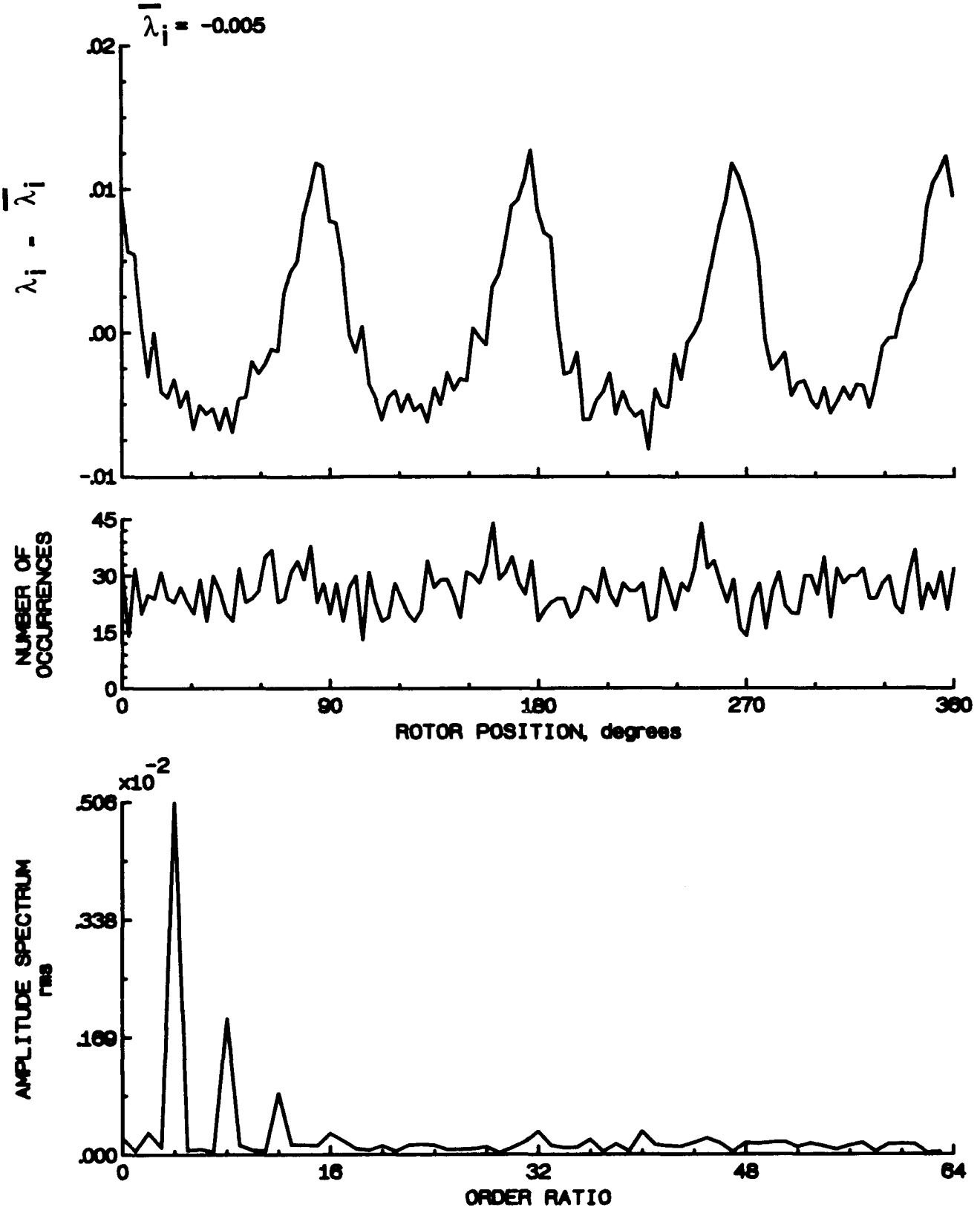

Figure 149.- Concluded.

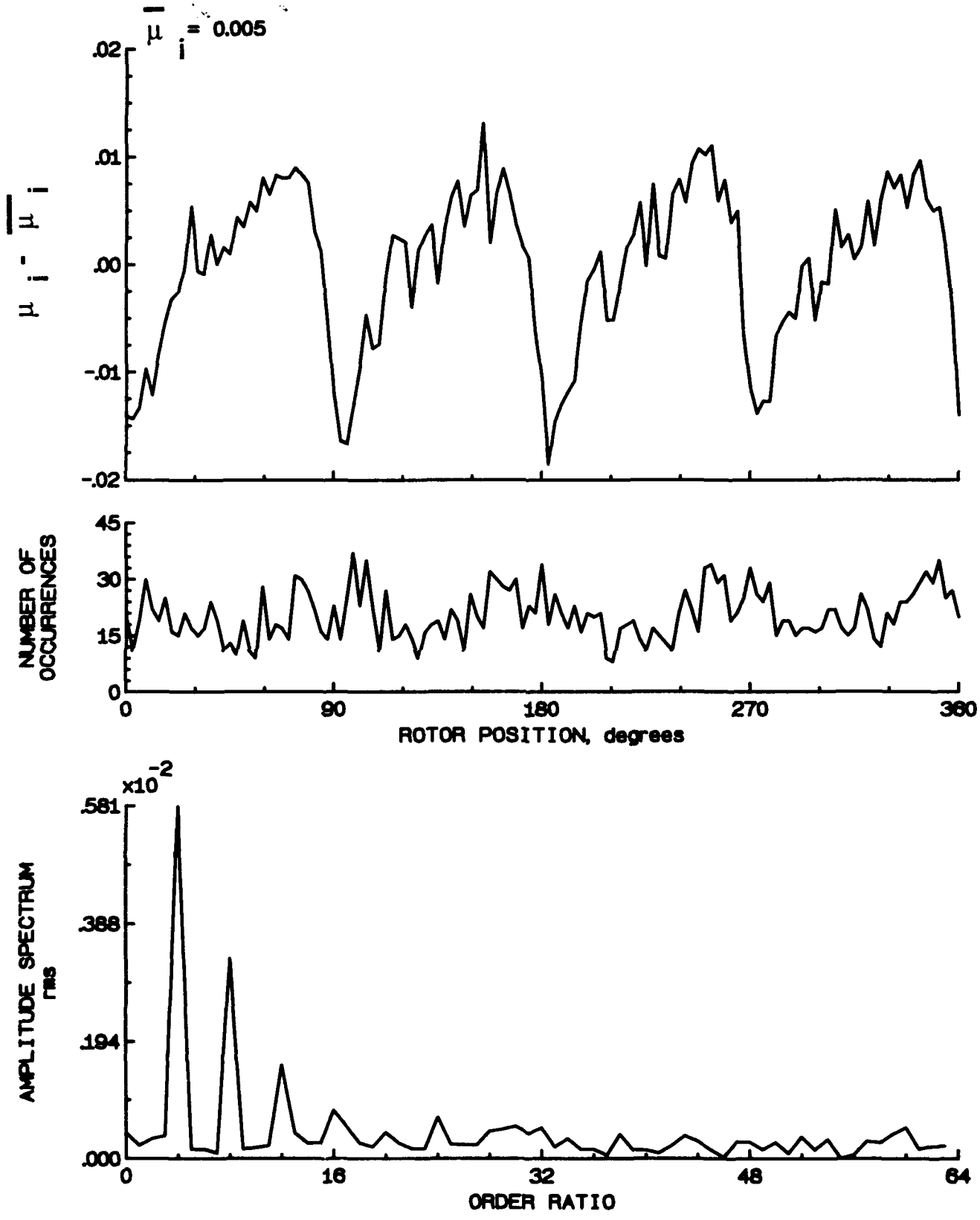

Figure 150.- Induced inflow velocity measured at 270 degrees and r/R of 0.70.

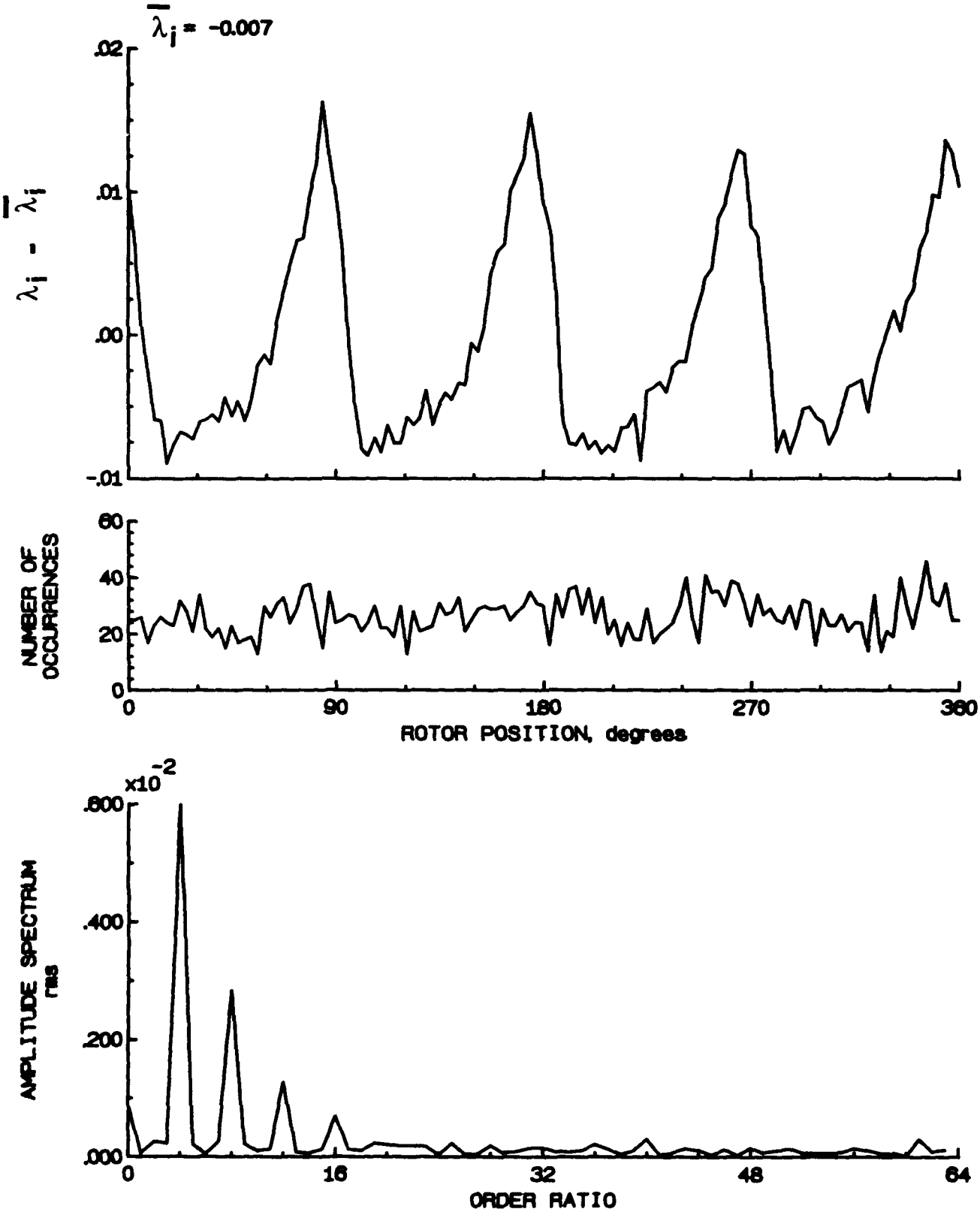

Figure 150.- Concluded.

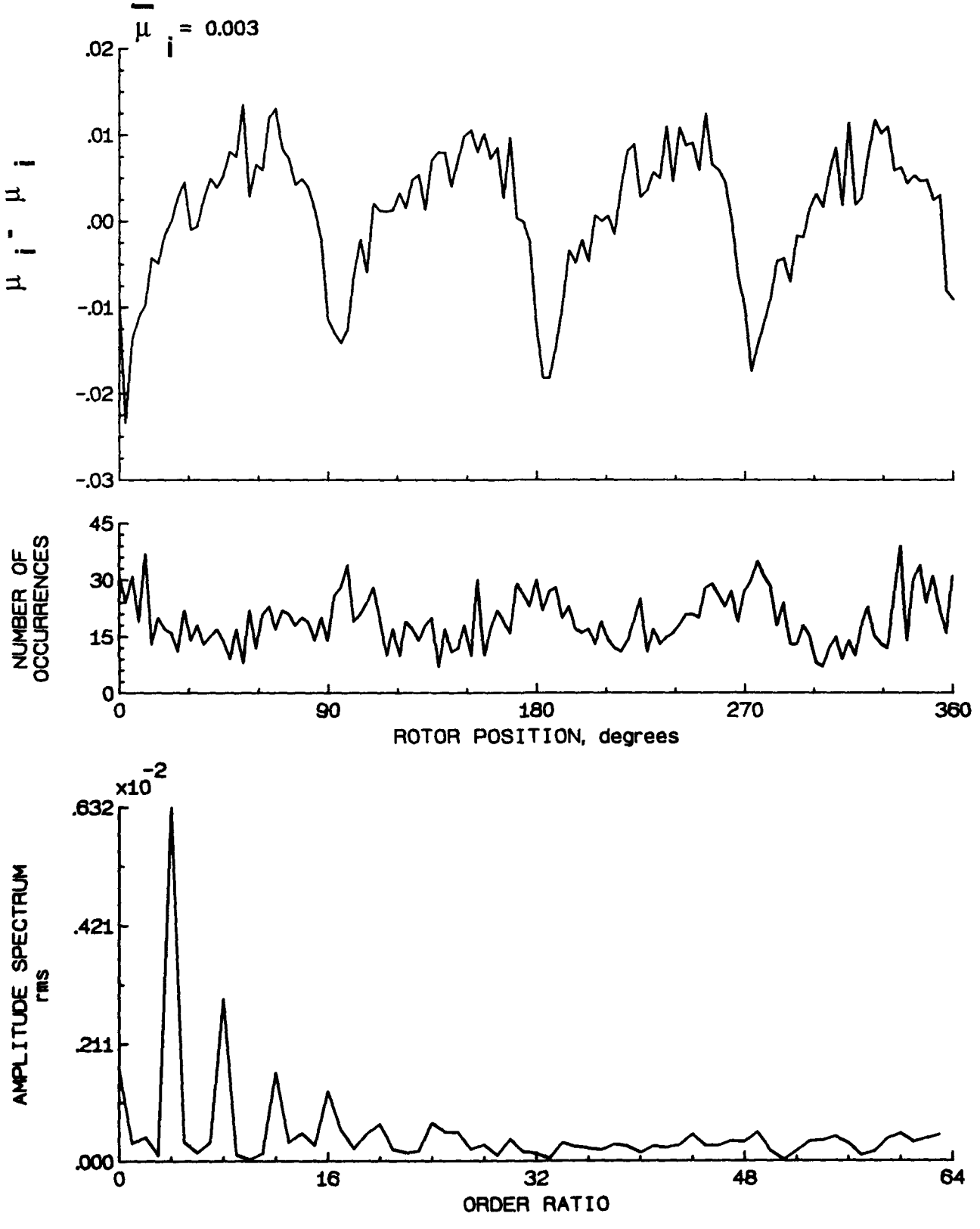

Figure 151.- Induced inflow velocity measured at 270 degrees and r/R of 0.74.

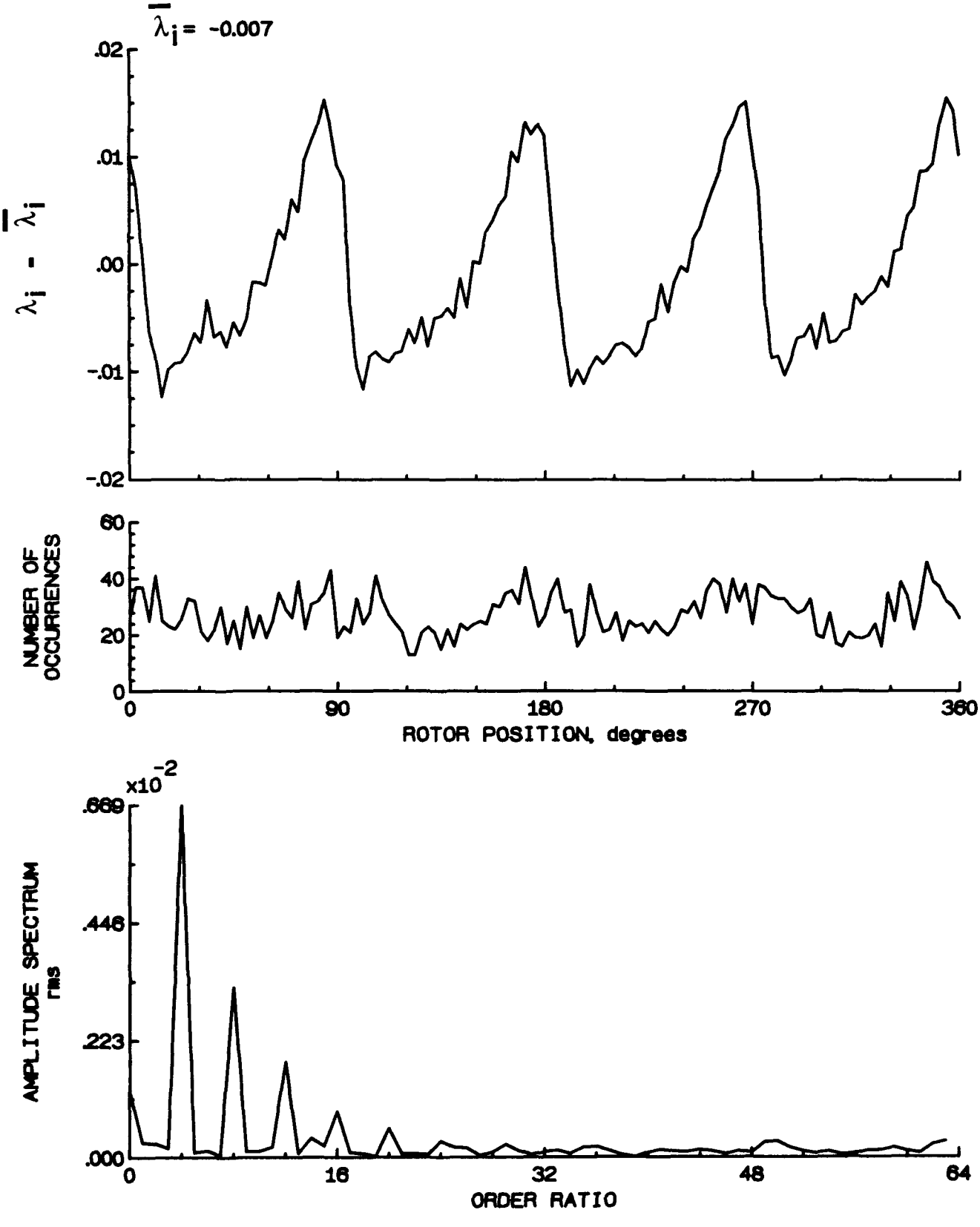

Figure 151.- Concluded.

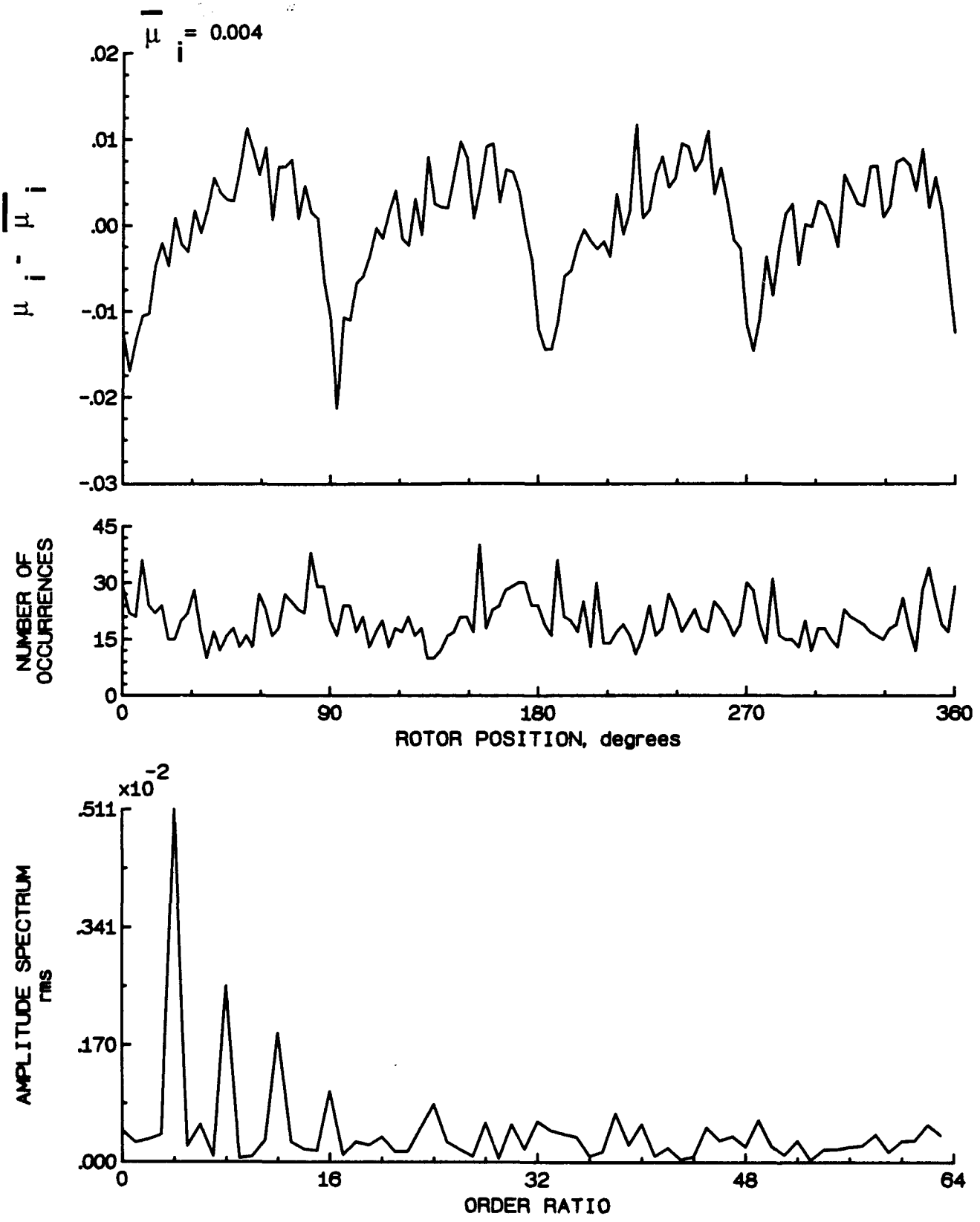

Figure 152.- Induced inflow velocity measured at 270 degrees and r/R of 0.78.

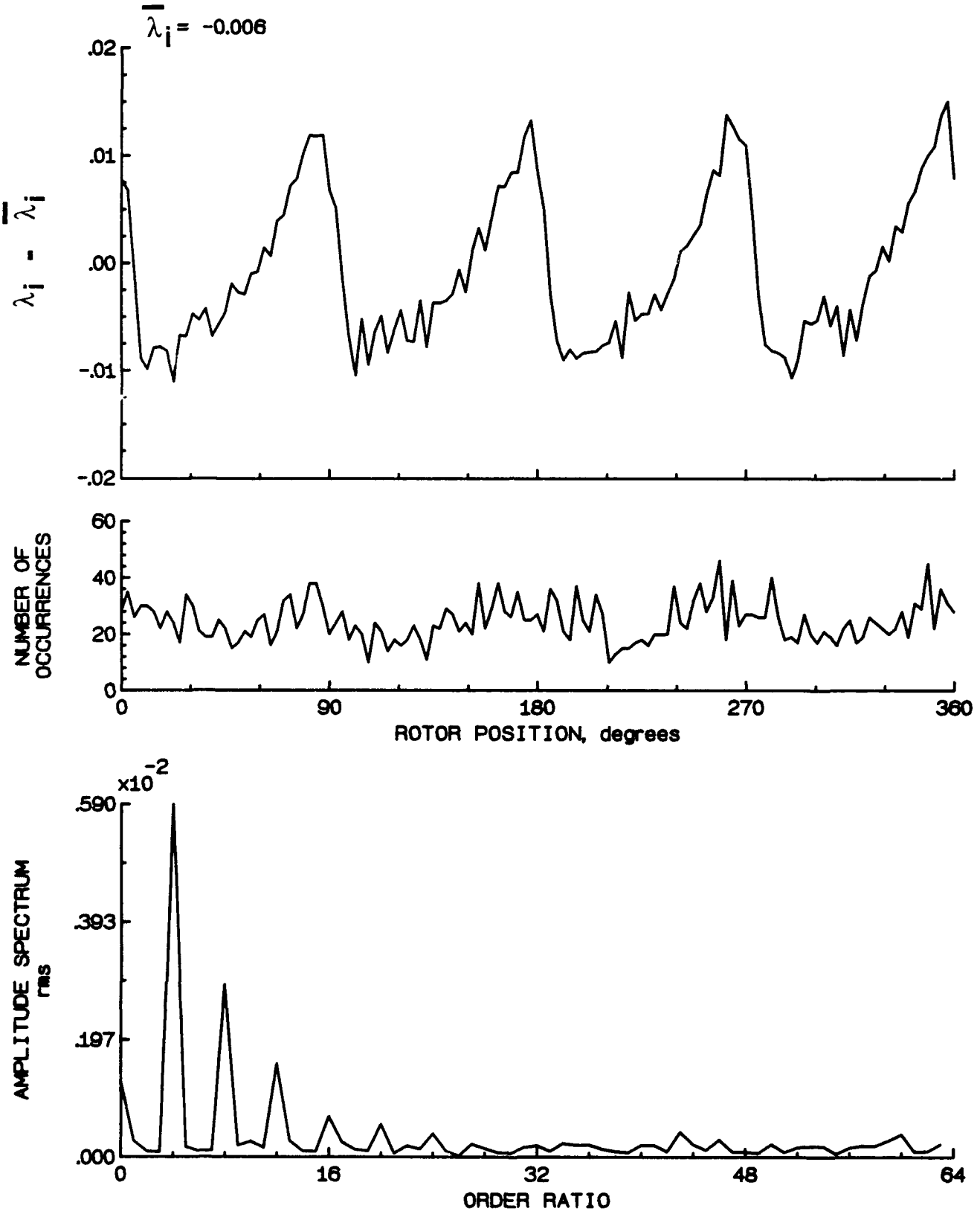

Figure 152.- Concluded.

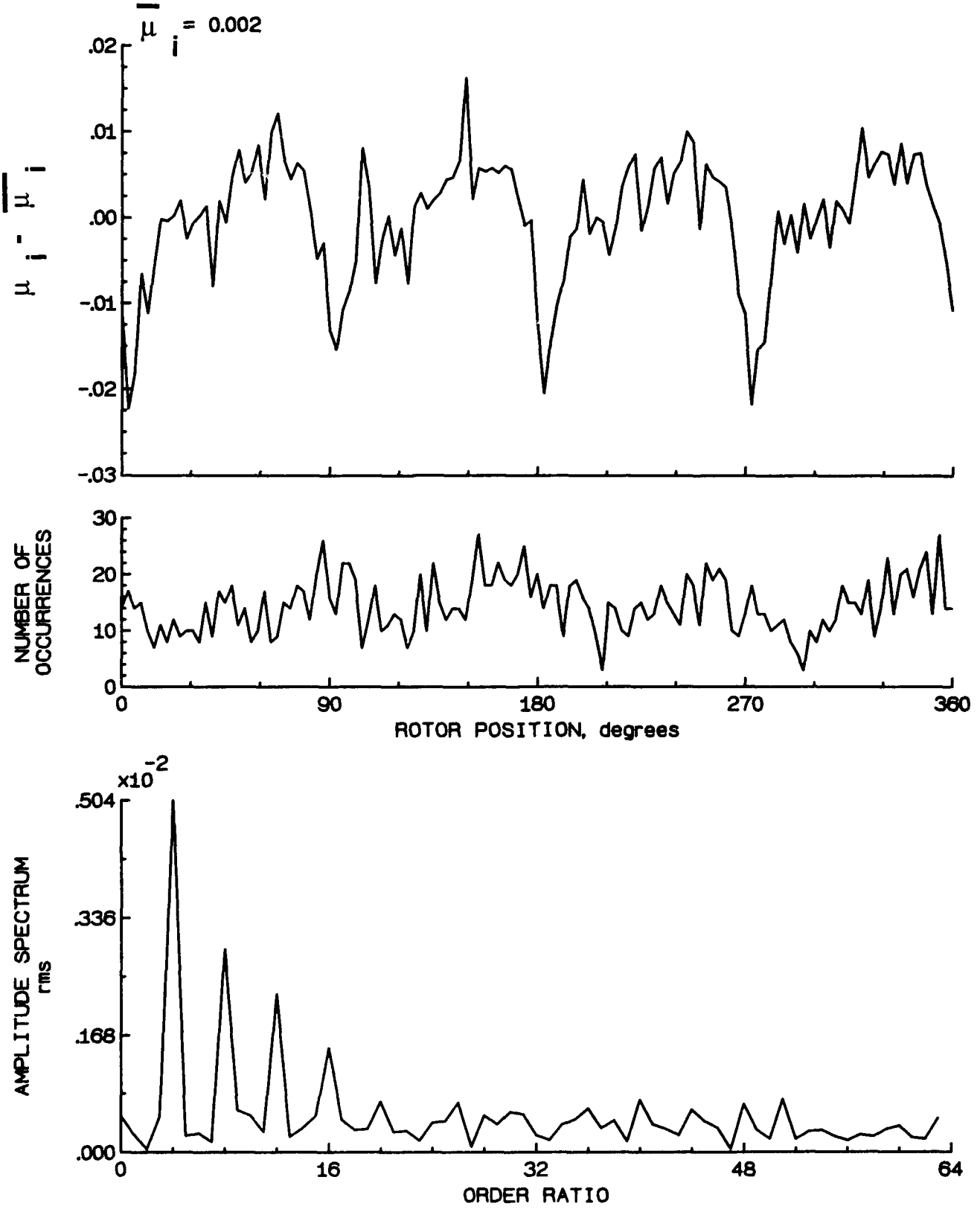

Figure 153.- Induced inflow velocity measured at 270 degrees and r/R of 0.82.

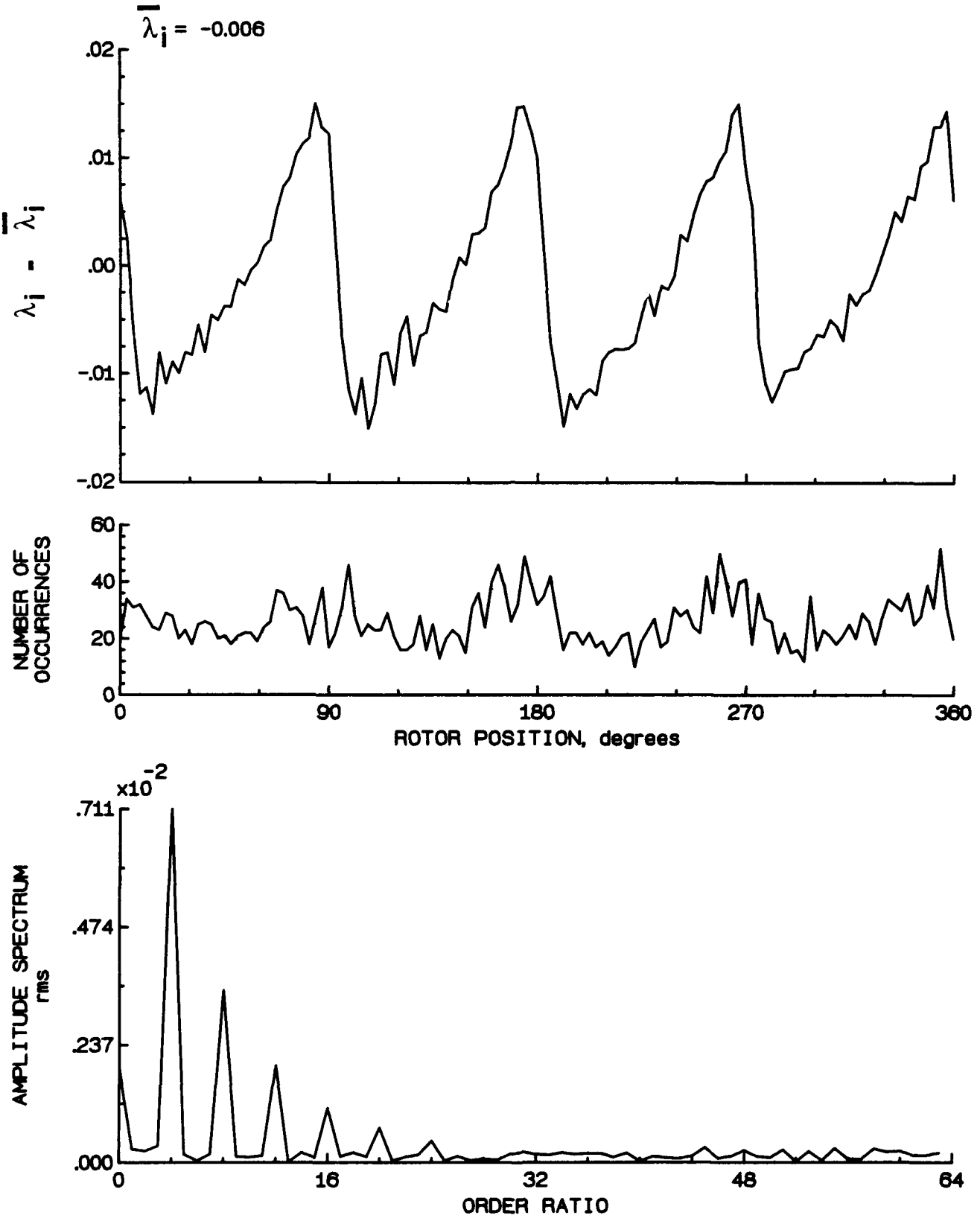

Figure 153.- Concluded.

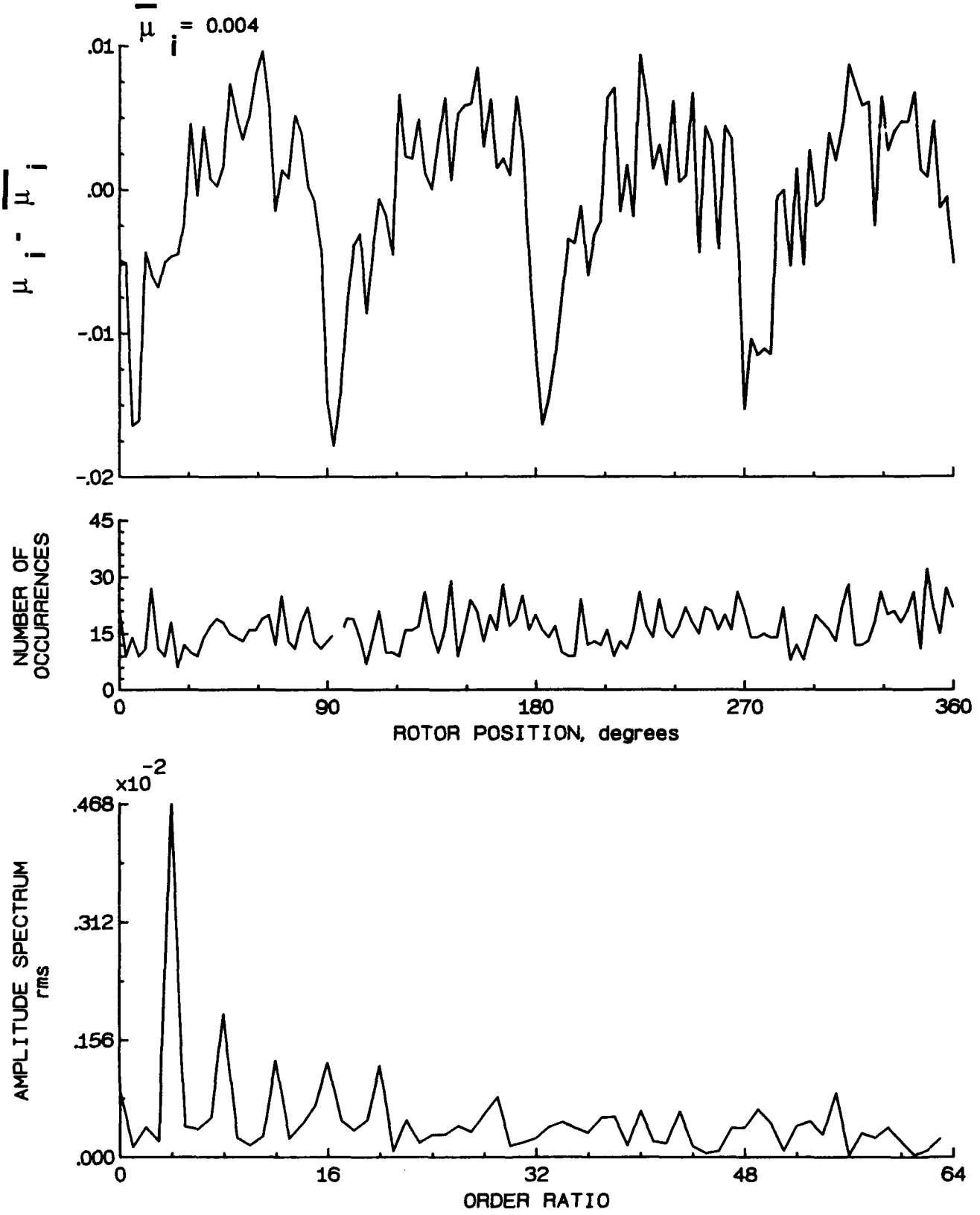

Figure 154.- Induced inflow velocity measured at 270 degrees and r/R of 0.86.

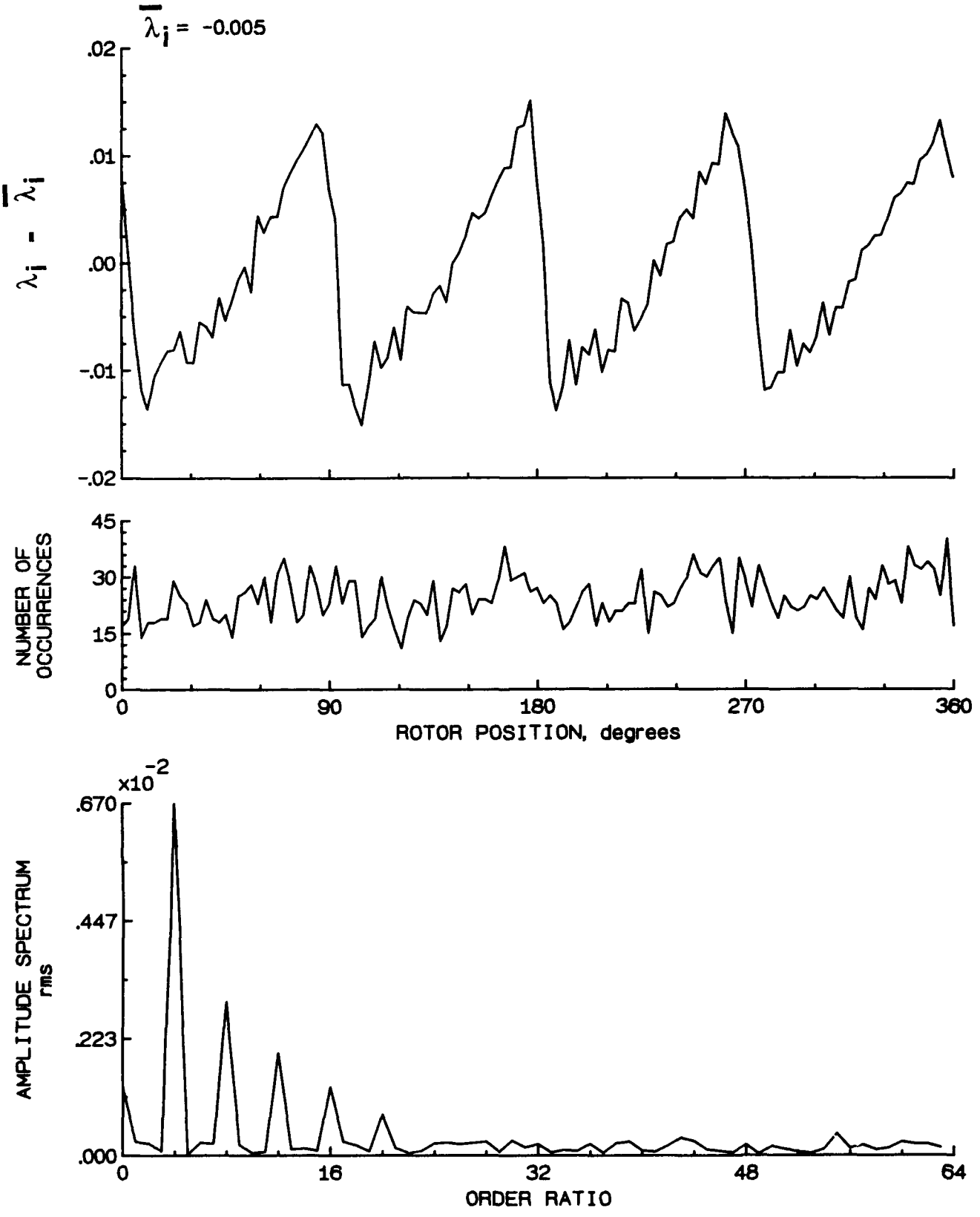

Figure 154.- Concluded.

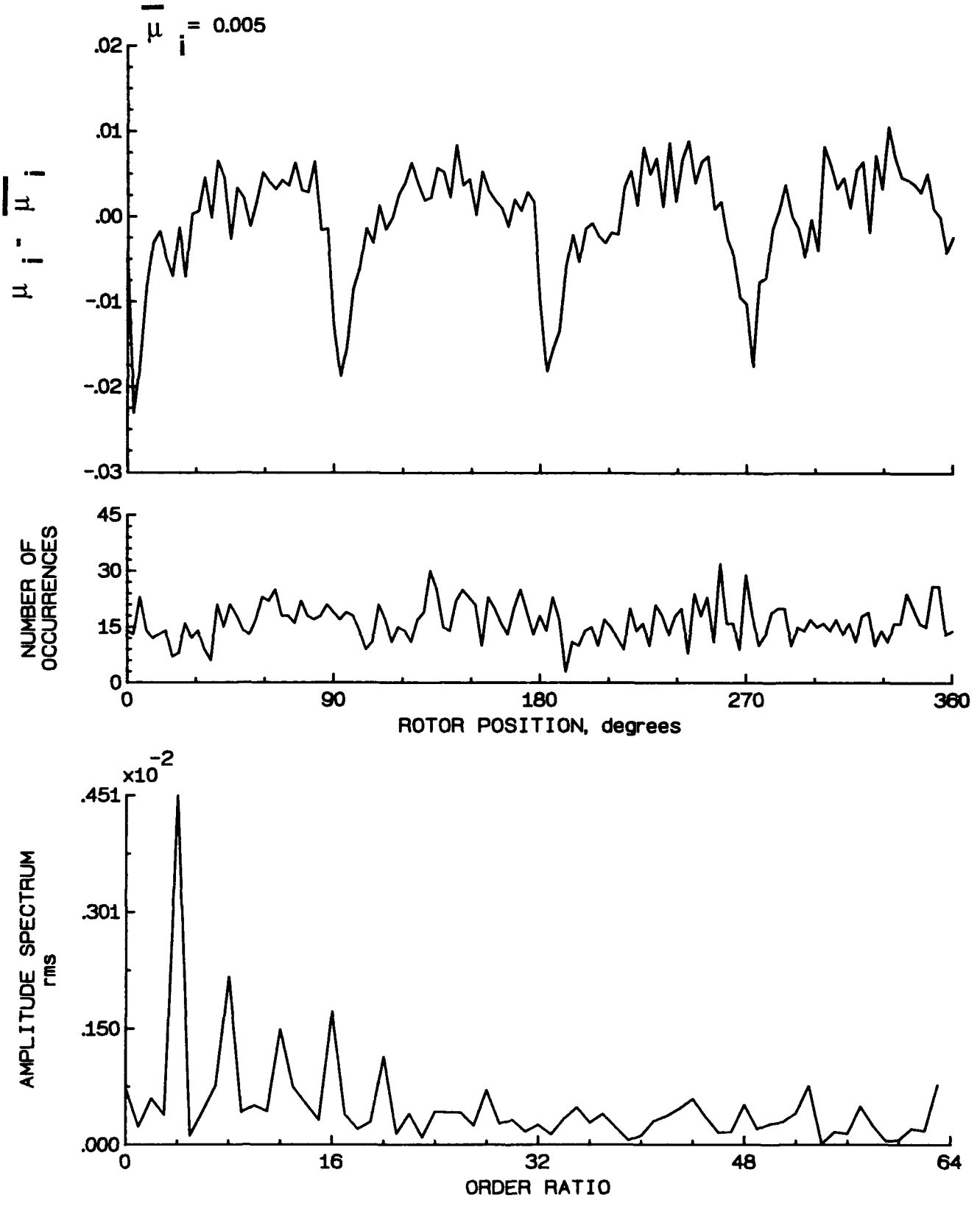

Figure 155.- Induced inflow velocity measured at 270 degrees and r/R of 0.90.

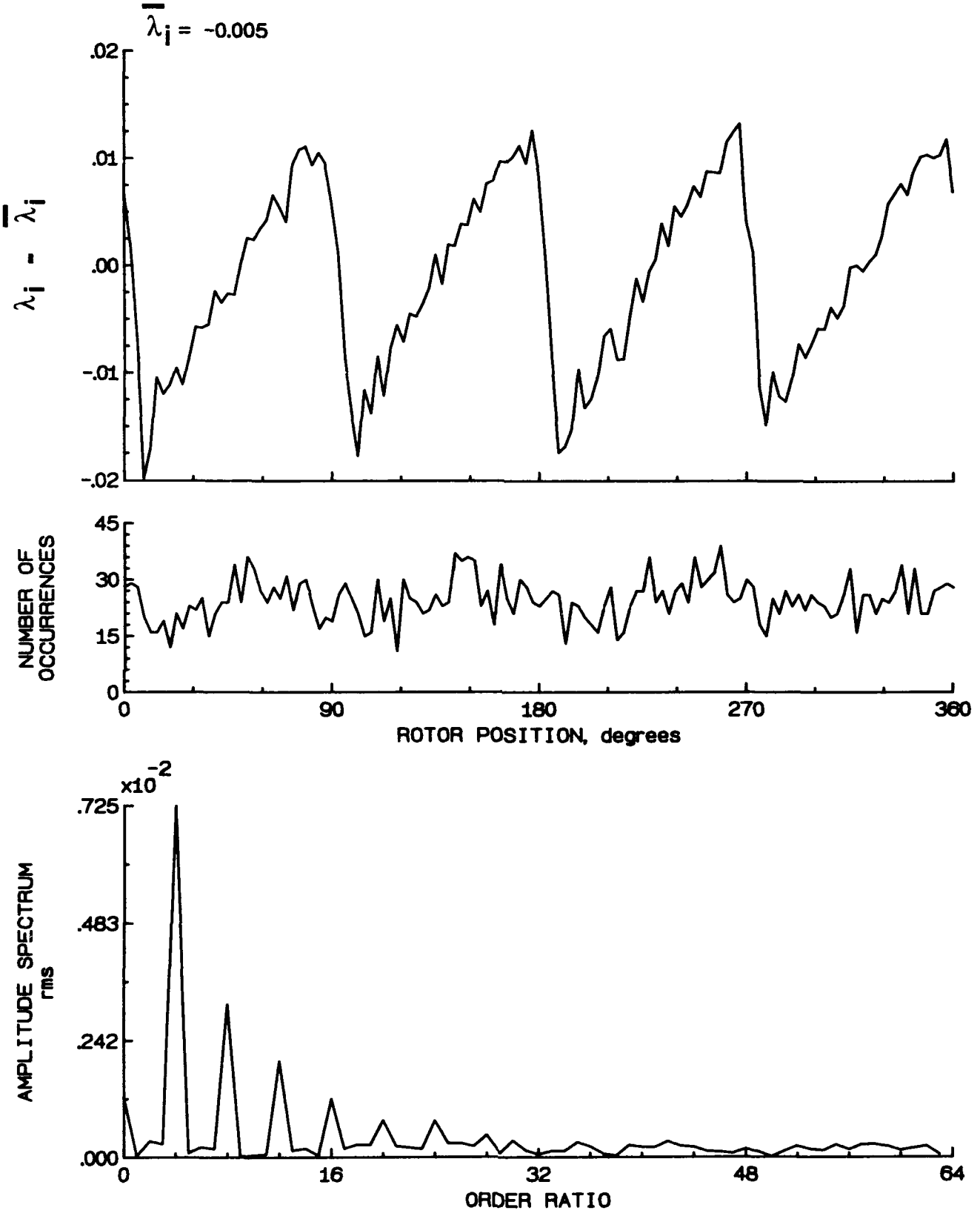

Figure 155.- Concluded.

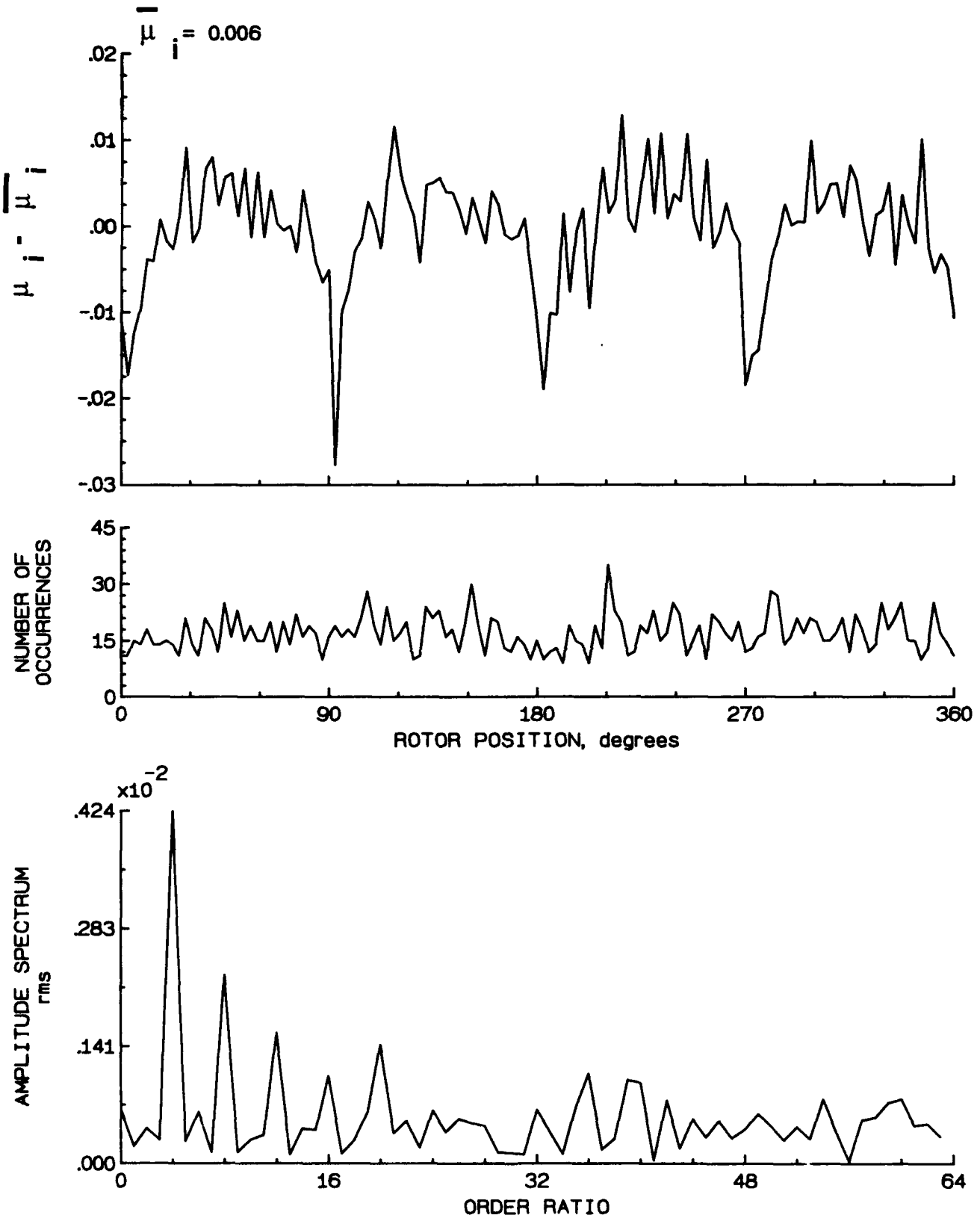

Figure 156.- Induced inflow velocity measured at 270 degrees and r/R of 0.94.

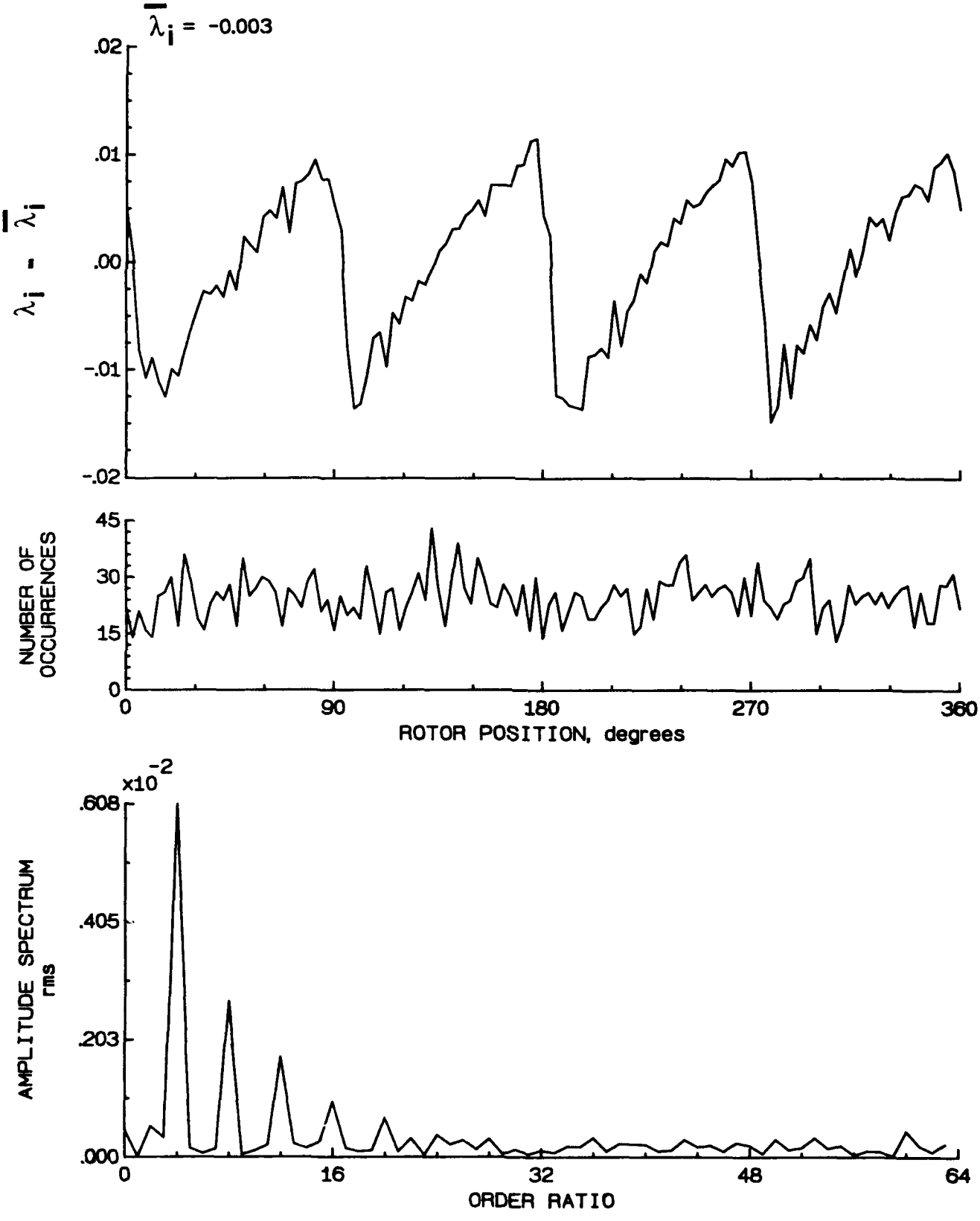

Figure 156.- Concluded.

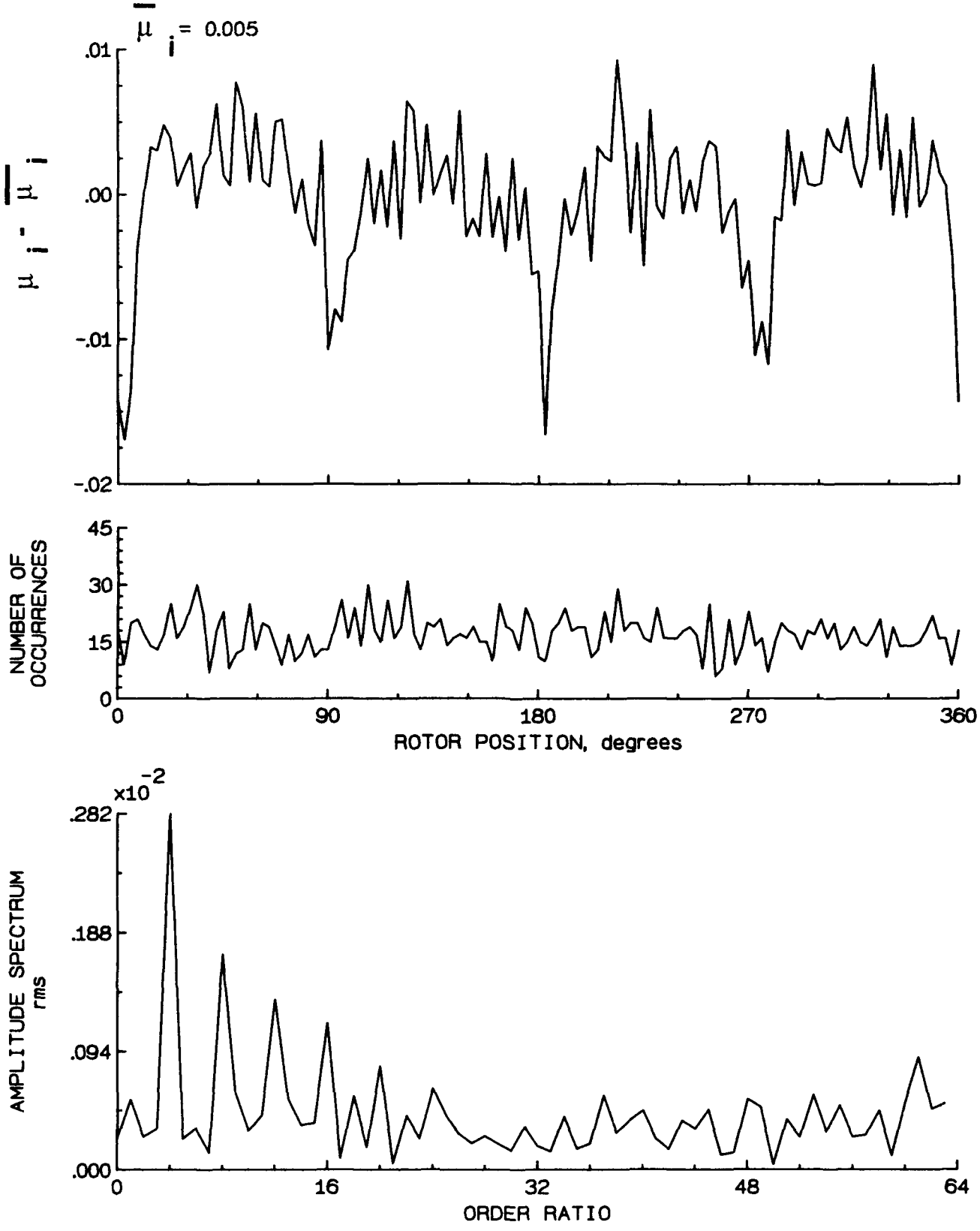

Figure 157.- Induced inflow velocity measured at 270 degrees and r/R of 0.98.

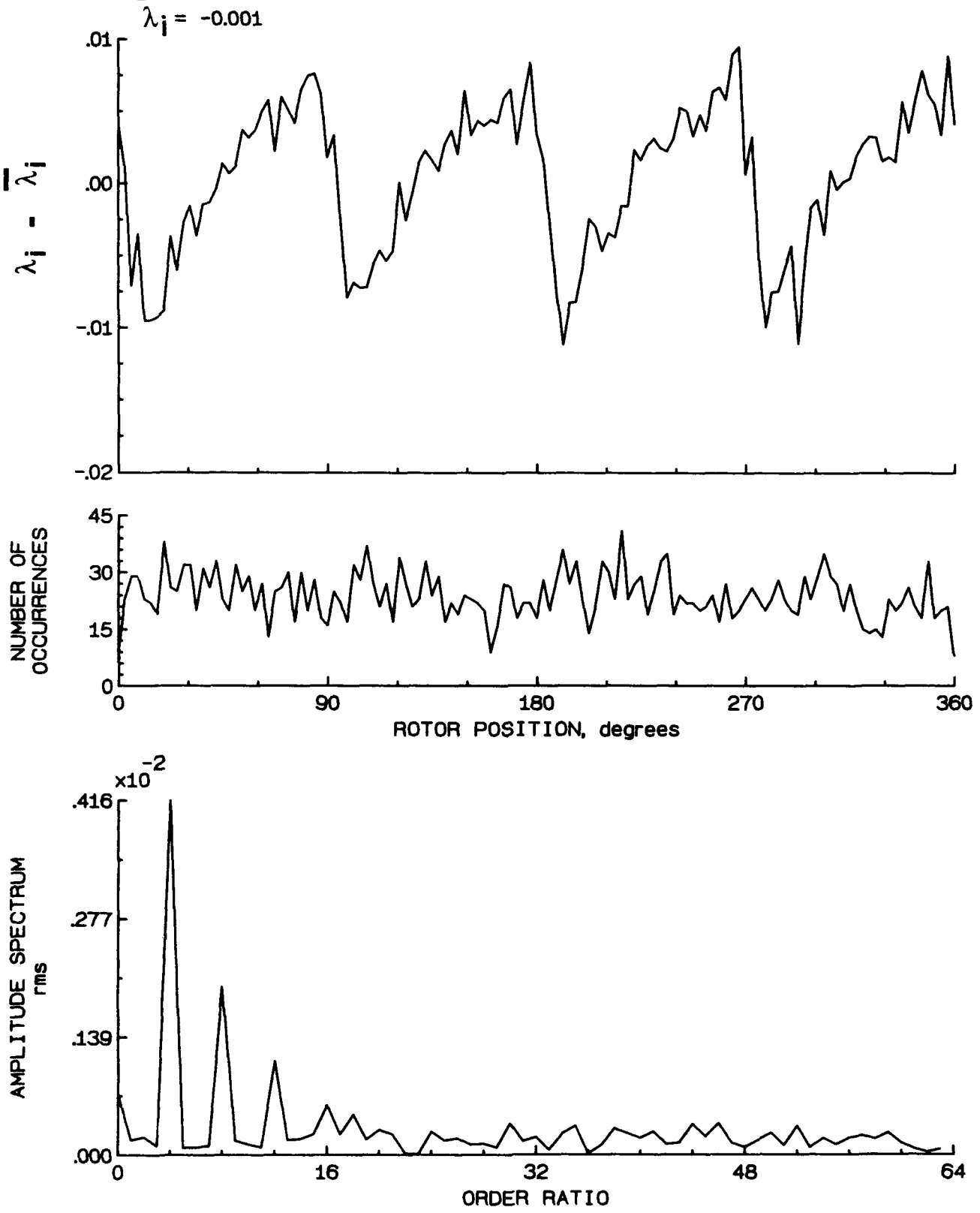

Figure 157.- Concluded.

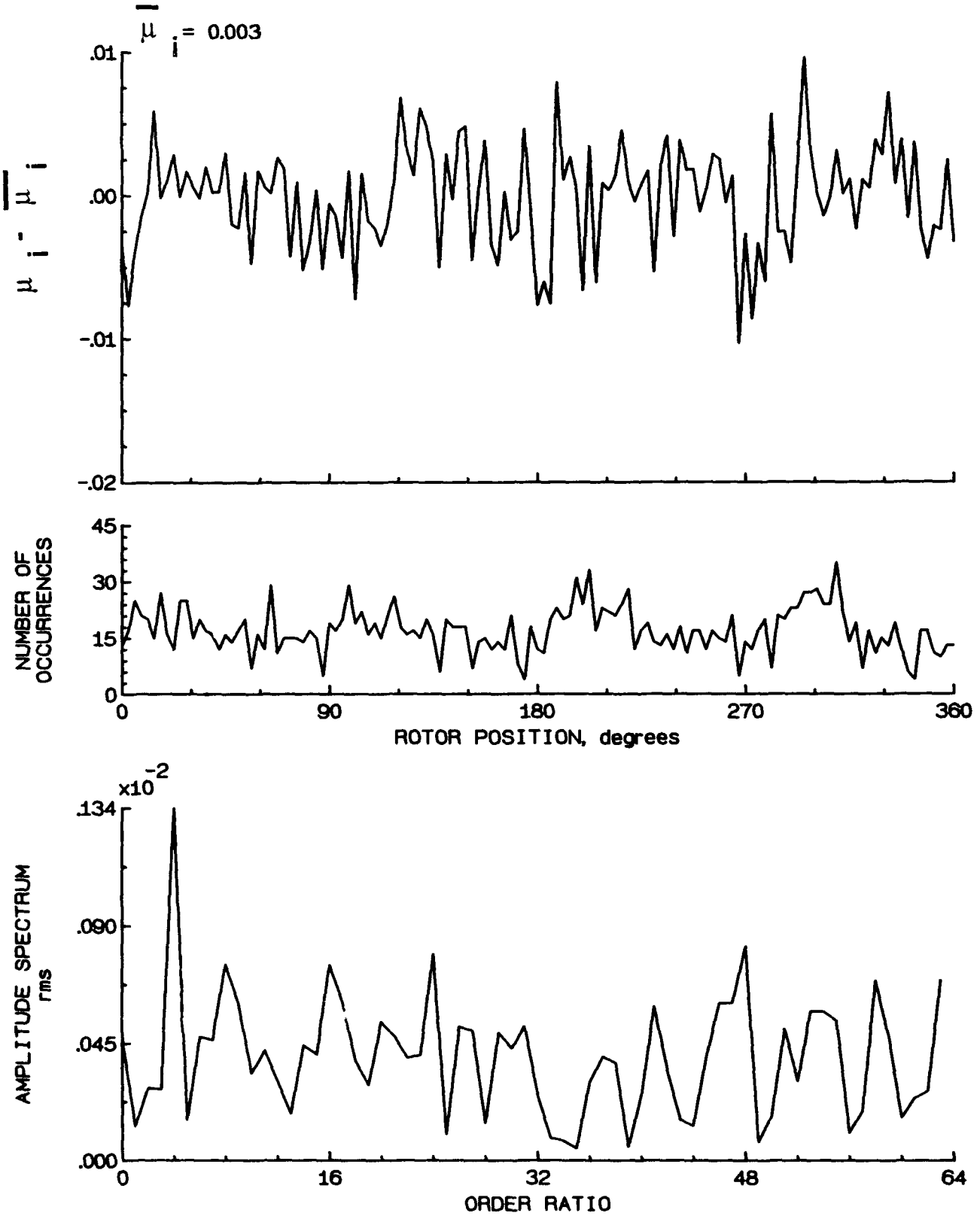

Figure 158.- Induced inflow velocity measured at 270 degrees and r/R of 1.02.

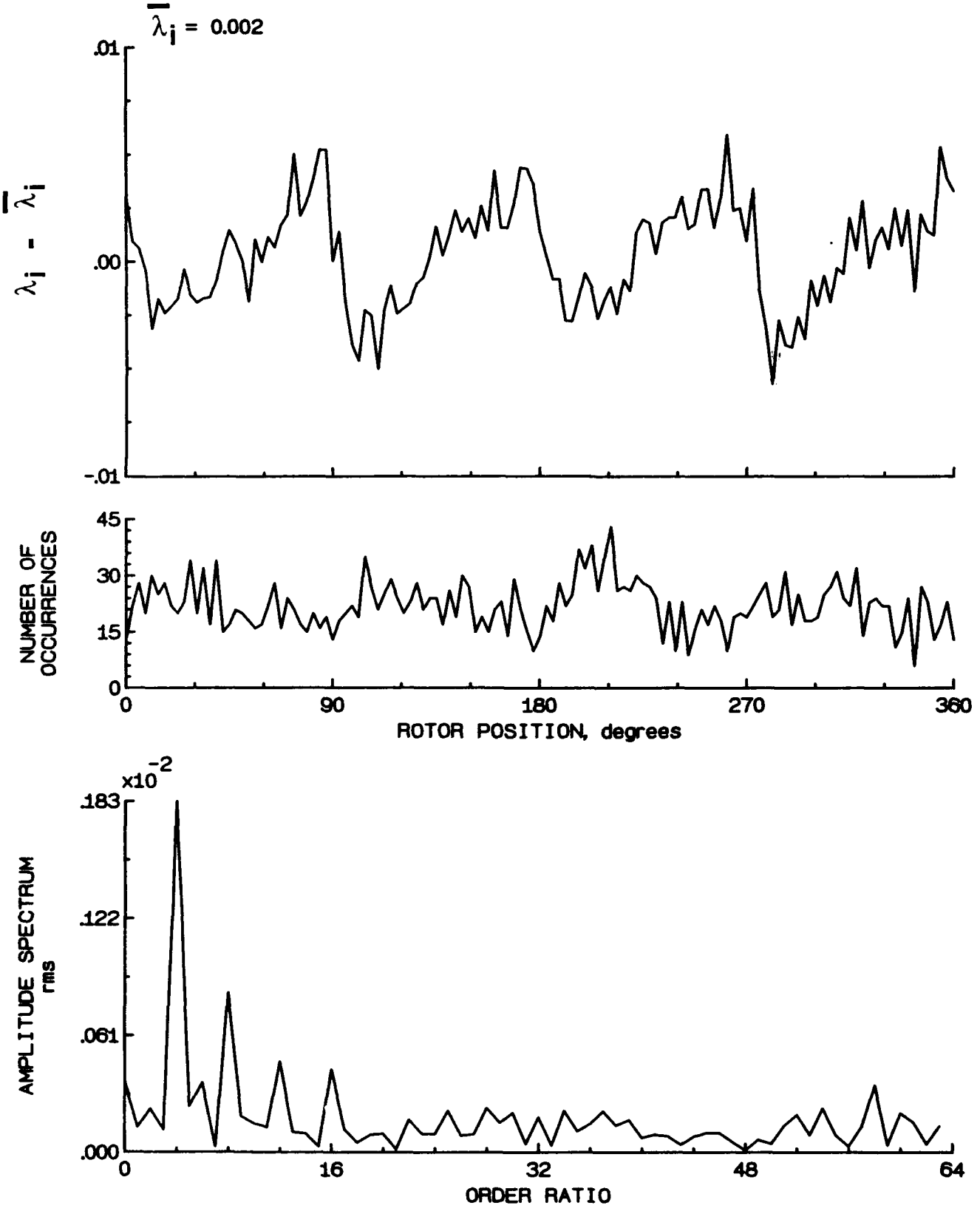

Figure 158.- Concluded.

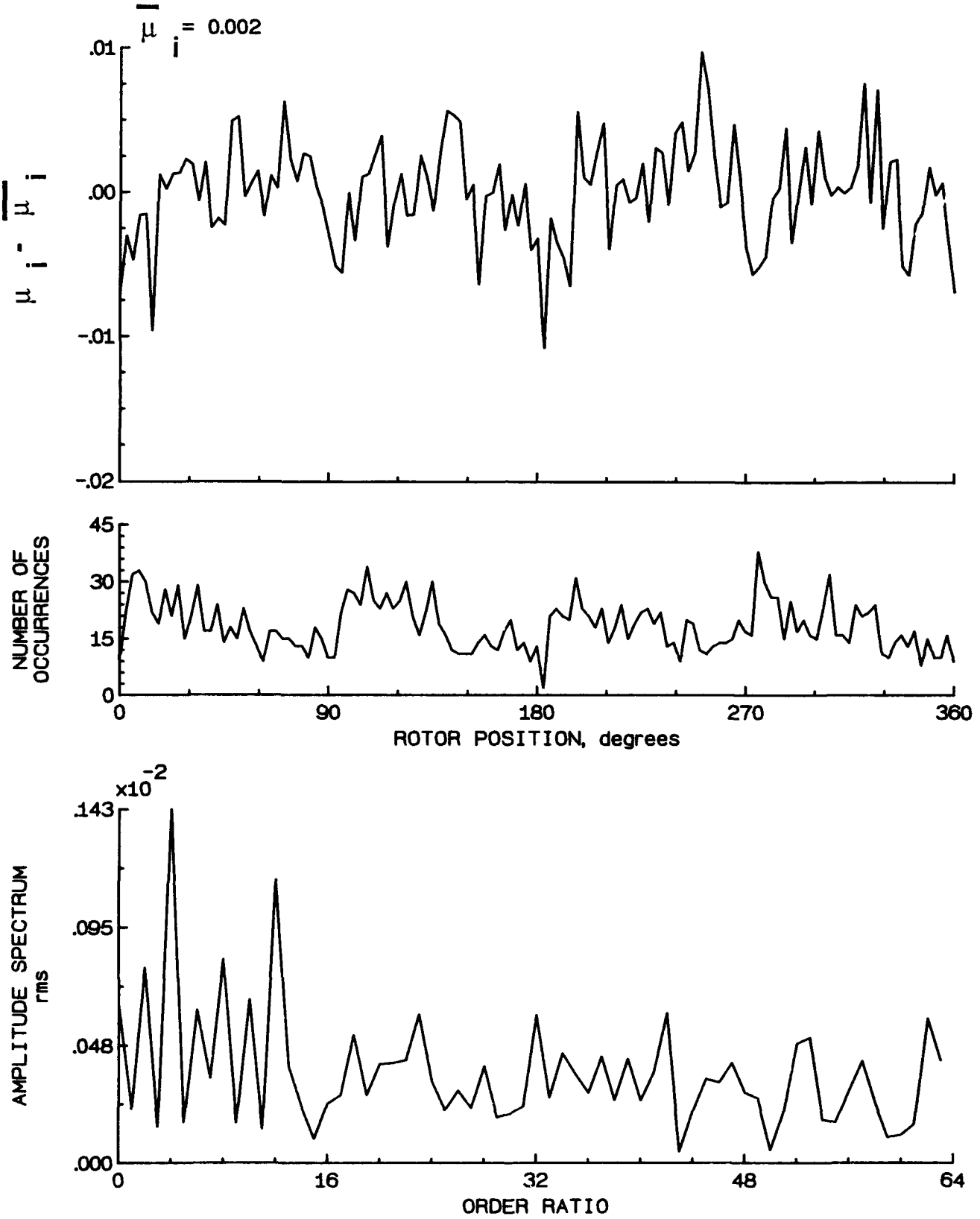

Figure 159.- Induced inflow velocity measured at 270 degrees and r/R of 1.04.

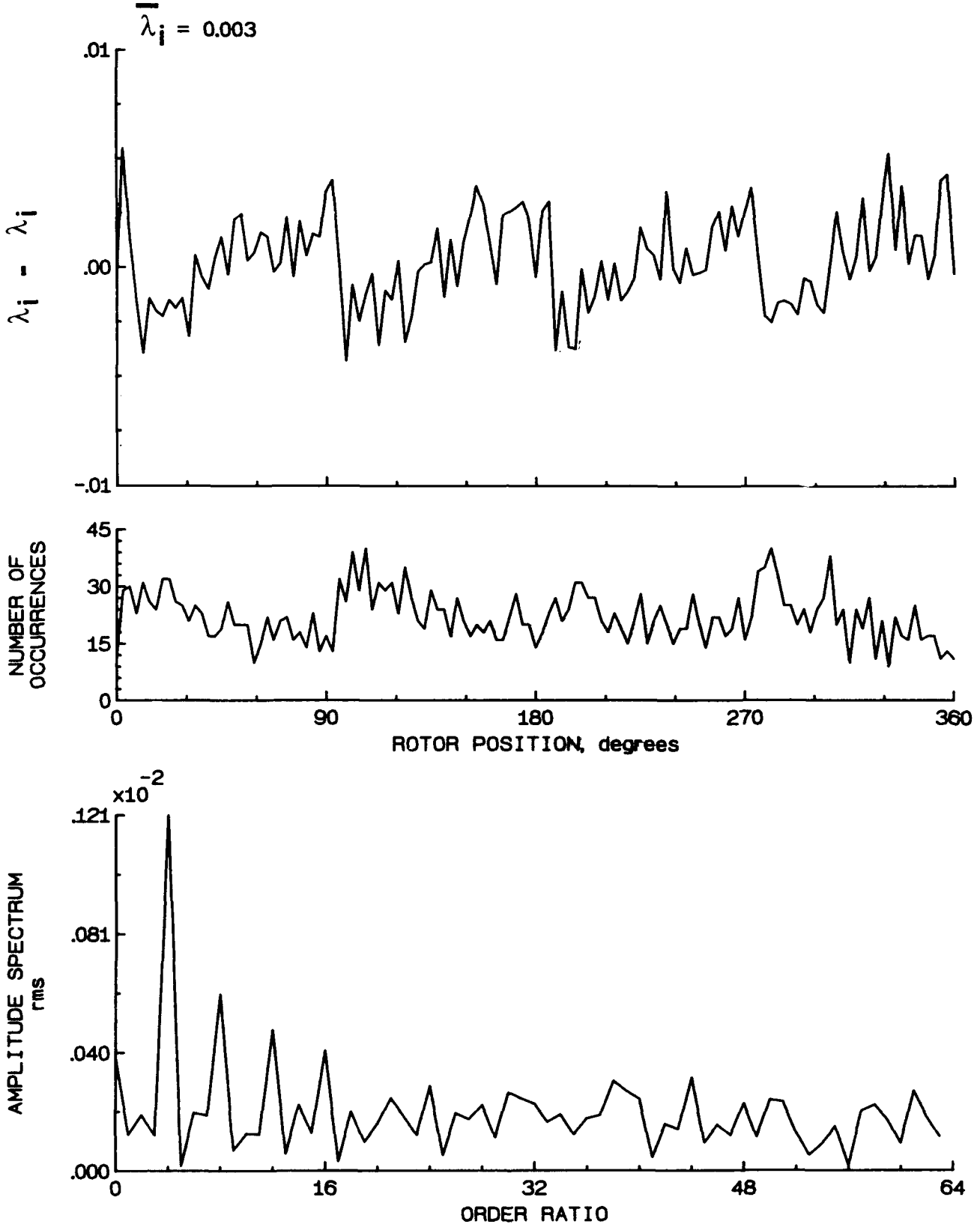

Figure 159.- Concluded.

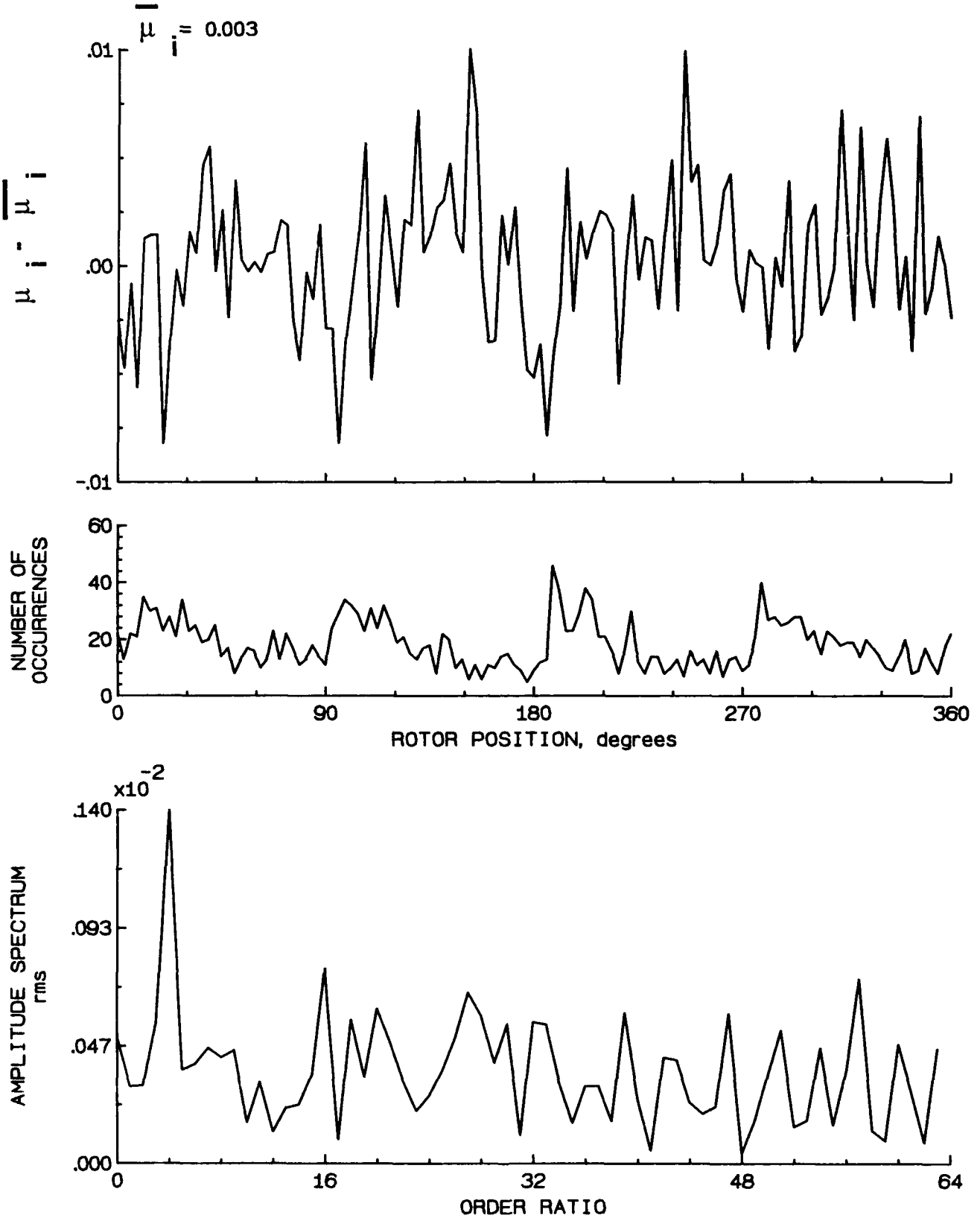

Figure 160.- Induced inflow velocity measured at 270 degrees and r/R of 1.10.

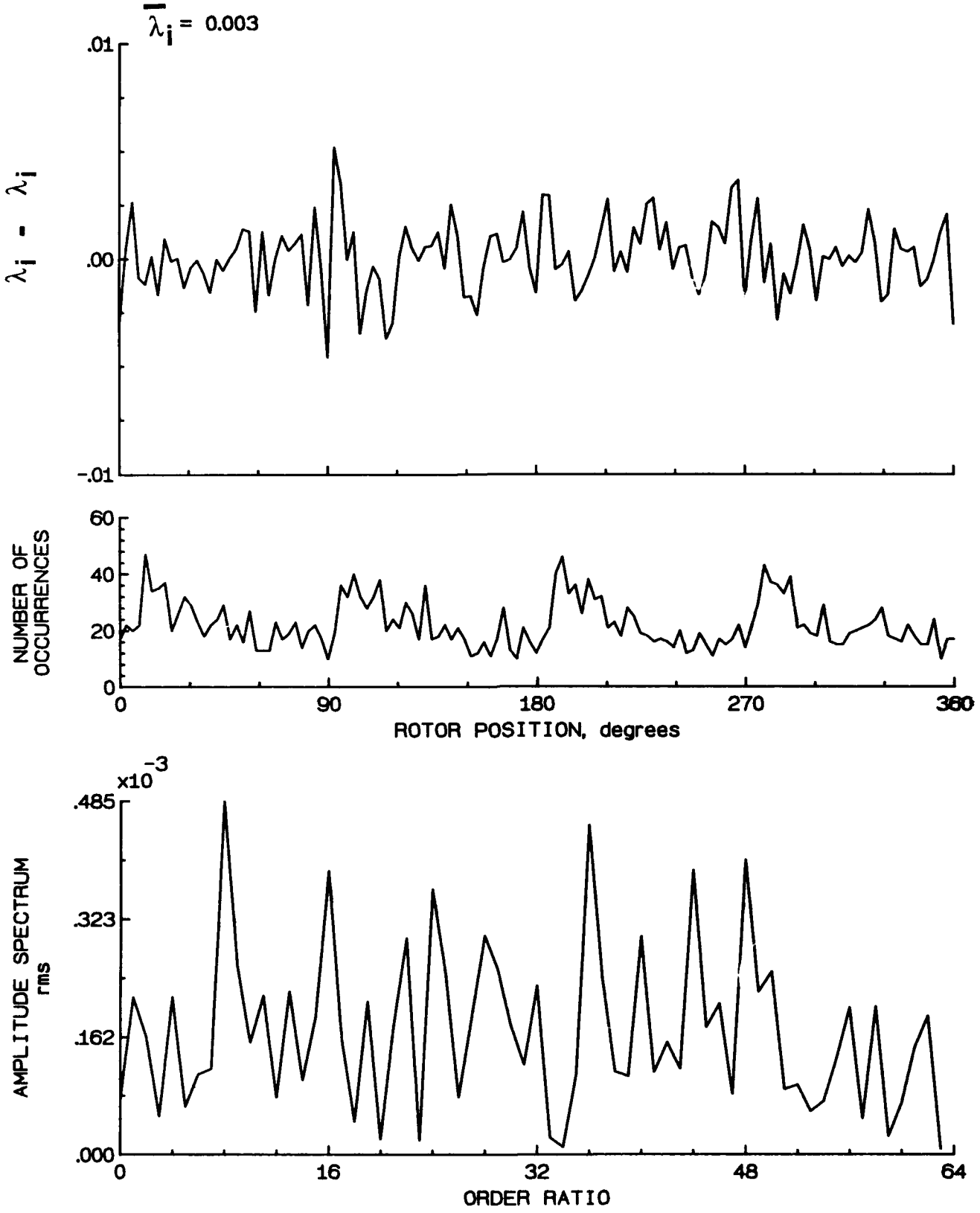

Figure 160.- Concluded.

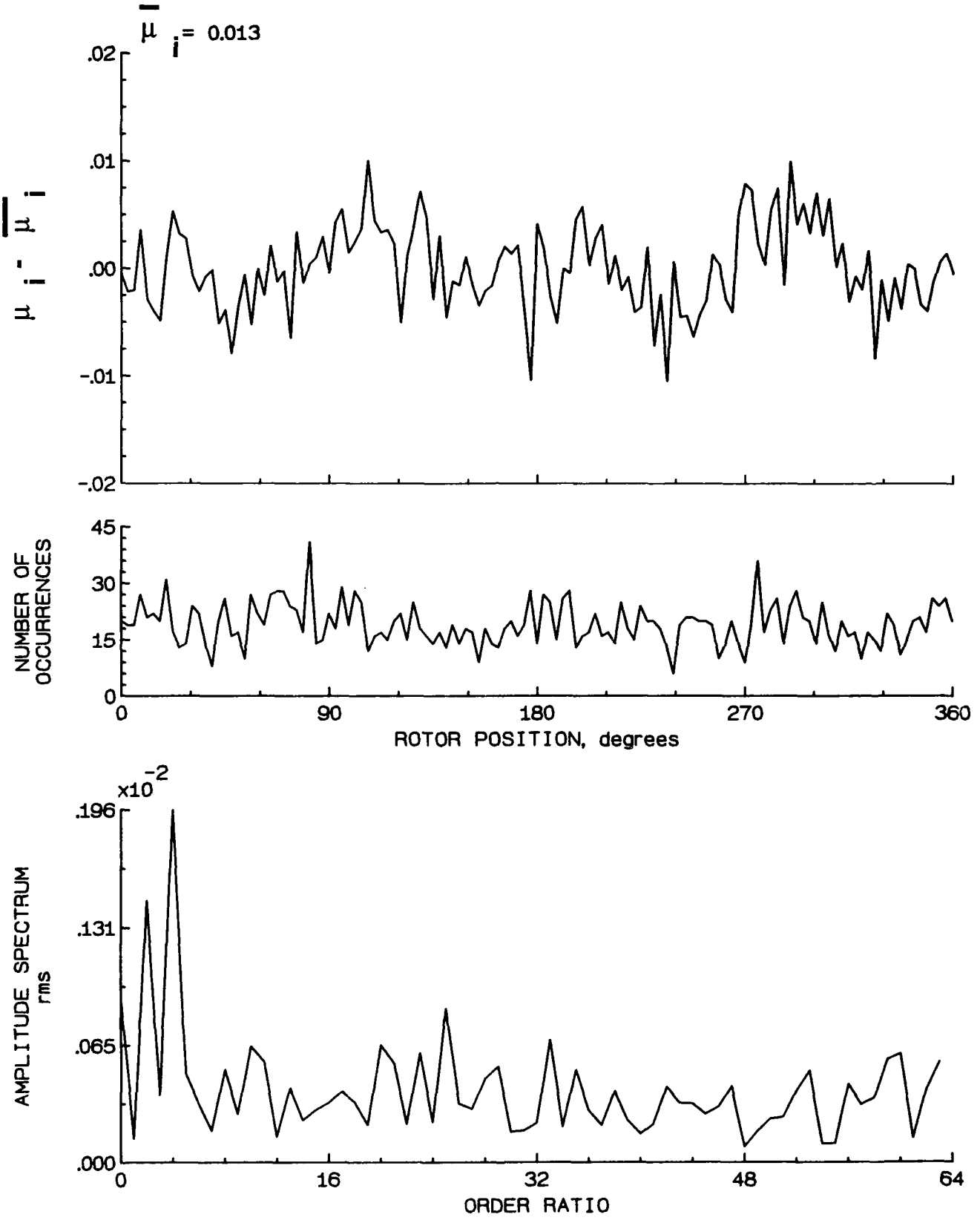

Figure 161.- Induced inflow velocity measured at 300 degrees and r/R of 0.20.

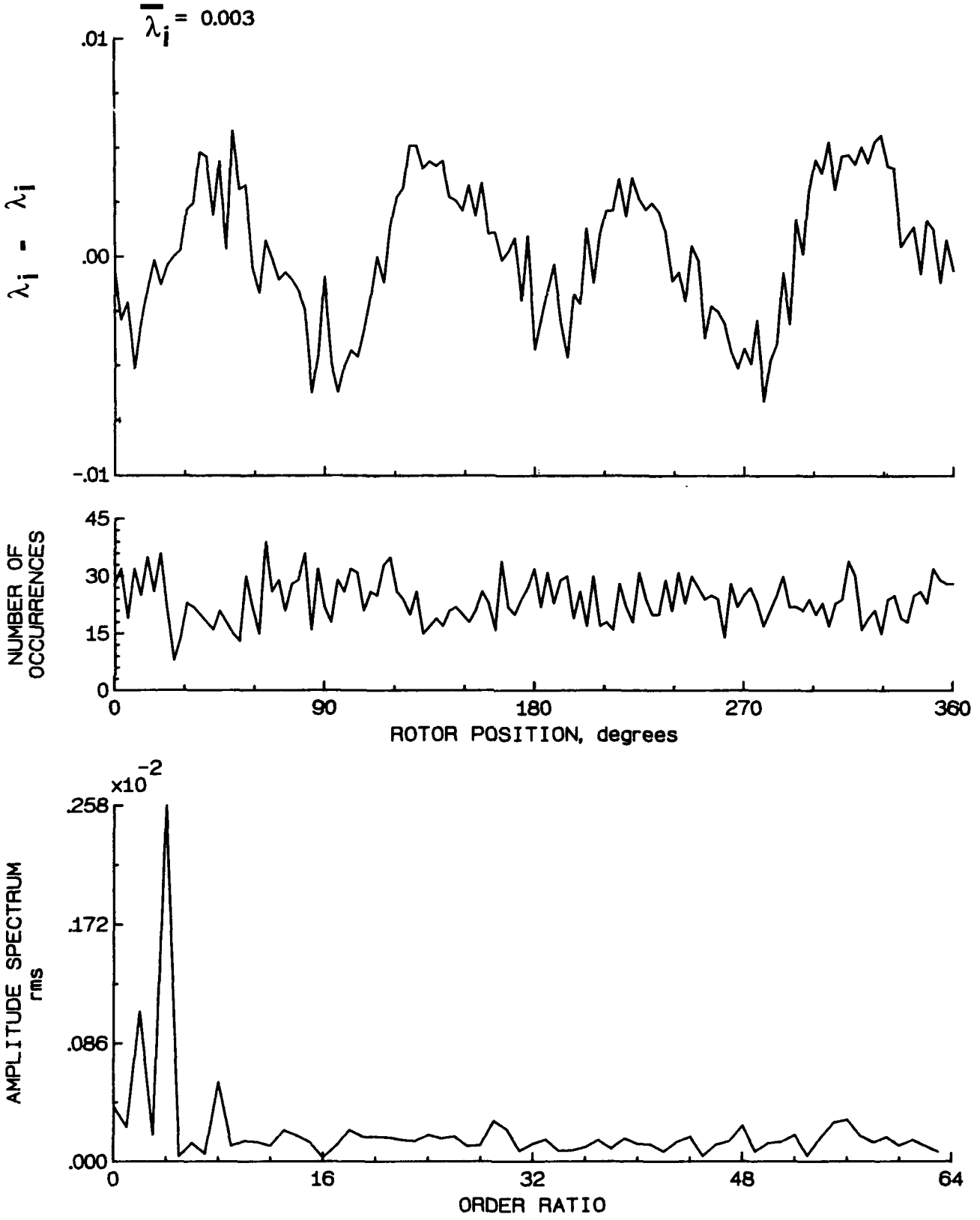

Figure 161.- Concluded.

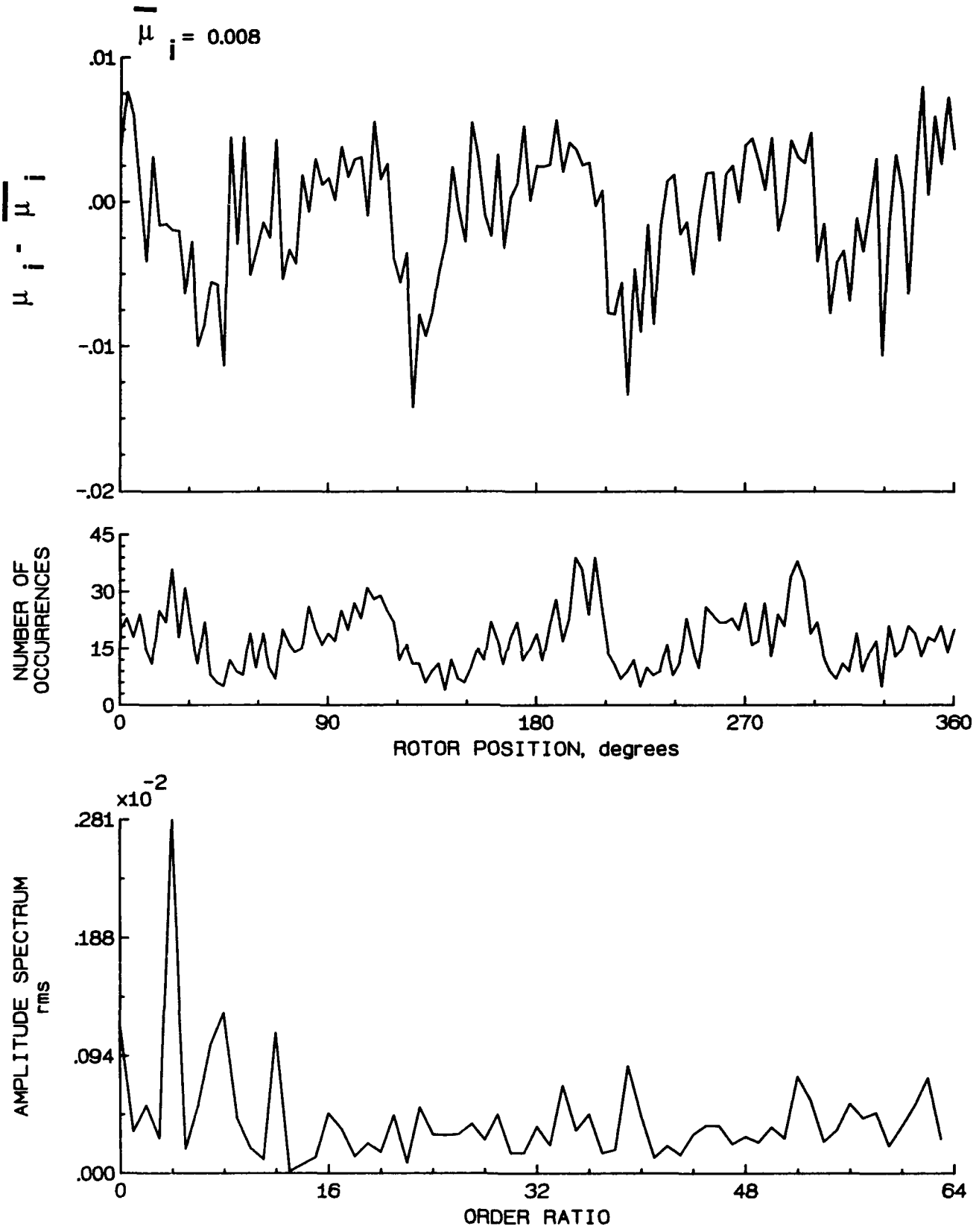

Figure 162.- Induced inflow velocity measured at 300 degrees and r/R of 0.40.

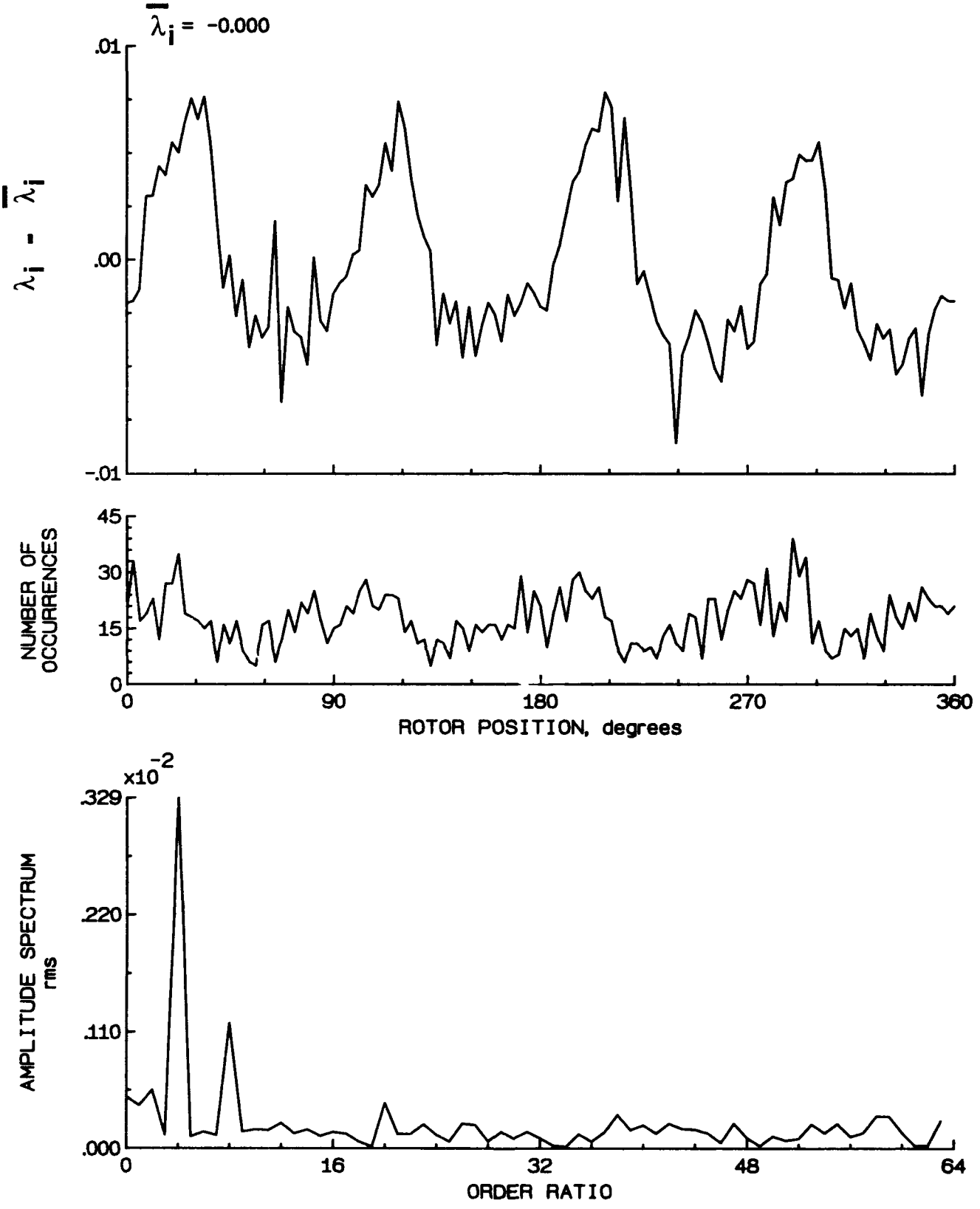

Figure 162.- Concluded.

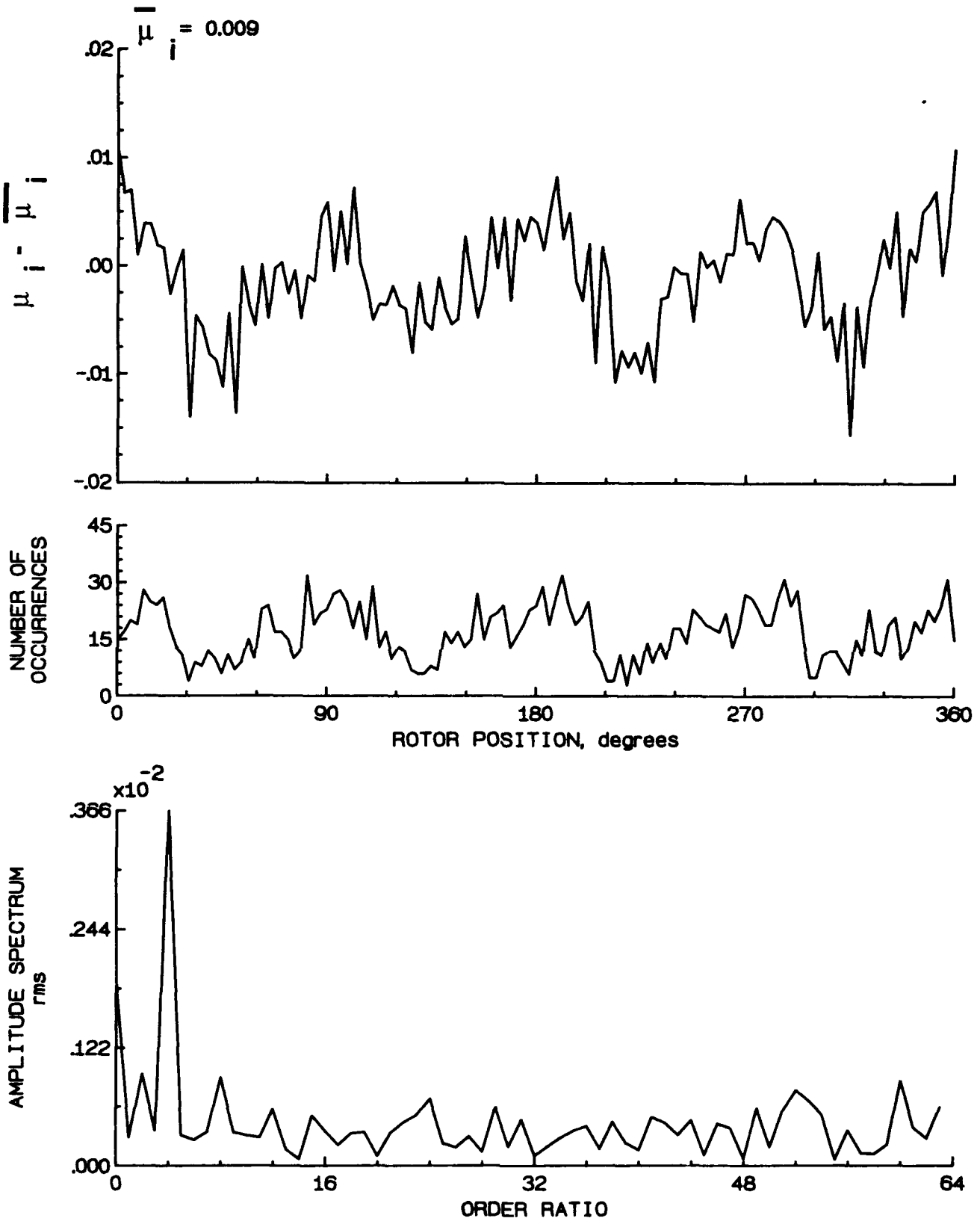

Figure 163.- Induced inflow velocity measured at 300 degrees and r/R of 0.50.

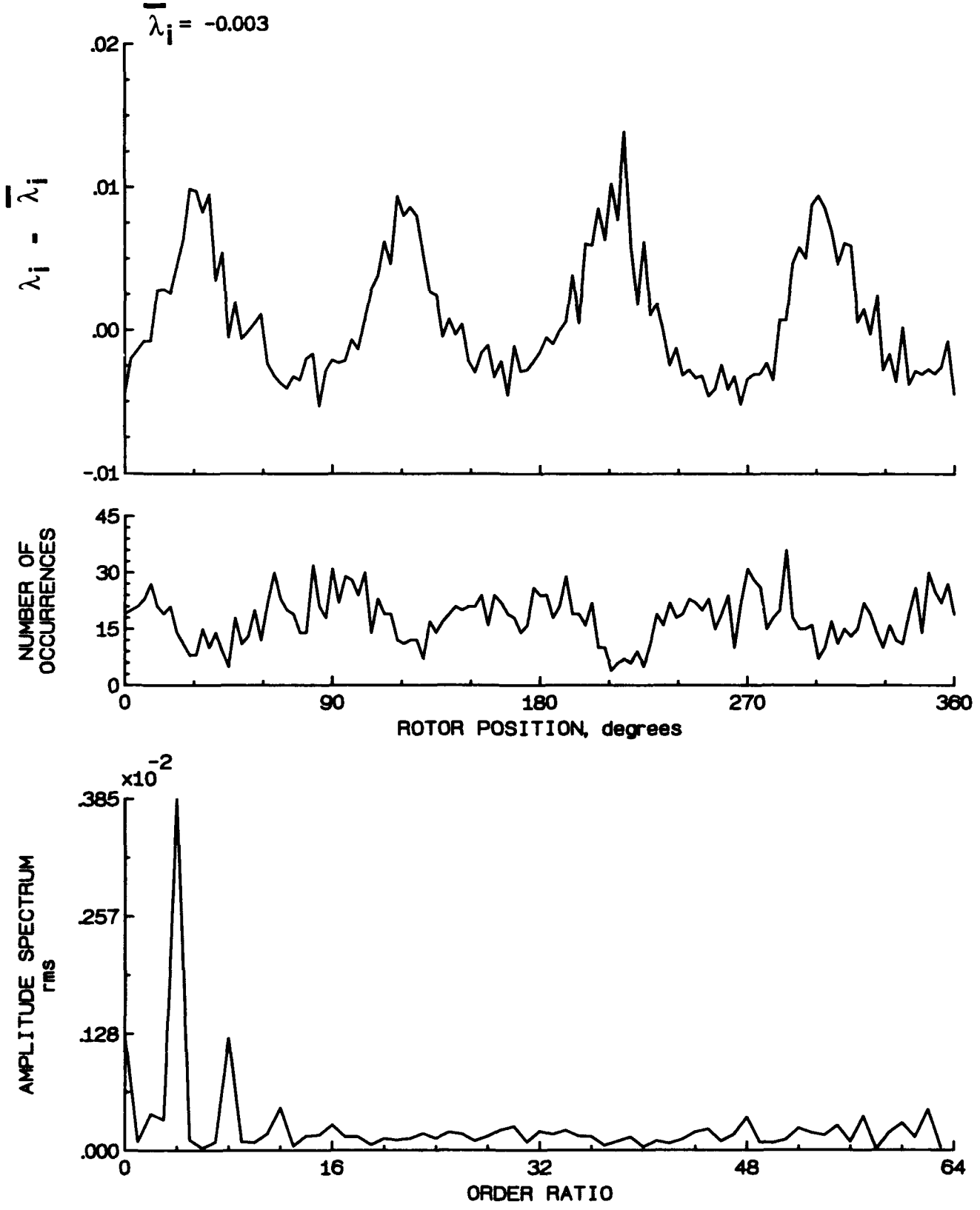

Figure 163.- Concluded.

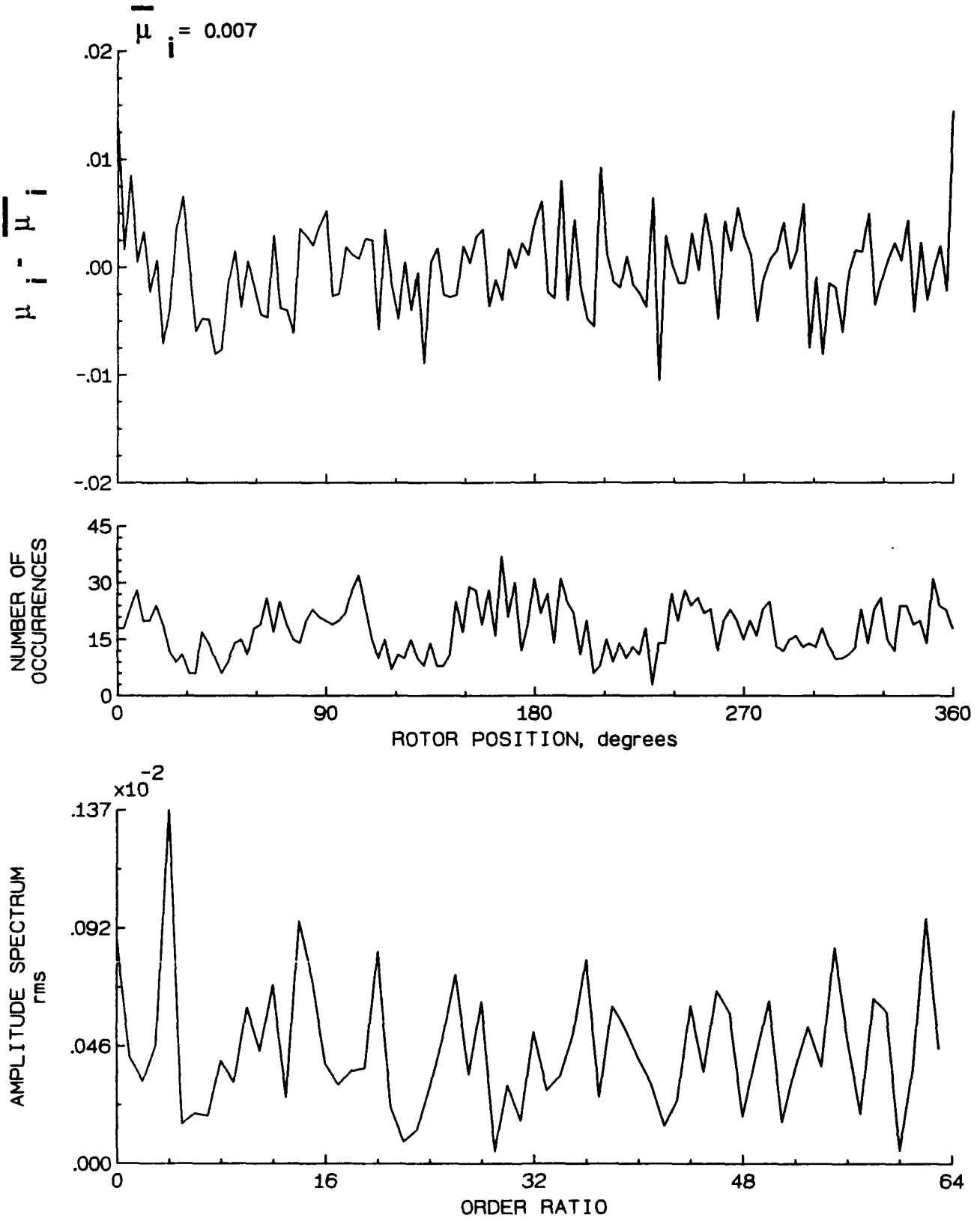

Figure 164.- Induced inflow velocity measured at 300 degrees and r/R of 0.60.

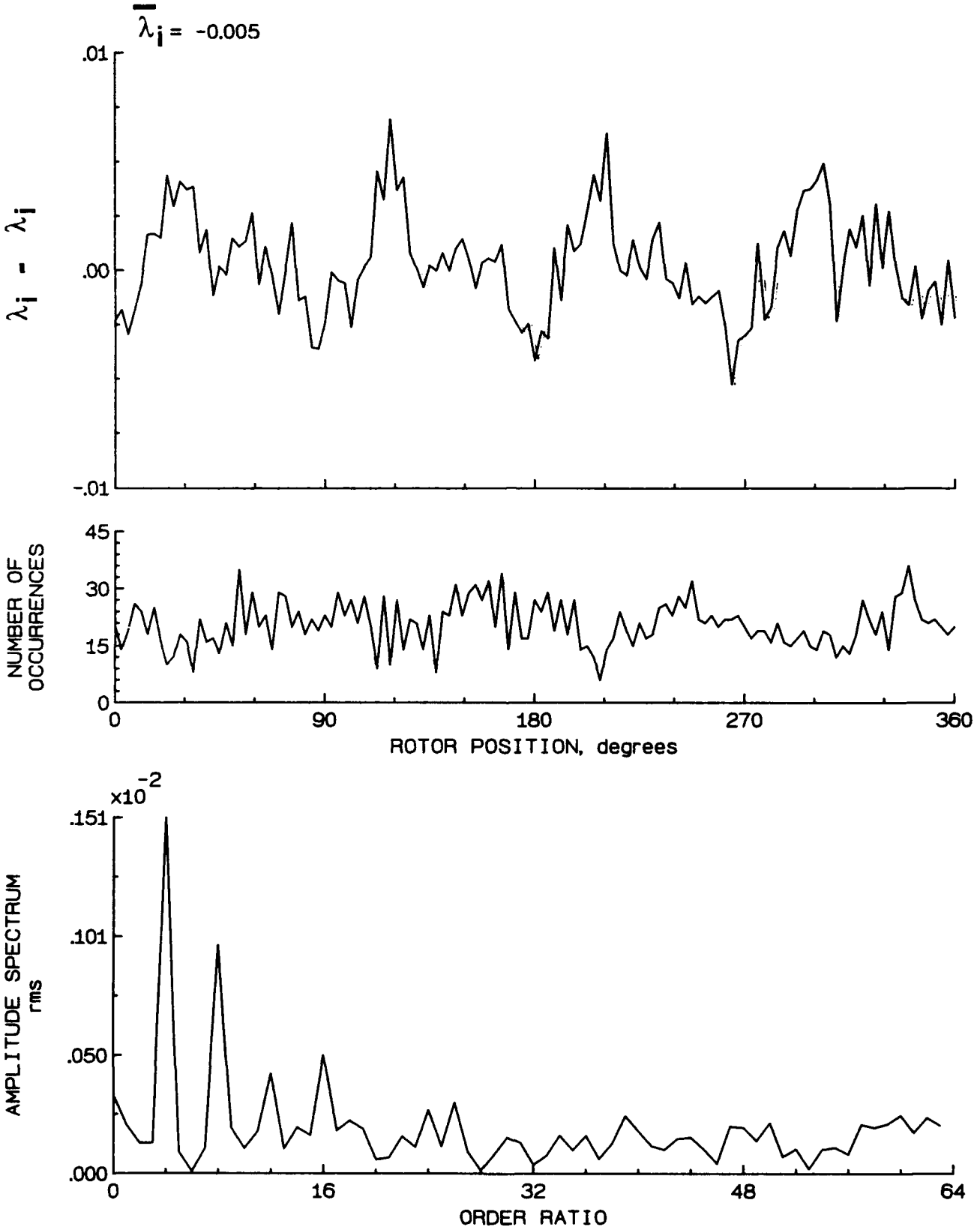

Figure 164.- Concluded.

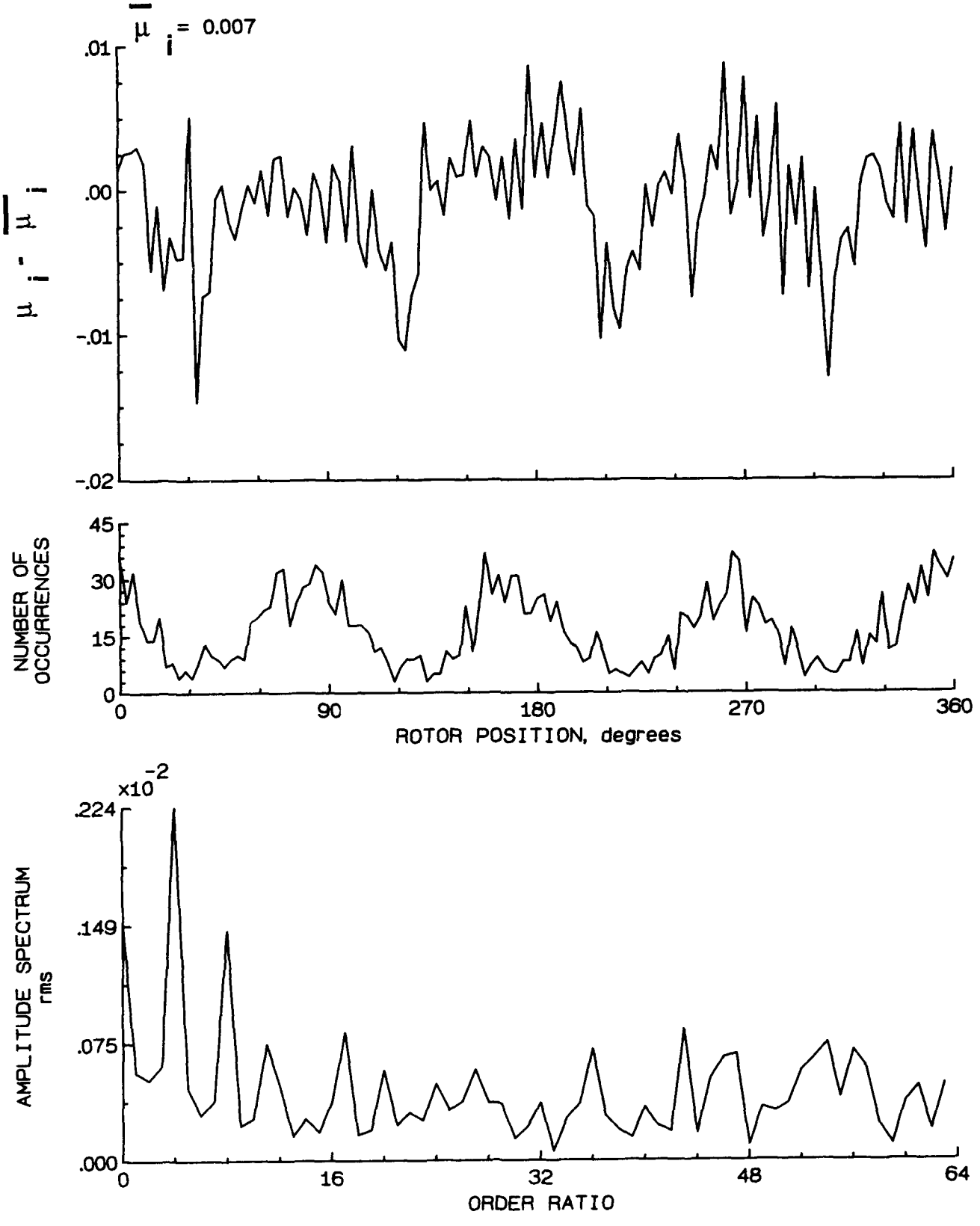

Figure 165.- Induced inflow velocity measured at 300 degrees and r/R of 0.70.

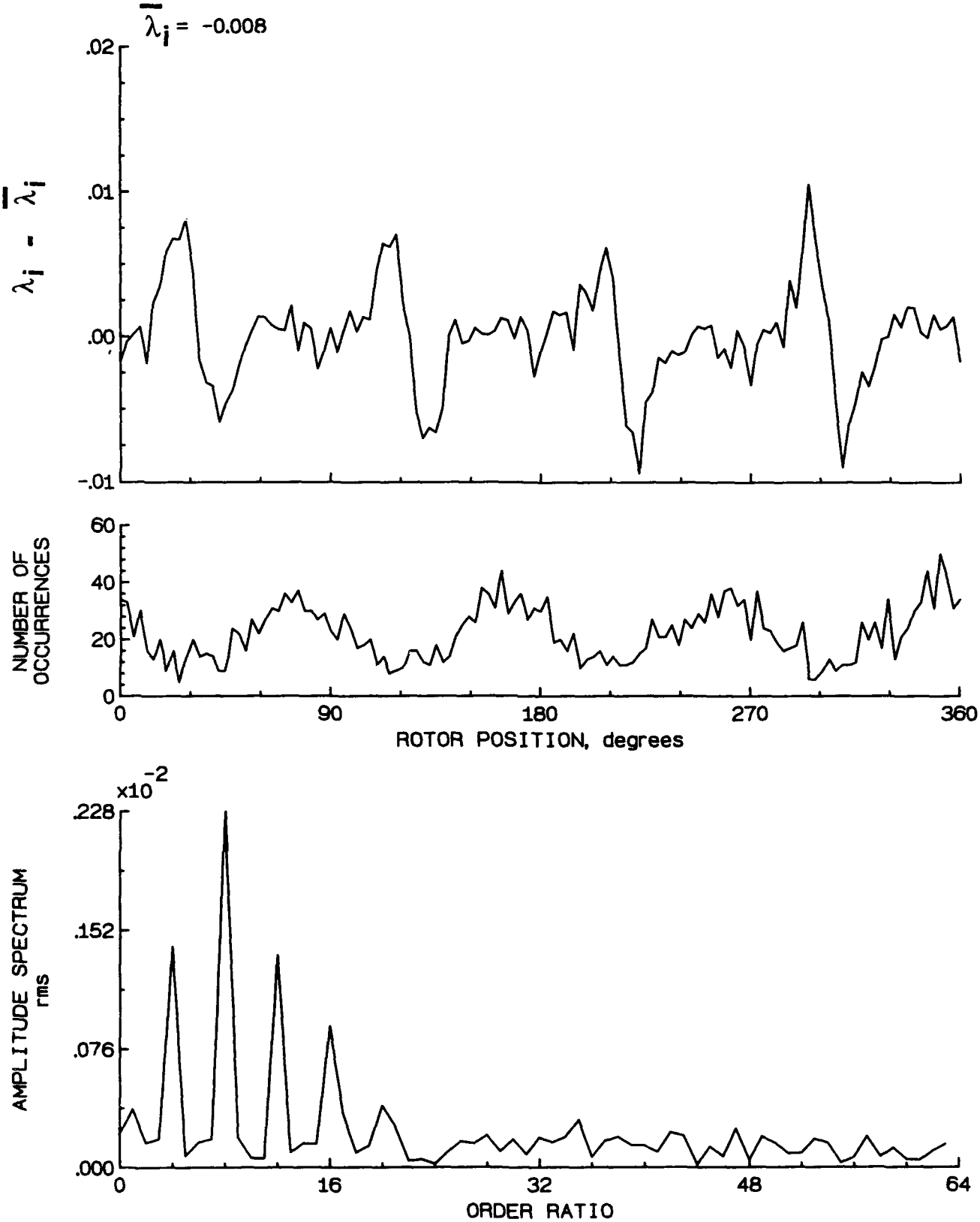

Figure 165.- Concluded.

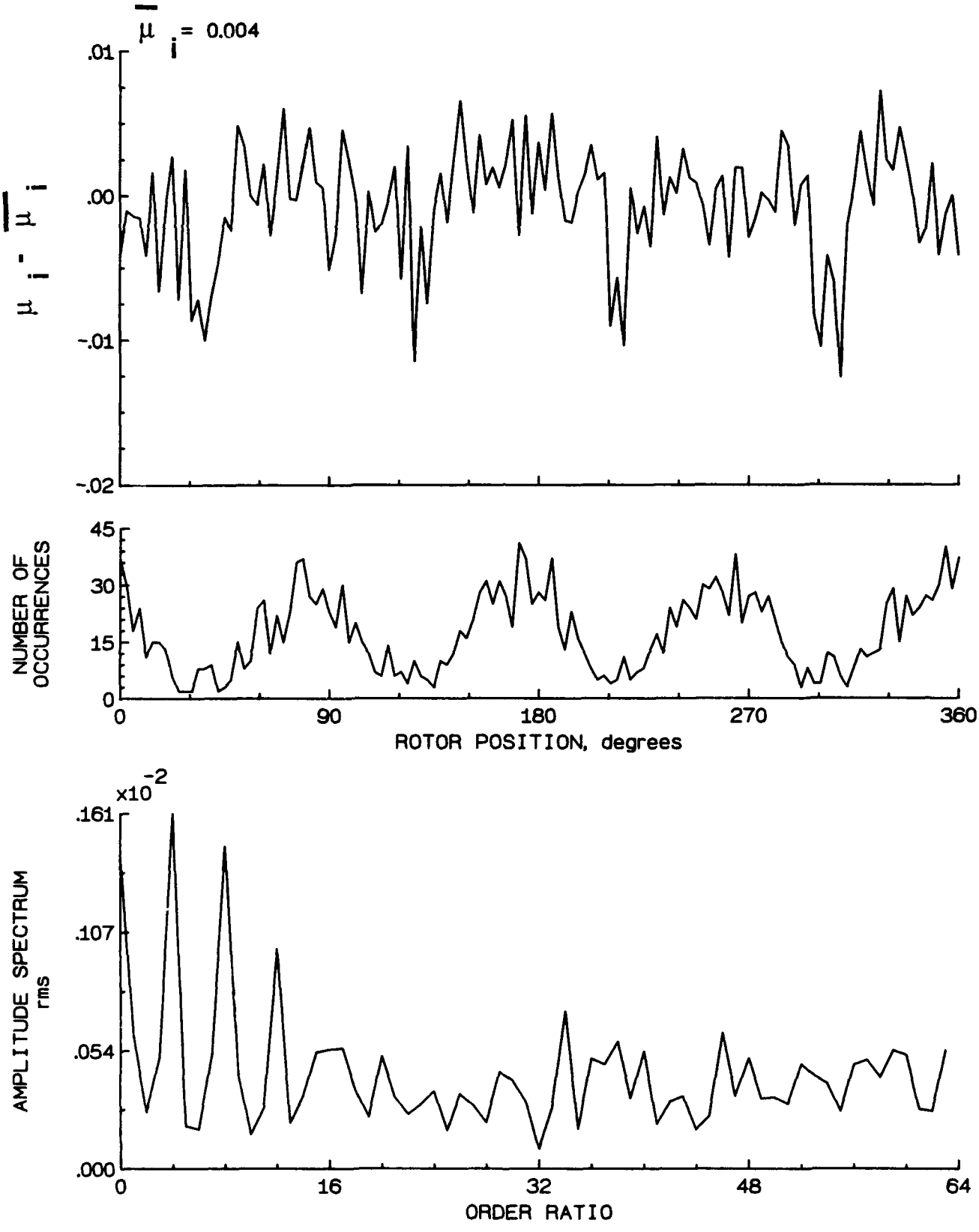

Figure 166.- Induced inflow velocity measured at 300 degrees and r/R of 0.74.

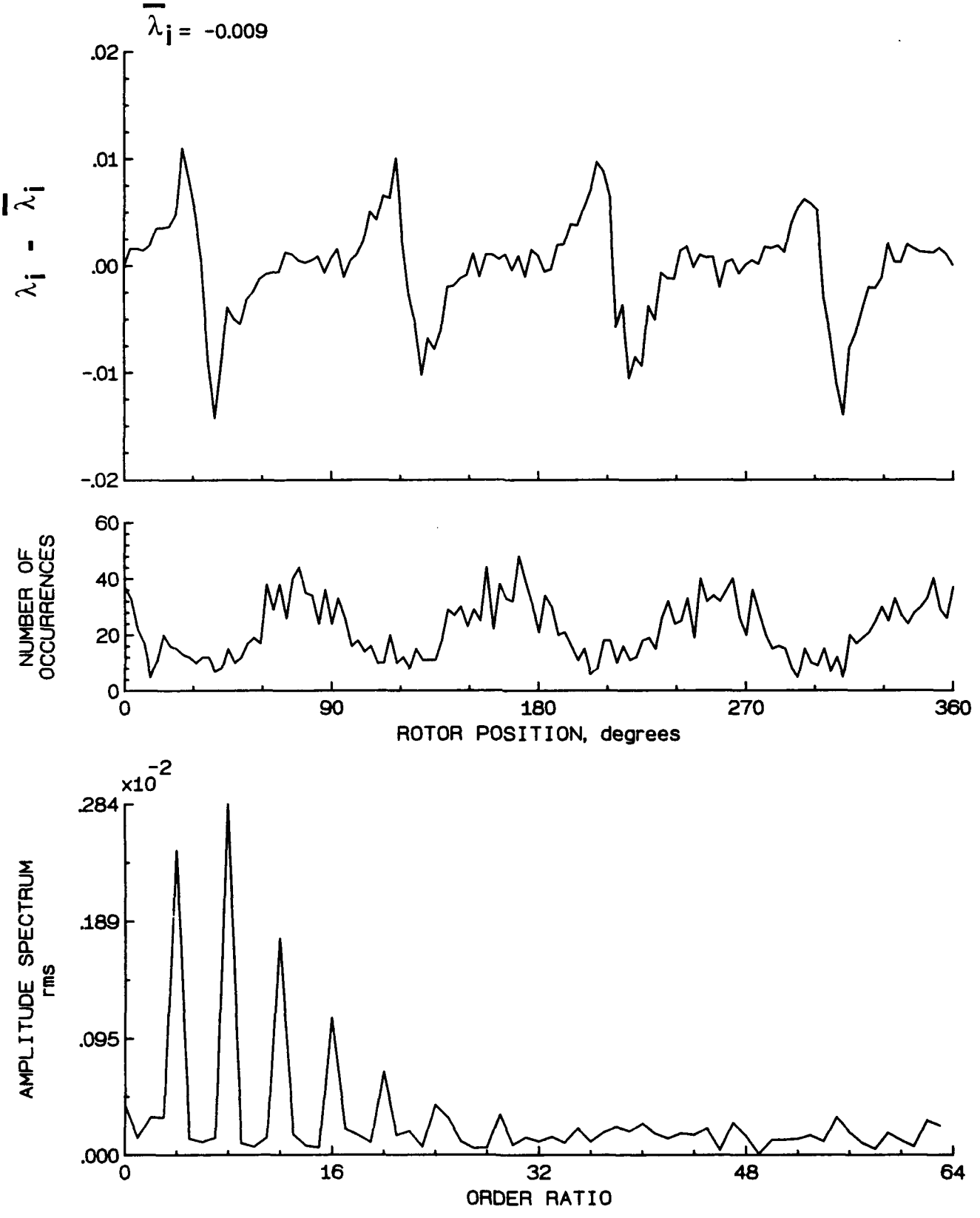

Figure 166.- Concluded.

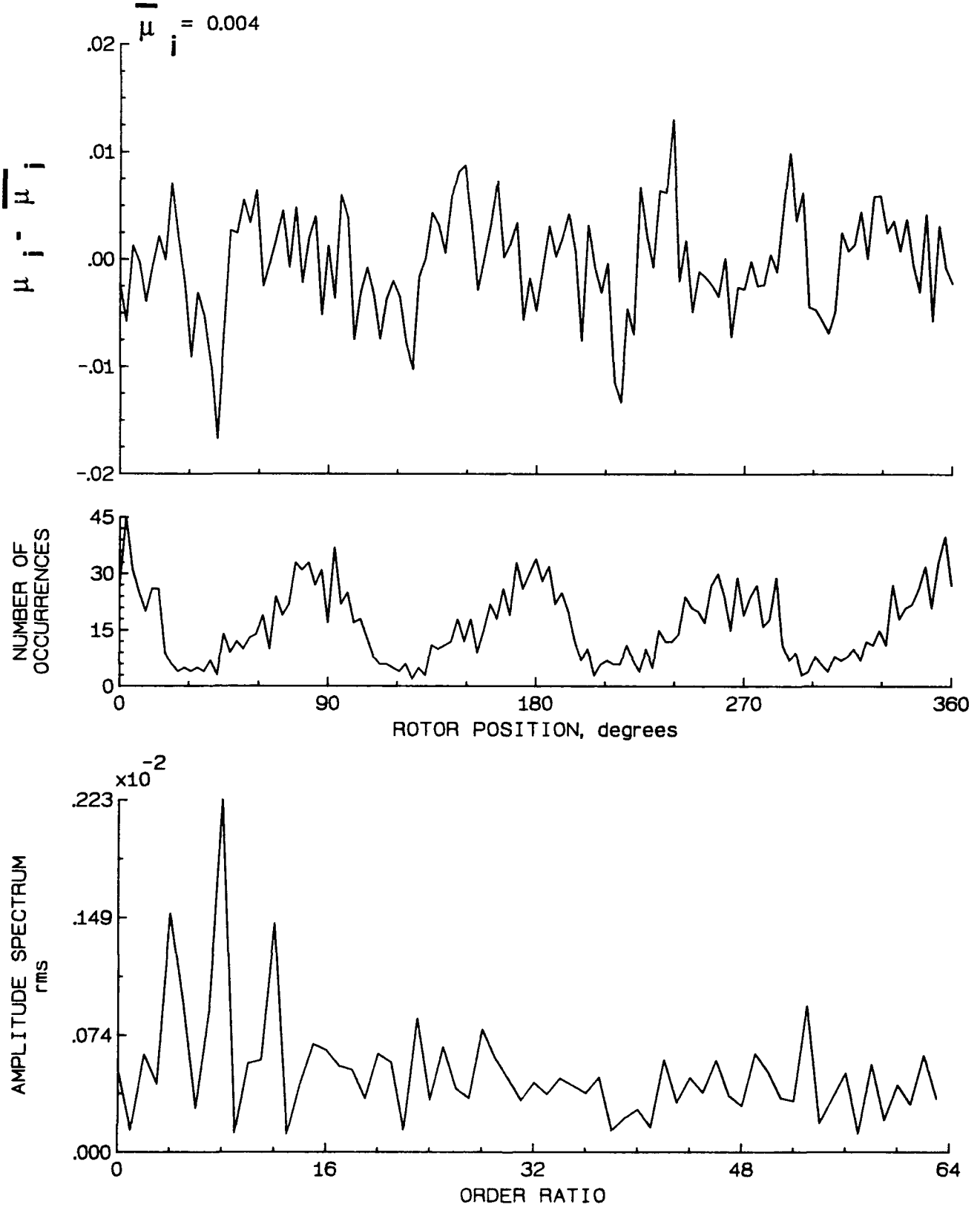

Figure 167.- Induced inflow velocity measured at 300 degrees and r/R of 0.78.

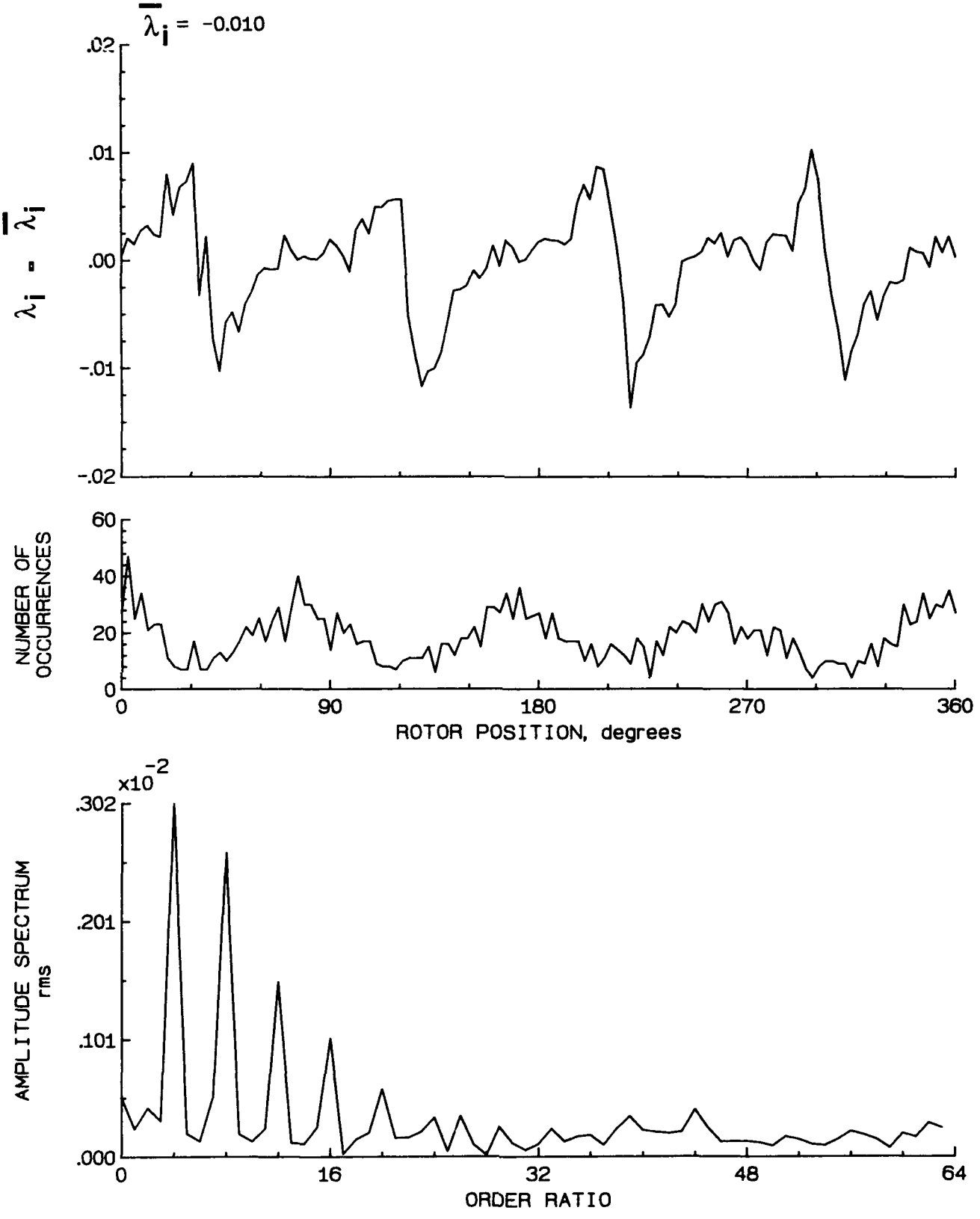

Figure 167.- Concluded.

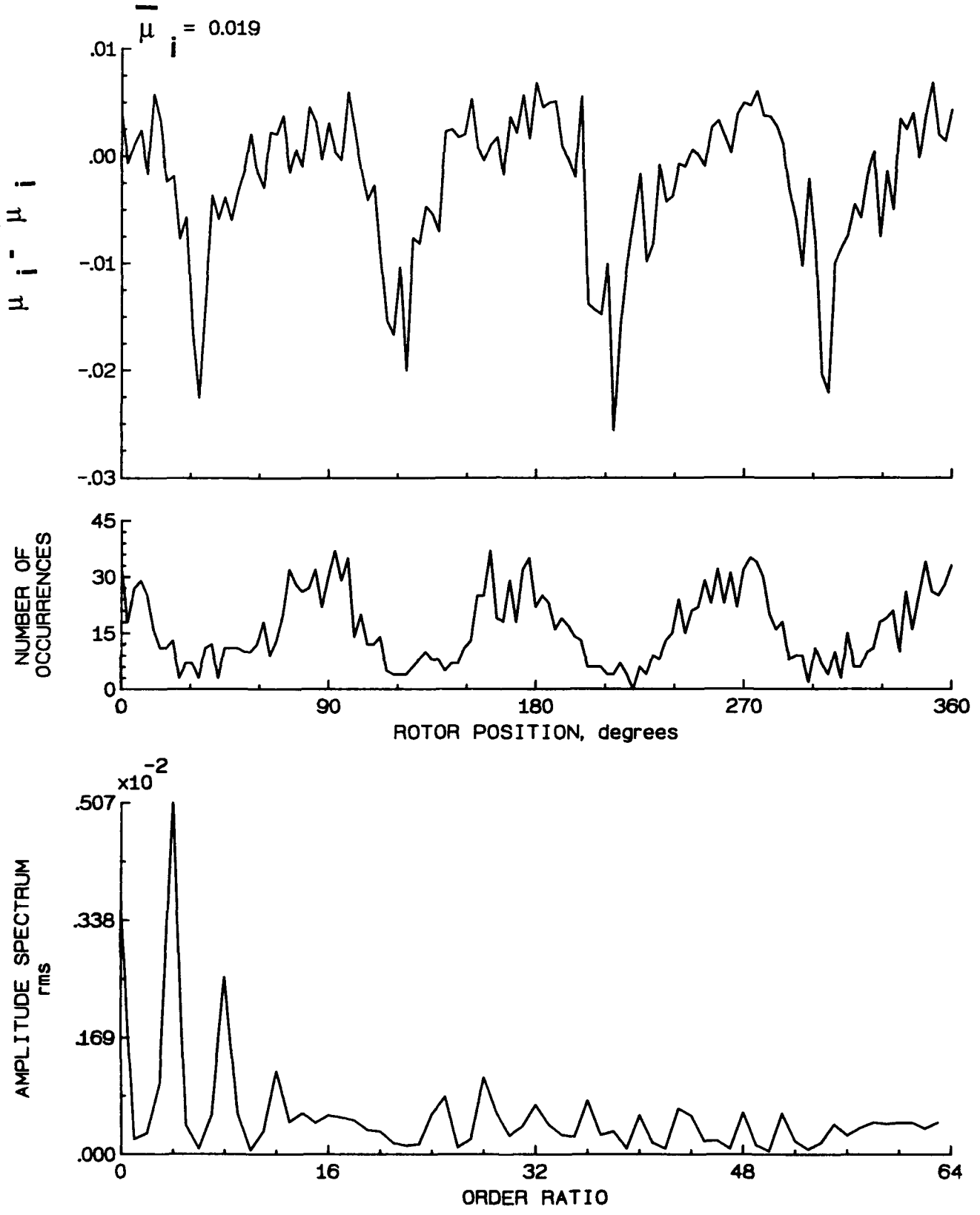

Figure 168.- Induced inflow velocity measured at 300 degrees and r/R of 0.82.

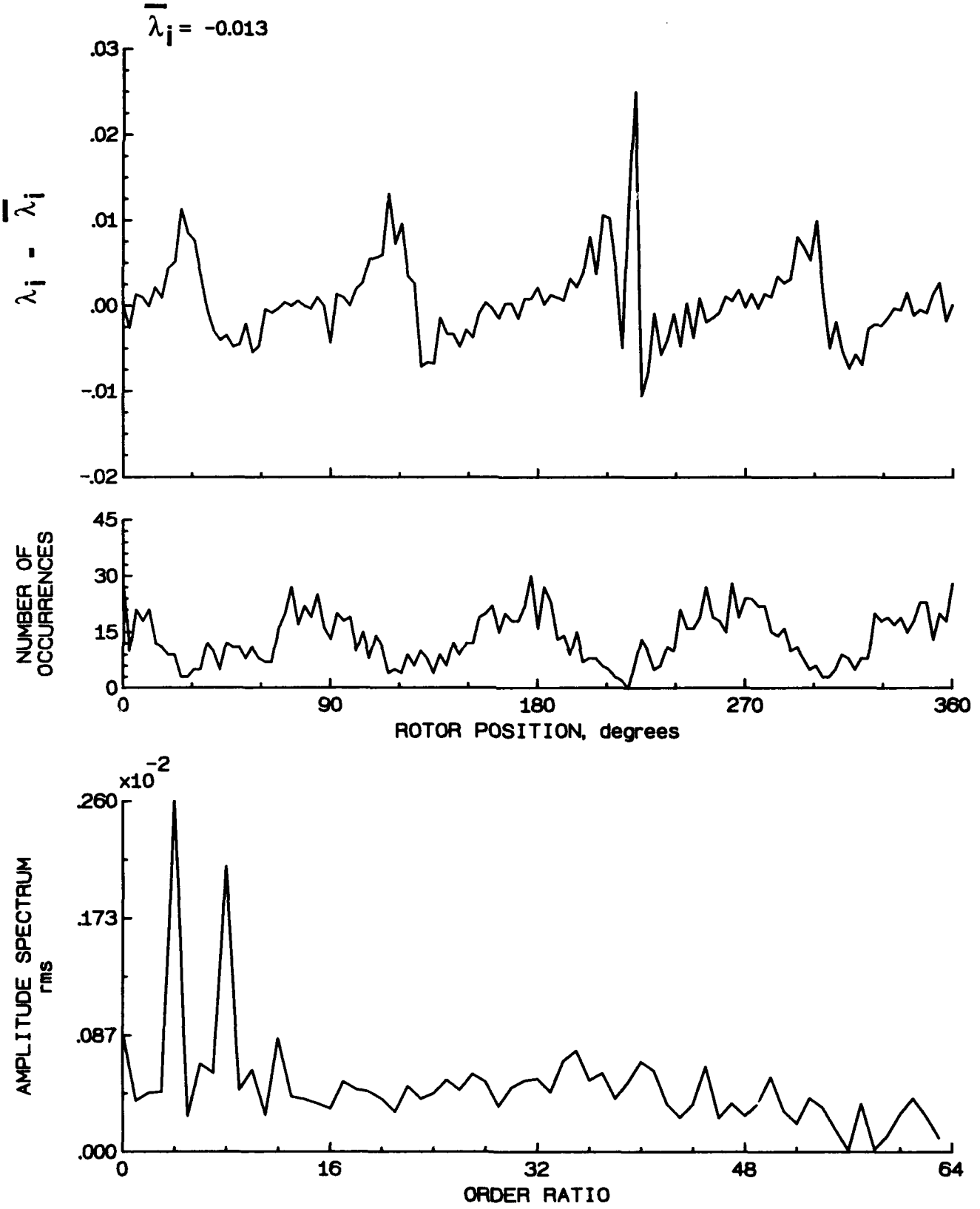

Figure 168.- Concluded.

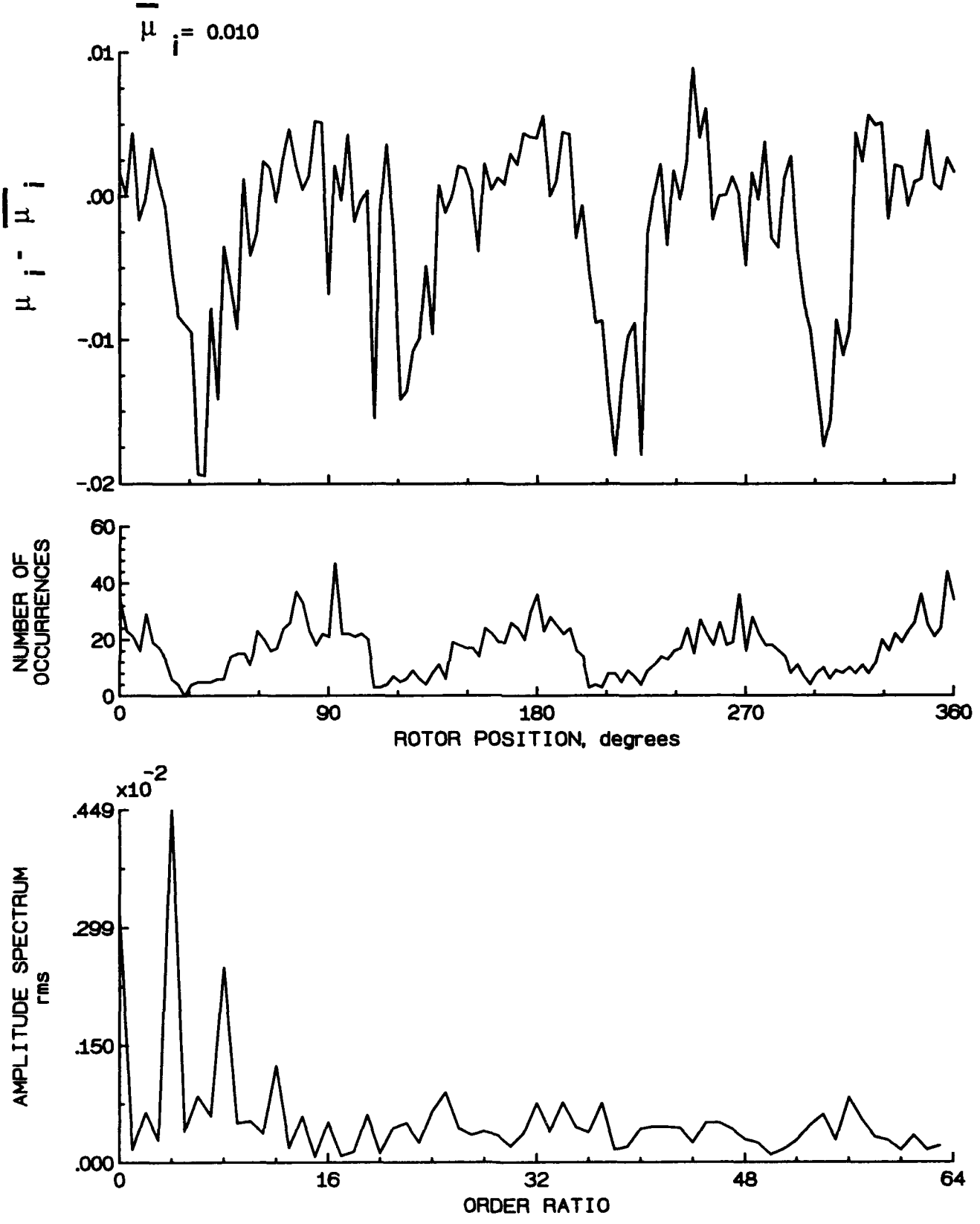

Figure 169.- Induced inflow velocity measured at 300 degrees and r/R of 0.86.

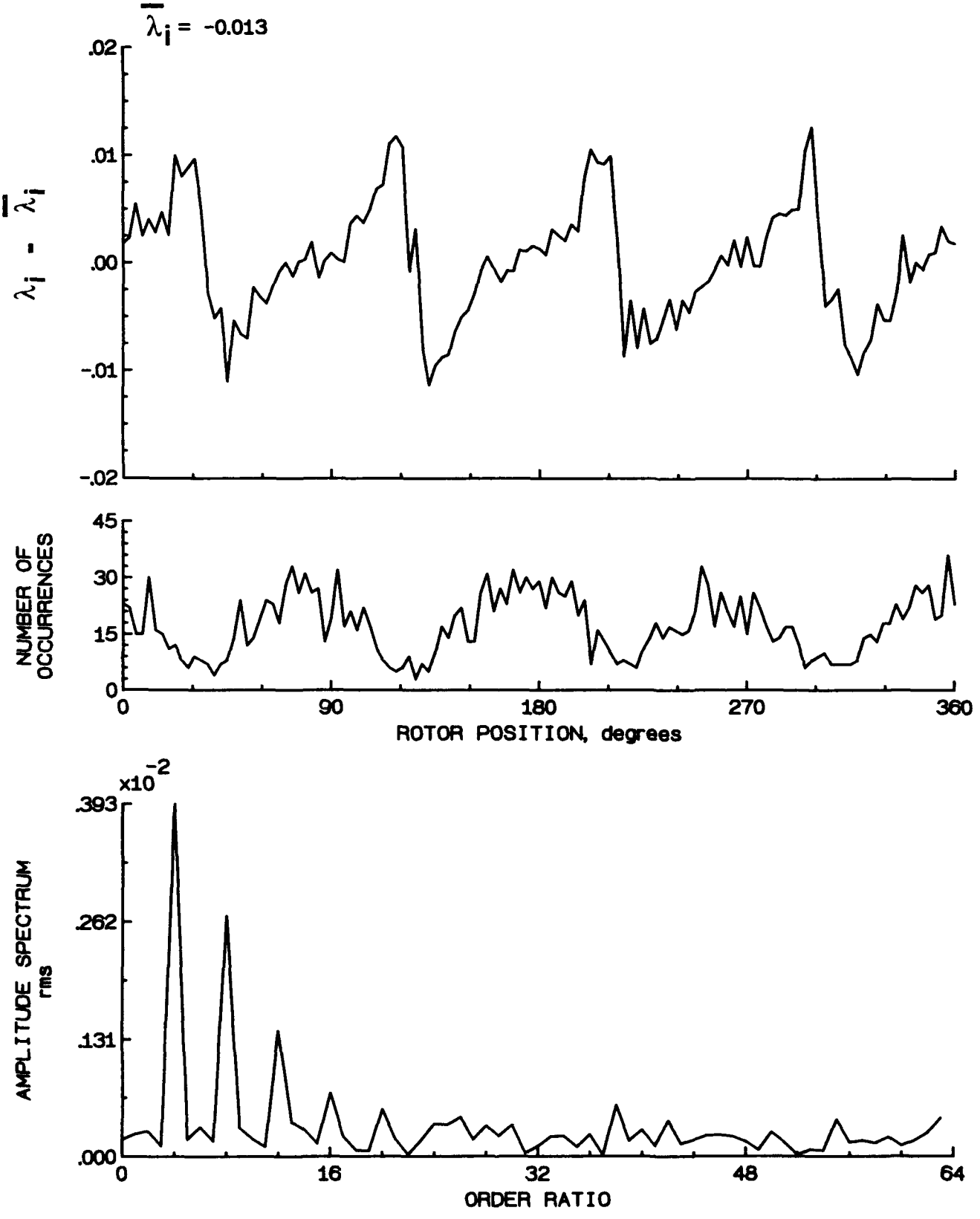

Figure 169.- Concluded.

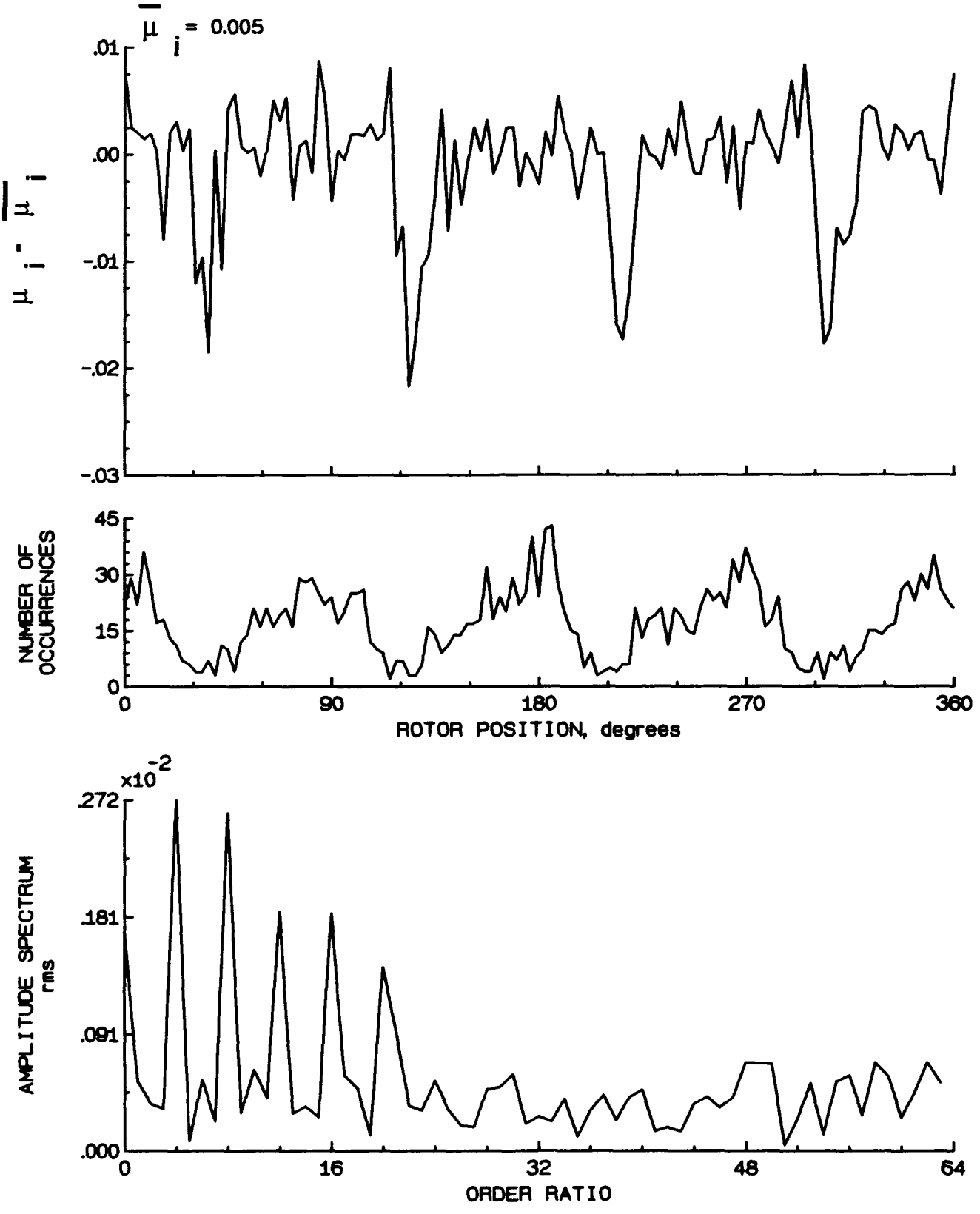

Figure 170.- Induced inflow velocity measured at 300 degrees and r/R of 0.90.

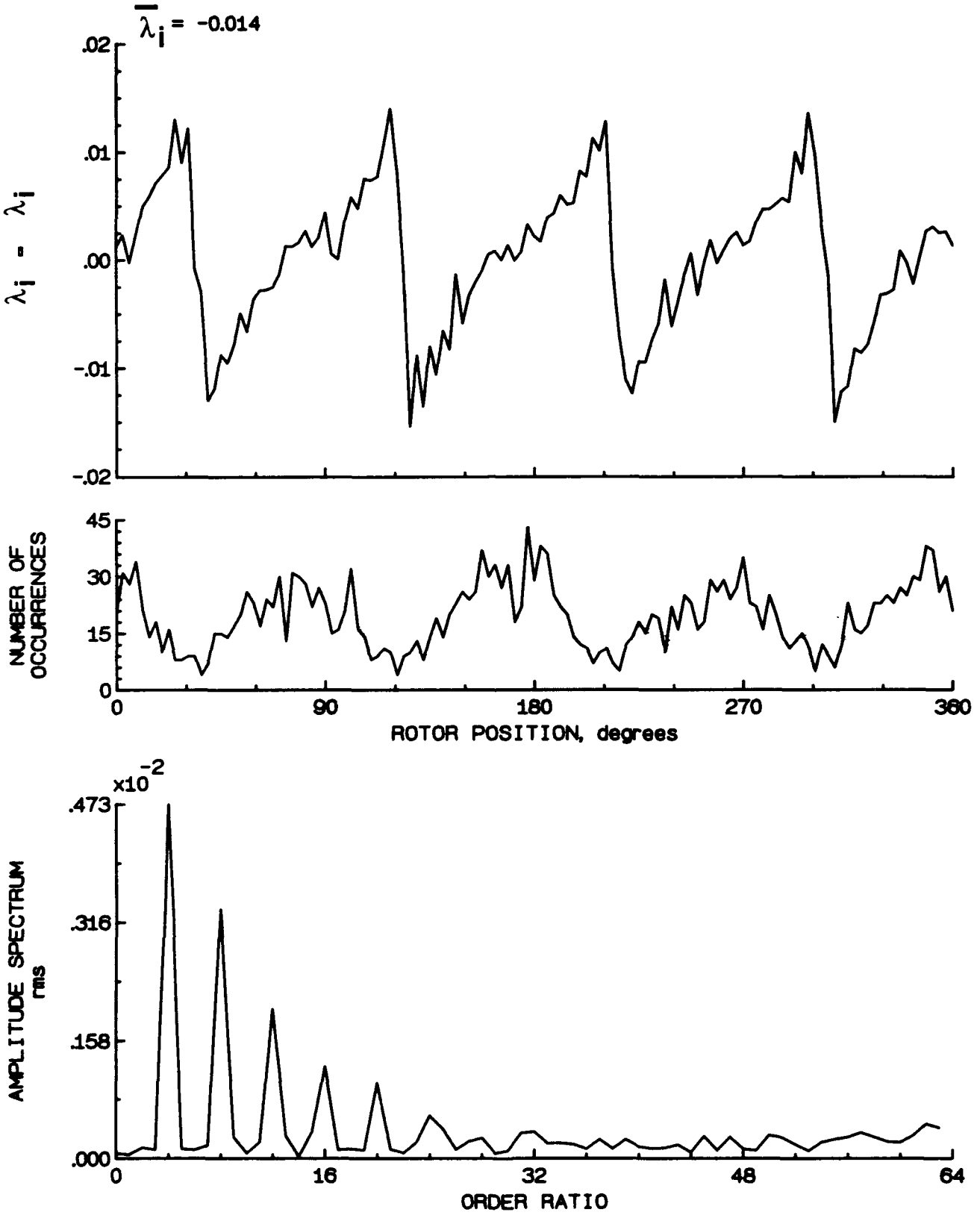

Figure 170.- Concluded.

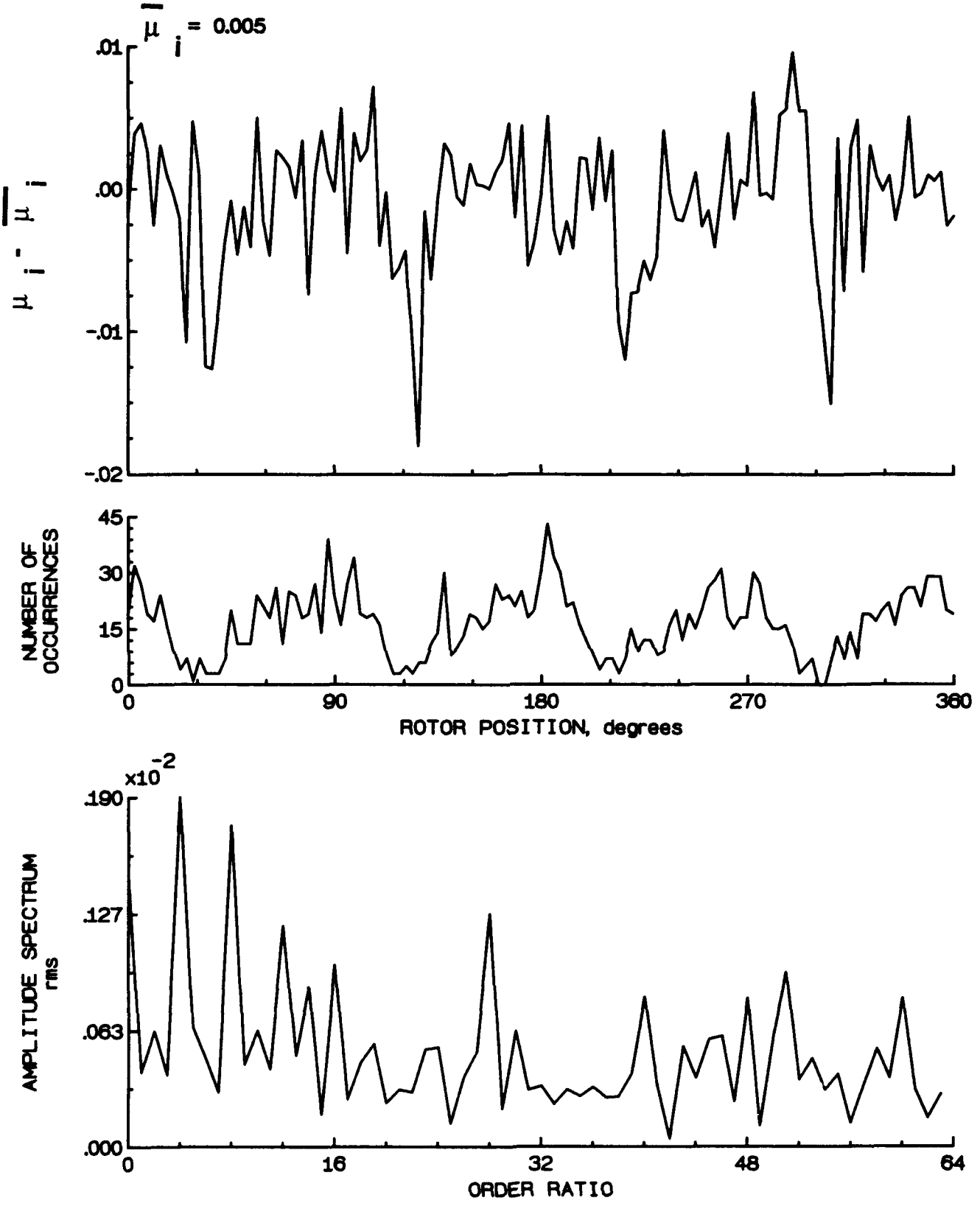

Figure 171.- Induced inflow velocity measured at 300 degrees and r/R of 0.94.

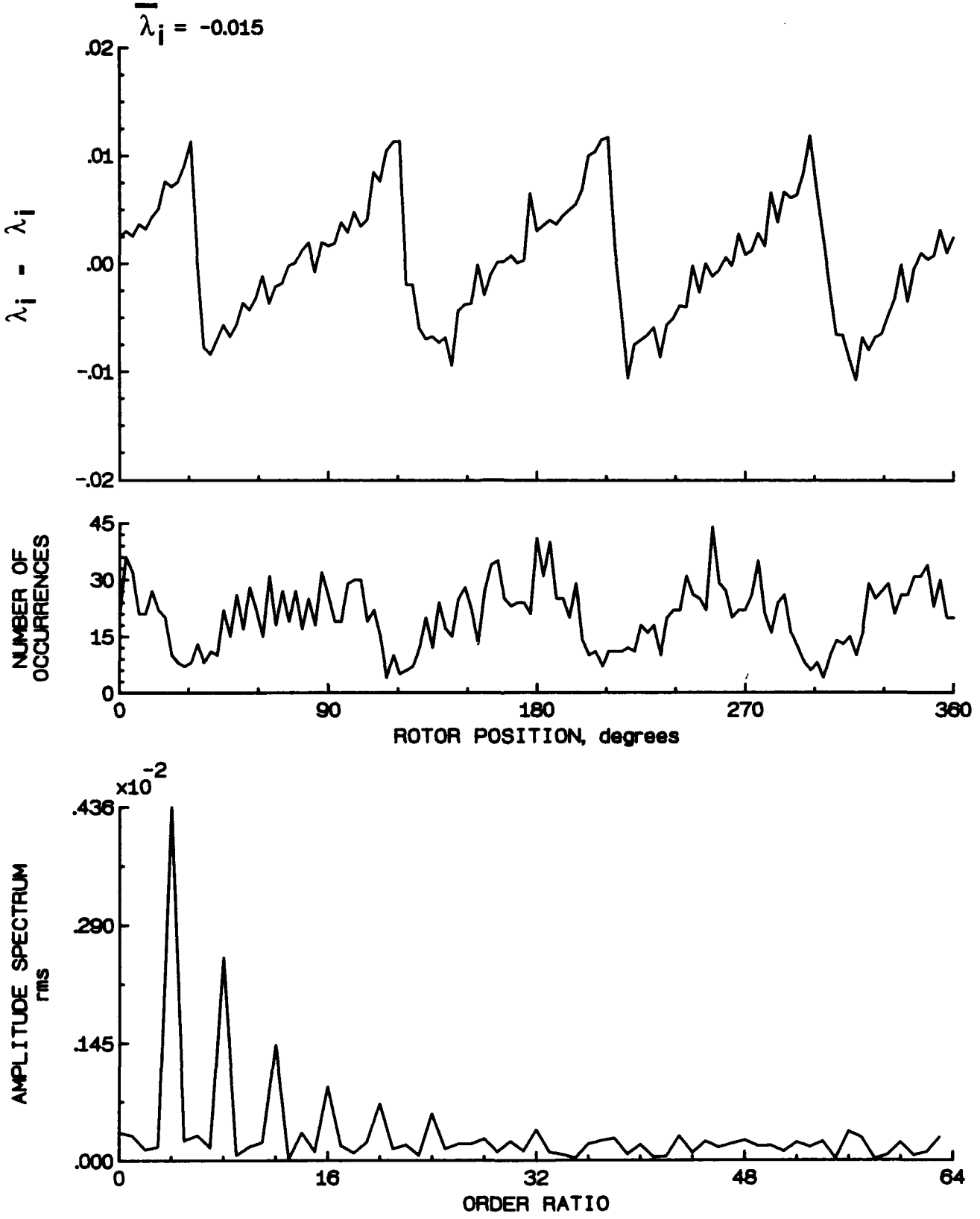

Figure 171.- Concluded.

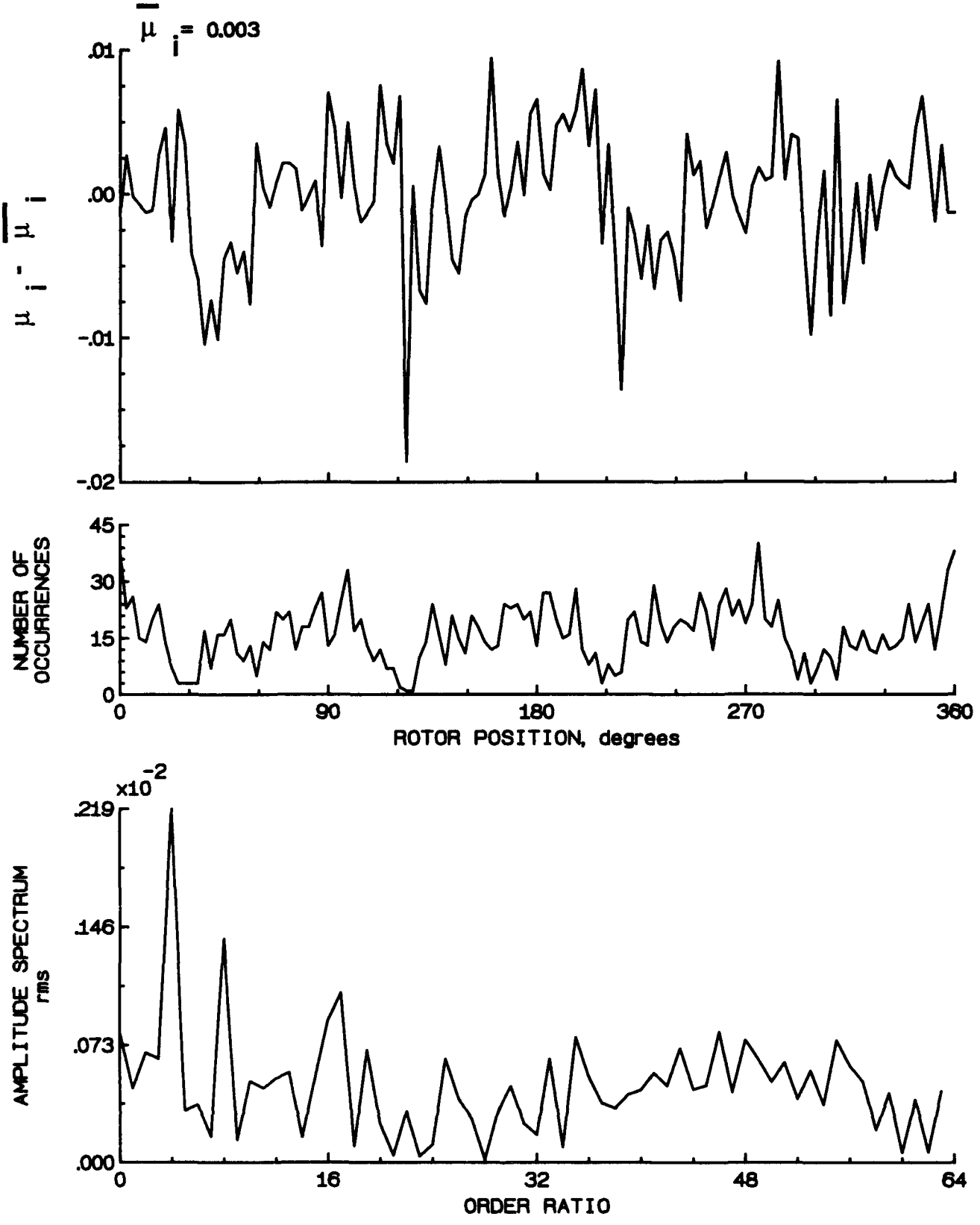

Figure 172.- Induced inflow velocity measured at 300 degrees and r/R of 0.98.

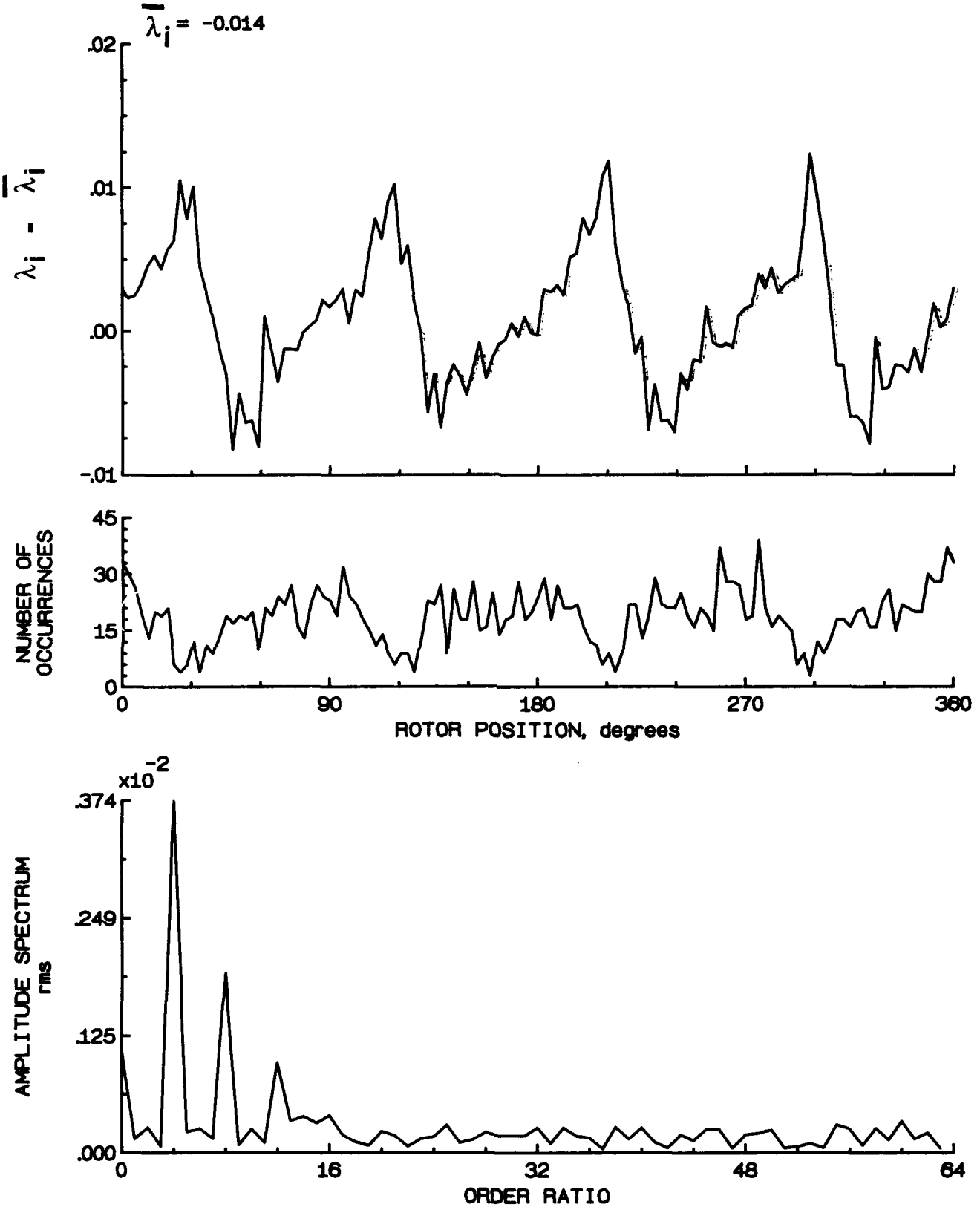

Figure 172.- Concluded.

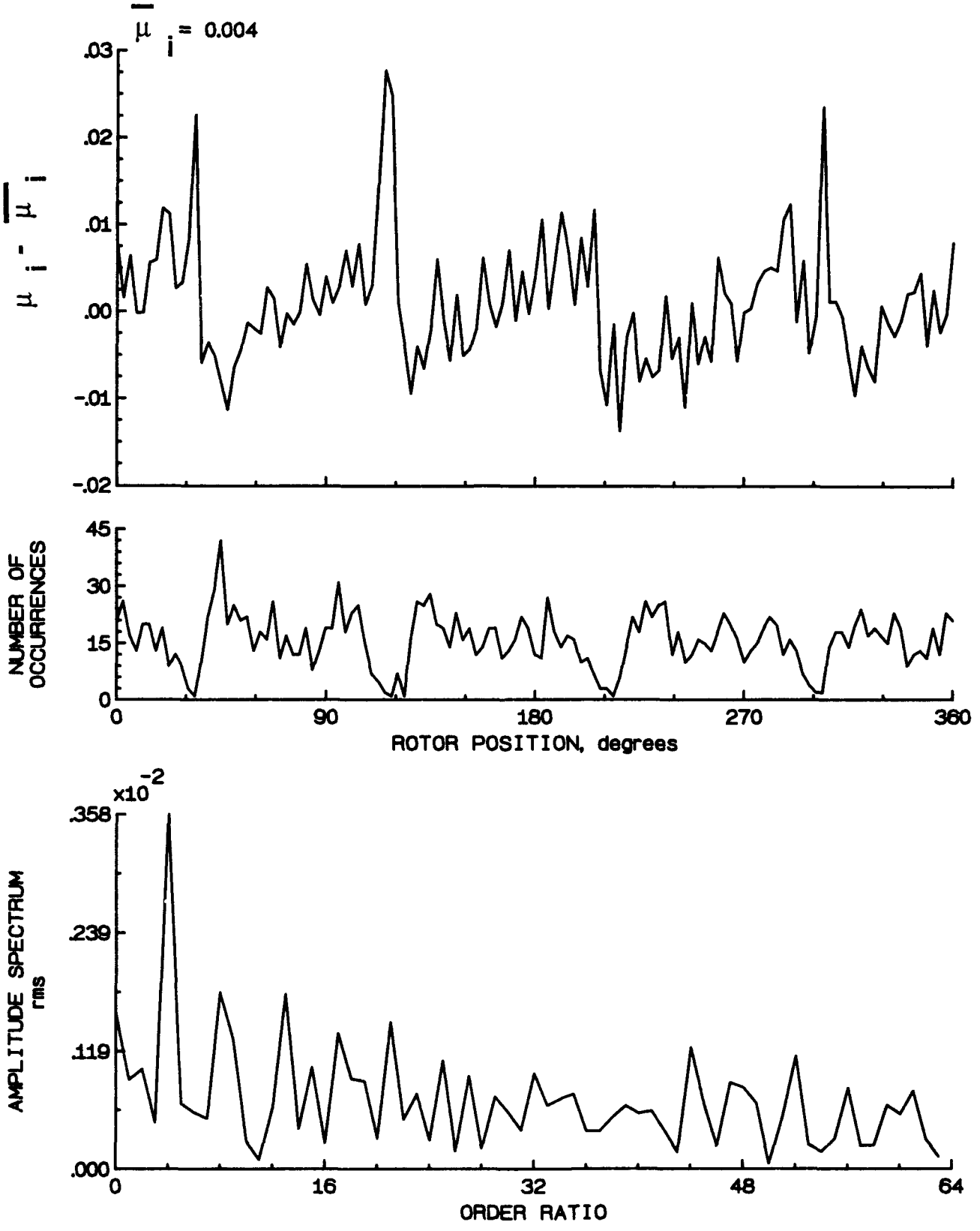

Figure 173.- Induced inflow velocity measured at 300 degrees and r/R of 1.02.

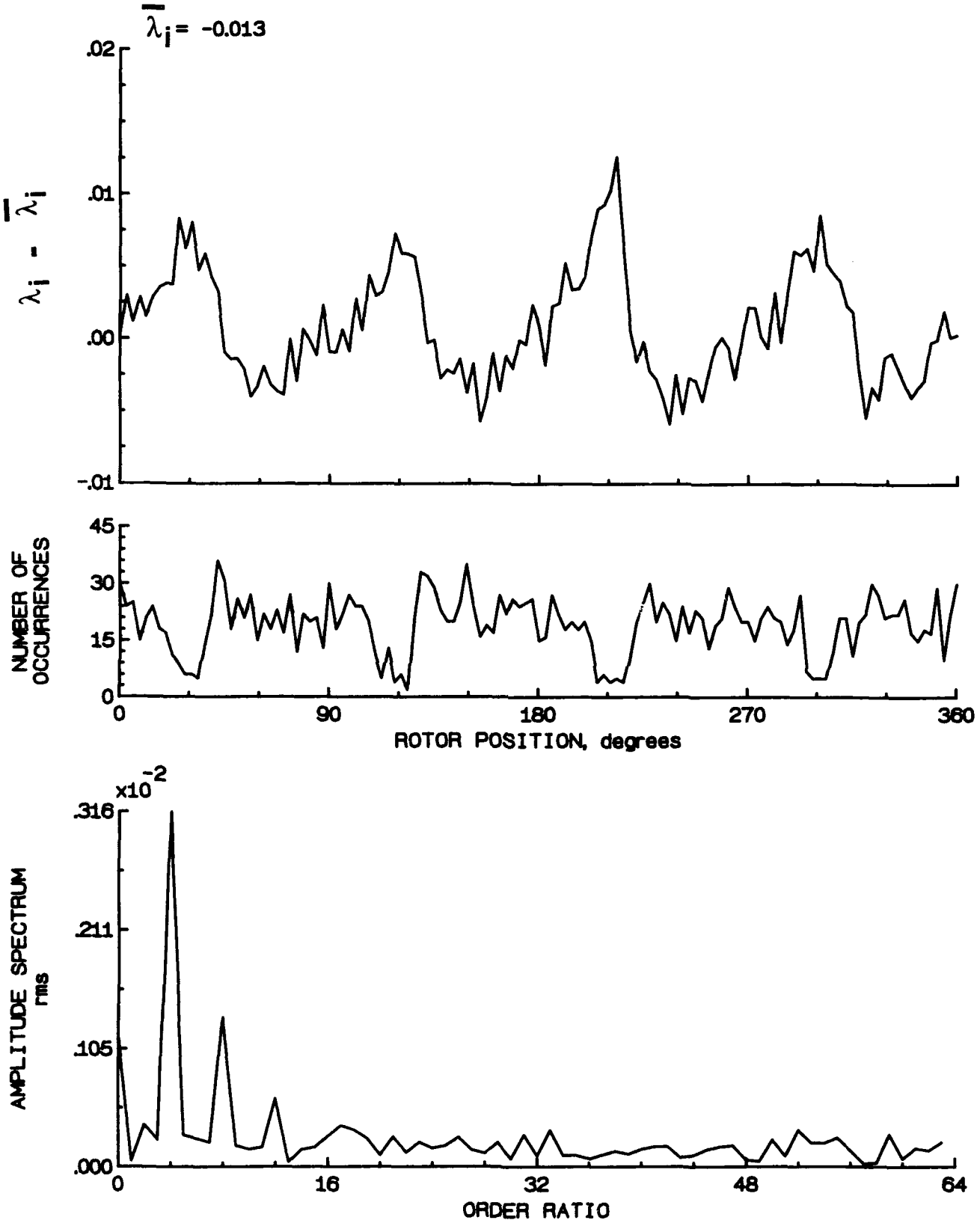

Figure 173.- Concluded.

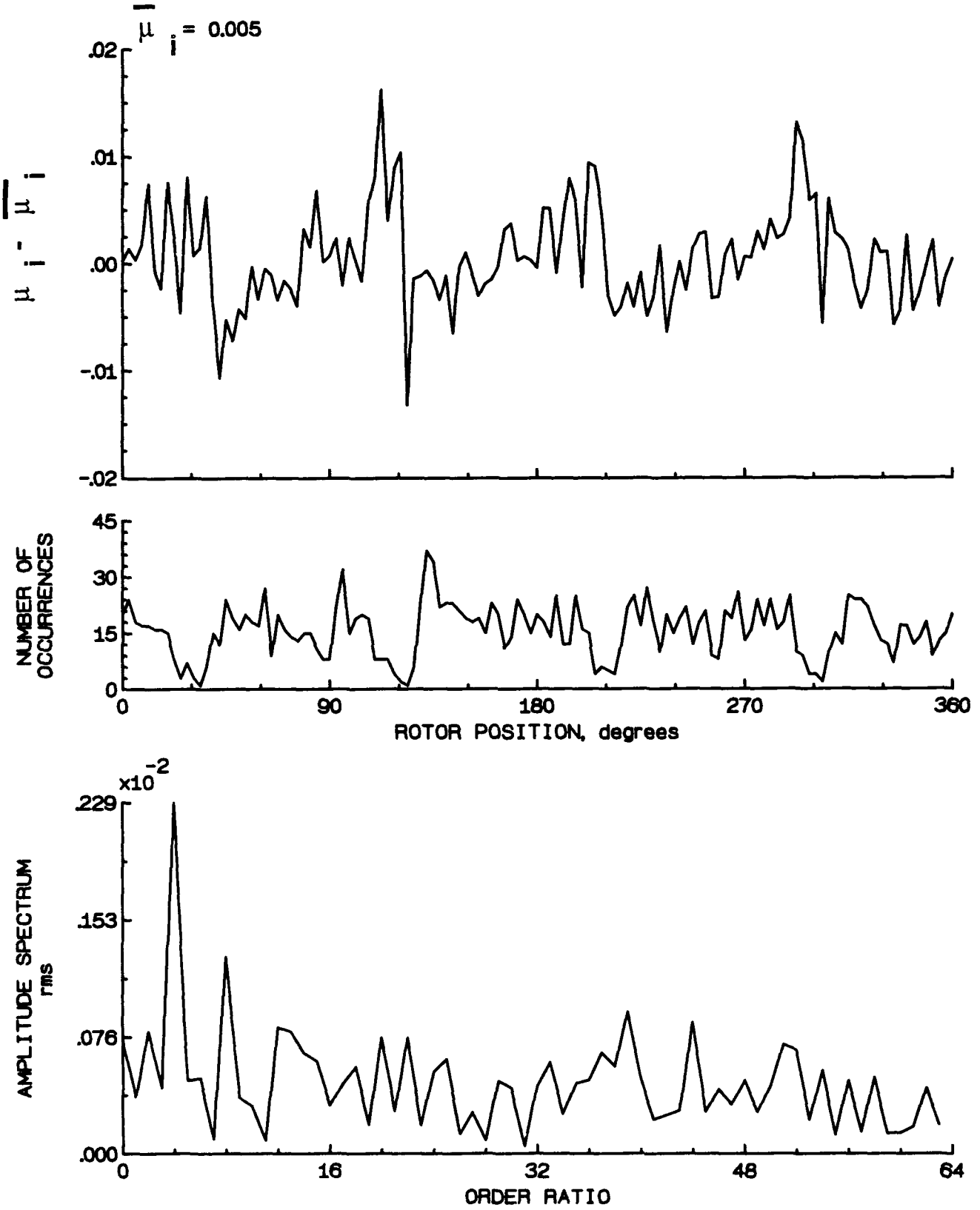

Figure 174.- Induced inflow velocity measured at 300 degrees and r/R of 1.04.

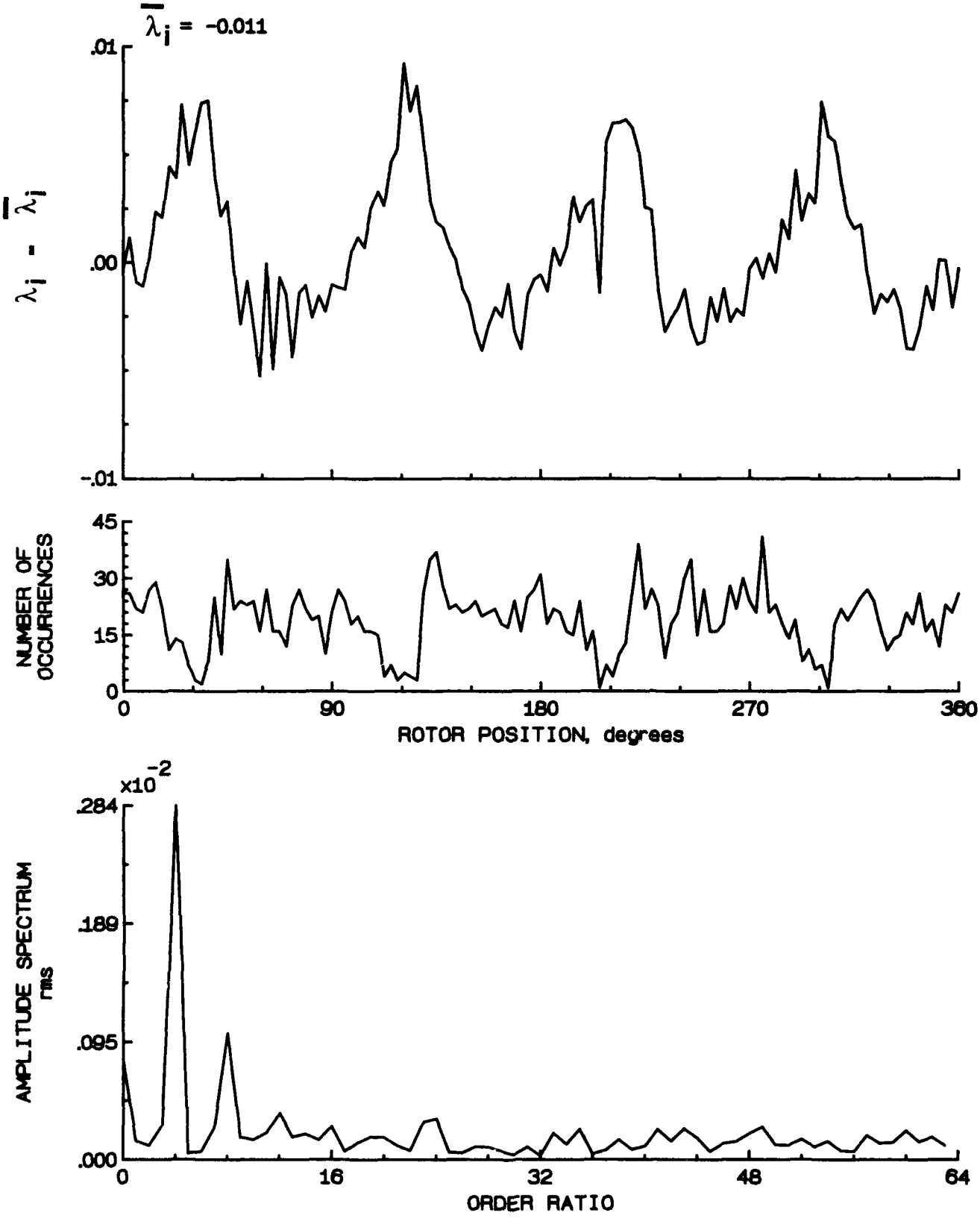

Figure 174.- Concluded.

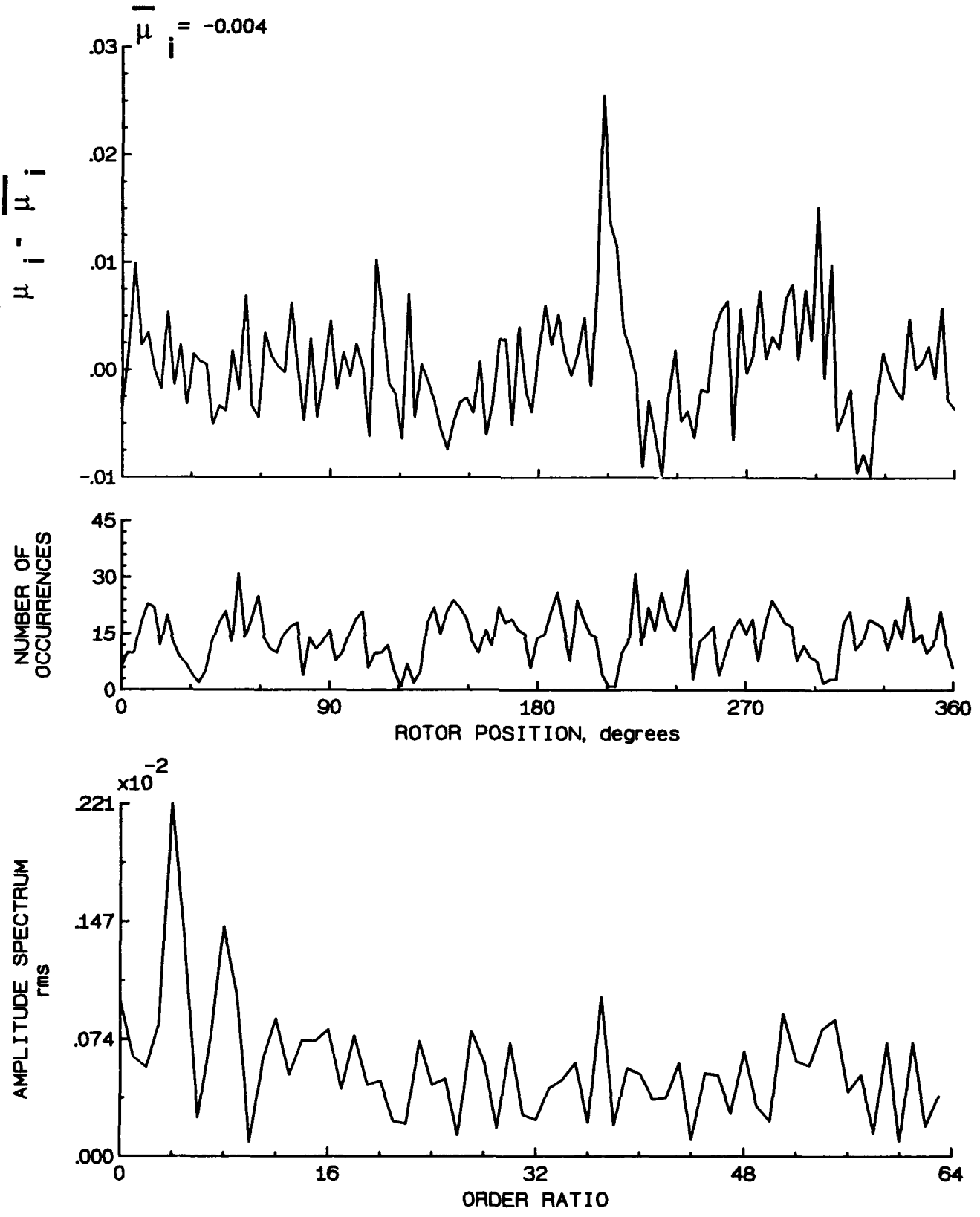

Figure 175.- Induced inflow velocity measured at 300 degrees and r/R of 1.10.

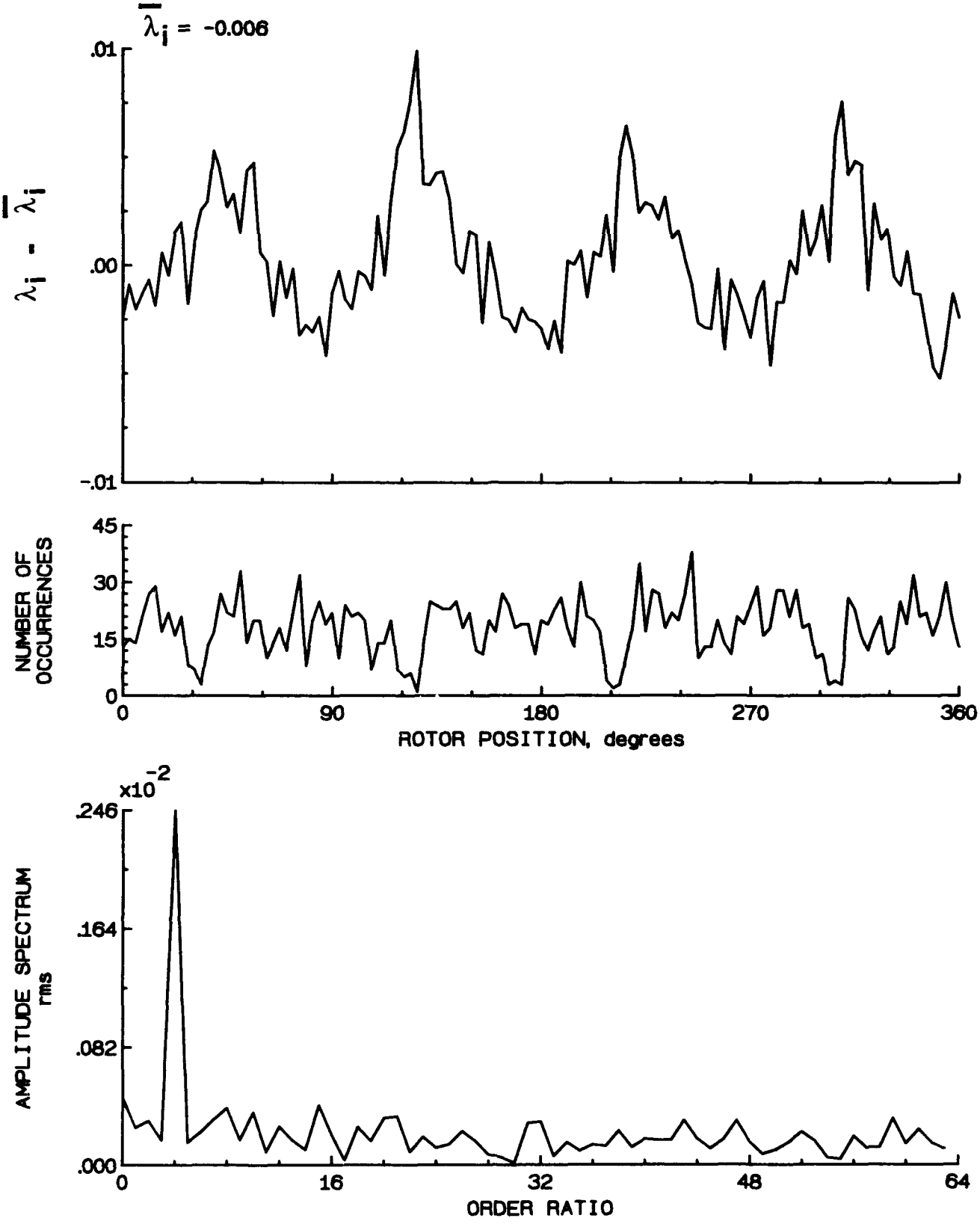

Figure 175.- Concluded.

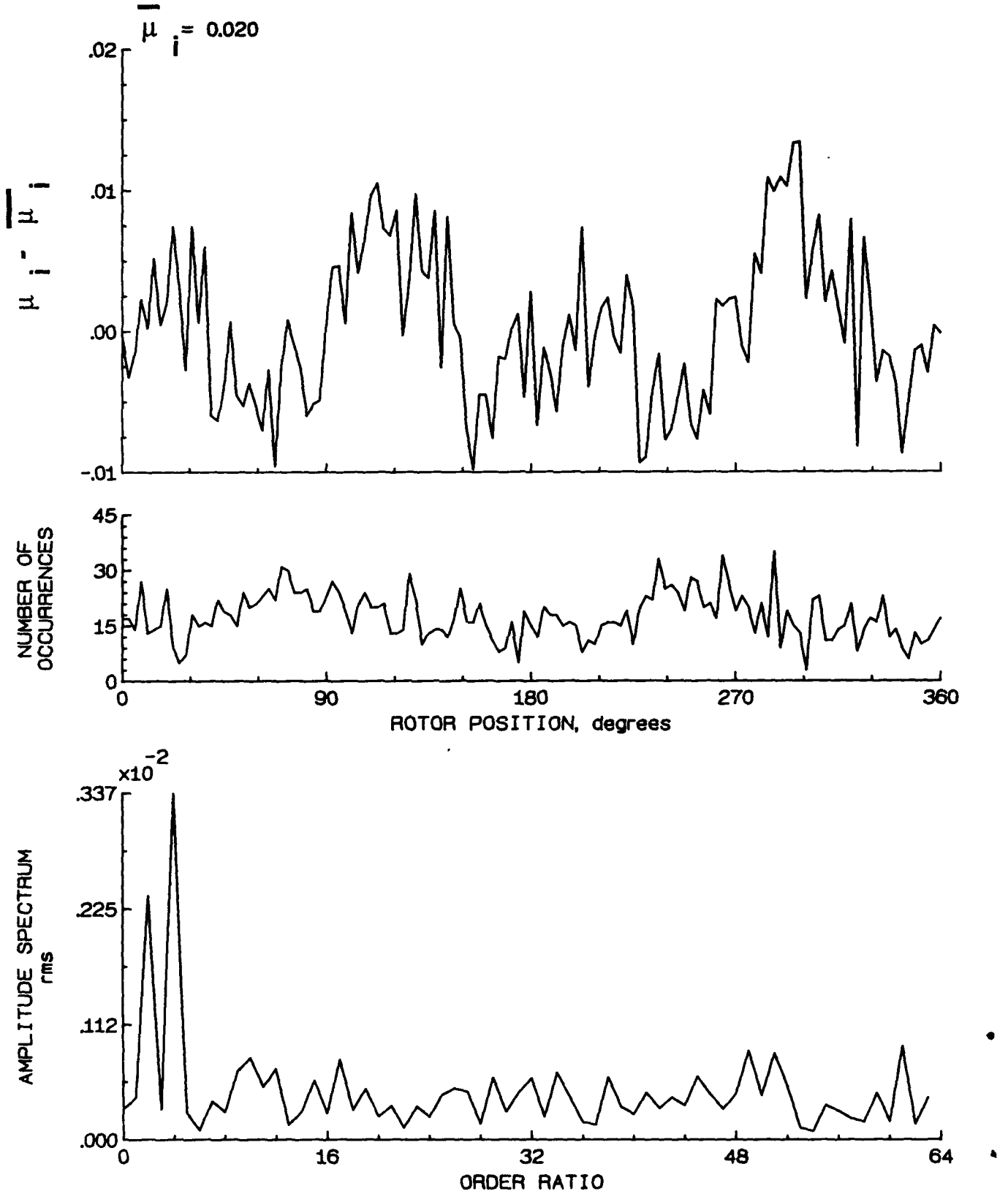

Figure 176.- Induced inflow velocity measured at 330 degrees and r/R of 0.20.

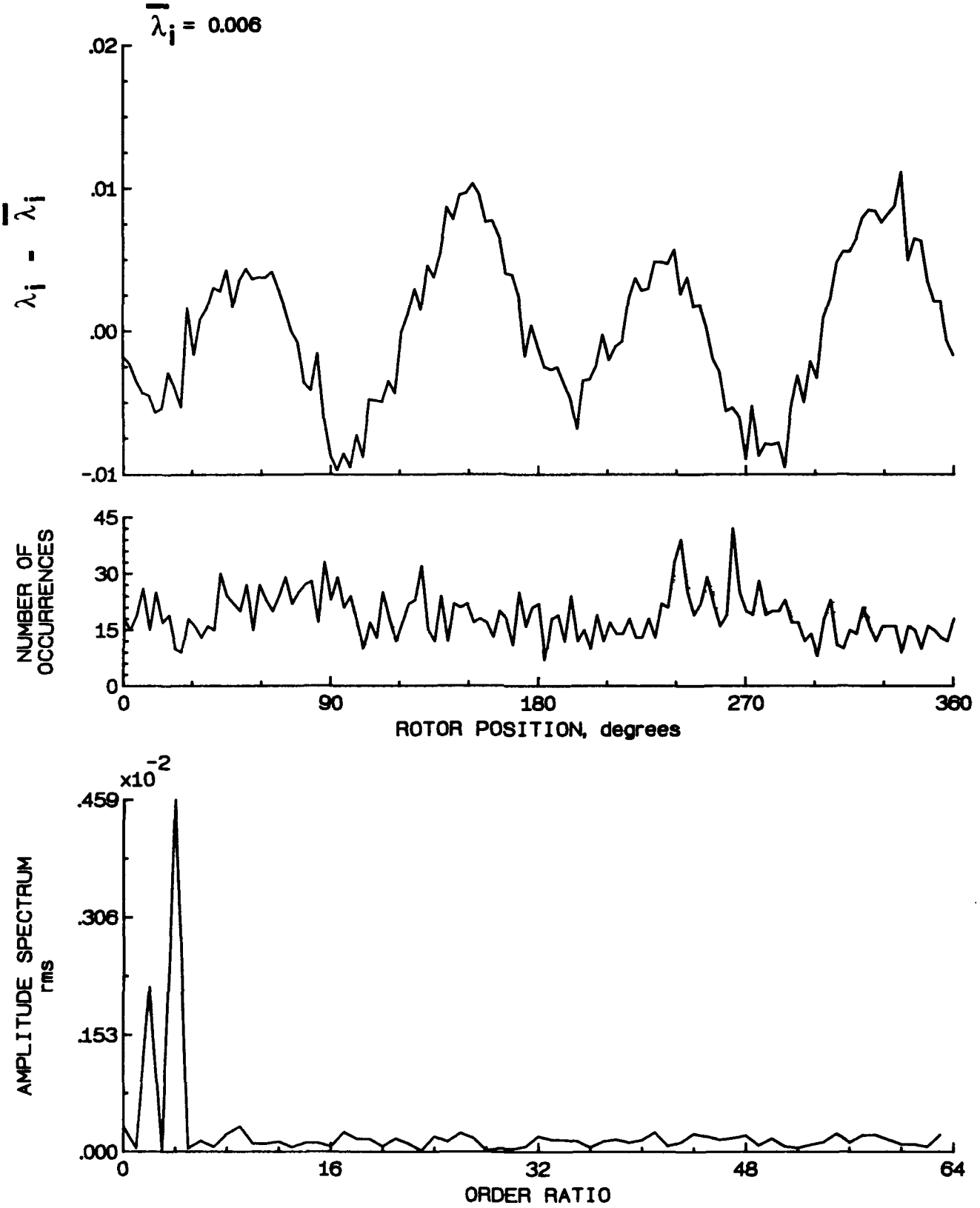

Figure 176.- Concluded.

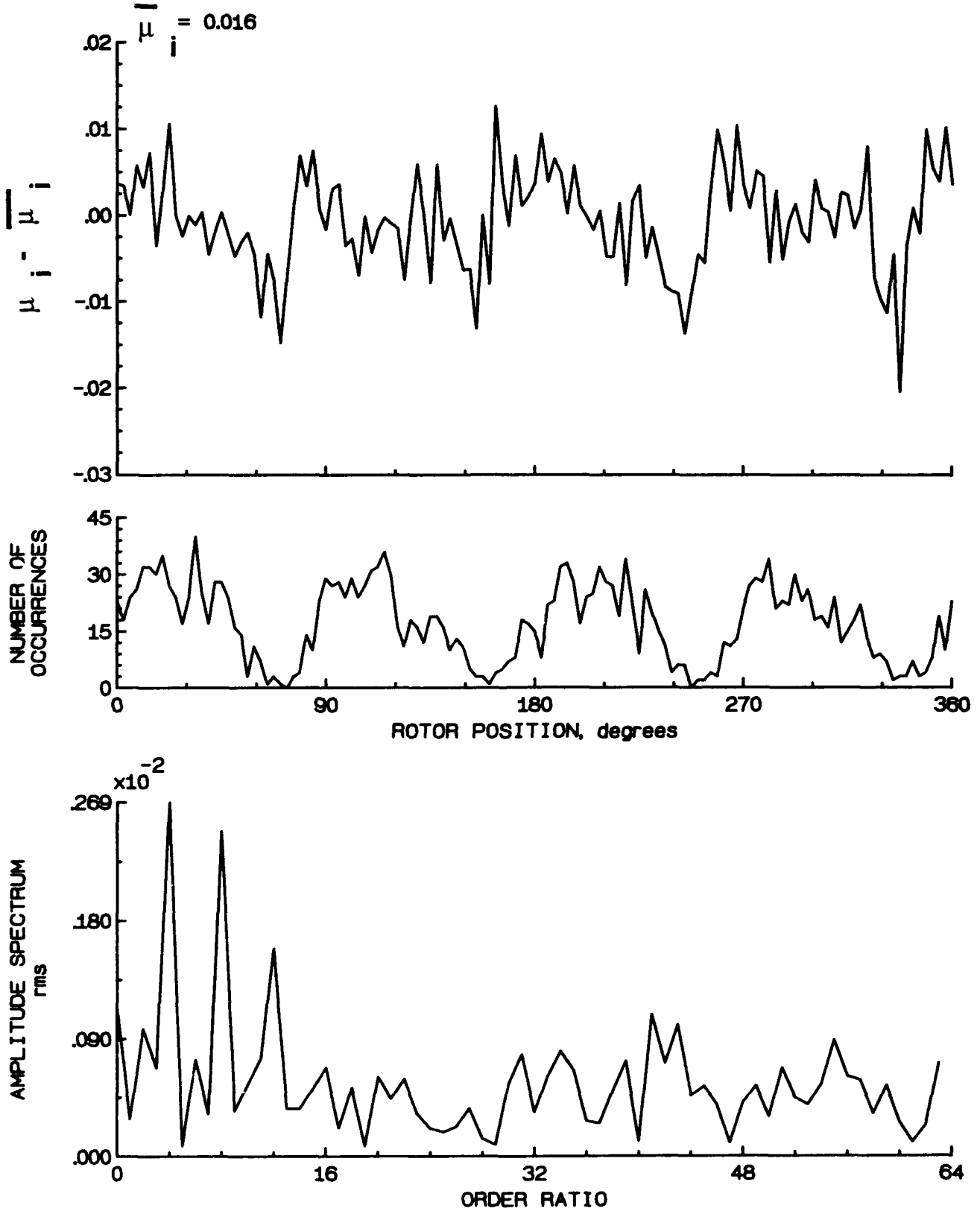

Figure 177.- Induced inflow velocity measured at 330 degrees and r/R of 0.40.

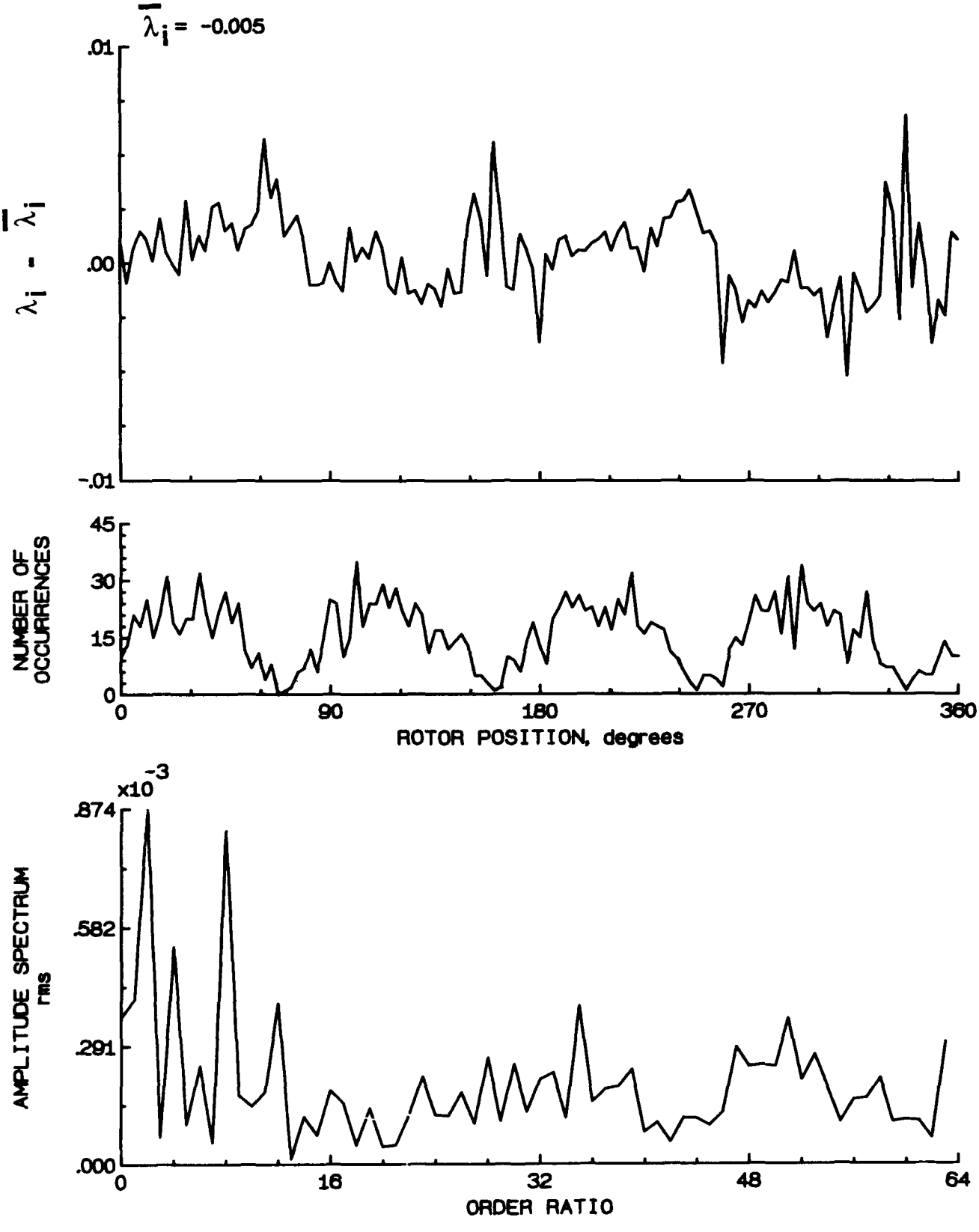

Figure 177.- Concluded.

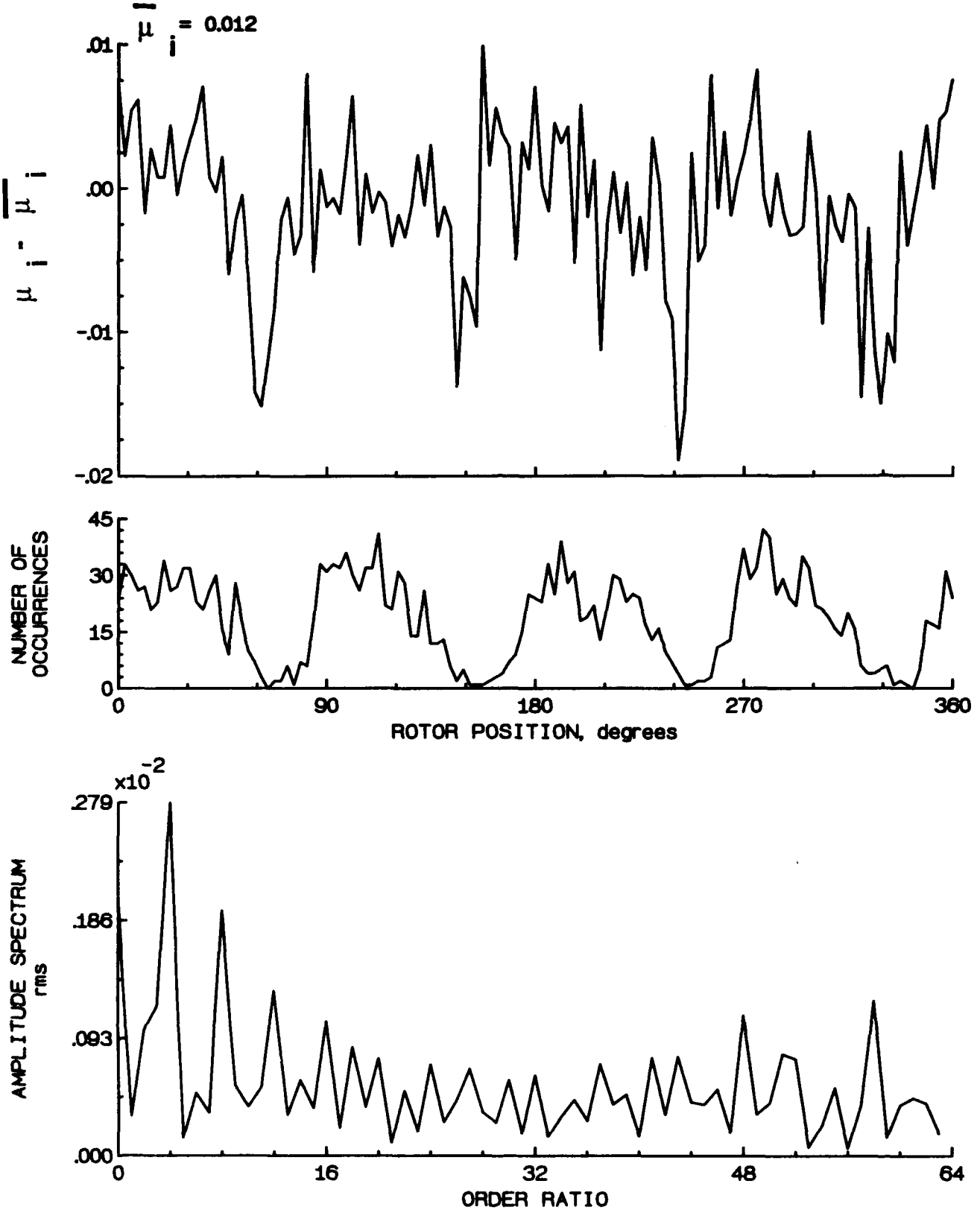

Figure 178.- Induced inflow velocity measured at 330 degrees and r/R of 0.50.

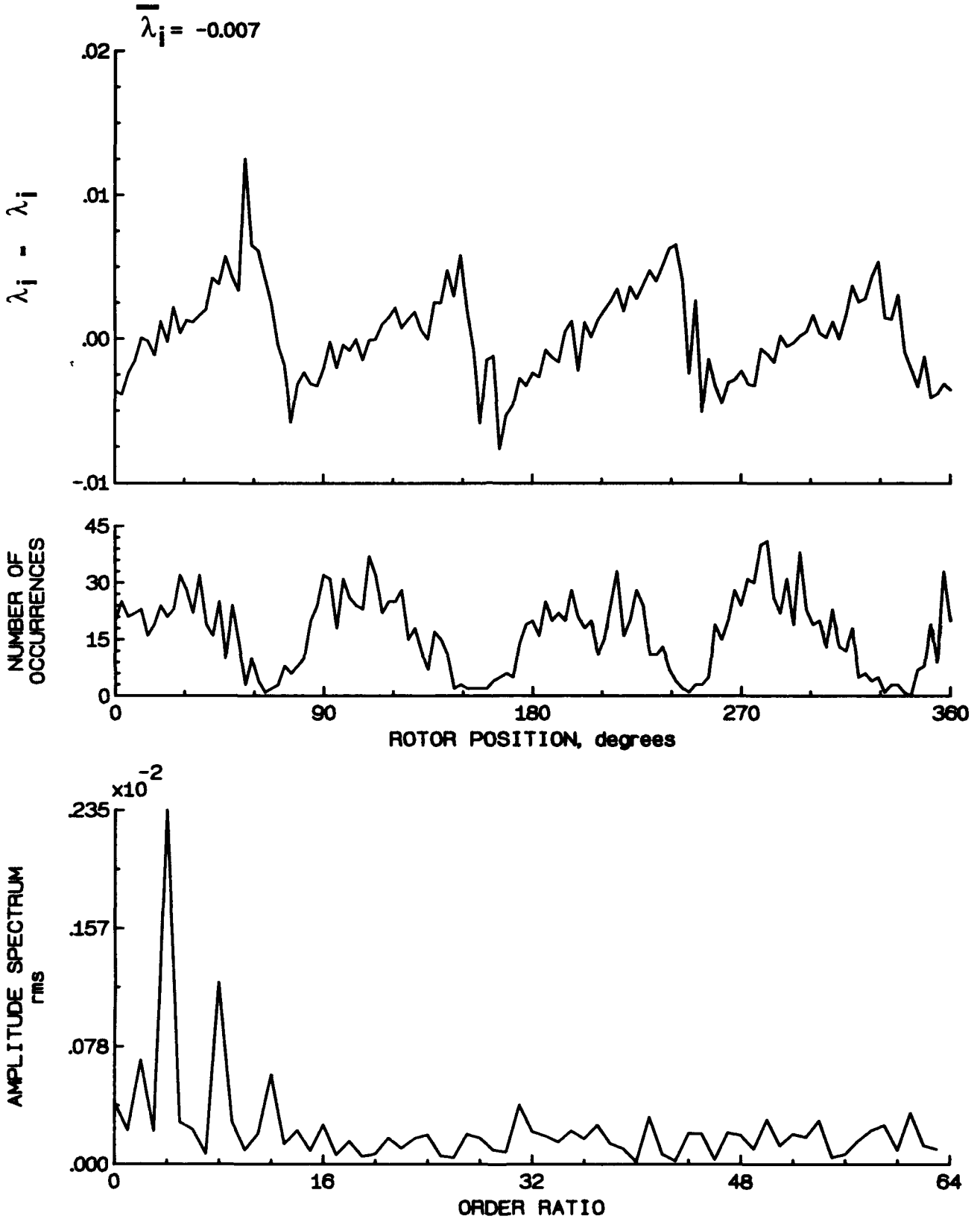

Figure 178.- Concluded.

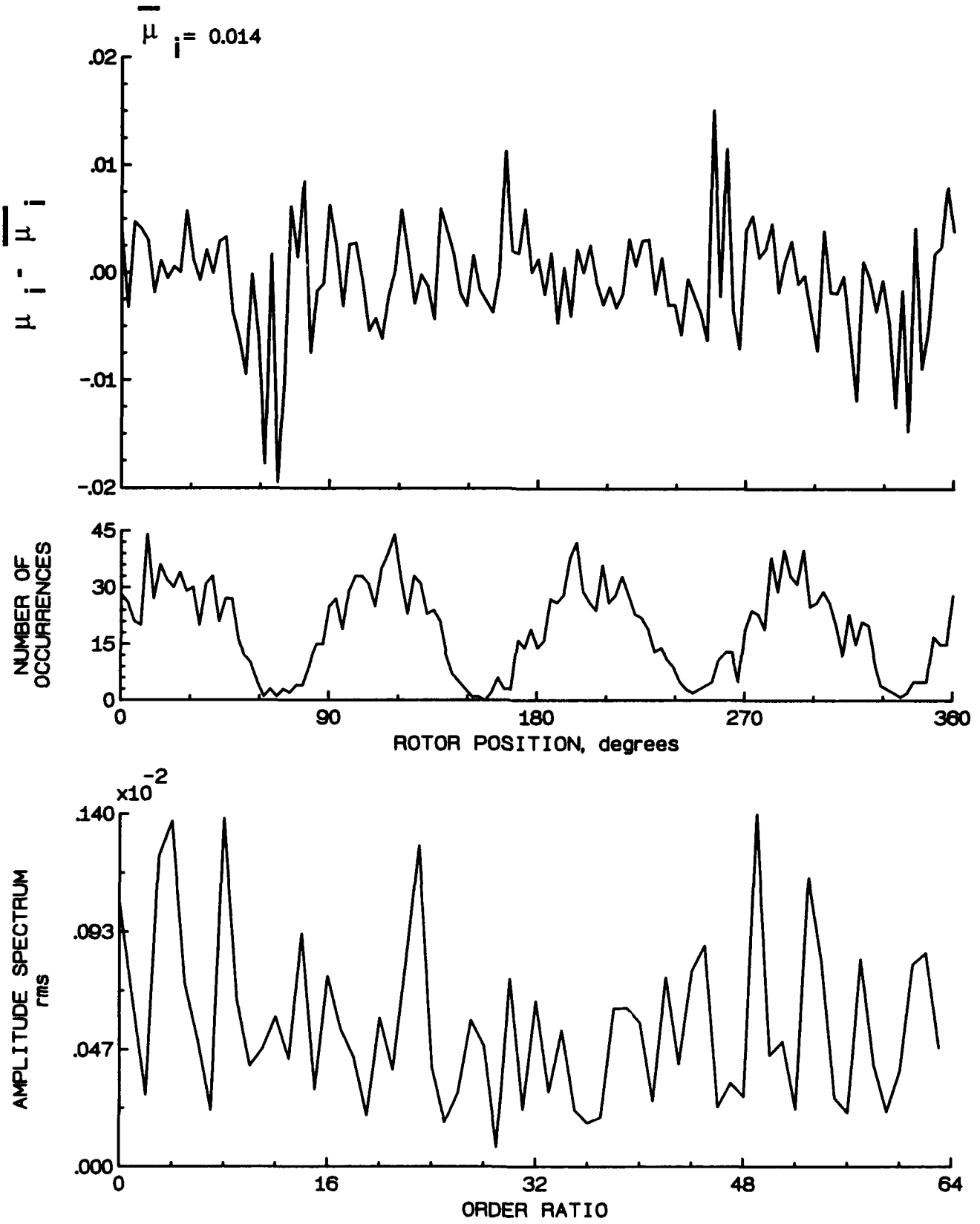

Figure 179.- Induced inflow velocity measured at 330 degrees and r/R of 0.60.

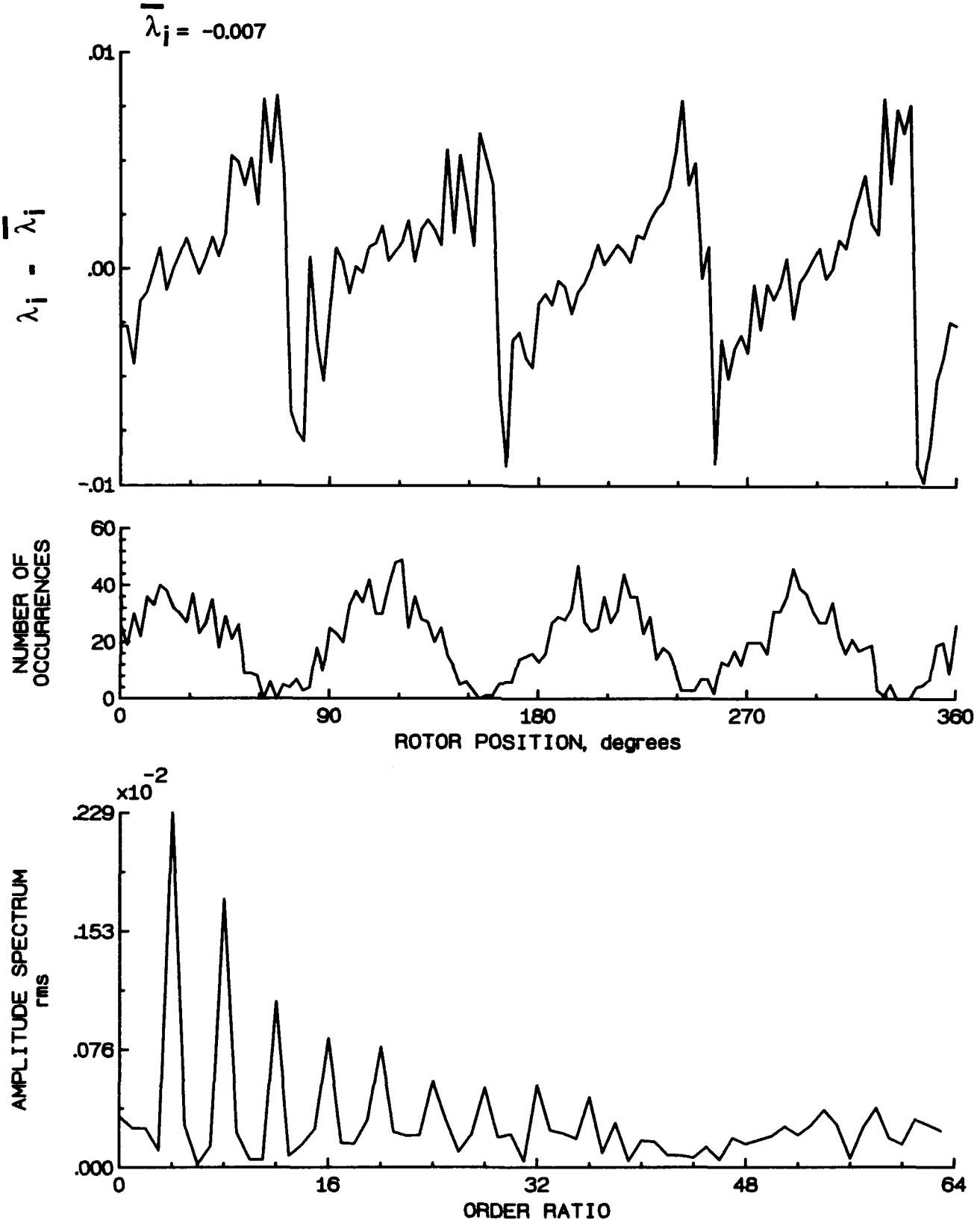

Figure 179.- Concluded.

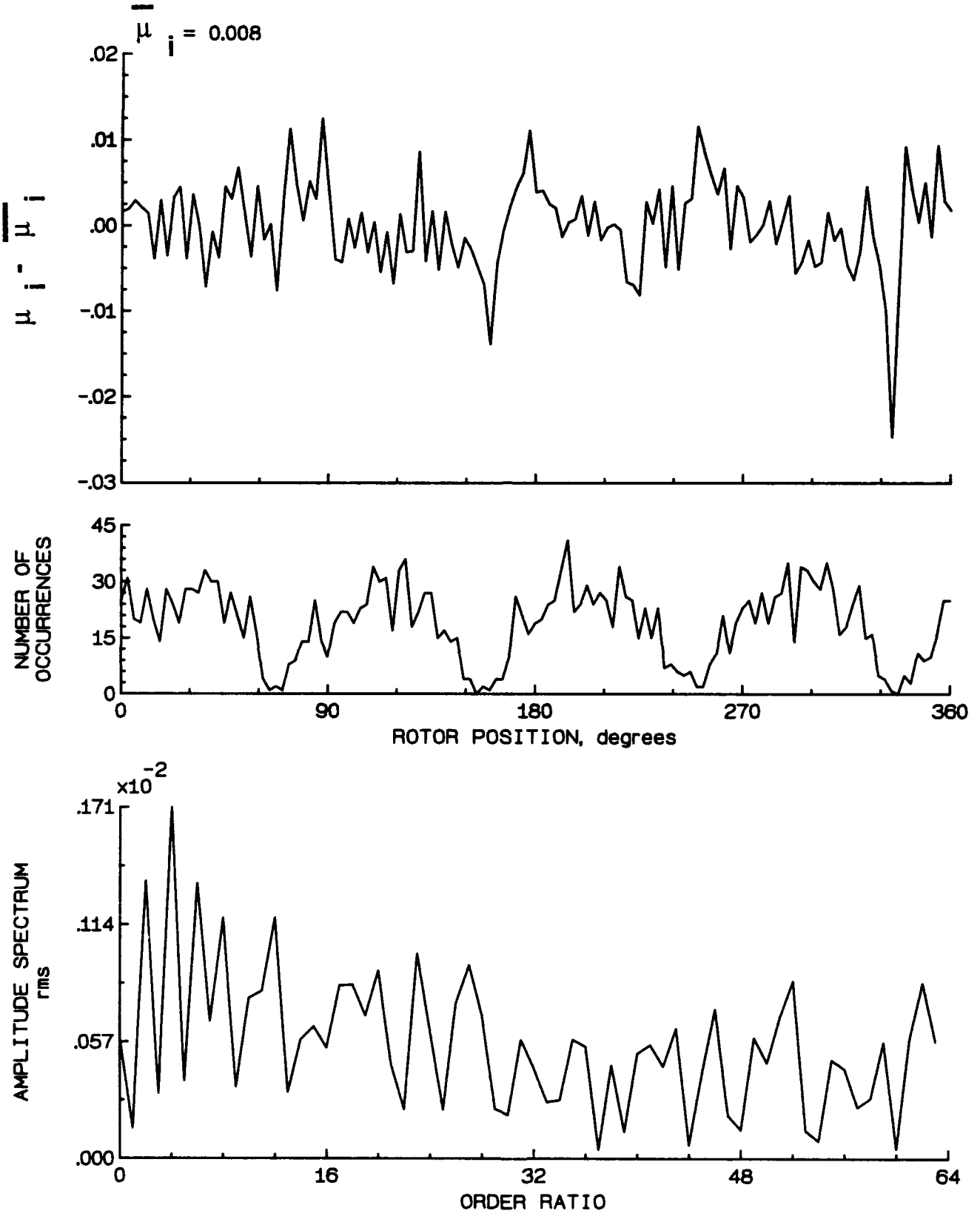

Figure 180.- Induced inflow velocity measured at 330 degrees and r/R of 0.70.

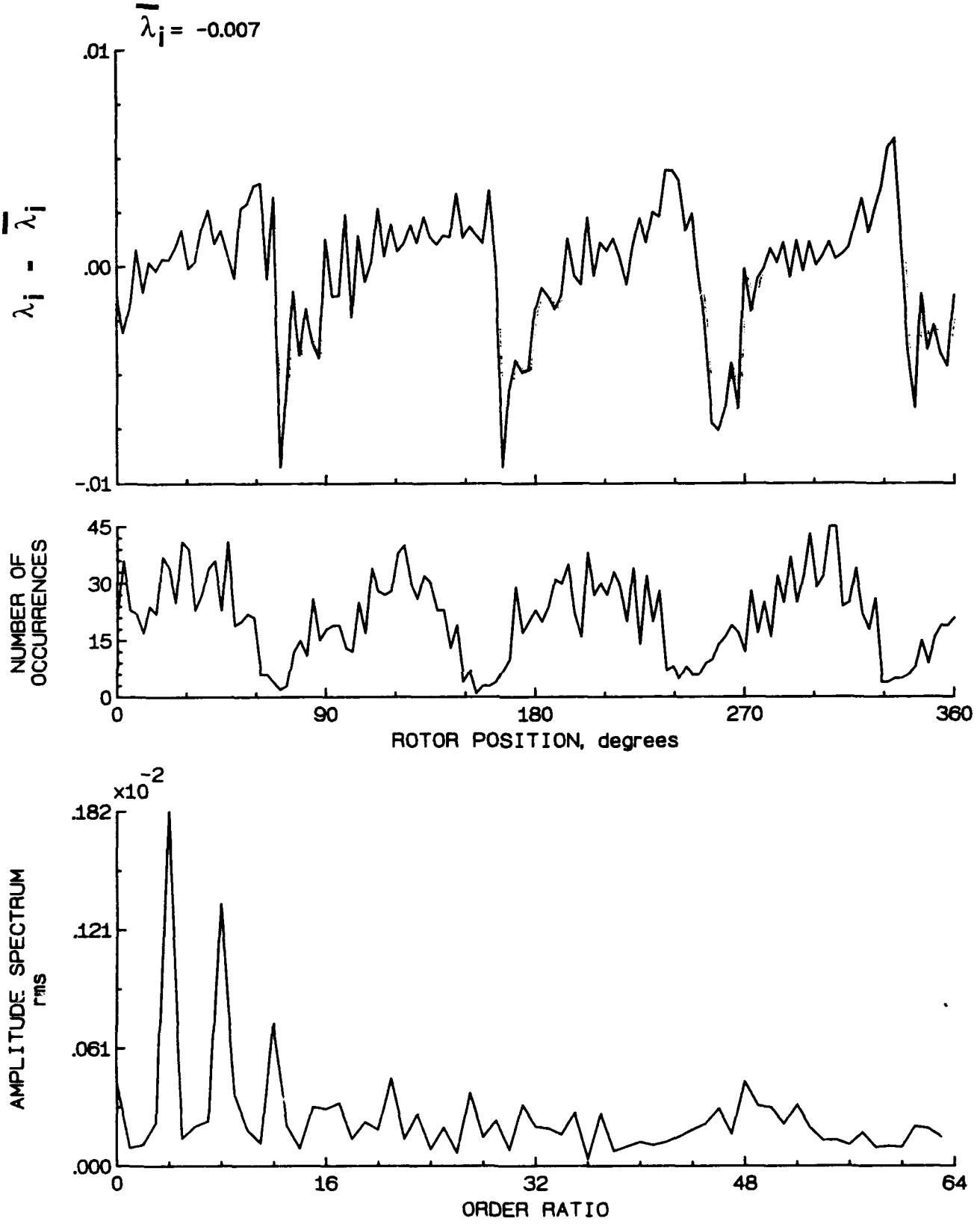

Figure 180.- Concluded.

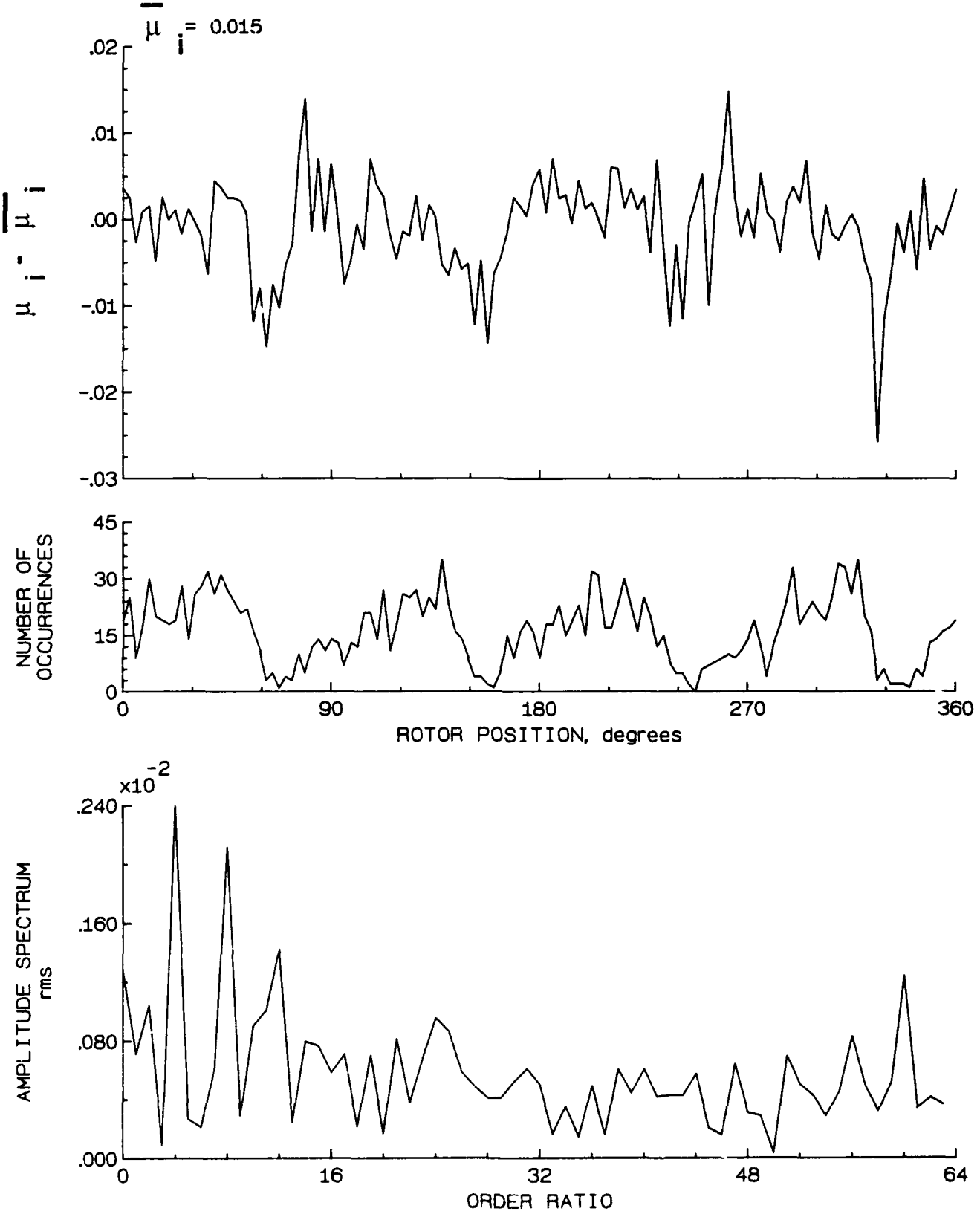

Figure 181.- Induced inflow velocity measured at 330 degrees and r/R of 0.74.

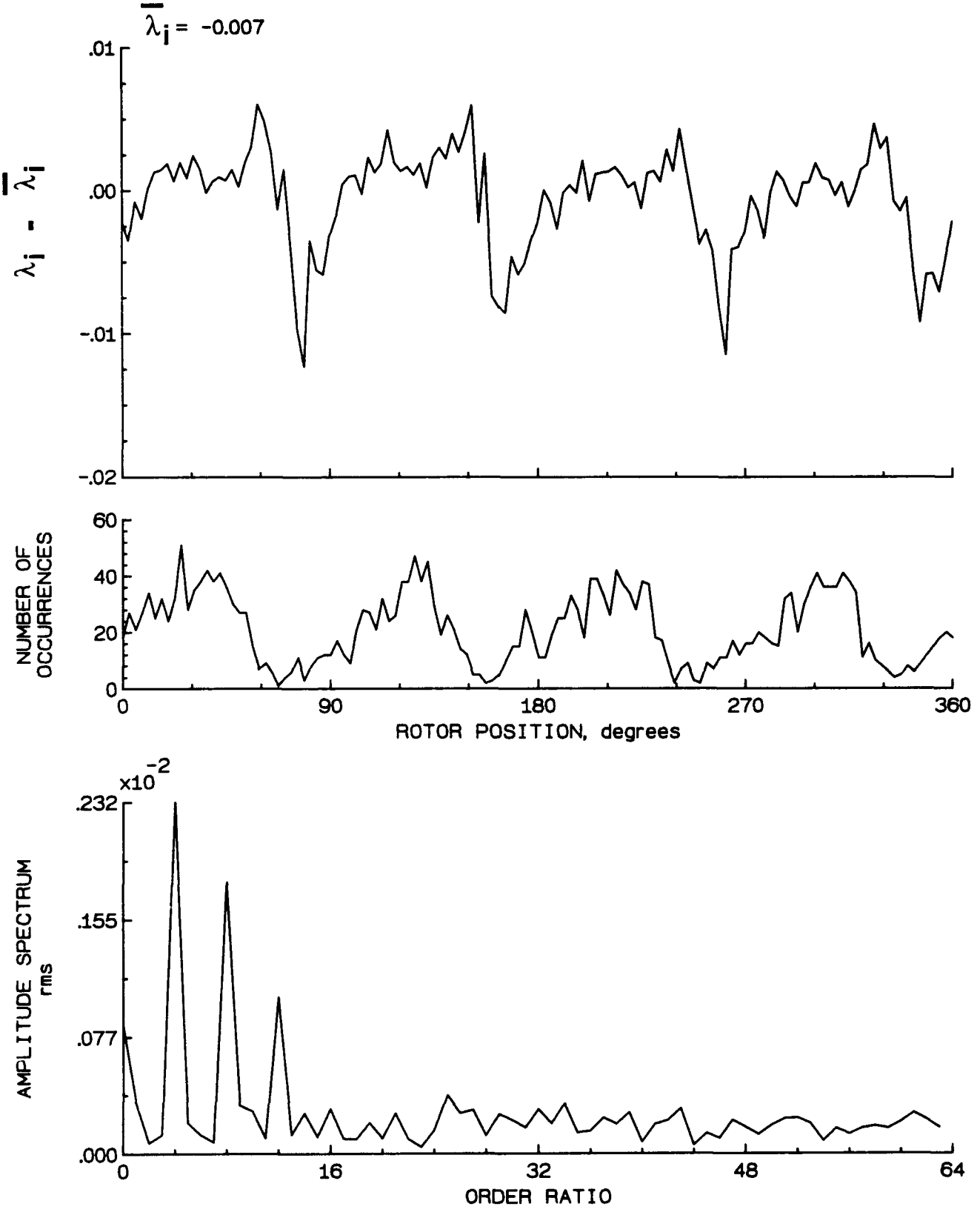

Figure 181.- Concluded.

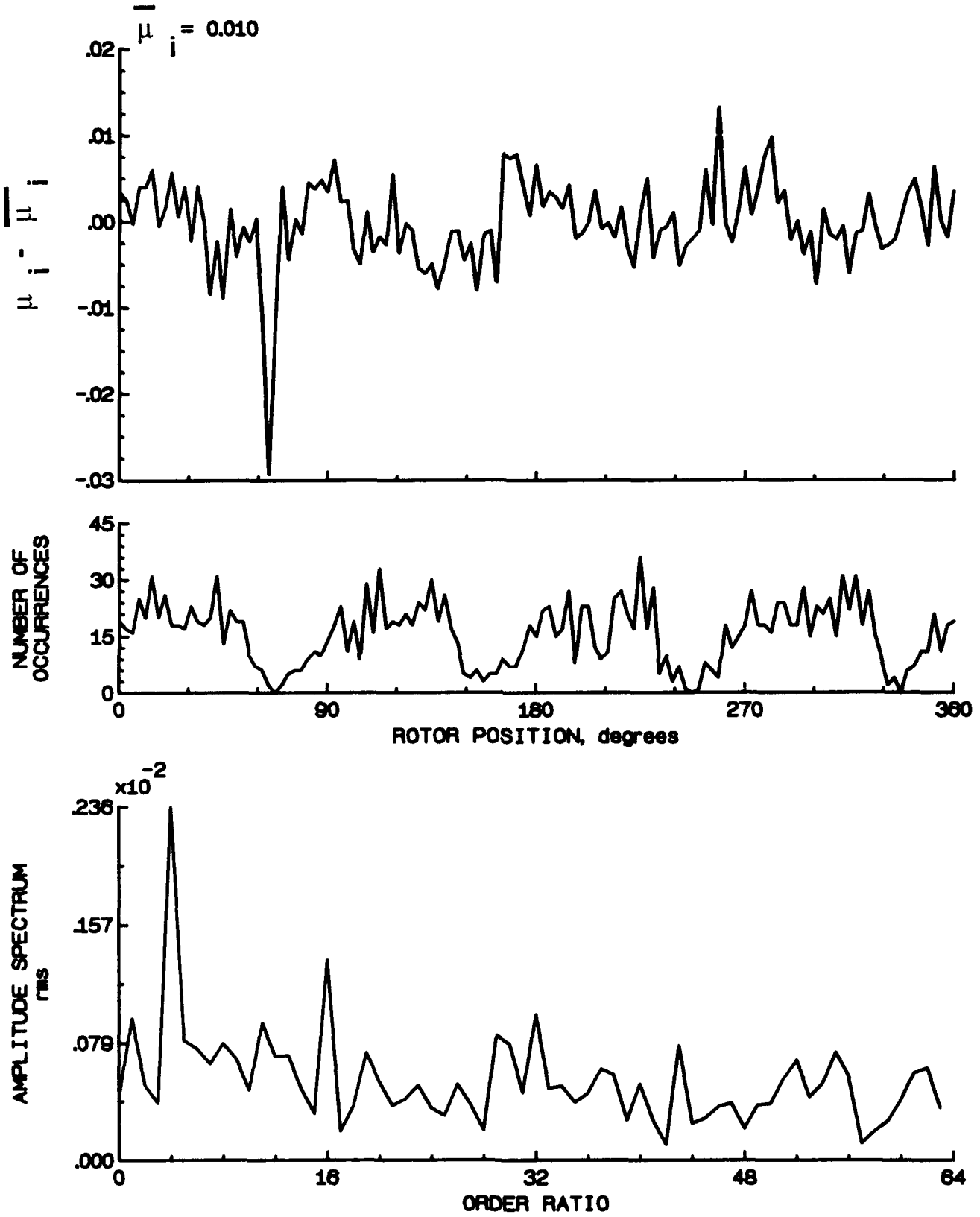

Figure 182.- Induced inflow velocity measured at 330 degrees and r/R of 0.78.

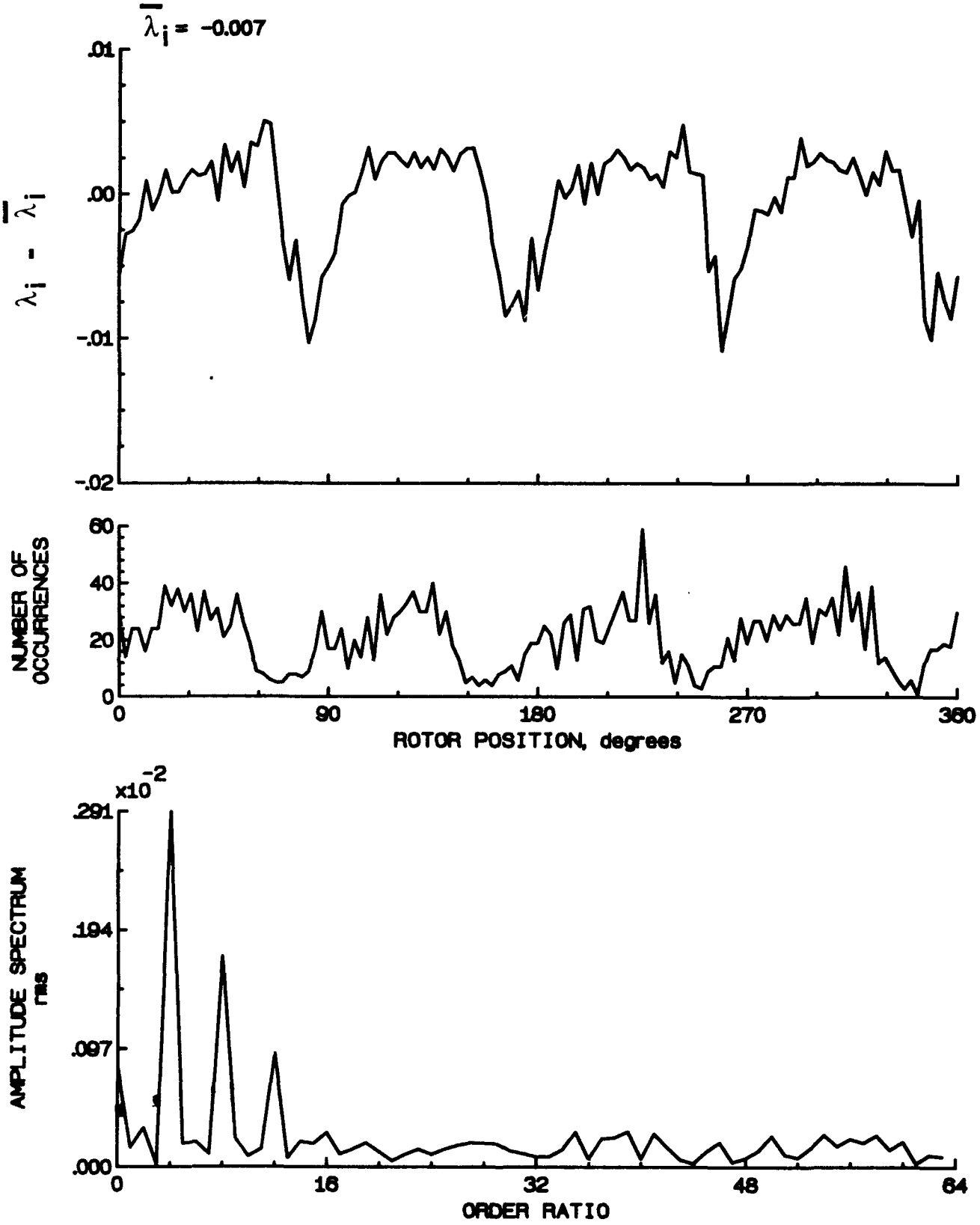

Figure 182.- Concluded.

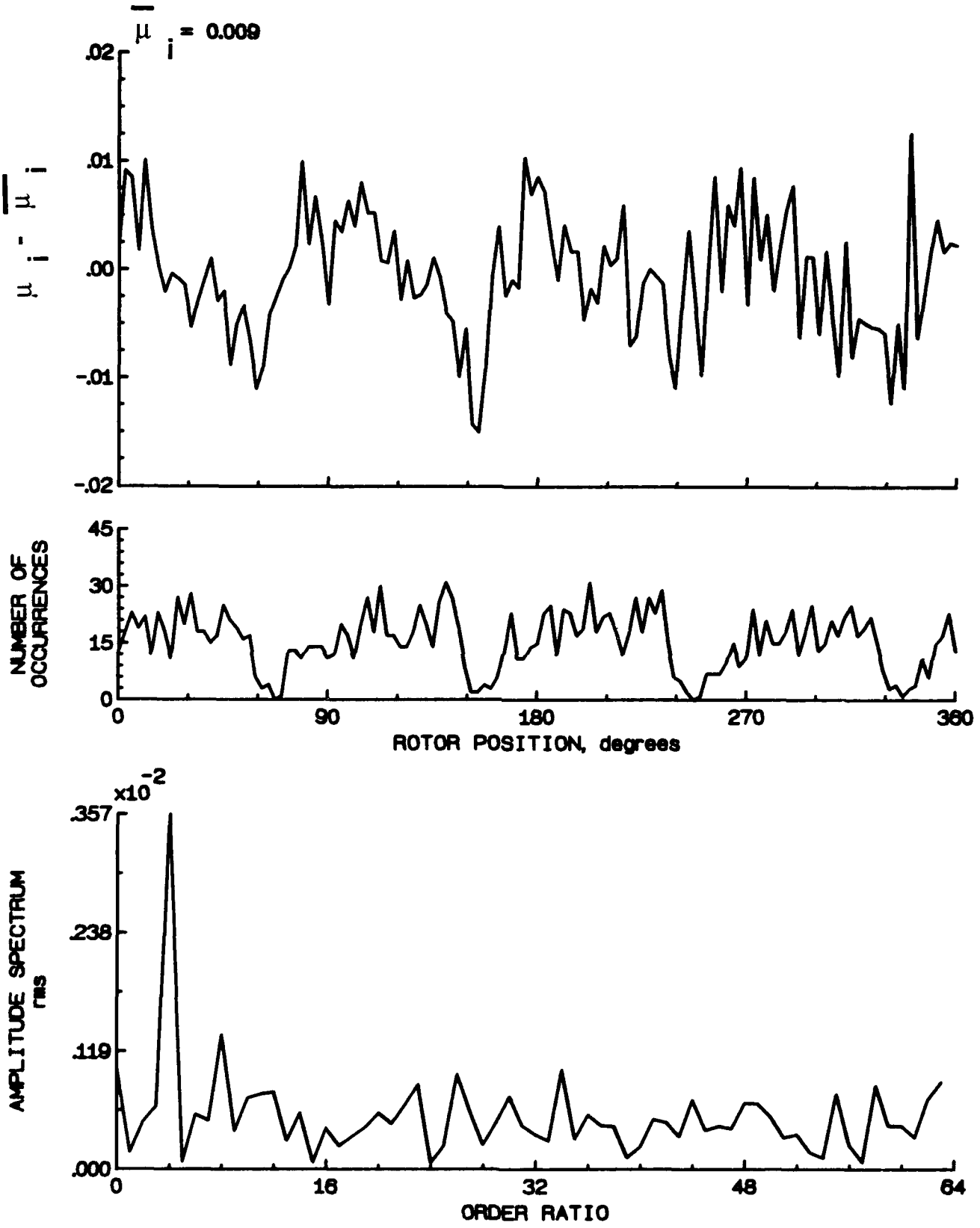

Figure 183.- Induced inflow velocity measured at 330 degrees and r/R of 0.82.

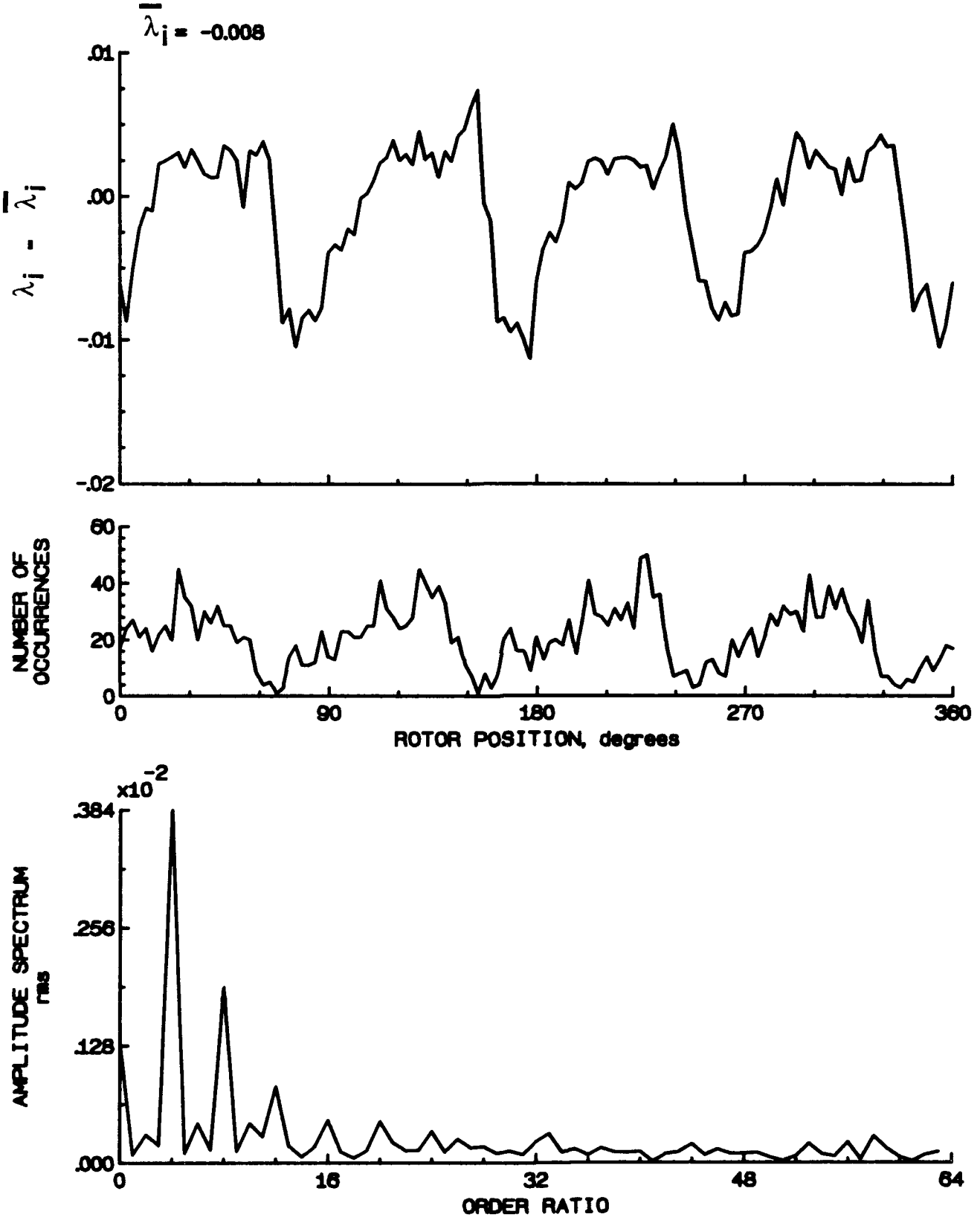

Figure 183.- Concluded.

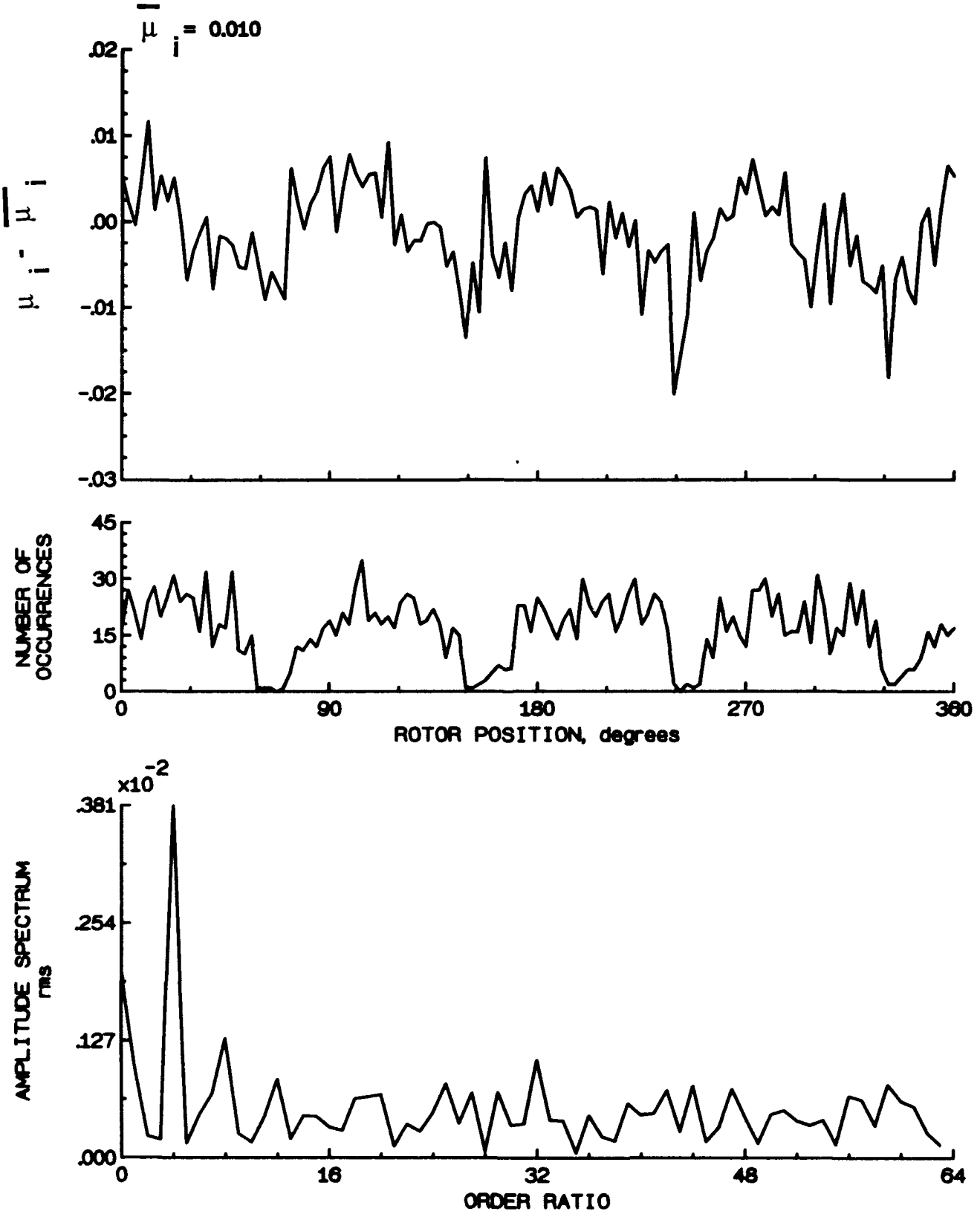

Figure 184.- Induced inflow velocity measured at 330 degrees and r/R of 0.86.

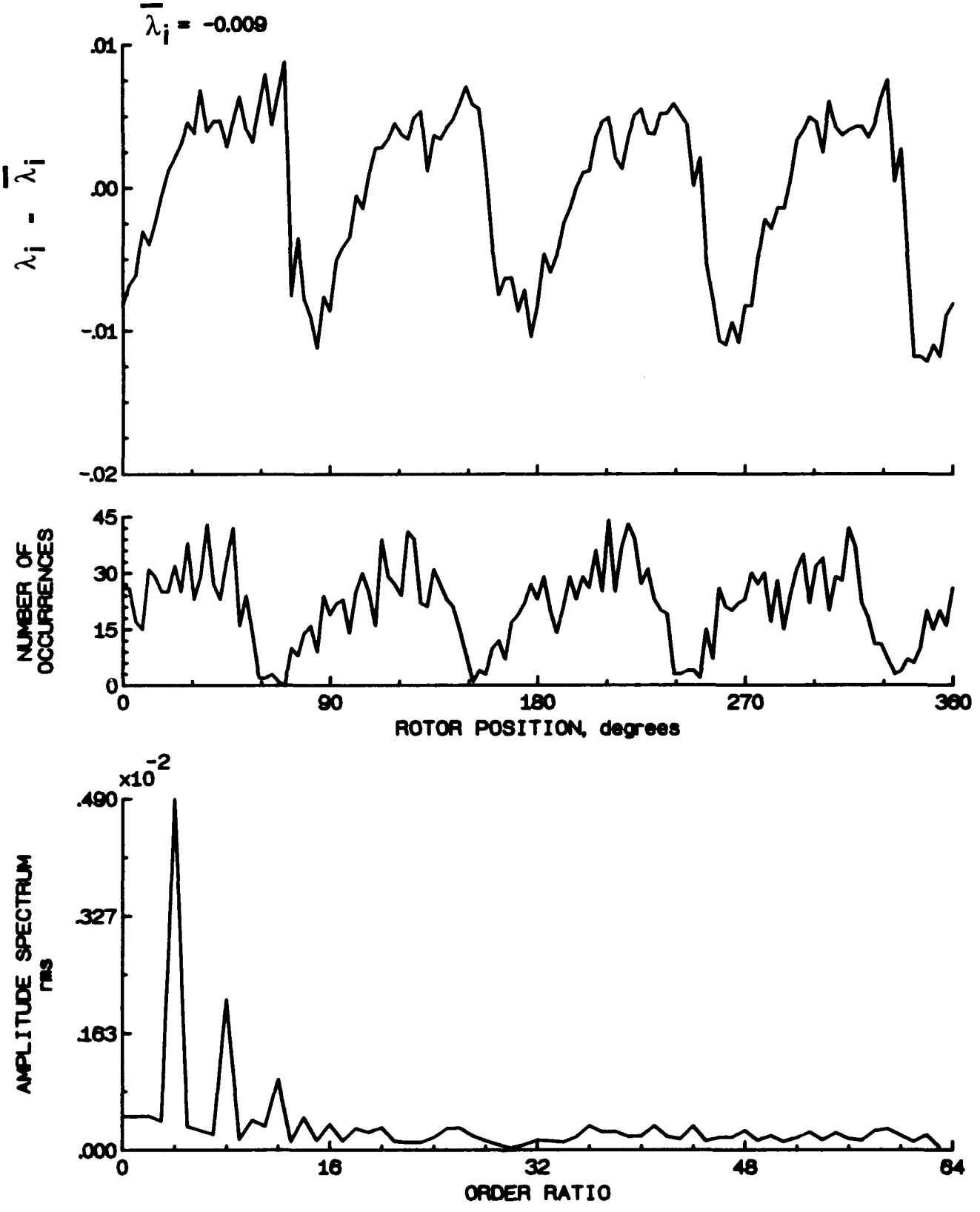

Figure 184.- Concluded.

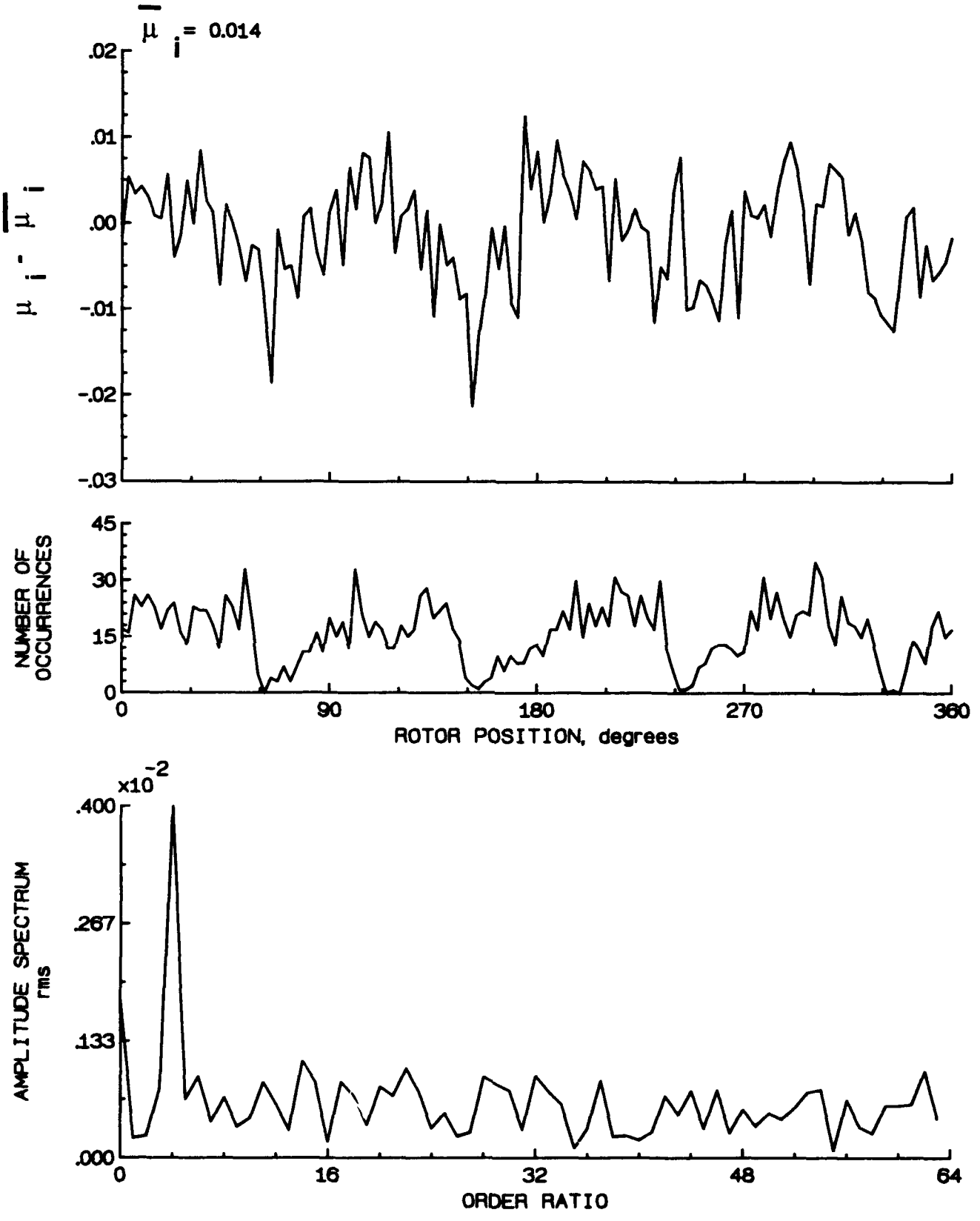

Figure 185.- Induced inflow velocity measured at 330 degrees and r/R of 0.90.

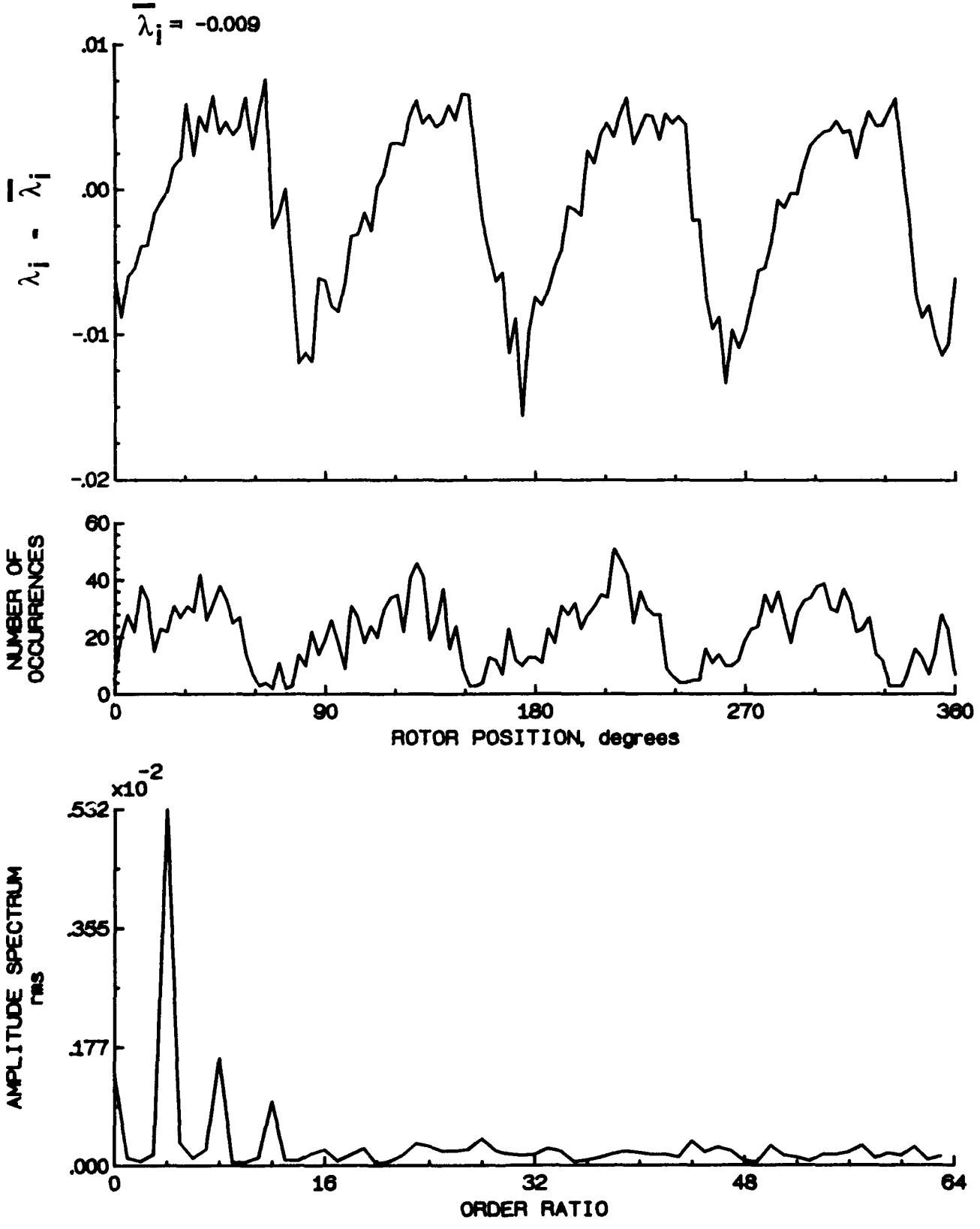

Figure 185.- Concluded.

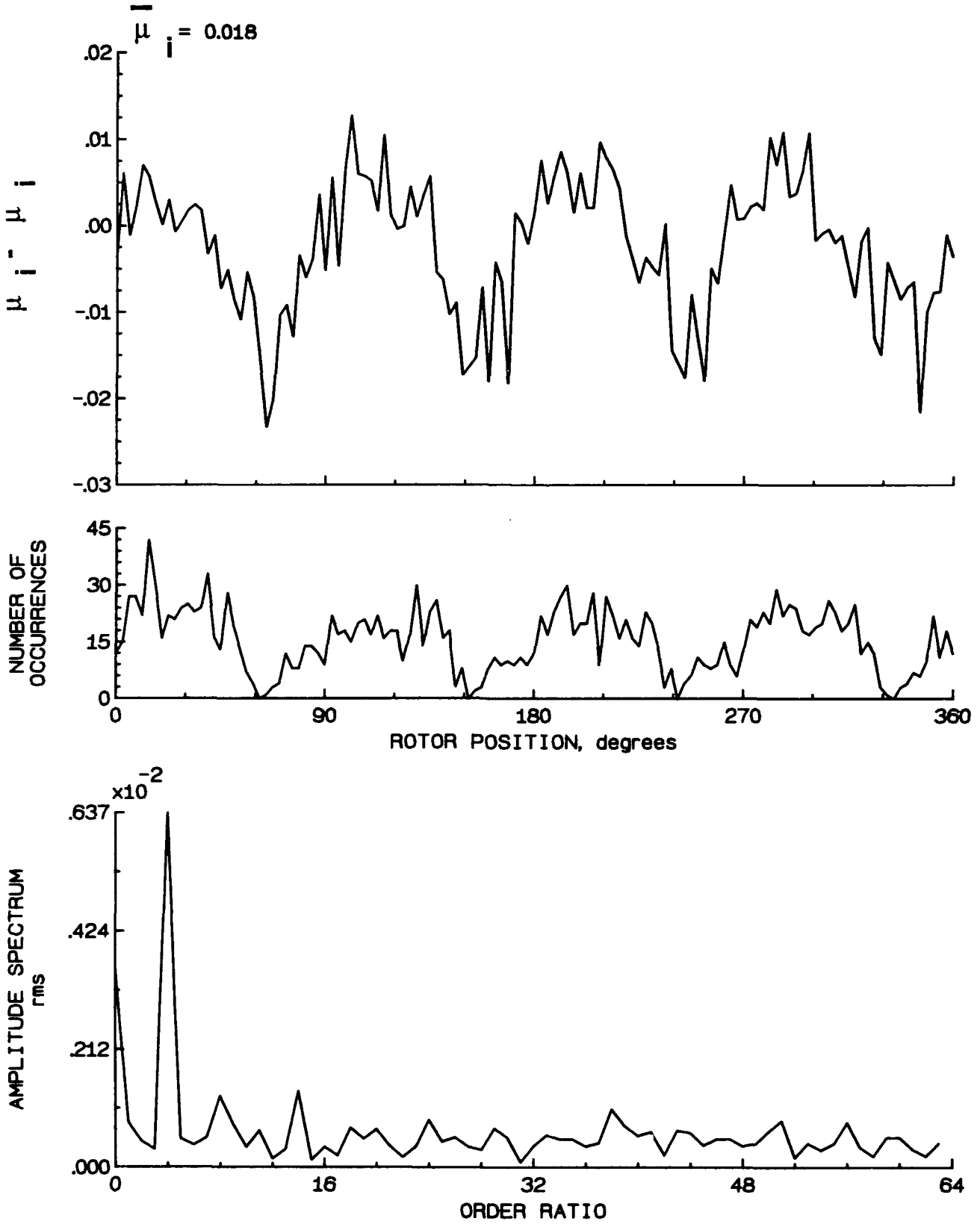

Figure 186.- Induced inflow velocity measured at 330 degrees and r/R of 0.94.

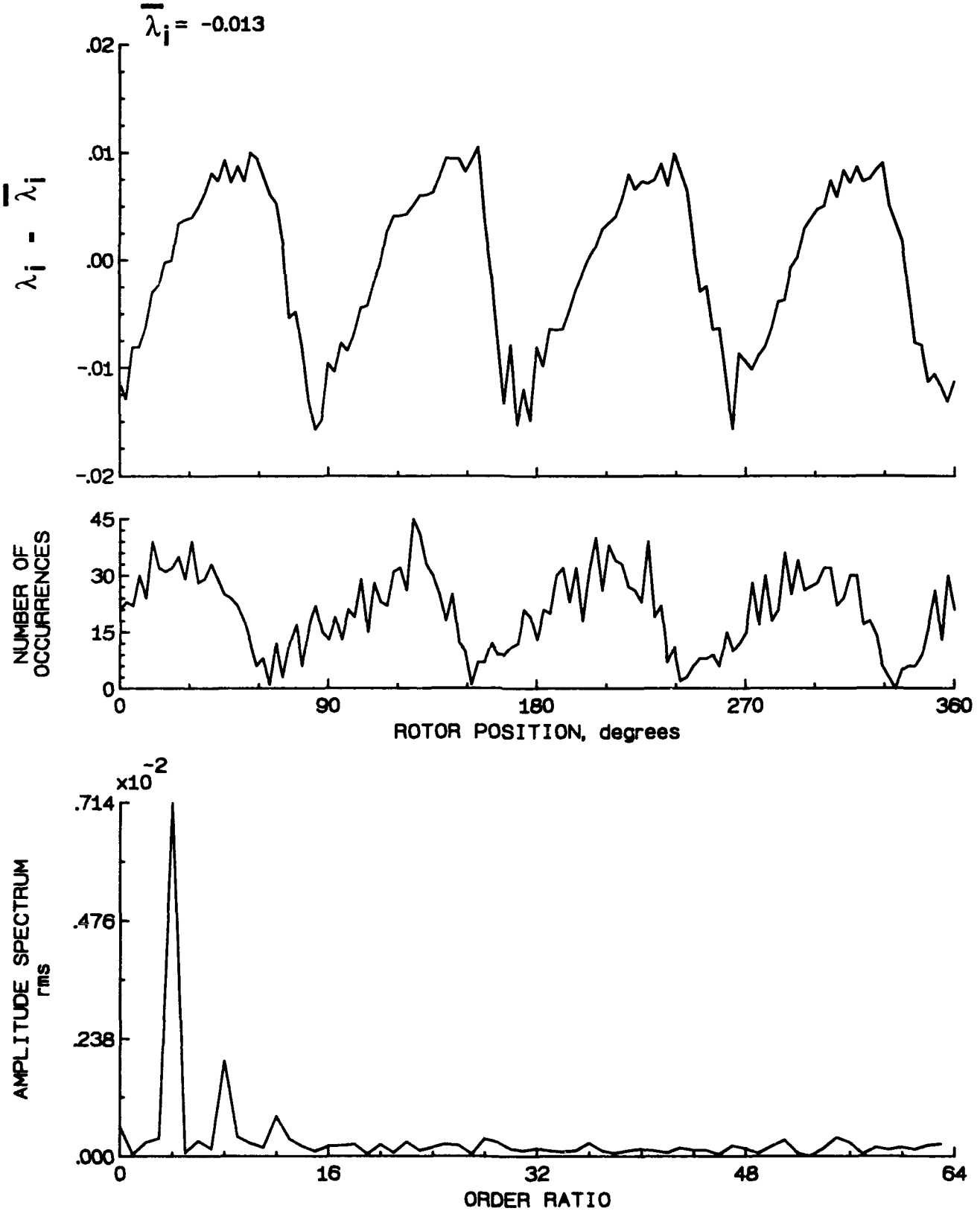

Figure 186.- Concluded.

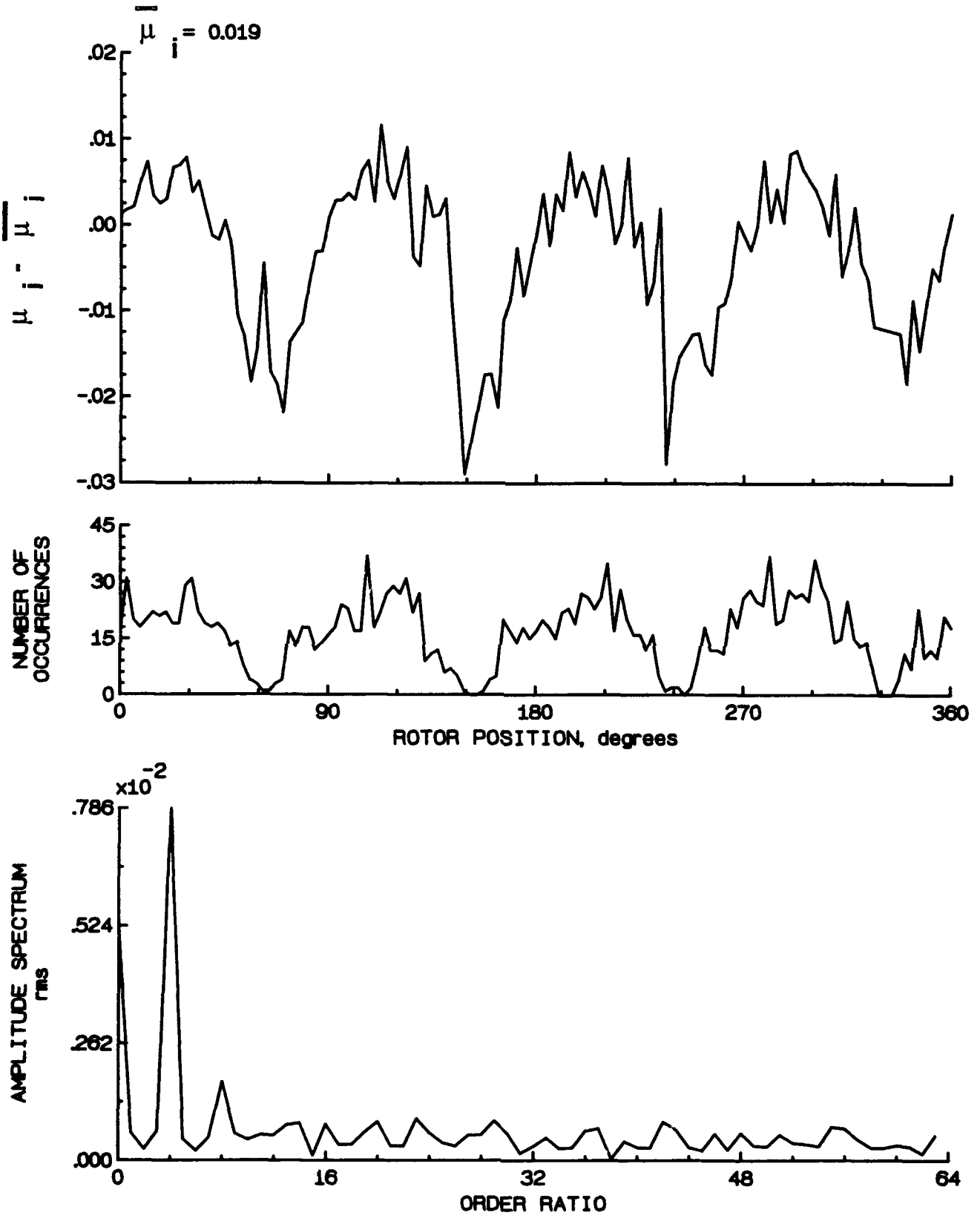

Figure 187.- Induced inflow velocity measured at 330 degrees and r/R of 0.98.

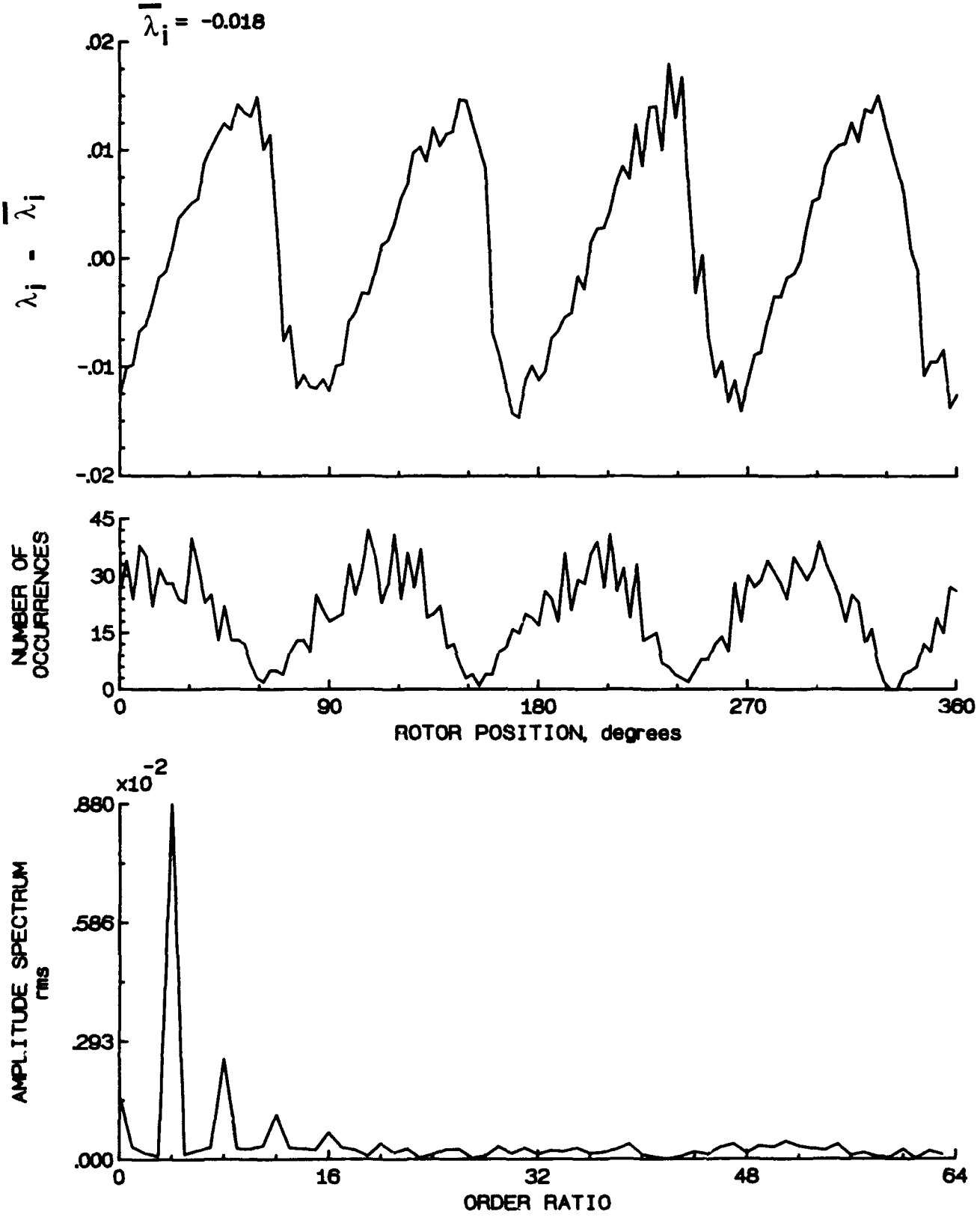

Figure 187.- Concluded.

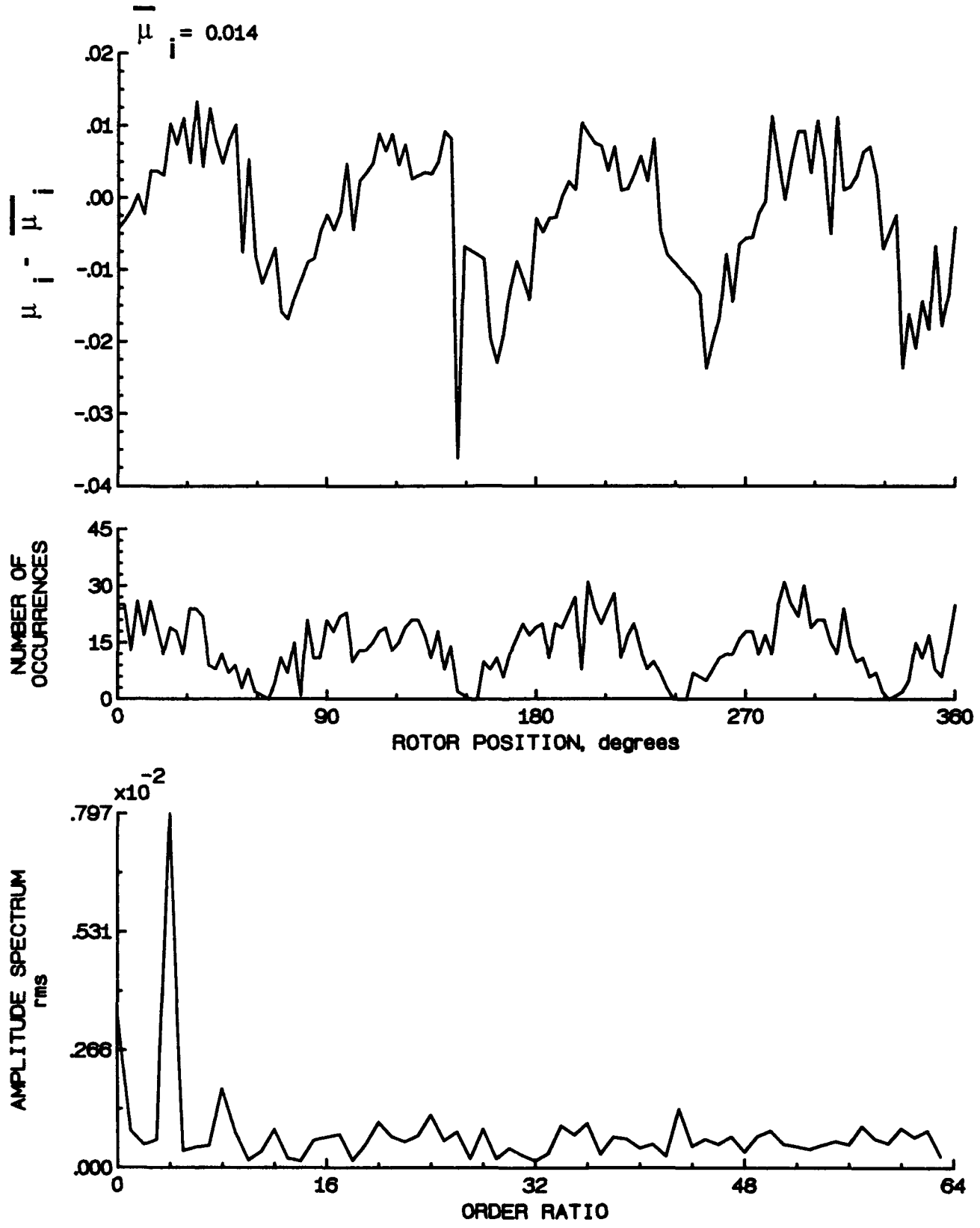

Figure 188.- Induced inflow velocity measured at 330 degrees and r/R of 1.02.

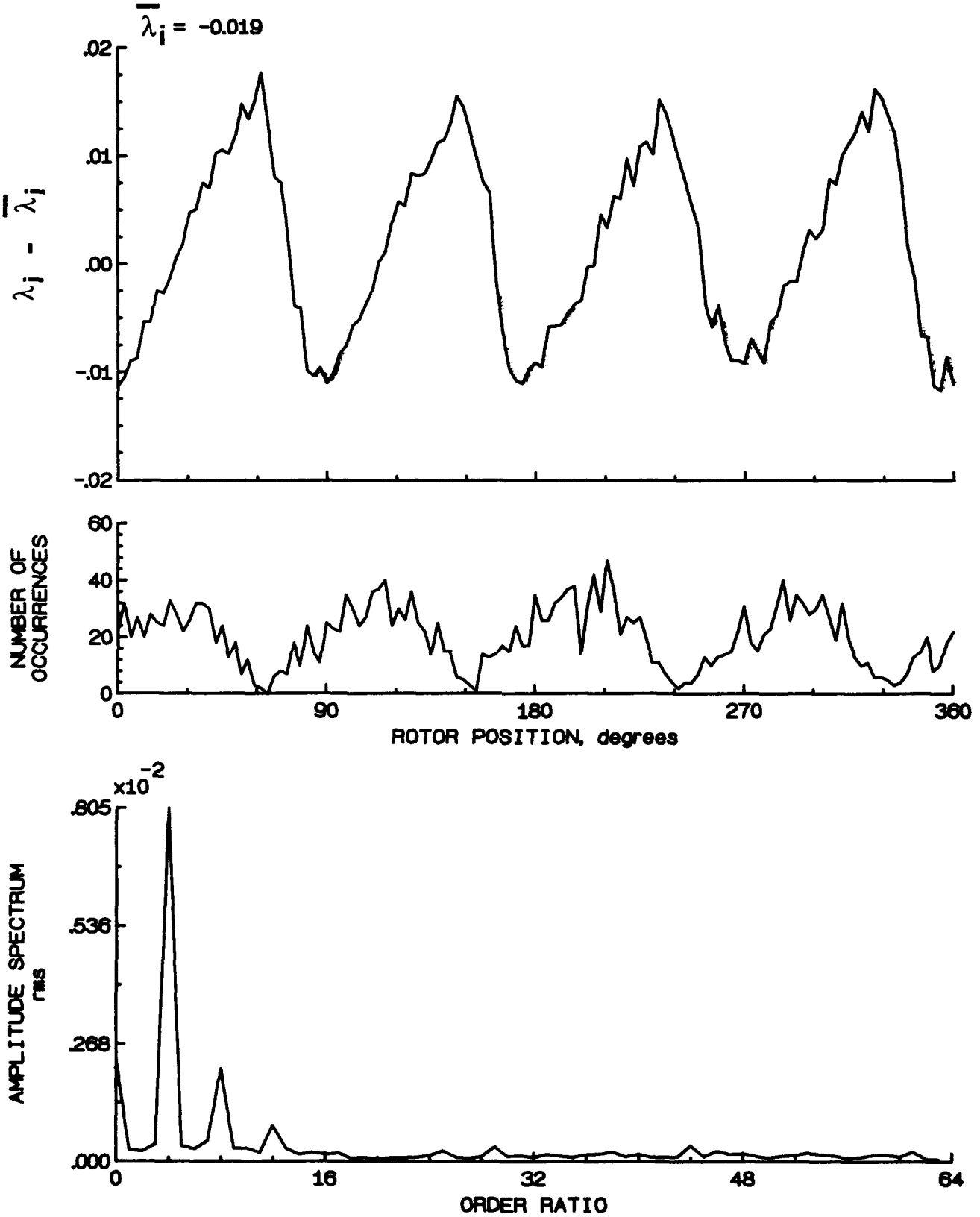

Figure 188.- Concluded.

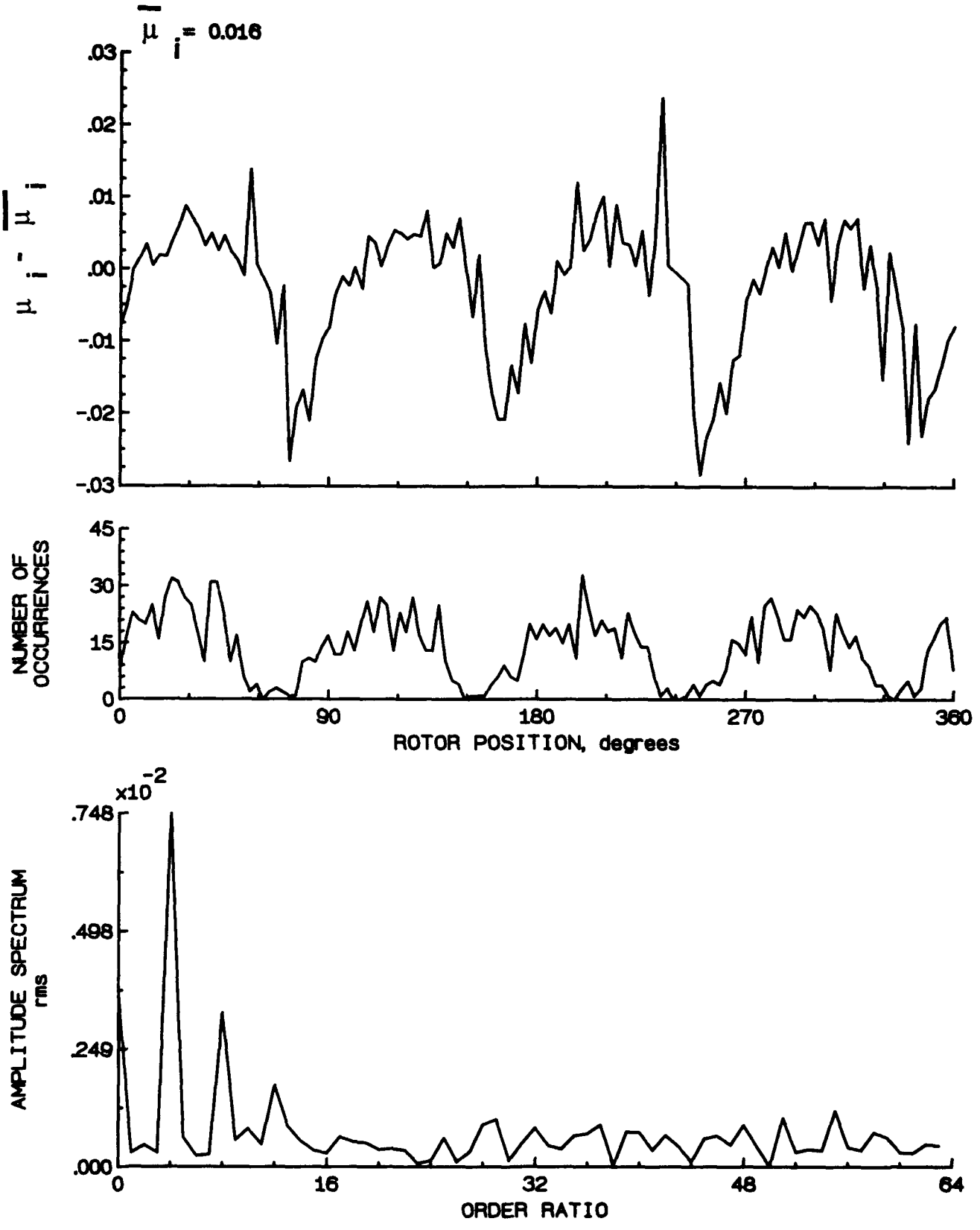

Figure 189.- Induced inflow velocity measured at 330 degrees and r/R of 1.04.

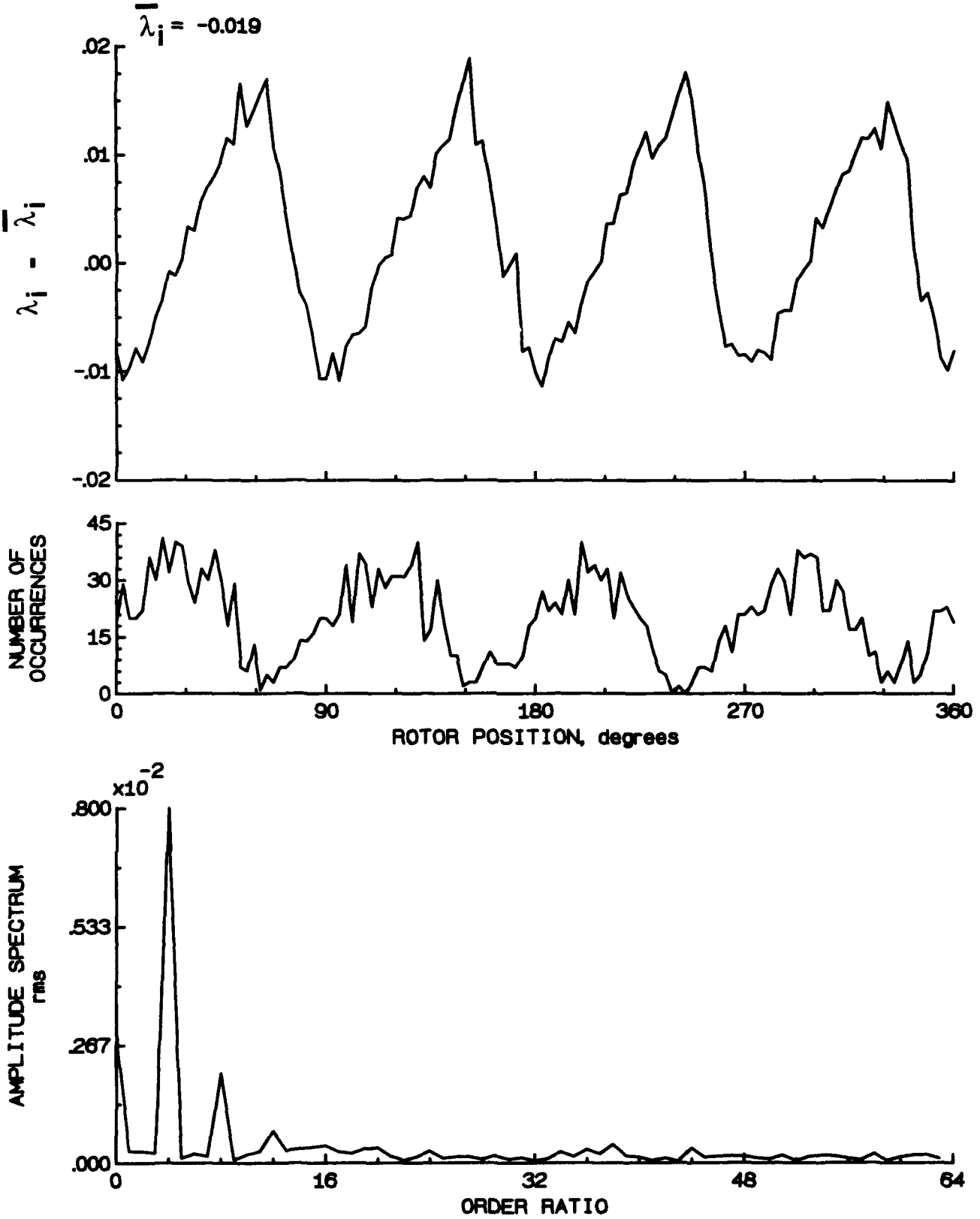

Figure 189.- Concluded.

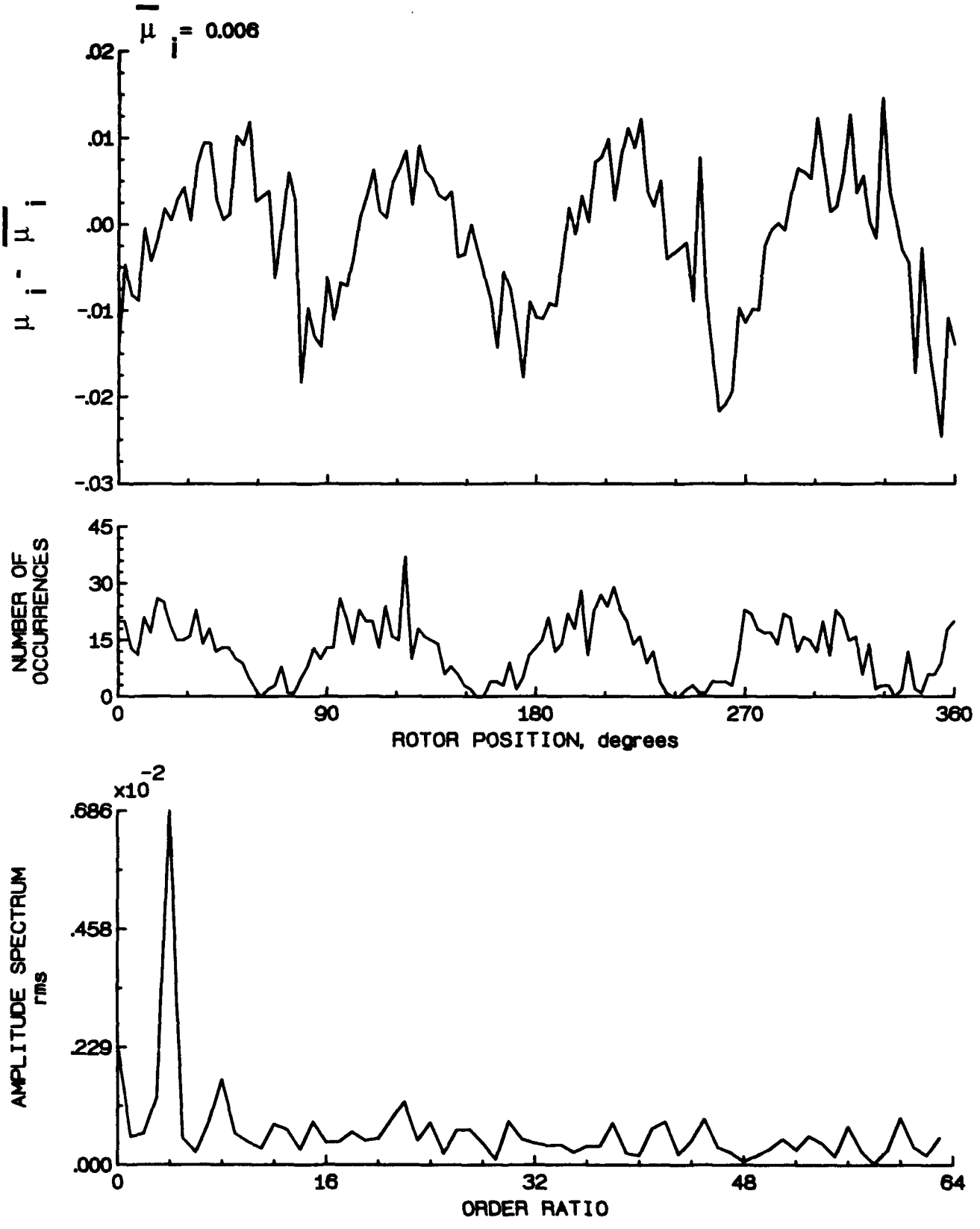

Figure 190.- Induced inflow velocity measured at 330 degrees and r/R of 1.10.

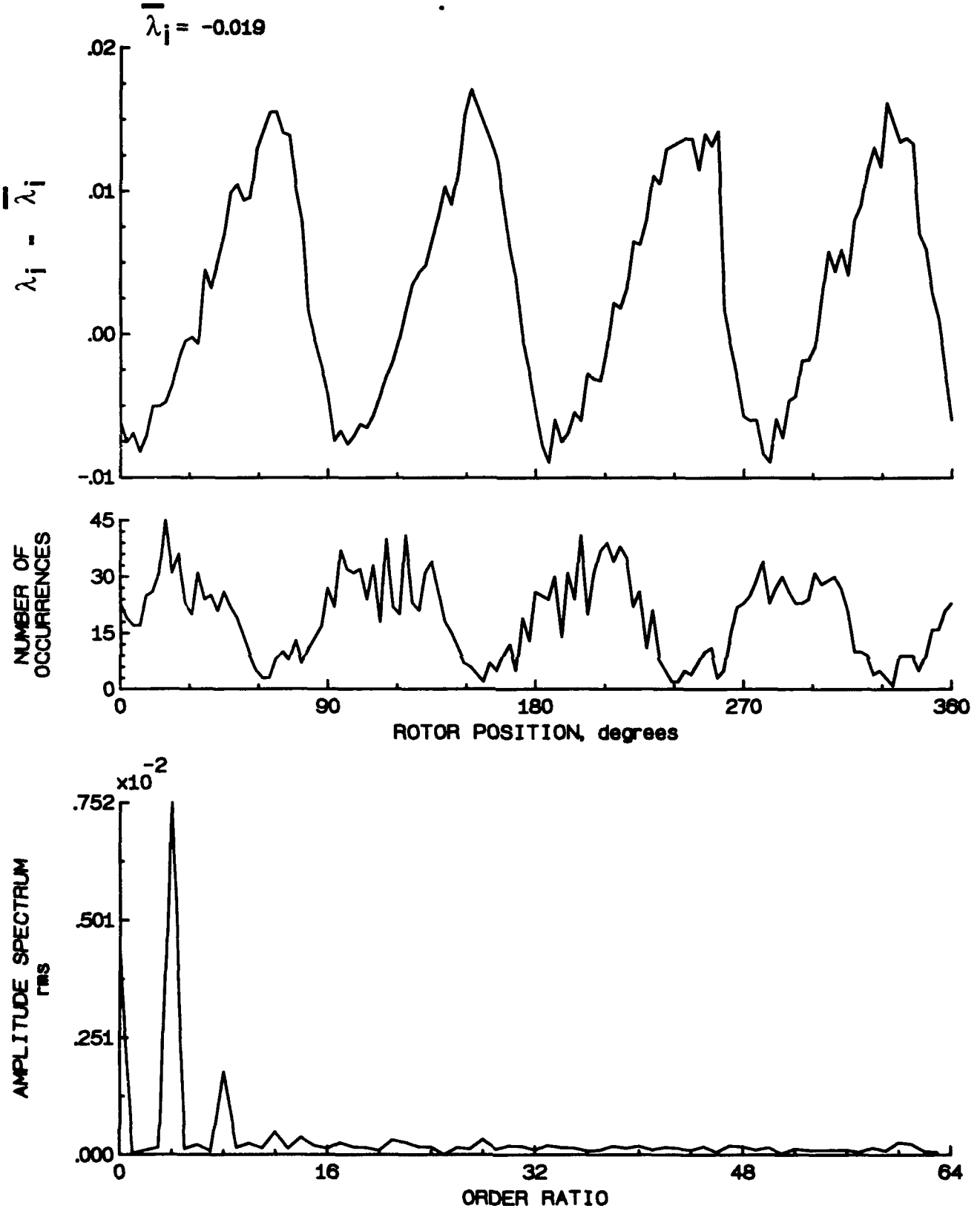

Figure 190.- Concluded.

NASA

Report Documentation Page

1. Report No.	2. Government Accession No.	3. Recipient's Catalog No.
NASA TM-101598 AVSCOM TM-89-B-001		

4. Title and Subtitle
Inflow Measurements Made With a Laser Velocimeter on a Helicopter Model in Forward Flight, Volume VI: Rectangular Planform Blades at an Advance Ratio of 0.35

5. Report Date
April 1989

6. Performing Organization Code

7. Author(s)
Danny R. Hoad, Susan L. Althoff, Joe W. Elliott, and Richard H. Sailey

8. Performing Organization Report No.

10. Work Unit No.
505-61-51-10

9. Performing Organization Name and Address
Aerostructures Directorate
USAARTA-AVSCOM
Langley Research Center
Hampton, VA 23665-5225

11. Contract or Grant No.

13. Type of Report and Period Covered
Technical Memorandum

12. Sponsoring Agency Name and Address
National Aeronautics and Space Administration
Washington, DC 20546-0001 and
US Army Aviation Systems Command
St. Louis, MO 63120-1798

14. Sponsoring Agency Code

15. Supplementary Notes
Danny R. Hoad, Susan L. Althoff, and Joe W. Elliott: Aerostructures Directorate, USAARTA-AVSCOM, Langley Research Center, Hampton, VA
Richard H. Sailey: Planning Research Corporation, Hampton, VA

16. Abstract

An experimental investigation was conducted in the 14- by 22-Foot Subsonic Tunnel at the NASA Langley Research Center to measure the inflow into a scale model helicopter rotor in forward flight ($\mu = 0.35$). The measurements were made with a two-component Laser Velocimeter (LV) one chord above the plane formed by the path of the rotor tips (tip-path-plane). A conditional sampling technique was used to determine the position of the rotor at the time that each velocity measurement was made so that the azimuthal fluctuations in velocity could be determined. Measurements were made at a total of 179 separate locations in order to clearly define the inflow character.

17. Key Words (Suggested by Author(s))	18. Distribution Statement
Rotor model Inflow Laser Velocimetry	Unclassified - Unlimited Subject Category 02

19. Security Classif. (of this report)	20. Security Classif. (of this page)	21. No. of pages	22. Price
Unclassified	Unclassified	390	A17